UNCLASSIFIED

AD **297 935**

Reproduced
by the

ARMED SERVICES TECHNICAL INFORMATION AGENCY
ARLINGTON HALL STATION
ARLINGTON 12, VIRGINIA
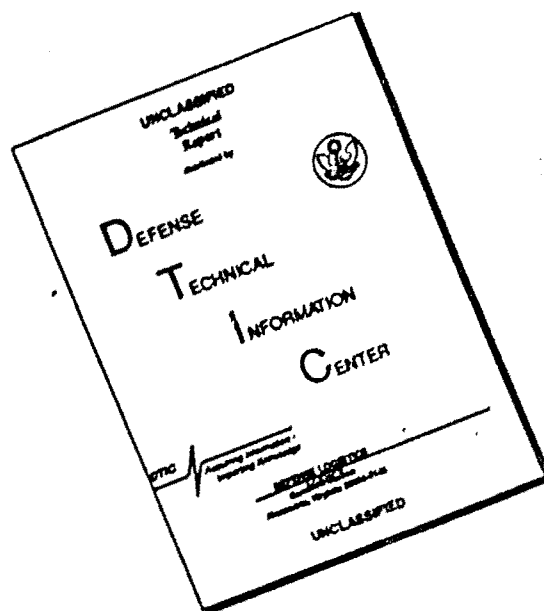
UNCLASSIFIED

DISCLAIMER NOTICE

UNCLASSIFIED
Technical
Report

DEFENSE

TECHNICAL

INFORMATION

CENTER

DTIC

UNCLASSIFIED

THIS DOCUMENT IS BEST
QUALITY AVAILABLE. THE COPY
FURNISHED TO DTIC CONTAINED
A SIGNIFICANT NUMBER OF
PAGES WHICH DO NOT
REPRODUCE LEGIBLY.

BLANK PAGES
IN THIS
DOCUMENT
WERE NOT
FILMED

Proceedings of the

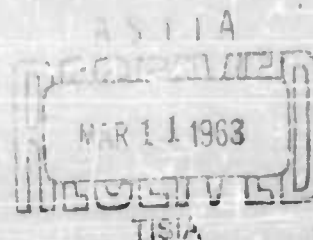# FLUID AMPLIFICATION SYMPOSIUM

October 1962

Volume I

DIAMOND ORDNANCE FUZE LABORATORIES
ORDNANCE CORPS ● DEPARTMENT OF THE ARMY
WASHINGTON 25, D. C.

Robert W. McEvoy
Lt Col, Ord Corps
Commanding

The Diamond Ordnance Fuze Laboratories is a Class
development, and engineering installation of the U. S. Arm.
Washington, D. C. Originally established in September 1953,
the Ordnance Corps, the Diamond Ordnance Fuze Laboratories
as the Ordnance Corps electronics laboratory, specializing in th
following areas:

) To perform research, development, and engineering on s
or automatically detecting targets of military significance,
local target evaluation, for accomplishing safing and
perfor...
ing function... for providing initiation signals in a manner t
imize weapons e... iveness.

(2) To perform the nece... research, development, a...
neering on components, subsyste... and systems of the type
to in Item (1) to achieve maximum imm... such systems to
conditions prevalent in a battlefield environ...

(3) To conduct a research program in fluid amplifica...
itary applications.

(4) To conduct instrumentation research and development
to the above.

.) To conduct basic research in the various required s...
fie... ated to the above.

In additio... ... major ...lity, DOFL operates a field...
located at ...os on... ... ... and ... Diamond Ord...
ation Facility at the Forest ... ... annex of the Walter Reed Army Med-
ical Center.

The findings in this report are not to be construed as an of...
Department of the Army position.

Proceedings of the
FLUID AMPLIFICATION SYMPOSIUM

Volume I

. M. Horton
Lt Col, Ord Corps   chnical Director
Commanding

The Diamond Ord.... . Fuze Laborate   ..... se research,
development, and engineering installation of : : ..... Army located in
Washington, D. C. Originally established in ... .. r 1953, under
the Ordnance Corps, the Diamond Ordnance F.... ... oratories serves
as the Ordnance Corps electronics laboratory, ... izing in the
following areas:

(1) To perform research, development, and   .. neer.ng on sys-
tems for automatically detecting targets of milita   ign icance, for
performing local target evaluation, for accompris   g safing and arm-
ing functions, and for providing initiation signals . manner to max-
imize weapons effectiveness.

(2) To perform the necessary research, deve   .. .., and engi-
neering on compon.nts, .ub...stems, and system   ... the type referred
to in Item (1) to .eh.   ... . sys.ems to the
conditions preva.... . a ...   .ed envi...... ...

(3) To conduct a .   .... n program in fluid a   .... mil-
itary application .

(4) To conduct in. ..mentation research and   .el.... .. related
to t. . bove.

(5) To conduct .   .. research in the various   .... .. .ientific
..elds related to the a...ve.

In ad....on to ... .. .or facility, DOFL operates ... d test area
located at Bloss... .   ., Maryland, and the Diar.... ... .nance Radi-
ation Facility a' the   ...st Glen Annex of the Wal.... R.. Army Med-
ical Center.

.. . . report are not to be c.... .. ... .fficial
                    . ... ..ent of the .. .. positi...

4

FOREWORD

A symposium on fluid amplification was held at the Diamond Ordnance Fuze Laboratories, Washington, D. C. on 2, 3, and 4 October 1962. The Proceedings of that symposium are issued in two volumes. Volume I includes all unclassified presentations. Volume II includes all classified presentations, which were given during the last half day of the symposium.

In addition to providing the first formal opportunity for the exchange of information regarding fluid amplification, an explicit objective of the symposium was to bring together the various persons interested in this new and yet unorganized field. The names and addresses of those who attended, except for personnel of the Diamond Ordnance Fuze Laboratories, are included in Volume I, for reference and to encourage further exchanges of information.

No record was made of the welcoming addresses delivered by Lt. Col. R. W. McEvoy, Commanding Officer, and B. M. Horton, Technical Director, Diamond Ordnance Fuze Laboratories, and their remarks are consequently not included. Their great interest in the field are perhaps sufficiently well known to make this omission excusable.

No attempt was made to edit the papers as presented at the Diamond Ordnance Fuze Laboratories; they were merely assembled and printed in the same order in which they were presented at the symposium.

CONTENTS

CONTENTS (Continued)

CONTENTS (Continued)

8

by

Brig Gen John G. Zierdt
Deputy Chief, R&D Directorate
U. S. Army Materiel Command

On behalf of the Army Materiel Command, I am glad to have this opportunity to welcome you to this first symposium on Fluid Amplification. I am pleased to be present at this assembly which represents government agencies and private concerns from coast to coast.

The concept of fluid amplification, that is, the control of high energy fluid streams by low energy flows, with no moving mechanical parts, was evolved by Mr. Horton less than four years ago. This concept constituted a major technical breakthrough in the sense that it represented a considerable advance in the state-of-the-art. This advance has removed many of the limitations on conventional military and commercial pneumatic systems and has enabled an extremely rapid extension of their capabilities. The use of low energy flow to direct and control high energy streams permits the design of pure pneumatic components, elements, and systems, capable of amplification, feedback, memory, logic functions, analogue computation, and digital computation. This, in turn, makes it possible to use pneumatic control systems, amplifiers, and computers where they could not be used before.

The work done here in your host agency, the Diamond Ordnance Fuze Laboratories, has already shown the great potential of this technology to the development of weapon systems and military hardware. The scientific staff at D.O.F.L. and we at A.M.C., who have cognizance and command supervision of their work, are aware of the tremendous advantages afforded by the simplicity, ruggedness, inherent high reliability, and virtual immunity to environment, even nuclear blast and the attendant high radiation levels, that are characteristics of the devices employing this new operating principle. These are essential requirements for military hardware.

When Mr. Horton and his associates first proved the feasibility of this new type control system, we recognized that his invention could open the way to rapid technological advances in civilian applications as well as in strictly military items. The decision was made at that time to release the information to American industry immediately, believing that this would lead to far faster development and greater

9

benefits to the country as a whole, both from the military and civilian standpoints, than could be achieved by cloaking this major breakthrough in military security. The diversity of representation here today bears out the wisdom of that decision.

You people have proven that you are quick to recognize and take advantage of the potential of this technique in your own specific fields. The response of industrial and scientific leaders to the challenge of new ideas and concepts is of great importance to those of us who are responsible for maintaining the competitive position of our nation in coping with those forces that are a continuing threat to our existence. The response to this challenge is indicated by the magnitude and scope of your effort in this new field and is evidenced by your presence here today. This acceptance of the challenge is indicative of the forward thinking attitude that is a mark of strength in American enterprise. We are heartened and our faith in the ability of our industrial leaders to take full advantage of the very latest technological advances to promote our economy is reaffirmed by the wide-scale recognition of the significance of fluid amplification techniques.

The Army Materiel Command has the responsibility for the scientific research and development work that is the basis for the design, production, and procurement of Army weapons and military materiel. We, therefore, fully appreciate the necessity for sound scientific investigation and for good communication between scientists. Such investigation and communication is particularly important in the prosecution of fundamental research in a stimulating new field such as that of processing control signals in fluid systems having no moving parts.

That is, of course, the object of this symposium. We encourage you to question, to challenge, to contribute. In this field which has, thus far, limited literature and limited exploitation there are few experts. We all have unsolved technical problems and unexplained experimental phenomena. Only by active participation can you exchange ideas and learn what others have done. The enthusiastic response of government agencies, universities, and private industries to the request for papers for this symposium, coupled with your individual participation as workers in this tremendously interesting and exciting field, should guarantee a profitable and stimulating meeting for all of us.

WALL EFFECT AND BINARY DEVICES

by

R. W. WARREN

of

Diamond Ordnance Fuze Laboratories

In general, there are two approaches to fluid amplification. In the first approach the large power jet is deflected by a small control stream, the amount of the deflection being proportional to the momentum of the streams. The second method is to use the entrainment characteristics of the stream and bounding walls to effect the deflection.

This is a short introduction to the way the flows and walls are used to obtain a bistable amplifier.

In Figure 1, a submerged stream is seen issuing from a nozzle between bounding walls. The stream entrains fluid from the interaction region, lowering the pressure. The entrained fluid is replaced by a counterflow of fluid from the ambient pressure. This is an unstable situation. Any small perturbation, turbulence or mechanical misalignment, will incline the stream closer to one wall than the other.

The stream entrains essentially an equal amount of fluid on each side. However, as the area available for counterflow is less on one side than the other, the pressure is reduced on that side creating a pressure difference across the stream. The pressure difference inclines the stream toward the low pressure region still further restricting the area available for counterflow. Thus a regenerative action is instituted which rapidly forces the stream to the wall, as shown in Figure 2. There is ambient pressure on one side of the stream and a low pressure separation bubble on the opposite side of the stream which is denied fluid to replace the entrainment. The differential pressure across the stream curves the stream to the wall. Where the stream contacts the wall the majority of the flow is diverted toward the outlet with a resulting high pressure on the wall. A small amount of the flow is curved back toward the nozzle where it circulates as a vortex to be reentrained by the stream.

The bistable amplifier is shown in Figure 3. If flow is introduced into the separation bubble through the right control, the point of attachment will move downstream but remain attached to the wall until the entrainment characteristics of the stream are satisfied. When there is sufficient control flow to satisfy the entrainment, the stream will

11

move to the center of the interaction region. Entrainment will lower the pressure on the left side of the stream and the stream will attach to the left wall.

An alternative method of switching the stream is to remove fluid from the left control. This, in combination with the entrainment, lowers the pressure on the left and the stream attaches to the left wall. If the control openings are large enough to admit sufficient flow from the atmosphere, the unit can be shifted by closing one control and opening the other. The stream moves to the side of the closed control, as the closed control limits the entrainment on that side. If the outputs of the unit are loaded, the pressure in the interaction region increases and there is an outflow from both controls. In this instance, if one of the controls is closed the stream attaches to the opposite wall. In other words, the controls have reversed. Actually the operation of the unit is the same, as the flow out of the open control limits the entrainment on that side and the stream attaches to the wall on the side where the entrainment is limited.

There is always a question as to the range of Reynolds numbers over which a unit can be operated. It was found that a stream of air would attach to the wall at a power pressure of .2" of water above atmosphere. This is approximately .007 PSIG. A Reynolds number was calculated for this pressure using the wetted perimeter of the nozzle, for L in the formula for the Reynolds number $R = \frac{\rho V L}{\mu}$. A Reynolds number of 200 was obtained by this method. The units have also been operated with a Reynolds number of over one million. The high level of operation occurs when the stream expands outside the nozzle sufficiently to attach to both boundary walls, as shown in Figure 4. The stream can still be controlled by admitting a control flow but the unit is no longer bistable.

A flow model of the stream is shown in the upper view of Figure 5. The power stream is issuing from a nozzle into the interaction region. There is a central core where the pressure is essentially unchanged from the source. This region has not felt the effects of the entrainment and the lower pressure in the interaction region. There is an outer mixing zone where the stream is entraining fluid, and an inner mixing zone which contains fluid entrained from the separation bubble or from the control. The middle view shows the velocity profiles of the stream across the core region at a point on the wall just downstream of the attachment point. The lower view shows the static pressures along the wall to which the stream is attached. It can be seen that there is a low pressure in the separation bubble which rises to the higher pressure at the stream reattachment point. The pressure goes still higher as the stream is diverted to flow along the wall and then the pressure decreases in the boundary layer to essentially the exhaust pressure.

When a unit is being loaded, the pressure in the boundary layer must rise above the pressure which exists just beyond the reattachment point

12

before it can affect the separation bubble and separate the stream from the wall. A pictorial view of a loaded unit is shown in Figure 6. The stream was originally going out the right outlet. When this outlet was blocked the pressure rose in the outlet and an increase in pressure proceeded down the boundary layer. The stream flowed around the splitter and out the left outlet. The splitter is far enough downstream so there is no turbulence at the reattachment point and the pressure in the right outlet does not exceed the pressure at the reattachment point so that the stream remains locked to the right wall while exhausting out the left outlet. As can be seen from Figure 6, a vortex is formed on the left side of the stream in the interaction region, which aids materially in stabilizing the flow. This feature of the unit is called memory, and is a function of the splitter position.

It is well known that a stream can become over-expanded and separate from the wall of a diffuser. This characteristic gives another mode of operation for a supersonic bistable element. In Figure 7, an over-expanded stream is seen which is separated from the left boundary wall by an oblique shock-wave. The oblique shock-wave adjusts the flow between the over-expanded region in the stream which is between 2 and 5 psia (pounds per square inch absolute) and atmospheric pressure on the other side of the shock-wave. Opening the right control to atmosphere or otherwise introducing flow into the right control will flip the power stream to the left wall.

There are many parameters which can be varied in a bistable fluid element. In addition to the pressure and flow, physical parameters can be varies also. The effect of varying some of the physical parameters is shown on Figure 8. On the right is shown the effect of moving the splitter downstream, increasing the receiver aperture, increasing the wall angle, and increasing the nozzle area. On the left is shown the effect of increasing the interaction region width and increasing the depth or aspect ratio. The effects of increasing the loading and the power jet pressure are also shown on this figure. Additional work needs to be done in evaluating the relationship of these variables.
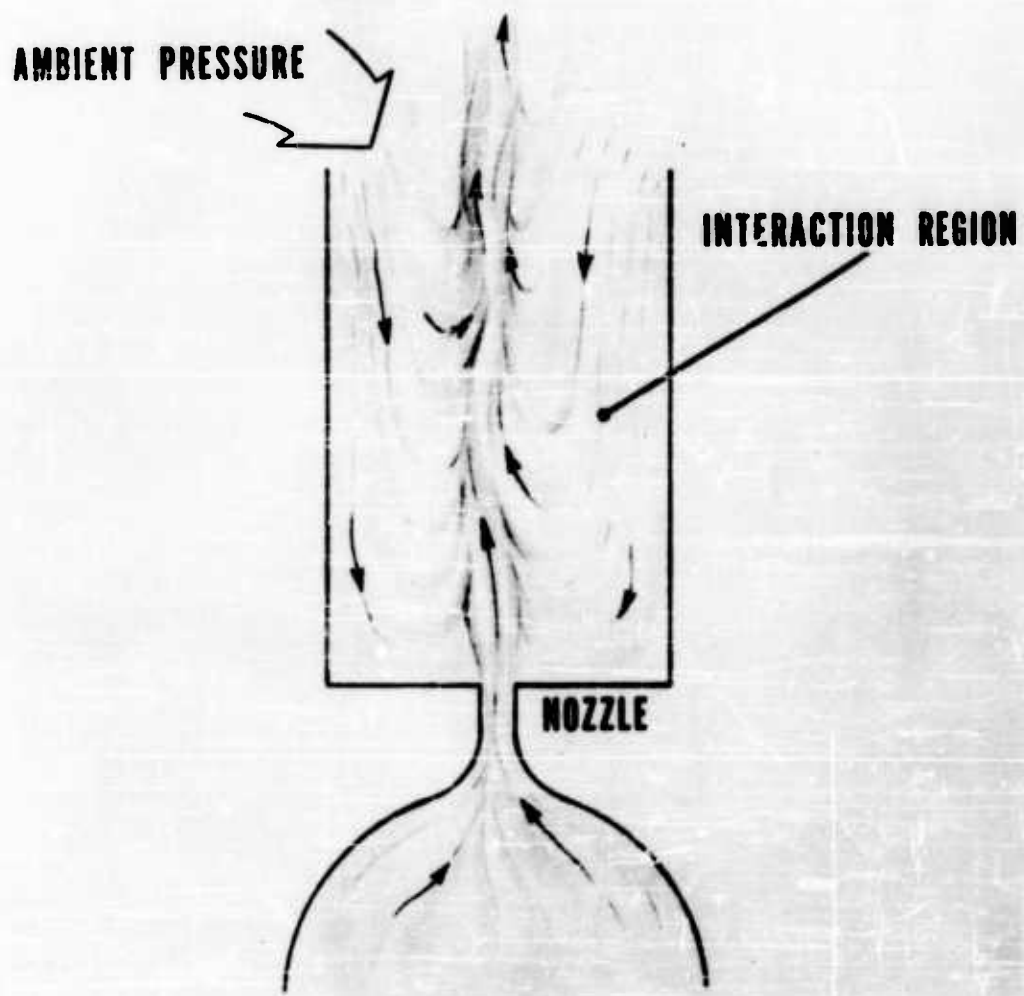
Figure 1. Initial fluid flow between parallel walls.

14
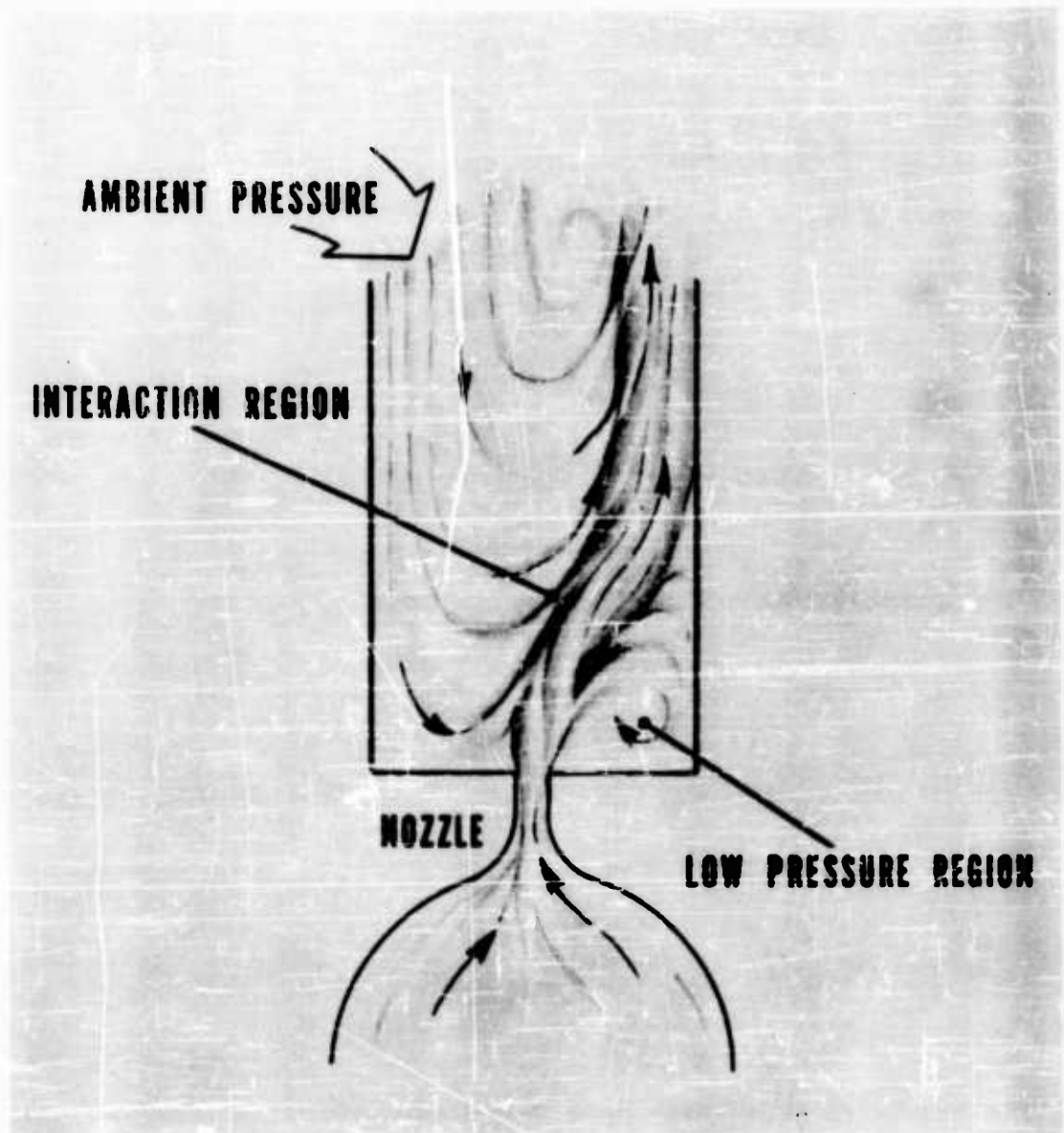
Figure 2. Final fluid flow between parallel walls.
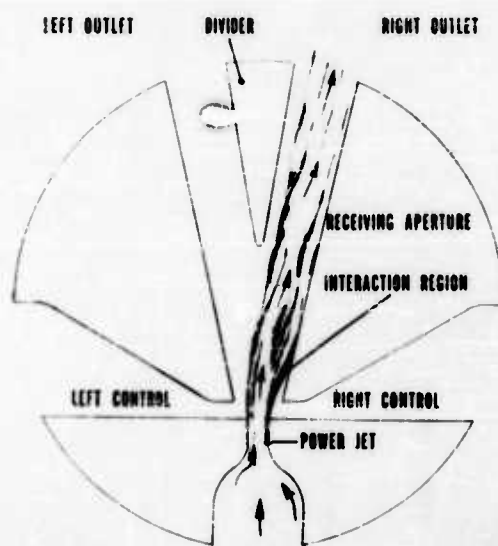
Figure 3. Fluid bistable element.
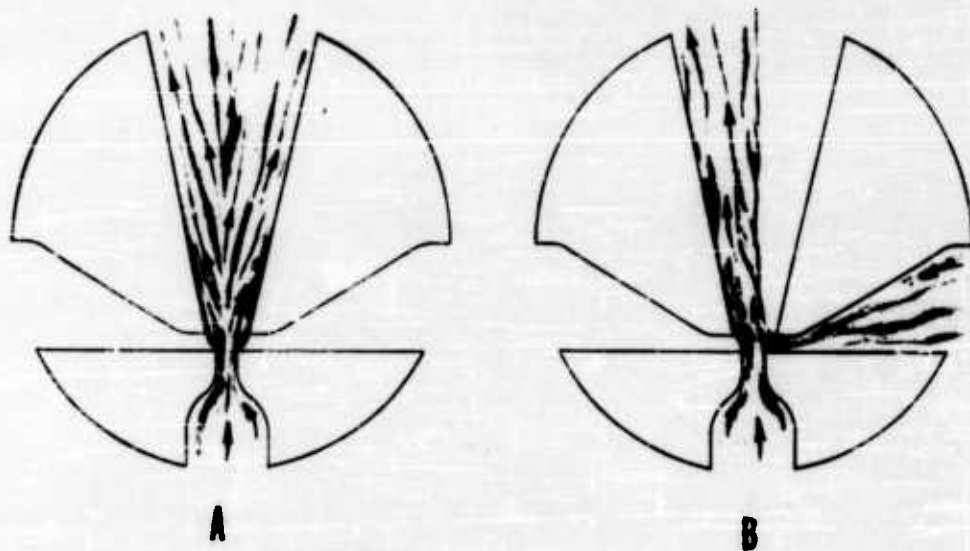
Figure 4. Control of completely filled bistable elements.

16
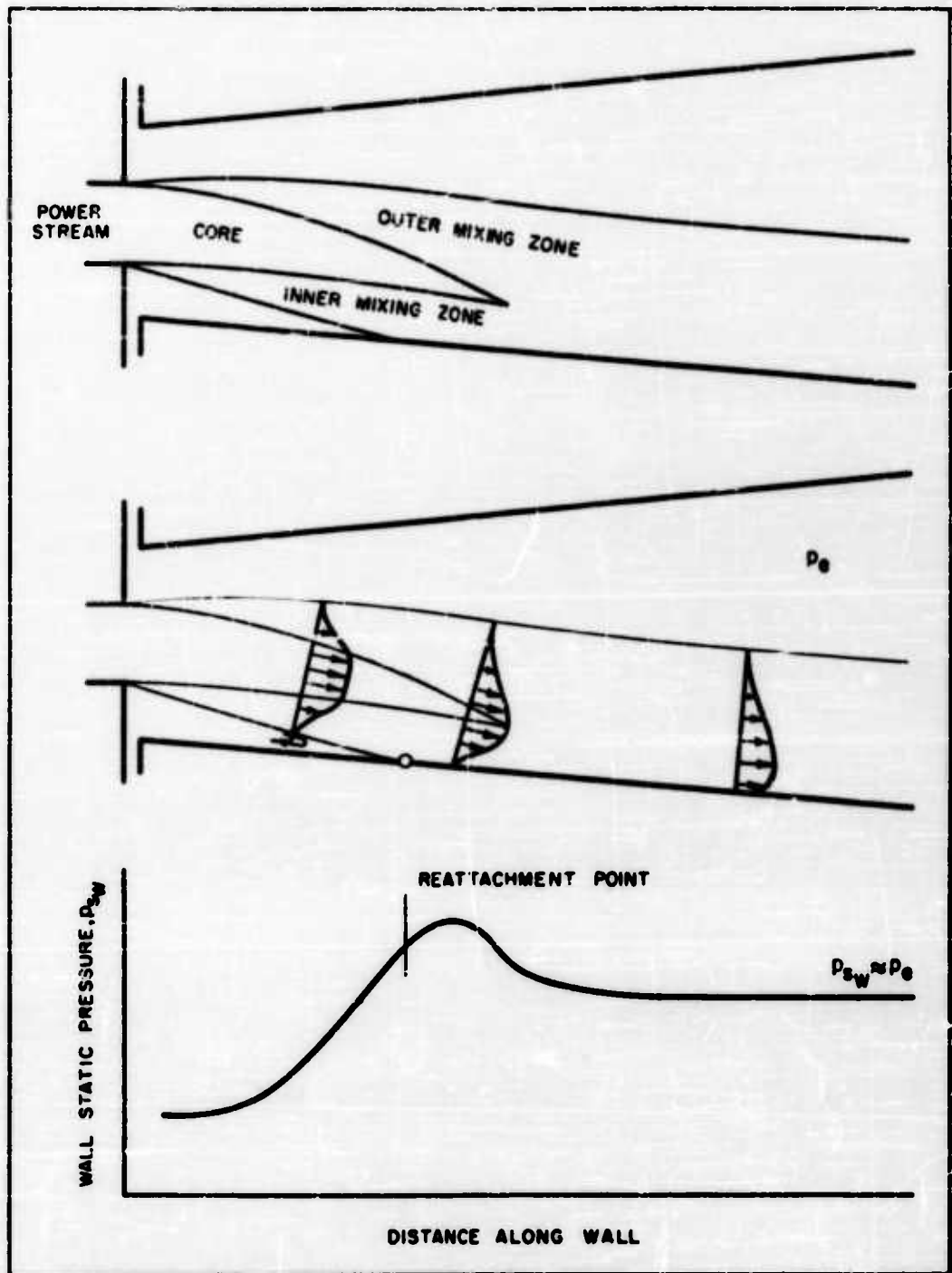
Figure 5. Flow model for interaction and profile adjustment regions.

17
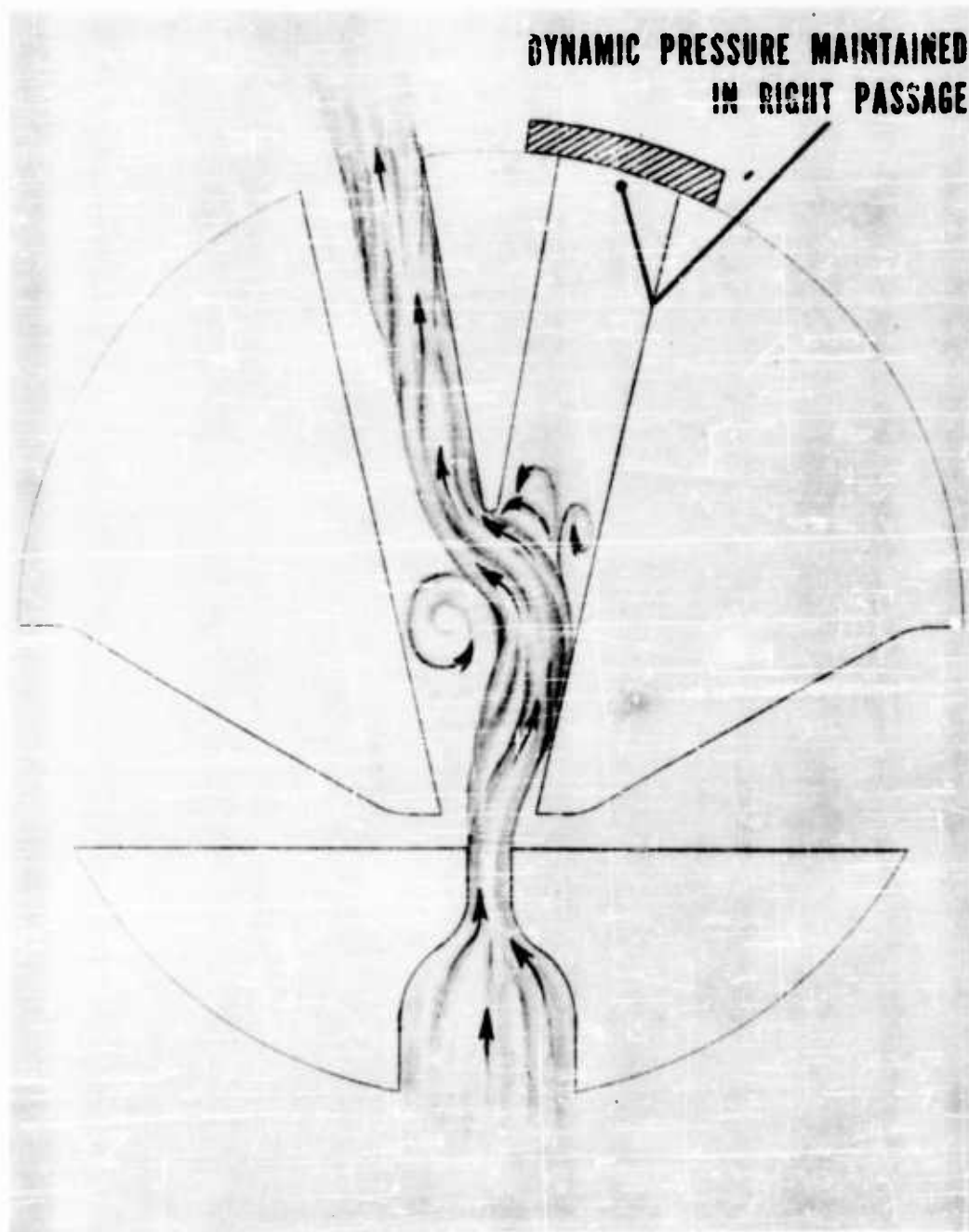
Figure 6. Memory characteristics of fluid bistable elements.

18
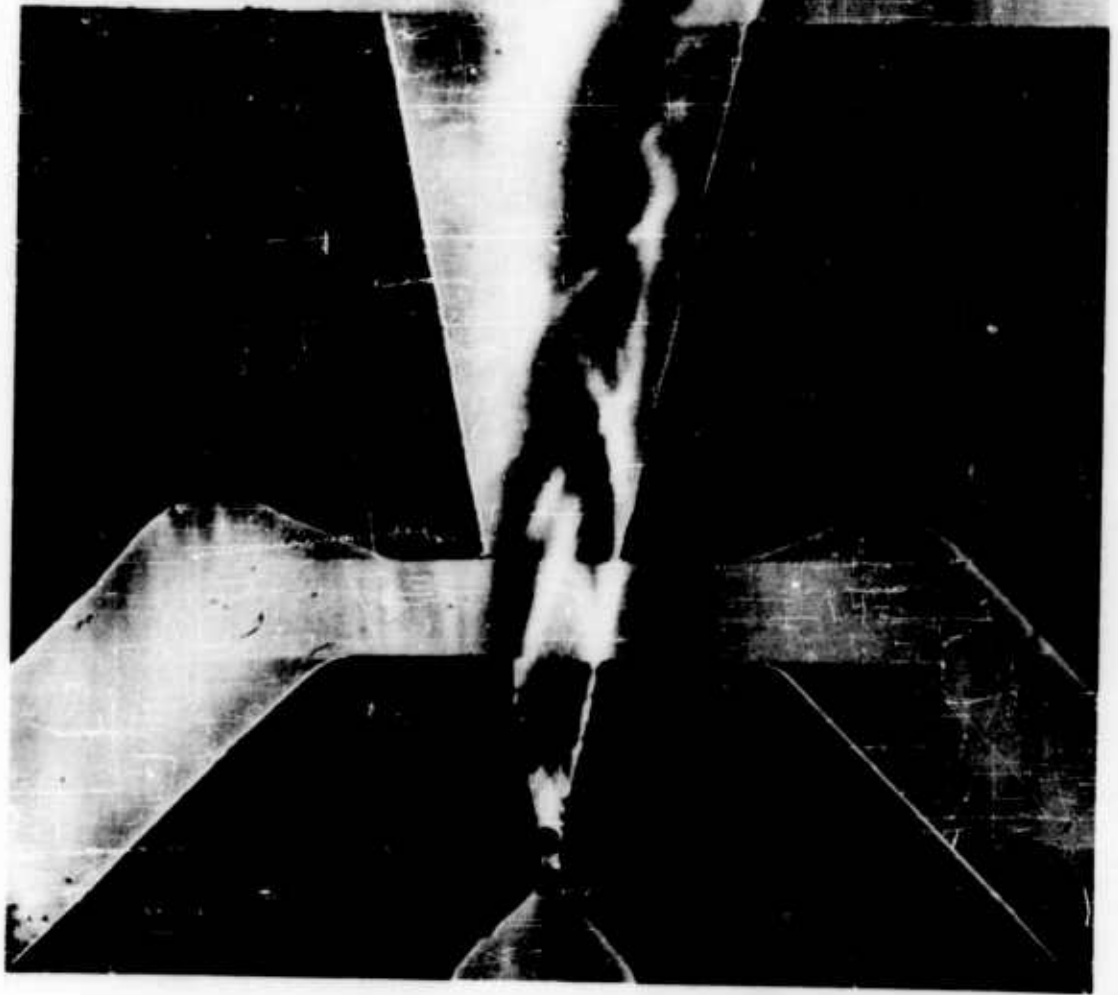
Figure 7. Schlieren photograph of bistable reaction jet.
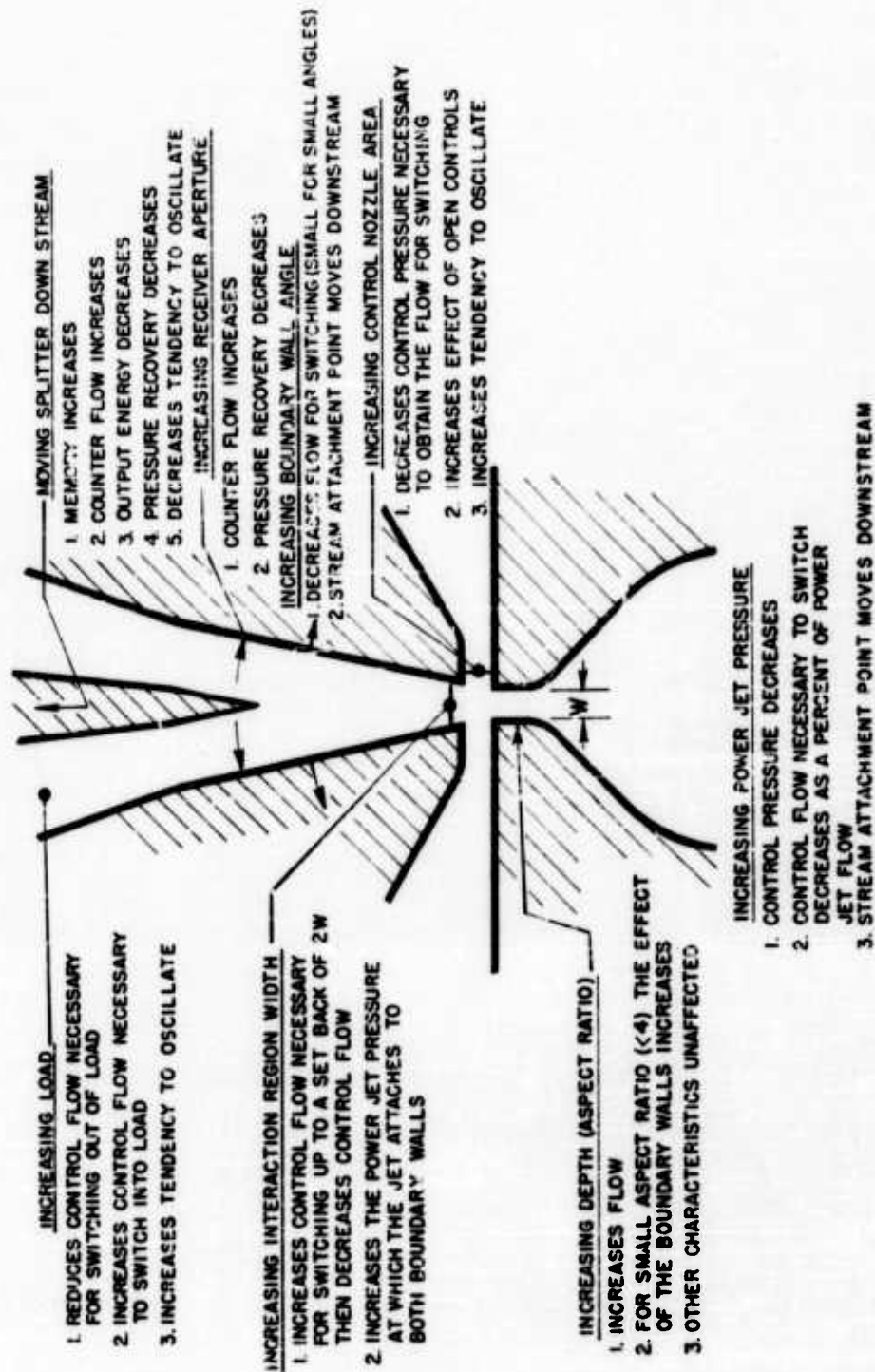
Figure 8. Effect of increasing dimensions of fluid bistable element.

AN INTRODUCTION TO PROPORTIONAL FLUID CONTROL

by

Silas Katz

of

Diamond Ordnance Fuze Laboratories

One of the objectives, here at DOFL, is to develop a proportional fluid control system without mechanical moving parts. To accomplish this requires both active and passive components without mechanical moving parts.

The active component, which is the basic building block of the control system, is the proportional fluid amplifier. This device provides a large fluid output signal that is proportional to a smaller fluid input signal. A basic single stage proportional amplifier is shown in Figure 1. High energy fluid from the power jet is directed into the interaction region. Control or low energy fluid is also directed into this region from jets on each side of the power jet. The direction that the power jet assumes after interaction with the control jets depends on the momentum flux of the power jet and the forces exerted by the control jets. At some distance downstream the jet is collected by two output apertures. There is an optimum position for these outputs. They must be far enough downstream to take advantage of the stream deflection and close enough to recover a reasonable amount of stream pressure. When the control pressures are equal, the power stream is not deflected. Then each output aperture collects the same quantity of fluid. A small change in one of the control pressures deflects the power stream and causes one output to collect more fluid than the other. Since the output difference is greater than the control difference which caused it, this is a stage of amplification.

The unusual shape of the interaction chamber shown in Figure 1 was deliberately chosen to prevent the power stream from locking-on to the walls and making the amplifier bistable. The shape and dimensions of the cutout areas have a considerable influence on the performance of the amplifier. Any fluid that is not picked up by the output collectors must be removed as efficiently and with as little disturbance as possible. When disturbances are present they may be reflected from the walls of the cutout back toward the power stream to produce a feedback effect. This could result in unstable

operation, oscillation, or reduced gain. In practice the two cutout side chambers are connected together to equalize the pressure across the power stream.

Figure 2 shows a Schlieren photograph of a power stream being deflected by a control stream. The deflecting force of the control streams may be generated in two ways. The force may be either a pressure force or a momentum flux force. Both force types are present in any proportional amplifier. In general, the low frequency input impedance of an amplifier with predominantly pressure type force is high. When the forces are predominantly momentum flux type the low frequency input impedance is low. In the particular geometry shown in Figure 2, momentum flux forces predominate. However, by bringing the controls in closer to the edges of the power jet, the pressure force is increased and the momentum flux force is decreased.

A more complex type of fluid amplifier is shown in Figure 3. Two stages of amplification are cascaded with one power supply. Power is supplied to the first stage only. The second stage obtains its power by picking off part of the first stage flow at the collector station. The outputs of the first stage become the inputs to the second stage. In operation an input signal at the control to the first stage is received amplified at the output of the second stage. The advantage of this configuration is increased amplification without an additional expenditure of supply fluid.

Passive components do not require a separate power supply. They produce their effects solely because of the fluid properties and a particular geometry. Some passive components are shown in Figure 4. In dealing with passive components it is convenient to use the electrical analogy. Thus, pressure is analogous to voltage and flow is analogous to current. Resistance is represented by an orifice or porous plug. The magnitude of the resistance depends on the viscosity of the fluid and the diameter of the orifice. Inertance is obtained with a length of tubing. Its magnitude depends on the density of the fluid, the length of the tubing and the cross sectional area of the tubing. Capacitance is obtained with a tank and depends on the volume of the tank. The function of these passive components is to operate on the signal waveform and produce some desired effect. For example, a combination of resistance and capacitance gives an output pressure which is approximately the integral of the input pressure.

At present the techniques described above are being used to build a high gain operational amplifier. In order to accomplish this several stages of amplification must be cascaded. The stages are directly coupled. That is, the outputs of a stage are fed directly into the inputs of the succeeding stage. Using this procedure amplifiers have been built with measured pressure gains in the neighborhood of 500.

22
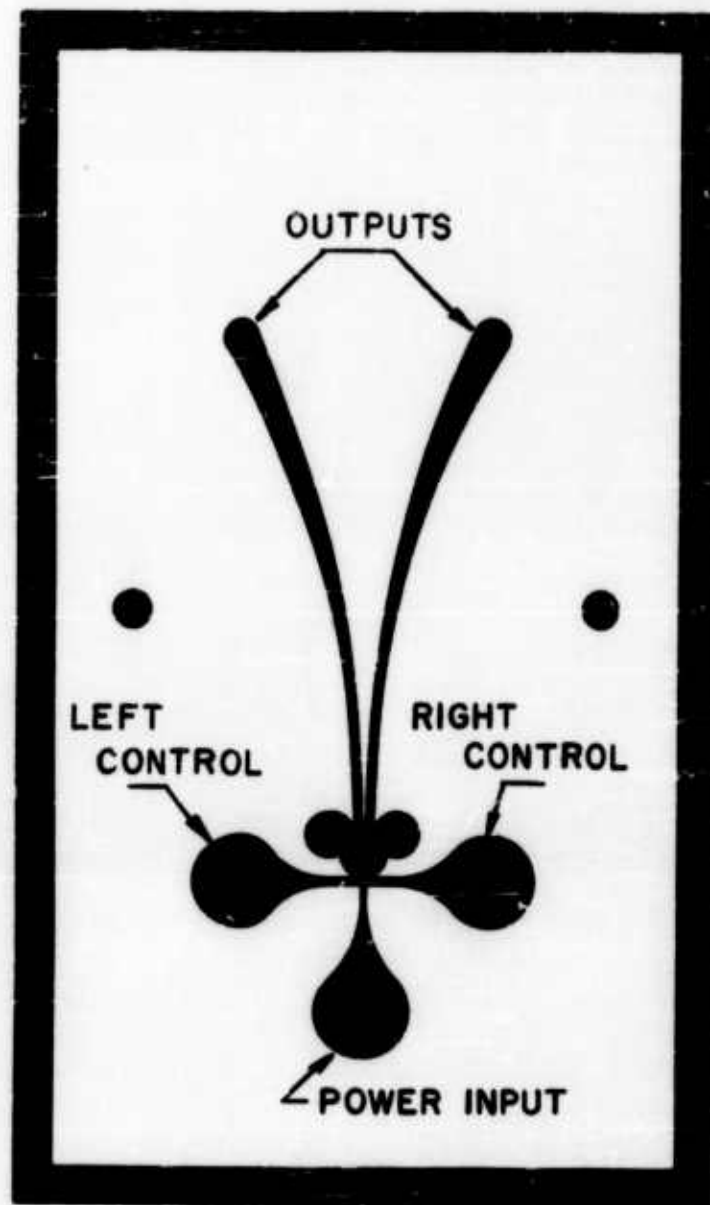
Figure 1. Proportional amplifier.

Figure 2. Deflected power stream.

24
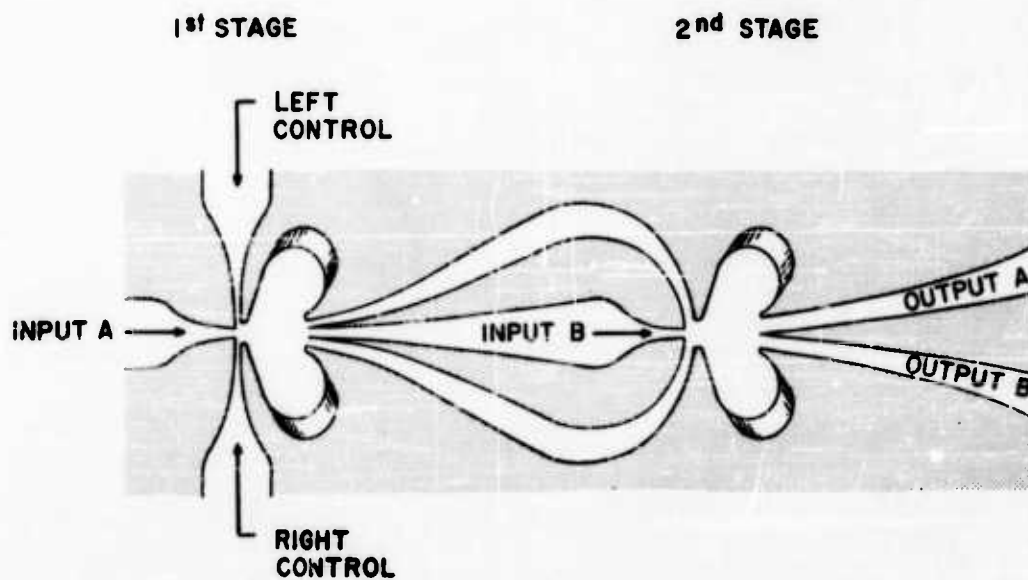
Figure 3. Two-stage open proportional amplifier with cas-
caded power inputs.
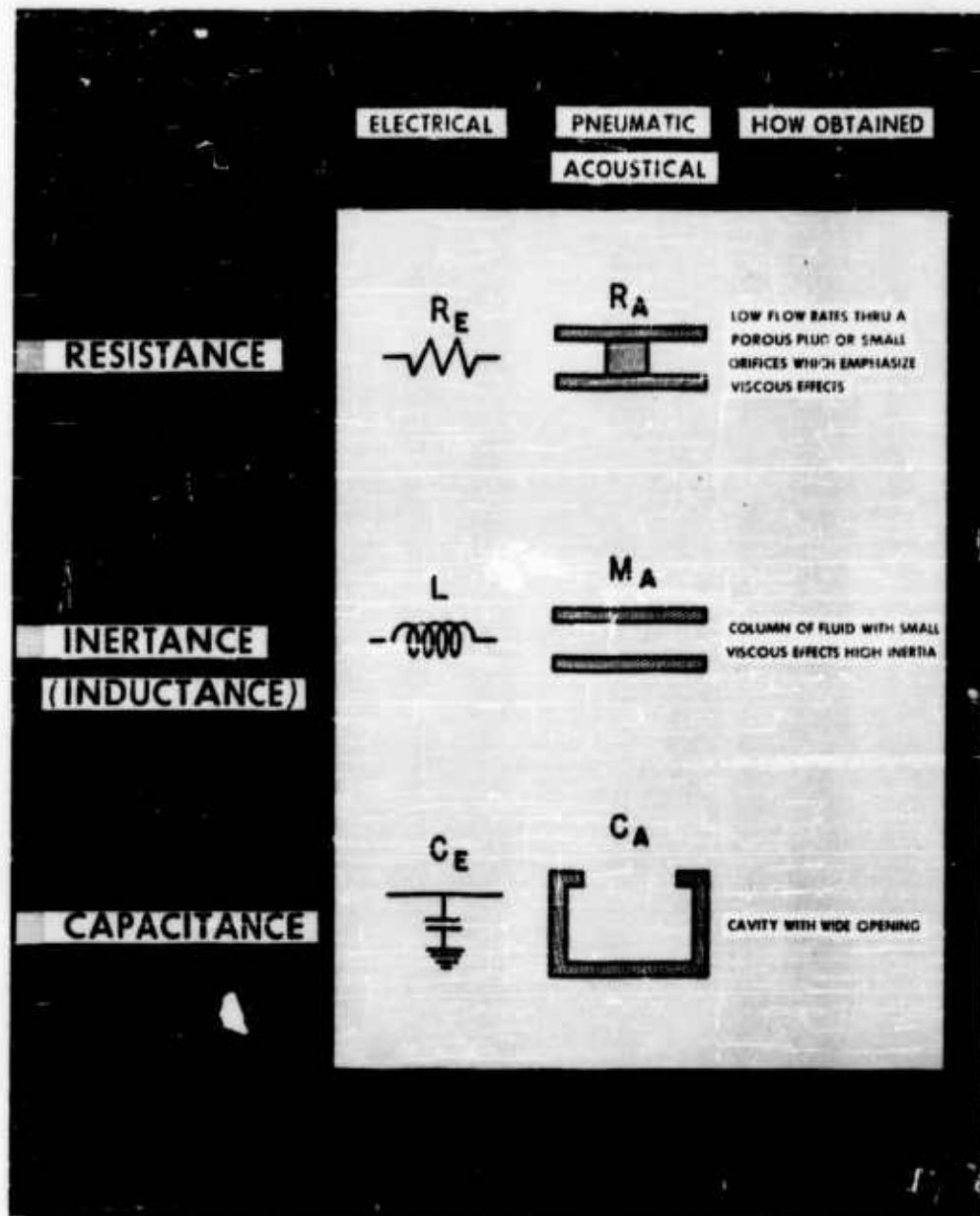
Figure 4. Analogies.

20

FLUID AMPLIFIER DEMONSTRATION VEHICLE

by

R. Richard Palmisano

of

Diamond Ordnance Fuze Laboratories

Abstract

A jet-propelled vehicle has been built which demonstrates the practicality of fluid-amplification for thrust vectoring. An account is also given of a 5-stage proportional fluid amplifier which is capable of amplifying control signals over 100,000 times. The amplifier output is used to steer the vehicle by deflecting the propelling jet stream. Both propulsion and steering of the vehicle are achieved without the use of mechanical linkage.

Requirements

In order to demonstrate the practicality of fluid amplification in guidance systems a suitable test vehicle was sought. Although the initial demonstration was intended to show the feasibility of fluid amplification as a means of thrust vectoring, a versatile conveyance was needed which could be readily modified to test and demonstrate a variety of fluid amplification devices under development. Since the available types of rockets and surface water craft were considered unsuitable, it was decided that an attempt should be made to build a demonstration vehicle having the following characteristics:

(1) Initially, it should be a directionally unstable vehicle which could be stabilized by a driver who operates the control system.

(2) It should be an air powered vehicle not requiring rocket fuel.

(3) The vehicle should be capable of giving a 2-dimensional demonstration on land.

(4) The demonstration should run for a relatively long period of time and be repeatable.

(5) The vehicle and control system should allow for future

27

changes and modifications to permit testing and demonstrating other
fluid amplification devices and systems under development.

Demonstration Vehicle

The vehicle built to meet these requirements is shown in Figures 1
and 2. This 850-pound vehicle carries a turbo-compressor powered by a
gas turbine engine which has a governed speed of 42,200 RPM. The
compressor supplies air at a constant pressure of about 40 psig and at
a steady rate of about 122 pounds per minute.

A 28-volt starting battery is mounted near the front of an aluminum
A-frame chassis. The engine fuel is JP4 and is carried in a 12-gallon
tank which is mounted centrally on the chassis, next to the battery.
This fuel capacity is sufficient for 12 minutes of operation. A driver's
seat was improvised on the fuel tank. The turbo-compressor is mounted
next to the fuel tank toward the rear of the vehicle.

The front wheel of the vehicle rotates about a fixed axis and is
therefore nonsteerable. Since the vehicle is propelled by a constant
thrust, the front wheel is equipped with a shoe-type brake which provides
the only means for the driver to keep the forward speed of the vehicle
within safe limits. This brake can be applied by the driver either
through an air cylinder operated by a valve on the dash panel or by a
foot-operated mechanical linkage which overrides the air cylinder. The
two rear wheels are oversized castors, free to swivel in any direction.
To further increase the instability of the vehicle, these rear wheels
were equipped with narrow steel bands. Very sight imperfections on the
surface of the runway would therefore tend to throw the vehicle off its
course and require a corrective signal from the driver. Since the CG of
the vehicle was far to the rear, its intentional, inherent instability
was further increased.

Propulsion and steering are achieved without the use of mechanical
linkage.

Figure 2 shows the oil tank in the foreground, compressed-air intake
screen to the left, and the large exhaust duct for engine exhaust gases
to the right. This exhaust contributes very little toward propelling the
vehicle. On the far left, mounted on the dash panel are two pressure
regulators with corresponding pressure gauges. It is by means of these
regulators that the driver sends directional control signals to the
5-stage amplifier.

The output of the compressor, i.e., the compressed air for propelling
the vehicle, passes through the 3-inch diameter stainless steel flexible
tube. The major portion of this flow of air passes through a converging
nozzle which has a throat opening 1/2 inch wide by 2 inches high. The
flow of air issuing from this nozzle provides the thrust required to

28

propel the vehicle. A 1-1/4 inch diameter copper line shown in the foreground supplies air to the 5-stage amplifier which is mounted below the thrust nozzle. A close-up of the thrust nozzle assembly may be seen in Figure 3.

The thrust-vectoring system including the relative flow rates is shown in Figure 4. The flow through the thrust nozzle is estimated at about 75 pounds per minute, producing a sustained thrust of about 44 pounds. As previously indicated, air is supplied to the 5-stage proportional amplifier through a 1-1/4 inch diameter copper line. The amplifier output is directed to either side of the thrust nozzle output by two curved passages whose cross section is 5/16 inch x 1-1/2 inches. Optimum position of the reaction vanes was determined experimentally in field tests.

It should be noted that the maximum input signal to the 5-stage amplifier is only .0045 pounds air per minute. These minute input signals are capable of controlling the much larger flows issuing from the two amplifier outputs. These amplifier outputs are in turn used to deflect (vector) the main jet issuing from the thrust nozzle which propels the vehicle.

Proportional Amplifier

A line drawing of a 2-stage proportional amplifier (Figure 5) shows how the outputs of the first stage serve as controls for shifting the input of the second stage. The area of each succeeding nozzle or passage is four times the area of the preceding nozzle. (This also applies to the output nozzle.) The concave ramps help overcome instability by providing proper chamber feedback.

The 5-stage proportional amplifier designed by B. M. Horton and S. J. Peperone and used in steering the vehicle is shown in Figures 6 and 7. The assembled unit is approximately 3 inches wide x 2-1/2 inches high x 18 inches long and when built of aluminum weighs about 9-1/4 pounds. A redesign of this unit indicates that an equivalent amplifier may be built weighing only 3-1/4 pounds should the need arise.

The exploded view of the amplifier (Figure 7) shows how air is supplied to all the power jet nozzles from one line, a 1-1/4 inch diameter copper tube shown at the upper left hand corner. The manifold plate supplying air to the first three stages also contains the control signal inputs to the first stage. The outputs of the first stage serve as control inputs for the second stage. The outputs of the second stage serve as control inputs for the third stage, and so on to the final stage, i.e., the outputs of one stage are used to deflect the input of the succeeding stage. The gaskets separate the flow in one stage from the other. The throats of the first control nozzles are .004 inch wide x .090 inch high. As previously noted, the final output passages are 5/16 inch wide x 1-1/2 inches high.

Demonstration

The work on this first phase of the project culminated in a demonstration given at Andrews Air Force Base for personnel of OCO. A short 16mm film strip of this demonstration is available. The first part of the film shows a restrained-type test in which the rear wheels were equipped with stops to limit their swivel movement and the front wheel was locked. This demonstration showed that a maximum control signal of less than 1/2 psi transmitted through the pressure regulators to the 5-stage amplifier was all that was required for a complete reversal of the vehicle's turning direction.

The second part of the demonstration film shows the vehicle in motion. With the rear wheel restrainers removed and with control signals transmitted to the 5-stage amplifier through the two pressure regulators, the cart is seen advancing in a straight line with the operator controlling the vehicle. This action demonstrates the feasibility of employing fluid amplification as a means of stabilizing a directionally unstable vehicle while in motion. As the vehicle advanced in a straight line, the front wheel brake was locked and the vehicle was put through a number of turning manoeuvres.

The third part of the demonstration shows manipulation of the vehicle when the control pressure regulators were by-passed by means of flexible plastic tubes. This enabled one to transmit the signal to the amplifier by placing his thumbs at the open ends of the two plastic tubes and varying the pressure in the line by controlling the amount of air allowed to bleed off. This action gave one the opportunity to actually feel the small magnitude of the control signals transmitted to the amplifier. Using this "thumbs" technique, the vehicle was steered in a straight line and then put through a series of turning manoeuvres as in Part Two of the demonstration.

Since the vehicle was propelled by a constant thrust (of about 44 pounds) from the nozzle, a safe forward speed of about 15 mph was maintained by applying the front wheel brake. The braking action on the single fixed axle front wheel located on the centerline of the vehicle had no effect on the steering.

Conclusions

The important feature in demonstrating this vehicle was <u>not</u> to show that thrust vectoring is possible; this has already been achieved in missile flight through the use of auxiliary fluid sources and complex electro-mechanical systems. The significant achievement, it is felt, lies in the fact that an extremely low-level signal has been amplified over 100,000 times in a 5-stage fluid amplifier without the use of a single moving part and without the use of an auxiliary power source. This clearly indicates the direct usefulness of these techniques to other hot-gas propulsion and control systems.

30
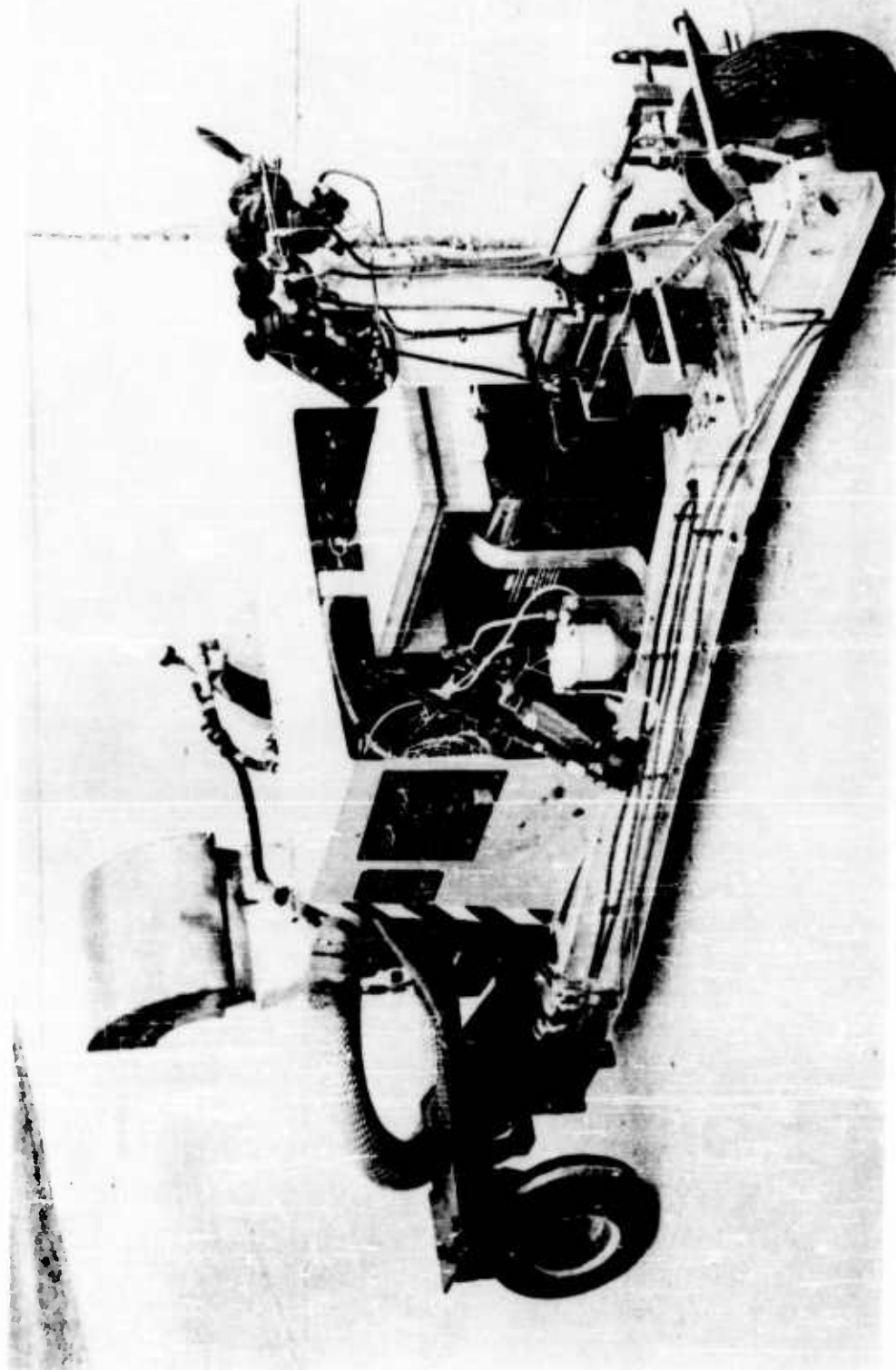
Figure 1. Three-quarter front view of fluid amplifier demonstration vehicle.

31
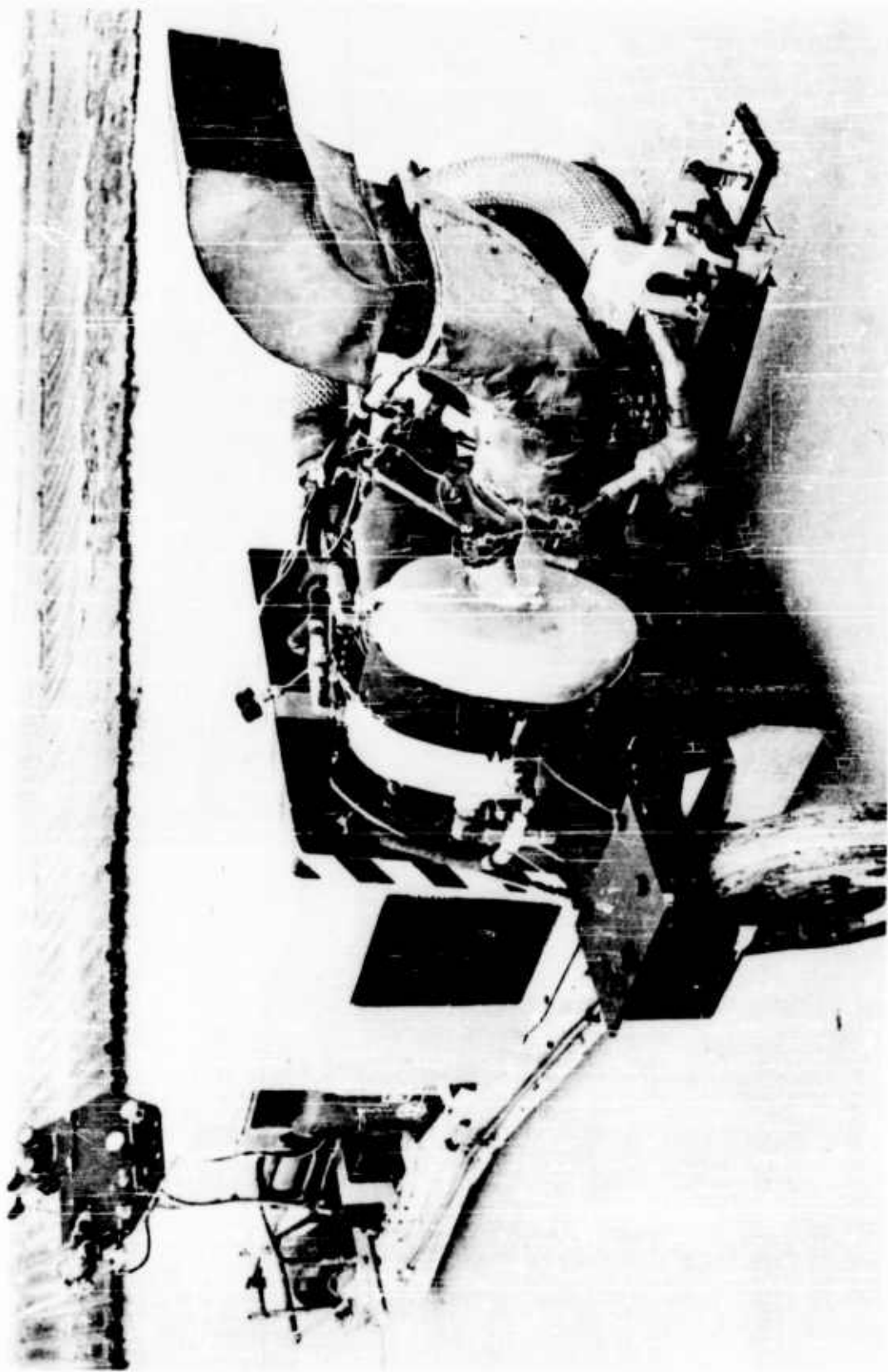
Figure 2. Three-quarter rear view of fluid amplifier demonstration vehicle.

497-62

Air supply from
turbine compressor

Amplifier output
ducts

Air supply to
5 stage amplifier

Thrust nozzle

Reaction vanes
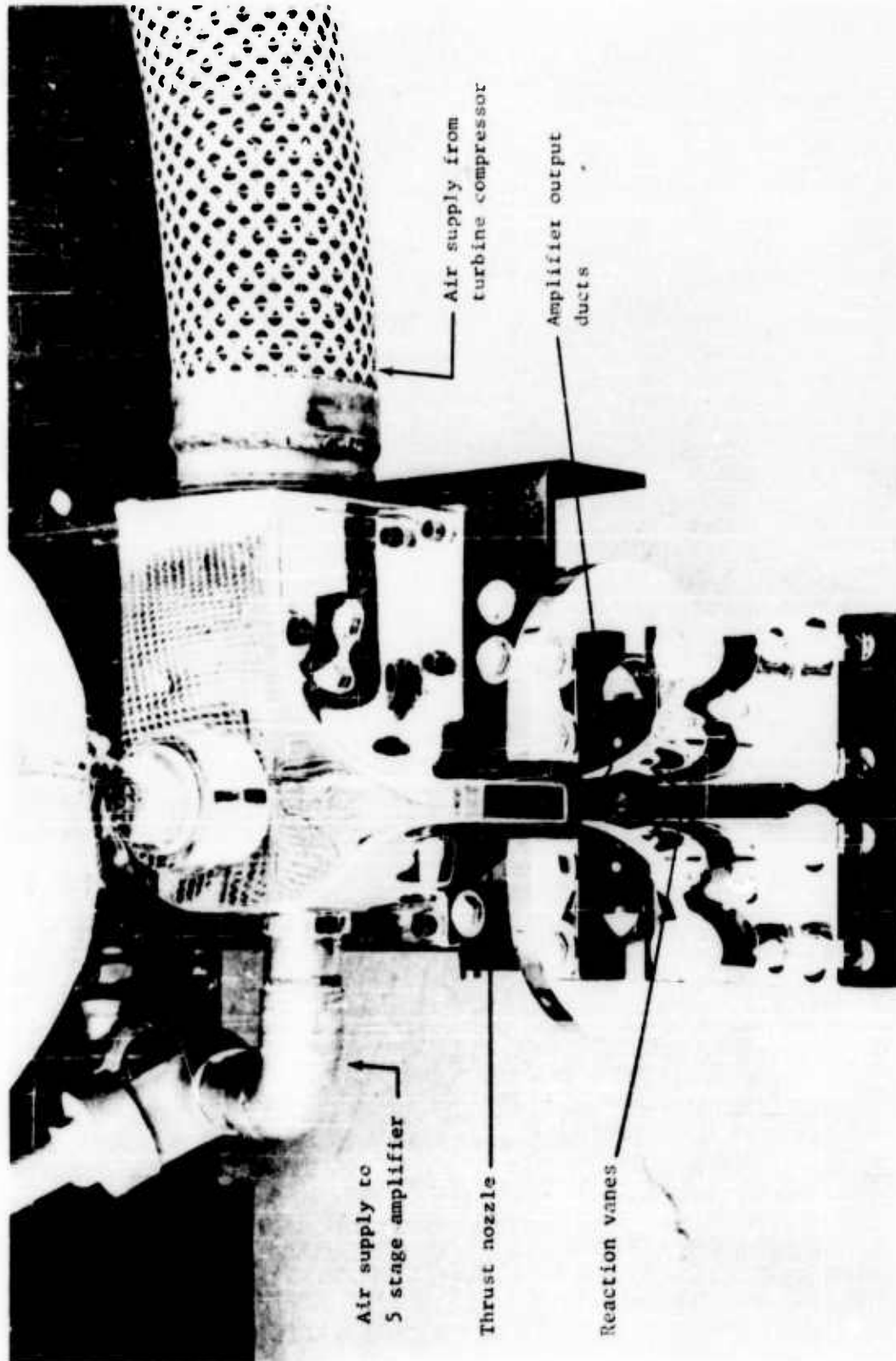
Figure 3. Thrust nozzle assembly.

498-62

33

AIR SUPPLY
TO 5-STAGE AMPLIFIER

INPUT CONTROL
SIGNAL (FLOW ≈ .0045
LB/MIN. MAX.) TO
5-STAGE AMPLIFIER

5-STAGE AMPLIFIER
OUTPUT AVAILABLE FOR
DEFLECTING THRUST
(FLOW ≈ 33.7 LBS/MIN.)

AIR SUPPLY FROM
TURBINE COMPRESSOR

5-STAGE AMPLIFIER

THRUST NOZZLE
(FLOW ≈ 75.7 LBS/MIN.)

THRUST ≈ 41.3 LBS

REACTION VANES
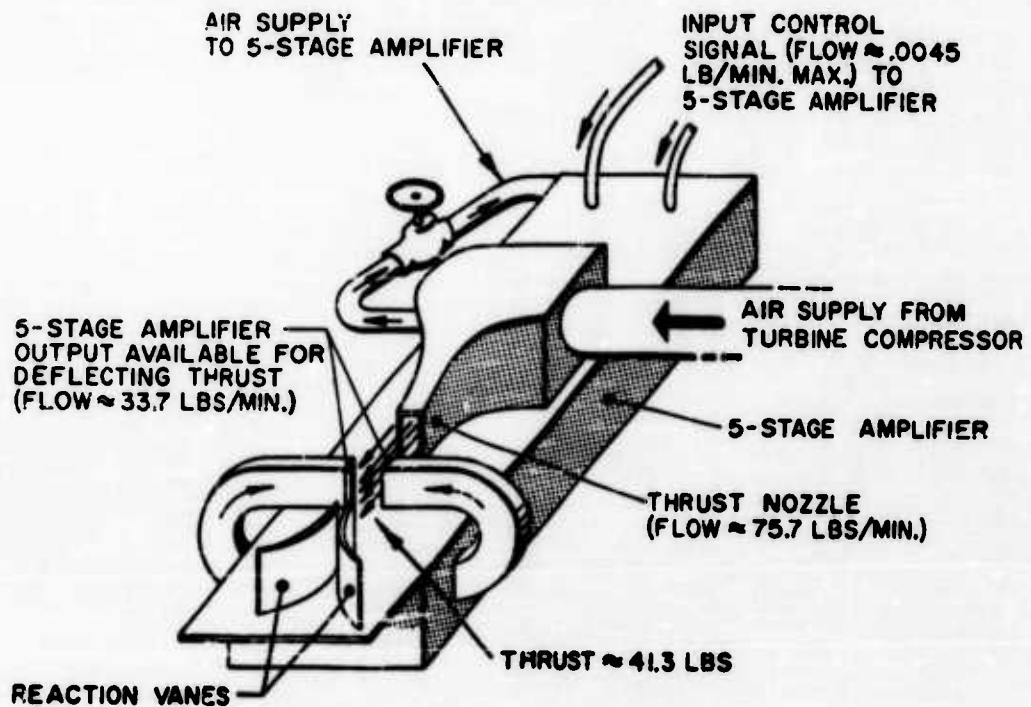
Figure 4. Thrust-vectoring system of jet demonstration vehicle using a 5-stage proportional fluid amplifier.

1st STAGE   2nd STAGE

LEFT
CONTROL

INPUT A →

INPUT B →

OUTPUT A

OUTPUT B

RIGHT
CONTROL
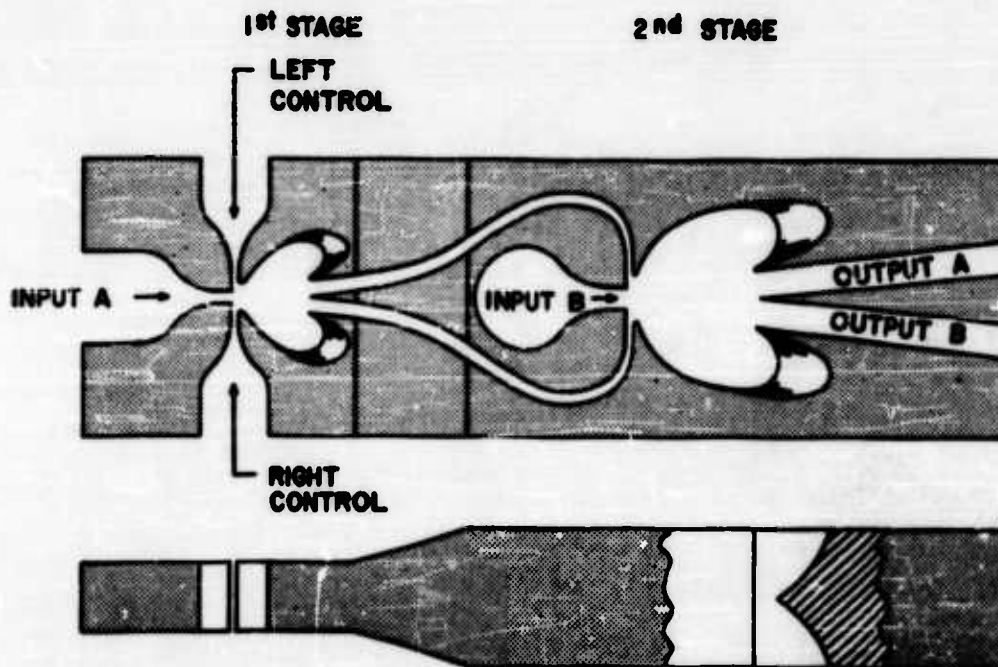
34   Figure 5. Two-stage closed proportional power amplifier.

Control inputs to first stage

Output duct

Air supply input
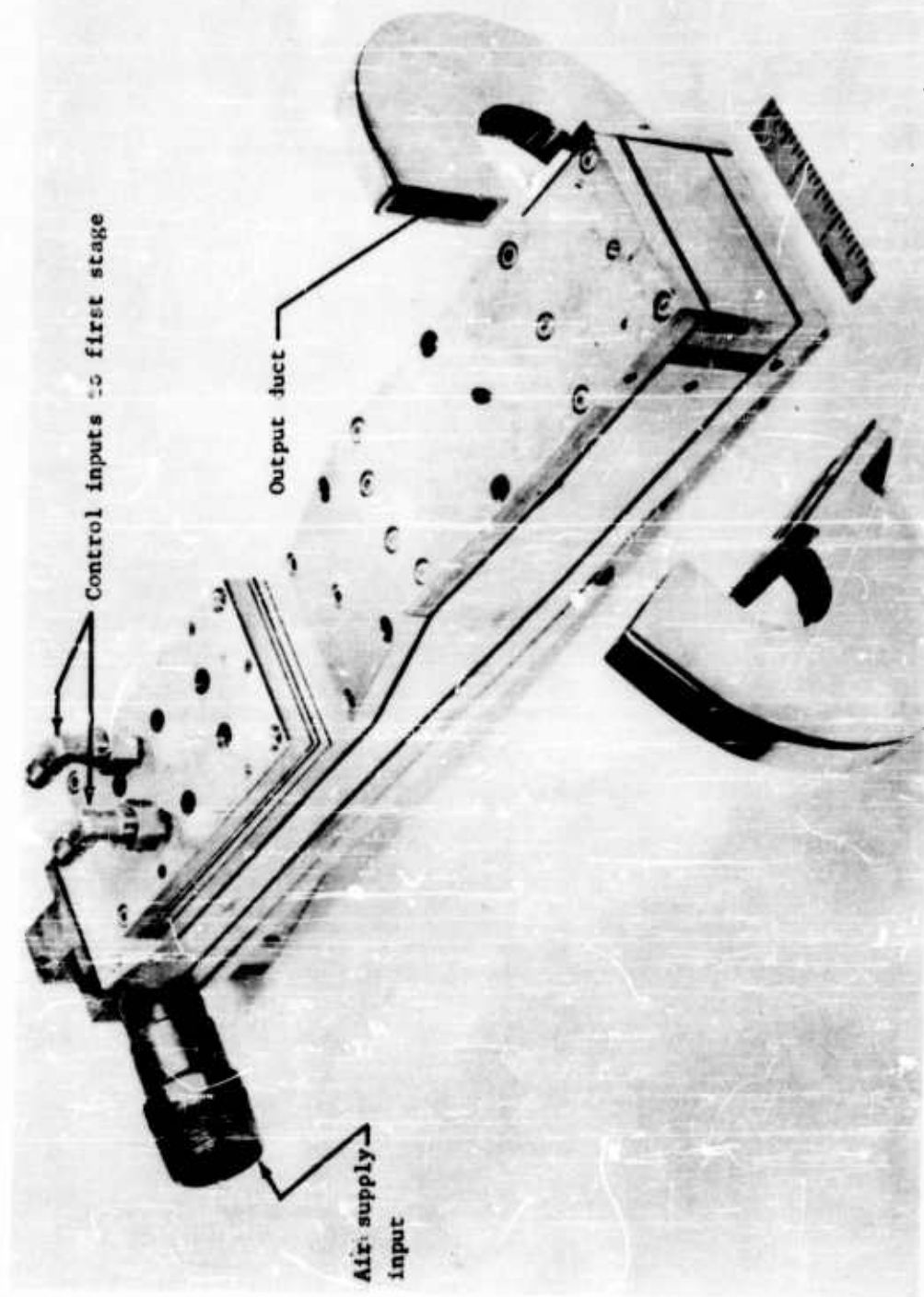
Figure 6. Five stage proportional fluid amplifier   772-62

35
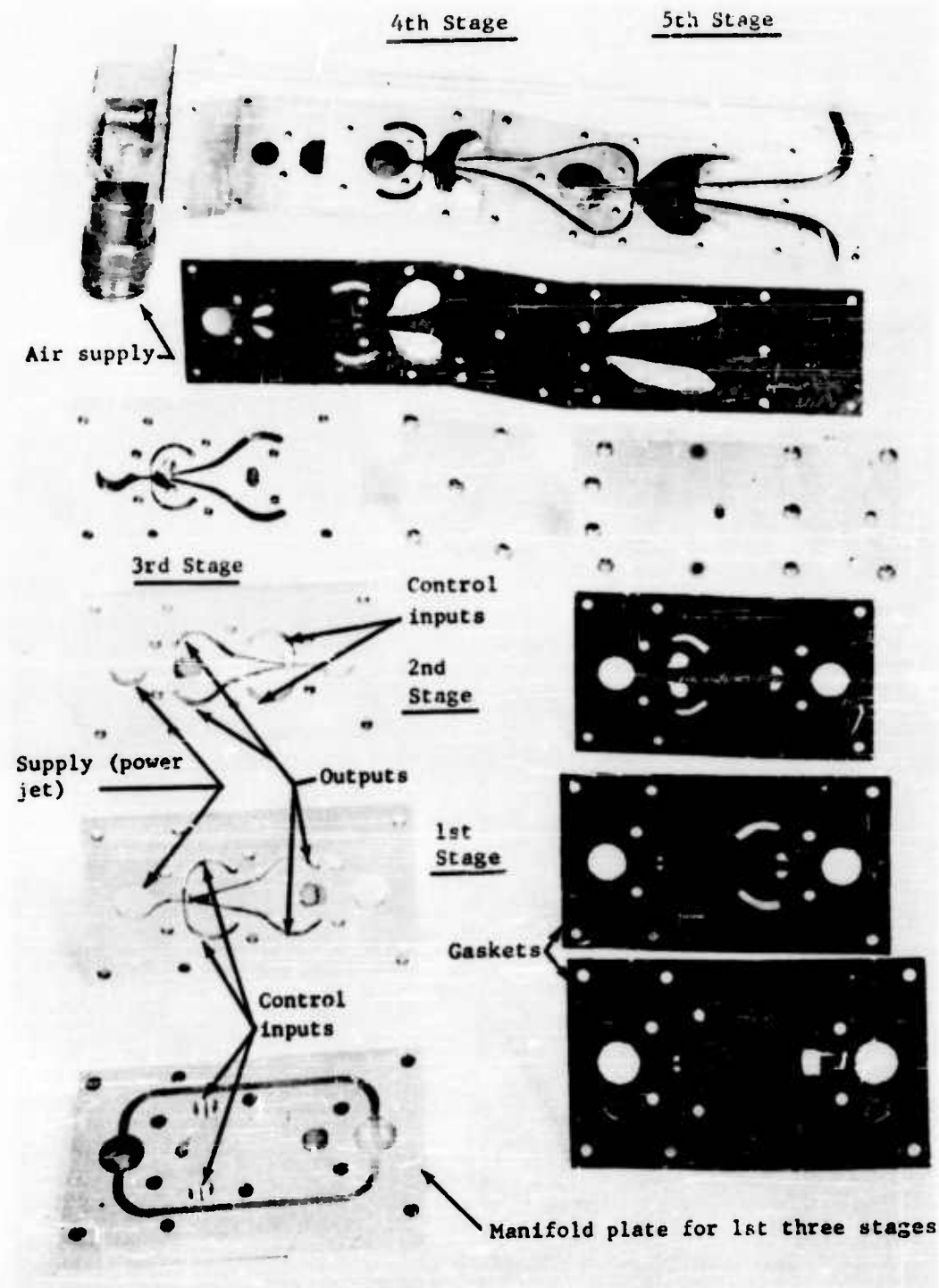
Figure 7. Five stage amplifier (exploded view).

771-62

THE HYDRAULIC ANALOGY

by

Ralph G. Barclay

of

Diamond Ordnance Fuze Laboratories

Introduction

The hydraulic analogy is the analogy that exists between two-dimensional compressible-gas flow and open-channel liquid flow. Open-channel liquid flow is flow of a liquid with no confining plane above the liquid. That is to say the surface of the liquid is open to the atmosphere and to all practical intents is a free surface.

DOFL Program in Hydraulic Analogy

DOFL has an internal effort and supports an external effort at The University of Maryland. In both cases the emphasis is on using the hydraulic analogy to investigate various fluid-amplifier designs.

References

The feature article in the June 1962 issue of _Applied Mechanics Reviews_ is, "The Hydraulic Analogy for Compressible Gas Flow" by J. W. Hoyt. It lists 126 references. The article gives the early history, tells of the general surveys and studies and mentions current applications of the analogy.

Use of Analogy in Study of Fluid Amplification

The main contribution of the hydraulic analogy to the study of fluid amplification is in providing a means of flow visualization. Complex flows can be observed with the hydraulic analogy using models which are very easily made and very easily changed. In this way the effect of various shapes can be quickly ascertained in a qualitative manner. Visualization is aided by the fact that the speed of flow in liquid is approximately a thousand times slower than the corresponding flow in the compressible gas. Transient flow conditions can thus be observed by the naked eye.

37

Photography

At the symposium a color movie was shown of various flow situations. Still pictures in black and white are inadequate representations of the phenomena shown. With this in mind we reproduce here only one of the scenes from the color movie.

Discussion of Accompanying Photograph

The picture which accompanies this write-up shows a hydraulic model representating the injection of a secondary flow into a primary propulsion nozzle for the purpose of changing the direction of the thrust from the primary nozzle. The liquid in use here is water which is dyed heavily and illuminated from below with diffuse light. The degree of shading of a particular point in the flow indicates the relative depth of the water. The depth of the water is analogous to the density of the gas in the corresponding compressible gas flow.

The light area which is roughly diamond-shaped to the right of the picture is the primary nozzle with the fluid flow directed upward on the page. The light tone indicates that the water in the nozzle and downstream of the nozzle is relatively shallow.

In the left lower part of the picture there is a bistable fluid amplifier. The power jet for this amplifier is directed at an angle of 45° with the binding-edge of the page against a splitter which has a rounded point. One output channel of the fluid amplifier is directed straight aft or upward on the page so when fluid is directed thru this output channel there is no appreciable side thrust. The other output channel of the fluid amplifier is directed into the main nozzle and is shown carrying the flow. A build-up of water-depth in the output is shown by the progressively darker tone of the flow in the output channel as it approaches the primary nozzle, and after it has entered the primary flow.

In the region of the power jet (lower left) there are two areas of approximately crescent shape. These are the control-flow reservoirs. There are channels (not visible in the picture) connecting these reservoirs to the interaction chamber of the fluid amplifier. The upper control reservoir has a darker tone which shows the presence of deeper water. This indicates that the control signal is being applied to this reservoir. The lower control reservoir shows the lighter tone which is the result of fluid being entrained away by the power jet.

Appraisal of the Analogy

The analogy is based on inviscid flow for both gas and liquid with only negligible vertical accelerations allowed in the liquid. The ratio of the specific heats for the "analog gas", as it is called, is 2.
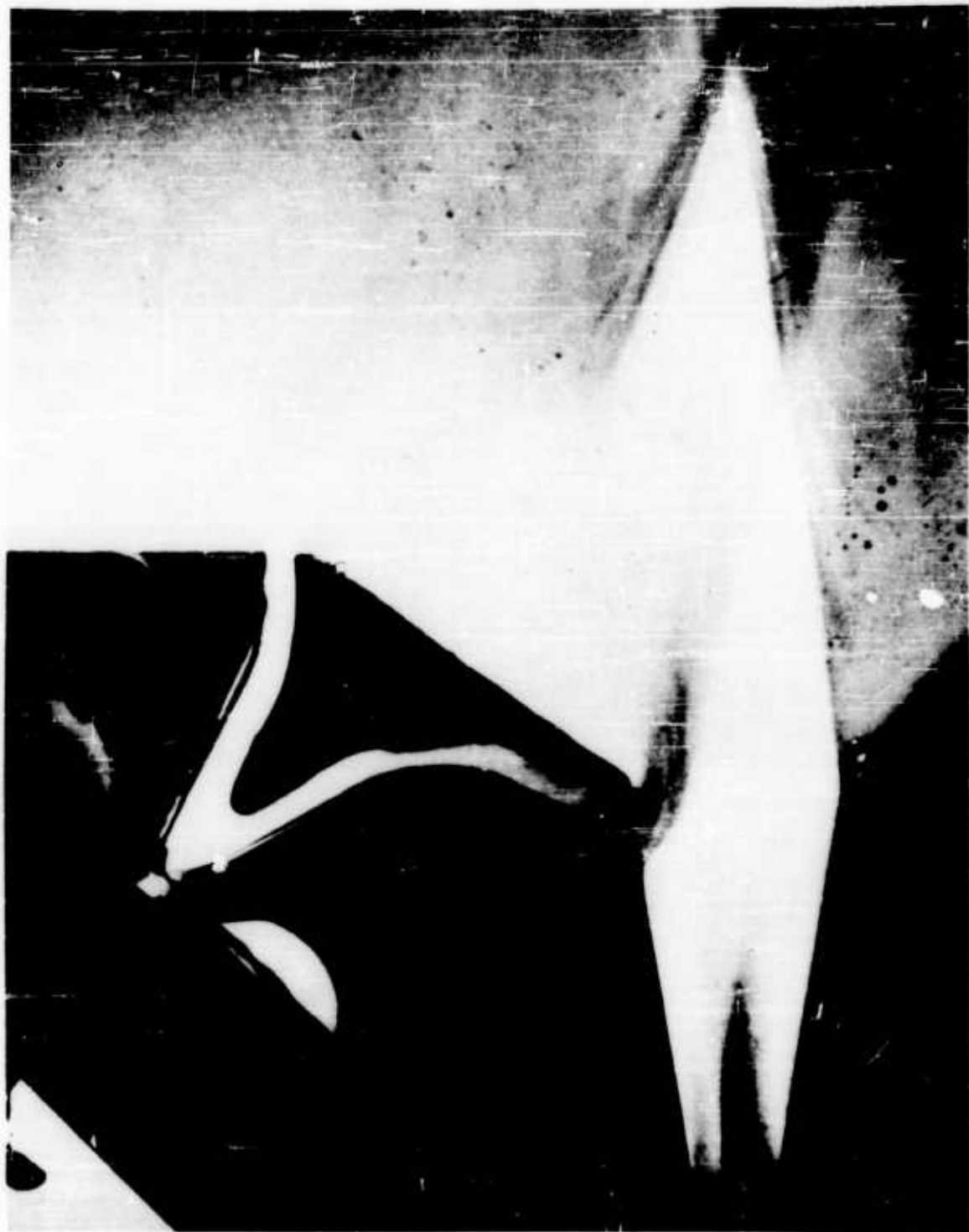
Naturally these limitations affect the quantitative results that can be obtained. However, since the analog regimes are so similar (flow of a fluid in each case) it seems possible to violate the strict requirements of the analog and still produce acceptable correspondence. We are able to produce the basic phenomena of fluid amplification in open-channel liquid flow. This yields a valuable preliminary evaluation tool for geometric investigations and idea generation.

PULSE DURATION MODULATION

by

R. W. WARREN

of

Diamond Ordnance Fuze Laboratories

Conventional digital control systems apply the full correction whenever the error signal is above a minimum threshold. If such a system were used with reaction jets to control a missile, there would be considerable overshoot, which would result in the application of the control signal in the opposite direction. Thus the missile would oscillate about the desired line of travel. To overcome this, an electronic system is in use wherein an oscillator causes the reaction jets to alternately emit from either side of the missile at constant frequency. When an error signal is introduced, the oscillating jet pauses for a longer or shorter time on either side to produce a reaction which is proportional to the desired correction. Thus, if the missile were to deviate to the right, the error would cause the reaction jet to remain for a longer time on the right and a shorter time on the left to produce the desired correction. When the error signal is small, the difference in time is small and when the error signal is large, the full correction is applied. If the frequency of oscillation is greater than twice the natural frequency of the missile, the oscillations are smoothed by the response characteristics of the missile.

An all-fluid pulse-duration modulation system has been developed which accepts fluid signals proportional to the error. An outline of the system is shown in Figure 1. It consists of an oscillator driving a buffer amplifier which drives the output bistable amplifier. The particular oscillator used is of an explicit feedback type. A small portion of the output is diverted into a capacitor. As the pressure in the capacitor increases, the flow in the control increases. When the control flow reaches a sufficient level, the oscillator switches to the opposite output. A portion of this output is diverted from the opposite leg into another capacitor and the process repeats. The frequency of oscillation can be varied by varying the capacitance. Instead of varying the volume of the capacitor, a bleed is used to delay the rise of pressure in the capacitor, thereby varying the time constant.

Like electronic oscillators, fluid oscillators normally change frequency as they are loaded. To overcome this, a technique similar to that employed with electronic oscillators is used. The oscillator is used to drive a buffer amplifier, and the buffer amplifier drives the load. Thus the oscillator only sees the comparatively constant load of the buffer amplifier. The outputs of the buffer amplifier are introduced into

capacitors. The capacitors are connected to the controls of the bistable amplifier. As the output from the buffer amplifier enters the capacitor the pressure rises and the flow into the control increases until there is sufficient flow to satisfy the entrainment characteristics of the bistable amplifier so that the stream switches to the opposite wall.

All of the output of the bistable amplifier issues out of one output, either the left or the right, and can be used as a reaction jet for purposes of control. If the error of the missile is sensed with a gyro, an air jet from the gyro can be divided between two adjacent orifices when the missile is on course, and as it deviates from the true course the flow will be more to one orifice than into the other. This variation can be fed into the left and right control inputs of the pulse duration modulation system. As shown in figure I, the control inputs are connected to the capacitors on the controls of the bistable amplifier. As the control signal on one side increases, the control signal on the other side will decrease.

For purposes of explanation let us assume that the control signal on the right increases and the signal on the left decreases. The increased flow into the right capacitor increases the control flow into the right control sooner and decreases it later as the output of the oscillating buffer amplifier enters and leaves this capacitor. The decreased control signal in the left capacitor delays the build-up of pressure and takes a longer time to provide the control flow to switch the power stream from the left wall. The net result is, that while the unit is oscillating between the two outputs at constant frequency, the cycle is not divided equally but instead the output reaction jet pauses for a longer time on the left and a shorter time on the right. This is shown by the output charts at the output of the unit. Flow increases upward and time increases to the right in each case. The level of flow from a pulse is constant at all times. The frequency is also constant as is shown by the time dots. When there is equal signal into the left and right capacitors the duration of flow is equal in each of the outputs. For the case cited with a decreasing signal in the left control and an increasing signal in the right control, Figure 1 shows the full output flow remaining for a longer time in the left output, and pausing for a shorter time in the right output.

The experimental setup is shown in Figure 2, with long leads and comparatively large capacitors. This system was operated at a frequency of from 30 to 100 cps when it had capacitors at the control inputs of the output amplifier. The system gain (that is, the change of output signal with the change of input signal) varied between 3 and 4. In an operational system additional amplifiers could be used at the output.

To increase the operating frequency, an experimental setup similar to Figure 3 was used. In Figure 3, the capacitors and the buffer amplifier have been deleted from the system. The error signals are fed directly into the separation bubble of the bistable amplifier. The separation bubble

42

serves as the capacitor. As this is a considerably smaller capacitor than was previously used, the operating frequency increased to 250 cps, even with the long leads. With flow gages on the outputs as shown in Figure 2 there was a very smooth change of output flow proportional to the error signals.
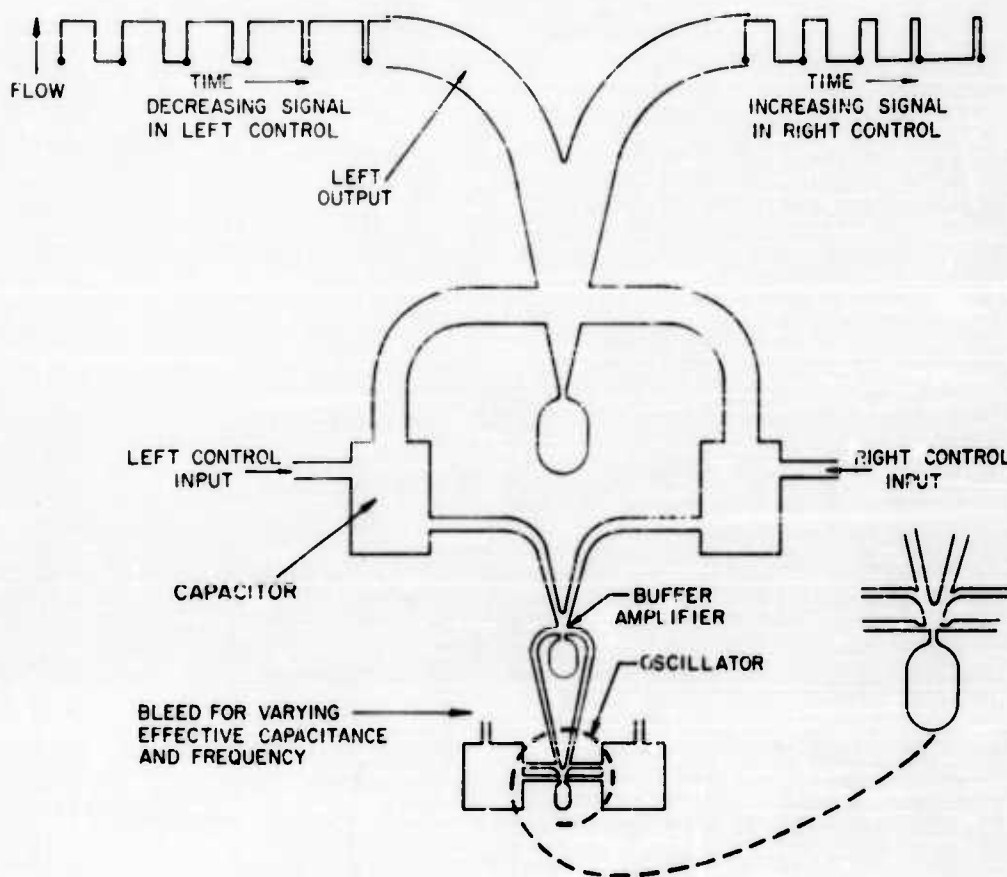
Figure 1. Pulse duration modulation (low-frequency)
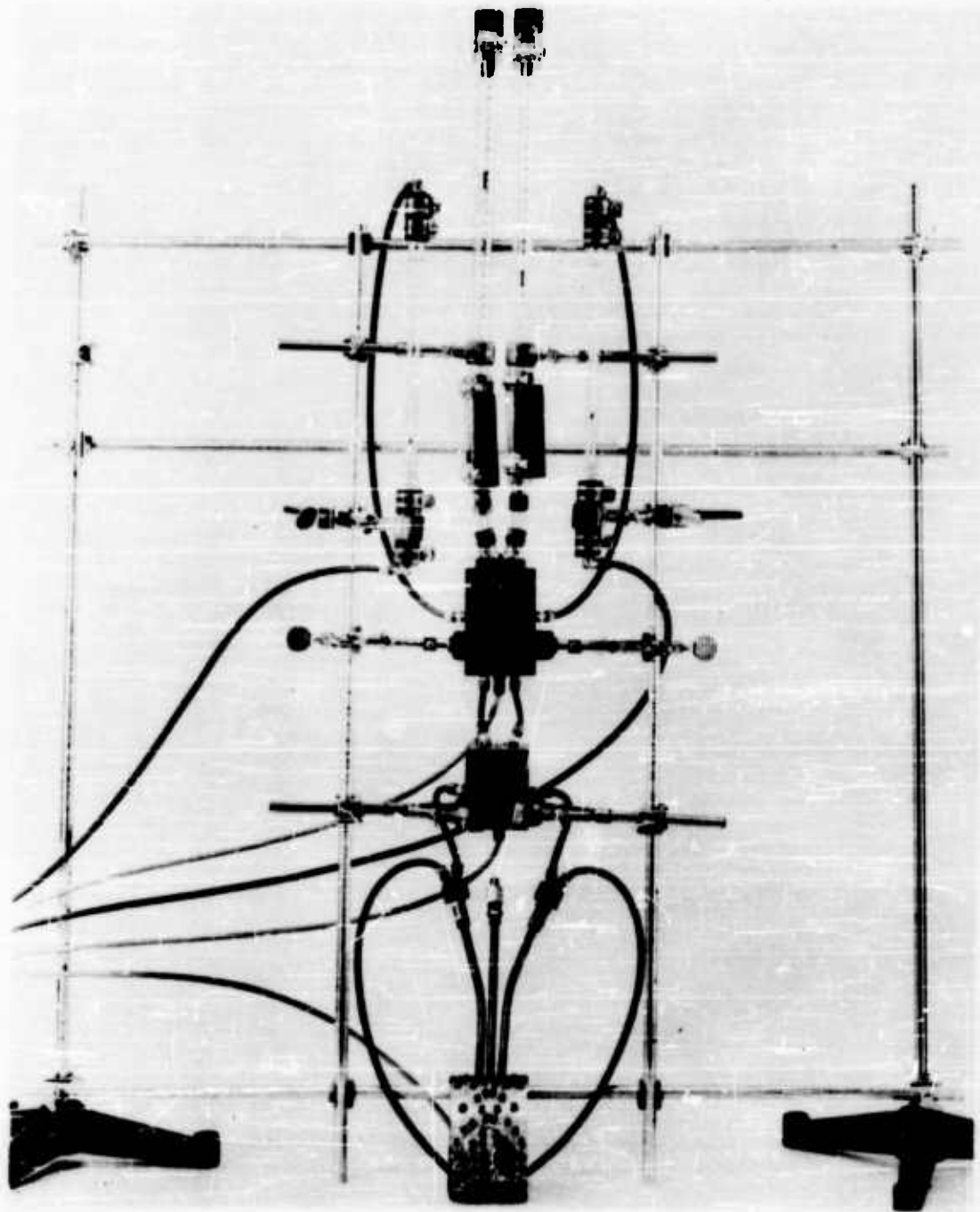
Figure 2. Experimental set-up.

44
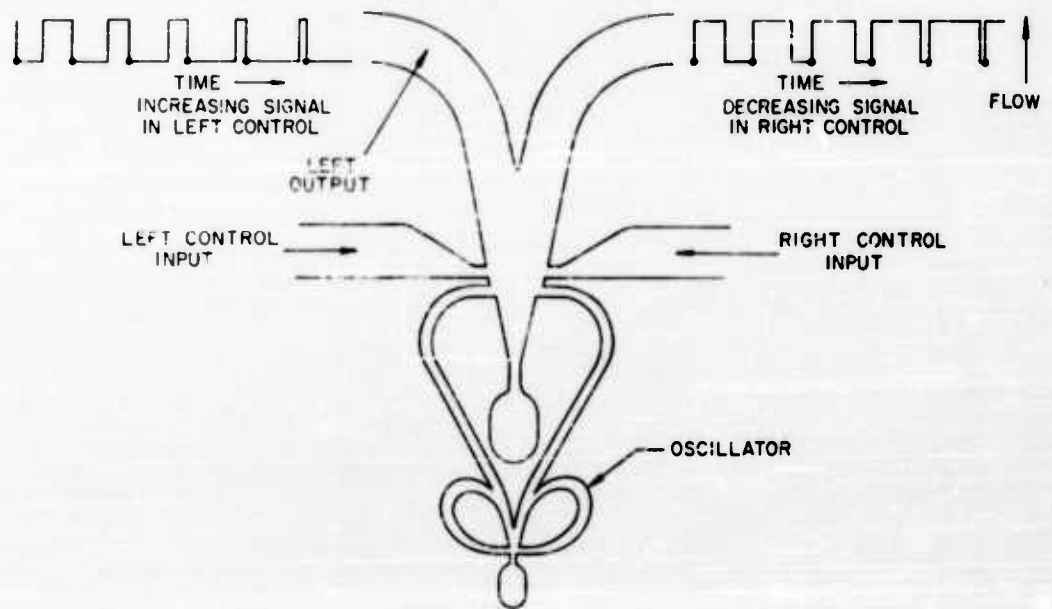
Figure 3. Pulse duration modulation.

A THREE STAGE DIGITAL AMPLIFIER

by

Carl J. Campagnuolo

of

Diamond Ordnance Fuze Laboratories

Abstract

This paper is concerned with the field of fluid amplification, the control of fluid streams by means of other fluid streams of less energy. This paper describes digital pneumatic elements, which are cascaded so as to obtain a high power output which can be controlled by means of a stream containing 10^{-3} of the output flow--a system consisting of three units in a cascade is discussed.

Introduction

One of the basic elements of fluid amplification is the boundary layer digital unit which is characterized by many parameters. It is the purpose of this paper to discuss some of these parameters in connection with a digital unit which is part of a three-stage digital system having a very high flow gain and a reasonable pressure recovery.

A boundary layer unit works on principles some of which have not yet been completely explained by classical fluid dynamics. The most important of these are wall-jet interaction and entrainment of fluid particles from the surroundings[1]*. Although a boundary-layer unit can operate in all three ranges of flow: subsonic, transonic, and supersonic, in this paper we are mainly concerned with the subsonic range of operations.

When a jet exhausts from a nozzle, turbulence is generated at the borders of the jet. Due to friction from shearing stresses against the surrounding fluid, the jet undergoes lateral diffusion and deceleration, and at the same time fluid particles are entrained by the jet.[2] The

---

*Numerical superscripts in the text refer to item numbers in the list of References which follows the text.

47

process of the mixing of the jet with the surrounding fluid causes the velocity distribution of the jet to change so that at a distance of about 6 nozzle widths the velocity profile approaches a Gaussian distribution. During the diffusion process, the kinetic energy of the jet transforms into kinetic energy of turbulence, which in turn is converted into heat energy. In this process the jet is decelerated while the surrounding particles are accelerated. This results in a net increase in the output flow. Even though the velocity of most of the jet decreases with distance from the nozzle, there is a zone called the core where the maximum velocity is constant.[2] This region is very evident in a bunsen burner where the bluish flame represents the core region of the burning gas. In this region the energy of the jet is the highest since no mixing with the outside has yet taken place.

The digital character of the boundary layer unit is brought about by the existence of a wall or fixed boundary. The jet emerging from the power nozzle attaches to one of the walls lowering the pressure between the boundary of the nozzle and the point of attachment at the wall (Coanda effect). The static pressure distribution of the attached wall jet is mostly a function of the set back and the angle of inclination of the wall. (See Fig. 1). The pressure varies from below ambient up to a maximum, and then drops slowly until at a long distance from the nozzle it approaches ambient. (See Fig. 2). The trajectory of the jet around the low pressure region or bubble is approximately the arc of a circle. The pressure within the bubble varies with distance from the jet because particles are constantly being taken away from the main stream. This bubble plays a very important role in a boundary layer element. The pressure in the bubble must be increased sufficiently by flow from the control nozzle before the jet will detach from the wall and move to the opposite channel. This is the factor responsible for the digital characteristics of these elements.

It is well known from classical aerodynamics that the presence of a wedge in a stream will cause the jet to oscillate as was first observed by Lord Rayleigh.[3] Consequently the presence of the splitter gives rise to resonant frequencies with associated harmonics, the cause and magnitude of which have been the subject of numerous investigations. This phenomenon increases the noise level of the unit. The oscillations are decreased by rounding the wedge. When this is done a higher pressure is obtained in the vicinity of the wedge which seems to reduce some of the modes of acoustic frequency oscillation associated with a jet-edge system.

A most important consideration in building these units is efficien We mean that there should be only a small loss of the total energy of t power jet. From Albertson's data for free jets in the atmosphere, it i evident that up to a distance of 6w (w = nozzle width) from the jet source the total energy decreases rapidly, and at large distances of

approximately 14w or 20w it decreases according to some exponential law. Also from the same data, it is evident that up to 6w the maximum velocity in the direction of the jet flow is constant and then further downstream it decreases exponentially. From such information one may conclude that in order to construct efficient units it is necessary to maintain the expansion chamber of the jet as small as possible and also have the divider no further downstream than 6w. Since high pressure efficiency is required at the output, the stream can be diffused very efficiently with a 12° angle. The diffuser must be kept short so as not to obtain separation of the stream from the wall and also to transform the velocity of the stream to pressure in a distance not over 6w. Elements fulfilling these conditions have been built and pressure recovery of about 70% and instan eous flow gains greater than 15 have been achieved in the subsonic range, up to 15 psig input pressure. (By pressure recovery is meant the amount of loading that the unit can sustain, measured in terms of the input pressure.)

A unit with the above characteristics is sensitive to rather small signals applied at the controls. In other words, it is easy to change the position of the stream from one channel to the other, and the energy expended in this process is small. Actually, in some of the elements atmosphere can supply sufficient flow and pressure to the controls to achieve bistable operation. This is possible because the pressure in the bubble of the attached stream is only 9 to 12 psia and the pressure surrounding the unit is over 14 psia. Consequently, if the control port is open, flow will enter from the atmosphere. If the flow is greater than the stream can entrain, the pressure in the bubble will increase until it becomes higher than the one existing on the opposite side of the stream and the jet will attach to the lower pressure wall.

Unfortunately an element of this type works very well only as long as no load is present at its output. If a small load such as another unit is present at the output, the static pressure at the output increases and this pressure propagates upstream in the jet, shifting the point of attachment of the jet upstream. This shrinks the entrainment bubble, and its pressure increases also, until it becomes higher than that on the opposite side of the jet. The stream will then shift to the other channel or, in some designs, will split between the two channels. Such effects are very undesirable if cascading of units is necessary to obtain the required gain.

Cascading of Units

In cascading units one must consider the function each amplifier performs in the system. Also it is imperative that the final operational characteristics of the system be known. In a high gain system, high instantaneous pressure efficiency of intermediate units is not so

important as the efficiency of the final stage. In a three-stage system where units are stepped up in flow capacity geometrically by a factor of 10, a flow gain of at least 1000 is expected. In such a system if the first two stages are made very efficient, it is found that the system is unstable.

It is, therefore, necessary that the pressure efficiencies of intermediate stages be sacrificed and the dividers of these stages moved to a position further downstream. This change increases the memory of the units. Aerodynamically, this means that the stream is caused to attach at a position further downstream. Then if the static pressure is raised by loading the output, even though the point of attachment will move upstream along the wall, it can move further before the jet detaches from the wall. Thus, stability for a large surge of input pressure is still possible. With the splitter downstream, the amplifier has a pressure recovery of about 30% and an instantaneous gain less than 10. In using such units in a system, some efficiency is lost but stability is gained.

At this point, it is necessary to say a few more words about memory units since they play a very important role in the system under consideration. Memory is obtained when the splitter is moved sufficiently downstream to allow the stream to turn and exhaust out the opposite outlet without creating turbulence at the attachment point. The stream remains attached to the wall even with the output of the amplifier completely blocked. The flow will exhaust from the opposite channel, but the pressure will remain in the blocked channel. If we reopen the blocked channel, the stream will exhaust from that channel. A memory unit is very important in a system since it is usually used as the driver for the subsequent units.

Positive feedback loops may be present when two units are coupled; proper use of this can increase the flow gain of the system. For example, in the three stage amplifier the system without feedback should have had a flow gain of 1000, but the actual gain obtained was greater than 2000. The feedback loop arises from the motion of particles interacting with the main stream. This entrainment becomes quite high as the splitter is moved downstream and approaches that of a free jet above 6w. This process can best be explained if we consider Figure 3 which shows three units connected together. The filled in region is the region of flow. In region 1 the pressure is low since the stream in the third stage is continually entraining particles. This low pressure will propagate down to region 2. At the same time, the stream in the second stage will also try to entrain particles from the leg having no output and to reduce the pressure there even further. If a condition of equilibrium exists between the two stages whereby the whole process cancels out, then stable operation is maintained. But if the entrainment required by stage three is such that stage two will be affected by it, then the outcome of the

50

process will be such that the stream in stage two will be detached from the wall and instability will occur, i.e., oscillations will take place. This is also true between stages one and two.

The system under consideration consists of three units differing one from the other by a factor of 10 in nozzle area. The first, second and third stages have areas of .001, .01 and .1 square inches respectively. Theoretically, according to geometrical analysis alone, we should have an instantaneous flow gain of 1000. By experiment it is found that the instantaneous flow gain for the subsonic range is greater than 2000. This is due to the fact that the feedback from the third stage to the second helps to detach the stream from the wall. The splitters in all units are positioned in ascending manner, the first one being 16w, the second 8w, and third 4w from the power nozzle.

The pressure recovery of the system as a whole is about 70%. This means that the system can operate into a maximum active load equivalent to 70% of the system input pressure. This system operates properly only in the subsonic range (up to 15 psig) and in that range can be controlled by access to the atmosphere.

In the present investigation, all the experiments are conducted on two systems. One consists of three elements connected together by means of flexible hoses, the other was built as a single unit with each digital element of the unit exhausting directly into the controls of the subsequent one. The controls are holes in which flow passes from one stage to the other by means of a vortex motion (Fig. 4). The vortex principle on the control has been chosen as a result of experiments conducted with water.

The test set up for the system consisting of three elements connected by means of tubing is shown in Fig. 5A. Pitot tubes surrounded by static pressure tap holes (Fig. 5B) are placed along each leg of the system, these pitot-static tubes help to determine the pressure distribution throughout the system. These probes are also important in determining the static pressure which is created at the output of one unit when exhausting into the controls of another.

The knowledge of this static pressure build up is very important in that it gives information about the load existing at that point. Fig. 6 shows a curve of this static pressure plotted against the input pressure; as is evident from this plot the static pressure is the highest between the second and third stages, which shows that the area of the control nozzle of the third stage is not large enough to accommodate all the flow. The static pressure is least at the output of the third stage since the unit is exhausting into the atmosphere. The static pressure between the first and second stages is relatively high due to the static pressure build up previously mentioned. Fig. 7

shows the total pressure in the output of each stage. The total pressure is the highest at the third stage since the very large flow momentum more than makes up for the low static pressure in the passage. It is well to note that the total pressure between the first and second stages is actually almost all static, since the motion of the fluid is very slow. Fig. 8 shows the Mach number distribution at the output of the second and third stage. Fig. 9 shows a photograph of the apparatus used to measure the pressure distribution by means of the static-pitot tubes. The three units are shown connected in series and a probe is shown mounted in each leg of the system. In the experiment, the three units had a common input pressure and the flows were measured by Brooks flowmeters or rotameters. Two flowmeters, good within 2% over the whole range, were connected in parallel to accommodate all the flow.

The system which is discussed in the remaining part of this paper is represented in Fig. 10. This is a three stage amplifier where each stage is connected by means of a vortex cylinder type output to the subsequent one. The whole system has a common input. A top view of the system is shown in Fig. 4. The pressure recovery of the system varies from 60% to 75%. The pressure recovery is measured with the aid of a gate valve placed at one of the outputs of the unit. When the valve is partly closed loading the output of the third stage, some of the dynamic pressure of the stream is transformed into static pressure which is measured in a tank with a gauge connected to it as shown in Fig. 5. In Fig. 11 two curves of pressure recovery are presented. When measuring pressure recovery, as the valve was being closed at the output, the static pressure was building up in the upper portion of the diffuser in the third stage. When this pressure became equal to that at the entrance to the diffuser, a resonant effect caused oscillations. When the resonant condition was eliminated, the final pressure recovery of the system was measured. The lower curve in Fig. 11 represents the pressure recovery for loading just short of oscillation, while the upper one represents the pressure recovery for a completely closed valve when the region of oscillation has been passed. Pressure recovery is given as the ratio of output to input pressures.

Output loading curves (flow vs. pressure) are shown in Fig. 12.

By means of the curves of Figs. 11 and 12, it is possible to compute the output power of the system. The output flow is measured by means of a flowmeter. Since the flowmeter is exhausting into atmosphere it reads mass flow directly. This mass flow is transformed back to volumetric flow at the pressure existing in the tank at the output of the system assuming an isothermal process.

Then, using the subscripts (1) to denote conditions in the tank and (2) to denote those in the flowmeter, the output power (P) is given by

$$P = pQ$$

$$p_1 \, Q_1 = \frac{p_{2(atm)}}{p_{1 \, (abs)}} \, p_1 \, Q_2 \quad , \qquad (1)$$
$$(gauge)$$

where p_1 is the gauge pressure of the air in the tank (Fig. 13). The pressure p_1 (abs) appearing in the ratio is a density correction since the flow Q_2 is measured with reference to the atmosphere.

In relation (1) we have assumed an isothermal process, hence

$$\frac{\rho_2}{\rho_1} = \frac{p_2}{p_1}$$

The maximum power output has been plotted against the input pressure in Fig. 14. It is evident from the graph, that the maximum power output is about a horsepower. By the same method the power input of the system was calculated, and the power efficiency as a function of input pressure is plotted in Fig. 15. The power efficiency is about 60% over the range considered. The losses are due mainly to pressure and flow degradation because some of the flow goes out the opposite channel when the system is loaded.

At this point it is necessary to introduce the term "switching power." It denotes the rate at which work must be done in order to detach the stream from the wall and switch it to the next channel. In order to measure the switching power of a system, an apparatus similar to the one described at the output is employed (see Fig. 5). The flow is measured by means of a Fisher and Porter flowmeter whose maximum range is .5 SCFM. A valve is provided after the flowmeter whereby the flow can be controlled. Following the valve is a small tank with a combination gauge connected to it. The pressure in the tank is measured initially when the valve is closed and then measured a number of times as the valve is opened slowly; in particular at the time when the unit is at the point of switching. The flow at switching is also measured. Hence, the instantaneous power to switch

is defined as

$$p_1 Q_1 = \frac{p_{2(atm)}}{\Delta p_{1(abs)}} \ p_1 (gauge) \ Q_2 \tag{2}$$

This power is that which passes out of the small needle valve at the instant of switching. In order to calculate the real instantaneous switching power, it would be necessary to know the total pressure at the output of the control nozzle at the instant of switching. This is not possible at present. But if it is assumed that the losses from the valve to the nozzle are very small and that the density of the gas doesn't change very much, then the switching power calculated is close to the correct one. In equation (2), p_1 is the gauge pressure at the instant of switching, while Δp_1 appearing in the ratio is the difference between the pressure existing in the tank before the valve is open and the pressure in the tank at the instant of flipping. In our case the source of power is the atmosphere. Since the pressure in the tank is below atmospheric, when the valve is opened the pressure difference between p_1 and p_{atm} is enough to create the flow necessary to switch the system. It is also possible to obtain switching power into the controls from a supply line through a regulator.

Switching power as a function of supply pressure is shown in Figs. 17A and 17B in different units. From these curves, it is evident that little power is needed to control the whole system up to 15 psig. The switching power is only a very small fraction of a watt. If we look back now at the power output (Fig. 14), we find that the instantaneous power gain increases rapidly and at 15 psig, is about 9000. The plot of power gain against input pressure is shown in Fig. 16.

Now that the power of the system has been discussed, it appears necessary to say a few words about the flow of the system. The whole system has a flow capacity of 64 SCFM at 15 psig (see Fig. 20 where the variation of flow with respect to input pressure is shown).

The flow gain of the system, i.e., the output flow divided by the switching flow, increases rapidly with pressure (Fig. 18) until it reaches maximum (3000) at about 8 psig and then drops slowly as the pressure is increased to 15 psig. The switching flow normalized in terms of the output flow is shown in Fig. 19 and this shows that the relative flow to switch the whole system decreases rapidly up to about 6 psig and then remains essentially constant up to 15 psig.

Figure 21 shows one experimental set up which may be employed to determine the basis characteristics of each of the individual elements. The pressures at the inputs and outputs are measured by means of transducers. The input and output flows are measured directly by

54

flowmeters and also computed from the pressure differences measured across orifice plates. The signal outputs from the transducers are plotted on an X-Y recorder. By this method plots are obtained directly by changing the input pressure continuously with a motorized valve. Once the characteristics of the elements are known, then it is a simple matter to match them together for given requirements.

Figures 22A and 22B show another set of apparatus by which the pressure distribution of a jet is measured with static taps placed one nozzle width apart along the wall. With this apparatus, it is possible to find the point of attachment of the jet and also to determine how it changes as some of the parameters are varied. The pressure distribution is read by means of manometers.

Some Further Problems

Although digital systems can be built and fluid amplifiers can be staged to obtain very high flow gains and power gains, more research in the following areas is necessary in order that theoretical analysis can be correlated with experimental results: The measurement of pressure profiles before entrance into a diffuser; the measurements of static pressure profiles along the boundaries of the amplifier; and the reduction of acoustic noise generated in jet-edge oscillations.

Acknowledgment

References

1. Bourque and B. C. Newman, Aeronautical Quarterly, Vol XI, August 1960.
2. M. L. Albertson, Am. Soc. of Civil Eng., Paper Nc. 2409.
3. Rayleigh, "Theory of Sound", (Dover Public. N.Y., 1945), pp 410.

BIBLIOGRAPHY

Olson, R.E.: "Studies of Pure Pneumatic Elements." United Aircraft
   Corporation, DOFL Contract Number DA-49-186-ORD-512, June 1961.

Brown, F.T.: "Sc. D. Thesis." M.I.T., Dept of Mech. Eng., May 1962.

Brown, C.B.: "Proc. Phys. Soc." (London) 49, 493 (1937).

Lighthill, M.J.: "Notes on the Deflection of Jets by Insertion of
   Curved Surfaces." R.M. 2105, 1945.

Glauert, M.B.: "The Wall Jet." Journal of Fluid Mech., Vol. 1, 1956.

Schlichting, H.: "Boundary-Layer Theory." 4th Edition.
   McGraw-Hill Book Company, Inc., N.Y., 1960, p. 605.

Sawyer, R.A.: "The Flow Due to a Two-Dimension Jet Issuing Parallel
   to Flat Plate." Journal of Fluid Mech., Vol. 9, Part 4, Dec. 1960.

Bailey, A.B.: "Use of Coanda Effect for the Deflection of Jet Sheets
   Over Smoothly Curved Surface." UTIA Tech. Note No. 49,
   Part I and II.

Figure 1

57

Figure 2

58

THREE STAGES
AMPLIFIER

III STAGE

II STAGE

I STAGE

Figure 3

THREE STAGE AMPLIFIER
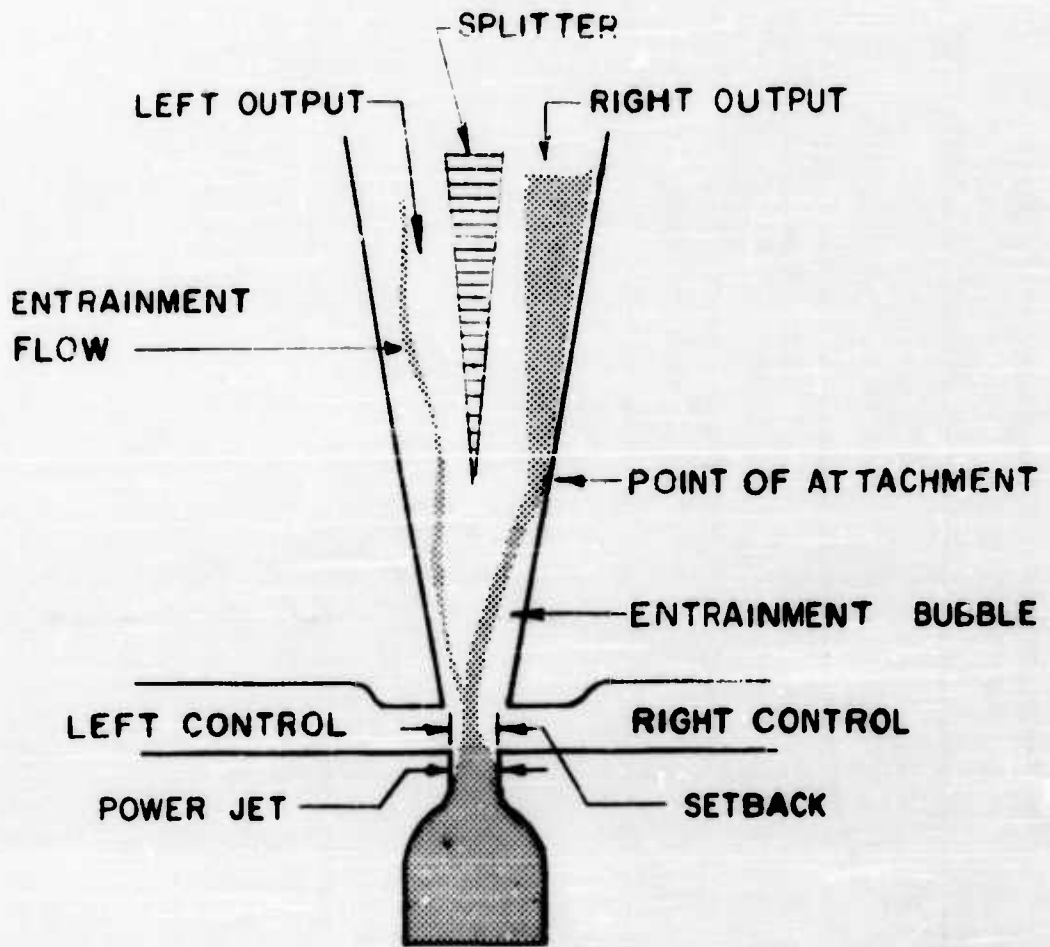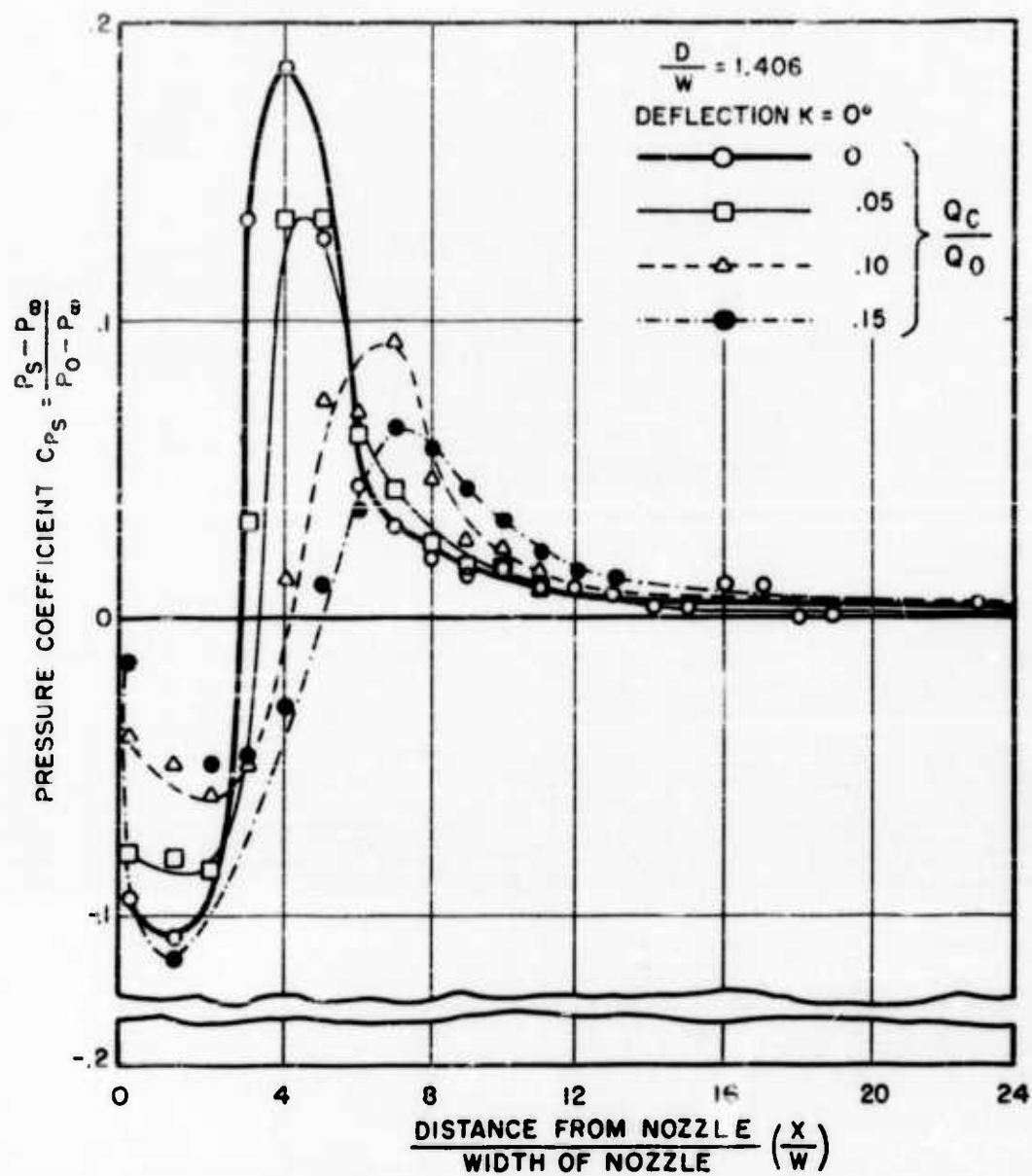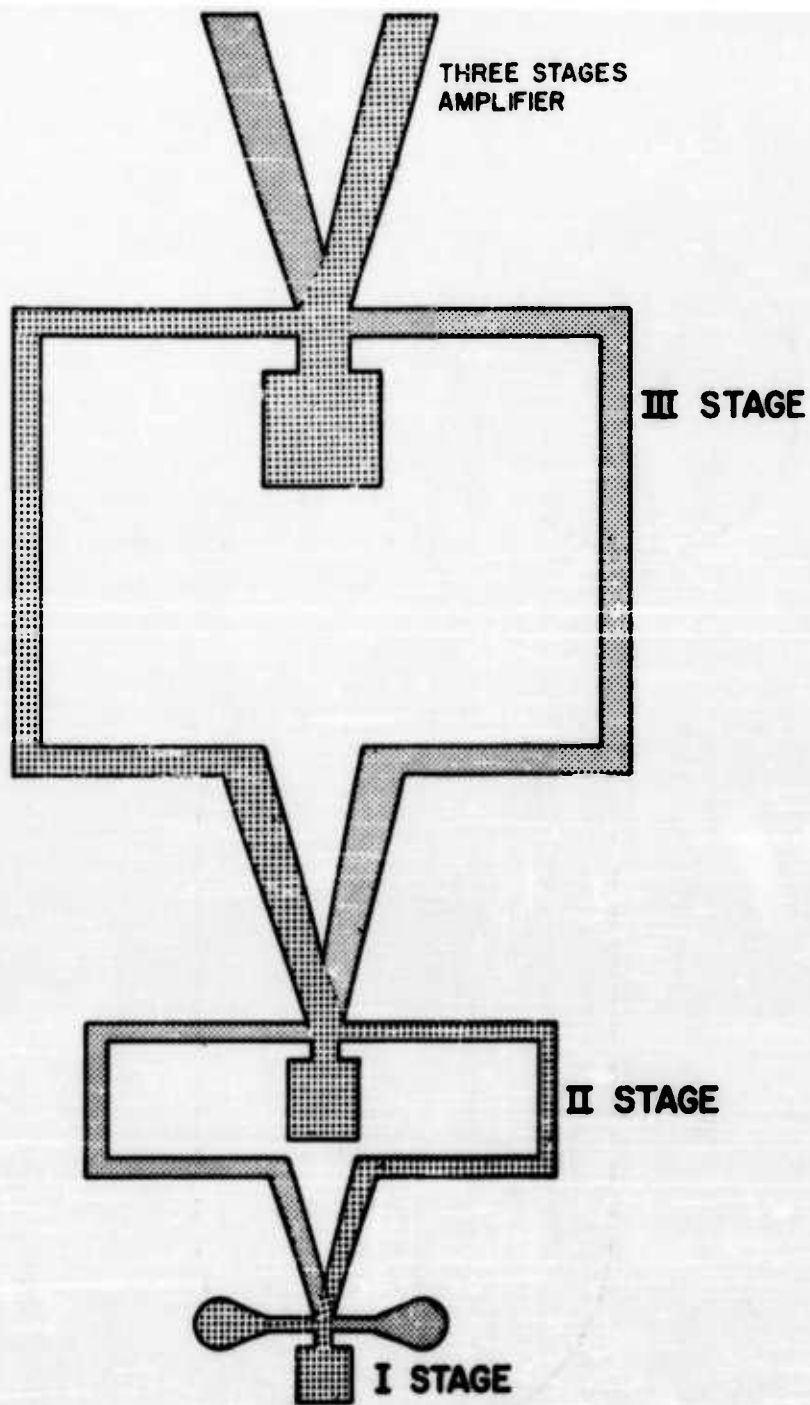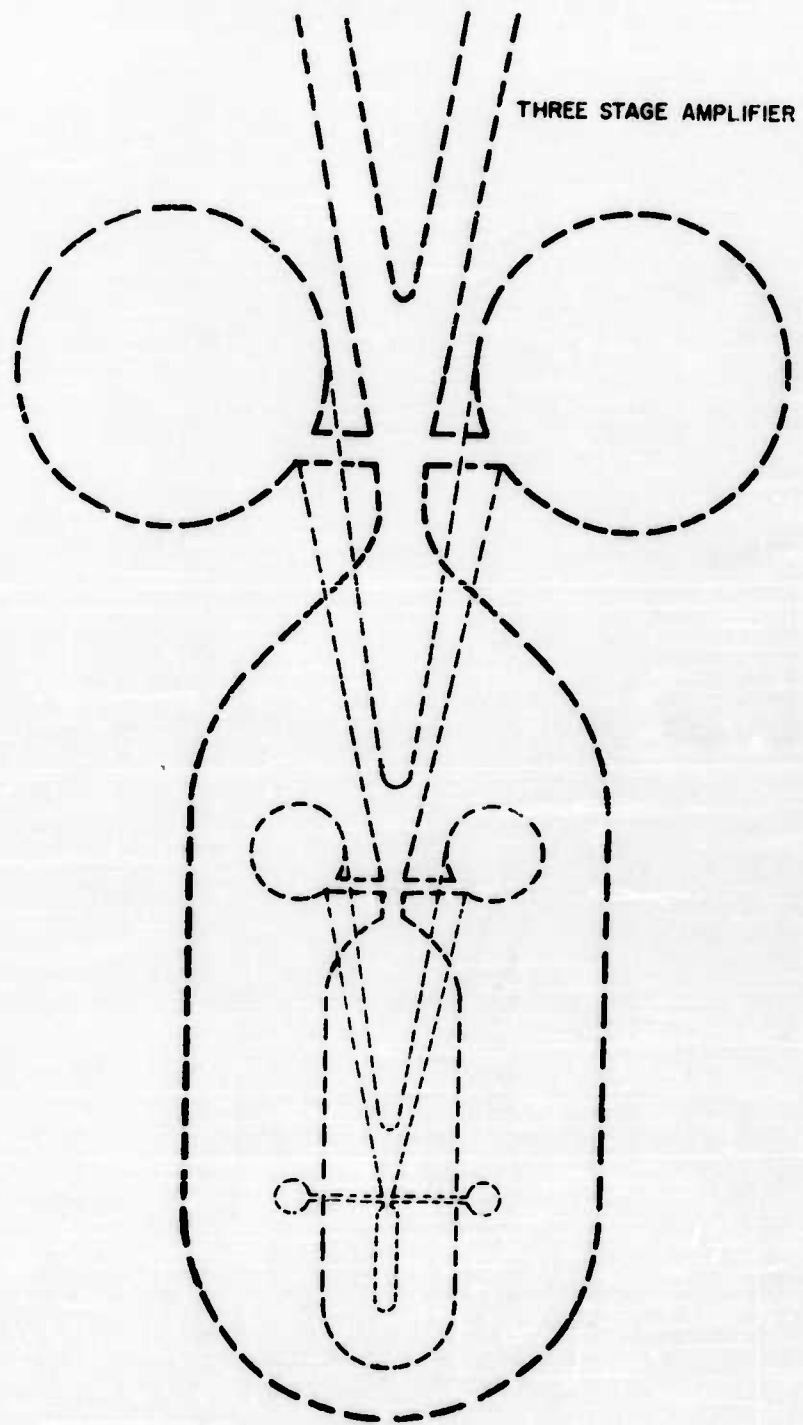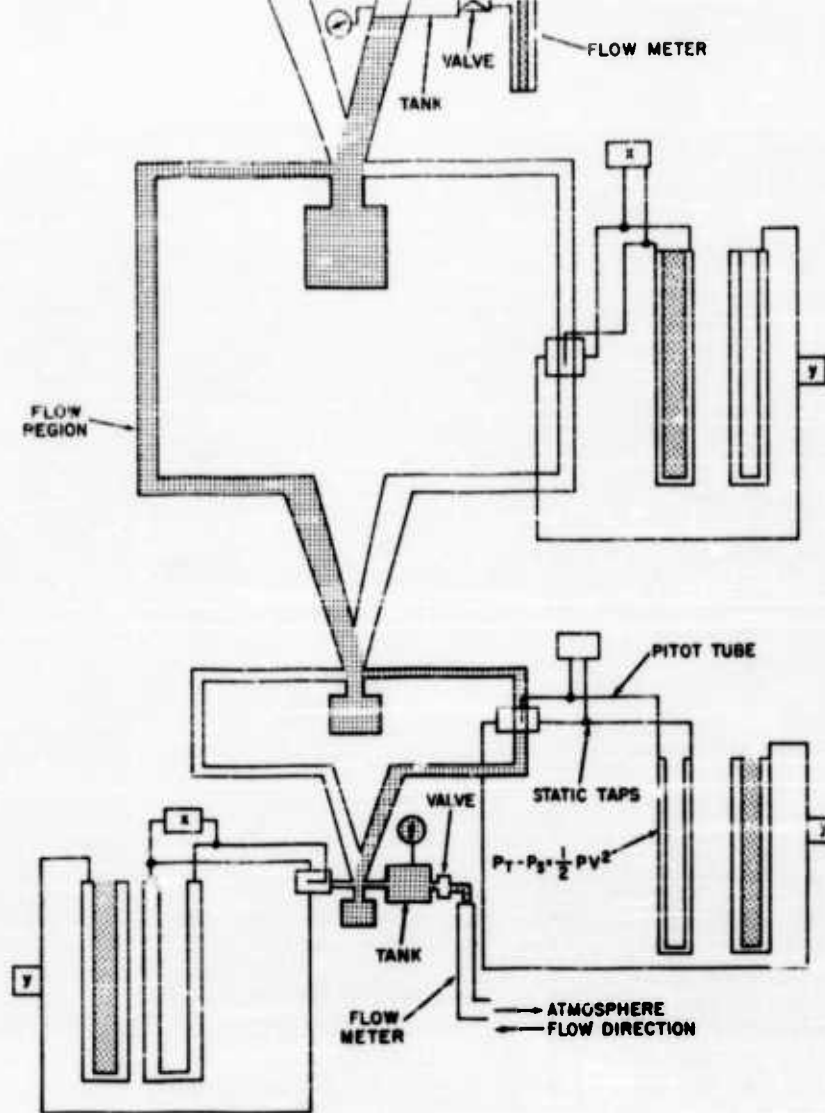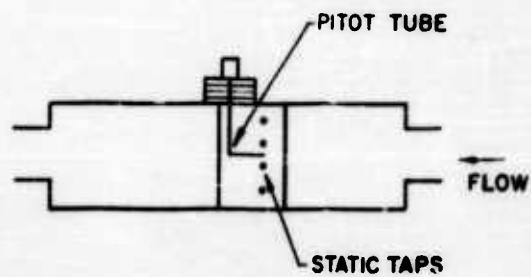
Figure 4

Figure 5a

Figure 5b

Figure 6

Figure 7

62
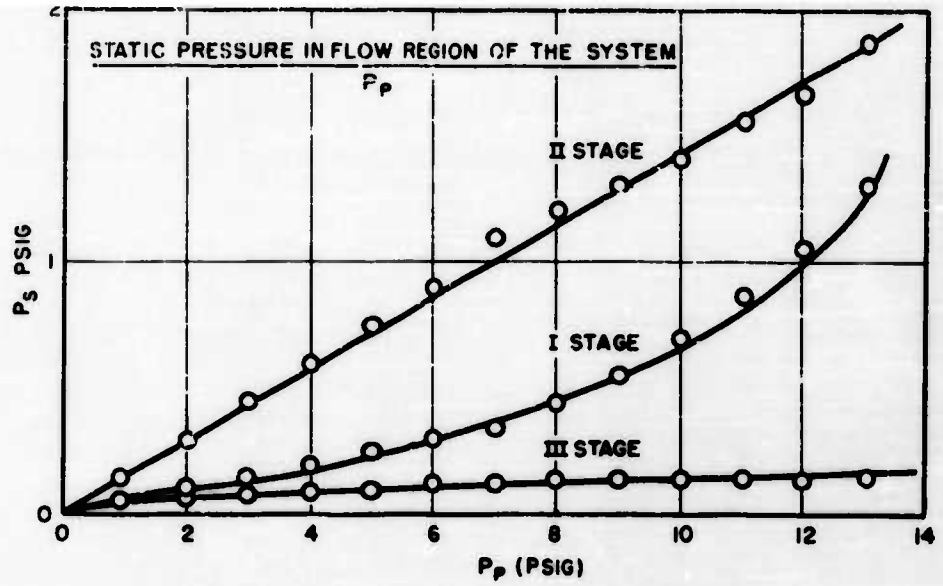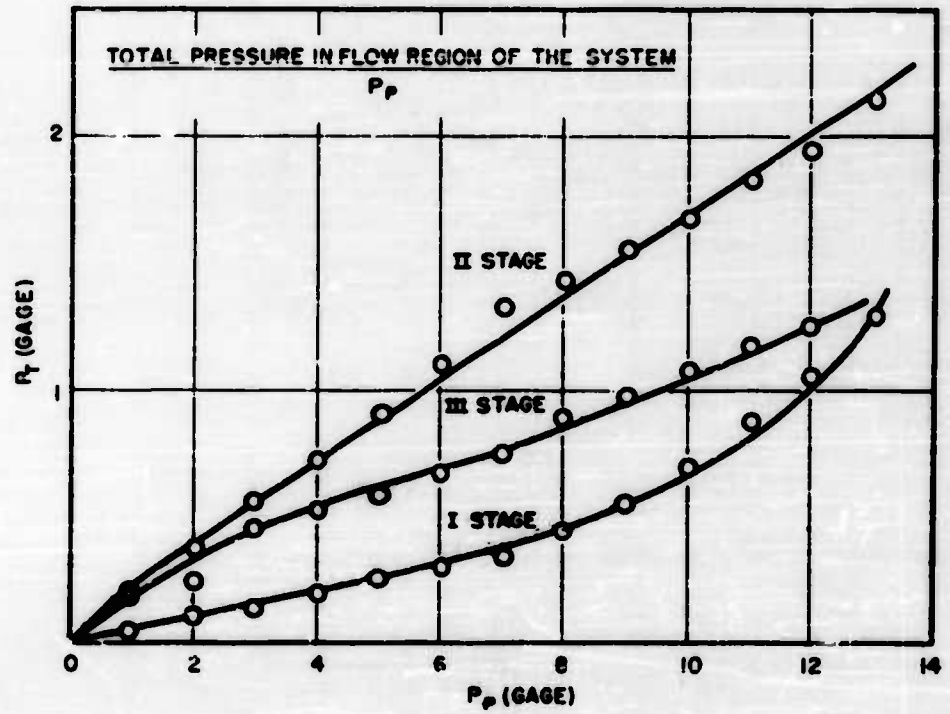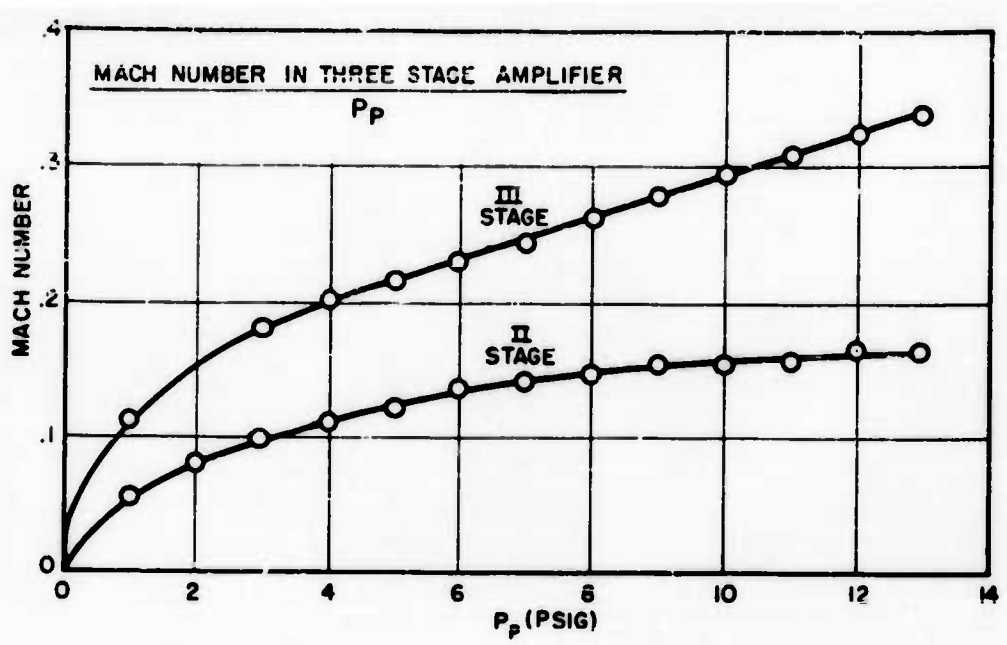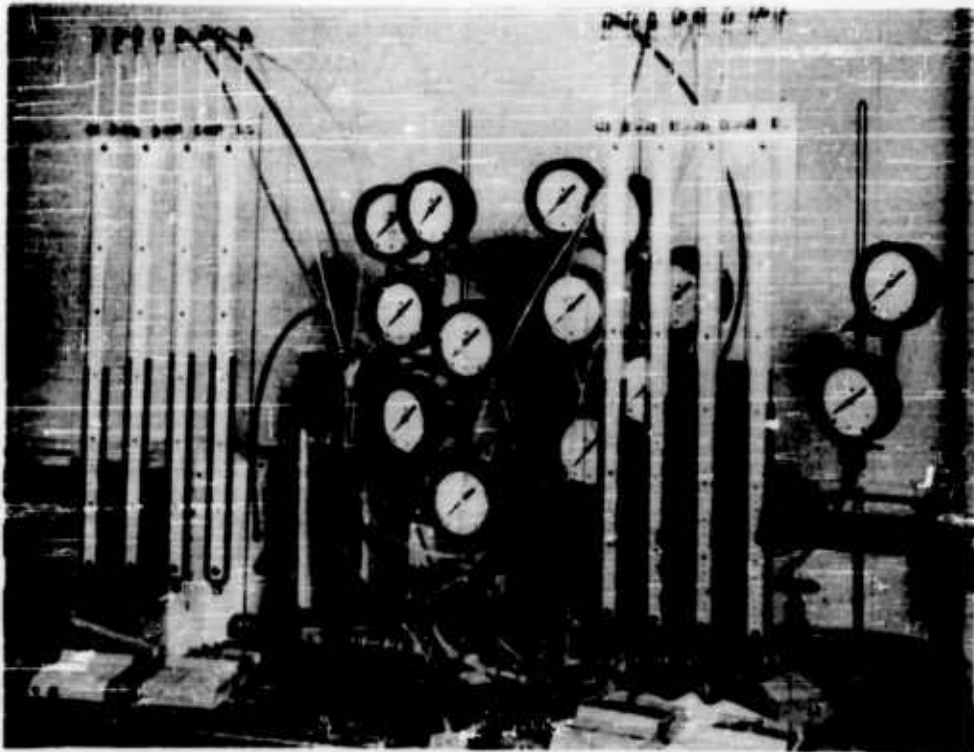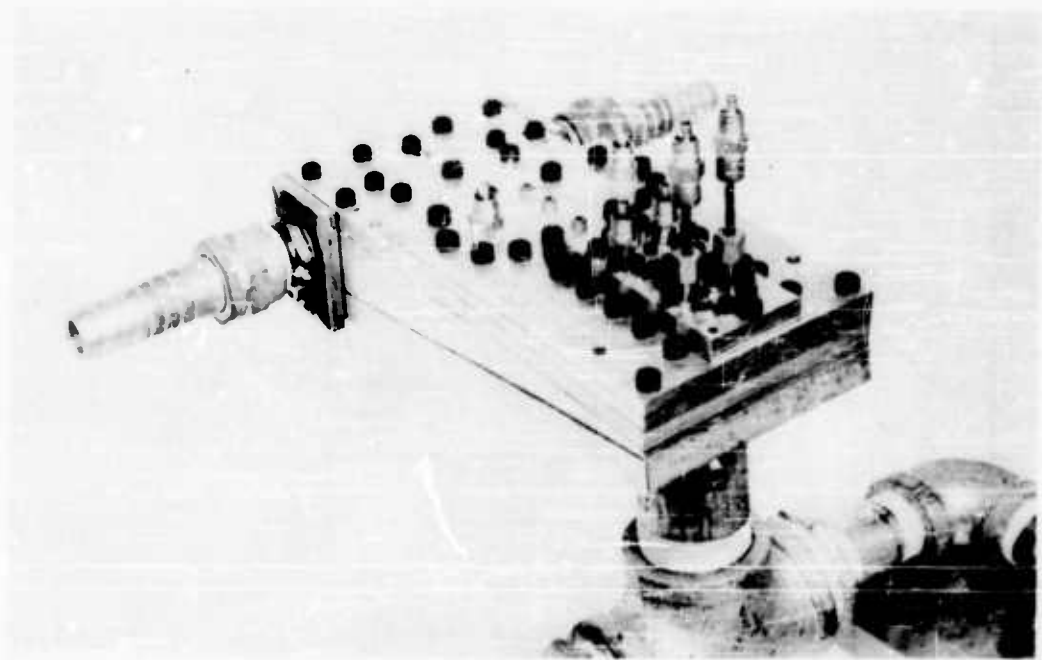
Figure 8
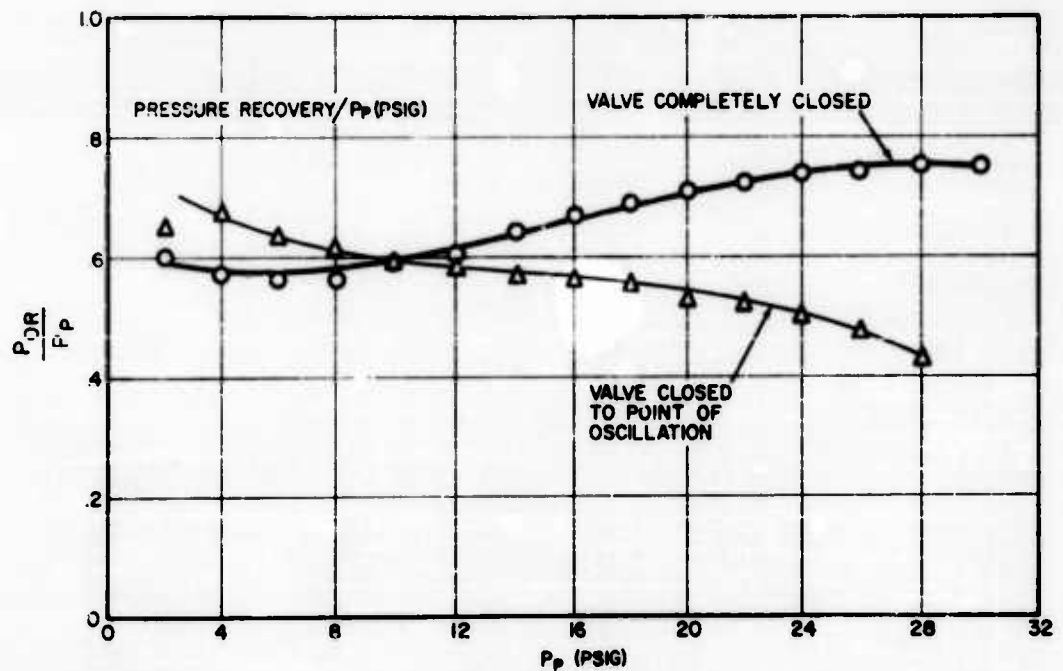
Figure 9

Figure 10

Figure 11

Figure 12

Figure 13

MAXIMUM OUTPUT POWER (WATTS)
VS
P_P (PSIG)
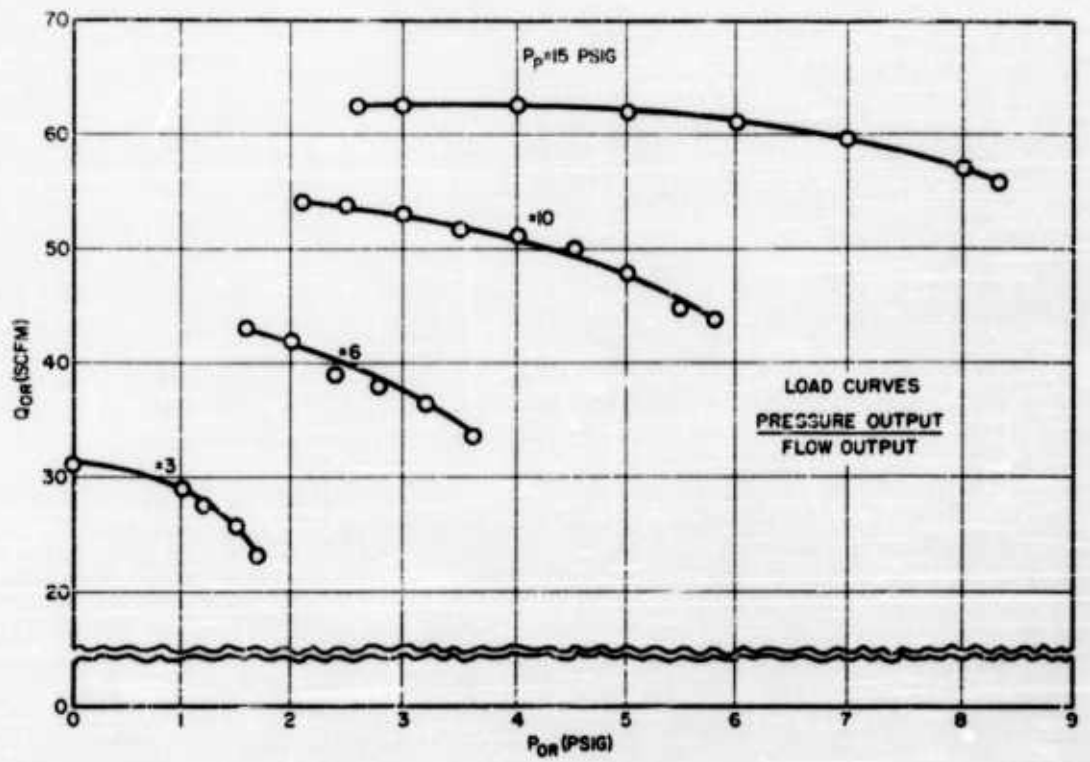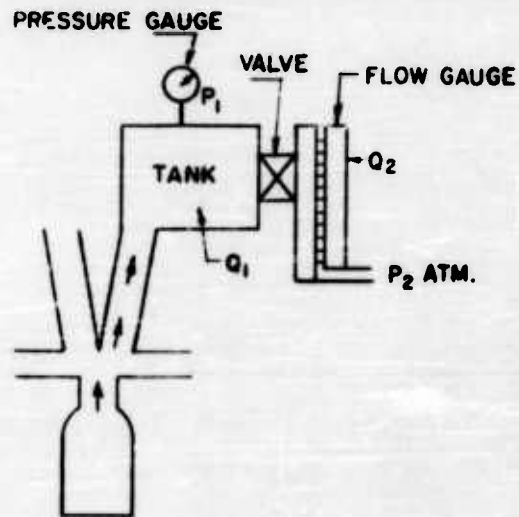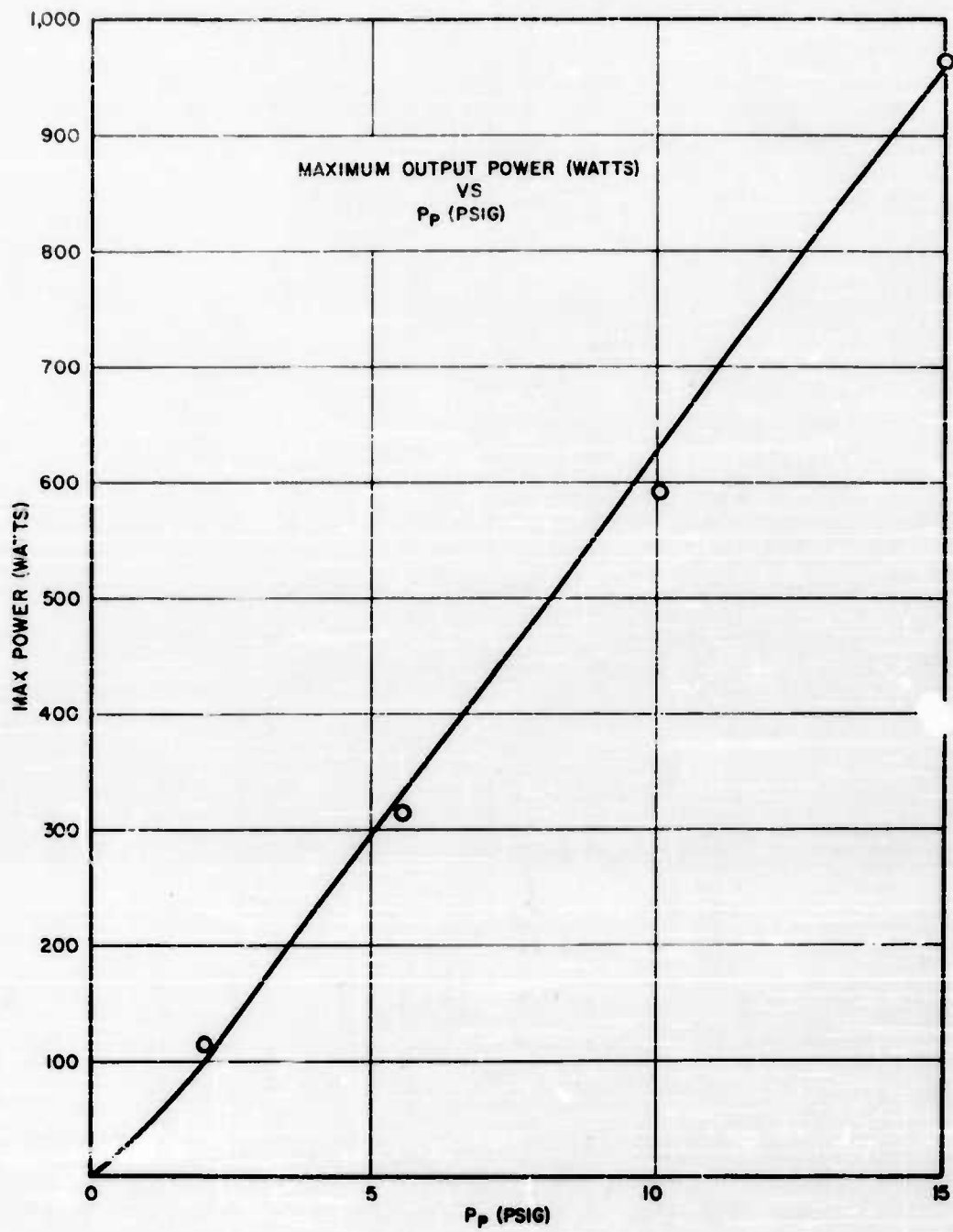
Figure 14

Figure 15

Figure 16

67

Figure 17 a

68

Figure 17 b

69

Figure 18

Figure 19

70

$$\frac{P_P}{Q_{OR}} = \frac{\text{INPUT PRESSURE}}{\text{OUTPUT FLOW}}$$
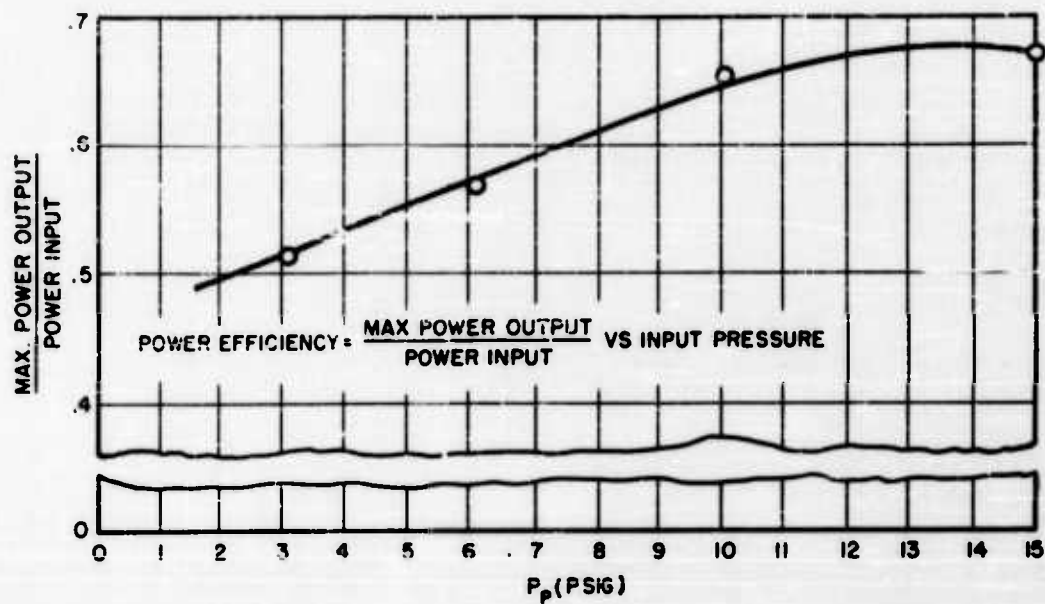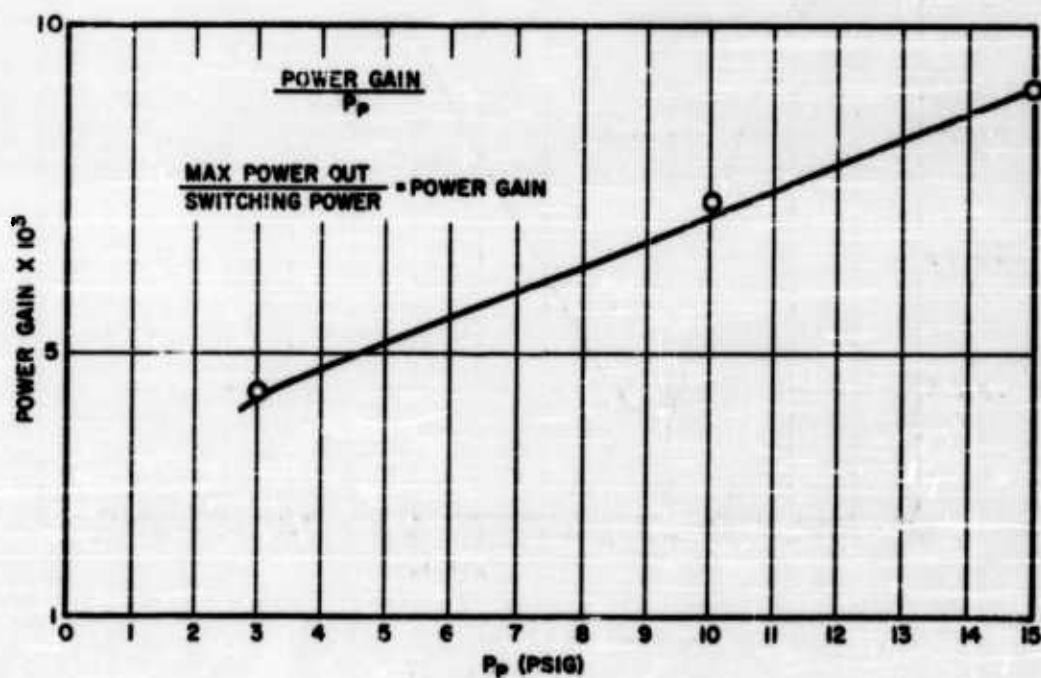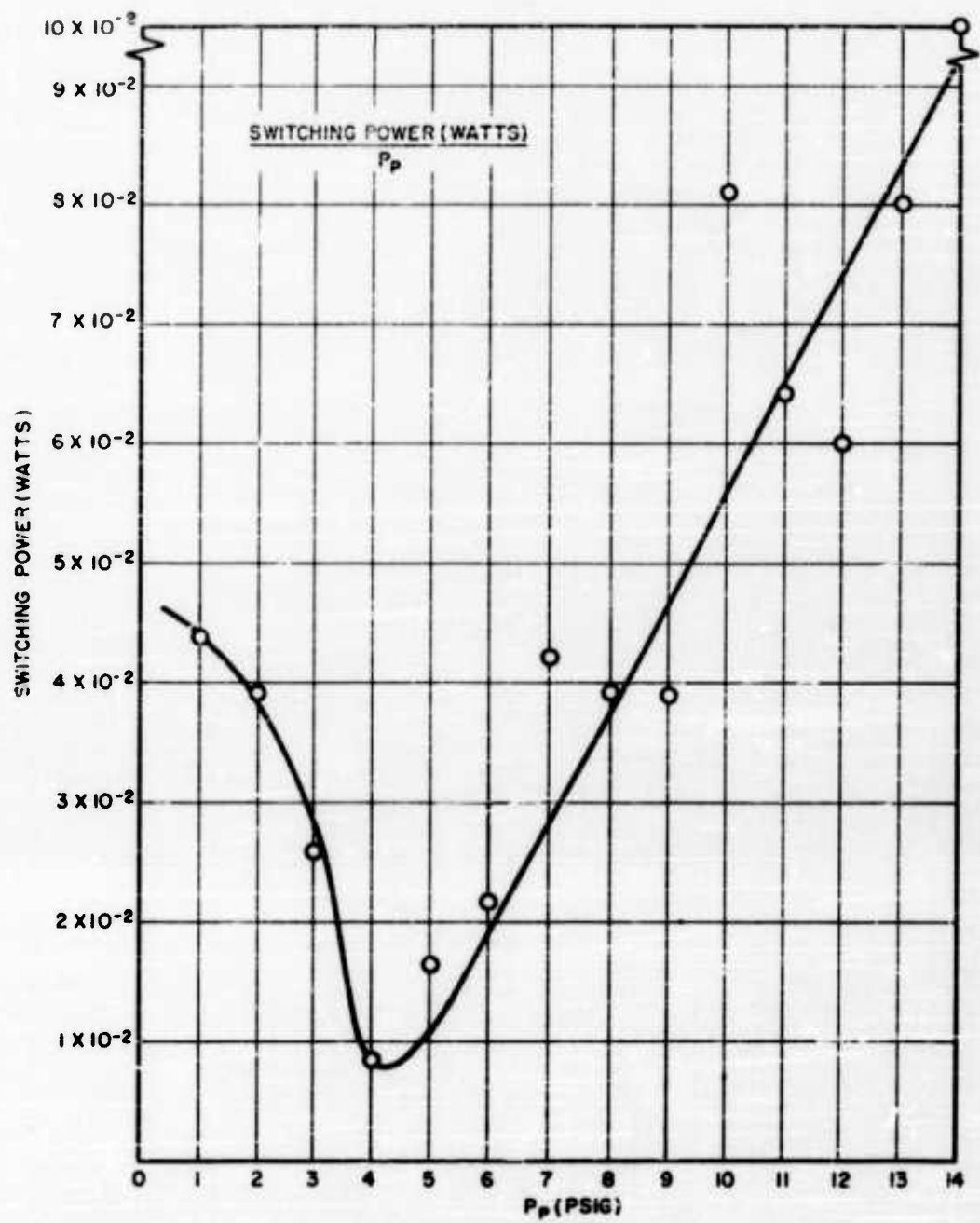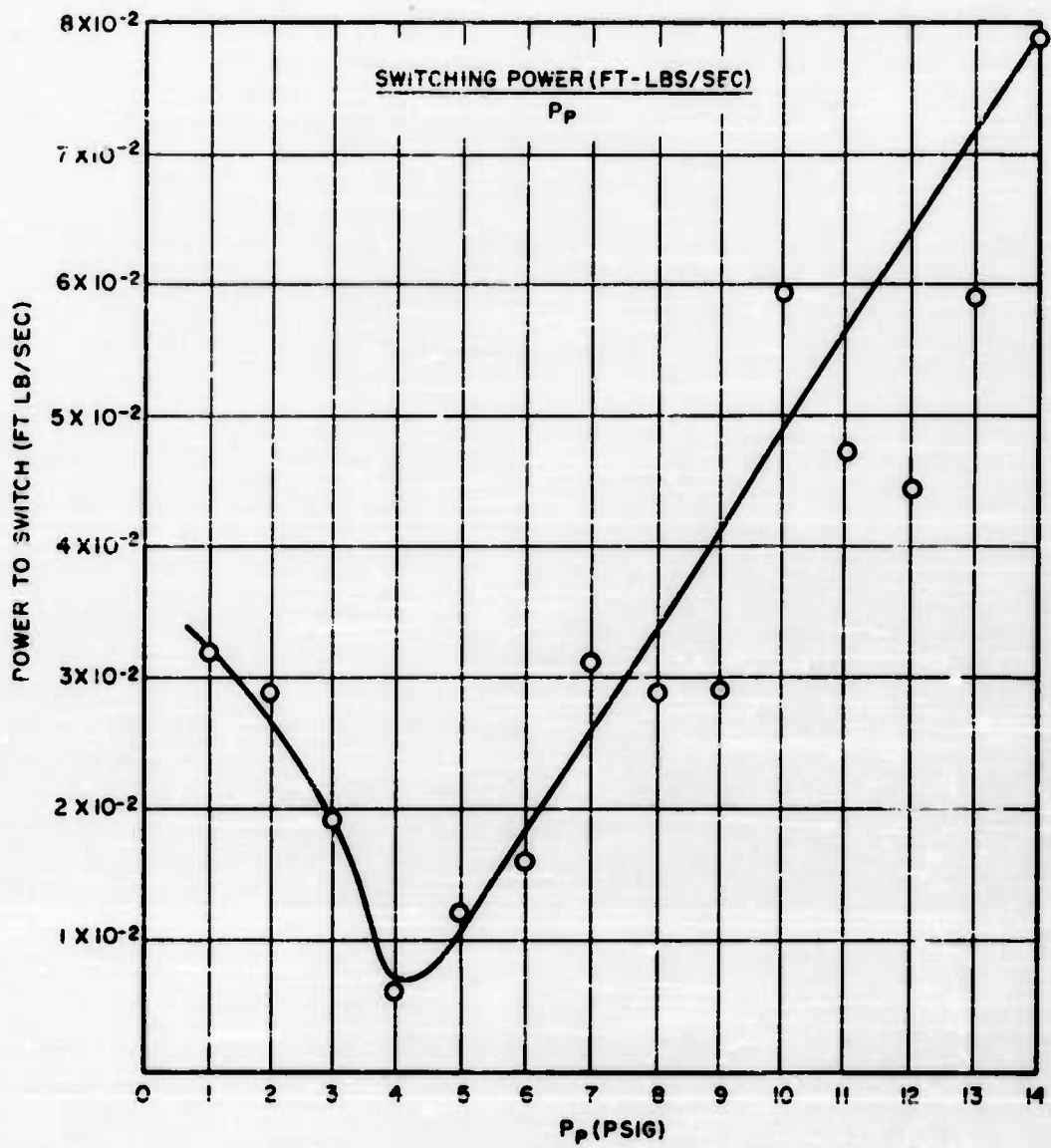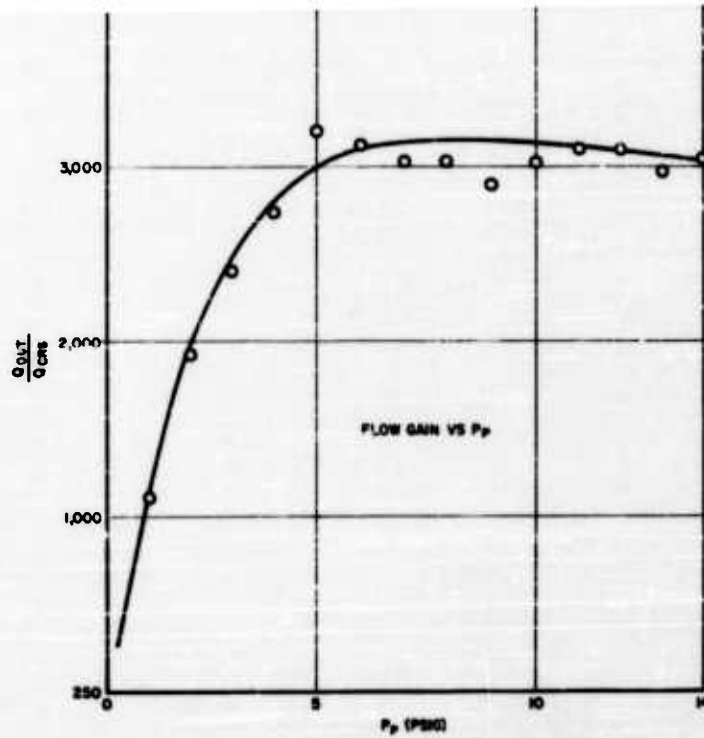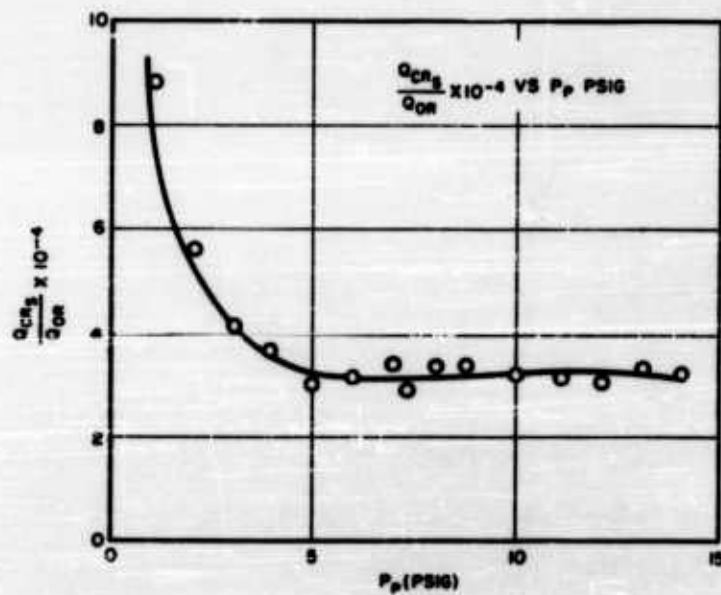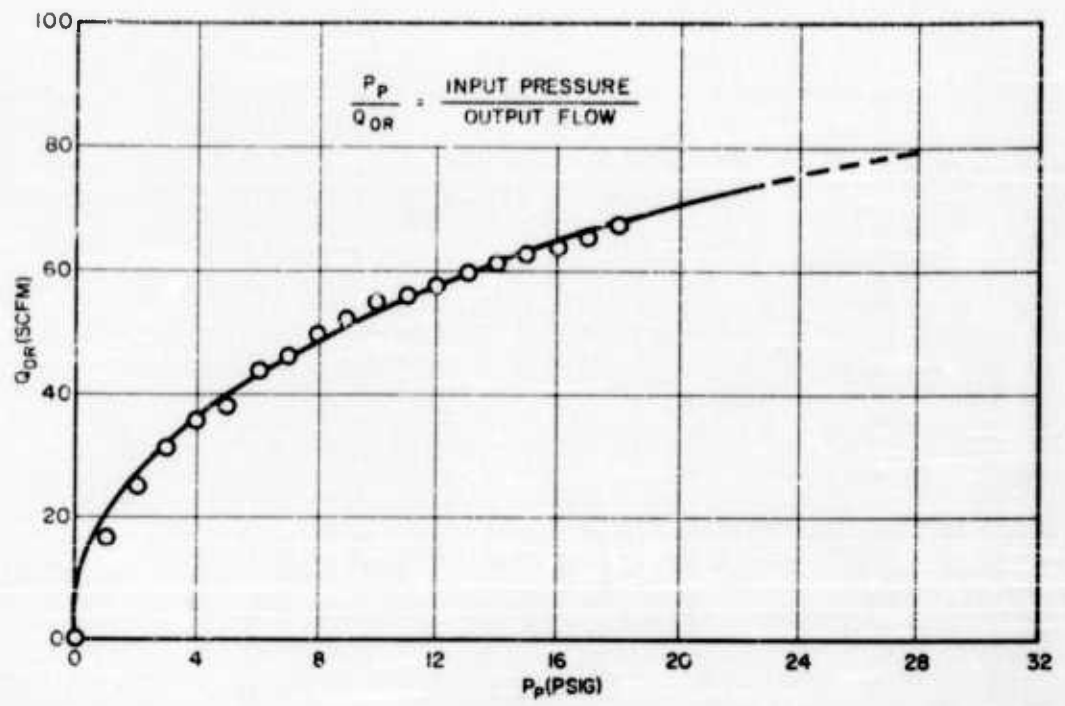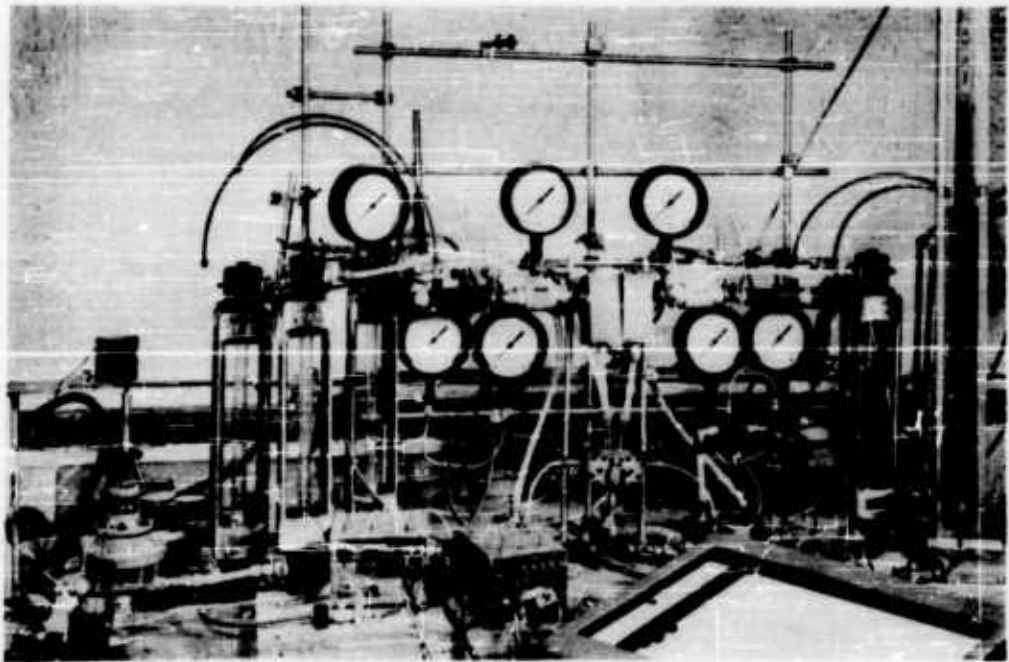
Figure 20

Figure 21

71
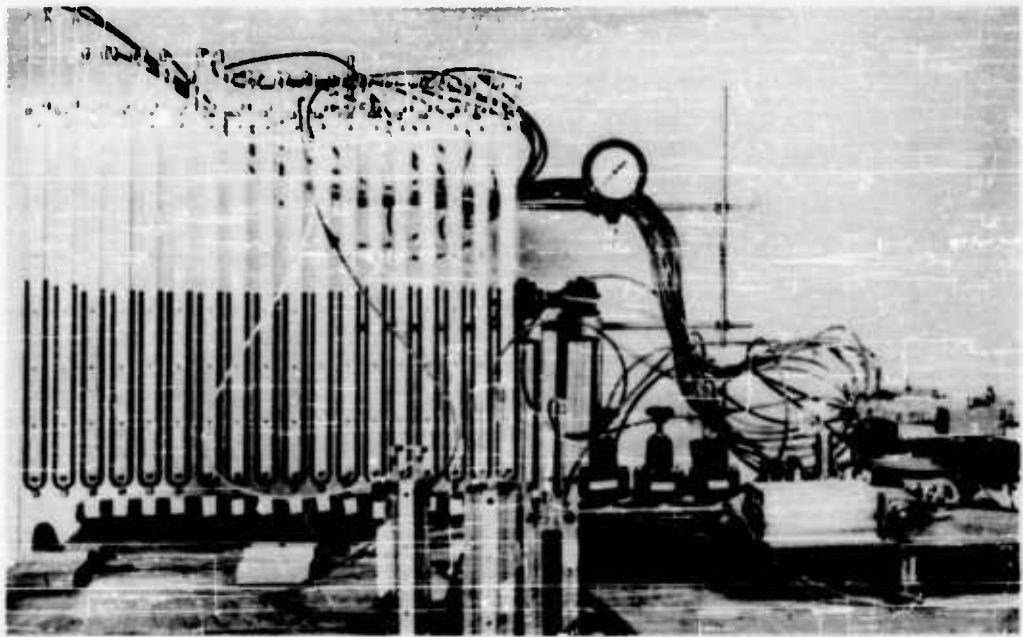
Figure 22a

Figure 22b

72

ROCKET THRUST VECTORING

by

Allen B. Holmes

of

Diamond Ordnance Fuze Laboratories

Abstract

An experimental program is being conducted at DOFL to investigate
the characteristics of a supersonic fluid amplifier discharging air at
high Mach numbers into the expansion cone of a rocket nozzle for thrust
vector control. Preliminary static firings of a cold gas Mach 3.2
nozzle with fluid amplifier controls were made during September of this
year. Direct measurements were made of the amplifier input flow,
induced lateral thrust, and switching levels.

Introduction

Today rockets are designed for maximum propulsive efficiency, with
maximum payload, and to follow extremely accurate trajectories. At
lift off and in outer space, external aerodynamic surfaces are ineffective
as control elements and some other means is required.

There are five major methods of controlling a rocket's trajectory.
These consist of: jet vanes, jetevators, gimbled or swiveled nozzles,
vernier rockets, and secondary fluid injection.

The first four of these have disadvantages such as exposing moving
parts to high temperature exhaust streams, requiring high actuating
forces, and having a relatively low frequency response.

A rocket is a thrust producing system which derives its thrust from
the ejection of hot gases generated from material carried in the system.
It has already been previously shown that a portion of this gas can be
bled from the combustion chamber and fed back into the expansion cone of
the propulsion nozzle for effective thrust vector control. However,
present hot gas injection systems require valves that are capable of
bleeding gas directly from the combustion chamber. These systems also
have the disadvantages of exposing moving parts to a high temperature
high pressure stream, and in the case of solid propellant motors the

intermittent operation of valves can affect the burning rate of the grain and cause a reduction in combustion pressure and overall performance.

DOFL's effort in this field is directed towards the utilization of fluid amplification techniques as applied to a chamber bleed thrust vector control system. This type of system has the advantage of not affecting combustion pressure and of having higher response rates, low actuating power requirements, no moving parts, and increased reliability. Proportional control can be attained with either a bistable unit which is pulse duration modulated or a proportional type fluid amplifier.

Object

Cold gas testing is presently underway on the prototype fluid amplifier which is shown in Figure 1. The unit was designed to have the following characteristics:

(1) No moving mechanical parts;
(2) Bistable operation;
(3) A flow gain of 500 (Flow gain in this case is defined as the primary nozzle flow rate divided by the control jet flow rate required to produce a given lateral to axial thrust ratio);
(4) A lateral to axial thrust ratio of about .05 for a secondary to primary flow ratio of .025.

Test Set Up

The amplifier was designed with interchangeable parts in order that changes could be made without interrupting tests. (Figure 2)

The power jet was designed to diverge in a plane normal to the interaction region. This was done to increase the aspect ratio of the nozzle, and therefore cut down on the viscous effects, due to the cover plates.

Figure 3 shows the amplifier mounted on the propulsion nozzle. The primary nozzle was designed with an expansion ratio of 5.12, and a primary flow rate of 3.5 lbs/sec. The theoretical axial thrust without injection was calculated to be equal to 220 lbs.

A three component thrust stand (Figure 4) was designed and built at DOFL. This stand is a framework in which three load cells are located in a single plane to determine the axial and lateral components of thrust. The nozzle assembly is held in place by flexure supports. These flexures behave effectively as pinned joints, but provide high compliance in all lateral directions. The spring constraints they impose on the system are very small relative to the forces being measured and can therefore be neglected.

74

Tests

It is to be noted that the purpose of these tests is to develop techniques for injecting the output of a fluid amplifier into the supersonic exhaust of a conical propulsion nozzle. Emphasis was placed on the compiling of information on the relative characteristics of each test system. A number of basic simplifying assumptions were made.

The basic assumptions were:

(1) Adiabatic isentropic flow throughout the entire system.
(2) Constant nozzle discharge coefficients.
(3) A constant location of the induced center of pressure on the primary nozzle wall.
(4) At secondary to primary flow ratios less than 0.05, the effect of the axial thrust component of the fluid amplifier was assumed equal to zero.

Test Results

Figure 5a is a schematic diagram of the fluid amplifier and nozzle. The general performance characteristics of this fluid amplifier thrust vector control system can be summarized in Figure 5b. This is a curve which plots induced lateral thrust against left and right control jet flow rate. The arrows indicate the order in which the process took place.

The best overall performance of the system occurred with an over-expanded power jet. Performance was determined on the basis of maximum induced lateral specific impulse. Lateral specific impulse can be defined as the induced lateral thrust per pound of total injected flow. A comparison was made between the induced lateral specific impulse and the specific impulse of a hypothetical nozzle expanding under ideal conditions at the same power jet pressure and flow rate. The lateral specific impulse with injection for this system was found to be about 1.25 times as great as an ideal hypothetical nozzle.

A point by point explanation of Figure 5b goes as follows: (a to b) the total power jet flow is ejected out the rear of the amplifier. At (b) there is just sufficient flow to switch the power jet flow into the primary nozzle and cause an abrupt increase in lateral thrust (b to c). The control jet flow is then reduced to zero (c to c'), causing a slight decrease in lateral thrust. When a small control flow (c' to d) is introduced, there is a slight increase in lateral thrust which is linear with respect to the increase in control flow. This flow switches the amplifier flow out of the primary nozzle, causing a sharp decrease in lateral thrust (d to e). The control jet flow is reduced to zero, thus completing the cycle.

75

Shadowgraphs

The shadowgraphs, Figures 6 and 7, correspond to points d and b on Figure 5b. The output of the amplifier produces a shock wave by appearing as a discontinuity to the primary stream. In effect the injected flow forms a wedge near the point of injection and causes the primary stream to separate from the nozzle wall. As the stream passes through this induced shock wave it decreases in velocity, increases in pressure, and tends to turn in the direction of the shock wave. This build-up in pressure in the separation region, plus the pressure and momentum of the injected stream, gives a resulting lateral thrust greater than a similar injection nozzle exhausting at the same pressure and flow rate, at 90° away from the primary stream.

Summary

In summary, the measured characteristics of the amplifier system were:

(1) The most efficient vectoring was achieved at a power jet pressure of 115 psia;

(2) A maximum lateral to axial thrust ratio of 0.014 was measured for a secondary to primary flow ratio of 0.01. (This corresponds to a force amplification factor of about 1.4.);

(3) The system had a flow gain of about 700;

(4) The amplifier had bistable operation at pressures up to 300 psig.

It is to be emphasized that these results are not indicative of optimum performance, but serve to illustrate the feasibility and adaptability of fluid amplification principles to Rocket Thrust Vector Control.

76
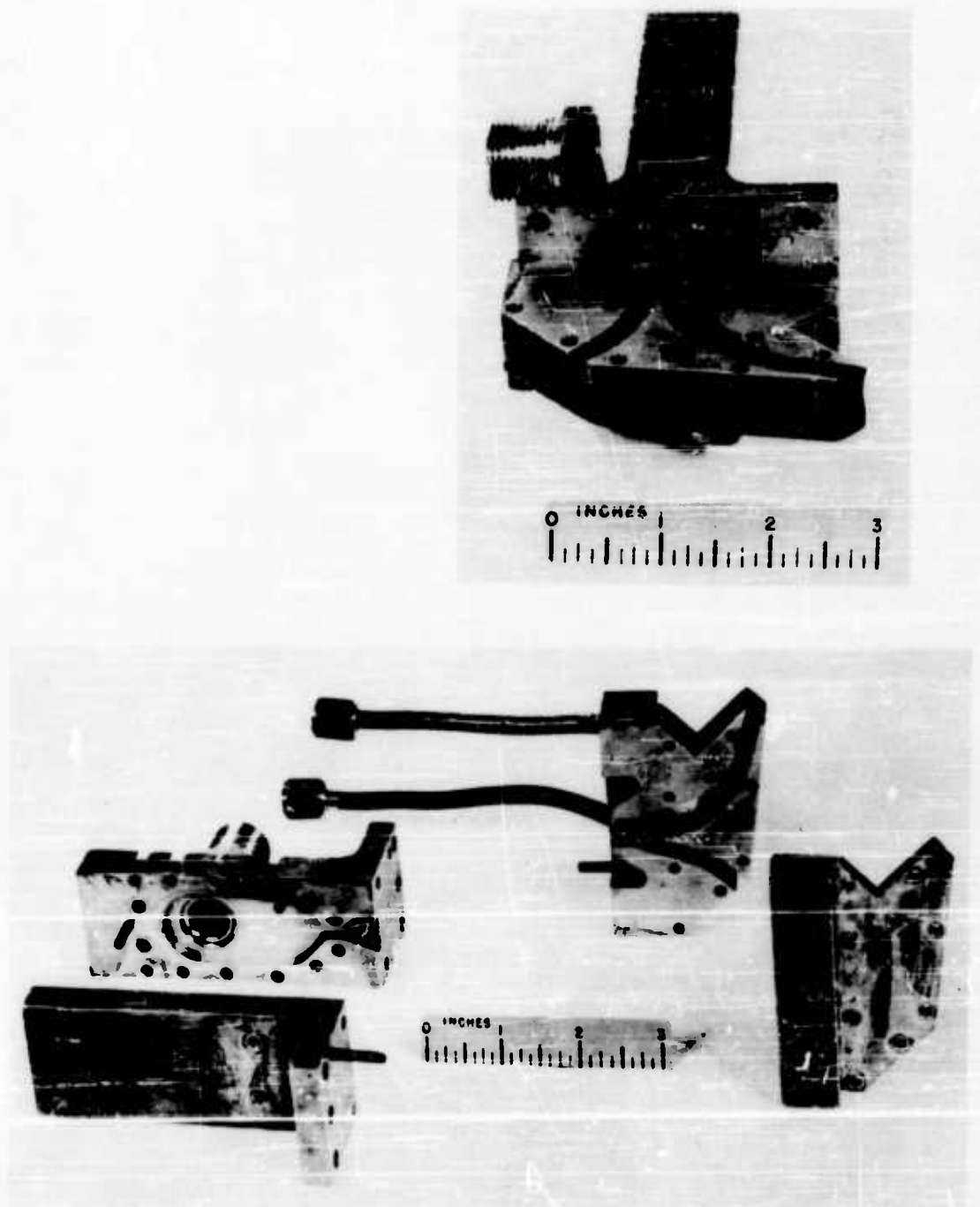
Figure 2. Bistable fluid amplifier assembly.
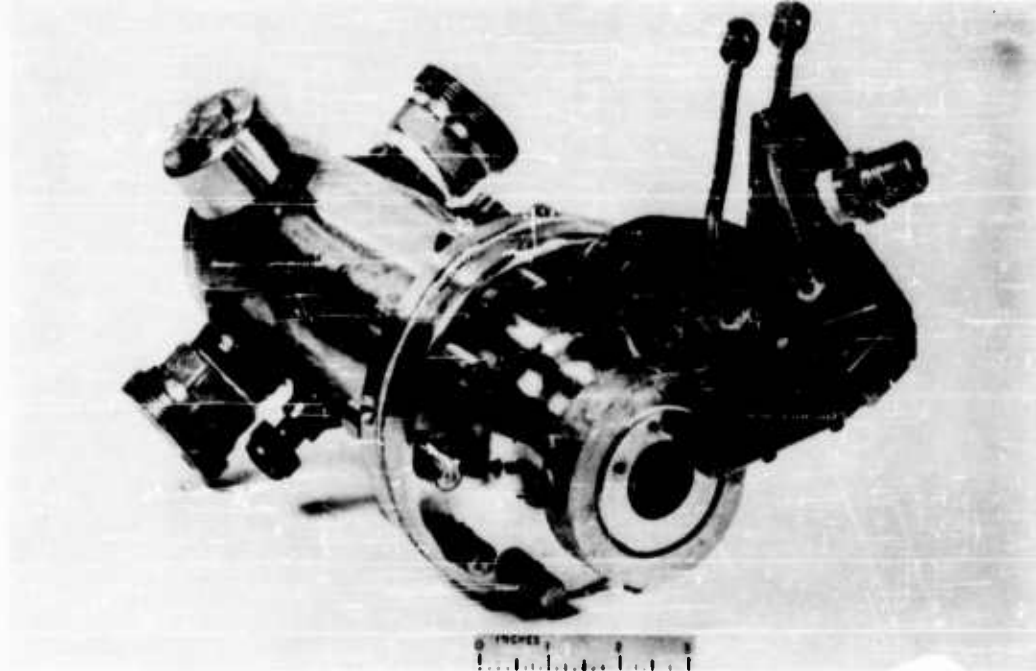
Figure 3. Fluid amplifier and thrust chamber assembly.
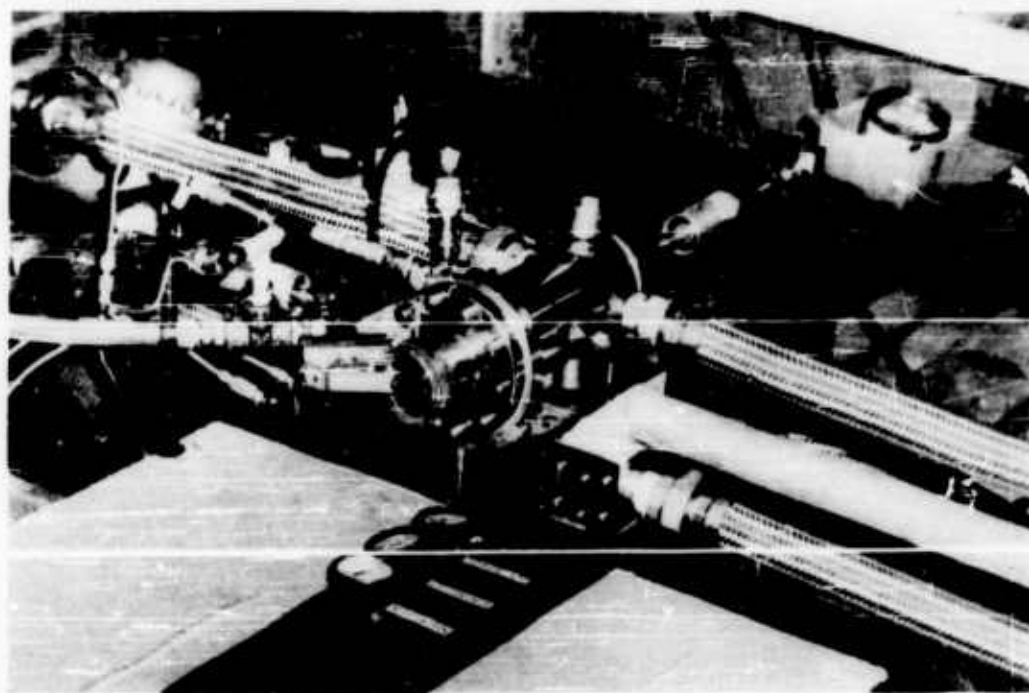
Figure 4. Thrust stand assembly.
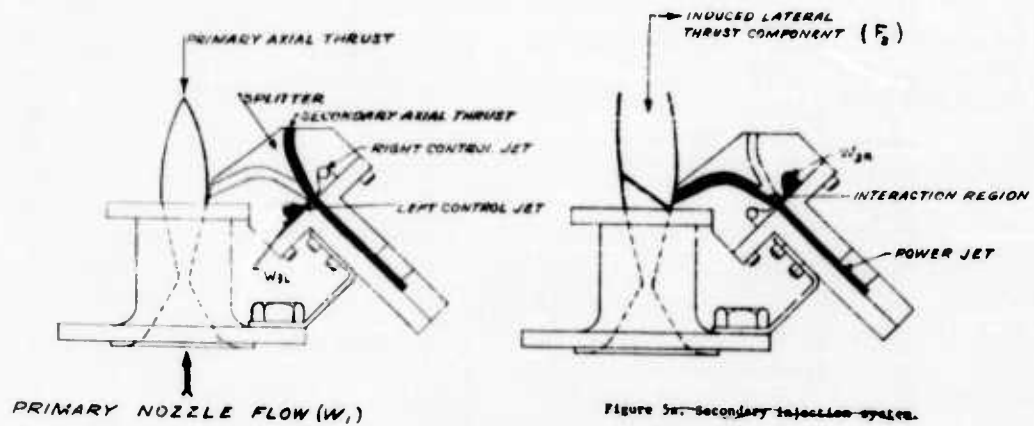
Figure 5a. Secondary injection system.
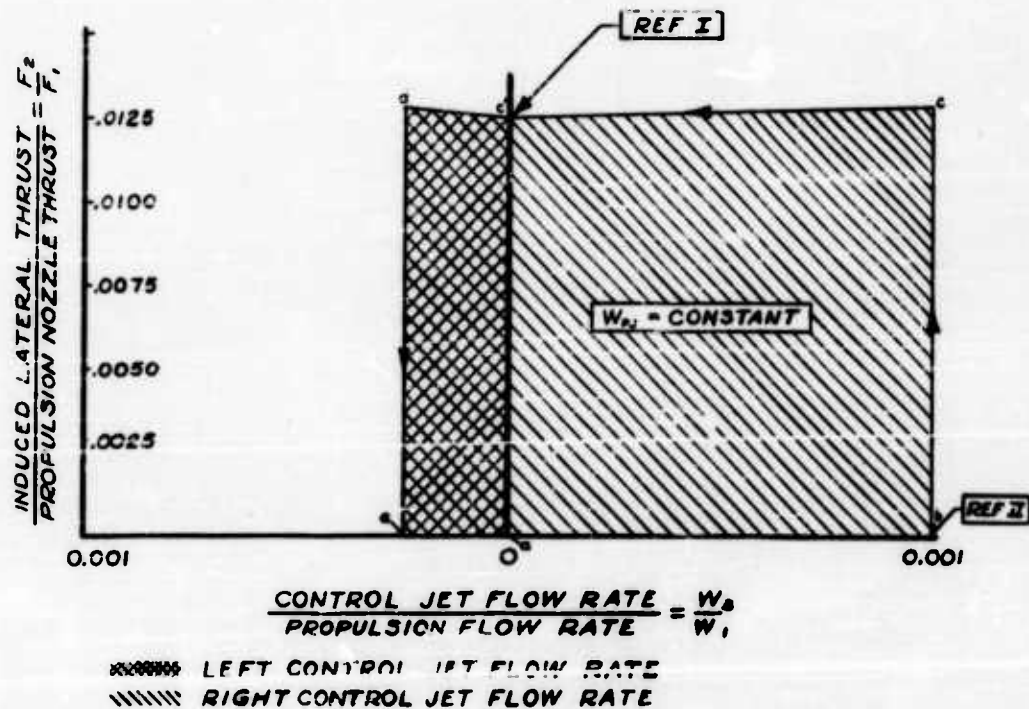
Figure 5b. Typical fluid amplifier switching characteristics model 1-A.

Figure 6.   Shadowgraph of deflected exhaust.

Figure 7.   Shadowgraphs of undeflected exhaust.

80

A FLUID-AMPLIFIER ARTIFICIAL HEART PUMP

by

Kenneth E. Woodward (1)
Lt Colonel Timothy G. Barila (M.C.) (2)
Captain Daniel E. Nunn (M.C.) (2)
George Mon (1)
Henrik H. Straub (1)

ABSTRACT

Fluid amplification, a recent Army invention concerned with the control of flowing fluids without moving parts, has been applied to the powering and control of an extracorporeal heart pump. Except for an artificial ventricle, two artificial heart valves and a flapper to control suction, the fluid amplifier pump has neither moving control parts nor electronics. The output is pulsatile, and its average rate of flow varies directly with filling pressure and inversely with vascular and other resistances, to achieve flow regulation. High reliability, long life and low cost are achieved. Early evaluation tests suggest its performance capabilities and hemolytic characteristics are at least equal to those of the better available heart pumps.

The Problem

The advent of open heart surgery has presented to the medical profession the opportunity of repairing damaged or diseased hearts that otherwise might soon fail completely. Many devices are involved in this type of surgery. One important apparatus is a pump that can assume the heart's role while the heart is being repaired. Existing pumps are fairly complicated both in design and in the methods of control.

Fluid amplification offers the possibility of design and control simplification for pulsatile types of extracorporeal heart pumps and a

---

(1) Diamond Ordnance Fuze Laboratories, Washington 25, D. C.

(2) Walter Reed Army Institute of Research, Washington 25, D. C.

more accurate duplication of the heart's physiological pumping functions. Because electronics can be eliminated and moving parts minimized, reliability can be measurably improved and production costs can be significantly reduced. These unusual qualifications recommended such a pump to the Army Medical Corps for field use.

Application of the pump might be expanded to include regional perfusion and the support of damaged or diseased hearts which if supported could recover.

Consequently the problem was to design an extracorporeal heart pump powered and controlled by fluid amplification principles. This paper describes the development effort to date. The pump, called the Army Artificial Heart Pump, is being jointly developed by the Walter Reed Army Institute of Research and the Diamond Ordnance Fuze Laboratories.

Design Requirements

The requirements for any extracorporeal heart pump may be broken down into three major categories. The pump must:

        a.   Duplicate the heart's essential pumping functions;
        b.   Possess adequate reliability and life;
        c.   Be appropriately packaged.

Each of these will be considered in detail.

        a.   Physiological Requirements

The pump must obviously possess enough of the essential functional pumping characteristics of the human heart to sustain life. Furthermore, irreversible blood damage can not be tolerated either during or after the pumping run. From an examination of the literature and existing pump designs, it appears that a single set of functional requirements for extracorporeal pumps in general has not been established. The authors in developing the fluid amplifier pump considered the following heart functions important:

        (1) Output Pressures and Flows

The pump must be capable of adequate perfusion of the subject. Moreover it seems desirable to have a single pump satisfy the needs of a relatively large range of subjects regardless of age or size. The pertinent cardiovascular pump parameters (pressures, flows, age, size, pulse and activity level) for the human male from age 1 through 80 are summarized in Figure 1. The ordinate is a cardiac flow index relating mean blood flow rate to total body surface area. Since the parameters of Figure 1 are collated from several medical texts, the information lacks a high degree of statistical significance. However,
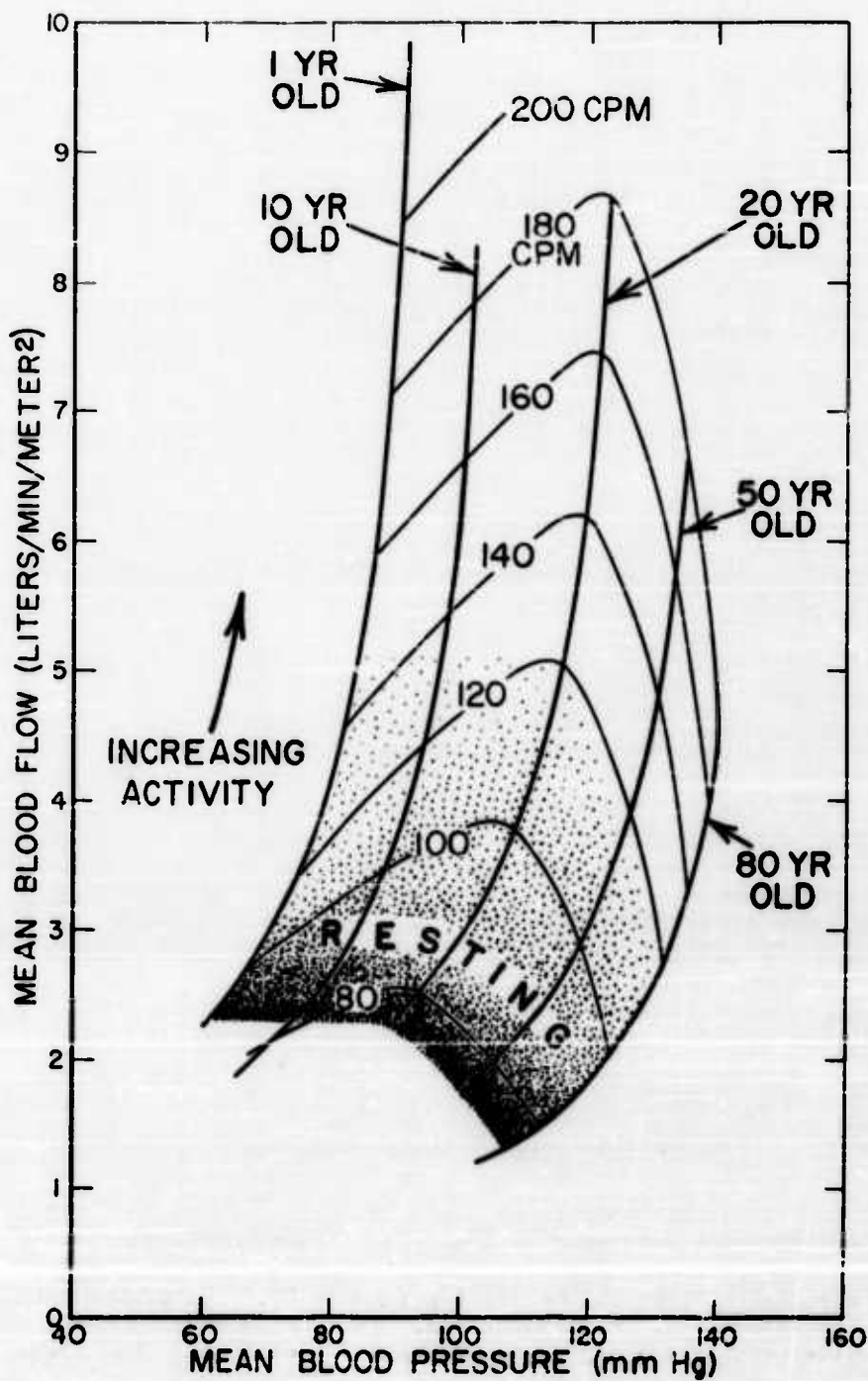
Figure 1. Cardiovascular characteristics (the human male).

it does establish the general output requirements for the pump. For operating room application, only basal or resting conditions are of concern.

(2) Load-Matching Capabilities

Reference 1 suggests that the human heart exerts just enough myocardial (muscle) force per stroke to achieve the necessary blood flows. Excess force causes excessive blood damage. An index of such trauma is the increase in red cell destruction. This index is called hemolysis. To control hemolysis and other blood damage the pump should be designed to propel blood with minimal force application.

(3) Pulsatile Blood Flows

Disagreement exists among cardiovascular experts relative to the need for pulsatile blood flows for extracorporeal pumps. The technically more easily constructed nonpulsatile pumps are currently most popular but both pulsing and steady-flow pumps presently function successfully for short periods - one to two hours only. It may be, however, that long-term perfusion requires pulsed flows. Reference 1 suggests that resonant principles may operate in the cardiovascular system. If so, the pumping system (including the catheter) must then be capable of duplicating the subject's normal pulse to exploit the elastic responses of the circulatory systems.

(4) Vasomotor Considerations

The heart is a relatively constant myocardial force pump because of vessel distensibility and the vasomotor characteristics of the cardiovascular system. Flow resistances are made to vary autonomously by the nervous and endocrine systems to suit the physical and emotional needs of the individual. To minimize the pump forces propelling the blood and to allow the pump to regulate its output in response to vasomotor changes in flow resistance, output flows must decrease with increased flow resistance and vice versa. To preclude packing or depletion of the two circulation systems, the output flow must also be made to increase with increased filling pressures, as in the case of the human heart.

(5) Other Functional Requirements

Filling of the human heart ventricle is achieved mainly by the difference between atrial and ventricular pressures during the period the difference is maximal. However, atrial contraction plays a small but significant part in the filling process (Ref. 2, p. 244) and serves to increase the flow rate of the heart by both increasing ventricular distention and compensating for valve resistance. For these

84

reasons and if cannulae* resistances are significant, it might be desirable to cause the pump to suck slightly in diastole. Additionally if the pump is to be used as an augmentation device for failing heart patients, the pump should be capable of synchronizing its pulses with that of the diastolic phase of the heart. By pumping blood during diastole, both peak myocardial forces and the work of the heart are diminished.

The pump should also cause as little blood damage as that caused by presently available commercial pumps. Blood damage arises not only from the use of unnecessarily large pump pressures, referred to above, but also from a variety of other phenomena, such as turbulence and shear, that are influenced by the mechanical design of the pump.

b. Reliability and Life Considerations

High reliability is an obvious necessity. It should be measurable and predictable and as independent as possible of operating conditions, the type of personnel responsible for the pump, and the kind of power source used. In the event of power failure, the pump should be designed to operate on stored energy. The pump should require minimum maintenance.

c. Packaging

The following design attributes would be generally desirable for the pump. It should be:

(1) Simple to operate and maintain
(2) Controllable with respect to pulse shape and rate
(3) Fabricated out of transparent materials to allow visual observation of performance. (impending ventricle failures can be observed.)
(4) Sterilizable preferably by autoclave methods
(5) Functional with negligible heat liberation
(6) Fabricated out of materials compatible with the blood
(7) Easily transportable
(8) Sealable to preclude blood contamination and air embolism
(9) Inexpensive to manufacture
(10) Operable with low audible noise levels

---

*Cannulae are small tubes inserted into the body cavity through which blood passes from and to the pump.

Existing Designs

Existing pumps and their performance capabilities offer to the designer a valuable source of experience and knowledge. Their advantages and disadvantages are considered in this section.

Present extracorporeal pumps may be classified with respect to the type of flows they produce, i.e., pulsatile or essentially nonpulsatile. Nonpulsatile pumps are the more uniform in design. They usually consist of a plastic or rubber tube or sleeve wrapped around or within a non-flexing cylinder. A roller driven by an electric motor squeezes the tube as it rolls around the cylinder. Blood is forced ahead of the roller. This type of pump has the following advantages:

1. Valves are eliminated
2. Minimal propelling pressures exist
3. Control mechanisms are relatively simple

Disadvantages may be:

1. A relatively short ventricle life
2. A lack of compactness

Pulsatile pumps are less uniform in design. They usually consist of a plastic or rubber ventricle squeezed by electric motors, pistons, electromagnets or pressurized fluids. Valves are required to control the blood flows. Such pumps have the following advantages:

1. Compactness
2. Long ventricle life
3. Pulse duplication potentialities

Disadvantages may be:

1. Excess propelling pressures
2. Valves which are both hemolytic and short lived
3. Relatively complicated control mechanisms

Exceptions certainly exist for both classes of pumps. Consideration of existing designs was found valuable in the development of the fluid amplifier pump particularly with respect to factors affecting hemolysis and ventricle life.

The Army Artificial Heart Pump

Figure 2 shows a recent Army Artificial Heart Pump design. It consists of a fluid amplifier attached to a housing containing a plastic ventricle and two plastic tricuspid semilunar valves. Two gages attached to the housing measure the amplifier and power supply pressures. Control
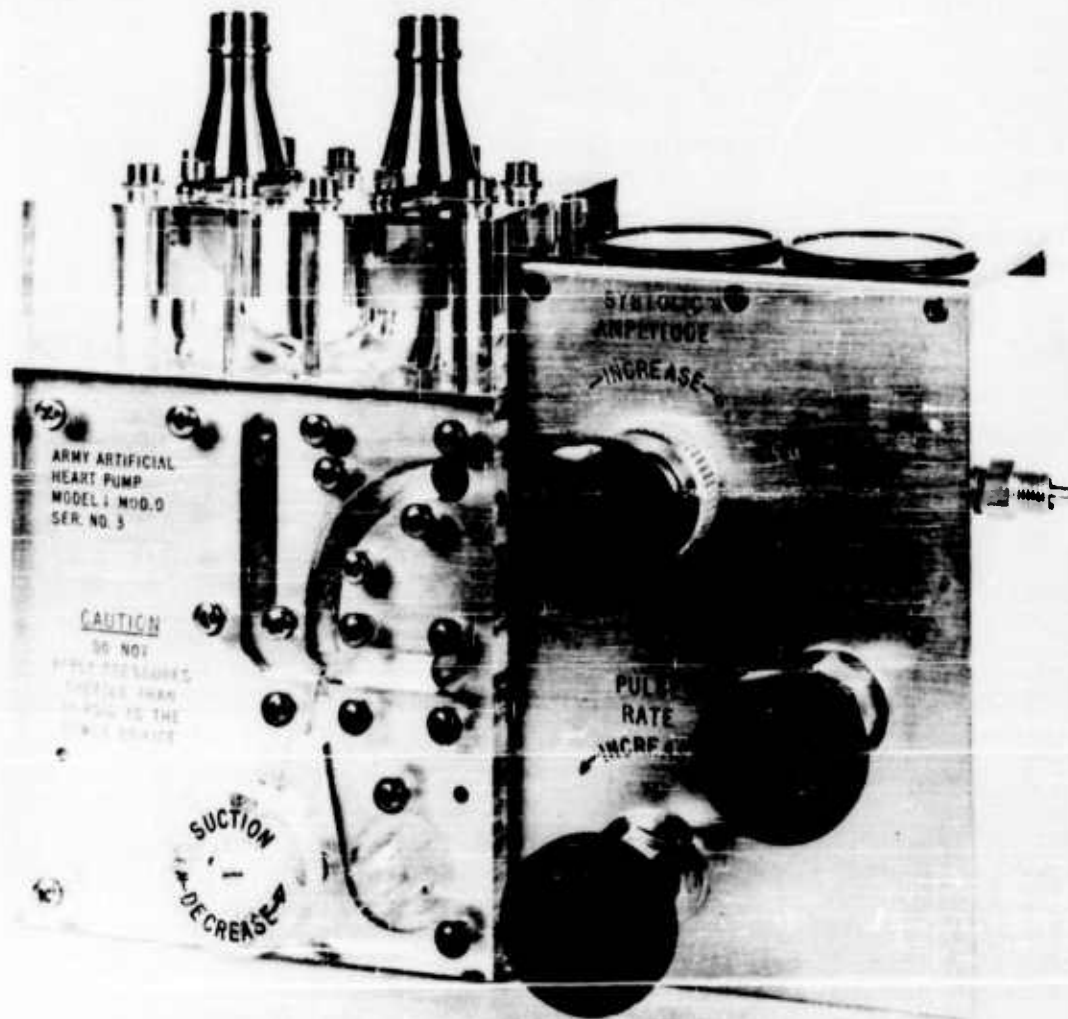
Figure 2. The Army artificial heart pump.

87

valves to regulate systolic pressures and pulse rate have also been introduced as well as a control to adjust the duration of the systolic pulse. These permit adjustment of the pump's output to the individual needs of the subject prior to or at the beginning of the pump run. (If the pump was intended to perfuse only a single subject with known peripheral resistances, the essential elements for satisfactory operation would be those shown in Figure 3. In this case the amplifier would be designed to accommodate the needs of the subject and the power supply without regulating valves.)

a. Operational Description

With the aid of the pump schematic shown in Figure 4, operation may be described as follows:

A fluid (air) enters the fluid amplifier after passing through a valve (the systolic amplitude control-A) which regulates the amount of air flowing. Upon leaving the power nozzle as a high velocity stream, the flowing air begins to entrain additional air. Because entrainment on either side of the stream does not occur at equal rates due either to unequal spacing of boundary walls or perturbations of the stream itself, the stream is forced to deflect toward the side of least entrainment by virtue of unbalanced pressures. Replenishment of air on the side now closer to a boundary wall is further impeded by this initial deflection of the power stream creating still lower ambient pressures in this region and greater stream deflections. Eventually the power stream is caused to "lock on" to the closer wall. The pump will start to pulse regardless of the wall chosen by the stream to lock on initially.

If the power stream locked on to the left wall upon admission to the interaction region, it would subsequently flow through the left receiver into the housing where the increase in air pressure squeezes the ventricle, as shown in the side view in Figure 4, until the upper port is uncovered. Air then flows through the deflection control line and by virtue of an exchange of momentum between it and the power stream, the power stream is deflected to the right receiver. In this process of squeezing the ventricle by air pressure, a cardiac systole has been duplicated.

After power stream switching has occurred, blood, forced by gravity, begins to fill the ventricle and in so doing closes the deflection port. The entrainment process begins with air being drawn both from the now closed deflection control line and through the left receiver from around the ventricle. As long as the ventricle is expanding, air is supplied in sufficient quantities to satisfy entrainment, and the power stream remains locked to the right wall. When the ventricle has been completely filled, air replenishment is impeded on the left side of the power stream. In the opposite control jet the pulse duration control (B) permits a metered amount of air to enter to prevent entrainment from dropping the pressure below a predetermined level. A pressure

88
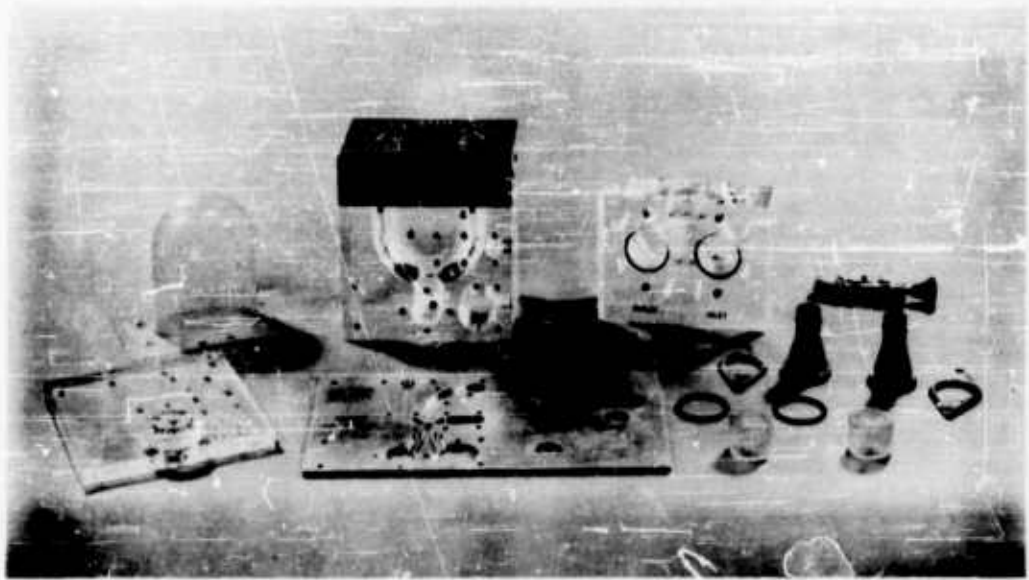
Figure 3. The disassembled pump.
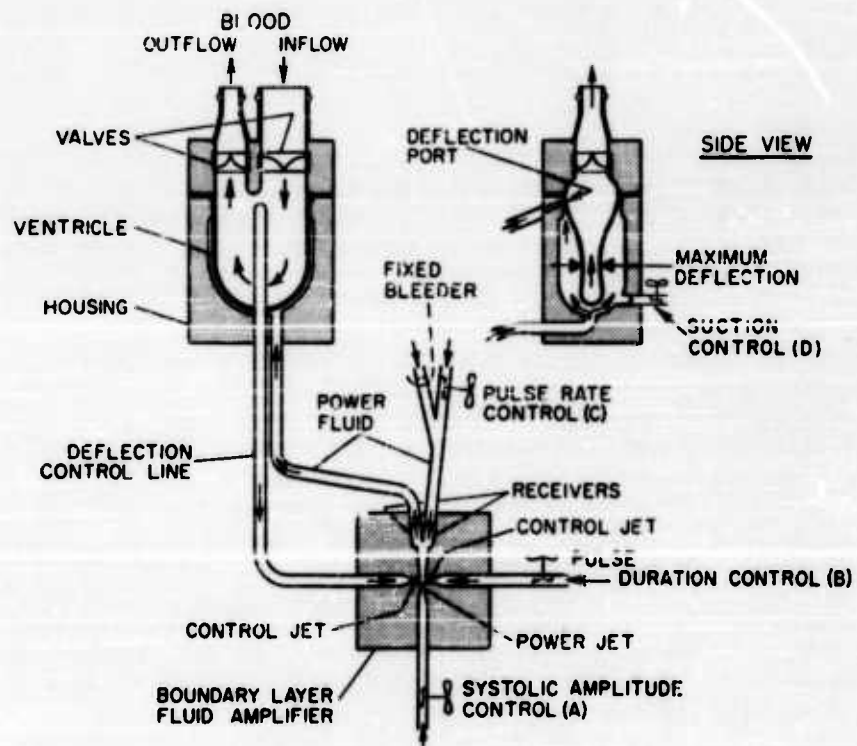
Figure 4. Heart pump schematic.

difference builds up between the control nozzles. When it becomes sufficiently great, a flow occurs in the right control nozzle great enough to deflect the power stream back to the left receiver. The cycle is now complete.

The pulse rate control (C) in the right receiver serves to create an adjustable load for the amplifier, and, as a consequence, pulse rate can be controlled. The fixed bleeder bypassing the pulse rate control precludes back pressures from building up great enough to switch the power stream. Control is achieved over the pump's systolic pressures by metering the amount of air entering the ventricle chamber. The pulse duration control, by regulating entrainment in the right control jet, allows the power stream to remain locked in the right receiver for adjustable periods of time thereby allowing the duration of the systole to be varied. The pulse duration control, the fixed bleeder, and the pulse rate control are open to atmospheric pressure. Adjustment of any individual control affects the functions of the others to some degree.

Output blood flows are made to vary directly with filling pressures by causing corresponding changes in the filled volume of the ventricle. By limiting the residual volume of the ventricle in systole, the desired effect is produced. This characteristic provides a regulation of filling pressures without electronic or other level sensing devices. Because of energy conservation, the output flows vary inversely with the flow resistances presented to the pump.

Minimal propelling pressures are realized by having the power stream produce flows which vary directly with the loads presented to the pump. The fact that stroke volume and pulse rate are controlled by the power stream offers the possibility of exploiting with a fair degree of precision the elastic responses of the vascular system by duplicating the appropriate stroke volume and pulse rate for any particular load and flow rate. The present pump can be made to approximate this for a variety of human situations by changes in ventricle stiffness.

Atrial contraction during diastole can be approximated by having the power stream entrain air through the left receiver from around the ventricle to produce slightly negative pressures. By allowing the power stream to suck air both from around the ventricle and from the atmosphere through the suction control, ventricular sucking can be regulated from near 0 mm Hg to much greater values.

An unusual characteristic of the pump is that a pumping mode similar to ventricular fibrillation can be produced. For power stream flows above certain energy levels (these levels can be varied), the power stream switches from receiver to receiver rapidly at about fibrillation frequencies because of insufficient ventricular filling time. Blood flows fall to zero.

90

b. Reliability and Life Characteristics

The fluid amplifier pump design should result in improved reliability and longer life for the following reasons:

(1) Only four moving parts are involved. There are no electronic components to fail. The passageways in the fluid amplifier are too large to clog easily.

(2) The basic fluid amplifier components can be reproduced with consistent accuracy.

(3) Maintenance is minimal. Lubrication is unnecessary.

c. Packaging

The packaging aspects of the pump are excellent. It consists of a minimal number of basic parts exclusive of assembly screws, pressure gages and valves. Apart from the fluid amplifier, dimensional tolerances are large. Both the housing and amplifier can be fabricated out of clear sterilizable plastics. Molding techniques can be used in the production of all pump elements. If required, the ventricle and valves can be thrown away after each use because of their low cost.

The present pump weighs 10-1/4 pounds and has a volume of (about) 150 cubic inches. These can be reduced considerably. It produces a muffled audible pulsing noise when operating. Quantity production costs for the complete pretested pump in its final design should be quite low when compared with the costs of available pumps.

Performance Results

Neither the engineering nor medical evaluation tests of the pump's capabilities have been completed. The pump appears to have the following performance characteristics:

1. It can produce blood pressures from near 0 to about 500 mm Hg.

2. Blood flows of about 1/2 liter/minute to nine or ten liters/minute are possible depending on circuit flow resistances and the ventricle design used.

3. Pulse rate can be varied from about 30 cpm to 180 cpm. The upper limit depends on flow resistance and the ventricle design.

The hemolysis rate appears to be less than that caused by two commercial pumps employed in comparison tests. The promising features

91

of design discussed above have proved functional and adequate during both partial and total heart bypass proof test experiments with animals.

It has been observed that autonomous changes in the peripheral resistance of the animal cause the output of the pump to change accordingly without adjustment of controls. Increases in peripheral resistance cause decreases in the pump's pulsing frequency and vice versa. Occluded veinous lines cause the pump to stop pulsing.

Decreases in filling pressure cause the pump to slow its pulse rate with a corresponding reduction in flow rate.

Through adjustment of propelling pressures and right control entrainment (the pulse duration control), both the duration and amplitude of the pump's systole can be varied. These changes have been observed in the arterial system of an animal.

Problem Areas

Apart from design improvements intended for future production models, three design problems need better solution in the R&D prototype described herein. One problem concerns valves. The life of the tricuspid semilunar types produced for the pump is relatively short, although their hemolytic characteristics are good. Other valve designs are being considered. The second problem involves the stability of the material used in the ventricles. Apparently the leaching of plasticizer from the material used causes the pulsing character of the pump to change. Thirdly a series of ventricles need to be designed to accommodate a range of subjects. Unfortunately a single ventricle design can not satisfy the range of needs between small animals and large humans.

Conclusion

A heart pump using fluid amplification principles has been designed that can approximate many of the human heart's pumping functions. It operates with few moving parts and no electronics. Reliability and life are consequently increased and production costs significantly decreased. Pumping and hemolytic characteristics are at least equal to those of available blood pumps.

Of particular importance to the Army in the field are the facts that the pump can be transported by hand, it can be completely disassembled and reassembled in minutes, and except for ventricles and heart valves all parts can be autoclaved. Its rugged construction permits toleration of rough handling. Power can be provided by tanks of compressed gas or eventually perhaps even by exhaust gases from internal combustion engines.

REFERENCES

1. Woodward, K. E., Barila, T. G., and Nunn, D. E., "Some Engineering
    Considerations of the Human Cardiovascular System",
    DOFL TM-62-5, 7 Feb 1962.

2. Best, H.C. and Taylor, N. B., "The Physiological Basis of Medical
    Practice", The Williams and Wilkins Company, Baltimore, Md,
    1961.

SURVEY ON COANDA FLOW[*]

by

Paul K. Chang

of

Aerophysics Co.
The Catholic University of America

SUMMARY

A survey of 31 available references of analyses and experiments was made on Coanda flow which clings to a curved or deflected surface and increases mass rate of flow. This survey may be useful to better understand the mechanics of this type of flow and for its practical use of fluid amplification.

- - - - - - -

Henri Coanda, a Rumanian engineer, conducted an experiment of jet flow using the following sketched device equipped with a curved surface in the form of an ogive cap.
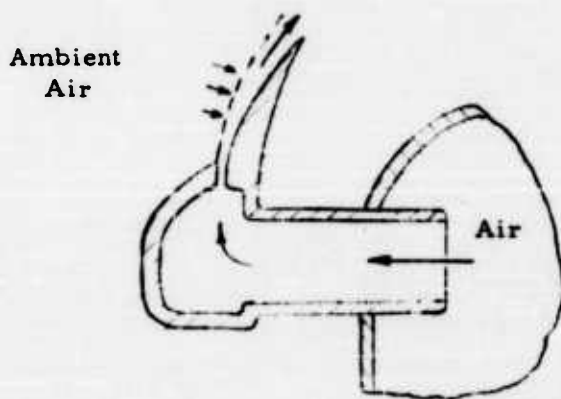
Ambient
Air

Air

Fig. 1. Coanda Nozzle

Air flowing through a channel was led to a slot and then to the upper curved surface. Coanda observed the following phenomena: (Reference 1)

The air jet is deflected toward the wall surface and jet flow clings to the cap. The ambient air over the ogive cap is depressed and is entrained to the jet fluid. If the curved surface is deflected further at a proper length to a new direction, the same phenomenon occurs again, although less strongly. Hence, by repeating the same deflection process it is possible to deflect the jet-flow direction to a large angle and to increase the mass rate of flow considerably.

Coanda invented useful gadgets exploiting these flow characteristics but did not elaborate to investigate scientifically.

The jet fluid flowing out from the narrow slot has a small thickness layer of fluid. Due to the limited thickness of the fluid layer the centrifugal force plays a role by pressing the jet flow toward the wall as the fluid accelerates along the curved surface reducing pressure. At the same time due to the viscosity of the fluid the ambient air is entrained to the jet. Downstream due to jet flow dissipation the jet flow deflects less strongly.

The jet flow issuing from a nozzle can be deflected and its mass rate of flow will be increased also by placing a single deflector or multiple deflector of straight plates joined at one end to the nozzle exit. In this case, jet flows over an inclined straight wall and remains attached up to a point of detachment where jet flow leaves the surface. This detachment point is located where the local surface pressure approaches the ambient pressure. These facts were observed by Von Glahn (Reference 2, 3) who investigated them scientifically. At the upstream of the detachment point, the surface pressure is lower than the ambient pressure, thus flow attaches upstream of the detachment point but downstream of the detachment point flow detaches from the surface because of higher pressure than that of ambient air. When the jet flow turns a sharp curve at the leading edge of a deflected plate, the velocity of fluid increases and consequently pressure decreases causing a suction effect. Therefore due to this suction, the surrounding air is rushed to the jet and because of viscosity entrainment occurs. But pressure rises reaching the ambient air pressure at a certain distance from the leading edge and pressure increases further as the fluid approaches the trailing edge. (Reference 2)

The above-mentioned phenomena may be called Coanda effect. Hence, the "Coanda flow" can be defined as a jet flow which clings to a curved or deflected surface and increases the mass rate of flow along the flow path. A nozzle, where Coanda effect is applied to gain the large mass rate of flow is called a "Coanda nozzle."

The entrainment of ambient air to the jet or absorption of external fluid to the jet is similar to the effect on aerodynamic sink. (Reference 4). Hence, the phenomenon of Coanda flow is that of an essentially wall jet involving sink effect. If Coanda flow is well understood and applied for practical use, a significant contribution to the development of fluid amplication can be made because wall jet is widely used for this purpose.

A survey of up-to-date available and pertinent references on Coanda flow and related subjects is briefly made here.

In order to compute performance of Coanda nozzle thrust of jet flow must be known. Since thrust is connected with dissipation of jet flow the following information may be useful.

On turbulent dissipation of jet flow, Caille (Reference 5) found that when a jet flows over the curved wall then, because of intensified secondary flow mixing, the dissipation rate was increased several times.

On turbulent jet flow through a nozzle Sigalla (Reference 6) observed that jet core begins to dissipate at a distance of about eight to ten times the test nozzle height downstream from the nozzle. Because of this dissipation the performance may be well defined based upon undeflected jet flow at or immediately near the exit nozzle.

By defining the performance of the Coanda nozzle as a ratio of lift to undeflected thrust, F_L, or as the ratio of axial undeflected thrust, F_z, and expressing it in the following simple equations, a good agreement among the experimenta and theoretical values was obtained as shown in Fig. 2.

The equations of the performance are,

$$F_L = \sin \theta$$

$$\text{and } F_z = 1 - \sin \theta \cdot \tan \theta$$

[1]   (Reference 2)

where θ is the angle of the deflected plate.

These equations are derived from the momentum equation of jet flow under the following assumptions: (Reference 7)

The whole primary jet expands to ambient pressure before intercepting the plate, which is two-dimensional, and only the surface affecting the flow. Counteracting moment as well as ejector secondary flows are negligible.
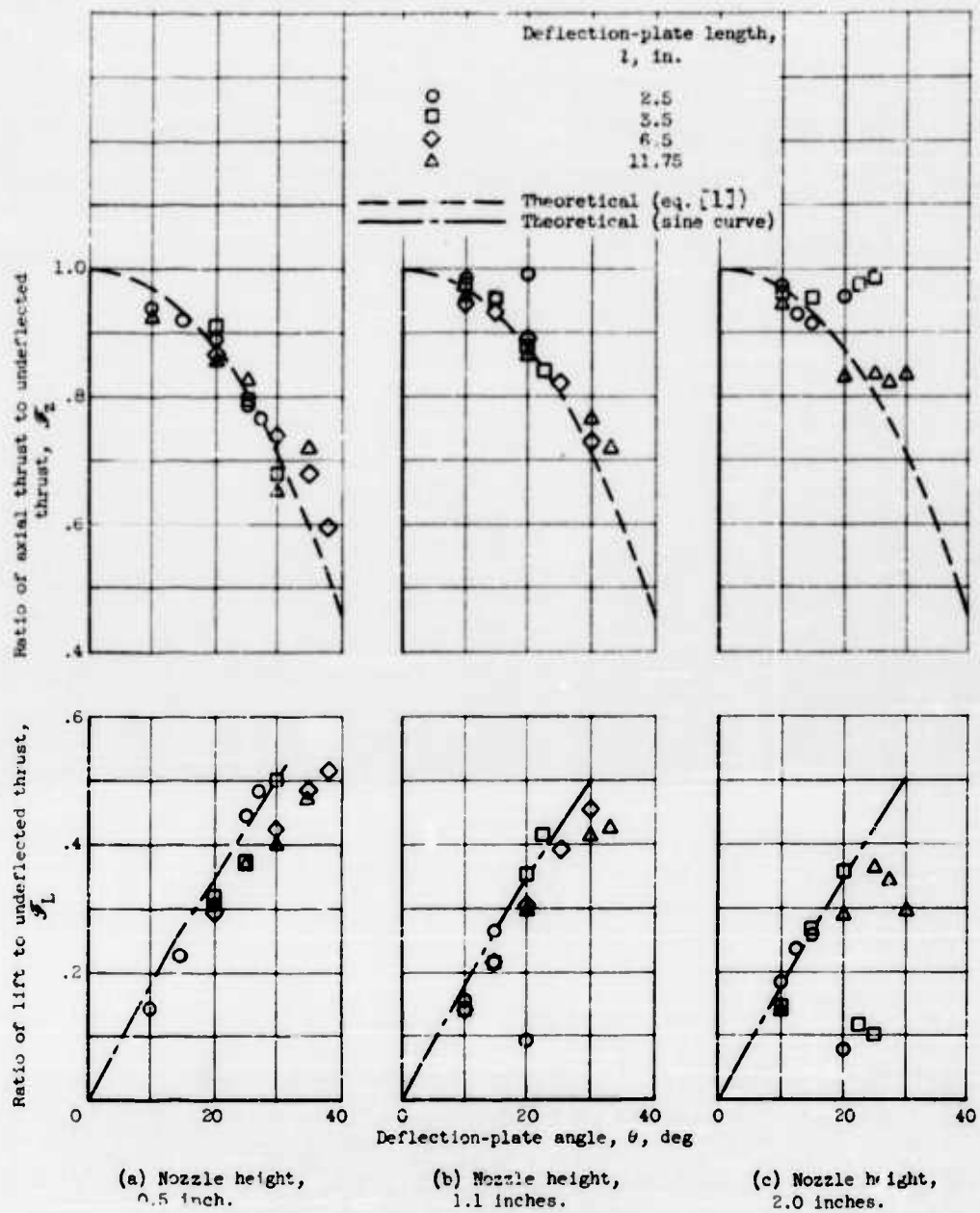
Figure 2   Typical performance of Coanda nozzles as function of deflection-plate angle.
Nominal pressure ratio, 2.1.

(Ref. 2)

98

I. Analysis of Incompressible Coanda Flow

The analyses comprises inviscid and viscous flow solutions.

a. Inviscid flow solution

Coanda flow was first analyzed by Metral (Reference 8). By using a technique of conformal mapping, Metral was successful in showing that the air jet flow along a single sharp-edged bend increases the mass flow rate. This result was verified by an experiment on automobile and motorcycle engines equipped with Coanda nozzles.

Voedisch's analysis (Reference 9) verified Coanda's findings -- the increased mass rate of flow issued from a nozzle and flowed along an inclined wall. Furthermore, Voedisch showed that the stationary ambient air is entrained along the primary jet.

Stratford (Reference 4), by analyzing the jet flap, found that direction of ambient air velocity is perpendicular to the jet boundary.

Lighthill (Reference 10) studied the clinging characteristics of an incompressible flow on a smoothly curved surface and applied his theory to the bends of a wind tunnel. Yen (Reference 11) applied the concept of free streamline and the Schwarz-Christoffel technique to the Coanda flow and extended Metral's work. Yen found that his analysis led to Metral's formulation when the smooth curve is reduced to a sharp corner and the Coanda effect is increased if the sharpness of the corner is increased.

These results of analyses with ideal fluid are not exact, and often are of little practical use, since the real flow differs from the ideal flow because of the viscosity of a fluid. Based upon the nonviscous flow solution, the viscous phenomenon such as jet flow detachment from the surface or reattachment to the surface can not be predicted.

b. Viscous Coanda flow

One of the essential features of Coanda flow is the ability of a narrow jet to attach to the surface, therefore the length of attachment or location of inception of detachment is an important problem to be investigated. The similar phenomenon to this is separation of flow with thick fluid layer. This problem has been studied much more extensively compared to the detachment of jet flow. Hence, a comparative study of these two phenomena, detachment and separation, may serve in the investigation of Coanda flow. In the following pages some of the differences of these flows are shown and in order to distinguish them, the terminology "detachment" is referred to as a narrow jet flow leaving the surface and "separation" to ordinary wide layer flow departing from the wall. Since separation is characterized by its velocity profile, the velocity distribution of

jet flow is studied first. The two-dimensional jet velocity distributions have been solved by Glauert (Reference 12) and Görtler (Reference 13).

Half Jet

Boundary Layer
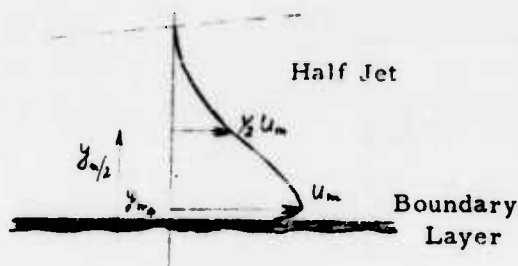
(Reference 19)
Fig. 3. Two-dimensional Turbulent Wall Jet

Glauert was successful in obtaining solution for laminar and turbulent radial and plane wall jets.

As shown in Fig. 3, the mean velocity profile of turbulent wall jet consists of an inner boundary layer ($y < y_m$) and outer half jet.

The approximate solution is given by a matching procedure of boundary layer flow for which the eddy viscosity varies with y to the outer flow for which eddy viscosity is assumed to be constant.

The inner profile given numerically by Görtler (Reference 13) is shown in Fig. 4.
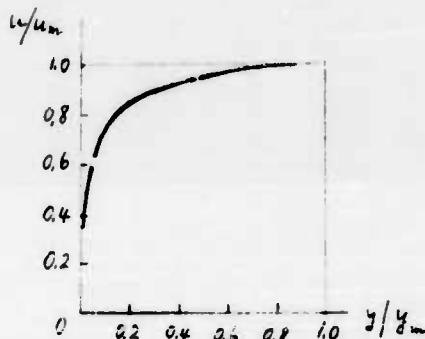
Fig. 4. Boundary Layer Mean Velocity Profile of Turbulent Wall Jet (Reference 19)

The outer profile which is similar to the free jet is given by

$$\frac{u}{u_m} = \text{sech}^2 \left\{ 0.88 \left(\frac{y - y_m}{y_{m/2} - y_m} \right) \right\}$$ [2]

This velocity profile of wall jet is different from the ordinary wide layer flow with its boundary layer velocity profile approximated by $u/u_e = (y/\delta)^{\frac{1}{7}}$ on the body surface submerged fully in the fluid. Thus, it can be seen that characteristics of separation and detachment would be different. For example, the position of turbulent flow separation on a sphere is at 110 degrees measured from the stagnation point but the turbulent jet detaches further downstream at 135 degrees (Reference 14). The flow behaviors downstream of separation or detachment are different too. Using a paper flag attached to the surface in the region of the separation bubble, Bourque (Reference 15) observed that reverse

100

flow occurred in the separation bubble since, because of reverse flow, the paper flag turned from the original position to an opposite direction. On the other hand Gates (Reference 16) observed that there is no reverse flow in the detachment region of Coanda flow.

For jet flow it is known that the detachment point of jet flow is located at a position farther downstream as the deflection increases. This characteristic is shown by experiments of Von Glahn and at the Catholic University of America (Reference 17).

Von Glahn found further that the jet detachment point is not affected by the downstream conditions and is dependent only upon the upstream condition. However, the point of jet detachment of the Coanda flow is independent of nozzle height parameter if $(p - p_0)/P_j$ is plotted verus l'/h^n, where p is the local surface pressure, p_0 is the atmospheric pressure, P_j the total jet pressure (gage), l' is the surface distance measured from the nozzle exit to a point on the deflection plate, h is the nozzle height, and $n = -a\theta + b$ (a and b are coefficients determined for each normal pressure ratio p_n/p_0, where p_n is the total jet pressure (abs) and θ is the plate deflection angle) (Reference 3). For flow separation, it is known that the point of laminar separation is a geometrically fixed position and is independent of Reynolds numbers in the region of laminar flow (Reference 18). But a test for a jet flowing around a small b/a, (b is width of the slot and a is radius of circular cylinder), 6 in. diameter cylinder shows that the detachment angle measured from the jet exit is linearly dependent to Reynolds number defined by $Re_{cyl} = \left[(P - p)\, b\, a/\rho\, \nu^2\right]^{1/2}$, up to 4×10^4, but in regions of the Reynolds numbers larger than 4×10^4; the detachment angle remains independent of Re_{cyl}. $P - p$ is the supply pressure relative to that of the surroundings, ρ is the density of the fluid and ν is the kinematic viscosity of the fluid. The parameter b/a is relatively unimportant because the experiment shows that with three different values of b/a, equal to 0.0067, 0.020 and 0.040, the scatters among the measured values of the detachment angles with respect to Reynolds numbers are small (Reference 19).

If discrepancies between the viscous phenomena of narrow thickness jet flow and thick layer non jet flow are clarified then knowleage gained from boundary layer theories and experiments on non jet flow may be used for Coanda flow and a faster development of Coanda flow theory could be obtained.

ii. Analysis of Viscous Incompressible Coanda Flow

Now on the analysis concerning viscous Coanda flow several references are cited.

Yen (Reference 11) pointed out the analysis of viscous Coanda flow is too

difficult to be solved. However, for two particular cases: Jet flow around a cylinder and two dimensional jet to an inclined flat plate, simple analysis including viscous effects as well as experimental measurements were made. (Reference 19). In jet flow around a cylinder, in the region of $Re_{cyl} > 4 \times 10^4$, Newman (Reference 19) used the following assumptions for his simple analysis.

1. The effect of skin friction on the jet momentum is small and negligible.
2. The radical velocity is very small compared to the circumferential velocity (boundary-layer approximation).
3. The velocity profiles u/u_m against $y/y_m/2$ are the same for all angles θ measured from the exist slot of the jet, where u is circumferential velocity, u_m is maximum value of u at a given station, y is distance measured perpendicular from the wall and $y_m/2$ is larger value of y for which $u = 1/2 \, u_m$. Thus velocity profile may be replaced by a uniform velocity profile of the same mass flow and the same momentum.

Newman (Reference 19) then computed surface pressure and the static pressure across the flow at $\theta = 90^o$.

The comparison of analytical results with experimental data shows that although the theory correctly predicts an adverse pressure gradient at the surface, the measured pressure is about 30 per cent low and the calculated pressure is too small near the surface but it becomes too large further out at $\theta = 90^o$.

In a two-dimensional incompressible jet flow to an inclined flat plate, Bourque (Reference 15 and 20) has developed several theories by using the principle of momentum and making allowance for the velocity distribution in the jet and its rate of spread. His theory is one of the simplest and gives the best results for values of free jet parameter S at angle $\times$, between the inclined plate and the axis of the slot, larger than 20°. For the analysis Bourque used a flow model of the reattaching jet on the flat plate and made the following assumptions to obtain the solutions:

1. The jet entrains fluid from the separation bubble in the same way as a fully developed free turbulent jet
2. The pressure within the bubble is constant and the center line of the jet is a circular arc.
3. Entrainment within the bubble ceases and the flow divides where the extended center line of the jet meets the surface of the plate.
4. The force parallel to the plate due to the skin friction of the forward and backward flow is negligible compared with the jet momentum.
5. The jet momentum is the same as that for a free jet discharging to atmosphere.

The variation of pressure within the separation bubble, the position of re-attachment, and the variation of mass flow from the slot with α, all at high Reynolds numbers were measured and computed. The comparisons of analyses and experiments show that the pressures differ by about 30 per cent, at high values of δ, the position of reattachment agrees fairly well, and for $\delta = 30$, and $\alpha > 15^\circ$ agreement on variation of mass flow is good. Bourque's theory presents an improvement of inviscious flow analysis of Metral (Reference 8).

For the future development of viscous Coanda flow analysis the existing work of Murphy (Reference 21) may be useful. Murphy solved laminar two-dimensional boundary layer along a curved surface including curvature effect.

III. Analysis of Compressible Coanda Flow

Metral and Zerner (Reference 22) noticed that a supercritical pressure is caused at the crest of surface, which is a function of a ratio of test nozzle height divided by the design nozzle height and supply pressure, and the supersonic Coanda flow is easily obtained.

As of this date, no direct analytical investigation of compressible Coanda flow has been carried out. However, some related problems are worked out in the past. Yen (Reference 23) studied the two-dimensional mixing problem of laminar flow and induction phenomenon by injecting a high-speed straight jet into a stationary fluid. His study shows that, if an asymptotic expansion and change of independent variables is introduced, two ordinary boundary-layer equations are reduced to a single ordinary differential equation. As a first approximation, Yen indicated that with the present knowledge of turbulent flow this solution of laminar mixing is applicable to a problem of turbulent mixing if the coefficient of viscosity is suitably modified. For turbulent flow eddy kinematic viscosity $\varepsilon = 134.7$ cm^2/sec at jet length $x = 17$ mm with a reference length $L = 1$ mm. This value is 1950 times larger than typical values obtained for the laminar coefficient of kinematic viscosity. This order of magnitude of ratio of turbulent eddy kinematic viscosity to laminar kinematic viscosity is the same for low subsonic as for supersonic flow (Reference 24). Yen (Reference 25) analytically studied two isentropic, two-dimensional, supersonic, parallel flows, consisting of primary flow near the surface and secondary flow above the primary flow. It was found that the Coanda effect could be utilized to improve the flow mixing.

IV. Experiment on Incompressible Coanda Flow

Several experiments on incompressible Coanda flow have been conducted in Europe, the United States, and Canada. In France, Henri Coanda, as previously stated, found and tested the Coanda flow, the results of which are reported in Reference 26. In the United States, the Coanda flow was tested at Purdue University

by Boyer (Reference 27) and Marwood (Reference 28). Their test results verified that two-dimensional Coanda flow clings to the surface. At Correll Aeronautical Laboratory the experiment by Foa and Markstein (Reference 29) on two-dimensional flow over a smoothly curved surface showed that it is possible to obtain thrust augmentation by the Coanda effect. Thrusts were measured normal to the jet, and measurements showed that the thrusts measured in a direction normal to the jet were 1.7 times higher than those thrusts measured in the direction of the nozzle axis with the surface removed. Sproule and Robinson's data (Reference 30) showed that the augmentation ratio (Coanda nozzle thrust/simple nozzle thrust) reached its maximum at 2.7 with an external ejector with a 200-mm throat diameter and with larger throat, augmentation ratio decreased, but the throat diameter less than 65 mm decreases this ratio less than 1.

Gates (Reference 16) tested both the two- and three-dimensional Coanda nozzle, which he calls the external ejector, and obtained the following results:

1. Turning efficiency is high.
2. With two-dimensional Coanda nozzle, ground effect is negligible to vertical lift, but ground effect increases the horizontal thrust by a factor of three.
3. Entrainment of ambient fluid is not vigorous and its direction is normal to the primary jet. This fact confirms Stratford's finding (Reference 4).
4. No static thrust augmentation can be obtained by a Coanda nozzle.
5. Supersonic velocities can be achieved inexpensively as Metral and Zerner noticed.

In the range of his tests Gates did not obtain the thrust augmentation although Foa and Markstein, as well as Sproule and Robinson, measured augmentation in certain flow regimes.

Young and Zonars (Reference 31) tested the Coanda nozzle and Coanda wing and found results similar to Gates' data. Although the Coanda wing reduced the drag, better results could be obtained by boundary-layer control.

Von Glahn (References 2 and 3) investigated two-dimensional Coanda flow with both single and multiple deflection surfaces and also with curved surfaces. In addition to the previously mentioned findings his lift measurements showed that the maximum ratio of lift to the undeflected thrust could reach 0.48 with a single flat plate, but that this ratio increased to 0.88 with many flat segments deflecting the jet flow to 90 degrees. The optimum plate length, which gives the maximum ratio of life to undeflected thrust, was found to be defined as that length whose surface pressure is equal to the ambient pressure at its downstream end. The optimum plate length also gives the maximum deflection angle with no detachment of jet flow from the surface.

V. Practical Application

Coanda claims that Coanda flow devices might be used for thrust augmentation, high lift, low drag wing, VTOL, and STOL.

Usines Chansson, a French motor-car radiator manufacturer, reports a gainful application of the Coanda flow wherein the flow is used to scavenge the exhaust gas in inducing air flow through a radiator and directing the exhaust gas through an annular Coanda nozzle. The flow augmentation, on a four-cylinder Citroen car engine, was about six times, and mass rate of flow was 20:1 with a 150 mm diameter nozzle (Reference 8). Coanda applied the Coanda effect to a rotary pump which was used a vacuum pump or compressor; as a vacuum pump, it was reported that 99.8 per cent vacuum was produced at an efficiency of 98 per cent (Reference 27).

An experiment, in which a Coanda slot was placed at the nose of a cigarette-shaped body which was submerged in water, showed that a reasonable propulsive efficiency was obtained (Reference 30). Metral and Zerner (Reference 22) found that a supercritical pressure can be obtained at the crest surface if a proper ratio of test-nozzle height divided by the design height and supply pressure are selected. Therefore, this phenomenon could be used as an inexpensive source of supersonic flow.

Henri Coanda (Reference 26) investigated both theoretically and experimentally the "Aerodyne" wherein the Coanda effect was applied. The Aerodyne is an ejector in which the primary air is delivered through an annular nozzle around the inlet periphery. The primary jet flow adheres to the curved wall and changes its direction to become axial. Then, a viscous entrainment increases the mass flow to a high degree. The purpose for which this Aerodyne is used is not known.

Nozzle Opening
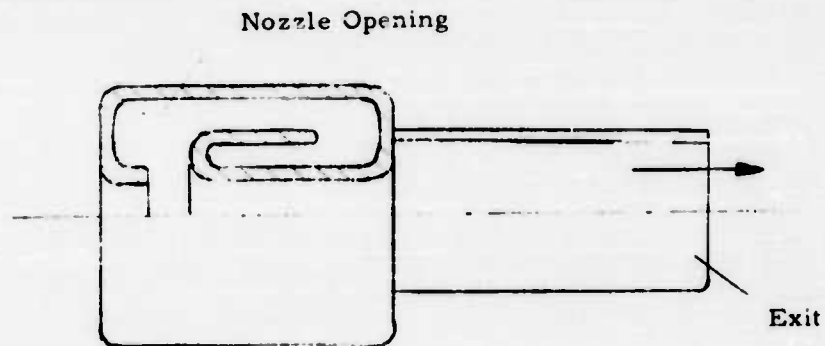
Fig. 5. Aerodyne

VI. Future Development

Coanda flow, as a jet flow clinging to the surface and entraining the ambient air, is a wall jet over a curved or deflected surface, involving a sink effect. Although it is very difficult to analyse the viscous Coanda flow when the distinctions on detailed mechanism of narrow jet and non jet viscous wide layer fluid flow on the curved surface are clarified, then mathematical solutions on viscous Coanda flow may be obtained. The solution of viscous Coanda flow will contribute greatly, accompanied by experience, to further development of mechanics of fluid amplification.

REFERENCES

1. Sferi-Coanda 1, Final Report, Contract No. AF 61(514)1409, ASTIA AD 204073 (1957).

2. Von Glahn, U. H., "Use of the Coanda Effect for Obtaining Jet Deflection and Lift with a Single Flat-Plate Deflection Surface," NACA TN 4272 (1958).

3. Von Glahn, U. H., "Use of the Coanda Effect for Jet Deflection and Vertical Life with Multiple-Flat-Plate and Curved-Plate Deflection Surfaces," NACA TN 4377 (1958).

4. Stratford, B.S., "A Further Discussion on Mixing and the Jet Flap," August 1956 Aeronautical Quarterly, Vol. VII (1956).

5. Sigalla, A., "Experimental Data on Turbulent Wall Jets," Aircraft Engineering (May 1958).

6. Caille, C., "Right Angled Emergency of Air from a Duct," Engineering Digest, August 1955, pp. 42-44 from Sulzer Technical Review, Winterthur, Switzerland, Vol. 38, No. 1 (1956).

7. McArdle, J.G., "Internal Characteristics and Performance of Several Jet Deflectors at Primary-Nozzle Pressure Ratio Up to 3.0," NACA TN 4264 (June 1958).

8. Metral, A.R., "Methods of Increasing Fluid Stream by Diverting it from its Axis of Flow," Coanda Effect (1939). A.M.C., Wright Field, Dayton, Ohio. Translation No. F-TS-823-RE. (1948) ASTIA ATI No. 18833.

9. Voedisch, A., Jr., "Analytical Investigation of Coanda Effect," AMC, Wright Field, Dayton, Ohio. Report No. F-TR-2155-ND (1947) ASTIA ATI No. 9881.

106

10. Lighthill, M. J., "Notes on the Deflection of Jets by Insertion of Curved Surfaces and on the Design of Bends in Wind Tunnels," British A.R.C.R. and M Mo. 2105 (1945).

11. Yen, K.T., "A Theoretical Evaluation of the Coanda Nozzle," Rensselaer Polytechnic Institute, TR AE 5501, Contract No. AF 18(600)-992 (July 1955).

12. Glauert, M.B., "The Wall Jet," Journal of Fluid Mechanics, Vol. 1, 1956, p. 625.

13. Görtler, H., "Berechnung von Aufgaben der freien Turbulenz auf Grund eines neuen Näherungsansatzes," Zeitschrift für angewandte Mathematik und Mechanik, Vol. 22, 1942, p. 244.

14. Eck, B., "Technische Strömungslehre," Second Edition, Springer Verlag, Berlin, p. 193 (1944).

15. Bourque, C., "Deviation d'un jet turbulent incompressible par un volet incline 'Effet Coanda'." Master's Thesis, L'universite Laval (August 1959).

16. Gates, M.F., "Static Lift-Characteristics of Jet Slots - A Clarifying Study of the External Ejector," Advanced Research Division of Hiller Aircraft Corporation, Rept. No. ARD-213 (1958). Final Report Contract No. Nonr-2428(00).

17. Barlow, G.R. and Lettendre, R.P., "Experimental Study of the Separation Point and Separation Bubble," Thesis for Bachelor of Aeronautical Engineering, Catholic University of America, Washington, D.C. (June 1959).

18. Chang, Paul K., "Laminar Separation of Flow Around Symmetrical Struts at Zero Angle of Attack," Journal of the Franklin Institute, Vol. 270, No. 5, November 1960.

19. Newman, B.G., "The Deflexion of Plane Jets by Adjacent Boundaries - Coanda Effect," Boundary Layer and Flow Control, pp. 232-264. Edited by G. V. Lackmann, Vol. I, Pergamon Press, New York, 1961.

20. Bourque, C. and Newman, B.G., "Reattachment of a Two-Dimensional, Incompressible Jet to an Adjacent Flat Plate," Aeronaut. Quarterly, Vol. 11, p. 201, 1959.

21. Murphy, J.S., "Some Effects of Surface Curvature on Laminar Boundary-Layer Flow," Journal of Aeronautical Sciences (May 1953).

22. Metral, A. and Zerner, F., "The Coanda Effect," (France) 1953. Translated by Technical Information Bureau, British Minstry of Supply TIB/T 4027.

23. Yen, K.T., "On the Laminar Mixing of a Two-Dimensional Compressible Jet," Rensselaer Polytechnic Institute, TR Ae 504, Troy, N.Y. (1954).

24. Pai, S.I., "Fluid Dynamics of Jets," D. Van Nostrand Company, New York (1954), p. 149.

25. Yen, K.T., "An Investigation of the Coanda Effect for Supersonic Flows," Rensselaer Polytechnic Institute, TR AE 5405, Troy, N.Y. (1954).

26. Sferi-Coanda, Final Report, Vol. II, Contract No. AF 61(514)1409, ASTIA AD 204 074.

27. Boyer, L.J., "Preliminary Investigation and Evaluation of the Coanda Effect," Technical Intelligence Division, AMC, Wright Field, Dayton, Ohio. Technical Report No. F-TR-2207-ND(1948). ASTIA ATI No. 26895.

28. Marwood, R.M., Jr., "An Experimental Investigation of the Coanda Effect," Thesis Project No. M-156, Contract No. W33-038-ac-17625. Purdue University Experimental Station, Lafayette, Ind. (1949). ASTIA ATI No. 80261.

29. Foa, J.V. and Markstein, G.H., "Theoretical Analysis of Flow Phenomena in a Pulse Jet," Cornell Aeronautical Laboratory Project SQUID, Semi-Annual Progress Report, Jet Propulsion Engines (1952).

30. Sproule, R.S. and Robinson, S.T., "The Coanda Effect," Combined Intelligence Objectives Sub-Committee, Air Material Command, Wright Field, Dayton, Ohio, (Oct.-Nov. 1944) ASTIA ATI No. 60515.

31. Young, D.W. and Zonars, D., "Wind Tunnel Tests of the Coanda Wing and Nozzle," Engineering Division, Air Material Command, Wright Field, Dayton, Ohio, A.F. Technical Report No. 6199, U 13481 (1950).

FLOW VISUALIZATION

by

Jorma R. Keto

of

Diamond Ordnance Fuze Laboratories

Abstract

Construction details are presented on two schlieren systems which have been used at DOFL, together with illustrated results of typical images obtained. A method of sealing interchangeable pure fluid elements to optical windows, permitting repeated use without renewal of materials or contamination of windows, is given. Techniques for aiding visualization in difficult situations are discussed.

Motion pictures are presented to illustrate the various schlieren techniques and the use of high speed photography in the visualizatic.. of transient phenomena.

Introduction

The subject of visualization of compressible fluid flow has been well covered in the literature (see bibliographies in References cited); consequently, this paper will discuss that technique which has seen the greatest use in DOFL, i.e., the schlieren system.

Figure 1 shows a schematic diagram of a Toepler schlieren system using lenses. The following arrangement is used. S_1 is a suitable light source (usually long and narrow); L_1 is a collimating lens that renders the light from a point source parallel before passing through the test section at O; L_2 is the "schlieren lens" that converges the light to form an image of the source at S_2 where a knife edge or "schlieren stop" is located; lens L_3 which is not always required, is used in combination with L_2 to image the test section at I. With proper adjustment of the knife edge, an image is produced in which the light intensity at each point is proportional to the density gradient at the corresponding point in the test section.

Lens Schlieren System

Figure 2 shows the arrangement for a schlieren system; lenses L_1 through L_5 are 7-in. f:2.5 Aero Ektar surplus lenses. The light source shown is a 0.010-in. diameter Libessart-type spark gap with a 25-w zirconium modeling light, focused through the gap by means of condensing lenses. The zirconium light is used for visual and motion picture observation; the spark is used for microsecond still photographs. The schlieren objective lenses L_1 and L_2 must be chosen for high quality, since surplus lenses are sometimes defective. Lens L_1 collimates the light passing through the fluid element being observed. Lens L_2 focuses the light on the schlieren stop (knife edge or filter) and, in combination with lens L_3, images the fluid element on the ground glass. The ground glass, used for visual observation, is removed for photography. Lens L_4 images the pressure gages into the plane of the ground glass by means of periscopic mirrors. The composite image is then relayed to the film by the combination of lens L_5 and the camera lens.

The sensitivity and quality of this system is relatively poor due to aberrations. Although supersonic flow is readily observed, other techniques are used to improve visualization, and are discussed below.

DOFL Mirror Schlieren System

The initial program of research in pneumatic devices set forth requirements that could be satisfied best by a schlieren system of greater sophistication than the lens system described above. This system had to be designed to permit resolution of flow in passages of 0.010 in. to 0.030 in. wide, with a maximum field of 8 in. in diameter. It was to be versatile enough to permit variations such as directional, nondirectional, phase-contrast, color, or monochromatic schlieren; also utilization as a polarizing or a diffraction grating-type interferometer. Though a very high sensitivity was demanded, it was necessarily restricted to 10^{-6} radians deflection as a practical limit.

Figure 3 shows a schematic diagram of this system. The components to the right of section A-A in the diagram are shown in Figure 4. (The component parts are identified with corresponding letter designations in Figures 3 and 4.) The console and electronic equipment shown in the left foreground of Figure 4 are used in operating the light sources. These sources consist of a high pressure mercury arc lamp (type BH-6) and a pulsed gaseous discharge lamp (type FX-12). The BH-6 is operated on alternating current for visual observation, or on direct current for motion pictures and photoelectric scanning of the image. The FX-12 is used for still photographs and high-speed motion pictures. Its ability to permit microsecond (or shorter) exposures at rates as high as 6000 per sec is necessary for the study of transient flows in the small passages of the pneumatic devices.

110

Visual observation can be made of the image on the ground glass of the 5 x 7 view camera, identified by (S) in Figure 4. This camera is adjustable to give a wide range of magnification and permits the use of either Polaroid packets or roll film and cut film (4 x 5 or 5 x 7) for still photographs. Additional photography is available with either a 35-mm still camera, or a motion picture camera, which can be mounted at position T. The motion picture cameras usually in this position are equipped with reluctance pickups to permit synchronized pulsing of the FX-12 lamp.

A photoelectric readout device can be installed in place of the motion picture camera. This consists of a single photomultiplier tube with a small pinhole window. The camera mount can be adjusted to permit any area of the schlieren image to fall on the pinhole. The pinhole can then be translated laterally with a cross feed, to which is coupled a precision potentiometer. In this manner a plot of image intensity versus distance can be made by an analog recorder, for steady-state flow.

Schlieren Test Section

The test section J (Figure 4) is shown in more detail in Figures 5 and 6. The light beam is divided into two paths at the test station - one through the pneumatic element being tested, and the other through a calibration standard. The standard is one of several long focal length lenses, the angular deviation of each being known across the diameter. (The focal lengths used are 238, 940, and 1600 ft.) A correction wedge is used to balance out any errors due to lack of parallelism of the windows used to cover the element being tested.

The pneumatic element to be tested is clamped between the windows by means of a "floating" annular hydraulic cylinder to attain a controlled uniform pressure. The window holders are removable to permit the use of a variety of round or rectangular windows. Figure 6 shows one type of window in which the air passes to or from the element by means of ports drilled through the windows. This method permits rapid exchange of low-cost elements produced by etching a photosensitive glass (Corning Fotoform B).

Sealing Pneumatic Test Elements

The behavior of a pure fluid element is dependent upon flow in the small area in the immediate vicinity of the control jets. Consequently, the flow in this area must be disciplined; leakage cannot be tolerated. Originally, units were supplied with tightly clamped transparent plastic windows that sealed well but introduced strong schlieren. Heavy glass windows were then tried, but the surface of the fluid element (made of brass) could not economically be rendered sufficiently flat. This

problem was resolved by machining the unit initially to ordinary shop tolerances, then coating it with a gasket of 0.010 in. extruded polystyrene foam sheeting. The gasket is applied with a water emulsion of vinyl acetate to provide a pressure-sensitive bonding material. The passageways are then cut free of the gasket with a hot wire.

The gasket material is composed of closed (unbroken) bubbles of polystyrene; consequently, it has an extremely low bulk modulus that permits it to conform to an uneven surface without areas of high stress in the windows. Also, the gasket has a good recovery and does not scratch the window; therefore, the unit can be clamped repeatedly, which permits frequent window cleaning. With a 30-psig pressure across a 1/16-in. wall, a leak rate of less than 30×10^{-6} scfm was measured.

Schlieren Images Obtained

Figure 7 shows a typical image obtained with the mirror system. Those who are not familiar with the interpretation of schlieren photographs may find the following method helpful. If one imagines the fluid within the passages as a milky liquid being illuminated at a grazing incidence from the direction of the knife edge (from above in Figure 7), the flow will appear to be in relief in such a manner that the higher the relief above the plane of the photograph, the greater the density of the gas. Various regions which give information of flow conditions can be seen in the photograph. Attached to the splitter is a shock wave. From the shock angle and the splitter angle one can determine flow Mach numbers before and after the shock, pressure coefficients, flow deviations, etc. In the nozzle one can see Mach waves from which flow characteristics can be determined and nozzle design modified. The fact that flow is filling both exit passages equally indicates that for this nozzle the backing or exhaust pressure was too low relative to the input pressure.

Figure 8 shows the same unit operating properly, with the flow separating within the nozzle, attaching to the wall and exhausting from one passage only. Details of flow separation within the nozzle can be studied as shown in Figure 9. In each of the flows illustrated the conditions are identical in regard to mass flows and pressure ratios. The nozzle is operating overexpanded, with flow separation and a shock occurring in exactly the same manner at the left side of the nozzle. Note, however, that the flow leaves the nozzle vertically in one case, and directed to the right in the other. Examination will show that flow separation occurs on the right wall of the nozzle also, and the final direction of flow is determined by the net effect of the deviated flow from both walls. The variation in separation at the right wall is caused by changes of backing pressure affecting the boundary layer buildup. In an actual unit the separation can be stabilized by allowing the flow to become attached to the downstream wall.

112

Aids to Improve Visualization

The schlieren pictures discussed thus far were taken by the mirror system of supersonic flow. In the case of a low sensitivity system or for "incompressible" flow, techniques can be used to aid schlieren visualization.

By introducing a volatile transparent liquid onto the surface of the window of a unit being tested in the schlieren system, the flow pattern can be visualized within errors imposed by inertial effects. Figure 10 shows a fluid element adapted with a hypodermic tubing aspirator nozzle for introduction of trichloroethylene. This technique works extremely well and requires little sensitivity of the schlieren system itself. Because of this, color can be used to enhance the visualization. (Chromatic aberrations of lenses and diffraction impair color schlieren when high sensitivity is required.) A point source can be used with a concentric green and red filter (similar to a Reinberg differential color filter for microscopy). Figure 11 shows a selected frame from 16-mm movie sequences taken at 150 frames/sec.

Flow lines can be visualized in the case of steady-state flow if "shop air" is used and oil vapor is present. The flow is left on and schlieren photographs taken of the traces that remain from the condensed oil as the droplets follow the flow in the glass-to-air boundary layer. Note the results of this technique in Figure 12. By taking time sequence movies at frame intervals of the order of six seconds, a complete flow pattern can be seen as the droplets creep along the boundary layer. It must be remembered, however, that this method shows averaged boundary layer flow, and not a complete time history of internal flow; furthermore flow in the boundary layer may be appreciably different from flow within the unit.

In some cases it is possible to introduce a "tracer gas" with an index of refraction differing from the flow being investigated. Heated air, or a gas such as helium can be used. Figure 13 shows the primary air being outlined by helium which is allowed to drift into the unit through the control orifices and is entrained by the primary flow. In this example, which was taken with the lens schlieren, the flow is incompressible, being at approximately Mach .04. One must remember, however, that in using this technique the flow visualized is the boundary between the tracer and the primary air rather than the over-all flow taking place.

Motion Pictures for Transient Visualization

The discussion at the Symposium was followed by a five minute 16-mm film showing examples in color or black and white of units in action. The scenes were as follows: 1) a fluid oscillator, taken with a very simple lens schlieren; 2) a momentum exchange unit using

helium; 3) a memory unit, visualized by means of trichloroethylene;
4) a bistable element photographed at 3,000 frames per second, using
the BH-6 mercury arc with direct current as a light source; 5) the
same sequence and frame rate as in scene 5, except the FX-12 lamp was
used, giving an exposure of about one microsecond per frame; 6) a
convergent-divergent nozzle, taken at 6,000 frames per second with
the BH-6 operating on D.C.; 7) a time sequence movie in which the
oil condensation technique is illustrated. Approximately two hours
running time were compressed into fifty seconds projection time.

References

1. DOFL Report TR-1041, "Fluid Amplification--2. Flow Visualization-
   Compressible Fluids," Jorma R. Keto, 20 August 1962.

2. NATO AGARDograph 23, "Optical Methods for Examining the Flow in
   High-Speed Wind Tunnels," D. W. Holder, R. J. North, G. P. Wood,
   November 1956.

3. Journal SMPTE, Vol. 61, No. 4, p. 503, October 1953.

4. Landenburg, Lewis, Pease and Taylor, "Physical Measurements in
   Gas Dynamics and Combustion," Princeton University Press, 1954.
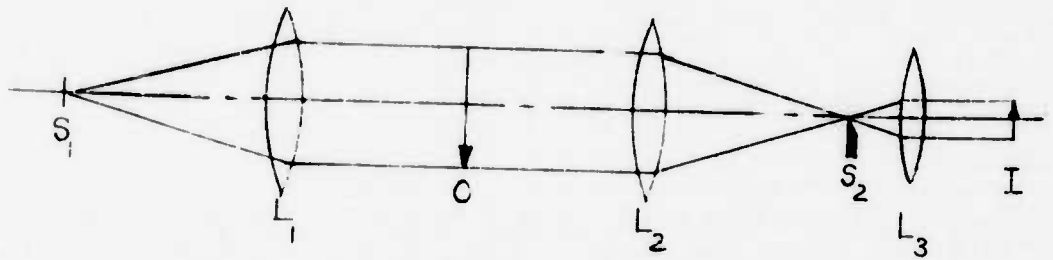
Figure 1. Schematic of schlieren system.
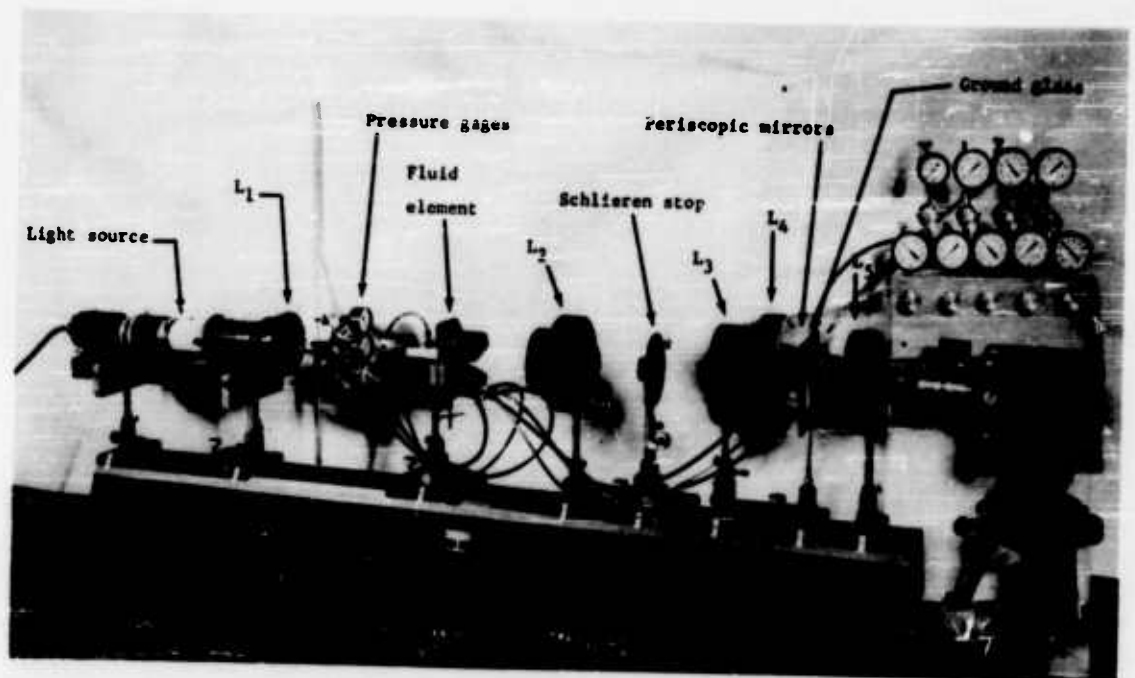
Figure 2. DOFL schlieren system using 7-in F:2.5 Aero
Ektar lenses.

115
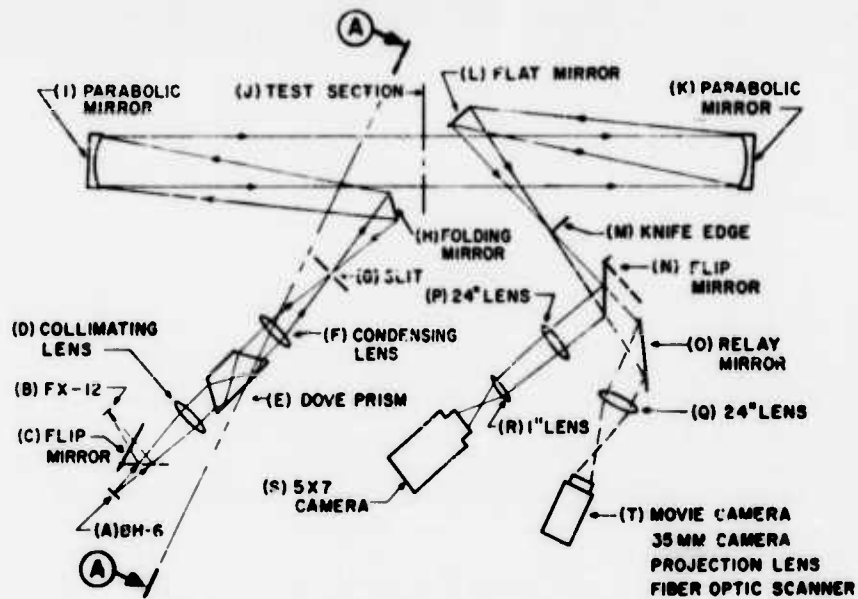
Schematic of DOFL mirror schlieren system.

Figure 3. Schematic of DOFL mirror schlieren system.
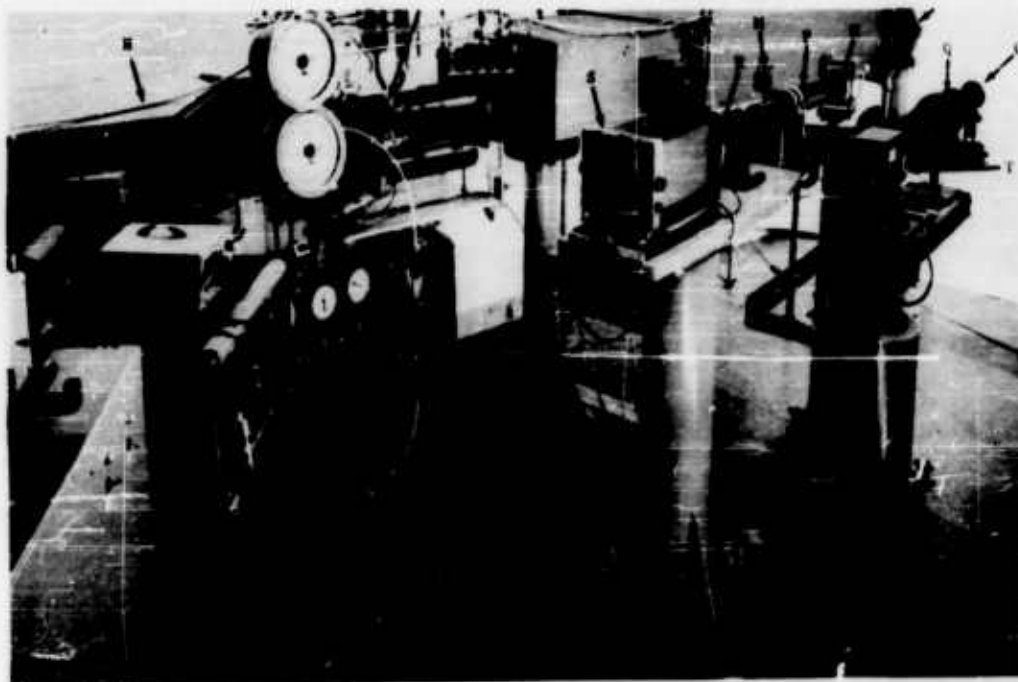
Figure 4. DOFL mirror schlieren system.

116
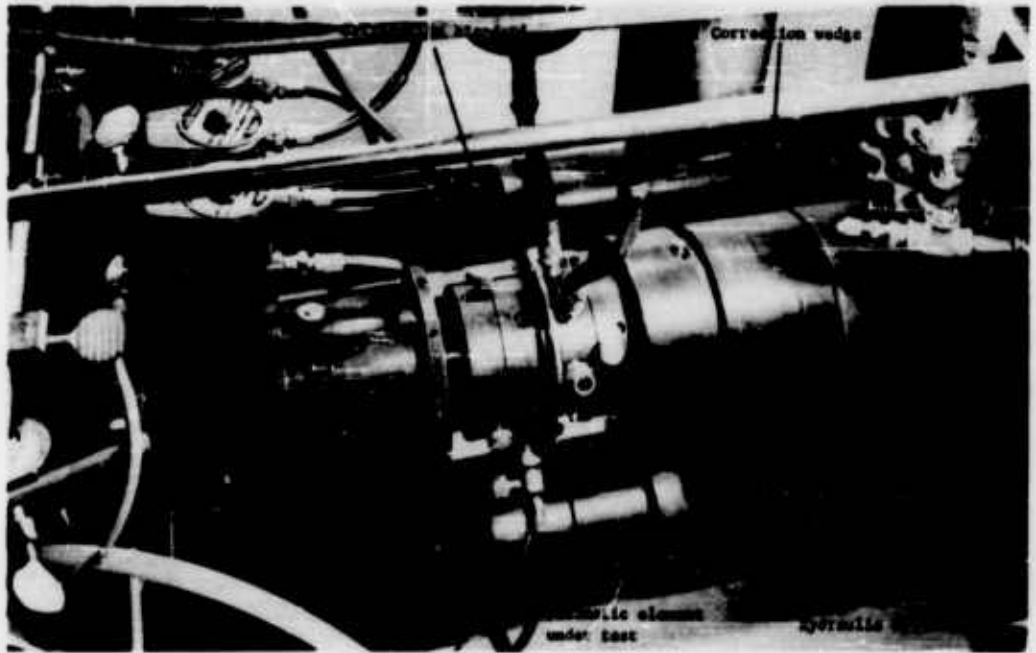
Figure 5. Test section of schlieren system.
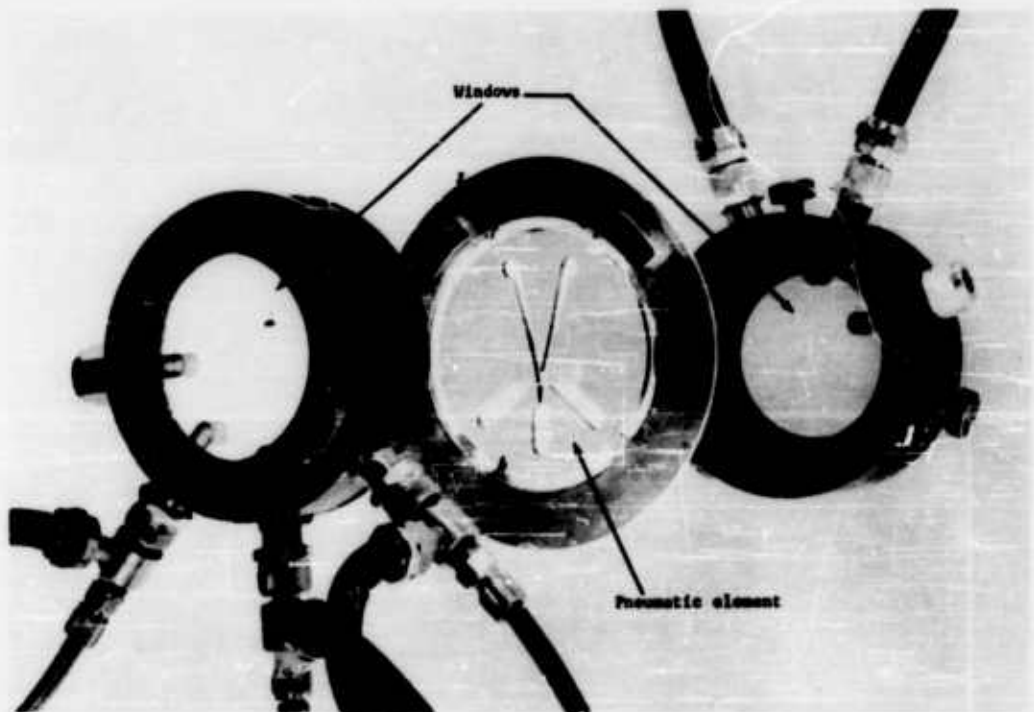
Figure 6. Exploded view of pneumatic element and test section windows.

117
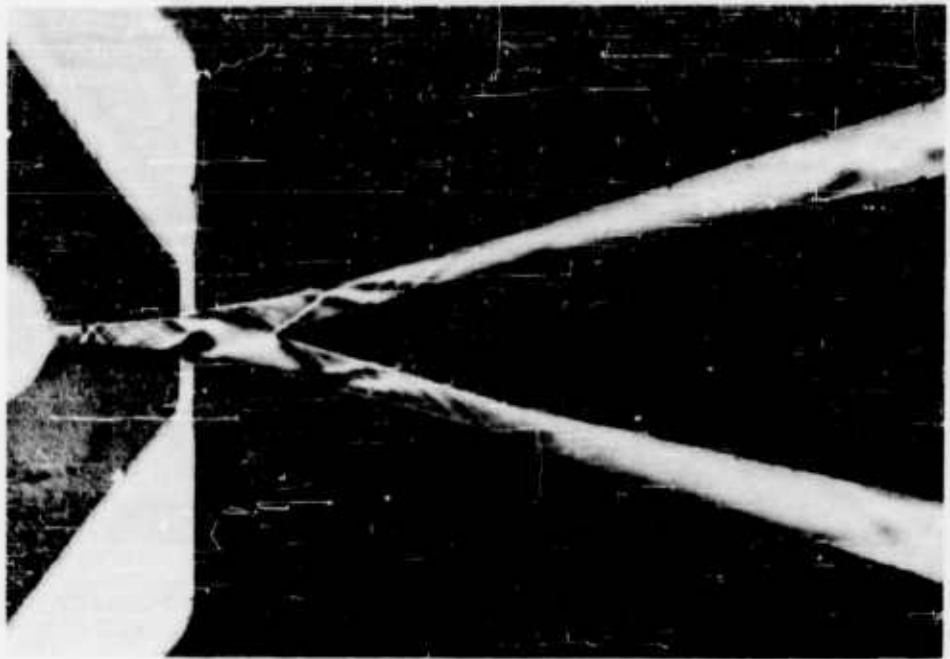
Figure 7. Supersonic unit. P/P_0 approximately .07, no control, throat = .030 in. wide.
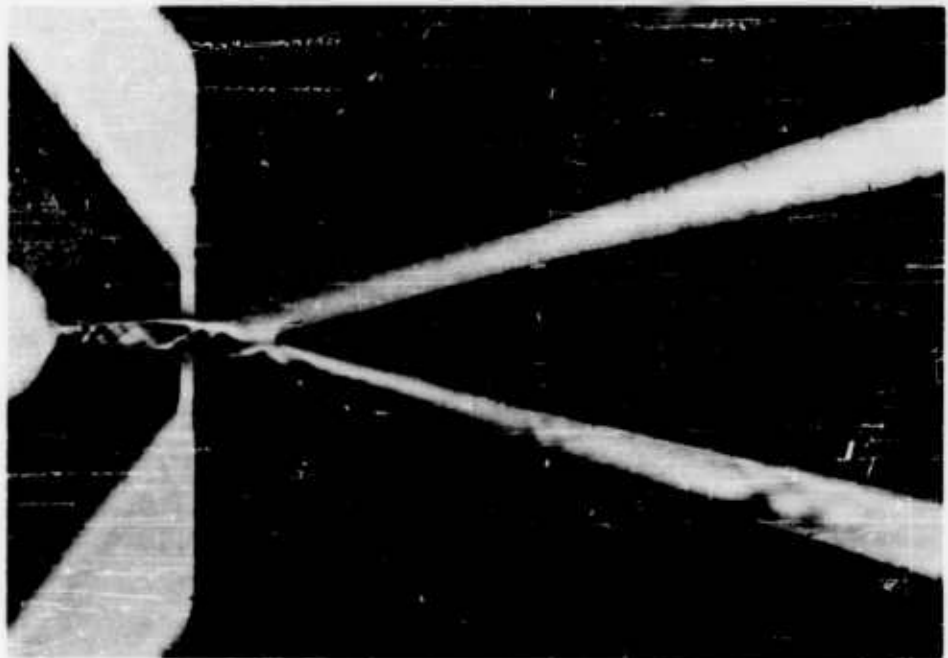
Figure 8. Supersonic unit. Pressure ratio adjusted for proper operation (no control).

118

Figure 9. Divergent nozzle showing flow separation. P/P_0 approximately .07, throat = .030 in. wide.

119
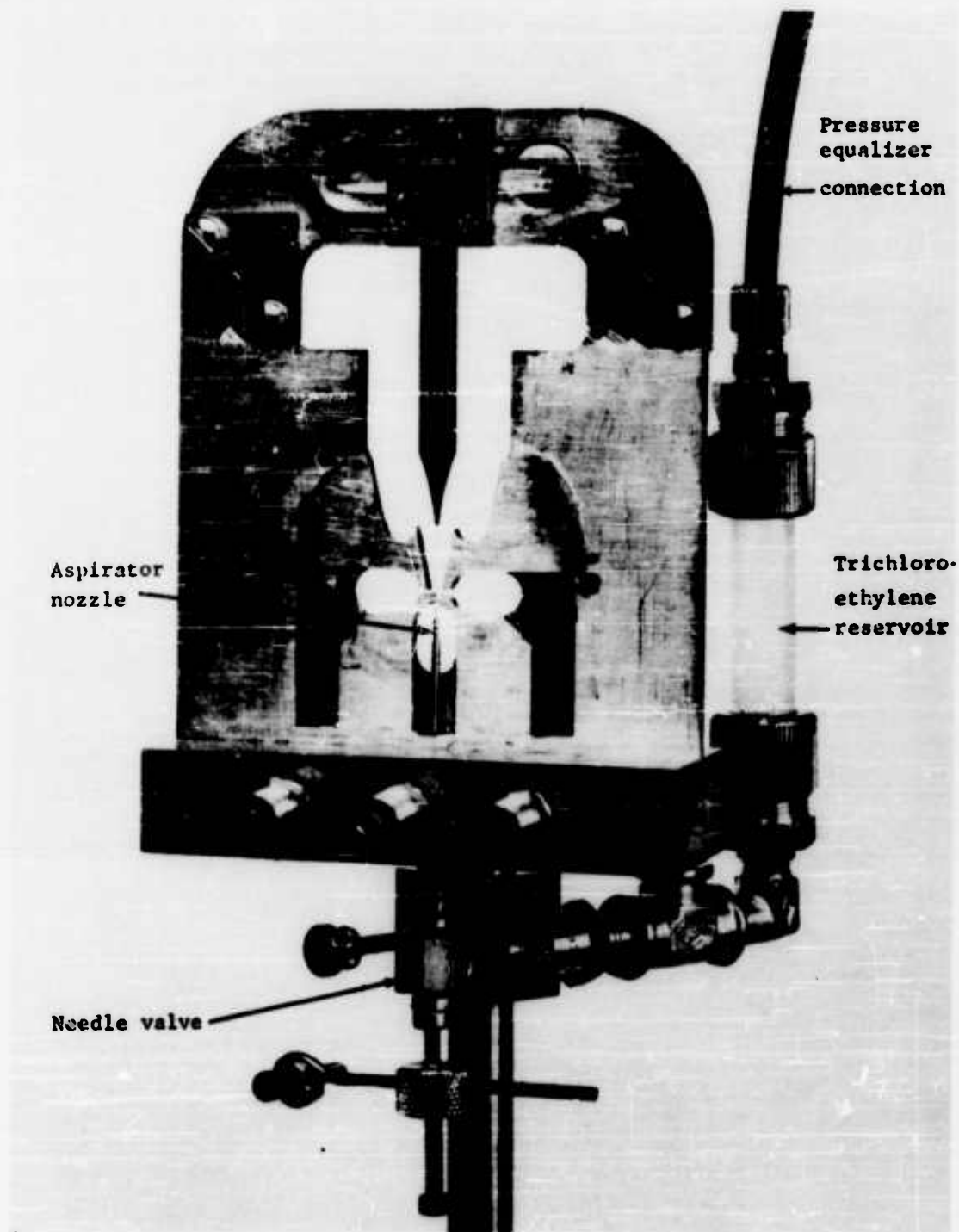
Figure 10. Method used to introduce trichloroethylene into element.
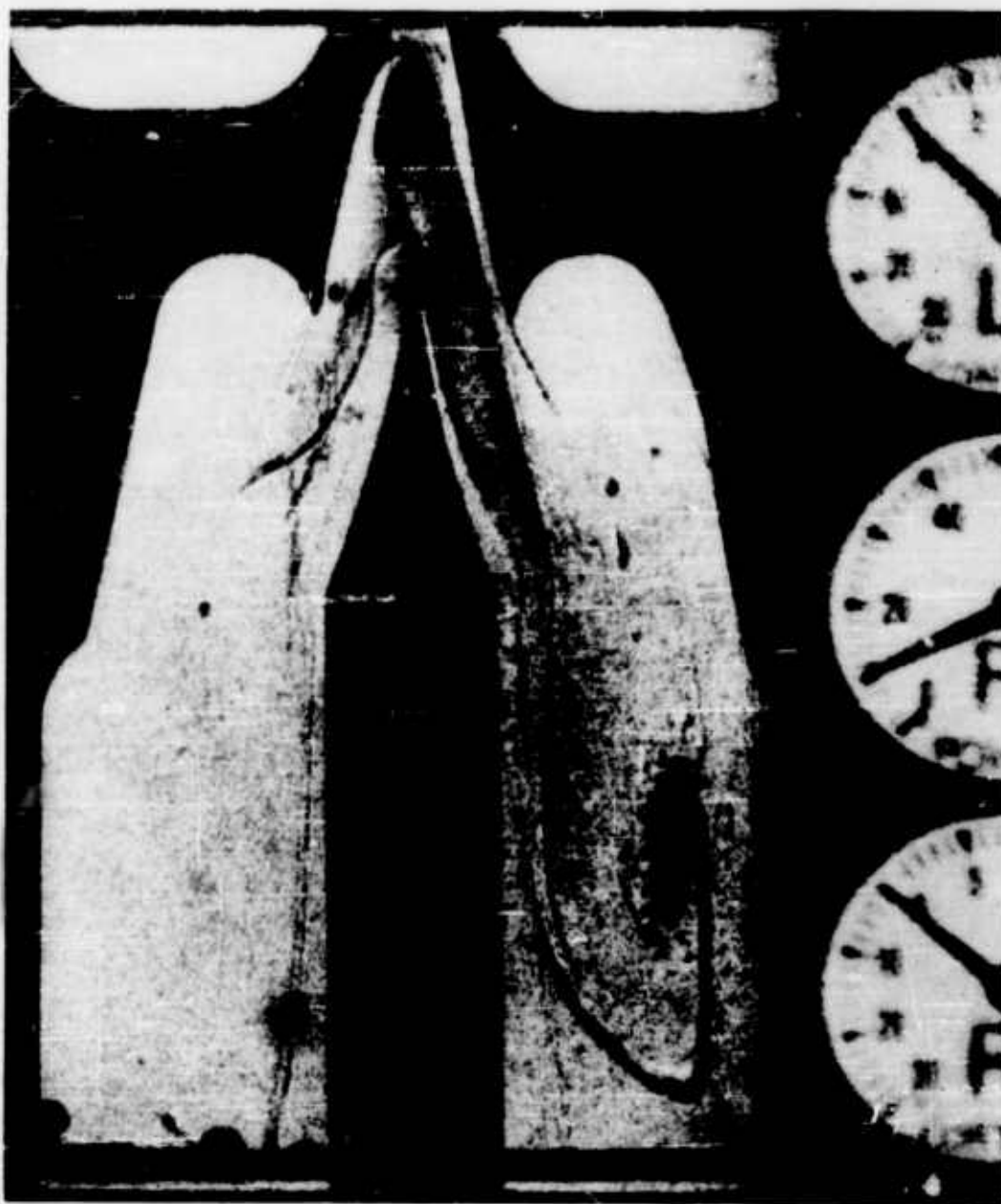
Figure 11. Bistable element, trichloroethylene aid.

121
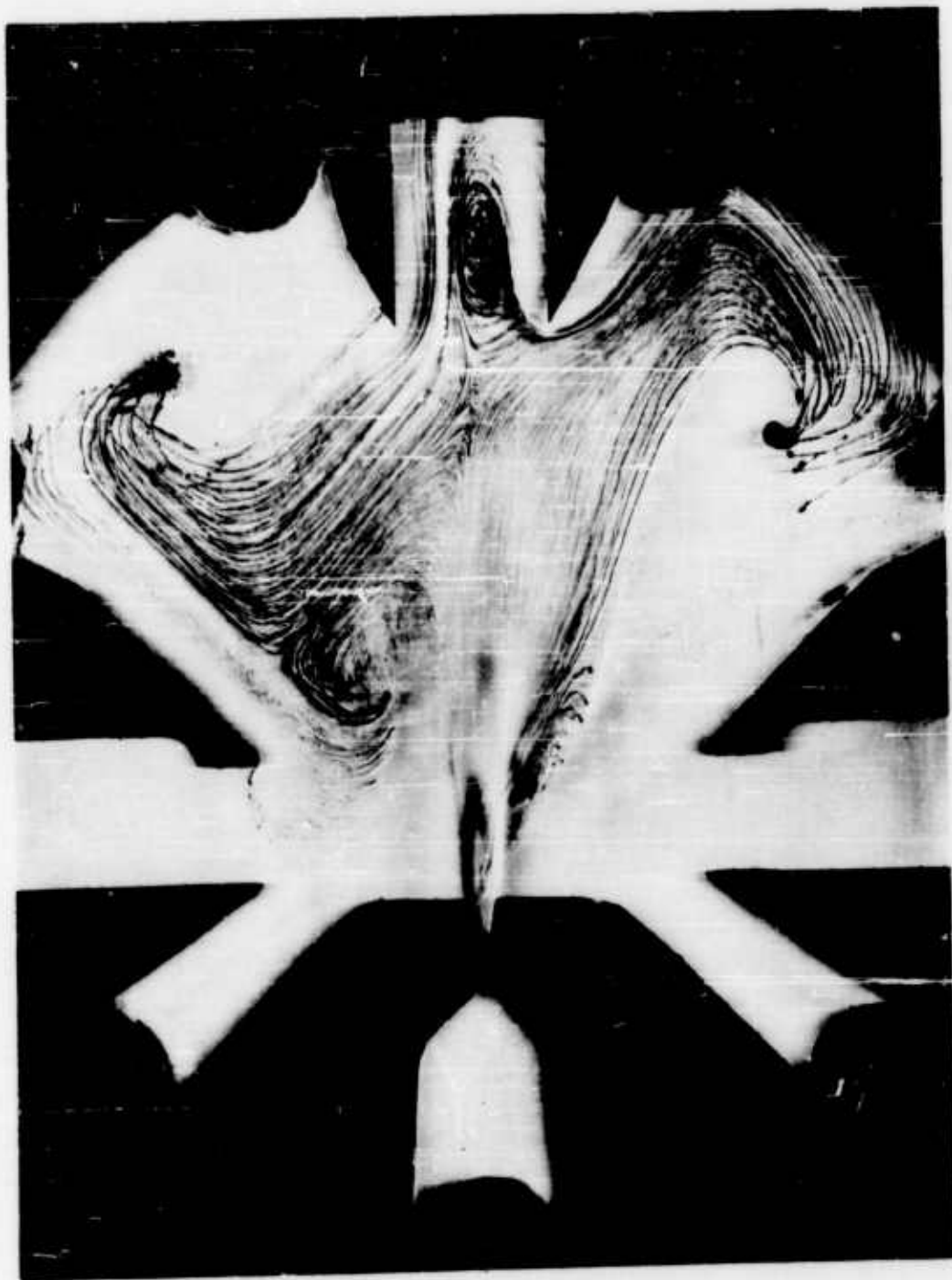
Figure 12. Boundary layer flow visualization by condensation of oil vapor.
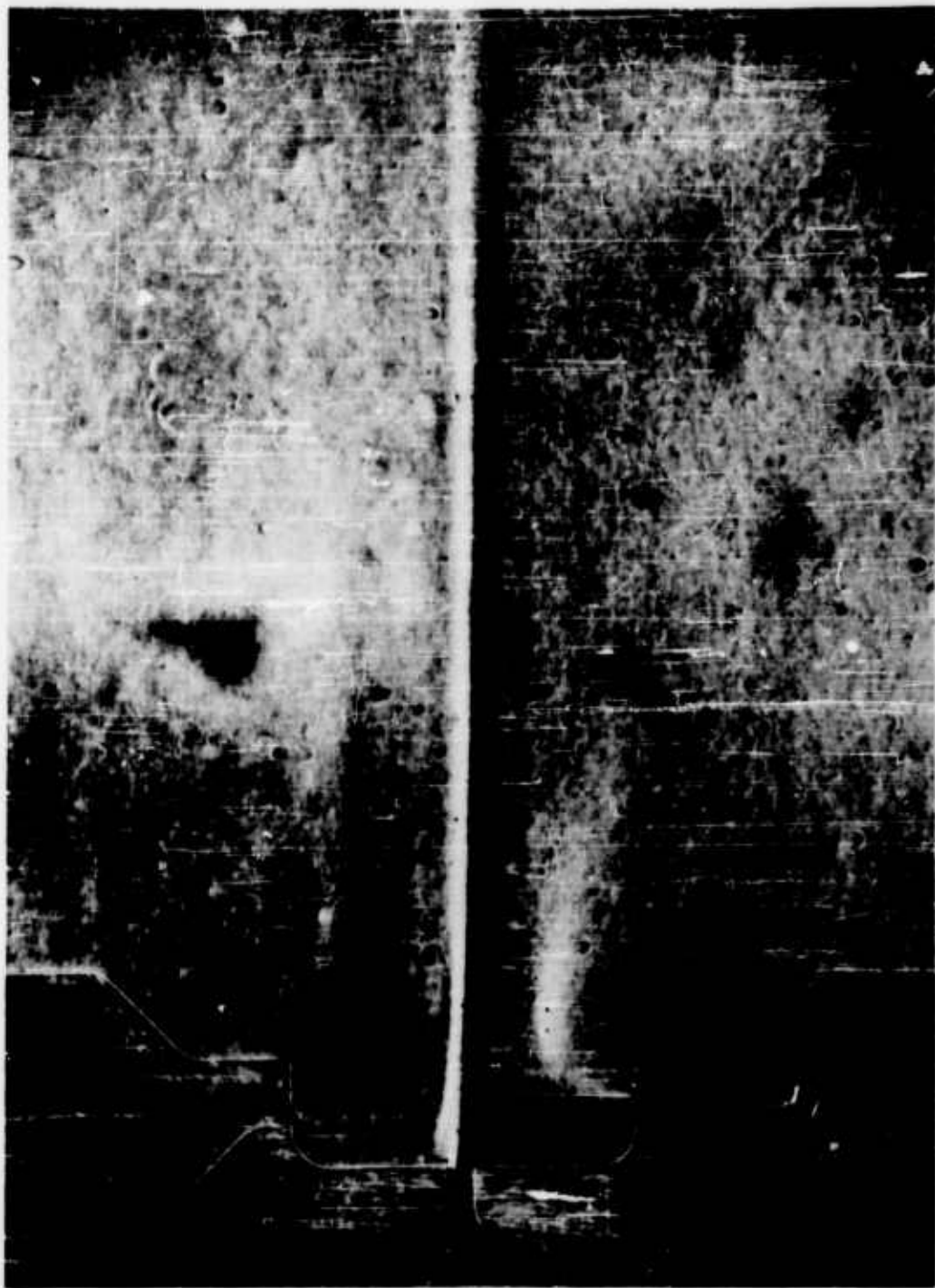
Figure 13. Primary air from power jet made visible by use of helium.
$$P/P_j = .9988$$

123

FLOW VISUALIZATION AND EXPERIMENTAL STUDIES OF A PROPORTIONAL FLUID AMPLIFIER

by

R.J. Reilly
J.A. Kallevig

of

Minneapolis-Honeywell Regulator Company
Military Products Group Research

Abstract

Experimental data taken on a particular type of closed, proportional fluid amplifier did not agree with analysis based on two different mathematical models. Visualization studies and detailed measurements in the interaction region of 3 fluid jets show that the power stream is accelerated after leaving the power nozzle. This fact is not predicted by either mathematical model and must be considered in future analytical investigations.

Early development of the proportional fluid amplifier was primarily on an experimental basis aimed toward determination of general operational characteristics and applicability of devices of this type. The need for analytical guidance in device optimization and system synthesis received early recognition. Horton and other early investigators based their mathematical description of the device on analogy to the submerged fluid jet. Initial work by Minneapolis-Honeywell investigated a refinement of the submerged jet model as well as other mathematical formulations. (Reference 1)

None of these mathematical models gave a really satisfactory prediction of the performance of the devices tested. In an effort to achieve a better understanding of the interaction of three fluid jets a series of flow visual-

ization experiments were performed. These studies indicate that the flow within the fluid amplifier differs significantly from the submerged jet. In particular, the flow patterns observed suggest the acceleration of the central portion of the power stream rather than the degradation of the velocity profile which occurs in the submerged jet.

To verify the observation made in visualization studies, a large, three jet, interaction model was constructed and instrumented. Preliminary measurements made with this model which show the existance of an accelerated core velocity are presented.

Review of Proportional Amplifier Operating Characteristics

During the early phase of development and evaluation, proportional amplifiers of widely varying size and configuration were operated on several different types of fluid. While the performance of each varied somewhat, nearly all showed performance characteristics similar to that shown in figure 1. This figure plots the change in output momentum versus the change in input or control momentum for a typical fluid amplifier. Output momentum is based on an average velocity over the receiving aperture area and power stream · momentum is chosen as the non-dimensionalizing parameter. The linearity of the central portion of this curve is striking. That this portion of the curve is truly linear and not merely a wishful line drawn through the data is demonstrated by figure 2 which shows the performance characteristic which results when the output flow of one proportional amplifier is used as the input signal of the second. The two amplifiers are identical except for size and not selected for compensating characteristics.

Analytical Formulations

Very early in the Honeywell fluid amplifier program it was evident that an analytical description of the proportional amplifier was necessary, both to guide the way toward optimum design of devices and to assist in organizing the experimental data according to significant flow and geometric parameters. Our first analytical attempt followed the work of Horton (Reference 2) utilizing the analogy to the submerged jet with minor improvements by numerical integration of the submerged jet velocity profile. In addition to the usual assumptions of two dimensional flow, steady flow and incompressible fluid, the submerged jet analogy assumes that there is a complete mixing of the power stream with the control streams and that no significant change in the symmetry of the velocity profile results from the asymmetric distribution of control

flow required for deflection of the fluid jet, figure 3.

The submerged jet mathematical model did not yield satisfactory agreement with the experimental results on the models tested, hence, to bracket the problem, a mathematical model, postulating an inviscid fluid and no mixing of the control and power streams, was analyzed, figure 4. Both of the above analyses are developed in detail in reference 1.

A comparison of the analytical results with data taken on one particular closed proportional amplifier configuration is shown in figure 5. Continuity requires that all of the fluid entering such a device must exit through the receiving apertures. Neither the submerged jet nor the inviscid model gives a really acceptable prediction of the performance of the actual device. The most notable discrepancy between experiment and theory is the fact that even the inviscid flow model does not yield an amplification which is as high as that determined by experiment. The inviscid model does, however, provide the linearity required by the central portion of the experimental performance curve so it is worthwhile to explore what is necessary in order that a linear performance curve is produced.

It is shown in reference 1 that the amplification or gain of a proportional amplifier can be written as

$$G_f = \frac{K}{k}(1+K)\frac{L}{y}R \qquad (1)$$

where:

K is the ratio of the total control mass flow to the power stream mass flow,

k is the ratio of a control nozzle area to the power nozzle area,

L is the distance from the power nozzle to the splitter,

y is the distance through which the jet is deflected perpendicular to the center line of the device,

R is defined as $$R = \frac{\dot{m}_{out_r} - \dot{m}_{out_l}}{\dot{m}_{out_r} + \dot{m}_{out_l}} \qquad (2)$$

128

the difference of the output mass flows divided by the total mass flow through the device. For a symmetrical velocity profile, R can be written in the following form:

$$R = \frac{\int_0^{y/L} \left(\frac{v}{v_0}\right) d\left(\frac{y}{L}\right)}{\int_0^{(y/L)_{max}} \left(\frac{v}{v_0}\right) d\left(\frac{y}{L}\right)} \qquad (3)$$

This integration was performed in reference 1 and is presented here in figure 6 for convenient reference.

Inspection of equation 1 shows that for a linear performance curve to exist, i.e. G_f = a constant, R must be a linear function of y/L. Equation 3 then shows that for R to be linear with y/L a uniform velocity profile must be presented to the receiving apertures, or the velocity profile must be changing in some mysterious way to make it appear so.

With the foregoing relationships one may work backward from experimental data to see what is required of the mathematical model if the performance curve of figure 5 is to be duplicated. An experimental velocity profile is constructed by determining R from the experimental data and then differentiating R with respect to y/L to obtain a velocity profile. The velocity profile so obtained is shown in figure 7, reproduced from reference 1. This figure shows that in order to satisfy the experimental curves under the assumed constraints it is necessary that the velocity profile presented at the receiving apertures not only be uniform but also accelerated rather than reduced in velocity as predicted by the submerged jet hypothesis.

Flow Visualization Studies

To assist in the formulation of a more suitable mathematical model and to guide the course of future experiments a series of flow visualization studies were conducted on a somewhat larger but geometrically similar proportional beam deflection amplifier. This model, shown in figure 8 used water as a working fluid and had provision for dye injection into the power stream and the control stream to make their respective flows visible. At the formal presentation a series of colored slides were shown which demonstrated the flow patterns obtained in a closed proportional fluid amplifier. The limitations of black and white reproduction processes precludes their presentation here.

In the first series of slides shown, the ratio of the control nozzle area to the power nozzle area is approximately .57 and the ratio of the total control momentum to power momentum at null is approximately 0.127. K, the ratio of the total control mass flow to the power nozzle mass flow, is .38. Reynolds number based on power nozzle width is of the order of 12,000 to 14,000. It is evident from this series of slides that nothing approaching complete mixing of the three streams occurs within this device. By close examination of the slides the identity of the 3 streams can be discerned several channel widths downstream of the receiving apertures. Further, what appears to be a slight contraction of the power stream can be observed in the interaction region. This contraction could be due to mixing of the streams or be a misleading phenomenon due to boundry layer effects on the top surface, or an acceleration of the central portion of the power stream as indicated by the above set of experiments.

A second series of photographs is shown for the same model modified so that the control nozzle areas are half what they were in the previous case.

130

The mass flow ratio was approximately the same, $K = 0.39$, and the momentum ratio rises to $M_{c_t}/M_o = .27$. This series of experiments shows a pronounced contraction of the power stream and, perhaps, somewhat more mixing of the 3 streams. Since a somewhat higher pressure was required to maintain the mass flow of the power stream at its previous level it became a matter of reasonable conjecture that the contraction of the power stream in the inter-action region indicated a corresponding acceleration of the central portion of the stream after leaving the power nozzle. It is interesting to note, however, that the momentum gain was virtually identical in both cases.

Section III

Detailed Jet Interaction Studies

Based on the flow visualization studies experiments a large variable geometry, three jet interaction model was fabricated to permit detailed studies of the interaction region. This model is shown in figure 9 and is of sufficient size to permit easy instrumentation without concern for the effect of the measurement probes on the flow field. The studies to be conducted on this model have begun with detailed traverses of the 3 jets alone and will proceed in orderly fashion, progressively adding downstream pieces until a configuration of the desired fluid amplifer is obtained. Measurements will be made after each modification of geometry to determine its effect on the interaction.

Some preliminary results of pitot static-static traverses of 3 interacting jets are shown in figure 10. The mass ratio, K, for these profiles is approximately 0.6. The area ratio, k, is 1.0, resulting in a momentum ratio of the two streams, M_{c_t}/M_o, equal to 0.18. Flow measurements were made with rotameters and the control flows balanced as well as possible, however, in the actual case, the curves of figure 10 were displaced somewhat from the

center line of the device. For presentation purposes they have been centered but the distortion of the profile for even this small asymmetry of the control flows is noticeable.

For this particular configuration, mass flow ratio and momentum ratio the submerged jet analogy of Albertson compares quite well with the experimental data as shown in figure 11. Since a mass ratio of one corresponds to a submerged jet of length 7.3 comparison could be made with the 6 D_2 and the 8 D_2 experimental data only (D_2 defines the width of the power nozzle).

Figure 12 shows a series of velocity profiles taken for mass flow ratio equal to approximately 1.0 with the same geometry as above. This gives a momentum ratio M_{c_t}/M_o equal to 0.5. Here it may be seen that the acceleration of the central portion of the stream indicated in the visualization studies appears. The maximum velocity reached by the central core of the profile exceeds the initial velocity of the power nozzle by 20% at the largest value. It is interesting to note that a total pressure survey of the center line velocity in this case shows an ever decreasing total pressure. In a model as large and open as this one, it is often easy to rationalize that the static pressure should be nearly constant everywhere except in the immediate vicinity of the nozzle exit, and the declining pressure survey should indicate a decrease in velocity. However, when the static pressure is measured, it is found to be declining more rapidly than the total pressure and hence an increase in the center line velocity is observed.

Conclusions:

1. Mathematical models of proportional fluid amplifiers based on submerged jet theory are not suitable for some amplifier configurations.

2. Interaction of the control streams with the power stream can produce acceleration of the power stream after it leaves the power nozzle.

132

References

1. Reilly, R. J. and Moynihan, F. A.; "Notes On a Proportional Fluid Amplifier". To be presented at the Winter Meeting, 1962 American Society of Mechanical Engineers.

2. Horton, B. M. to R. J. Reilly; "Personal Communication", October 1961.

3. Albertson, M. L., Dai, Y. B., Jensen, R. A., Rouse, Hunter; "The Diffusion of Submerged Jets", Transactions of American Society of Civil Engineers, Vol. 115, 1950.

Figure I

134

TWO PROPORTIONAL AMPLIFIERS
IN CASCADE
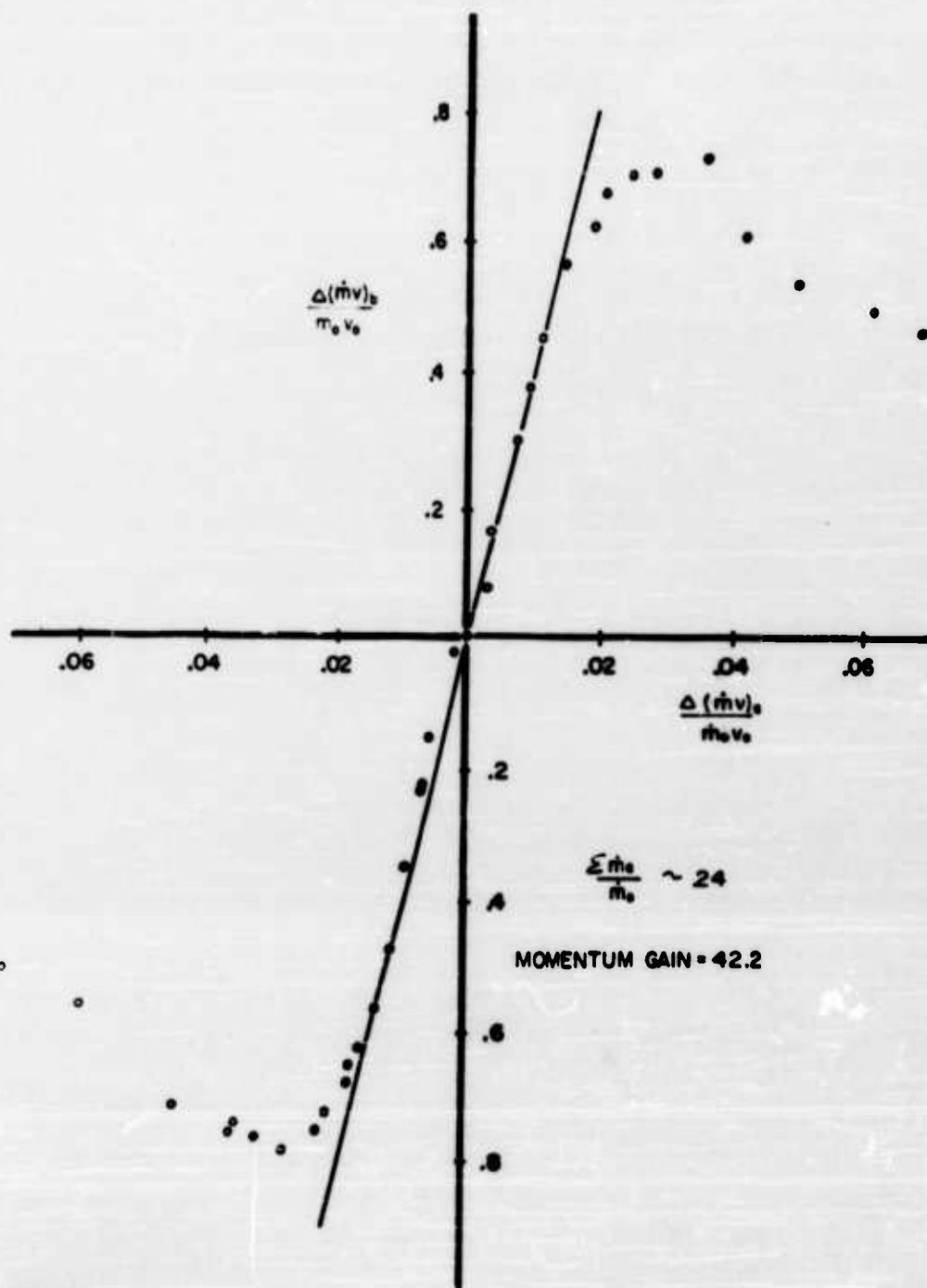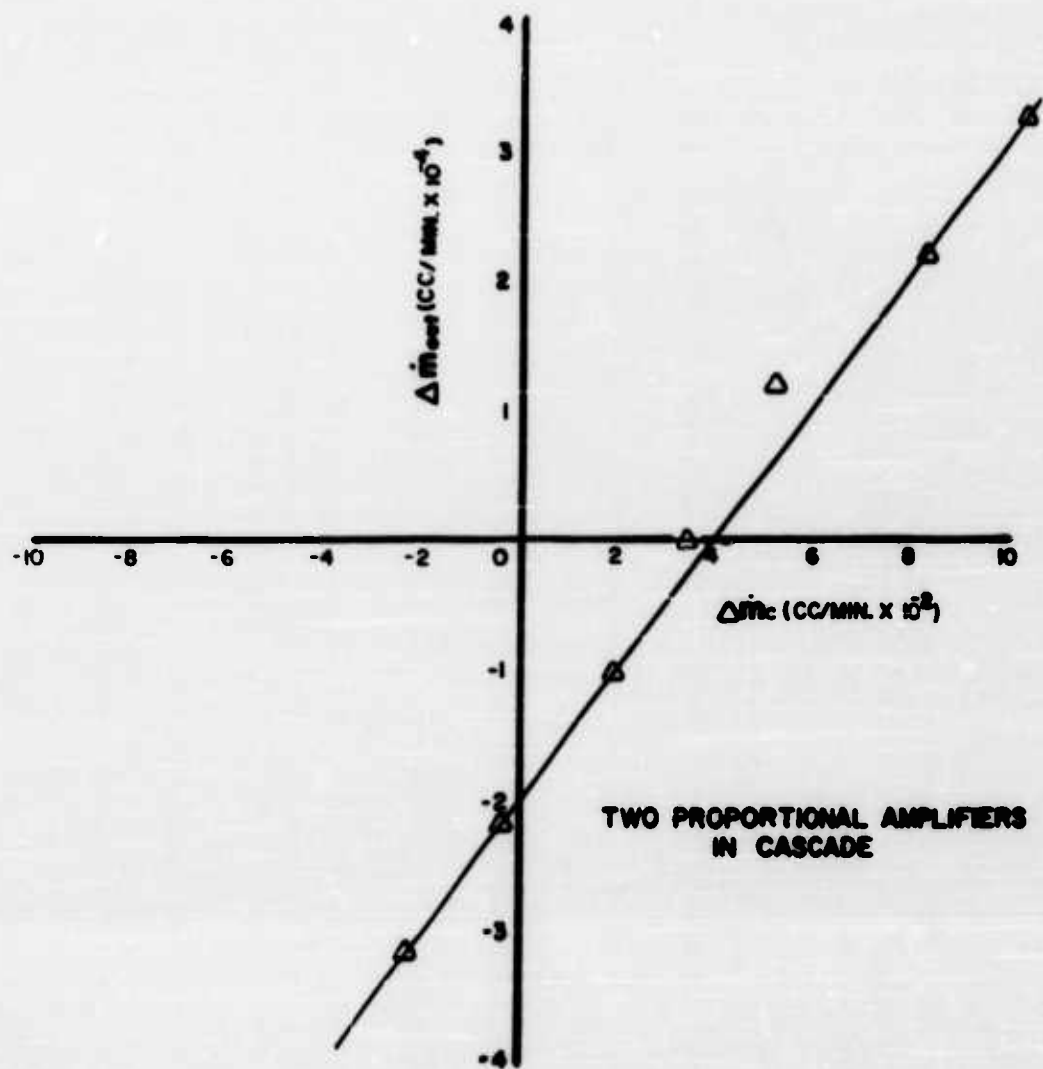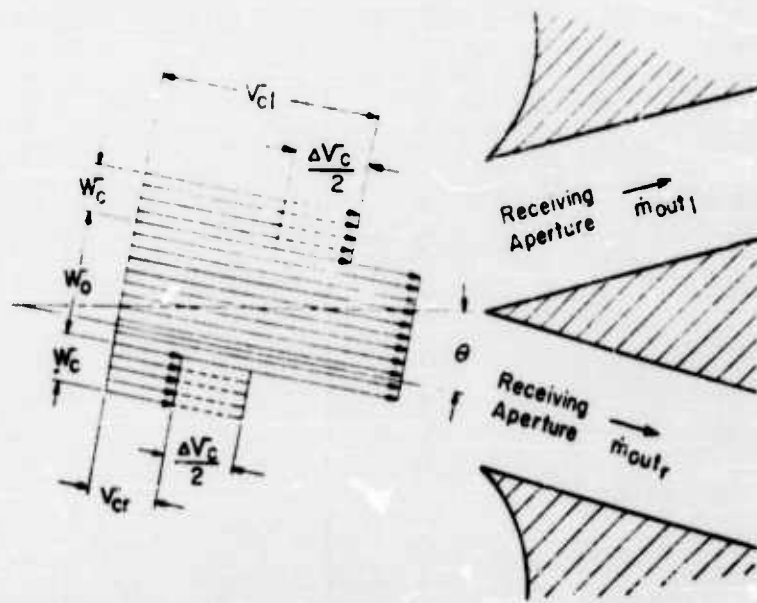
Figure 2

Figure 4 INVISCID MODEL VELOCITY PROFILE

$$LOG_{10} \ (v/v_0\sqrt{L/w_0}) = 0.36 - 18.4(y/L)^2$$

(REFERENCE 3)
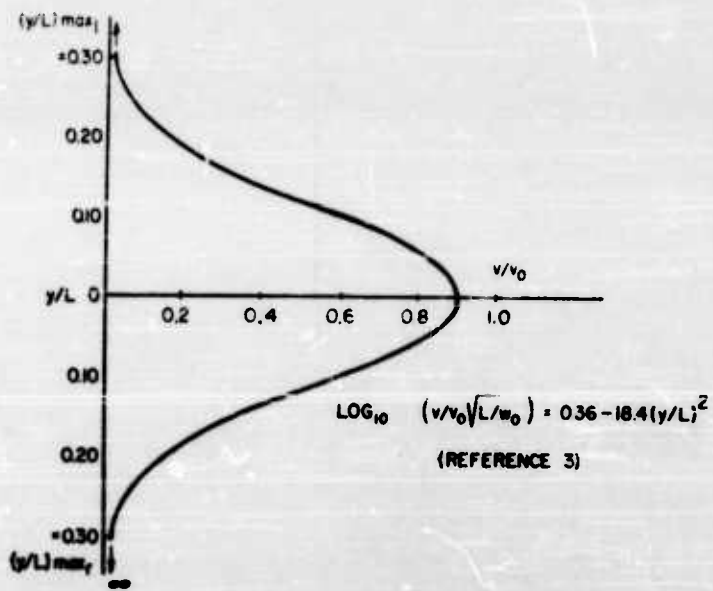
Figure 3   VELOCITY PROFILE FOR A SUMERGED
JET, $L/w_c = 6.0$

136
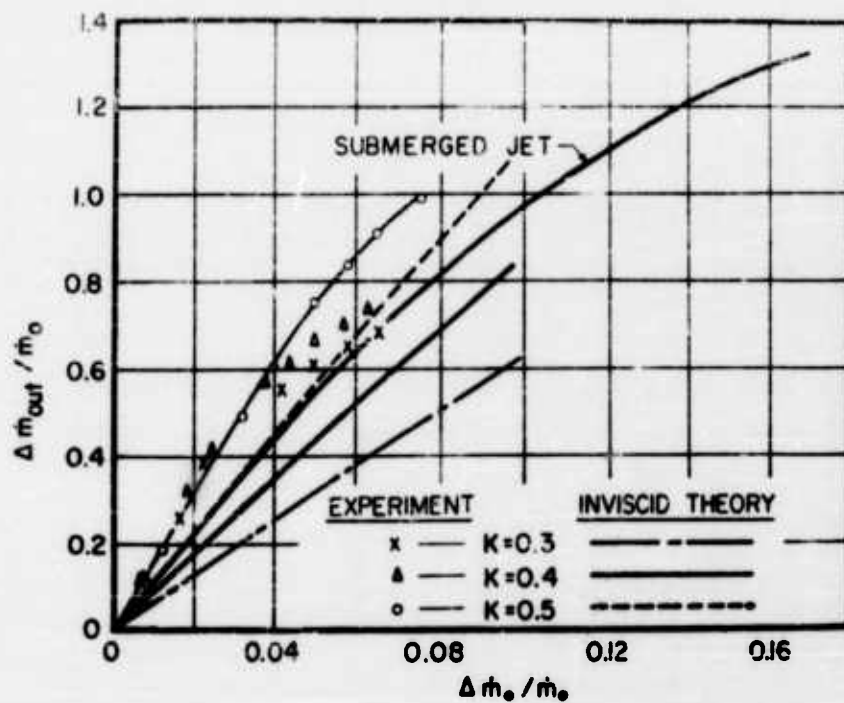
Figure 5. Analytical and experimental performance curves.
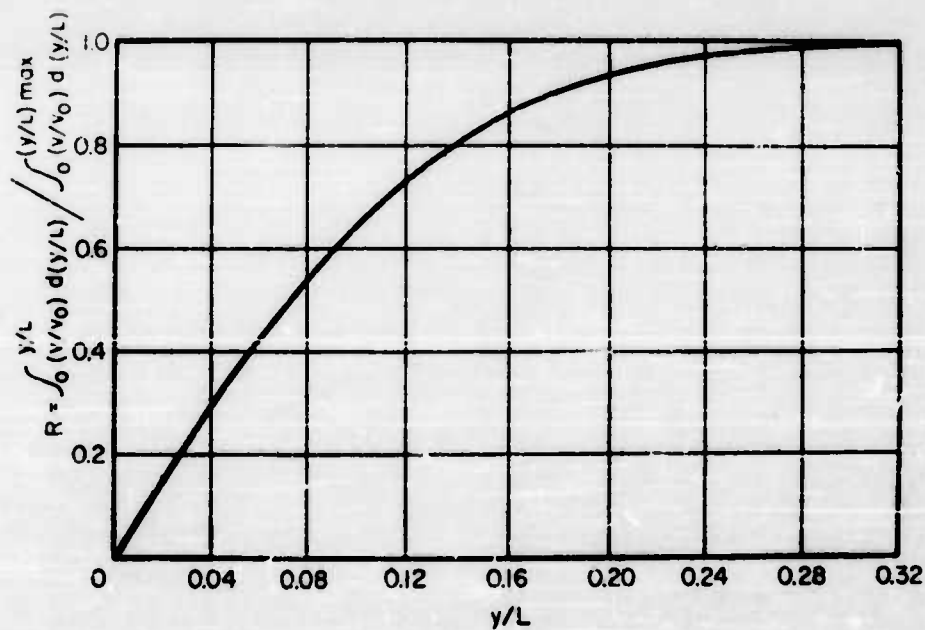
Figure 6. R as a function of y/L.
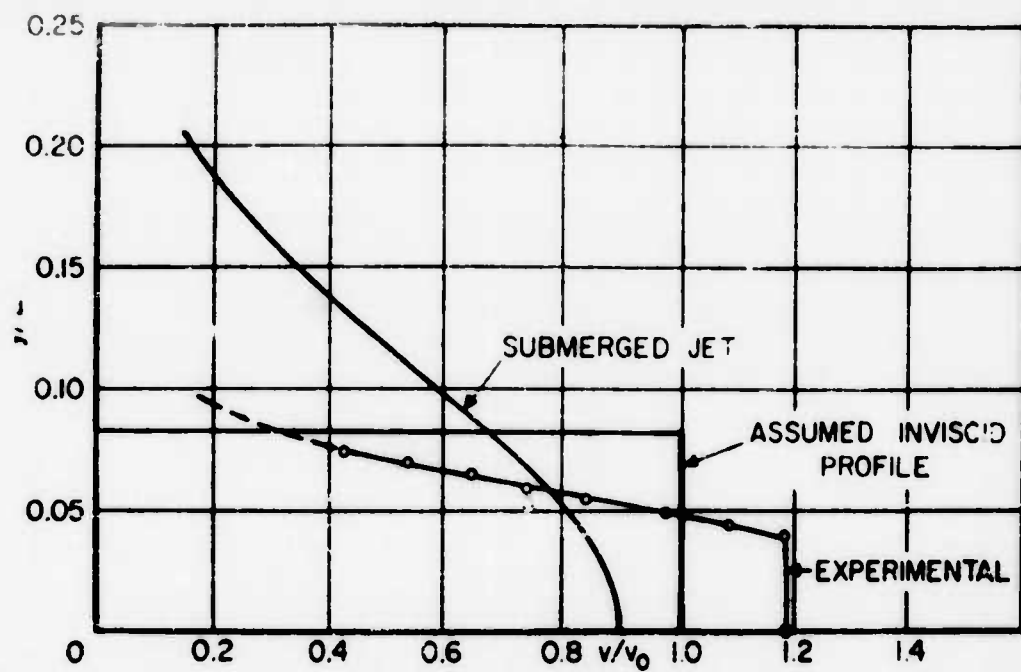
Figure 7. Comparison of jet profiles.
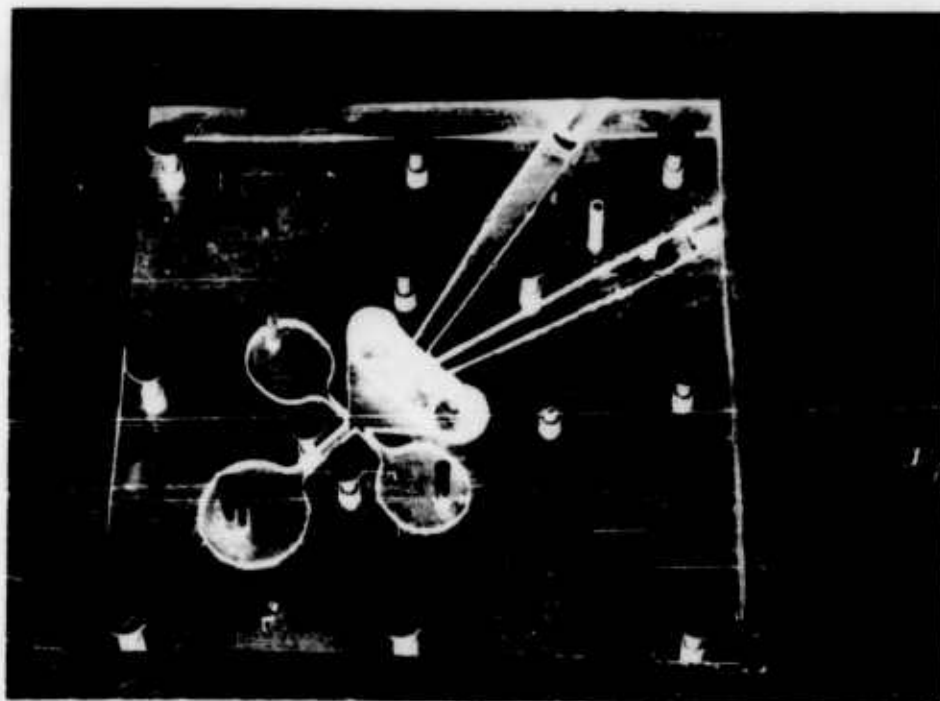
Figure 8. Flow visualization model.

138
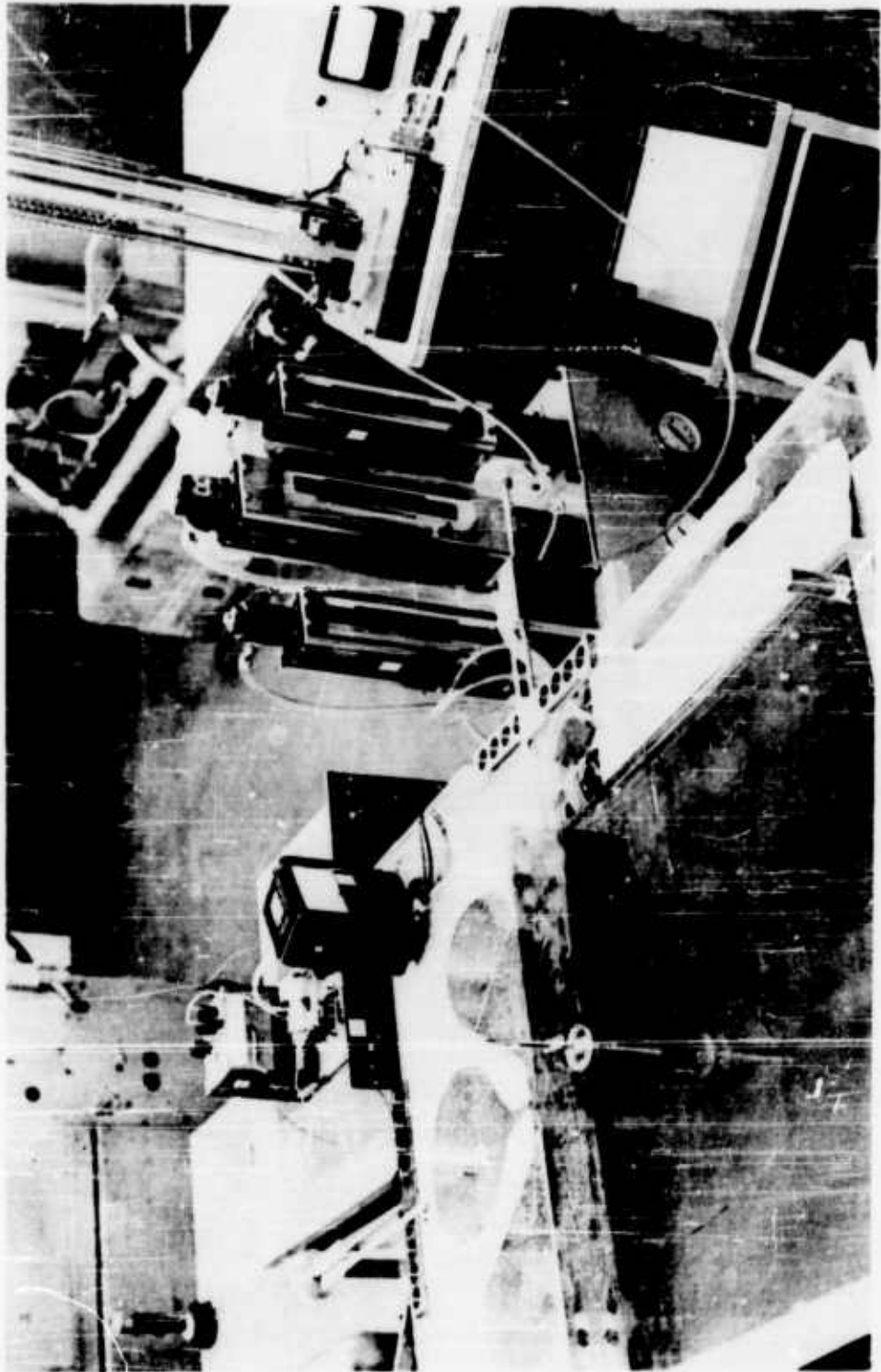
Figure 9. Jet interaction model.

139
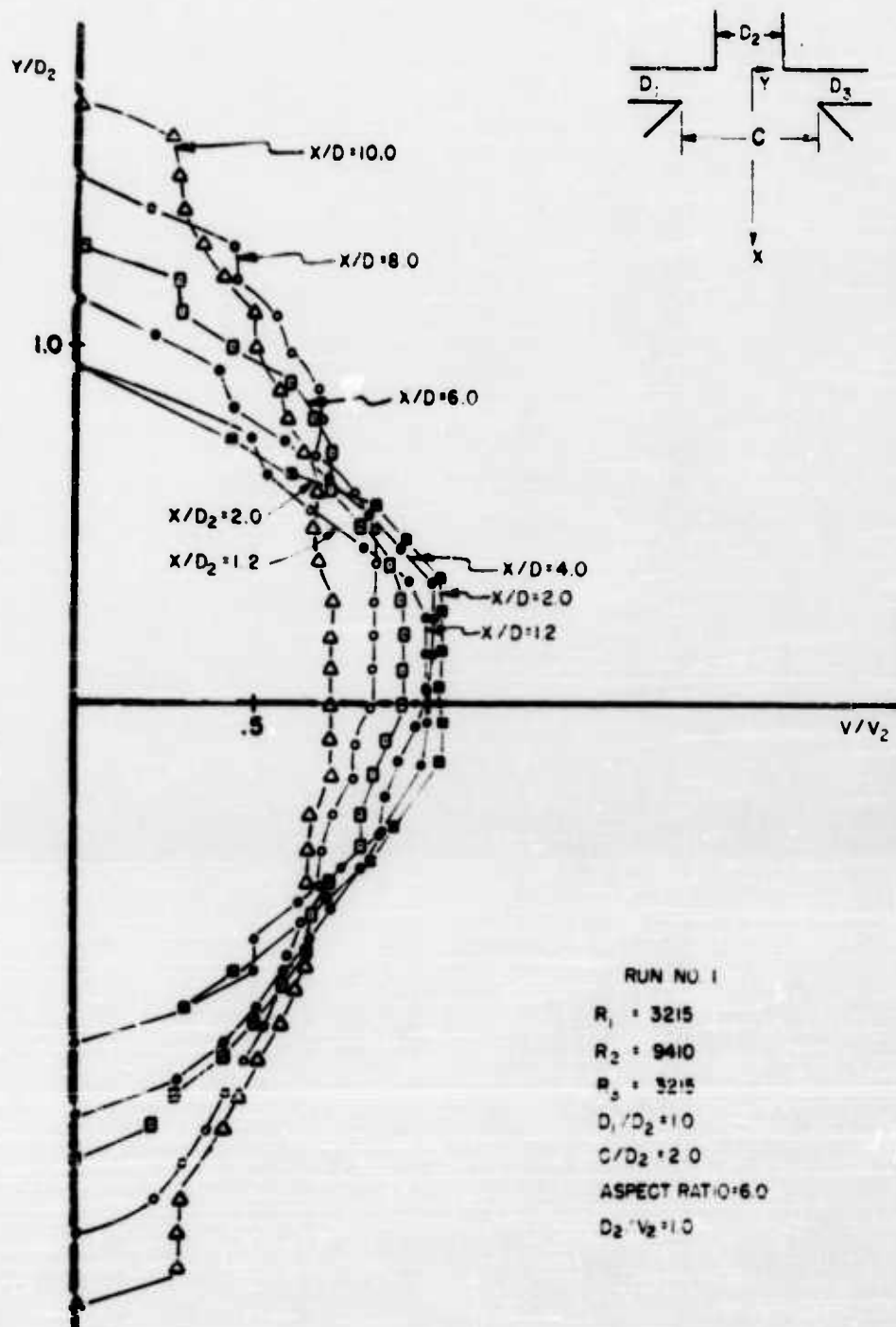
Figure 10. Experimental jet profile.

140
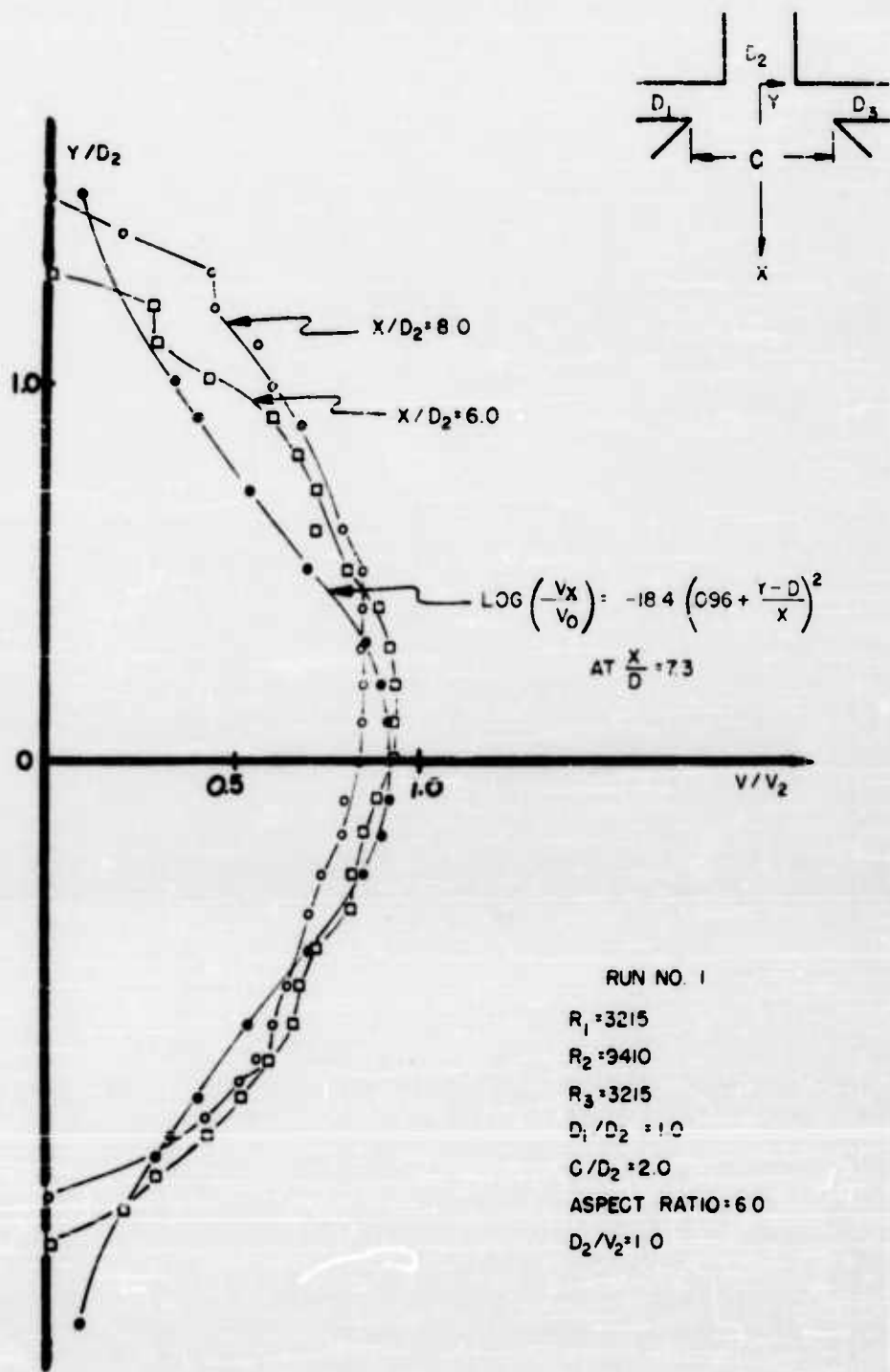
Figure 11. Comparison of experimental jet profiles with submerged jet theory.
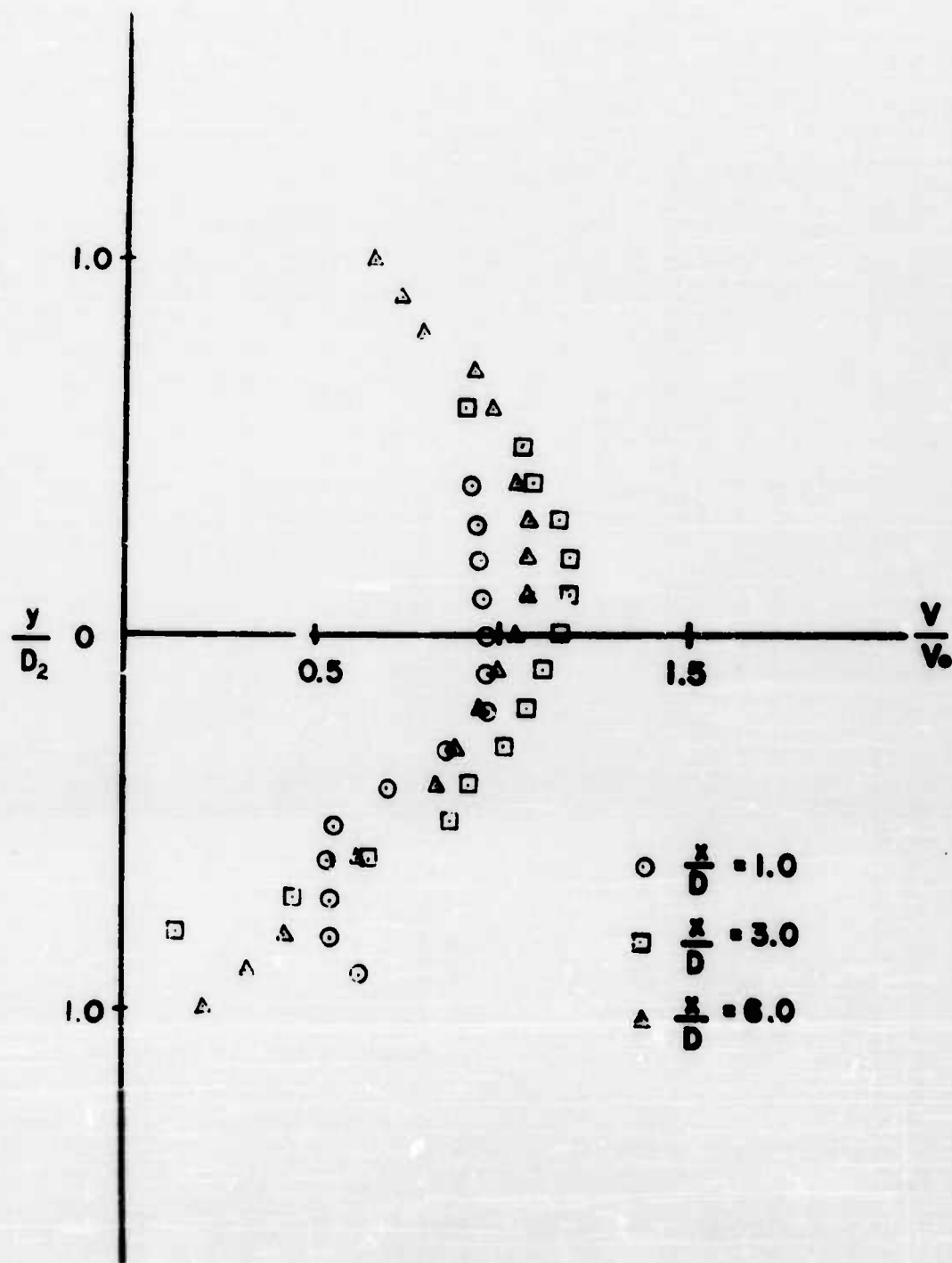
Figure 12.   Experimental jet profiles.

142

PRODUCTION OF FLUID AMPLIFIERS

BY OPTICAL FABRICATION TECHNIQUES

by

R. W. Van Tilburg

of

CORNING GLASS WORKS

Abstract:

A presentation is made of the results of a study of the applicability of optical fabrication techniques to the production of fluid amplifiers.

Advantages and limitations of Fotoform materials as they are related to the fabrication of fluid systems are discussed, along with data relating process variables and performance.

Designs submitted by The Diamond Ordnance Fuze Laboratory were optically transferred to sensitized glass plates, and the resultant patterns were chemically machined to the desired depth. A sufficient number of identical units were produced to permit evaluation of the effect of process variations on amplifier performance.

Variables inherent in the process were measured prior to sealing, and a table of dimensional variations and side wall and channel bottom roughness is shown. After sealing, operational characteristics were determined, and curves are presented. In this program, nozzles in the dimensional range of .020" x .080" to .030" x .090" were used with air as the fluid. All flows were subsonic. Production equipment was utilized for all fabrication, and the ranges of variation shown are typical for volume processing.

Results indicate that it is possible to fabricate the complex fluid amplifier designs rapidly and relatively inexpensively, and this can be done with a material which is dimensionally stable, capable of high temperature operation, unaffected by nuclear radiation, and impervious to most corrosive liquids and gases.

Introduction:

Although the process for making Fotoform products has been in commercial existence for more than five years, few applications have been investigated during that time which are more naturally suited to the process or material than the fabrication of pure fluid systems.

As indicated by the title, the primary purpose of this presentation is to discuss the production of fluid amplifiers by optical fabrication techniques. Production of a difficult product has been demonstrated with a proven process in a material which is uniquely suited to durable and reliable systems.

In introduction, it should be pointed out that a substantial part of the work leading to this discussion has been sponsored by the Diamond Ordnance Fuze Laboratories, and that all of the fluid amplifier designs discussed were submitted by DOFL personnel.

It is generally conceded that if the theoretically sound concept of pure fluid systems is to become a factor in the control and computation industries, an economical manufacturing process must be developed. Complex designs, such as the DOFL Test Pattern shown in Figure I, are not readily fabricated by high speed mechanical machining methods.
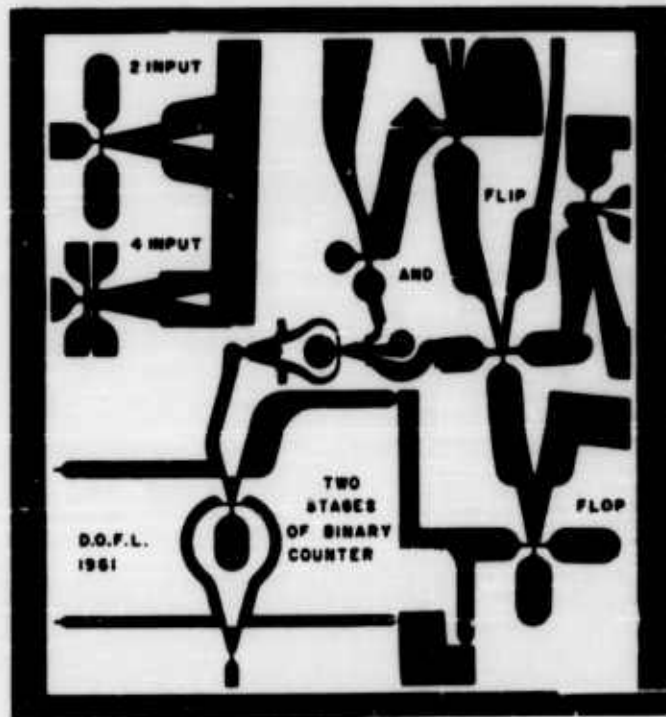
FIGURE I
DOFL Test Pattern - Average nozzle size approx-
imately 0.020"

144

The problem is further complicated by the fact that highly min-
iaturized devices such as the reproduction of the test pattern in
the size shown in Figure II are a prerequisite to maximum component
density and minimum system power consumption.

FIGURE II

DOFL Test Pattern - Average nozzle size approx-
imately 0.005"

Nozzles as small as five by twenty thousandths of an inch, such
as the one shown in Figure III, compared to a human hair, at fifty
times actual size, must be readily and precisely reproducible in a
material which is durable and thermally stable, and which can be
processed at a cost which will permit competition with established
electronic and mechanical devices.

FIGURE III

50 X magnification of cross section of nozzle
chemically machined in Fotoform glass and compared
to a human hair.

Perhaps the most difficult step encountered to date in the fabrication of high density fluid systems is the assembly of a multiple of miniaturized sub-plates containing active elements, through-holes and cross-over channels. Designs must be reproduced precisely to permit accurate registration of the through-holes, and any leakage of fluid within the system would quite probably render it useless. Not only is it necessary to guarantee the seal at fabrication, it must be guaranteed for the life of the device.

Digital type devices will not function if a short circuit exists between the power nozzle and either of the control channels; and in truly miniaturized systems, the partition separating these nozzles would not be over .010" wide. Assembly must be such that the systems will operate for years without the fear of a seal failure due to the loosening of bolts, the deterioration of gaskets, or the warpage and shifting of the laminated plates under thermal stress.

Fabrication Techniques:

The process for making Fotoform plates consists essentially of two steps: optical reproduction and chemical machining. Any design, no matter how complex, which can be drawn in black and white and photographed, can be reproduced. Light is passed through a standard negative into a sensitized glass plate which is then subjected to a thermal development cycle. The exposed portion is transformed into a crystalline phase which is approximately twenty times more soluble in dilute hydroflouric acid than the base glass. Since the rate of solution of the crystalline material is known, it is possible to machine to accurate depth by regulating the length of time the pattern is exposed to the acid.

Miniaturization of the patterns can be accomplished optically by simply reducing the negative, and design modifications can be made on the art work without fear of disturbing the acceptable portion of the circuit.

One of the really outstanding features of the process relative to the fabrication of the complex, miniaturized fluid systems is the ease with which through-holes can be introduced into the plates for interconnection to cross-over channels and other circuits in a multi-layer laminated system. The glass can be passed completely through the process more than once; and it is, therefore, possible to process the plate first with only the holes, and chemically machine them entirely out. The circuit pattern may then be superimposed on the hole pattern, developed, and chemically machined to the desired depth.

146

Due to the time consuming thermal development cycle, the process time is approximately twelve hours from art work to the finished piece; but in quantity production, continuous lehrs are used and an economical rate can be maintained.

For applications where extreme environmental conditions of shock or heat will be encountered, it is possible to convert the entire machined plate to a ceramic phase. This conversion is accomplished by flood exposing the entire plate and then passing it through a somewhat hotter thermal cycle than that used to develop the pattern. The resulting ceramic material is three times as strong as the glass, and will maintain its shape at temperatures as high as 500°C.

Although not directly associated with optical fabrication of fluid systems, it should be noted that both Fotoform and Fotoceram pieces are capable of being fuzed together into a monolithic structure at temperatures which will not destroy the basic patterns in the machined plates. This property of glass makes it possible to seal any number of plates so effectively that they become a solid, honeycombed mass which cannot be mechanically separated.

Although the process of thermal lamination precludes the possibility of disassembly of components for repair, it also substantially lessens the likelihood of the laminated plates separating under the most extreme operating conditions. In answer to the obvious question, if the systems should show a tendency to become fouled with foreign matter, any material, with the exception of glass, can be removed from the nozzle areas by flushing the entire system with an appropriate solvent, and this can be done in less time than would be required to disassemble, clean, and reseal, and with more assurance of success.

The final step in the fabrication of such a system is the attachment of the inlet and outlet part to the device. Since these component devices must be readily assembled and disassembled in the field, thermal fusion is not possible, but glass to metal sealing has been developed to the point that high temperature metal tubes with adapters to any standard tubing system can be firmly attached during fabrication.

Fotoform and Fotoceram Materials:

Although glass is generally considered to be a fragile material which must be handled with extreme caution, it becomes one of the most durable materials known when properly utilized.

It will maintain its integrity under extreme corrosion, vibration, and thermal conditions, and when converted to the ceramic phase, will withstand relatively high levels of impact.

A Fotoceram fluid system will retain its shape at temperatures in excess of 500°C, and if thermally laminated, heat will tend to strengthen the seal, rather than weaken it. Both the glass and the ceramic are impervious to most liquids and gases, are not affected in this application by nuclear radiation, and are dimensionally stable over long periods of operation.

Single Fotoform plates which have been etched to a substantial depth are admittedly weak and must be handled with a reasonable amount of care, but single plates are used primarily for development and testing, and the addition of each plate to a laminated system substantially increases its strength.

Dimensional Tolerances:

Almost the entire history of the process for making Fotoform products has been associated with products requiring only through-etching, in which the entire pattern is removed by machining from both sides simultaneously. As a result of this, limited data are available to establish dimensional tolerances for partially machined fluid amplifier patterns.

Efforts are underway to establish tolerances for fluid amplifiers, and these will be discussed later. For the present, it can be said that dimensions are generally being held as well as or better than in the standard process.

For the standard process, holes and channel widths up to 1/4" are maintained to $\neq$ .001", and diameters and widths between 1/4" and 1" are held to $\neq$ .002". Center to center dimensions are held within $\neq$ .003" in a 5" x 5" plate, and the tolerance maintained in depth control is $\neq$ .002" throughout a 5" x 5" plate.

In general, no dimension should vary by more than .002" from the target value, and in miniaturized systems variations from element to element are substantially less than .002", and within a given element are measured in ten thousandths. For example, the nozzle shown in Figure III which was selected completely at random from one of several elements fabricated for testing, was intended to be .005" wide, and .020" deep, with a nozzle area of .0001 square inches. As fabricated, it measures .0045" at the bottom, .0062" at the top, and .0193" in depth. The actual area is .000103 square inches, or approximately three per cent from the intended area. Measurements made on the other two nozzles of this bi-stable device show no variations over .0002" in any dimension.

148

These tolerances are for Fotoform materials only, and cannot be extrapolated to sizes over 5" x 5". During the thermal cycle used to convert to Fotoceram material, temperatures are reached which permit some sacrifice of dimensional control during ceraming. Dimensions within an element are reasonably stable, but center to center tolerances for spacing over three inches might approach ± .005".

The thickest glass sheet currently available is 1/4", and therefore, the thickest plate which can be made is somewhat less than this. With simple patterns which can be chemically machined completely through the glass without any segments becoming detached, it is possible to etch several identical patterns entirely through, and stack the plates one upon the other to an almost unlimited depth. For all practical purposes, however, the maximum depth to which the pattern can be recessed is about 0.125".

As previously stated, the rate of solution of the crystalline material is approximately twenty times that of the glass, and this means that, for every .020" of depth, the surface side walls will etch away .001". This results in side wall taper of approximately three degrees in all nozzles, channels, and holes, and places certain limitations on pattern design.

Referring to Figure IV, which is a DOFL Pattern designed to determine the extent of these limitations, several facts are immediately obvious.
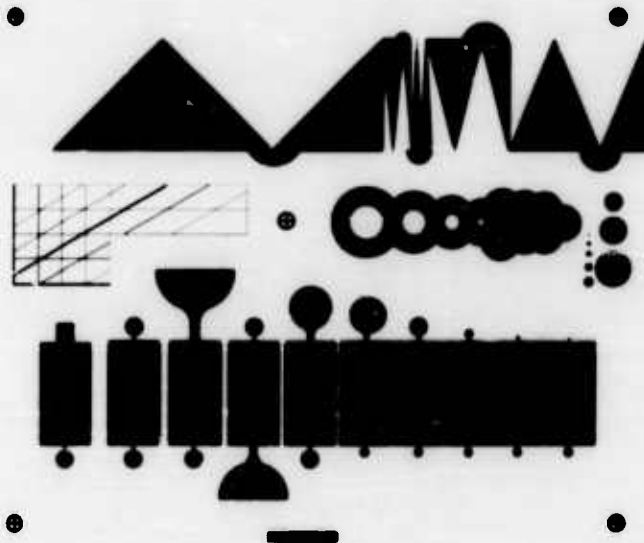
FIGURE IV
DOFL Test Pattern used to establish fabrication process limitations.

149

In the case of the narrow glass partitions separating the machined out rectangles, the .001" and .002" walls disappear almost as rapidly as the pattern, and the .005" wall, which is inadequate for sealing as is, does not last much longer. The .010" partition is marginally adequate for the shallow miniaturized systems, but for all practical purposes, it is necessary to separate all channels which operate under a pressure differential by a partition .020" wide. Obviously, the same situation is true for any posts which might be desired in open areas.

Nozzles must be designed at least .010" longer than necessary, because they will erode from both the interaction chamber side, and the nozzle chamber side. In the pattern, the two extremely small nozzles disappeared almost immediately, and the small nozzles on the opposite side of the chamber soon lost their identity.

The most difficult area to compensate for is that of the sharp wedges, used as splitters. As the pattern is dissolved, the wedge is attacked from both sides as well as the leading edge and soon loses its shape. If possible, sharp protruding angles must be avoided, but, when essential, they can be obtained by designing a radius on the end of the wedge which is calculated to disappear at the desired depth.

Narrow channels and small holes also present somewhat of a problem. In order for the chemical machining process to take place, it is necessary to maintain a supply of fresh acid at the interface. With the long narrow channels, and the very small holes, this is not possible; and the erosion rate is markedly reduced. Blind holes and channels with a width of less than .010" will lag in depth.

The .005" nozzle maintained the desired rate because it is exposed on two sides to relatively large chambers which permit the free flow of acid through the nozzle opening.

To date, no process limitations have been encountered which must be overcome by major design changes.

Design Tolerances:

An extensive program is underway to determine the effect of process variations on fluid amplifier performance so that improvements can be made to better adapt the process to the production of pure fluid systems.

150

Several proportional pressure amplifiers of a design supplied
by DOFL personnel were fabricated over a period of time by
different technicians to establish a group of devices repre-
senterive of the process. These underwent exhaustive testing.
The procedure was repeated with a digital memory device, also
designed by DOFL.

Ten of each of these devices were selected at random and com-
plete dimensional data were taken on a traveling stage optical
comparitor capable of measurement to a few ten thousandths of
an inch. These measurements were listed in order of magnitude
to permit rapid correlation with performance data.

In addition, traces of surface contour and roughness were
generated on a proficorder and listed in order of magnitude
for the same purpose.

Glass cover plates were sealed to the units both mechanically,
with various types of gaskets, and semi-permanently with epoxy
cement until it was found that better reproducibility from
seal to seal could be obtained with the latter method. Thermal
sealing of the cover plate was not employed because the per-
manent nature of such a seal does not permit disassembly of
the device after testing for inspection.

Standard static testing devices, including manometers, labor-
atory type test gauges, rota meters, pressure transducers,
and X-Y type recorders were installed, and procedures were
established for the generation of curves which would be rep-
resentative of the device, as well as the design, and which
could be used to establish relative levels of operation for
comparison with fabrication process variables.

Proportional Pressure Amplifier Performance:

Figure V includes a silhouette of the proportional device, a
normalized curve representing the test data, and a summary of
test conditions.

The device was fabricated exactly as shown, with relief
holes completely through the units centered in the circular
areas just downstream of the control nozzles. The power
nozzle is nominally .020" wide, and .060" deep, and the
control nozzles and receiver apertures are .030" wide and
.060" deep.
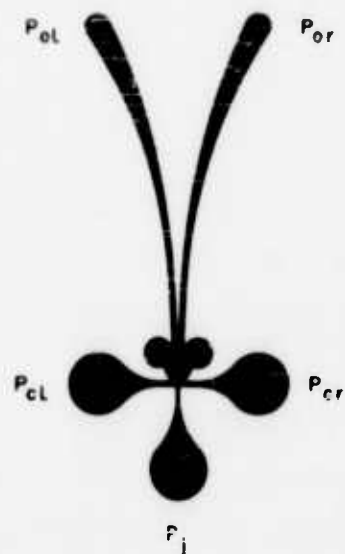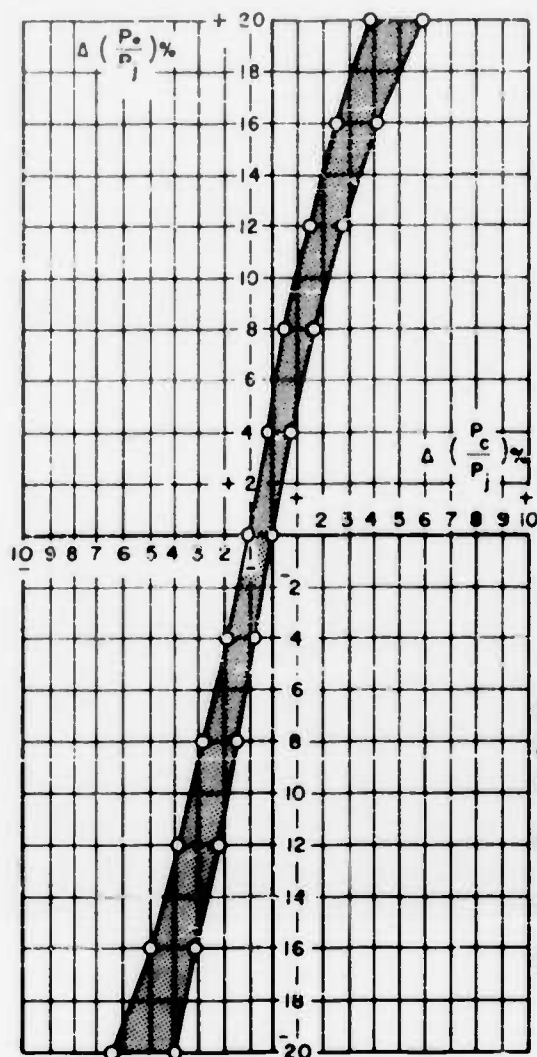
FIGURE V

Silhouette of proportional pressure gain amplifier
and chart showing range of pressure gain curves
for ten units.

For purposes of this comparison it was decided to generate a
curve of control pressure differential vs. output pressure dif-
ferential, the slope of which is the pressure gain of the unit
for the particular set of fixed conditions chosen.
152

Power jet pressure (P_j) was set at 5 psig, and the left control jet (P_{cl}) was set at 0.545 psig. The right control jet P_{cr} was driven from 0 psig to 1 psig. Back pressure was developed in the output legs by placing restrictions of an area equivalent to the area of the receiver apertures downstream. Air was used as the fluid.

Ten pressure gain curves were generated, and values of output pressure differential ($P_{or}-P_{ol}$) were determined for different values of control pressure differential ($P_{ol}-P_{or}$). These values were normalized by dividing by the power jet pressure, and plotted. The outside points were connected resulting in the broad curve shown. All of the curves were not parallel to these lines and a pressure gain range of 4.3 to 5.7 is represented.

The volume of dimensional and surface roughness data taken is such that it is not practical to include a complete analysis. However, the power nozzle variables listed in Table I are representative of the units tested, and clearly show the lack of correlation between the process variables and the pressure gain.

TABLE I

Proportional Pressure Amplifiers, A Summary of Pressure Gain, Dimensional and Surface Roughness Data.

Power Nozzle		Dimensions in inches				Average Roughness in micro inches	
			Width				
Unit	Gain	Top	Bottom	Average	Depth	Sidewall	Bottom
390	5.5	.0230	.0185	.0208	.060	124	18
509	5.1	.0239	.0199	.0219	.061	105	14
393	5.0	.0238	.0188	.0213	.063	89	16
396	4.9	.0237	.0189	.0213	.060	90	15
398	4.9	.0236	.0188	.0212	.060	102	8
394	4.8	.0238	.0185	.0211	.062	93	19
399	4.7	.0235	.0191	.0213	.060	100	9
494	4.6	.0238	.0202	.0220	.061	94	12
395	4.4	.0234	.0188	.0211	.060	105	3
508	4.3	.0237	.0204	.0220	.061	92	10

As indicated, the unit is slightly unbalanced, and a control pressure differential in the range of .03 pounds, or 0.6% of the power jet, is required for balancing. Throughout the central area of the curve the range of control pressure differential for the ten units, required to establish a given output pressure differential, was under 2% of the power nozzle pressure or less than 0.1 pound.

Even though all ten of the devices behave quite similarly, it is not possible to establish a relationship between performance and process variables, and there is apparently a variation in assembly technique which is over-riding dimensional and surface variations.

Bi-Stable Amplifier Performance:

Figure VI includes a silhouette of the bi-stable device, curves representing the test data, and a summary of test conditions.

The device was fabricated as shown, with all three nozzles .020" wide, and .080" deep. The receiver aperture areas are 0 100" wide, and .080" deep.

For purposes of comparison it was decided to plot the control pressure differential required for switching against power jet pressure.

With the left jet (C_1) open to the atmosphere, equal resistance applied to the output legs (O_1 and O_r), and the stream locked to the right wall, the right control jet was increased until the device switched. This procedure was repeated at 1 psig increments of power jet pressure (P_j) from 1 psig to 11 psig.

All of the points were plotted, and the extreme points were again connected to show the range. In this case, however, the curves differed in slope only, and did not cross as in the case of the proportional units.

As indicated, the range of control pressure differential required for switching increased from .04 pounds at a power jet pressure of one pound to 0.34 pounds at a power jet pressure of eleven pounds, and substantial room for improvement exists at the higher pressures. However, when the control differential values are reduced to a percentage of the power jet pressure, as was done in the lower curve, it can be seen that the control pressure differential required to switch one pound of power jet pressure remains quite constant, and that all ten of the units fall within a range of 4% of the power jet pressure.

No correlation can be established between fabrication process variables and performance variables with these devices, as was the case with the proportionals, and again it appears that there is an over-riding variable which must be detected and eliminated.

154
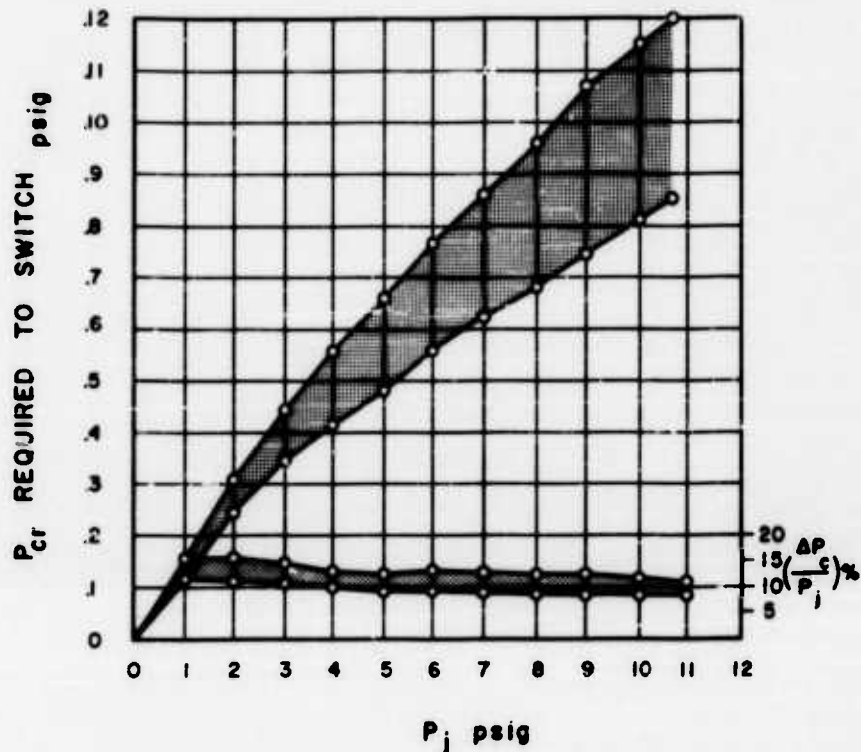
FIGURE VI
Silhouette of Bi-stable amplifier and chart showing
range of control pressure differential required for
switching. Data taken from ten units.

Conclusion:

Optical fabrication techniques make possible the fabrication of the
extremely complex patterns associated with pure fluid systems, and
the availability of Fotoform glass makes it possible to fabricate

155

these systems in a material which is durable, stable, and can be fuzed into a monolithic structure which cannot be separated at the seal to permit short circuits.

Fabrication techniques have been developed to the point that process variations in the sub-plates have less of an effect on performance than assembly variations, and the total variation has been reduced to the point that economic production of pure fluid systems will become a reality as soon as adequate functional designs become available.

Any fears that fabrication costs will retard the entry of fluid systems into the control and computation markets should be quickly dispelled by the fact that the process and equipment used to fabricate complete fluid amplifier plates are in use every day supplying the electronics industry with circuit boards for mounting expensive components.

156

"OPTIFORM", OPTICAL MACHINING OF PURE FLUID SYSTEMS IN PLASTICS

by

Romald E. Bowles
John R. Colston

of

Bowles Engineering Corporation

ABSTRACT

Optiform is a low-cost, fast, production technique for machining con-
stant-depth Pure Fluid Systems in plastic. The optical machining is accom-
plished by using a master silhouette to define the areas of a conditioned sheet
of plastic which are exposed to ultraviolet light and consequently polymerized.
The unexposed areas remain soft and are washed away using a sodium hydroxide
solution. From the standpoint of Pure Fluid Systems, Optiform has limitations
as to maximum temperature (150°F) and minimum size of components which can
be processed as a production line product, i.e., with limited inspection. The
basic circuit plate is assembled with a transfer plate and a manifold plate to
provide a rugged package having a thick aluminum surface front and rear and
can be further protected by addition of an aluminum channel like a picture
frame to protect the edges of the assembly where the plastic edge is exposed.
Standard Clippard fittings tapped into the aluminum base plates provide an
easy means for connecting the system inputs and outputs to auxiliary equip-
ment. With Optiform and a file of silhouettes of components of known perform-
ance characteristics, one can assemble a pure fluid control system at the
drawing board with high probability that the first of the resulting low-cost,
short-lead-time production models will function properly.

INTRODUCTION

Optiform is a low cost process for machining constant-depth forms in
plastic. It has been developed specifically for production of Pure Fluid
Systems. The plastic can be used with most gases and fluid hydrocarbons (but
not with water) as a working fluid. The paper covers the following points:

What is Optiform?
How is the Optical Machining Accomplished?
What are the Limitations from the Standpoint of Pure Fluid Systems?
How does an Optiform Plate Become as Assembled Pure Fluid Control
  System?

WHAT IS "OPTIFORM"?

Optiform is a low-cost process for machining constant-depth forms in plastic. It is suitable for production of Pure Fluid Systems. The plastic can be used with gases and fluid hydrocarbons but is not recommended for use with water as the working fluid.

The raw material is a DuPont photopolymer widely used in the printing industry under the trade name of Dycril*. The printing industry process is not suitable for Pure Fluid Components or Systems because the resulting sidewall slopes are excessive and there is wide variation in channel depth. The Optiform plates are designed for use in Pure Fluid Systems. The raw material is available bonded to aluminum or steel in several thicknesses and sizes; however, we have standardized on one class for the present time. The standard Optiform plate is 9" x 12" x .150". The .150" $\pm$ .002" thickness includes .042" $\pm$ .002" of plastic, an adhesive layer, and a .100" thick aluminum base plate.

HOW IS THE OPTICAL MACHINING ACCOMPLISHED?

Four Steps of the Process

Conditioning

The plate is first conditioned in a controlled atmosphere to establish the plastic sensitivity to ultraviolet light as a function of depth (Fig. 1a).

Setup and Exposure

Next the "master silhouette" is clamped to the unexposed plate in a vacuum frame and the assembly is exposed to ultraviolet light (Fig. 1b). The silhouette areas which are clear permit the ultraviolet light to irradiate the plastic and polymerize it so that those areas become hard. The silhouette areas which are opaque shadow the plastic so that those areas remain soft.
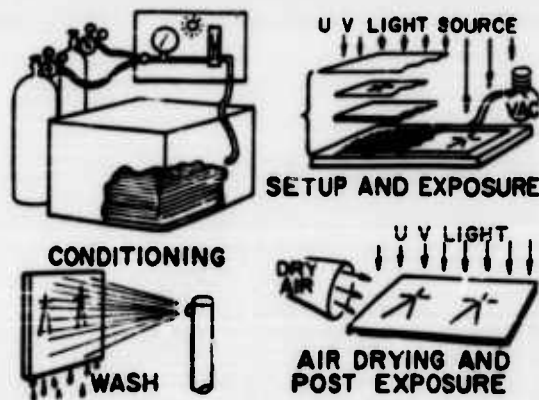
Fig. 1 OPTIFORM "A" PROCESS

* Donald B. Hurd, Printing Plate Laboratory, E. I. DuPont De Nemours and Co., Photo Products Department, 1309 Noble Street, Philadelphia, Pennsylvania

158

Wash

Next the exposed plate is sprayed with a sodium hydroxide solution to remove the soft unexposed plastic and thus create the desired channels (Fig. 1c).

Drying and Post Hardening

Finally the washed plate is air dried and further exposed to ultraviolet light so as to achieve maximum strength and hardness of the remaining plastic (Fig. 1d). Figure 2 presents curves based on very limited data showing how the plastic's strength is affected by temperature and humidity. We recommend use of this plastic below 150°F. Shop quality air is acceptable as a working fluid as are most gases and fluid hydrocarbons. While we have operated Optiform systems for short periods using water as a working fluid, we do not recommend such use for extended periods of time as the plastic appears to soften, swell, and lose strength.
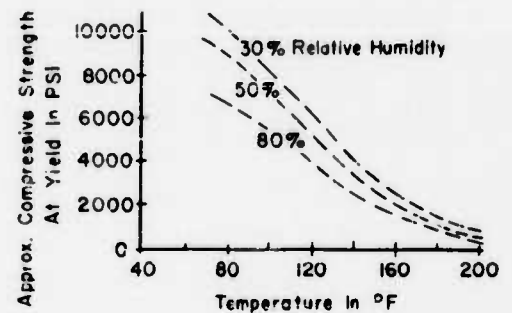
Fig. 2 EFFECT OF TEMPERATURE AND HUMIDITY ON THE PHOTOPOLYMER PLASTIC

The Master Silhouette

Preparation

Conventional automated machine tools use punched tape, magnetic tape and punched cards as a control to establish the machined product contour. Similarly, in optical machining a slide or silhouette is used as the control. After one develops a component of known performance characteristics, its silhouette can be duplicated (large scale) photographically or on an ozalid machine using clear transparent stable base film. With time, a file of silhouettes of such components is readily established and can be used to construct the silhouette of a desired system on the drawing board. Interconnections can be inked in and the large scale system silhouette is then ready to be photoreduced by a precision process to provide a full-scale master silhouette.

59

Example

Figure 3 shows the silhouette of a standardized binary counter stage component and the silhouette of a subsystem built up from such standard silhouettes of components as described above.

Suitable Material

The final full scale silhouette must be on a material which is suitable for the production line. The Kodak Autopositive film on .004" clear estar base is a suitable material for an Optiform process

Fig. 3 MULTI STAGE BINARY COUNTER

"master silhouette." This film is matched to the "Optiform Process A" production line. The transparent areas transmit the correct amount of ultraviolet light and the opaque areas are properly opaque in the ultraviolet spectrum.

This transparancy is the "suitable master silhouette" which should be furnished in a standard 10" x 12" size for production of a standard 9" x 12" Optiform plate.

WHAT ARE THE LIMITATIONS FROM THE STANDPOINT OF PURE FLUID SYSTEMS?

Performance

First, it is emphasized that this process has been used to make working pure fluid components and systems. Some comparison and performance data are presented in the papers of Humphrey-Metzger, Dexter, and Bauer which are part of this symposium. Units are undergoing operation life tests. The output wave form of a logic element is being monitored and has shown no change in over 70 million cycles. No change is anticipated.

Changes in silhouette are sometimes necessary in making a transition from a machined model to an Optiform model. In particular such changes may be necessary if the aspect ratio (nozzle height ÷ nozzle width) is different in the two models. To bypass such effects we now do almost all of our experimental work using Optiform models, cutting away material and filling with clay to make quick contour changes. When the final design is reached, a photograph is taken to use as a guide in drawing the master silhouette. As would be expected there are limitations as to what configurations can be repeatibly reproduced by the process. These are discussed later. The overall Optiform

process is a compromise based on the performance characteristics of beam deflection type pure fluid amplifiers. Some component designs may be more critical dimension-wise than those already tested even though they have the same scale. Therefore we cannot say Optiform is suitable for every type pure fluid element. We can say that Optiform has been suitable for the pure fluid components we have tried, wherein the acceptability is based on performance as a fluid component.

Tolerance

Standards

Let us consider each dimensional tolerance which affects performance and assign numbers to these tolerances. This has advantages when one must make a transition from one production technique to another. In a pure fluid component the critical regions from a performance standpoint are associated primarily with characteristics of the nozzles, interaction region, and divider leading edges (Figures 4 and 5). In the following, two numerical values are presented for each physical characteristic which currently appears to be important. In each case the value A represents the current evaluation of reliable repeatability for Optiform Process A and the value B represents an idealized generalized goal, i.e., if we had such a capability we would not feel justified in spending money to further improve the process based on what we currently know and forcast about pure fluid systems. This does not mean that the "B" values are required by Pure Fluid Systems but rather that such dimensional control would open up many additional areas of application. It is emphasized that the "B" values are only an opinion and are not based on detailed tests.

Sidewall location

It is necessary that one be able to predict sidewall location on a basis of the master silhouette dimensions. It is also necessary that sidewall location not vary excessively with height above the channel floor.

Figure 5 indicates the character of sidewalls which result from the Optiform Process A.
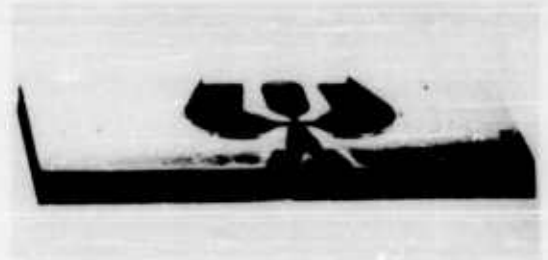
Fig. 4 CROSS SECTION OF FLUID AMPLIFIER

161

"A" In Optiform the wall center-line is displaced +.001" from the edge of the opaque silhouette. This displacement is a character-istic of the process and is repeat-able as a result of our production line quality control. If desired one can allow for this displacement in the nozzles and critical areas of the silhouette. We normally do not compensate for this feature when nozzle width is of the order of .020" because the units can be scaled undersize if desired without hurting their performance characteristics.
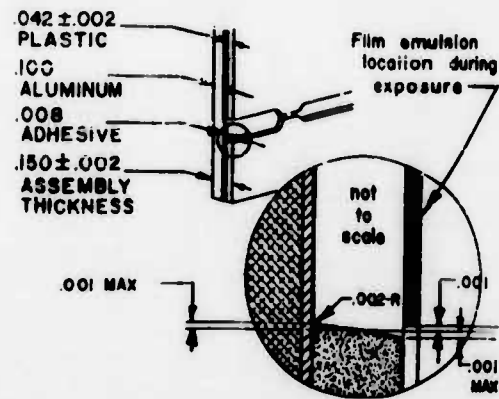
Fig. 5 PROFILE OF OPTIFORM PLATE

"B" In an idealized process the wall centerline should be identified within +.0001" of the edge of the opaque silhouette.

Deviation of sidewall from the vertical

"A" The sidewall contour is subject to both process effects and batch effects. Process effects depend upon how rigidly the production line is con-trolled and is therefore part of the Optiform process control. Batch effects are a function of the raw material available and are beyond control process. For example, in Figure 5, it is illustrated that the sidewall of an Optiform channel will have a .002" radius fillet at the root of the wall. This is a function of the process. It is also shown that the Optiform sidewall may deviate up to $+3^{\circ}$ from the vertical. In such case the root of the sidewall may be up to .001" closer to the opaque silhouette and the crest of the wall up to .001" farther from the silhouette than the wall centerline. In Optiform the sidewall does not have a constant slope; however, by process control we maintain sense of the sidewall slope. Sidewall slope contour is definitely also a function of the batch of raw material which we receive. We have tested batches wherein the sidewall is vertical within $\pm$ .0005" for a .042" wall height. As the raw material supplier becomes better acquainted with the needs of Optiform and the relationship of his process controls to these needs we anticipate an improved final product. Batches which test to less than $\pm$ .001" are felt to be acceptable for .042" deep Pure Fluid Systems. This is a mean slope of less than $+3^{\circ}$. Batches with greater deviation are not accepted for the Optiform process.

"B" In an idealized process this slope would be $+1/10^{\circ}$.

162

Surface roughness

This is an unknown factor which affects the character of the boundary layer flow.

Sidewall roughness

"A"   16-63 microinch in Optiform A.

"B"   0-5 microinch idealized goal, useful in laminar flow conditions.

Bottom of channel roughness

"A"   0-16 microinch in Optiform A

"B"   0-5 microinch idealized goal, useful in laminar flow conditions.

Fillet radius at root of wall

The importance of a fillet at the root of a wall depends upon the aspect ratio. For large aspect ratios such a fillet has little importance; however, we have encountered measurable performance changes apparently due to slight full-width fillets when using aspect ratios of 8. These effects appear at the extreme high pressure operating limit of the device. In a digital unit the result is to lower the maximum operating pressure limit.

"A"   .002" maximum in Optiform process A.

"B"   .0001" idealized goal.

Minimum channel width: short channel

In optical machining the minimum channel width is limited by aspect ratio, (channel depth ÷ channel width). As a rule of thumb one generally avoids an aspect ratio less than two and would like an aspect ratio of the order of four in the nozzle throat. Such aspect ratios provide a jet which is substantially two dimensional and which is not spread unduly by top and bottom wall friction within the interaction chamber. If the nozzle throat width is .010" or greater no dirt problem is anticipated for shop quality air. With an aspect ratio of four or greater it may be feasible to reduce the throat width to .005" without a dirt problem. With a "clean" system nozzle a throat width of .002" is of interest. The area of a component is proportional to the square of the throat width. Thus a reduction of nozzle width from .020" to .010" increases the component density on a plate by a factor of four. In addition the power consumption of a unit will be reduced approximately by a factor of two if nozzle width is reduced from .020" to .010". All of the above assume no change of channel depth. If the aspect ratio is kept constant than the

volume density of components is proportional to the cube of nozzle width and power consumption per unit is roughly proportional to square of nozzle width. System speed capabilities are roughly proportional to nozzle width in that the distance over which a signal must be transmitted is approximately proportional to nozzle width. Thus the minimum channel width is important on a basis of cost, weight, volume, system power requirements, and system speed.

Figure 6a illustrates a converging nozzle. The dimension W is the nozzle width and the length indicated as 2W is a straight section desirable for control of jet direction.

"A"   For a short channel of .042" depth and length 2W, minimum width is .020" in Optiform process A. We have worked with Optiform nozzles down to .010" wide; however, they do not yet have the repeatability we believe necessary for a production process.

a) NOZZLE   b) WEDGE

c) WALL   d) POST & HOLE

Fig. 6 QUALITY CONTROL POINTS

"B"   An idealized goal is W= .002". This would permit a major improvement in component density and system speed. Pure Fluid Systems have a built in cooling system and do not encounter the heating problems often associated with high component density electronic packaging.

Minimum channel width: long channel

"A"   For a long channel of .042" depth, minimum width is .025" in Optiform process A. Narrower long channels sometimes result in spotty full width fillets at the root of the channel.

"B"   .0005" is an idealized goal useful in precision resistor designs.

Minimum corner radius

Male wedge

The exit corner of a nozzle effects direction of jet flow and the sensitivity to control signals. If the exit corner is very sharp it is easier to repeat fluid performance characteristics than it is if the corners are rounded. Thus from a nozzle exit standpoint, see Figure 6a, it is desirable that such 90° wedges have extremely sharp radius of curvature at the corner. The divider

164

on the other hand is normally a sharp male wedge. At such a sharp apex one encounters a problem of structural strength and ability to predict location of the divider leading edge.

Consequently while Optiform provides a male corner radius capability of .002" or less, a sharp wedge should be artifically blunted as shown in Figure 6b if the included angle α is less than 30°.

A male wedge is illustrated in Figure 6b with an apex blunted by a flat "b". It is recommended that in Optiform Process A if the male wedge angle α is less than 30°, a .010" bluntness be designed into the wedge apex. This firmly establishes the apex location and provides ample strength.

"A"   .002" in Optiform process A (see recommendation above for $\alpha < 30^{\circ}$).

"B"   .0001" idealized goal based on .002" nozzle width.

Female wedge

The corner radius of a female wedge is usually less critical in a pure fluid system design. Consequently this capability has been sacrificed in compromising parameters of the production line.

"A"   .010" minimum radius in Optiform process A.

"B"   .001" idealized goal.

Minimum wall thickness

Walls are used to guide the flow of fluid and to separate two channels of different pressures. As wall thickness is decreased the well becomes less stable structurally and the top surface becomes harder to seal against leaks. In Optiform, wall stability and location become a problem before one encounters poor top surface problems.

"A"   For a .042" wall height the .015" minimum or a 5° minimum wedge angle is recommended on a general basis for Optiform, see Figure 6c.

"B"   .002" minimum is an idealized goal for a structurally stable sealable wall.

Minimum Post diameter

Posts are used both as support columns and to establish particular flow conditions in a system.

"A"   For a height of .042" we are able to provide a stable full height post down to a .012" minimum diameter in Optiform process A.

"B"   .001" diameter capability would be useful for current designs.

Minimum hole diameter

Isolated small holes are not used as often as holes adjacent to and connected with larger open areas. The isolated full .042" depth hole is indicative of such a capability.

"A"   .030" minimum diameter is recommended for Optiform process A. Smaller diameters do not always wash the full depth.

"B"   .0001" minimum diameter is an idealized goal based on the .002" nozzle width goal.

Physical properties

"A"   Optiform plates have serious limitations. In particular, they cannot tolerate high temperature and cannot, for any length of time, use water as a working fluid without change in dimension or strength. Figure 2 illustrates some of the effects of temperature and humidity on strength of the plastic used for Optiform plates. The following physical properties are based on very limited data and are approximate values for 77°F and 50% relative humidity. The raw material supplier is assembling additional data.

tensile strength	9,500 psi
compressive strength	9,500 psi
compressive strength at yield	9,400 psi
modulus of elasticity	100,000 psi
compressive bulk modulus	150,000 psi
surface hardness	D82 to D86 shore
density	.042 lb/in^3
thermal conductivity	1.61 BTU in/hr ft^2 F^o

"B"   The ideal material for a pure fluid system depends upon the individual application. A generalized ideal material does not exist; however, stainless steel looks very good.

Limitations on idealized goals

The above capabilities of the Optiform Process A and the idealized goals (our opinion only) offer a guide as to generalized dimensional tolerances which one might encounter in pure fluid systems work. They have not been firmly tied to the component operating characteristics. Indeed one component might tolerate ± .1" tolerances in the interaction region whereas a different type of

166

component might exhibit an unacceptable change of characteristics unless tolerances of $\pm$ .001" were maintained. The values presented are generalized very broadly and should only be used within this limitation.

HOW DOES AN OPTIFORM PLATE BECOME AN ASSEMBLED PURE FLUID CONTROL SYSTEM?

Parts

Figure 7 shows a front and rear view of an Optiform circuit plate. This particular sample is the result of an exercise we conducted some time ago to establish the problems of transition to a finished piece of hardware.

The assembled system consists of: (1) a circuit plate, (2) a transfer plate (having through holes appropriately located at P+ locations to supply power to each element, and holes at P_O locations to extract a components output signal for transfer as an input to another component in the circuit

Fig. 7 FRONT AND BACK OF OPTIFORM CIRCUIT

plate, and holes at the corresponding P_C locations to insert control signals being transferred), and (3) manifold plate which both distributes P+ to the correct transfer holes and provides channels which connect the output signal transfer holes to the appropriate control signal transfer holes.

Assembly

These three plates can be assembled by clamping using gaskets. Care should be exercised, as with any plastic models, that the clamping pressure is not so high as to cause cold flow of the plastic. We prefer to bond the three plates together using adhesives. This avoids cold flow of the plastic and we think also provides a greater reliability than is obtained using gaskets.

Connections to Other Equipment

The aluminum backup plate is readily punched and tapped for more conventional fittings. We have found that Clippard hose fittings* are very suitable

---

*10-32 to 1/8 hose fitting, Part # 11752. Clippard Instrument Laboratory, Inc., 7390 Colerain Road, Cincinnati 39, Ohio.

167

as input-output connections to either plastic tubing or rubber hose to connect the assembled pure fluid system with other apparatus.

The Final Package

The completed assembly presents a strong structure with rugged aluminum exterior surfaces except at the edges. If desired a picture frame type channel can be wrapped around the 9" x 12" package to protect all of the plastic material from external damage.

SUMMARY

Optiform is a low-cost, fast, production technique for machining constant-depth Pure Fluid Systems in plastic. The optical machining is accomplished by using a master silhouette to define the areas of a conditioned sheet of plastic which are exposed to ultraviolet light and consequently polymerized. The unexposed areas remain soft and are washed away using a sodium hydroxide solution. From the standpoint of Pure Fluid Systems, Optiform has limitations as to maximum temperature (150°F) and minimum size of components which can be processed as a production line product, i.e., with limited inspection. The basic circuit plate is assembled with a transfer plate and a manifold plate to provide a rugged package having a thick aluminum surface front and rear and can be further protected by addition of an aluminum channel like a picture frame to protect the edges of the assembly where the plastic edge is exposed. Standard Clippard fittings tapped into the aluminum base plates provide an easy means for connecting the system inputs and outputs to auxiliary equipment. With Optiform and a file of silhouettes of components of known performance characteristics, one can assemble a pure fluid control system at the drawing board with high probability that the first of the resulting low-cost, short-lead-time production models will function properly.

INSTRUMENTATION FOR RESEARCH AND DEVELOPMENT IN PURE FLUID SYSTEMS

by

Ronald L. Humphrey
Eric E. Metzger

of

Bowles Engineering Corporation

INTRODUCTION

Some flow and pressure measurements in Pure Fluid Systems can be made with instruments adapted from other fields --- others require new types of instruments. Examples of both are discussed in this paper.

THERMISTOR ANEMOMETER

A hot thermistor anemometer has been developed and shown to be very useful as a Flow-No Flow indicator with the thermistor mounted in a channel type probe. This instrument has been designed as a visual (light) flow indicator for use with displays and as an indicator of the existence or non-existence of flow in very low-power fluid devices and systems. This instrument also has proved useful in development work and production checking.

Figure 1 shows the Flow-No Flow indicator and a channel probe. The indicator is simply a bridge using a single transistor as both a bridge balance detector and a switch to turn the light on and off. This instrument is constant-current operated and needs a direct-current power supply.

Figure 2 shows the indicator's typical sensitivity curve of flow versus level adjust setting. The instrument is usable over a velocity range of 0.5 to 500 ft/sec. The steep slope seen in Figure 2 illustrates the capability of the instrument to indicate the difference between two flows from 0.5 to 5 ft/sec in approximately 0.5 ft/sec increments. The frequency response of the instrument is DC to 10 cps. This is quite satisfactory considering that the typical response of the human eye is 12 to 14 cps. The device may be used with most gases, excluding only those which would attack the probe body, thermistor or wire materials. Operation has been found satisfactory over a temperature range from zero to 30°C for ambient and gas.

The standard probe body used is made of plexiglas or epoxy and designed to fit 1/4 inch o.d. tubing and insure a smooth transition from tubing to probe. The flow sensor is a standard thermistor 0.007 inch in diameter. The thermistor could be mounted in any channel, such as in Optiform models, where gas velocities are within the instrument limitations.

One of many applications was a series of flow indicators displaying the outputs of a five-stage pure fluid binary counter.

A LOW COST HOT WIRE ANEMOMETER

A hot-wire anemometer has also been developed and become very useful as a Hot-Wire indicator with the wire mounted in a channel probe. This instrument has been designed to be used in conjunction with an oscilloscope for displaying pneumatic wave forms.

Figure 3 shows the Hot-Wire indicator and a channel type probe. The indicator is simply a bridge with a balance adjustment. The instrument is constant-current operated and needs a direct-current power supply.

Figure 4 shows the indicator's typical sensitivity curve of velocity versus output voltage in millivolts. Figure 4 also shows that this instrument can readily indicate small changes over a velocity range of one to 500 ft/sec. With this instrument the DC versus AC velocity may be easily measured and compared by simply monitoring the DC output of the device when it has been initially balanced to zero at zero flow. The frequency response of this instrument is DC to 300 cps (-3db) at a velocity of 160 ft/sec. At lower velocities the response is less (approximately DC to 115 cps at a velocity of zero ft/sec). These curves are shown in Figure 5. The frequency response was obtained by using the standard square-wave calibration technique. This instrument may be used with most gases, except those which would attack the probe body or wire materials. Operation has been found satisfactory over a temperature range of 20 to 25°C for ambient and gas.

The standard probe body is the same as used with the Flow-No Flow indicator. The flow sensor is a 0.0002 inch diameter gold-plated tungsten wire approximately 0.300 inch in length, with an approximate R_{cold} of 15 ohms. Tungsten wire offers needed strength for mounting, while the gold plating reduces oxidation of the wire surface and allows a more reliable R_{cold}. The length reduces end effects of the mounted wire thereby increasing the frequency response of the uncompensated wire. Hot wires are not limited to this type mounting and have been mounted within the plastic elements being monitored.

Figure 6 is a block diagram of a switching time measurement circuit using three standard Hot-Wire indicators for measuring the switching time of a pneumatic "OR" gate. This diagram shows the "OR" gate in a pneumatic circuit operating under true load conditions.

Figure 7 shows the oscilloscope trace of the switching measurement made on the "OR" gate shown in Figure 6. The switching time was measured to be 0.5 milliseconds, with a point-to-point switching time of approximately 0.2 milliseconds. Point-to-point switching time is the time that it takes the power jet to switch from one side of the divider point to the other side of the divider point.

Figure 8 shows the output of a pneumatic "OR" gate made of Optiform as measured with a standard Hot-Wire indicator. The sweep rate is 20 milliseconds per centimeter.

The Hot-Wire indicators have also been used to measure signal-to-noise ratios and output wave forms of various pneumatic elements and systems.

In many applications of this Hot-Wire indicator, the DC flow was sufficient to saturate the wire and thereby make it less sensitive to small AC flow changes. However, a technique was developed which reduced the DC flow and mainly passed AC flow, therefore extending the useful range of the hot wire. This involved placing holes and slots along the length of pneumatic tubing leading to the hot wire. Very little AC flow distortion has been noticed due to the holes and slots being present in the tubing.

MINIDUCER

A miniature piezoelectric transducer for aerodynamic and acoustic pressure measurements is being developed. The transducer is made from a modified lead zirconate titanate ceramic material. The size of the transducer is 0.030 x 0.060 x 0.250 inches with 0.030 x 0.060 inches being the size of the sensitive area. This area is important where resolution is a problem.

Figures 9 and 10 show the Miniducer in three states. The pressure sensor is shown unmounted, mounted in a pneumatic flip-flop, and as an acoustical transducer.

Figure 11 shows the sensitivity curve of a Miniducer mounted as a pressure sensor in a pneumatic flip-flop. Sensitivity checks were made at various points from 0.1 to 10.0 psig. The instruments used for this calibration curve were a Kistler Charge amplifier and a Brush recorder.

Figure 12 shows the free-field frequency response of a Miniducer mounted for acoustical measurements. The acoustical driver for this measurement was a DuKane tweeter, and the output of the transducer was fed into a Kistler Charge amplifier and then to a Tektronix oscilloscope.

Figure 13 shows the Miniducer output while being driven by a 30 KC signal from the DuKane tweeter.

FIBER OPTICS MONITOR

A Schlieren system has been adapted to make high-frequency measurements in small elements and systems. The Schlieren field was examined by a Fiber Optics Monitor, consisting of four channels containing light guides, photomultipliers, and amplifiers. The Monitor is shown in Figure 14. The time of arrival of pneumatic signals was measured with this instrument by the detection of the change of illumination in the Schlieren field produced by variations in density gradients in the air flowing through the pneumatic element under test. The sensitivity and bandwidth of photomultipliers made them ideal for detecting small changes in light level in these experiments, but they are unwieldly when small sources of light must be examined. This difficulty was overcome by using the light guides to conduct the light from the Schlieren field to the photomultiplier cathode. These light guides consist of many optical fibers bundled together to form an efficient and flexible light conductor 3 feet long with a light, mobile entrance aperture 1/16 inch in diameter.

Figure 15 shows the experimental arrangement used, with the observer looking into the exit aperture of the Schlieren. The focal length of this Schlieren is 80 inches with an aperture of 6 inches. It was manufactured by the Unertl Optical Company of Pittsburgh for use in our laboratory.

A plastic Pure Fluid element is shown in Figure 16. Figure 17 shows the element under test. The solenoid valves shown on the slide were driven by a cycling timer, so that they were nearly 180 degrees out of phase. No particular effort was made to insure exactly 180 degrees phase shift, nor to establish exactly what the phase shift of the control jet pressures actually was during the experiments. The timer was run at 1-1/2 cps, with a separate trigger pulse for oscilloscope synchronization. The two states of the switching element are shown in Figures 18 and 19, which are photographs of the Schlieren image. The position of the light guides in relation to the channels cut through the element is shown in Figure 20, which is the image of the channels with two light guides in place. These images were masked to 18 mm to exclude all extraneous parts of the fluid element, which left the sections shown here magnified 4x by the Schlieren system itself.

The change in output of the Fiber Optics Monitor when the element was switched is shown in Figures 21 and 22. The ripple is 60 cycle from the Schlieren light source. An analysis has not been made of the structure of the switching transient. The data shown indicates a switching time of less than 7 milliseconds. The signals indicate, however, that the first effects on both the output channel flows appear in a much smaller time.

SUMMARY

The field of Pure Fluid Systems has been somewhat handicapped by a lack of suitable instrumentation. The general problems have been related to:

      (1) small passageways
      (2) cost per channel
      (3) sensitivity
      (4) high speed transient characteristics

Each instrument discussed in this paper was designed for a specific purpose. For example:

Thermistor Anemometer --- A visual indicator for quickly checking a large number of flow passageways.

Hot Wire Anemometer --- Indicators used in conjunction with oscilloscopes. They can be used to study the wave forms of various pure fluid components.

Miniducer --- Miniature piezoelectric pressure sensors for use in small channels.

Fiber Optics Monitor --- Combines high response with small sensors for the study of transients of density in the air flowing through pure fluid elements or systems. (Used cooperatively with shadowgraph, schlieren, or interferometer.)

With the previously mentioned instruments it is economically feasible to monitor a large number of channels, i.e., locations on a qualitative or quantitative basis.
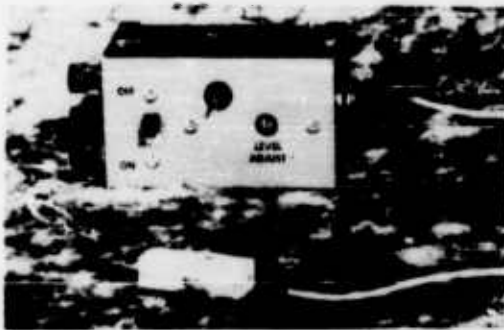
Fig. 1 FLOW-NO FLOW INDICATOR
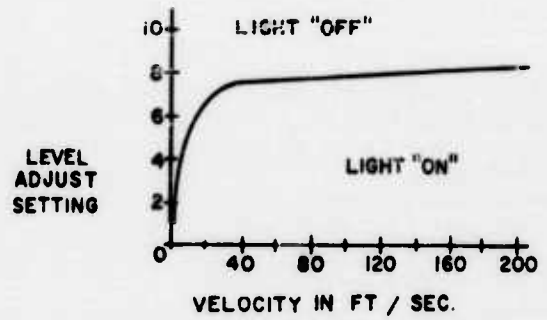
Fig. 2 TYPICAL FLOW-NO FLOW INDICATOR SENSITIVITY
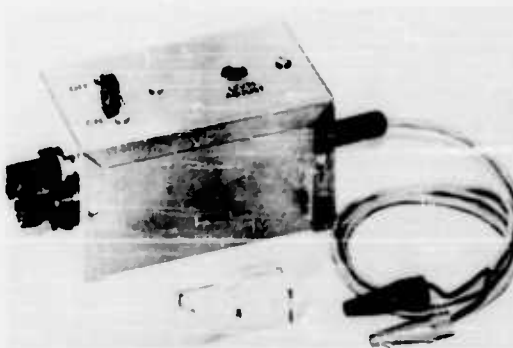
Fig. 3 HOT WIRE INDICATOR
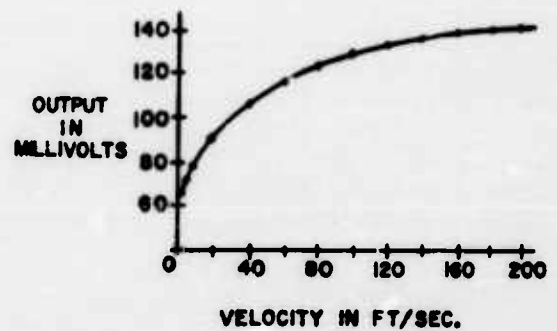
Fig. 4 TYPICAL HOT WIRE SENSITIVITY
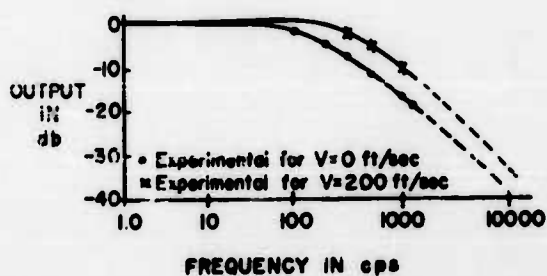
Fig 5 FREQUENCY RESPONSE OF .2 MIL DIA. x 300 MIL LONG GOLD PLATED TUNGSTEN WIRE
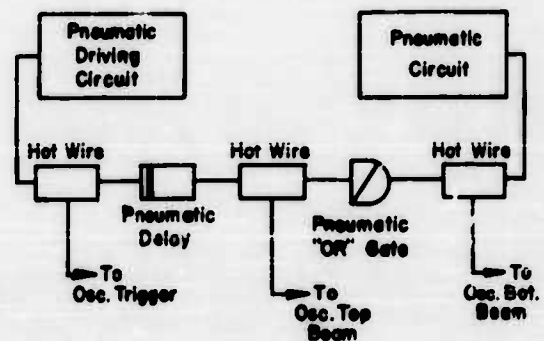
Fig. 6 SWITCHING TIME MEASUREMENT CIRCUIT
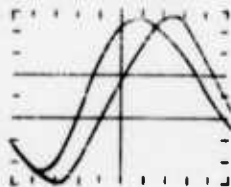
Sweep Rate: .5ms/cm
Switching Time: .5ms

"OR" Gate Driven By 250cps
Pneumatic Oscillator
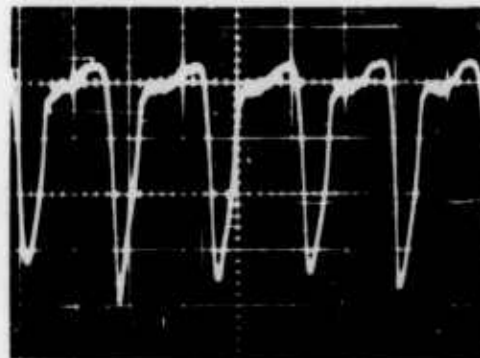
Fig. 7 "OR" GATE SWITCHING TIME MEASUREMENT

Fig. 8 OUTPUT OF OPTIFORM "OR" GATE
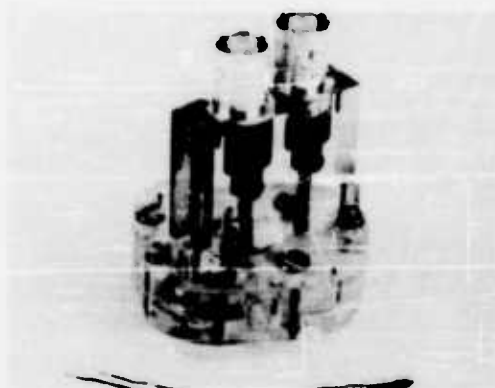
Fig. 9 MINIDUCERS, MOUNTED AND UNMOUNTED
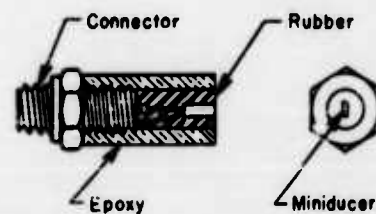
Fig 10 ACOUSTIC MINIDUCER
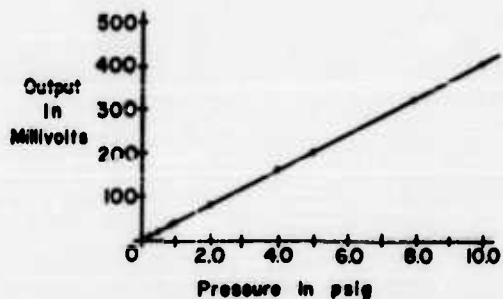
Fig. 11 MINIDUCER SENSITIVITY CURVE
(Miniducer Mounted In Flip-Flop)
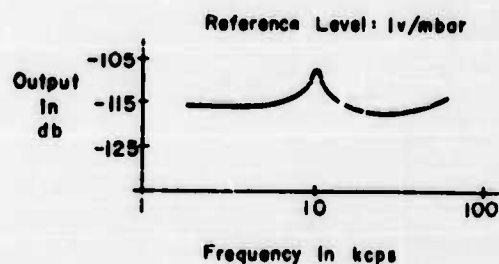
Fig. 12 FREE FIELD MINIDUCER FREQUENCY RESPONSE

175
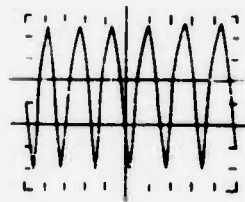
Sweep Rate:
20 msec/cm

Driven By 30 kc
Acoustical Signal

Fig. 13 WAVEFORM OUTPUT OF MINIDUCER
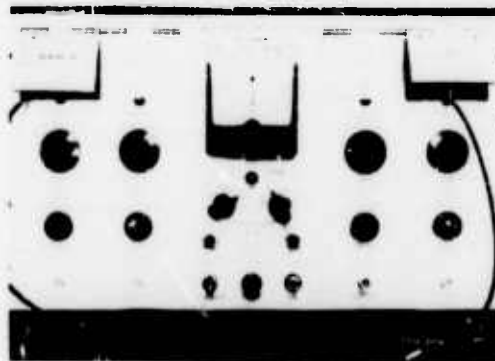
Fig. 14 OPTIC FIBER MONITOR

Fig. 15 SCHLIEREN/OPTIC FIBER MONITOR,
EXPERIMENTAL ARRANGEMENT

Fig. 16 PLASTIC PURE FLUID ELEMENTS
USED IN SCHLIEREN/OPTIC FIBER
MONITOR EXPERIMENT
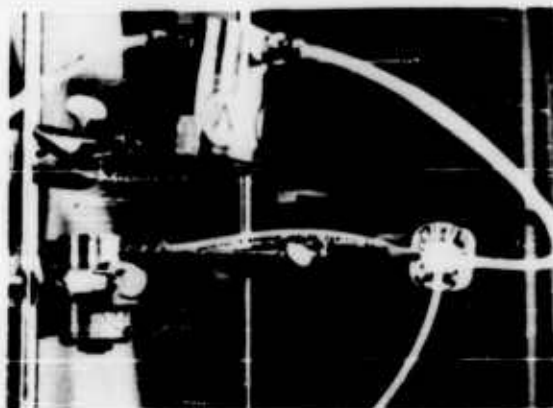
Fig. 17 PLASTIC PURE FLUID ELEMENT

Fig. 18 ELEMENT WITH FLOW SWITCHED
TO THE RIGHT OUTPUT

176

Fig. 19 ELEMENT WITH FLOW SWITCHED
TO THE LEFT OUTPUT

Fig. 20 ELEMENT CHANNEL IMAGE SHOWING
POSITION OF THE LIGHT GUIDES
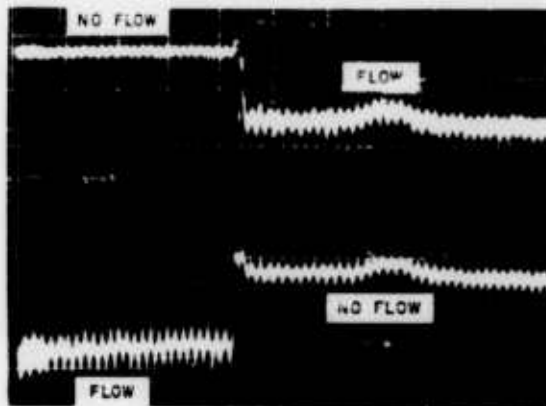
Fig. 21 OPTIC FIBER MONITOR OUTPUT
TRACE. TIME BASE 50ms/cm
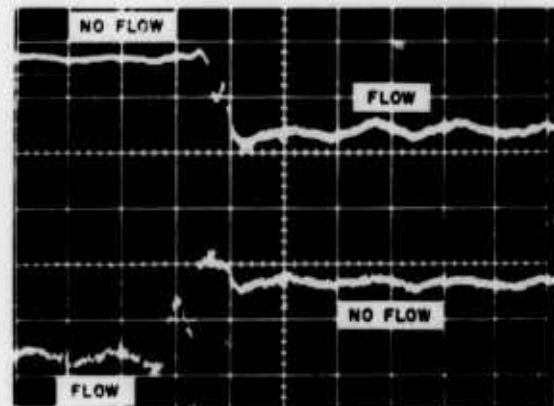
Fig. 22 OPTIC FIBER MONITOR OUTPUT
TRACE. TIME BASE 5ms/cm

177

CHARACTERISTICS OF TWO-DIMENSIONAL
COMPRESSIBLE ATTACHED JETS

by

R. E. Olson

of

United Aircraft Corporation
Research Laboratories

ABSTRACT

Analytical and experimental studies of the characteristics of two-dimensional, compressible jets attached to an adjacent boundary wall were conducted with air as the working fluid. A theoretical flow model is presented and methods for predicting the jet characteristics based on this model are discussed. Experimental measurements of the flow profiles within the jet at various axial stations both upstream and downstream of the reattachment location for Mach numbers of 0.90 and 2.0 are presented. Correlations of the experimental results on the basis of the analytical concepts are made for certain regions of the jet. Measurements of pressure recovery characteristics of a diffuser located downstream of reattachment are presented and compared with pressure recoveries calculated on the basis of average conditions at the diffuser inlet.

INTRODUCTION

An evaluation of the performance of pure-pneumatic elements, particularly digital elements, requires information regarding the characteristics of two-dimensional attached jets (i.e., jets originally unattached which subsequently attach on one side to a boundary wall). The flow profiles throughout the jet and the pressure recovery characteristics of diffusion systems capturing portions of the jet are of particular interest since these characteristics determine the power efficiency of an element. Quantitative procedures for predicting flow profiles in jets attached to plates are not available and related work is generally limited to subsonic flows (e.g., Ref. 1). Furthermore, although previous studies of diffusers for

subsonic and supersonic wind tunnels and propulsion systems (e.g., Refs. 2 3 and 4) have provided analytical procedures for predicting diffuser pressure recoveries, the applicability of these procedures to diffusers having extremely nonuniform inlet profiles, as would be the case in most pure pneumatic components, has not been demonstrated.

Accordingly, investigations have been initiated to study the flow profile development characteristics of two-dimensional attached jets and the pressure recovery characteristics of diffusion systems capturing jets of this type. The results presented herein represent the initial portion of these investigations, which were undertaken as part of a general investigation of the performance of pure-pneumatic elements being conducted for the Diamond Ordnance Fuze Laboratories under Contract DA-49-186-ORD-912.

ANALYTICAL CONSIDERATIONS

A theoretical flow model for a two-dimensional attached jet is presented in Fig. 1. In this model the jet exhausts from a nozzle and reattaches to one of the bounding walls thereby enclosing a separated region or separation bubble. The upper portion of the figure shows the jet divided into four zones: the core, the inner and outer mixing zones, and the boundary layer. Viscous effects predominate in the inner and outer mixing zones and in the boundary layer, whereas the core can be considered to be inviscid.

Also shown in this portion of the figure are typical velocity profiles at the various axial stations in the stream. Between the nozzle exit and the reattachment point, the jet entrains fluid from the separated regions bordering the jet, and the turbulent mixing which results produces velocity profiles characteristic of those for a free jet. At reattachment a portion of the flow in the jet is not able to withstand the associated pressure rise (shown in the lower portion of the figure) and is reversed back into the separation bubble. If flow is introduced into this separation bubble from an external source, steady-state conditions will still exist if this additional flow can gain sufficient momentum by mixing with the main stream to negotiate the pressure rise associated with reattachment. If this is not possible, the amount of fluid in the separation bubble will continue to increase until the entire stream separates from the wall. This mechanism will cause the flow to switch and become attached to the opposite wall. At the reattachment point the velocity profile near the wall is characteristic of that for incipient separation (i.e., the velocity gradient is zero at the wall). Downstream from the reattachment point the high-energy portion of the stream mixes with the low-energy flow near the wall, and a typical power-law type boundary layer velocity profile is established in the portion of the stream near the wall. The inner mixing zone diminishes in height due

180
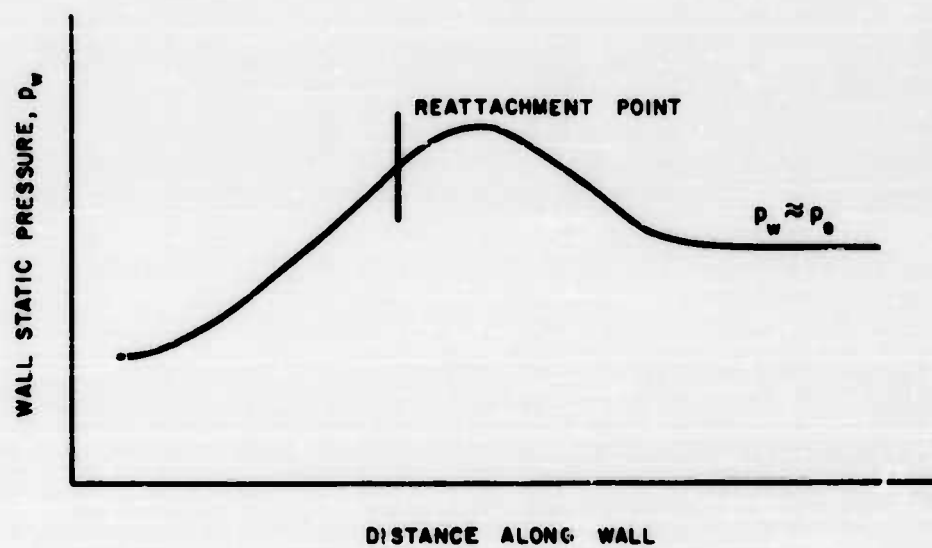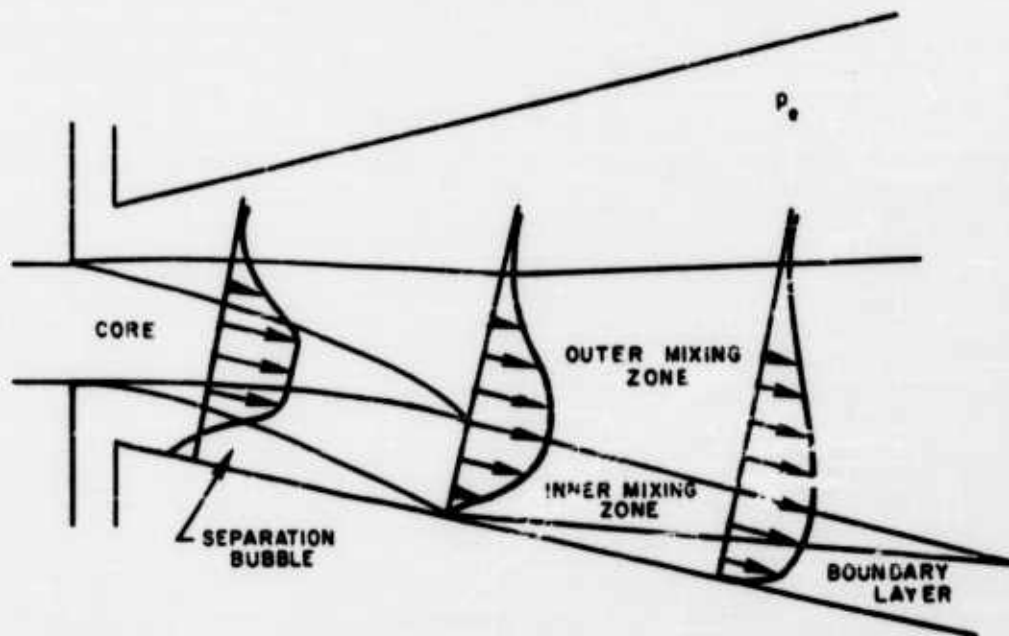
FIGURE 1 SKETCH OF FLOW MODEL

to the boundary layer growth and the spreading of the outer mixing zone. In the outer mixing zone where the profile is similar to that for a free jet. flow is continually being entrained along the outer boundary thereby causing this region to spread. At some downstream station the inner boundary of the outer mixing zone intersects with the outer edge of the boundary layer and the mixing zone becomes nonexistent. At subsequent downstream stations, complete velocity profile similarity exists with the profile for the upper portion of the stream being similar to that of a free jet and the portion of the stream near the wall having a power-law type profile.

Presently, the velocity profile development in these various zones can only be qualitatively established. Quantitative procedures for computing these characteristics requires additional knowledge of jet mixing in the presence of pressure gradients and boundary walls, and knowledge of the boundary layer growth characteristics of reattached flows.

EXPERIMENTAL STUDIES

A schematic diagram and photographs of the test rig employed for these tests are presented in Figs. 2 and 3 respectively. The test rig was two dimensional throughout its length and was provided with hinged sidewalls 3 in. apart. A portion of these sidewalls was glass to enable schlieren observation. Removable nozzle blocks were provided to obtain both subsonic and supersonic jet Mach numbers. Subsonic jet Mach numbers were obtained with a smooth-approach convergent nozzle. Convergent-divergent nozzles designed for uniform flow at the exit were employed to obtain supersonic jet Mach numbers. The exit height, w , for all nozzles was equal to 0.50 in., thereby providing an aspect ratio (distance between side-walls divided by the nozzle height) equal to 6.0. The boundary walls downstream of the nozzle blocks were adjustable to vary both setback and wall angle. Airflow was supplied at an upstream total pressure of approximately 22 psia and a total temperature of 80 F for all tests and was exhausted through laboratory vacuum pumps.

Fifty pressure taps were provided along one of the boundary walls to measure the wall static pressure distribution. The variable-position pitot pressure probe shown in Fig. 3 was employed to obtain surveys through the stream without a diffuser installed. This probe was motorized in the direction perpendicular to the boundary walls and in the streamwise direction but was positioned manually in the direction perpendicular to the side plates. The position of the probe in the motorized directions was recorded by an automatic data-recording system on punched cards.

FIGURE 2   SCHEMATIC DIAGRAM OF TEST RIG FOR ATTACHED-JET TESTS

183

WITH PROBES INSTALLED

STATIC PROBE

VARIABLE POSITION
PITOT PROBE

WITH DIFFUSER INSTALLED
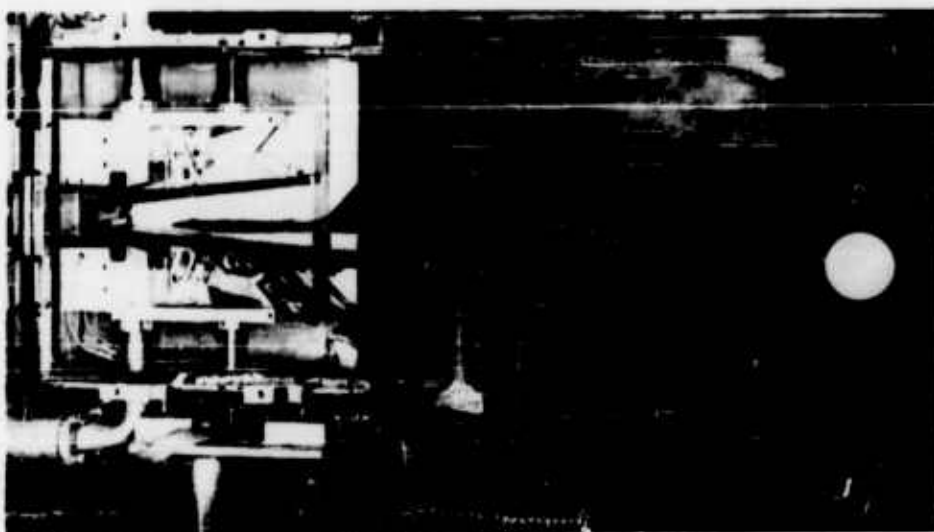
FIGURE 3   PHOTOGRAPH OF TEST RIG FOR ATTACHED-JET TESTS

184

This rig was designed to accommodate diffuser models attached directly to the boundary walls. A typical diffuser model is shown by the dashed lines in Fig. 2 and a photograph of the model emp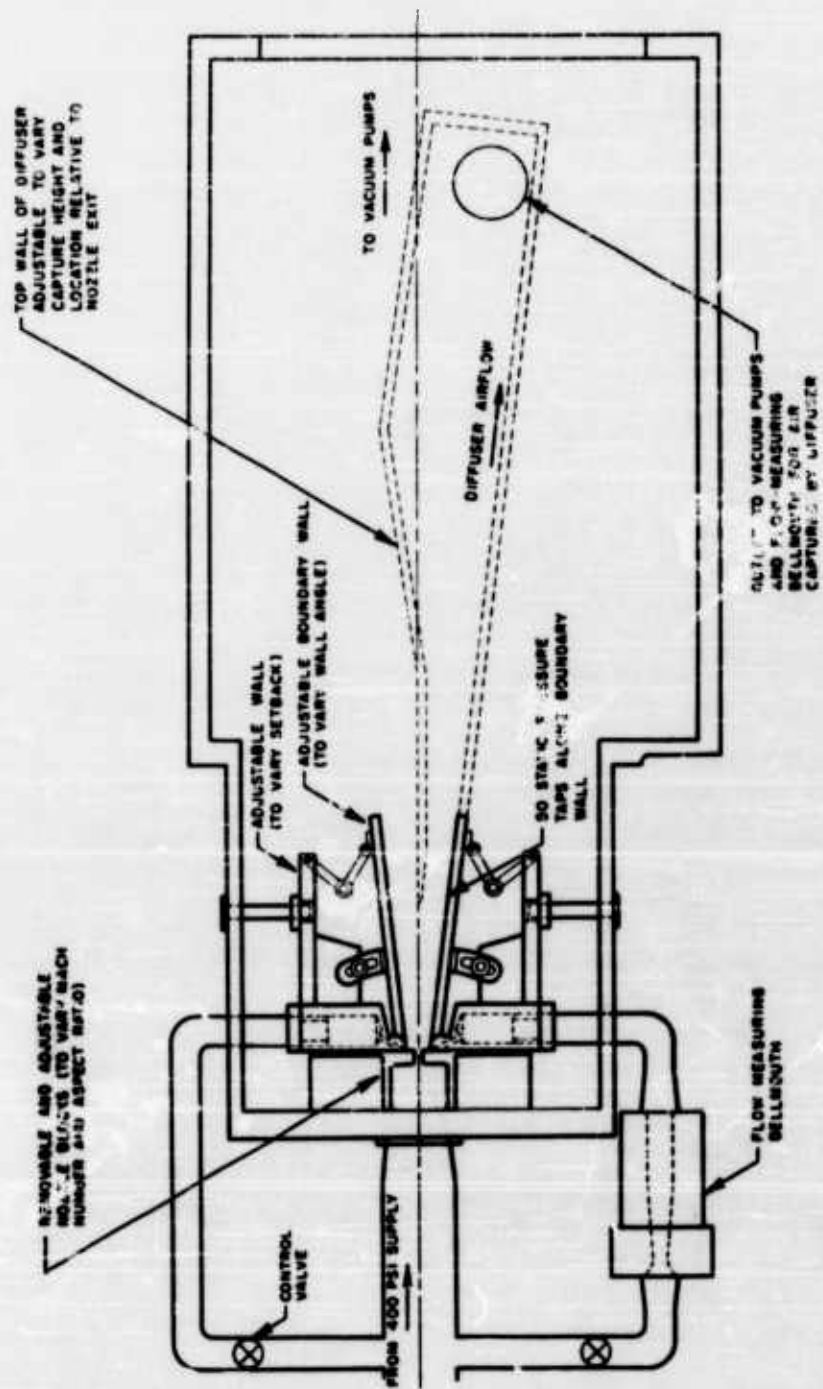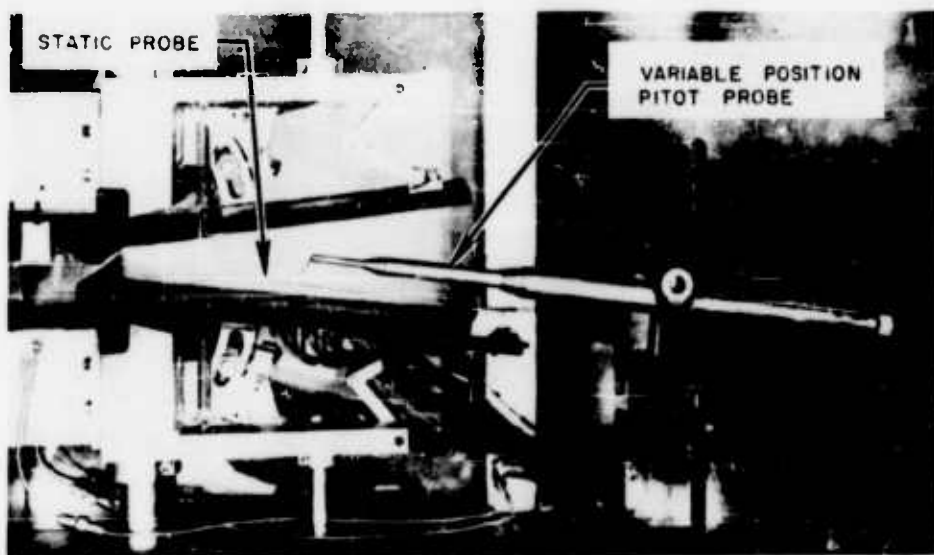loyed for the tests reported herein is presented in Fig. 3. Sealing of the diffuser at the side plates was accomplished with flat rubber gaskets. For tests with the diffuser installed, a flow-measuring bellmouth was provided between the diffuser exit and the vacuum supply. Diffuser back pressure was controlled with a throttling valve downstream of the bellmouth.

In determining the velocity or Mach number profiles in the jet without the diffuser installed, both the pitot and static pressures at each point must be known. Conventional probes for obtaining static pressure could not be employed because of the extreme sensitivity of these probes to flow angularity and the adverse interference effects caused by the probe support, particularly at transonic Mach numbers. Therefore, a special probe was developed to obtain static pressure measurements along the jet centerline (defined as the locus of points of maximum stream velocity). This probe comprised a slotted hypotube which was bent to the contour of the jet centerline. The location of this centerline was determined from the position of the maximum pitot pressures obtained from limited pitot pressure surveys. A second movable hypotube with a static pressure orifice was contained within the first. The slot in the first hypotube was oriented so that the static pressure orifice faced the side plate. The hypotube extended upstream into the plenum chamber and downstream to the end of the boundary walls. This technique eliminated the probe body interference effects and reduced the adverse effects of flow angularity. Both the pitot and static pressure probes are shown in Fig. 3.

The approximate equation of motion in the direction perpendicular to the stream shows that the static pressure gradient is zero at the wall or outer extremity of the jet where the streamwise velocity is zero. By differentiating this equation it can also be shown that the curvature of the static pressure profile is zero at the point of maximum stream velocity where the velocity gradient is equal to zero. These static pressure gradients and the measured static pressures at the outer extremities of the jet and on the jet centerline were employed to establish the static pressure profiles. On the outer boundary of the jet, the static pressure was assumed equal to the measured pitot pressures. On the inner boundary of the jet, the measured wall static pressure was used. Typical static pressure profiles together with their corresponding measured pitot pressure profiles are presented in Fig. 4 for stations both upstream and downstream of the reattachment point. It should be noted that all pitot pressure surveys were taken perpendicular to the jet centerline. The Mach number and velocity distributions were computed using one-dimensional compressible flow relations assuming constant total temperature throughout the stream.

FIGURE 4   TYPICAL PITOT AND STATIC PRESSURE PROFILES

186

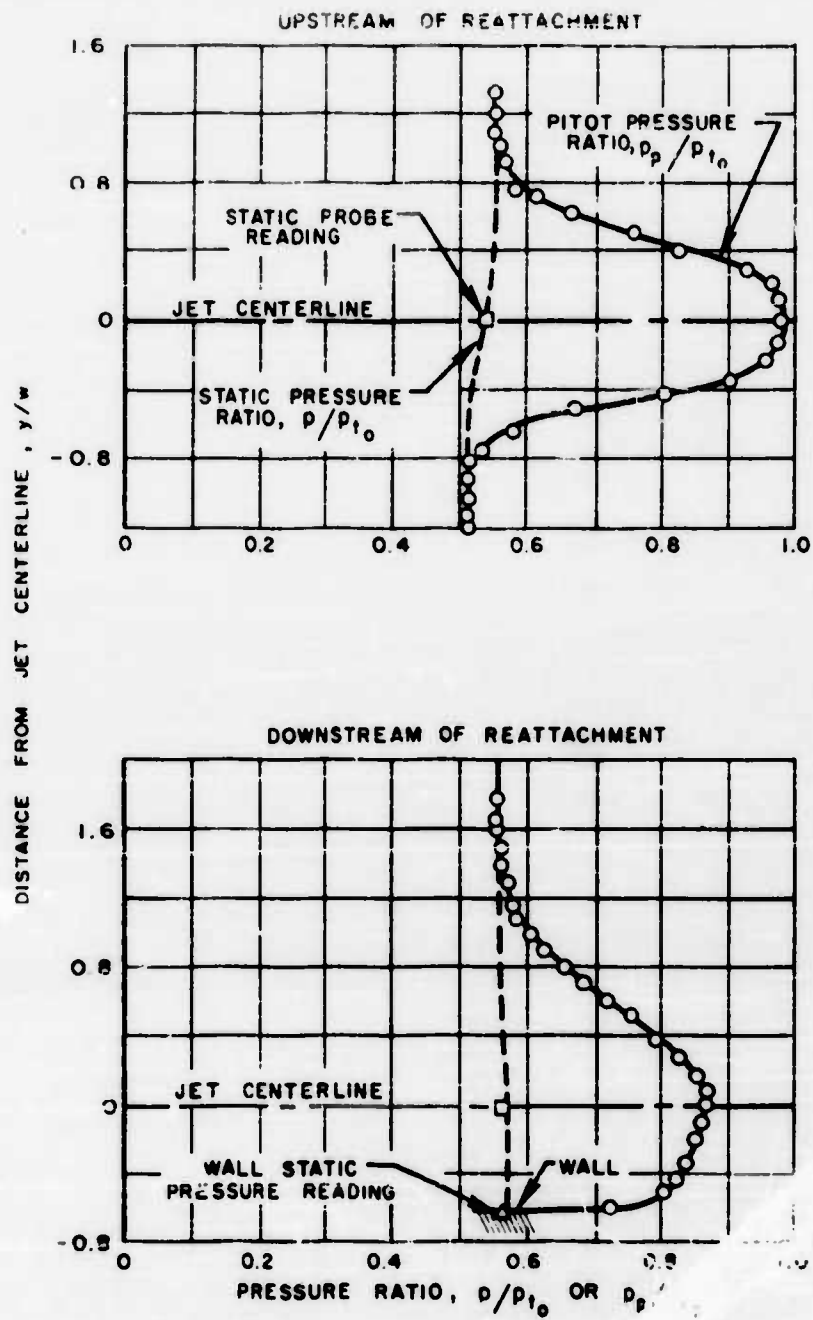Velocity profiles obtained at various distances along the jet centerline are presented in Fig. 5. It should be noted that the profiles shown were obtained perpendicular to the jet centerline and for cases upstream of reattachment or near reattachment are not perpendicular to the wall. The characteristic velocity profiles at the various stations throughout the jet, mentioned previously under "ANALYTICAL CONSIDERATIONS" are evident in this figure. The increase in the distance to reattachment as the Mach number is increased can also be seen.

Static pressure distributions on the wall to which the stream is attached are shown in Fig. 6. The reattachment point locations shown in the figure were determined by placing a mixture of lampblack and oil evenly on the surface of the boundary wall and subsequently maintaining test conditions for a period of time necessary to establish a flow pattern. Using this technique, the lampblack and oil mixture is "wiped away" in regions of high velocity and deposits in stagnation regions. The effect of Mach number on the reattachment location mentioned previously is more clearly evident in this figure. Two additional characteristics of interest are also shown. The first is that the ratio of the pressure at reattachment to the minimum pressure upstream of reattachment increases as the jet Mach number increases. This characteristic is consistent with reattachment data for a semi-infinite stream flowing over a rearward-facing step (Ref. 5). The second is the character of the static pressure distributions downstream of reattachment. For the supersonic Mach number, the wavy character of the pressure distribution indicates the presence of oblique shock waves.

Mach number distributions along the jet centerline are presented in Fig. 7. The existence of the repetitive shock and expansion patterns for the supersonic Mach number jet is clearly evident in this figure. These shock patterns which are characteristic of those for an imperfectly expanded jet arise because of the flow turning required. The effect of this turning for the subsonic Mach number jet is indicated by the variation in centerline Mach number for values of $x/w < 6$.

Integrated average total pressure characteristics of the jet at two axial stations are presented in Fig. 8 for the two jet Mach numbers investigated. (All pressures are absolute values). For a jet Mach number 0.90, the maximum average total pressure that could be obtained by capturing a portion of the jet is shown to decrease with increasing distance from the nozzle exit as would be expected since the maximum total pressure in the jet is decreasing. For a Mach number 2.0, however, the maximum average total pressure available is approximately equal for the two axial stations. This occurs since the station with the lowest x/w is upstream of reattachment and therefore includes a portion of very low energy fluid close to the wall thereby decreasing the maximum average total pressure available. In addition the maximum average total pressure available in the stream at a given streamwise station downstream of reattachment is seen to decrease with increasing Mach number. The major portion of this decrease can be attributed to shock losses.
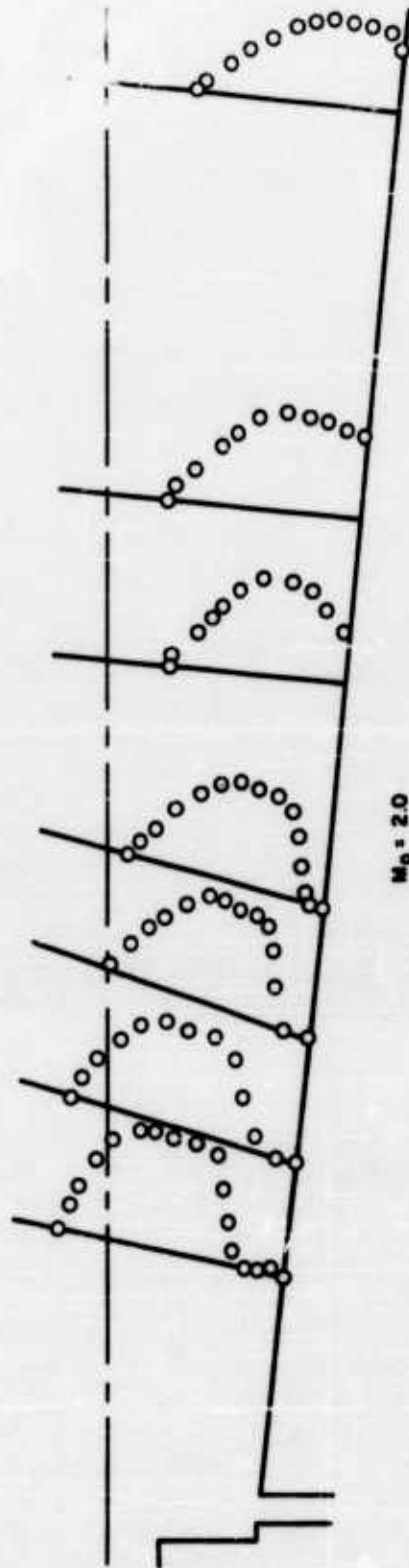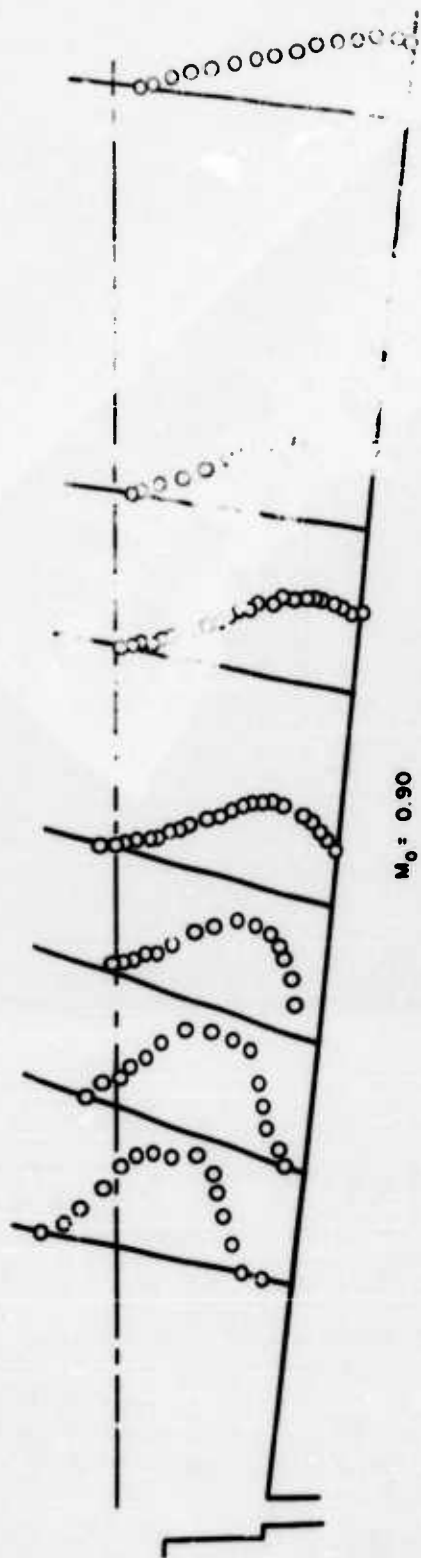
FIGURE 5 EXPERIMENTAL VELOCITY PROFILES

$M_0 = 0.90$

FIGURE 5 EXPERIMENTAL VELOCITY PROFILES

$M_0 = 2.0$

$M_0 = 2.0$

188
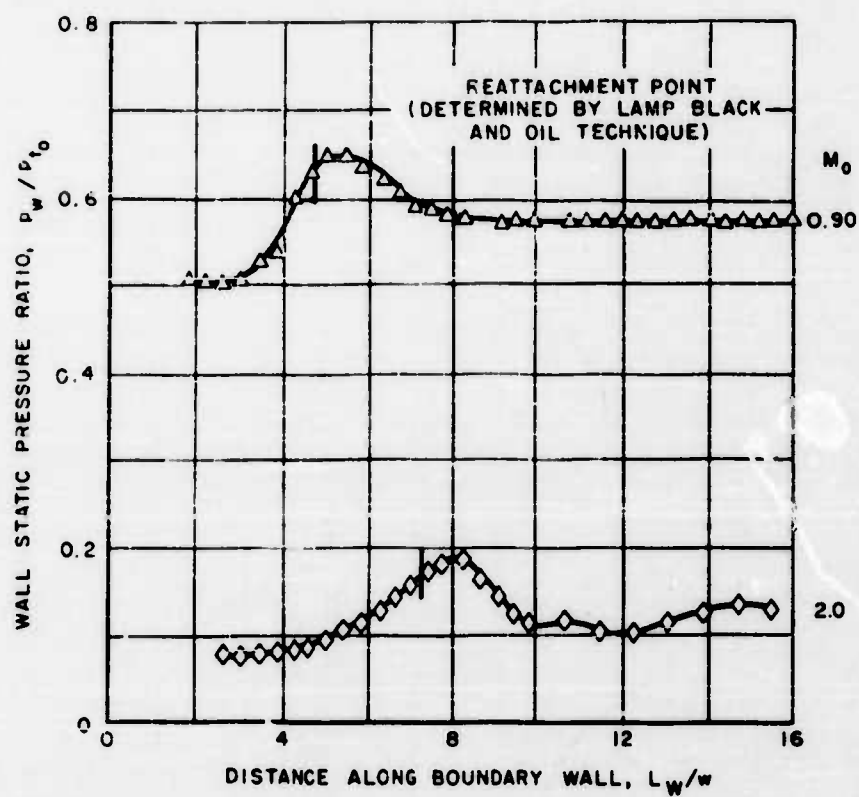
FIGURE 6   STATIC PRESSURE DISTRIBUTIONS ALONG BOUNDARY WALL
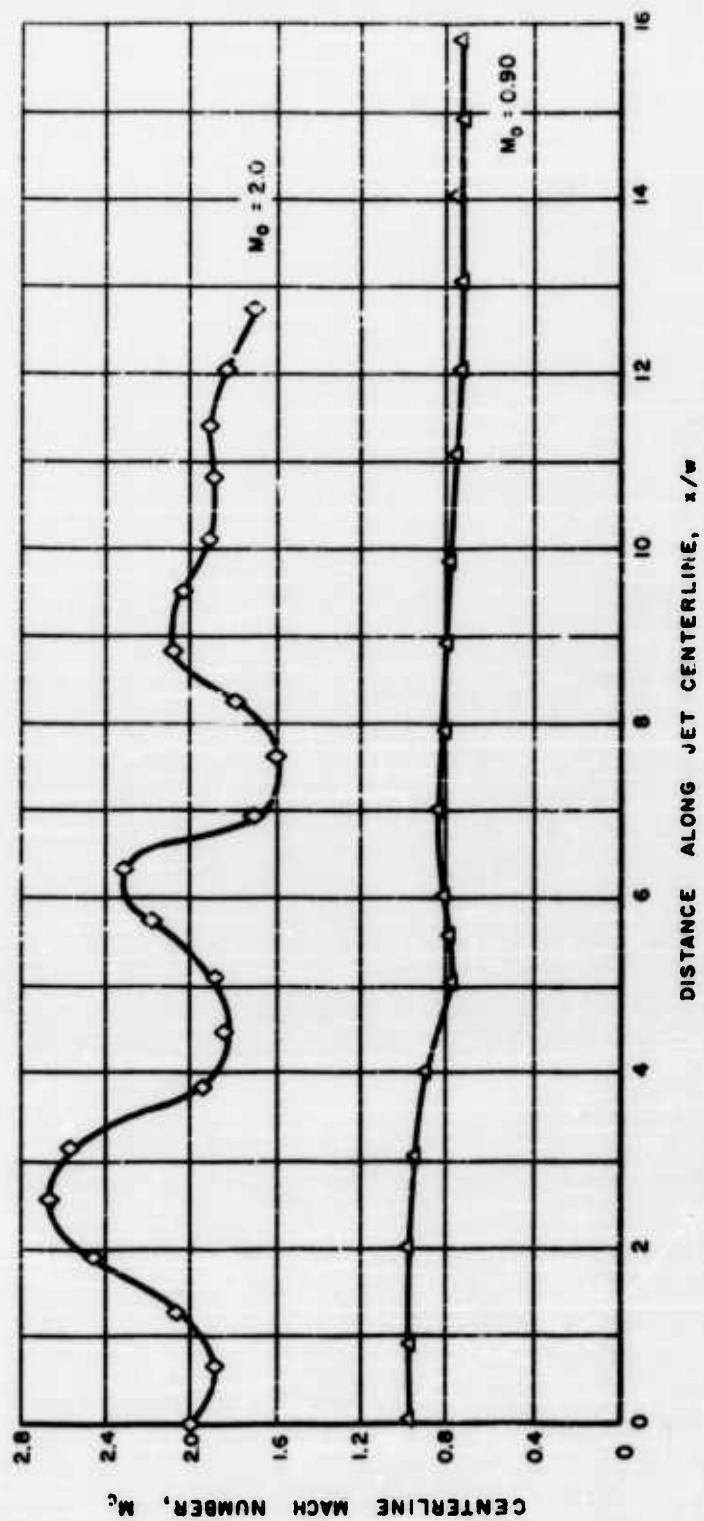
FIGURE 7 CENTERLINE MACH NUMBER DISTRIBUTIONS

190
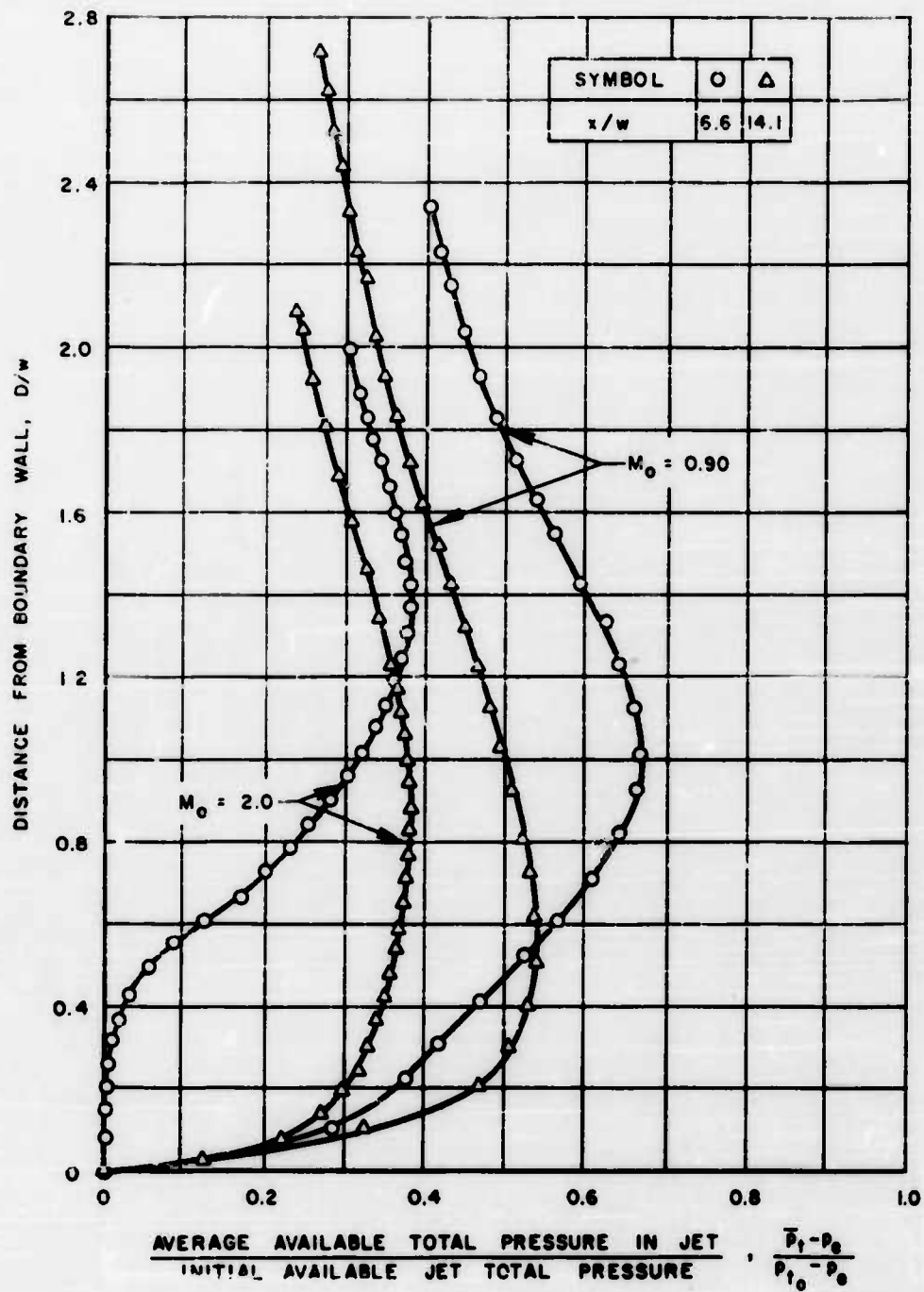
FIGURE 8 AVERAGE TOTAL PRESSURE CHARACTERISTICS

191

SYMBOL	D	△	▽	△
x / w	6.6	8.6	10.1	14.1

CLOSED SYMBOLS - $M_0 = 2.0$
OPEN SYMBOLS - $M_0 = 0.90$
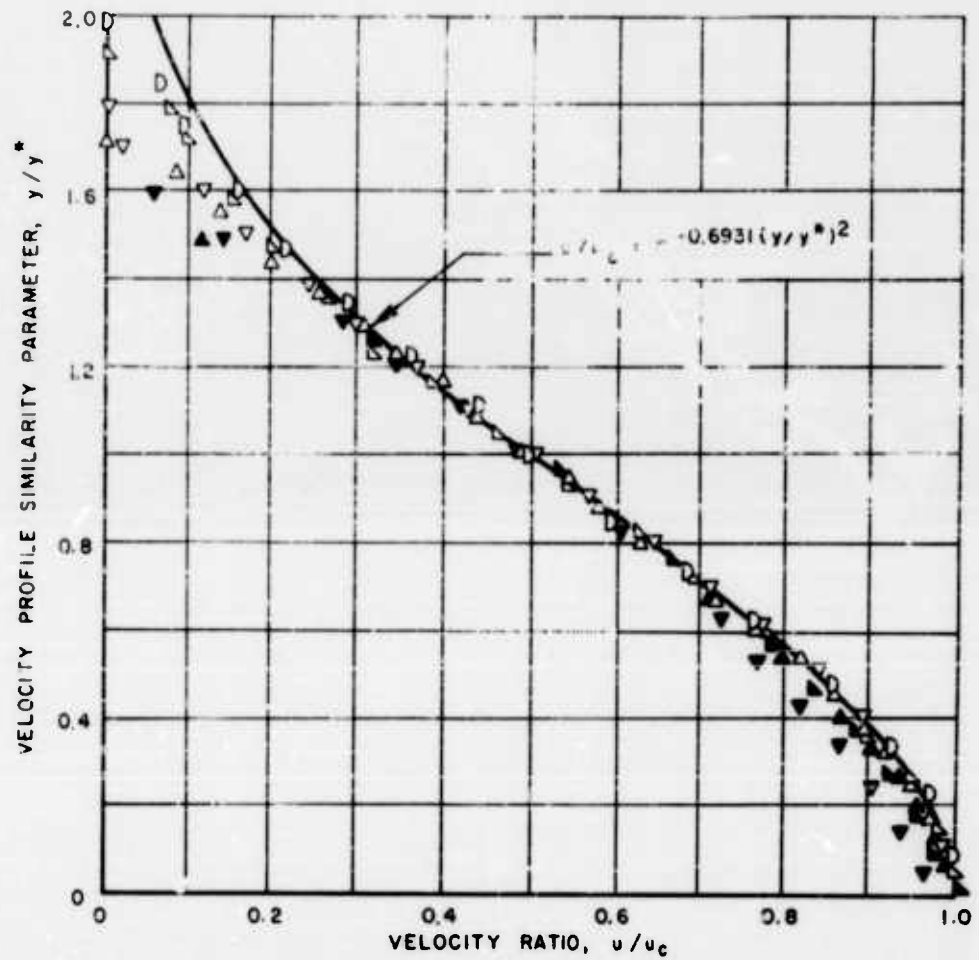
FIGURE 9   NONDIMENSIONAL VELOCITY PROFILES DOWNSTREAM OF
REATTACHMENT IN OUTER MIXING ZONE.
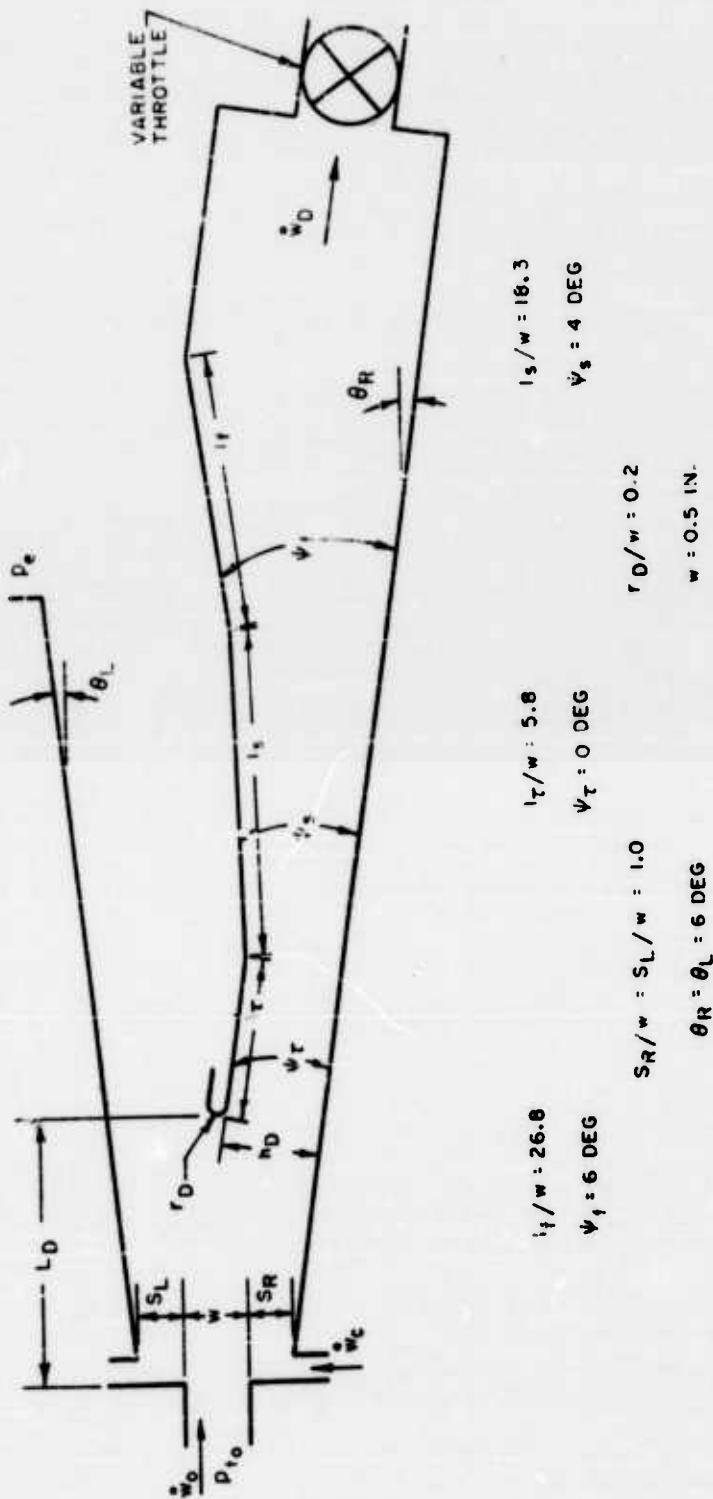
FIGURE IC SKETCH OF DIFFUSER MODEL

VARIABLE THROTTLE

$\dot{w}_D$

P_e

θ_L

θ_R

$\dot{w}_0$ P_{t_0}

$\dot{w}_c$

L_D

S_L w S_R

r_D

h_D

$l_t/w = 26.8$
$\psi_1 = 6$ DEG

$l_\tau/w = 5.8$
$\psi_\tau = 0$ DEG

$l_s/w = 18.3$
$\psi_s = 4$ DEG

$S_R/w = S_L/w = 1.0$
$\theta_R = \theta_L = 6$ DEG

$r_D/w = 0.2$
$w = 0.5$ IN.

193
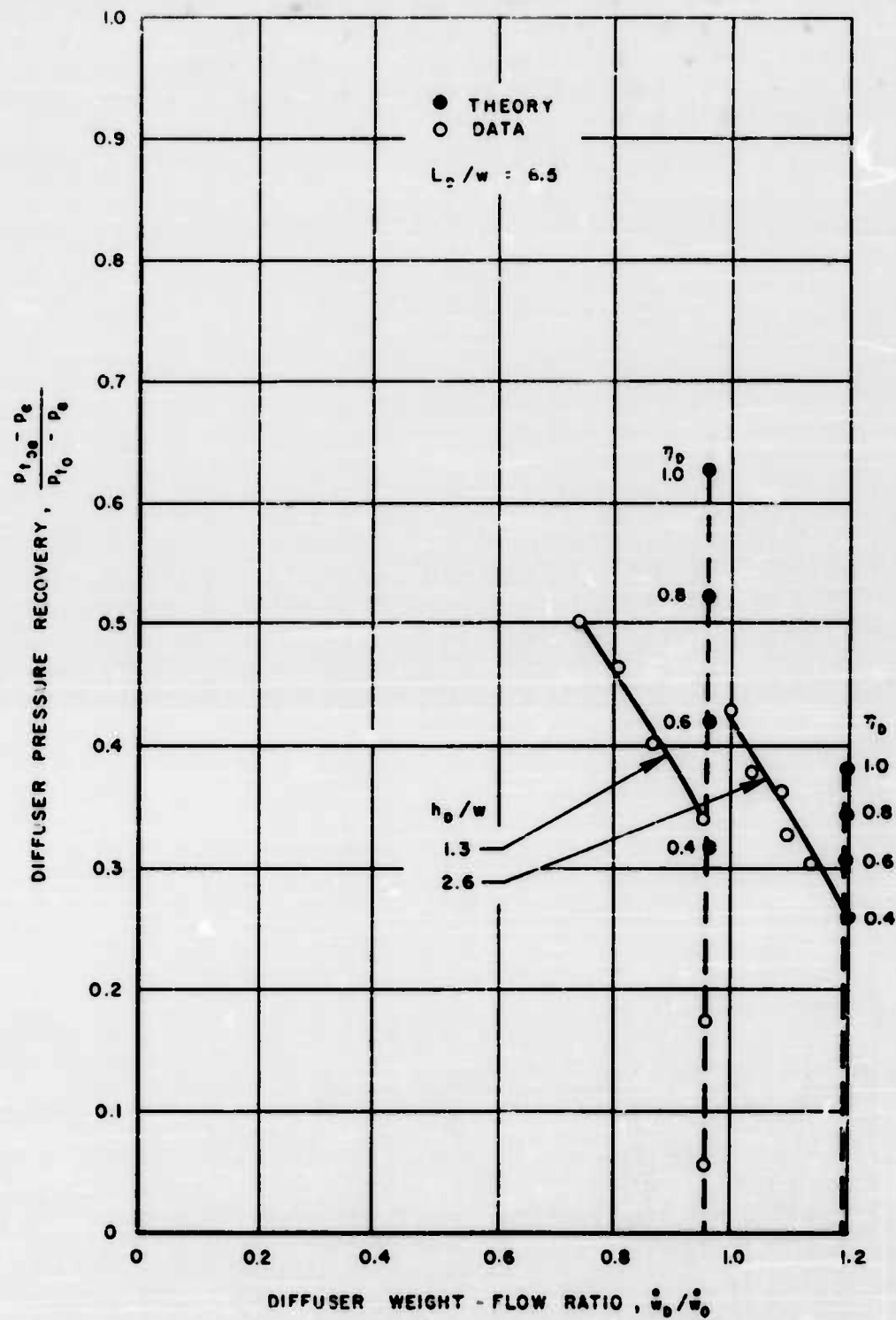
FIGURE II DIFFUSER PRESSURE RECOVERY CHARACTERISTICS

194

As mentioned previously under "ANALYTICAL CONSIDERATIONS", procedures for predicting the velocity profiles for attached jets require a knowledge of jet mixing in the presence of boundary walls. Attempts to gain insight into the nature of the velocity profile development downstream of reattachment in the outer mixing zone were made by determining if velocity profile similarity existed in this region and in particular to determine whether or not these profiles were similar to those for a free jet. This was done by determining the vertical scale factor which would make the slope of the velocity profiles at the mid-velocity point ($u/u_c = 0.5$) equal to the value for the nondimensional free-jet velocity profile (Ref. 6). This scale factor was then employed to nondimensionalize the profiles in the outer portion of the jet for all stations downstream of reattachment. The resulting profiles are presented in Fig. 9. Similarity is shown for all measured profiles except near the outermost portion of the stream where the data are scattered. This scatter was probably caused by the extreme sensitivity of the calculated velocities to the measured values of the static pressure. In addition, the calculated velocity ratios and the empirical curve for a free jet are not in agreement near the outer portion of the stream, probably due to the close proximity of the boundary wall to which the stream is not attached.

In the portion of the stream near the wall, velocity profile similarity is not obtained in the range of x/w investigated. This lower portion of the stream consists of a boundary layer near the wall and a mixing layer of unknown character which separates the boundary layer portion of the flow and the free-jet portion of the flow. This mixing layer decreases, however, for increased downstream stations and would be expected to disappear. Further work is needed to investigate the nature of this mixing layer which exists between the reattachment point and the region of similar profiles far downstream.

Tests were also conducted at a jet Mach number of 0.60 with a diffuser installed on the sidewall downstream of the jet reattachment point. A sketch showing the diffuser model employed for these tests is presented in Fig. 10. The diffuser model consisted of a constant-area throat section ($\psi_T = 0$) followed by a subsonic diffuser having an initial divergence angle of 4 deg ($\psi_1 = 4.0$ deg). The purpose of the constant-area section was to allow the profile to adjust to a stable boundary layer profile on the wall nearest the free boundary of the jet before diffusing. Previous data on subsonic diffuser performance have indicated that if this is done the tendency to separate in the subsonic diffuser and the associated loss in subsonic diffuser efficiency are reduced.

Tests with the diffuser installed were performed by throttling the exit of the diffuser passage while at the same time adjusting the flow rate into or out of the exhaust plenum to maintain the pressure on the free boundary of the jet, p_e, at a constant value. Tests were initiated with the throttle in the full-open position and continued until the throttle was closed or until the jet

switched to the opposite wall and flowed into the exhaust plenum. For each throttle setting, measurements of diffuser weight flow and diffuser exhaust static pressure were obtained. From these measurements the continuity-average total pressure at the diffuser exit was calculated.

In general, when the Mach number approaching the lip of the diffuser has a relatively low subsonic value, one of three flow regimes (termed Case I, II, and III) may be encountered. For Case I, the subsonic flow approaching the diffuser lip is entraining air from the region outside the undisturbed streamline (i.e., the streamline which was at the location of the diffuser lip without the diffuser installed); for Case II, the diffuser captures all of the flow which was in the stream at the station without the diffuser installed; for Case III, flow is spilled around the lip of the diffuser. With high subsonic or supersonic Mach numbers approaching the lip (i.e., with the lip moved from the outer stream boundary toward the center of the stream), only Cases II and III are encountered because the inlet is effectively choked.

Presented in Fig. 11 are the results of tests with the diffuser installed for a jet Mach number of 0.90. In these tests the diffuser was located immediately downstream of reattachment. Results are presented for two diffuser heights, h_D/w, relative to the boundary wall. For an $h_D/w = 2.6$ the entire stream was captured whereas for an $h_D/w = 1.3$ only a portion of the stream was captured. The vertical dashed lines were calculated by integrating the measured flow profiles obtained without the diffuser installed out to the diffuser lip position. For an $h_D/w = 2.6$ the open symbols to the left of the dashed lines represent the Case III flow regime. No data were obtained for Case I with this configuration because of limitations on the air-handling capacity of the exhaust-plenum bleed valve which was installed during this series of tests. The solid symbols were obtained by integrating the measured total pressure profiles without the diffuser installed to obtain average total pressure. Calculated values for various assumed subsonic diffuser efficiencies are shown. With the diffuser lip located closer to the wall so that only a portion of the stream was captured, the flow approaching the lip has a high subsonic Mach number and Case I flow was not obtained because the diffuser was effectively choked as shown by the vertical array of open data points. For this diffuser position the stream separated from the wall just upstream of the diffuser for diffuser weight-flow ratios slightly less than those for the lowest values plotted.

The integrated weight flows obtained from profile measurements without the diffuser installed are in excellent agreement with the weight flows measured with the diffuser installed. The degree of agreement between the open and closed symbols with respect to critical diffuser pressure recovery (highest pressure recovery with no flow spillage) depends on the subsonic diffuser efficiency, η_D. The best agreement is obtained with $\eta_D > 0.40$ for $h_D/w = 1.3$ and $\eta_D = 0.40$ for $h_D/w = 2.6$. These relatively low subsonic diffuser efficiencies can be

196

attributed principally to the poor inlet profiles existing near reattachment where the diffuser was located. The somewhat poorer diffuser efficiency with the greater capture height is probably due to the poorer velocity profiles at the diffuser inlet existing on the outer boundary of the jet.

From the preceding discussions of the tests with the diffuser installed, it is seen that the diffuser pressure recoveries for no flow spillage can be predicted by employing the average flow properties obtained from measured profiles in the jet without the diffuser installed and an assumed subsonic diffuser efficiency. The values of diffuser efficiency obtained for the tests reported herein are slightly lower than those obtained with well designed diffusers having well developed inlet profiles. It is believed that improved diffuser efficiencies can be obtained with more refined diffuser designs. Additional experimental and analytical investigations, however, would be necessary to obtain these refined designs.

LIST OF REFERENCES

1. Sawyer, R. A.: The Flow Due to a Two-Dimensional Jet Issuing Parallel to a Flat Plate. Journal of Fluid Mechanics, Vol. 9, Part 4, p. 243, December 1960.

2. McLafferty, G. H., F. L. Krasnoff, E. D. Ranard, W. G. Rose and R. D. Vergara: Investigation of Turbojet Inlet Design Parameters. UAC Research Laboratories Report R-0790-13, December 1955.

3. Kepler, C. E.: Investigation of the Performance of a Variable-Geometry Diffuser for the AEDC Propulsion Wind Tunnel. UAC Research Laboratories Report R-0667-26, August 15, 1955.

4. Cnossen, J. W. and R. L. O'Brien: Investigation of the Diffusion Characteristics of Supersonic Streams Composed Mainly of Boundary Layers. ASD Technical Documentary Report, ASD TDR 62-528 (to be published).

5. Beheim, M. A.: Flow in the Base Region of Axisymmetric and Two-Dimensional Configurations. NASA TR R-77, 1961.

6. Olson, R. E.: Interim Report on Aerodynamic Studies of Pure Pneumatic Systems. Diamond Ordnance Fuze Laboratories Report (to be published).

198

D	Distance from boundary wall measured perpendicular to jet centerline
h_D	Diffuser inlet height measured perpendicular to boundary wall
l	Length of subsonic diffuser section
L_D	Distance between nozzle exit and diffuser inlet measured parallel to nozzle centerline
L_W	Distance along boundary wall
M	Mach number
M_c	Mach number on jet centerline
p	Static pressure
p_e	Static pressure on free boundary of jet
$\bar{p}_{D_i}$	Average static pressure at diffuser inlet
p_p	Pitot pressure
p_t	Total pressure
$p_{t_{De}}$	Diffuser exit total pressure
$\bar{p}_{t_{Di}}$	Average total pressure at diffuser inlet
p_w	Boundary wall static pressure
r_D	Diffuser inlet radius of curvature
S	Distance between boundary wall and inner contour of nozzle at nozzle exit
u	Velocity parallel to jet centerline
u_c	Velocity on jet centerline
w	Total height of nozzle at exit

$\overset{\circ}{w}_c$	Control jet weight flow
$\overset{\circ}{w}_D$	Diffuser weight flow
$\overset{\circ}{w}_0$	Initial jet weight flow
x	Distance along jet centerline
y	Distance perpendicular to jet centerline
η_D	Subsonic diffuser efficiency, $\left(\dfrac{p_{t_{De}}}{\bar{p}_{t_{Di}}} - \dfrac{\bar{p}_{Di}}{\bar{p}_{t_{Di}}}\right)\bigg/\left(1 - \dfrac{\bar{p}_{Di}}{\bar{p}_{t_{Di}}}\right)$
θ	Angle of boundary wall relative to nozzle centerline
ψ	Angle of subsonic diffuser section

Subscripts

f	Denotes final subsonic diffuser section
L	Denotes upper boundary wall
R	Denotes lower boundary wall
s	Denotes initial subsonic diffuser section
T	Denotes throat section of subsonic diffuser
o	Denotes conditions at nozzle exit

Superscripts

*	Denotes conditions where $u/u_c = 0.5$

THE APPLICATION OF FREE JET MIXING
THEORIES TO FLUID AMPLIFIER ELEMENTS

by

Glen W. Zumwalt

of

School of Mechanical Engineering
Oklahoma State University

INTRODUCTION

It is often possible to design fluid amplifier systems on the basis of
experimentally-derived component characteristics, without recourse to jet-
mixing theory. But this is becoming increasingly difficult--and dangerous.
When a component is "scaled-up," the fluid pressure level changed, or oper-
ating temperature varied, Reynolds number effects may appear. If transition
to (or from) turbulence is involved, discontinuities or instabilities in
component characteristics are likely. When secondary flows are present
(e.g., control jets), extrapolations of operating characteristics become even
less justified. Multiplied complexities accompany multiple-stage amplifiers.
The effects of differing combinations of fluid properties in the two inter-
acting streams demand an understanding of the basic phenomena involved.

Jet mixing analysis is not, of course, a new field. Several well sub-
stantiated theories exist which have been successfully applied to various
aerodynamic, duct-flow, and ejector types of problems. It would seem reason-
able to adapt these to use with fluid amplification elements wherever possible.
We must anticipate, however, that the peculiarities of fluid amplifiers (e.g.,
small sizes, rapid transients. extremes of temperature) may not permit direct
application of the theories.

It is the purpose of this paper to examine the status of two well-accepted
mixing theories, one laminar and one turbulent, in order to (1) make immediate
application where possible, (2) delineate inherent limitations, and (3) suggest
profitable extensions of the theoretical treatments. The discussion shall be
limited to two dimensional, perfect gas jet-flows, where the jet "core" is
supersonic.

REQUIREMENTS FOR A THEORY

Figure 1 shows a basic model for a boundary layer type of fluid amplifier
component (Ref. 1). A theory which would adequately treat this flow type must
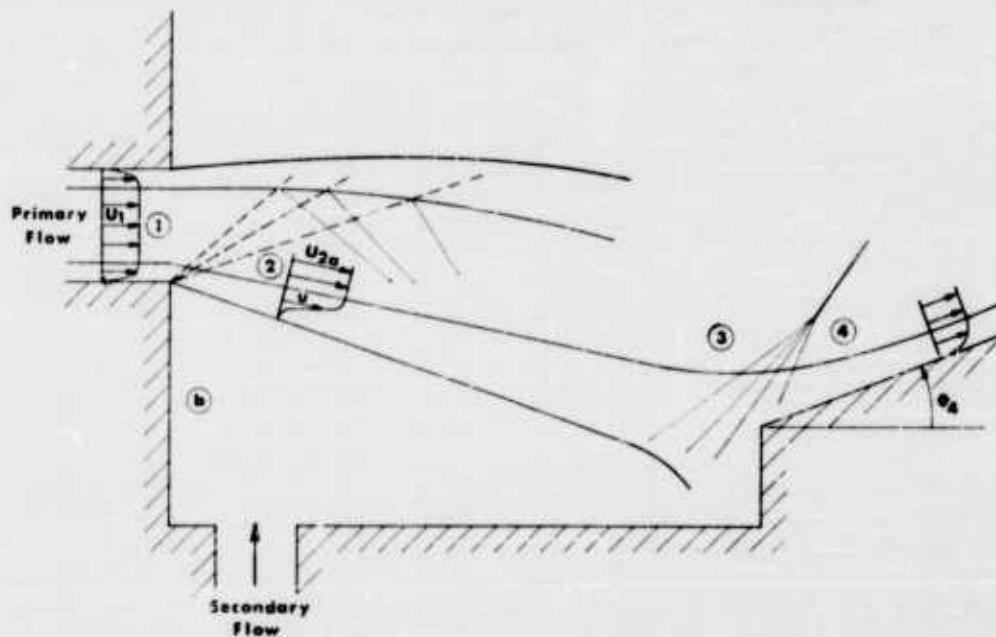meet the following requirements:

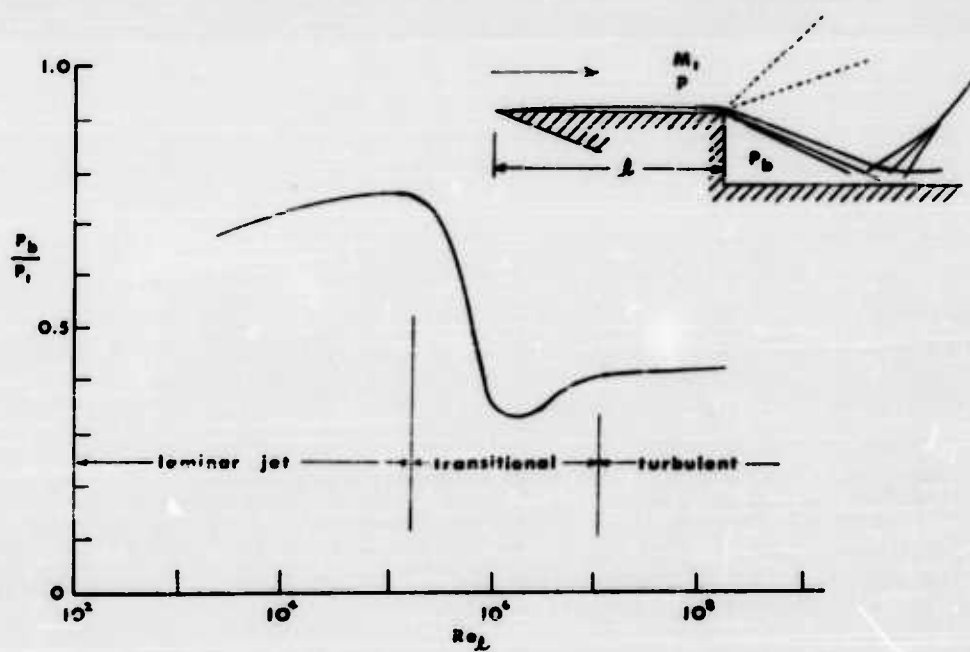Figure 1. Basic model for boundary layer type component.

Figure 2. Effect of transition location on separated pressure. (M ≈ 3).

1. Specify the turn mechanism at the separation corner: flow from ① to ②.
2. Define the mixing region characteristics in region ② to ③; e.g., velocity profile and pressure gradients.
3. Specify the recompression mechanism at the wall reattachment (if any): region ③ to ④.
4. Relate the above to secondary mass flows.
5. Consider the effect of the initial boundary layer at ① on the above four phenomena.
6. Consider the effect of laminar-to-turbulent transition location.

In order to be generally useful, it would also be desirable that the theory:
7. Apply to various gases
8. Consider the effect of temperature differences in primary and secondary fluid streams.
9. Be applicable when different fluids flow in the two streams.

Many of these requirements are met, or are capable of being met in theories developed to treat base pressure problems. The general theory of Crocco and Lees (Refs. 2 and 3) dealt with the entire spectrum of compressible free jets from purely laminar to purely turbulent. By this theory, it was possible to predict the qualitative relationship between pressure on a back step and the turbulent transition location, as characterized by length Reynolds number. Figure 2 shows this relation, with its strange reversed trend in the transition region, providing a warning to those who would design within this region. The theory, however, suffered in practice from its requirement of up to five empirical constants or functions. Therefore, it has not been widely used for quantitative work.

THE CHAPMAN-KORST APPROACH

The two theories which have proven to be most useful in external flow base pressure analysis are those of H. H. Korst (turbulent) and D. R. Chapman (laminar). These were developed independently and almost simultaneously in the early 1950's. They utilize nearly identical theoretical flow models shown in Figure 3. Here the flow is divided into three sections: (1) a frictionless free-stream, (2) a dissipative layer consisting of either a guided or free boundary layer, and (3) a dead-air region formed by the separation of the boundary layer due to a sudden recession of the guiding wall. For sonic or supersonic flow at the separation corner, a Prandtl-Meyer expansion takes place in the free stream from ① to ②. In region ②, pressure equality is assumed between the free-stream and the dead-air region, i.e., constant pressure across the jet mixing region. A pressure gradient or flow direction change between ② and ③ can result from the impingement of interference lines from other fluid boundaries. The direction change at nearly constant pressure can be tolerated by the theory. At the end of the free jet, wall reattachment and recompression take place. The pressure in region ④ is impressed upon the viscous layer by the adjacent free stream. Chapman assumed this recompression to be that resulting from a reversible compression turn from ③ to ④. Korst used an oblique shock turn from ③ to ④. These differ only slightly for low Mach numbers (less than 3 at section ③) since the turning angle is small.

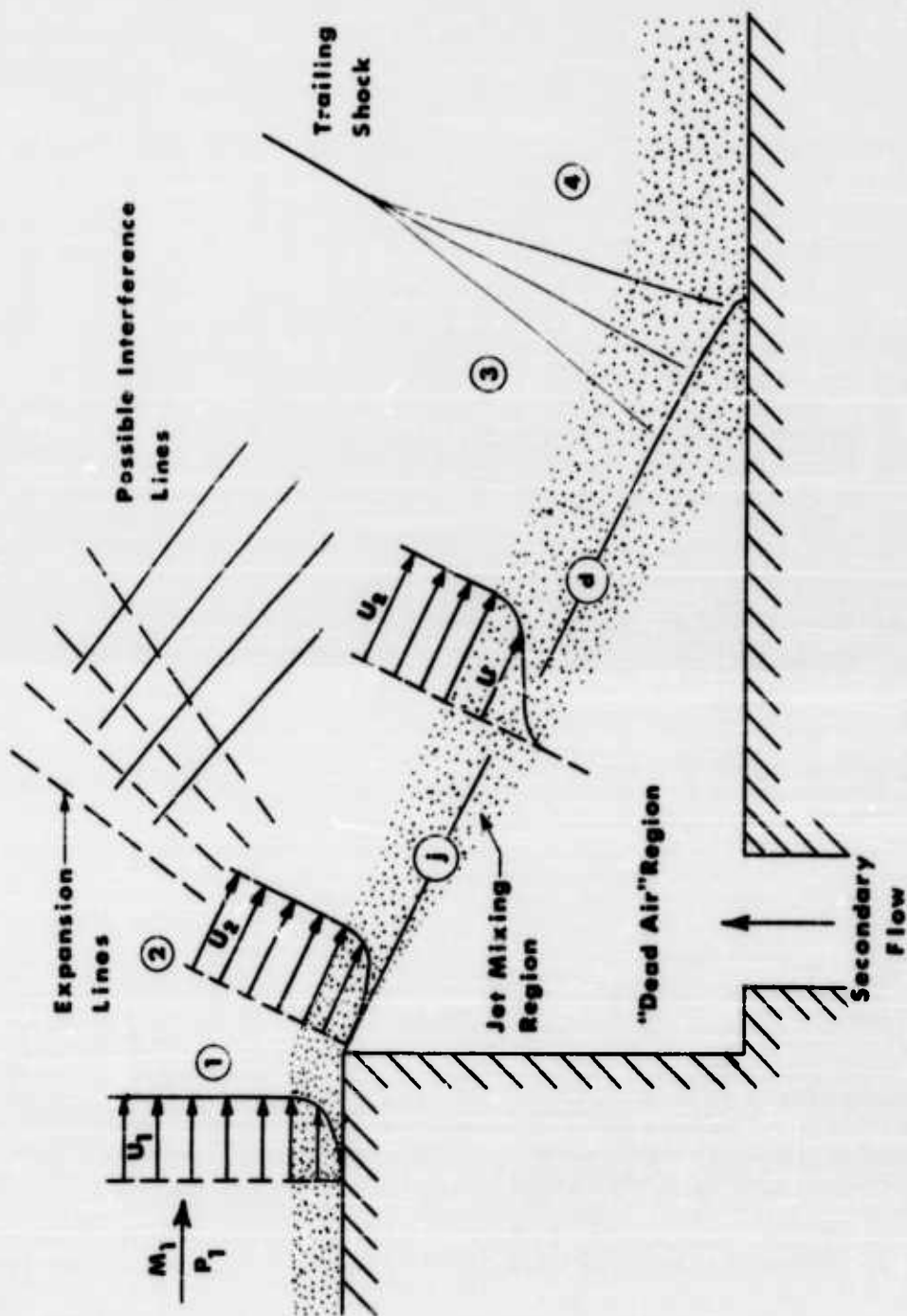Figure 3. Korst - Chapman flow model.

A streamline, j, can be identified which divides the amount of mass passing over the corner at ① from that mass flow entrained by the viscous action of the free jet. A second streamline, d, can be identified which has just sufficient kinetic energy at ③ to penetrate the pressure rise to ④. Streamlines above this one have higher kinetic energies and enter the recompression zone ④ with a remaining velocity. Streamlines below have lower kinetic energies and are unable to escape through the recompression, but are turned back to recirculate in the (nearly) dead-air space. If there is no secondary flow, the conservation of mass in the dead-air region requires that the j and d streamlines be identical. Chapman did not include the possibility of secondary flow, but Korst distinguished between these two streamlines and pictured the space between them as a sort of corridor through which mass would flow into or out of the trapped "dead-air" space. All that remains for a stable pressure solution is knowledge of the velocity profile in the viscous layer in the vicinity of the reattachment. Fortunately, the profiles approach a fully-developed shape, independent of streamwise location (except for width) if the jet is sufficiently long compared to the boundary layer thickness to allow the influence of the initial boundary layer to die out. This "thin boundary layer" situation gives a unique pressure-geometry solution independent of scale for two-dimensional back-steps. The mixing theories were derived to provide profile information for this solution.

TURBULENT FREE-JET MIXING (KORST)

A theory for constant pressure, turbulent mixing of an isoenergetic free jet was developed by H. H. Korst at the University of Illinois (Ref. 4). Application of this theory to two-dimensional, isoenergetic base pressure type problems were made in Refs. 5 and 6, and tables were computed to make secondary flow problems tractable (Ref. 7). Extension to non-isoenergetic jets (differing stagnation temperatures in the free stream and "dead-air" regions) was made by Page (Ref. 8), by including energy equation in the basic development. Tables and curves were then published to permit rapid calculations for general non-isoenergetic back-step type flows, (Ref. 9) and the methods presented in Ref. 10. Further extensions were made to include the streamwise momentum of a secondary flow (Ref. 11 and 12) and the interaction of two supersonic streams separated by a rearward-facing surface (Refs. 12 and 13). Similar axi-symmetric problems were treated in Ref. 14. The most complete resume of all this work is given in Ref. 10. Transient base pressure situations have also been successfully treated (Refs. 15 and 16).

The mixing theory starts with an equation of motion simplified as in most boundary analyses. Since turbulence is present, the eddy viscosity (or "turbulent exchange co-efficient") term appears. A functional form is given for the eddy viscosity, following Görtler, and a transformation of co-ordinates is introduced to simplify the differential equation. A solution is then obtained for the velocity ratio (local velocity divided by adjacent free-stream velocity) as a function of a position parameter $\eta = \sigma y/x$ where x and y are intrinsic co-ordinates in the streamwise and normal directions, and σ is a similarity parameter. The σ parameter represents the rate of jet spreading with length and is a function of Mach

number and fluid. The resulting "fully developed" profile which is asymptotically approached is:

$$u/u_2 = \frac{1}{2} (1 + \mathrm{erf}\, \eta).$$

A second term added to the right side of the equation gives the decaying initial boundary layer contribution.

Conservation of mass and momentum are sufficient to specify the j streamline velocity and the location of the intrinsic streamlines with respect to the boundary of an inviscid jet having the same properties as the free stream. Tables and charts giving integrated mass flow below a given streamline permit secondary flows to be calculated. These integrations are functions of the total temperature ratios of the two streams for non-isoenergetic cases.

For fluid amplifier application, the above can be summarized as follows:

TURBULENT MIXING THEORY STATUS (KORST)

VATIATIONS WHICH HAVE BEEN TREATED:
1) Secondary Flow at Zero Momentum.
2) Heat Transfer to Dead-Air Region.
3) Various Gases.
4) Interaction of Two Streams
5) Transient Conditions.

TREATED IN SPECIAL CASES ONLY:
1) Momentum Effect of Secondary Stream.
2) Influence of Oncoming Boundary Layer.

LIMITATIONS:
1) Constant Pressure Along Mixing Region.
2) Empirical Data: For Secondary Flow Solution Jet Spreading Parameter Needed. This is Function of Fluid and Mach Number.

LAMINAR FREE-JET MIXING THEORY (CHAPMAN)

The theory of laminar mixing developed by Dr. Dean R. Chapman of Ames Laboratory, NACA/NASA, was presented in Ref. 17, and applied to base flow problems in Ref. 18. More extensive application and evaluation is given by Chapman in Ref. 19 and more recently by Beheim in Ref. 20. The method has not been developed to nearly the same extent as the turbulent theory for two reasons:

(a) Laminar separated flows are not so likely to occur, since they are notoriously unstable. At atmospheric conditions and moderate supersonic velocities, laminar mixing regions experience transition to turbulent within a few tenths of an inch. However, Chapman warned (Ref. 19) that high altitude hypersonic flight conditions would return laminar free jets

to prominence in aerodynamics. Similarly, small sizes, low densities, and high temperatures will tend to present fluid amplifier designers with stable laminar jets.

(b) The second cause for incomplete development came from a fortuitous simplification in the solution for simple back-step base pressure. The velocity ratio of the j (dividing) streamline was found to be almost constant for air, nearly independent of adjacent free-stream Mach number and only slightly influenced by the specified temperature-viscosity relationship. This permitted the expressing of base pressure in a simple equation dependent only on Mach number and pressure of the oncoming stream (section ① of Figure 3). Thus, part of the incentive for detailed development was removed.

Chapman also began with a simplified equation of motion,

$$\rho u \frac{\partial u}{\partial x} + \rho v \frac{\partial u}{\partial y} = \frac{\partial}{\partial y} \left(\mu \frac{\partial u}{\partial y} \right)$$

This, together with the continuity relation and a simplified energy equation, was solved with the aid of the following approximations or simplifications:
a) Perfect gas.
b) Prandtl number is unity.
c) Viscosity is related to temperature by $\frac{\mu}{\mu_2} = C \left(\frac{T}{T_2} \right)^{\omega}$, where C is a constant depending on T and T_2, and ω is a constant.ˣ The exponent, ω, is 0.76 for air, but little effect is seen on the velocity by the use of $\omega = 1.0$, a simple linear relation.
d) The boundary layer at the separation corner is negligible in thickness so that similar profiles exist in the separated flow mixing zone.

A transformation of co-ordinates was effected by use of the stream function and a solution for the velocity profile could be found by numerical integration. The resulting velocity was expressed as a function of a modified stream function. No single profile resulted, but a family having M_2, the adjacent free-stream Mach number, as the parameter. The profiles can be converted to physical co-ordinates by means of a simple quadrature. (See Ref. 17 for profiles.)

Although secondary flow problems have not been considered in the formulation of the theory, the possibility of doing so is intrinsic in the theory (Ref. 21). A brief development of this is given in the Appendix. Further extension to be applicable to gases other than air requires only

---

* This exponential relation for viscosity-temperature has since become quite widely used in boundary layer analysis.

a satisfactory viscosity-temperature relation. The interaction of two supersonic streams should also be capable of treatment. Although much more difficult the non-isoenergetic laminar jet mixing should be possible to analyze by the Chapman approach.* Experimental verification should be sought, however, before confidence can be established in each of these extensions.

One feature of the Chapman-Korst model requires some discussion. The d streamline which stagnates at a reattachment wall is pictured as performing this recompression isentropically. When one notes that the streamline is in a viscous region with thermal gradients, it seems clear that the flow along a streamline is neither adiabatic nor reversible. Yet experimental verification seems conclusive that isentropic relations describe the pressure-velocity exchange. In Ref. 10, a discussion and explanation appears, in which the isentropic, but diabatic and irreversible, process is shown to be likely for turbulent, isoenergetic mixing. However, it remains questionable for highly non-isoenergetic mixing and for large secondary flow rates.

In summary, then, for fluid amplifier usage:

LAMINAR MIXING THEORY STATUS (CHAPMAN)

NOT WELL DEVELOPED DUE TO:
1) Limited Occurence.
2) Simple Solution Resulted For Base Pressure.

VARIATIONS WHICH SHOULD BE TREATABLE:
1) Secondary Flow
2) Heat Transfer to Dead-Air Region
3) Various Gases.
4) Interaction of Two Streams.

LIMITATIONS:
1) Constant Pressure Along Mixing Region.
2) Simple Viscosity-Temperature Relation.
3) Prandtl Number of One.
4) No Initial Boundary Layer.

EXAMPLE OF APPLICATION

An example of the application of the turbulent theory to a boundary layer type component has been calculated. The configuration is shown in Figure 4. Here a M = 2 air flow separates from the walls of a nozzle producing uniform, parallel flow. For this example, the ambient pressure has been made equal to the nozzle exit pressure. If this were not true, disturbance lines would originate at the opposite (top) separation corner,

---

* Chapman has suggested that this can be done. (Ref. 17, p.5)

Figure 4

EXAMPLE OF CALCULATED
COMPONENT PERFORMANCE

209

Figure 5

EXAMPLE OF CALCULATED
COMPONENT PERFORMANCE

$$\frac{P_{amb}}{P_i} = 1$$

$$M_i = 1.8$$

BREAK-AWAY LENGTH, $\frac{L}{h_g}$

$\frac{\Delta C_g}{h_g}$
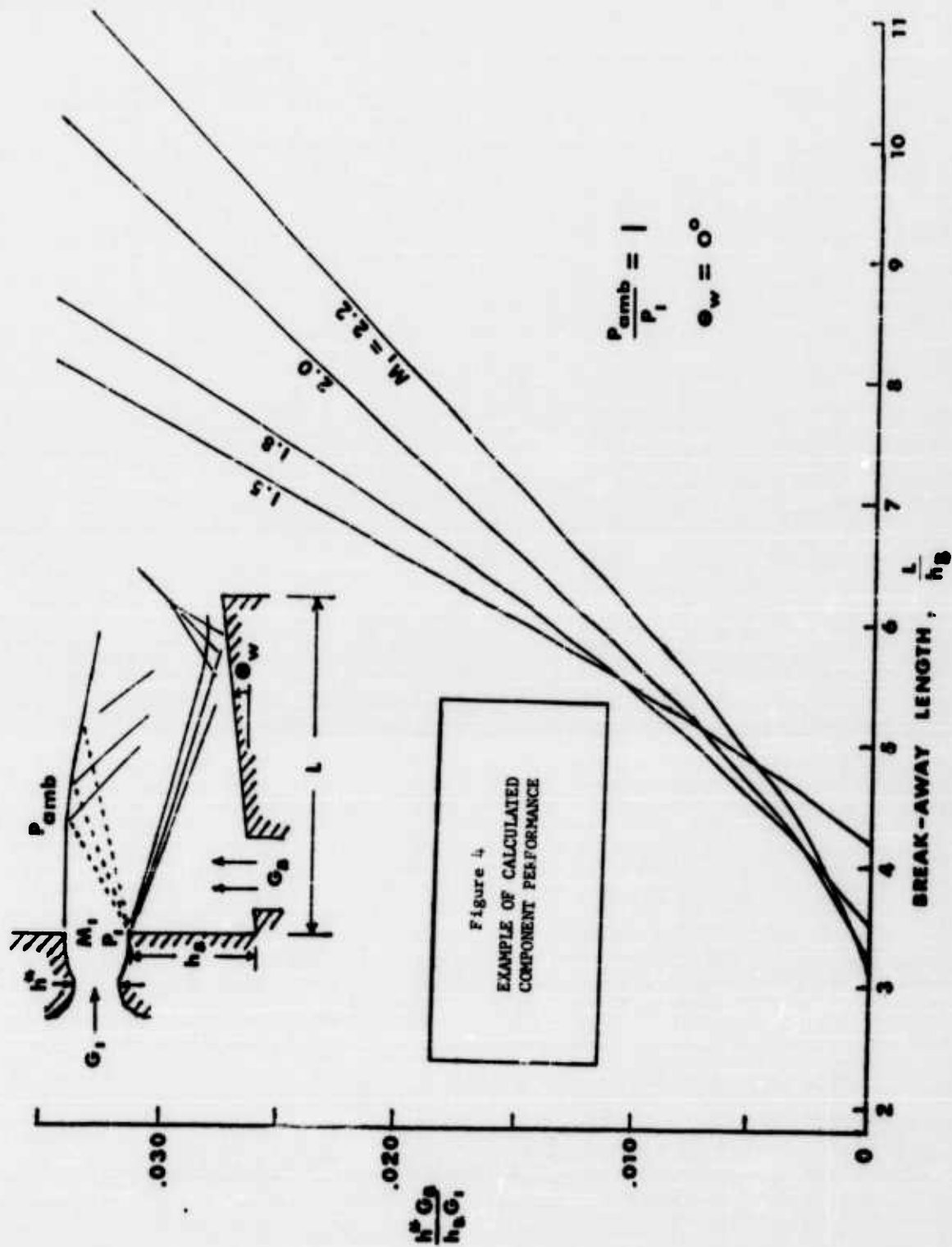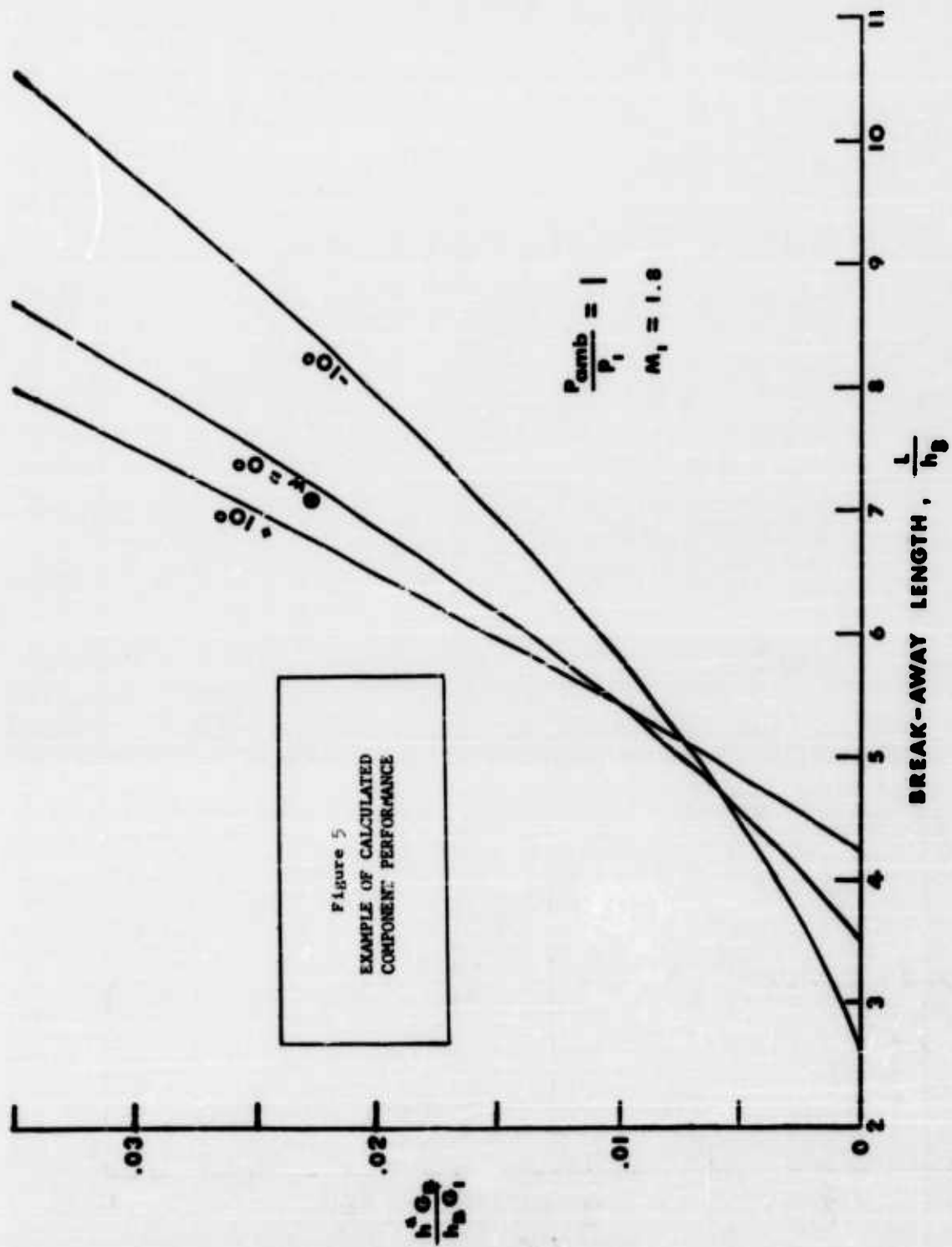
and the free jet would be curved. The curved path of an inviscid jet boundary under similar conditions would then be found by the method of characteristics, and the recompression turning angle would be given by this path.

For the straight jet boundary assumed here, the reattachment point is a function of the pressure and the geometry. For fixed wall geometry the pressure in the separated region can be increased by adding a secondary flow of mass, thus moving the reattachment point downstream. When the center of the mixing region * reaches the wall termination, break-away of the jet from the wall is eminent.

The calculations can be performed with the aid of standard isentropic flow tables plus Figure 13 of Ref. 10. The effect of secondary stream momentum is not included in this analysis, but would cause the break-away to occur at slightly lower G_B values. Such a calculation can be performed for laminar regions by utilizing the relations presented in the Appendix.

CONCLUSIONS

The two jet mixing theories discussed herein can be applied immediately with confidence to many plane flow fluid amplifier problems. In order to treat a wider range of such problems, it is the author's recommendation that the following work be attempted by those concerned with fluid amplifiers:

Experimental Work:
1. Verification of the predicted laminar jet entrainment rates. The theory predicts that laminar entrainment is proportional to the square root of the jet length, rather than being proportional to the first power of length as is well verified for turbulent jets.
2. Determination of jet spreading rate parameters for turbulent free jets for gases other than air, and for air at high temperatures.
3. Evaluate the effect of secondary flow on the laminar jet stability.
4. Evaluate the effect of heat transfer across the jet (non-isoenergetic mixing) on laminar free jet stability.

Analytical Work:
1. Alter Chapman's theory to include the influence of
   (a) the initial boundary layer.
   (b) differing stagnation temperatures (non-isoenergetic mixing).
   (c) various gases.
   (d) transient conditions.

---

* Actually, the "d" streamline.

211

2. Study the effect of impinging compression or expansion waves on turbulent profiles. (may be experimental, also.)
3. Calculate boundary layer influence decay rates for several representative cases.
4. Attempt to include the effects of transverse momentum of secondary flows in the analysis.
5. Extend the analytical model to include the "fully developed" jet, i.e., no remaining isentropic core.
6. Define the range of applicability of the assumption of isentropic recompression of the "d" streamline.
7. Explore the possibility of making a similar analysis of subsonic free jets.

212

REFERENCES

1. Bowles, R. E., B. M. Horton, and R. W. Warren, <u>Fluid Amplifier Handbook</u>, <u>Section 1</u>, <u>Chapter I</u>, <u>Introduction</u>. Diamond Ordance Fuze Laboratories, Washington, D. C., 1960.

2. Crocco, L., and L. Lees, <u>A Mixing Theory for the Interaction Between Dissipative Flows and Nearly Isentropic Streams.</u> Journal of the Aero. Sci., V. 19, 1952, pp. 649-676.

3. Rom, Josef. <u>Theory for Supersonic, Two-Dimensional, Laminar, Base-Type Flows Using the Crocco-Lees Mixing Concepts.</u> Journal of the Aero. Sci., V. 29, Aug. 1962. pp. 963-968.

4. Korst, H. H., R. H. Page, and M. E. Childs. <u>Compressible Two-Dimensional Jet Mixing at Constant Pressure</u>. Univ. of Illinois, (Engrg. Expr. Sta.,) ME-TN-392-3; OSR-TN-55-99, Contract AF 18(600)32, April 1955, (For Sale, $10.00 per copy).

5. Korst, H. H., R. H. Page, and M. E. Childs. <u>A Theory for Base Pressures in Transonic and Supersonic Flow.</u> Univ. of Illinois, Engrg. Exper. Sta., ME-TN-392-2, OSR-TN-55-89, Contract No. AF 18(600)392, March 1955.

6. Korst, H. H., <u>A Theory for Base Pressures in Transonic and Supersonic Flow.</u> Journal of Appl. Mech., V. 23, 1956. pp. 593-600.

7. Korst, H. H., R. H. Page, M. E. Childs. <u>Compressible Two-Dimensional Jet Mixing at Constant Pressure Tables of Axiliary Functions for Fully Developed Mixing Profiles.</u> Univ. of Illinois, Engr. Expr. Sta., ME-TN-392-3; OSR-TN-55-99, Contract No. AF 18(600) 32, April 1955, (For Sale, $10.00 per copy).

8. Page, R. H., and H. H. Korst. <u>Non-Isoenergetic Turbulent Compressible Jet Mixing with Consideration of its Influence on the Base Pressure Problem.</u> Proc. of the Fourth Midwestern Conf. on Fluid Mech., Purdue Univ., Sept. 1955. pp. 45-68.

9. Korst, H. H., and W. L. Chow. <u>Compressible Non-Isonergetic Two-Dimensional Turbine Jet Mixing at Constant Pressure, Auxiliary Intergrals, Heat Transfer and Friction Coefficients for Fully Developed Mixing Profiles,</u> Univ. of Illinois, Engrg. Exper. Sta., ME-TN-392-4, Contract No. AF 18(600)392. January 1959.

10. Korst, H. H., W. L. Chow, and G. W. Zumwalt, <u>Research on Transonic and Supersonic Flow of a Real Fluid at Abrupt Increases in Cross Section.</u> (Final Report). Univ. of Illinois, Engrg. Exper. Sta., ME-TN-392-5; Contract No. AF 18(600) -392, December 1959.

11. Wu, C. Y. <u>The Influence of Finite Bleed Velocities on the Effectiveness of Base Bleed in the Two-Dimensional Supersonic Base Pressure Problem.</u> Ph.D. Thesis, Dept. of Mech. Engrg., Univ. of Illinois. 1957.

12. Chow, W. L. On the Base Pressure Resulting From the Interaction of a Supersonic External Stream with a Sonic or Subsonic Jet. Journal of the Aero. Sci. V. 26, Mar. 1959.

13. Korst, H. H. and W. Tripp. The Pressure on a Blunt Trailing Edge Separating Two Supersonic Two-Dimensional Air Streams of Different Mach Numbers and Stagnation Pressures, but Identical Stagnation Temperatures. Proc. of the Fifth Midwestern Conf. on Fluid Mechanics, Univ. of Michigan. Apr. 1957, pp. 187-199.

14. Zumwalt, G. W. Analytical and Experimental Study of the Axilly-Symmetric Supersonic Base Pressure Problems. Ph.D. Dissertation, Dept. of Mech. Engrg., Univ. of Illinois, 1959.

15. Ihrig, Karl. A Study of the Base Pressure Problem for Supersonic Two-Dimensional Flow in which the Approaching Stream has Transient Properties. Ph.D. Thesis. Dept. of Mech. Engrg., Univ. of Illinois. 1961.

16. Zumwalt, G. W. and H. H. Tang. Blast Wave Effect on Missile Base Pressure. Research Report Prepared for the Aero-Thermodynamics Dept. of Sandia Corporation, Albuquerque, N. M., by the Office of Engineering Research, Okla. State Univ., Stillwater, Okla., Rpt. No. SBW-1, June 1961.

17. Chapman, D. R., Laminar Mixing of a Compressible Fluid, NACA Report 958, 1950.

18. Chapman, D. R., An Analysis of Base Pressure at Supersonic Velocities and Comparison with Experiments. NACA Report 1051, 1951.

19. Chapman, D. R., D. M. Kuehn and H. K. Larson, Investigation of Separated Flows in Supersonic and Subsonic Streams with Emphasis on the Effect of Transition. NACA TN 3869, 1957.

20. Beheim, M A. Flow in the Base Region of Axisymmetric and Two-Dimensional Configurations. Lewis Research Center, NASA-TR-R77, 1960.

21. Tang, H. H. and G. W. Zumwalt Adaptation of Chapman's Laminar Jet Mixing Theory For Use in Non-Steady Base Pressure Problems. Research Report Prepared for the Aero-Thermodynamics Dept. of Sandia Corporation, Albuquerque, N. M., by the Office of Engineering Research, Okla. State Univ., Stillwater, Okla. Rpt. No. SBW-2, June 1962.

An extension of the Chapman laminar jet mixing theory can be made to permit the calculation of mass passing between two streamlines in the mixing region. This calculation is necessary for problems involving secondary flows or transient conditions.

Referring to Ref. 17, we shall adopt the simple viscosity-temperature relation

$$\frac{\mu}{\mu_\infty} = C \left(\frac{T}{T_\infty}\right)^\omega ,$$

where μ is the absolute viscosity, T stream temperature, and C and ω are constants. The subscript ∞ refers to the adjacent free stream and the unsubscripted symbols refer to local condition in the mixing region. Dimensionless variables used are:

$$u^* = \frac{u}{u_\infty}$$

$$\zeta = \frac{\psi}{\sqrt{u_\infty \nu_\infty \, xC}}$$

Here ν is kinematic viscosity, x the length of the separated flow, and ψ the stream function. Thus, ζ is a modified stream function. In Ref. 17, a plot of u^* vs. ζ is given.

The mass rate per unit width flowing between the two streamlines "d" and "j" is

$$G_B = \int_{y_j}^{y_d} \rho u \, dy ,$$

where ρ is density and u and v are velocity components in the x and y directions.

From the definition of the stream function,

$$\left(\frac{\partial \psi}{\partial x}\right)_\zeta dx + \left(\frac{\partial \psi}{\partial \zeta}\right)_x d\zeta = \left(\frac{\partial \psi}{\partial y}\right)_x dy + \left(\frac{\partial \psi}{\partial x}\right)_y dx .$$

$$\left(\frac{\partial \psi}{\partial y}\right)_x = \frac{\rho}{\rho_\infty} u$$

$$\left(\frac{\partial \psi}{\partial x}\right)_y = - \frac{\rho}{\rho_\infty} v$$

215

From the definition of ζ.

$$\left(\frac{\partial \Psi}{\partial x}\right)_\zeta = \frac{1}{2}\zeta\sqrt{\frac{u_\infty \nu_\infty C}{x}}$$

$$\left(\frac{\partial \Psi}{\partial \zeta}\right)_x = \sqrt{u_\infty \nu_\infty x C}$$

Thus:

$$\frac{1}{2}\zeta\sqrt{\frac{u_\infty \nu_\infty C}{x}}\,dx + \sqrt{u_\infty \nu_\infty x C}\,d\zeta = \frac{\rho}{\rho_\infty}(u\,dy - \upsilon\,dx)$$

With x held constant, dy can be expressed:

$$dy = \frac{\rho_\infty}{\rho}\frac{1}{u}\sqrt{u_\infty \nu_\infty x C} = \frac{\rho_\infty}{\rho}\frac{\nu_\infty}{u}\sqrt{Re_x C}\,d\zeta$$

Substituting in the mass-flux equation:

$$G_B = \rho_\infty \nu_\infty \sqrt{Re_x C}\int_{\zeta_j}^{\zeta_d} d\zeta = \rho_\infty \nu_\infty \sqrt{Re_x C}\,(\zeta_d - \zeta_j)$$

Some values of C for air are suggested in Ref. 17 as functions of M_∞. Ref. 19 presents a discussion of the u_j^* value, which for air is almost a constant 0.587 for Mach numbers between 0 and 5. Thus, ζ_j can be found from Figure 2 of Ref. 17 to be a small negative number (about -0.01).

Thus, for known free stream conditions, G_d and $u_d = f(\zeta_d)$ are in a fixed relationship. The recompression pressure, which must be matched with u_d, provides the accompanying free stream condition. These must be satisfied simultaneously for a stable secondary flow solution.

INTERACTION OF TRANSVERSELY IMPINGING JETS

by

Darshan S. Dosanjh[*]
William J. Sheeran[**]

Mechanical Engineering Department
Syracuse University

Summary

Experiments on the interaction of transversely impinging jet flows were performed in which a low pressure control jet flow interacted with a relatively high pressure power jet flow. The ratio of the control jet to the power jet supply chamber gauge stagnation pressure was varied. Both two-dimensional and axisymmetric jets were used. Shadowgraphs of the power jet alone as well as of the corresponding interacting jet flows were recorded to establish the nature of, and changes in, the shock structure. The two-dimensional jet flows were traversed by a pitot tube to record pitot pressure at various locations downstream of the power jet exit.

It was observed that the impingement of only two per cent control jet flow was sufficient to change the normal shock front of the highly underexpanded two-dimensional jet flow to a repetitive oblique shock structure. A considerable increase in the corresponding maximum pitot pressure downstream of the previous location of the normal shock was recorded. Possible importance of this phenomenon to fluid amplifiers using such highly underexpanded power jet flows is pointed out.

---

[*] Professor of Mechanical Engineering

[**] Graduate Student, Mechanical Engineering Department

217

The behavior of the impinging axisymmetric jet flows was observed to be considerably different from that of the two-dimensional case. This as well as other observations such as the deflection angles, pressure recoveries, entrainment characteristics etc., of the interacting jet flows are discussed.

Symbols

α	Jet flow deflection angle measured with reference to transverse pivot point of $x/w = -25$.
b	Jet width
C.J.	Control jet
d	Jet nozzle exit diameter
δ	Jet flow deflection angle measured with reference to intersection point of power and control jet nozzle axes.
G	Pressure gain of pneumatic amplifier
P	Static pressure
P_a	Ambient pressure
P_0	Stagnation pressure
P_{OC}	Control jet settling chamber stagnation pressure in psia
$\overline{P_{CC}}$	Control jet settling chamber stagnation pressure in psig
P_{OP}	Power jet settling chamber stagnation pressure in psia
$\overline{P_{OP}}$	Power jet settling chamber stagnation pressure in psig
P_{TJ}	Local jet flow pitot pressure
P_{TJC}	Local jet flow centerline pitot pressure
P.J.	Power jet
ρ	Density
T_{OC}	Control jet settling chamber stagnation temperature
T_{OP}	Power jet settling chamber stagnation temperature
θ	Angular location
u	Velocity

218

w   Jet nozzle exit width

x   Distance measured along power jet nozzle centerline from power jet exit

y   Distance measured along control jet nozzle centerline from control jet exit

Introduction

In the last decade the problems associated with the interaction of jet flows with external flow fields have assumed increasing importance. Such problems are important in the reduction of noise from rockets and high speed jet aircraft[1], lift augmentation techniques[2], cooling of re-entry vehicles[3], mixing of liquid propellants in rocket engines[4] and thrust vectoring of rocket exhausts. More recently there has been the development of fluid operated control and computation systems, both here in the United States and in Russia[5,6]. The basic sub-system of most of these systems is the fluid amplifier which serves a purpose similar to the electronic amplifier in that it directs and controls the fluid flow energy. In a pure pneumatic amplifier a low energy jet flow (input or control jet) is used to direct a high energy jet flow (output or power jet) to a receiver or transducer. The pressure gain, G, of such a pneumatic amplifier may be defined as:

$$G = \frac{\text{Incremental pressure delivered to receiver}}{\text{Control jet pressure needed to direct the power jet to the receiver}}$$

From the existing experimental and analytical literature on free jet characteristics, it may be proposed that for the pneumatic amplifier

$$G = G(P_{OP}, P_{OC}, x/w, s, b, \ldots)$$

where P_{OP} and P_{OC} are the absolute stagnation pressures in the supply chambers of the power and control jets, respectively; x is the axial distance from the
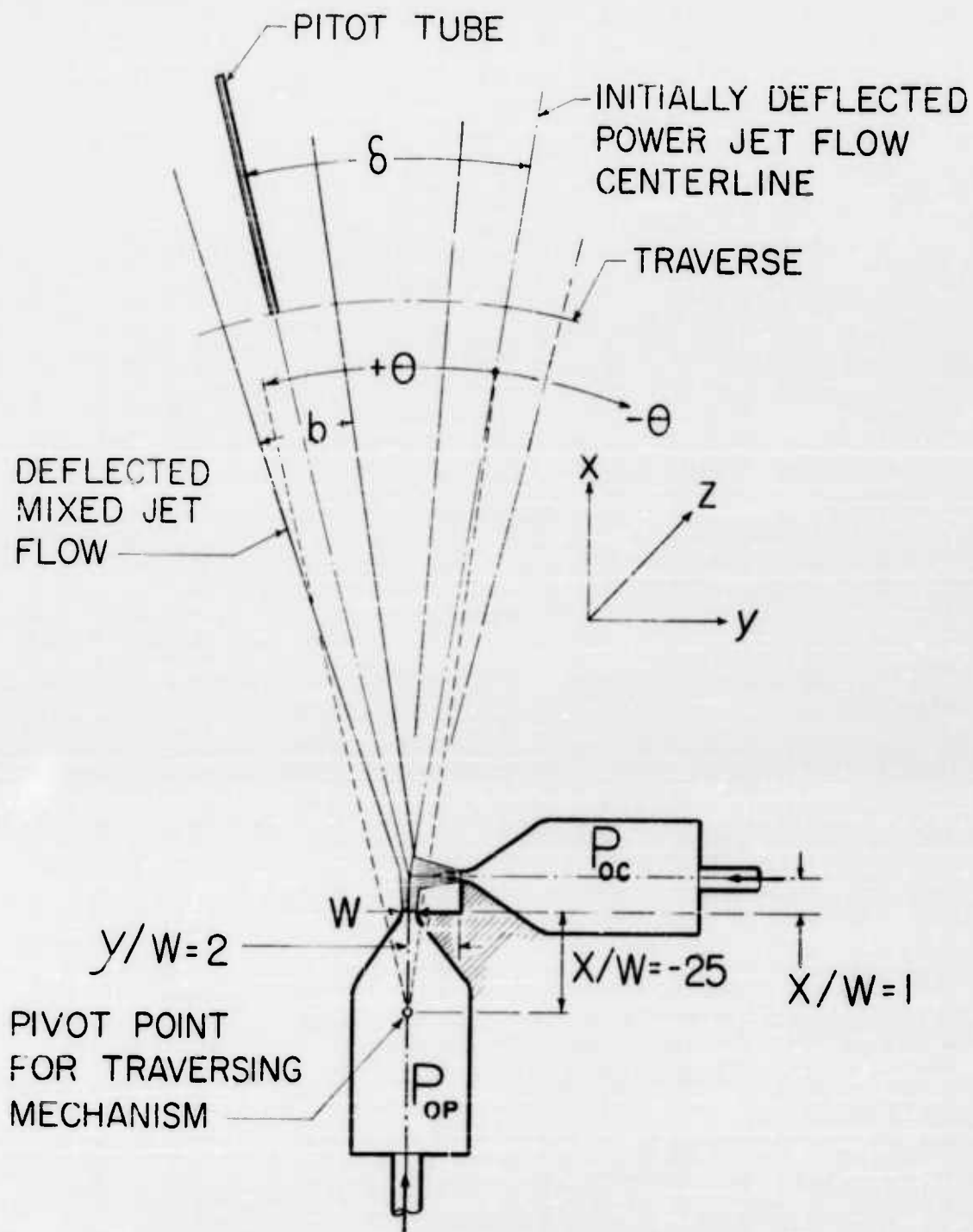
Figure 1. Illustration of interacting jets and important flow parameters.

220

power jet exit; w is the jet nozzle width; δ is the angle of deflection; and b is the jet flow width. (See Fig. 1 for this notation as applied to one of the arrangements used in these studies.) If the interacting jet flows are supersonic with their attendant shock structure, additional complexities arise in attempting to predict the behavior of such an amplifier.

To shed some light on these problems basic investigations of the interaction of high speed jet flows have been carried on in the Mechanical Engineering Department at Syracuse University, on an off and on basis for the last two years. The studies were initiated under the support of the Diamond Ordnance Fuze Laboratories in order to evaluate the interaction of high speed jets in relation to their possible use in pneumatic amplifiers. Under DOFL support from June 1960 to June 1961 the experimental facility was constructed and preliminary data were taken. During July and August of 1961 experiments were continued under support of the Mechanical Engineering Department. More recently a ten week study was carried on by Mr. Jeff Asher an undergraduate at Syracuse University and a holder of a National Science Foundation Undergraduate Research Stipend. A complete account of the experimental work done from June 1960 to August 1961 was reported in the Syracuse University Research Corporation Report DSL R-65, "Interaction of Confined Two-Dimensional Transversely Impinging Jets"[7] which was submitted to DOFL in August of 1961. The present paper includes some of the basic experimental findings of the past two years including the behavior of the shock structure, pressure recoveries, entrainment characteristics, and deflection angles of the interacting jet flows.
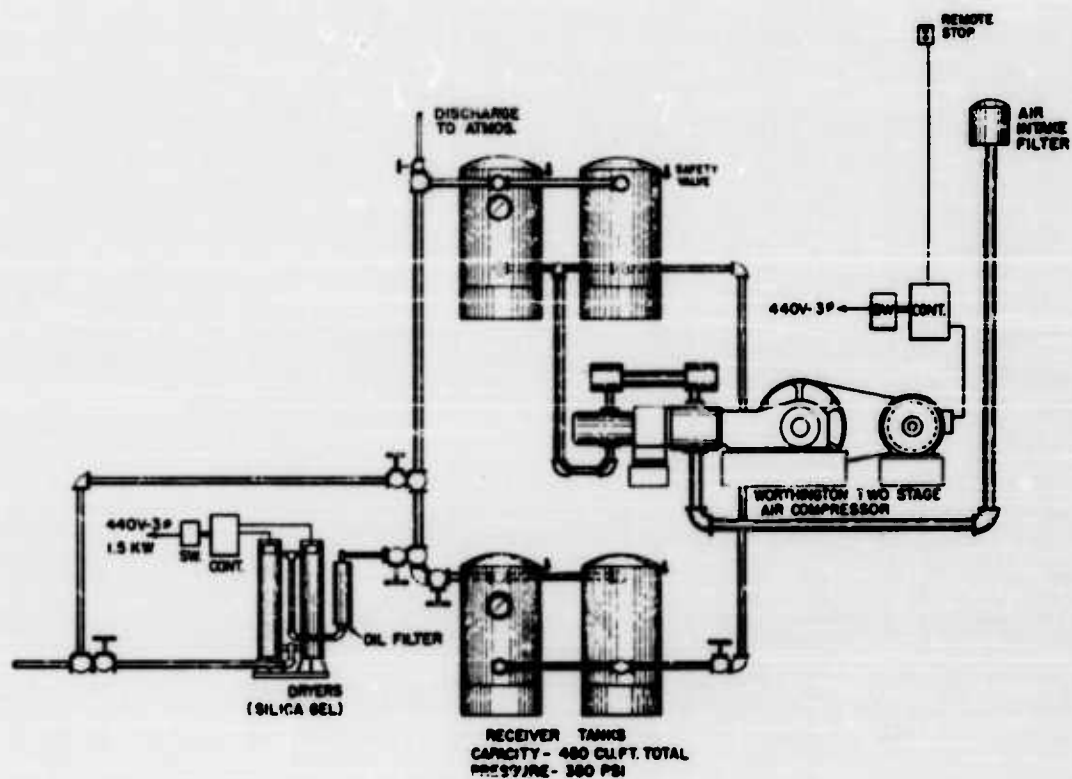
Figure 2. Schematic Diagram of Compressed Air System

Experimental Facility

1. Compressed Air Facility and Pressure Control System

The schematic arrangement of the compressed air facility used in these studies, including the compressor, storage tanks, oil filter, and dryer is shown in Fig. 2. The two-stage air compressor has a pumping capacity of 270 cfm with a maximum obtainable pressure of 350 psig. The compressed air storage tanks have a total capacity of 450 cu. ft.. The air flowing from these tanks passes through an oil filter and an electrically reactivated dryer which employs silica gel and molecular sieves as drying agents. As a result of the long flow path involved between the storage tanks and jet nozzles, the air supply process was found to be isothermal. From the throttled isothermal expansion flow relation, and for the jet areas involved, it was found that for just choked jet flows almost 8 hours of run time is available with this system.

In gathering the experimental data on the interacting jets it was imperative that the supply pressures of the power and control jets be independently controllable to any level and that this pressure remain constant at the desired setting even when the main storage tank pressure falls over an extended range, say 350 to 5 psig, during the run. Micro-flow diaphragm control valves were used for precise control of the stagnation pressure in the settling chambers of the jets over the entire anticipated range of operation, 0-350 psig. The arrangement of the control valves along with their control system is shown in Fig. 3. With the 1/32" x 3/8" jet exit area used in these studies, a maximum weight rate of flow of 4.5 lb/min at a settling chamber pressure of 300 psig was to be controlled. Since it was planned to use smaller jet exit areas and subsonic exit velocities, the range of possible weight flow rates necessitated the use of two different control valves for each

Figure 3. Block diagram of test facility.

224
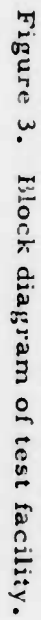
of the two jets. A high mass flow rate valve which could control from 0.3 to 4.5 ppm was installed in parallel with a low mass flow rate valve which could control 0.009 to 0.9 ppm, for each jet supply system. Since the power and control jets were used at various independent settings they had independent control systems. One pressure pilot was installed to control both the high and low mass flow rate valves in each jet supply line since only one of the two valves was to be used at a time.

2. Jet Arrangements and Test Section

The details of the two-dimensional jet nozzles used in these studies are shown in Fig. 4. All the two-dimensional nozzles used were identical in construction having small 3" x 3/8" x 5/16" supply chambers which converged to the 1/32" x 3/8" (aspect ratio of 12) nozzle exits. The leaking of air and the deflection of the converging nozzle side elements, with the attendant increase in exit area, at the higher pressures offered the main design problems for the nozzles. After much trial and error a suitable groove-gasket arrangement was found to completely seal the nozzle blocks. The converging pieces of the final design were such that only a 2.5 per cent increase in the exit area occurred at a supply chamber pressure of 200 psig.

The sketch of Fig. 1 shows one of the jet arrangements used and Fig. 4 shows the test section used in conjunction with this particular arrangement. The power jet and control jet nozzle centerlines were perpendicular to each other, as they were in all the arrangements, with the control jet nozzle axis located at $x/w = 1$ downstream of the power jet exit and the control jet exit located at $y/w = 2$ from the power jet nozzle axis. The jet width w is the 1/32" exit dimension, x is measured along the power jet nozzle axis from the power jet exit and y is measured along the control jet nozzle axis from the

Figure 4a. Jet arrangement and probe traversing mechanism.
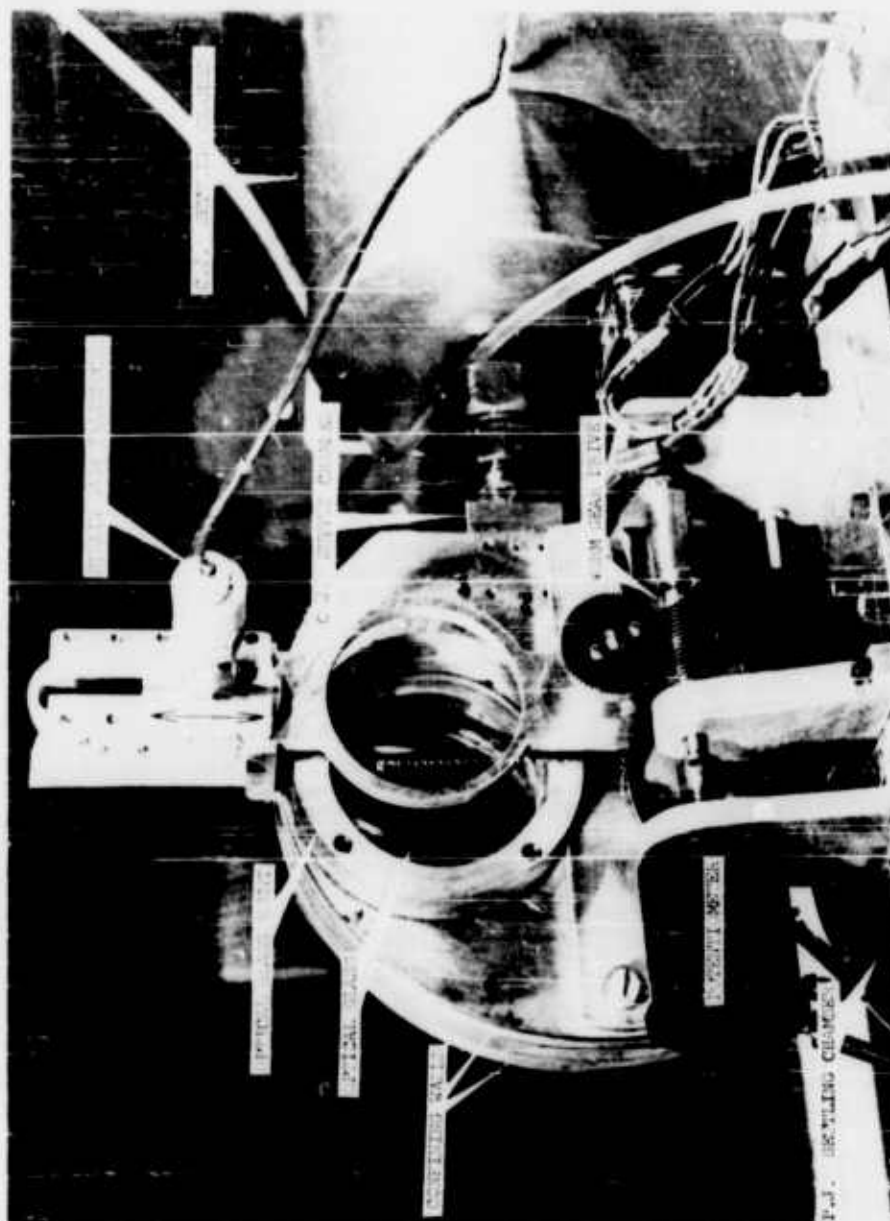
Figure 4b. Test section and traversing mechanism for 1-2-1 and 1-2-1D arrangements.

227

control jet exit. As shown in the sketch, no gap was provided for free entrainment of air between the power and control jet nozzles. Since the other side of the power jet was unobstructed, the resulting entrainment to the jet flow was asymmetric for this particular arrangement. This arrangement was referred to as the 1-2-I arrangement; the first figure, 1, refers to the x/w distance from the power jet exit to the control jet nozzle centerline; the second figure, 2, refers to the y/w distance from the control jet exit to the power jet nozzle centerline; and the letter, I, stands for insert which indicates no entrainment allowed between the nozzles. This arrangement along with the others used is also illustrated in Fig. 5.

To eliminate the entrainment asymmetry of arrangement 1-2-I some data were recorded with a dummy jet nozzle in position as shown in Fig. 5, this arrangement being referred to as 1-2-ID. The other arrangements shown in Fig. 5 were used in a different test section than that shown in Fig. 4, which was for the 1-2-I and 1-2-ID arrangements; however, the jet nozzle construction was similar. The flow characteristics of the 12-12-0 arrangement (letter 0 indicates free entrainment between nozzles) are compared with those of the 1-2-I and 1-2-ID arrangements. The majority of the results discussed in this paper, however, were recorded with the 1-2-I and its associated 1-2-ID arrangement.

The test section and traversing mechanism for the 1-2-I and 1-2-ID jet arrangements are shown in Figs. 4. A curved pitot probe was employed for pressure measurements so as to minimize obstruction to the flow by the probe. The sensing portion of the probe, the tip of which could be located at various axial distances, x/w's, downstream of the power jet exit, was $3/8$" long with a 0.0285" outside diameter. The outside diameter of this sensing portion gradually opened in a distance of 1 1/8" to the full 3/16" outside diameter

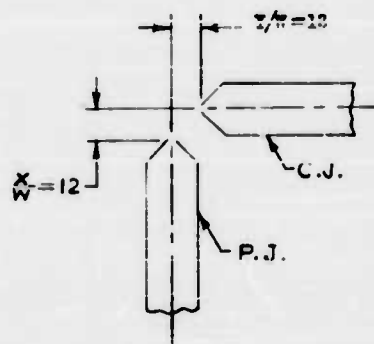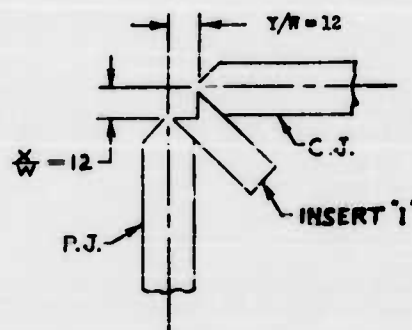228
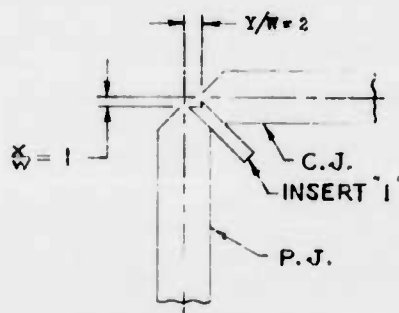
ARRANGEMENT 1-2-1   ARRANGEMENT 1-2-1D
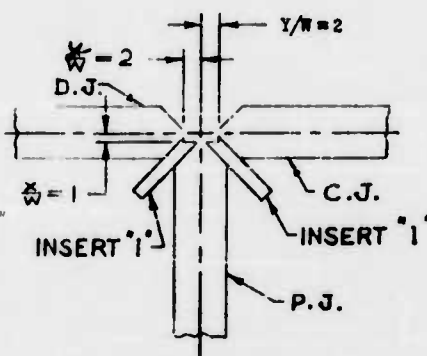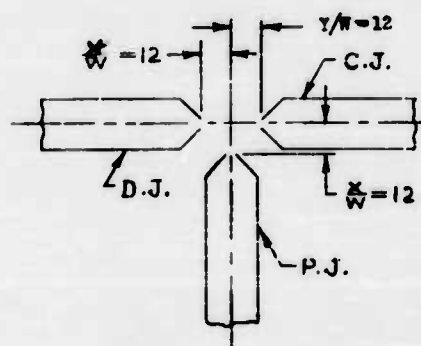
ARRANGEMENT 12-12-0   ARRANGEMENT 12-12-1

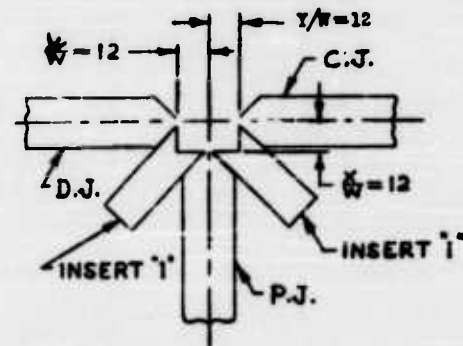ARRANGEMENT 12-12-0D   ARRANGEMENT 12-12-1D

Figure 5. Jet arrangements.

229

of the main pitot tube stem. It was found that any interference by the curved probe itself on the recovery jet flow pitot pressures was negligible compared to the pressures actually recorded. A strain gage pressure transducer was mounted either directly on the end of the probe, as shown in Figs. 4, or remote from the tube; the particular arrangement depending on the magnitude of the pitot pressures encountered. For recovery pitot pressures less than 100 psig a smaller transducer mounted directly on the end of the probe could be used, while for pitot pressures greater than 100 psig a higher capacity transducer had to be used. The larger transducer was too heavy for the traversing mechanism, therefore, it was connected to the pitot tube through a short flexible high pressure tube. The traversing mechanism for this test section pivoted about the point $x/w = -2$ (see Fig. 1), giving a nearly straight pitot tube traverse at right angles to the jet flow centerline, for most of the flows encountered in these studies.

To avoid the very difficult problem of affecting a leak proof seal between the glass windows and the metallic nozzle blocks for high operating pressures, and to avoid stressing the interferometric quality optical glass itself, it was decided not to have the glass cover the nozzle exits. Also the impingement point of the interacting jet flows was not exposed. The test section used in connection with the 12-12-0 and its associated arrangements (Fig. 5) was similar in construction to the one shown in Figs. 4 but did not have the glass windows for photographic work.

3. Instrumentation and Procedure

The experimental arrangement for recording pressures and temperatures is shown in Fig. 6. The general arrangement of the overall instrumentation is
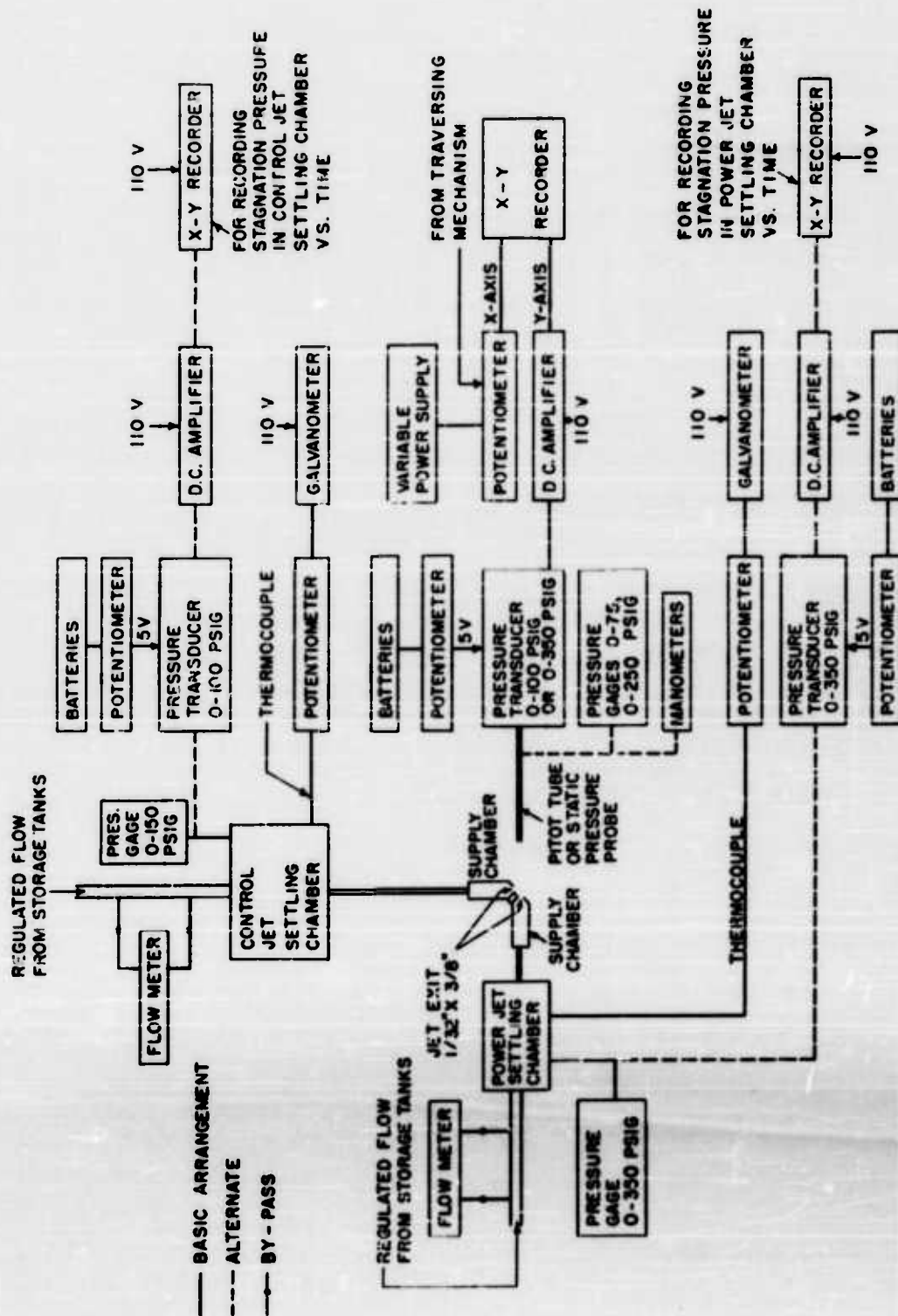
230

Figure 6. Experimental arrangements for recording pressures and stagnation temperatures.

231

shown in Fig. 3. However the interferometer was not used in these investigations; only shadowgraphic data were recorded.

The power and control jet supply chamber absolute stagnation pressures, P_{OP} and P_{OC} respectively, were measured in large settling chambers connected to the jet nozzles by short rigid fittings. Calibrations revealed that the losses in stagnation pressure occurring between these large settling chambers and the corresponding small nozzle supply chambers just ahead of the jet exits (see detail drawing of Fig. 4a) were negligible (maximum loss, 1/4 per cent of settling chamber pressure). The large settling chambers were constructed from heavy 4" diameter steel pipe about 2 feet long with outlet transitions which tapered smoothly in a conical shape from the 4" diameter down to the 1/2" diameter connection to the two-dimensional nozzle block.

The pitot tube strain gage pressure transducer arrangement was discussed earlier in connection with the test section. The pressure recording instrumentation is shown in Fig. 6. The transversing mechanism (Figs. 4) moved at such a slow speed that when the smaller transducer mounted directly on the end of the probe was used the response time of the pressure recording system was confirmed to be fast enough to allow the automatic recording of the jet pitot pressure as a function of angular location (see Fig. 15 for an original x-y recorder data sheet). The angular location was indicated by the output of a potentiometer attached to the transversing mechanism drive shaft. When the heavier transducer, mounted remote from the pitot tube, was used the pressure response of the system was slowed noticeably so that a point to point traverse, rather than a continuous one, was necessary. All the transducers used in the studies were calibrated frequently under all expected ranges of operation. If an independent check on the x-y recorder data was desired a manually operated pitot tube - manometer or pressure gage combination was used.

Stagnation temperatures in the settling chambers of both jets, T_{OP} and T_{OC}, were recorded at frequent intervals during the operation of the jets by thermocouples mounted at the midsections of the large settling chambers. It was established that these stagnation temperatures did not vary much from the ambient room temperature. However, the smaller supply chambers of the individual jets gradually cooled when the jets were operated; quantitative measurements of this effect were not made.

During the course of these investigations spark shadowgraphs of the interaction of the jet flows were taken. Recently it was found that Kodak Contrast Process Ortho film developed at higher temperature and longer time than recommended gave high contrast shadowgraphs. In previous studies the very fast Kodak Royal X-Pan film was used with an attendant loss in contrast. To emphasize the shock structure in the flows the film was mounted as close as possible to the flow while to emphasize the turbulence and sound emission characteristics of the jet flows it was mounted farther away. Considerable difficulty was experienced with oil in the air supply during the photographic observations, particularly for the shadowgraphs taken this past summer. Part of this oil contamination has been traced to the oil in pressure gages used for measuring settling chamber pressures.

Experimental Observations and Discussions

1. Collapse of Normal Shock in Highly Underexpanded Power Jet Flow

During the course of the investigations with the 1-2-1 arrangement and convergent nozzles, power jet settling chamber pressures of 200 and 300 psig were used. The usual shock structure present in highly underexpanded jet flows was observed[8,9,10]. The shadowgraph of the power jet flow alone for $\overline{P_{OP}}$ = 200 psig, as shown in Fig. 7a, illustrates this shock structure which consisted
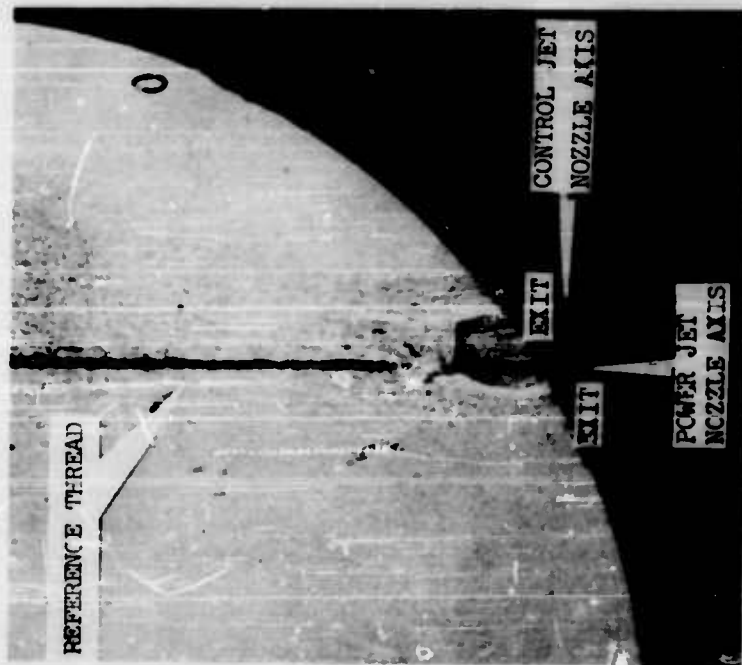
(7a) 0 per cent control
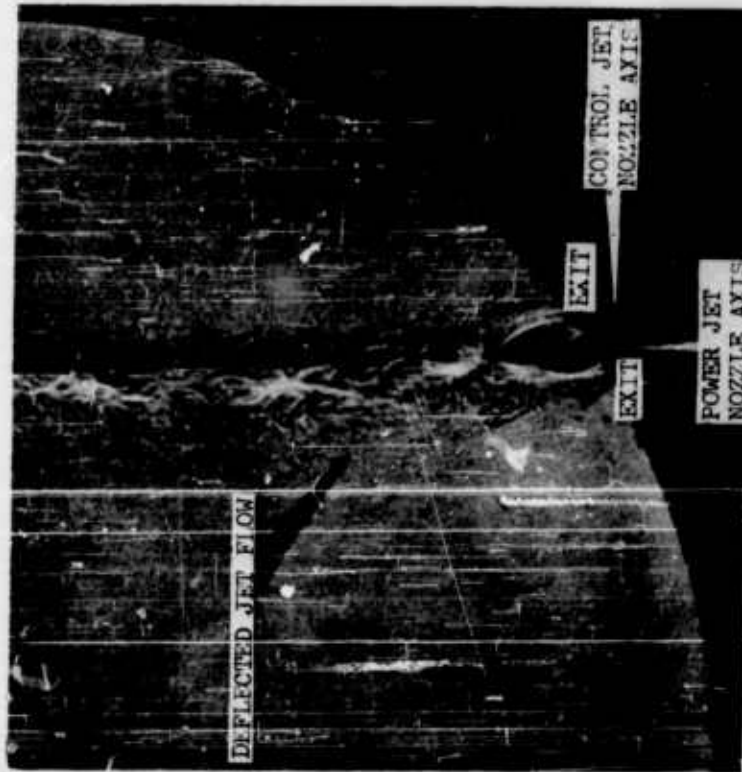
(7b) 10 per cent control

Figure 7.

Shadowgraph of interacting two dimensional jet flows.
Atmospheric pressure = 29.52" of Hg.   Room temperature = 71°F
POP = 214.50 psia $T_{OP} = 71°F$, $T_{OC} = 71°F$
Arrangement 1-2-1

234

of intercepting shocks which extend from the nozzle exit downstream to the location where they are connected with a normal shock. At $\overline{P_{OP}}$ = 200 and 300 psig this type of structure essentially consisted of only one cell; it did not repeat in the downstream direction as it may in less highly-underexpanded flows. Indicated in Figs. 7a and b are the power and control jet nozzle axes as well as the approximate positions of the jet exits which are not exposed by the optical window as stated earlier. The reference thread indicates the power jet nozzle centerline.

These studies revealed that when a relatively low energy control jet flow was transversely impinged on the highly underexpanded two-dimensional power jet flow, with the impingement point between the location of the normal shock and the jet exit, the shock structure of the highly underexpanded power jet flow was radically changed. The normal shock disappeared yielding the familiar repetitive oblique shock or diamond structure observed in less underexpanded jet flows. This behavior is illustrated in Fig. 7b where a 10 per cent control flow impinged on the power jet flow shown in Fig. 7a. Per cent control is defined as $100\,\overline{P_{OC}}/\overline{P_{OF}}$.

For $\overline{P_{OP}}$ = 200 psig the normal shock was located at x/w = 7.7 and the control jet flow impinged at x/w = 1. It was observed that as little as 2 per cent control flow addition was sufficient to cause the normal and intercepting shock pattern to change to the oblique or diamond shock structure for $\overline{P_{OP}}$ = 200 psig. The shadowgraph confirming this is shown in Fig. 8b; Figs. 8a and c correspond to Figs. 7a and b for zero and 10 per cent control. The heavy dark line appearing in Figs. 8 is a reference line which is parallel to, but not coincident with, the power jet nozzle axis. The shadowgraphs of Fig. 8 were taken with Kodak Contrast Process Ortho film which gave much better contrast than those of Fig. 7 which was taken with Kodak Royal X-Pan. However
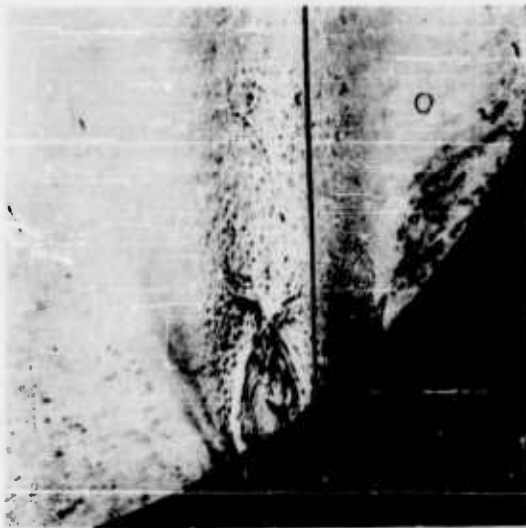
235

Figure 8b. 2 per cent control.

Figure 8c. 10 per cent control

Figure 8a. Shadowgraph of interacting two-dimensional jet flows.
0 per cent control   Atmospheric pressure = 29.46" of Hg.
P_{OP} = 214.47 psia   Room temperature = 71°F
Arrangement 1-2-1

in Figs. 8, the streaks due to the oil in the supply air are apparent.

In order to record the effects of this shock structure change on the jet flow pressure distribution for $\overline{P_{OP}}$ = 200 psig, pitot tube traverses were taken at x/w = 10 (i.e. downstream of the normal shock location at x/w = 7.7 in the power jet flow alone). A shadowgraph taken with the probe at x/w = 10 did not reveal any detectable change in the shock structure shown in Figs. 7 and 8. The plot of the ratio of the local jet flow pitot pressure to the power jet settling chamber pressure, P_{TJ}/P_{OP}, versus the angular location in the jet flow, θ, is shown in Fig. 9. The angular location, θ, is measured to either side of the zero per cent control power jet flow centerline and with respect to the pivot point of the traversing mechanism at x/w = -25, (see Fig. 1). The negative angular locations are measured toward the control jet side, the direction of impingement of the control jet flow being indicated on the plot by an arrow. The location of the actual power jet nozzle centerline was at θ = +1.25 approximately, indicating that the zero per cent control power jet flow is initially deflected towards the control jet nozzle because of the restricted entrainment from the control jet side.

The central low pitot pressure region in the zero per cent control curve corresponds to the jet flow that passed through the normal shock. The pressure in this region is only about 21.5 psia indicating a large loss in the jet flow stagnation pressure across the normal shock. The higher pressure peaks on either side of the central region correspond to the flow that crossed the intercepting shocks at very oblique angles and therefore experienced a relatively less severe entropy rise (stagnation pressure loss).

The effect of the addition of 2 per cent control jet flow on the shock structure for $\overline{P_{OP}}$ = 200 psig and the corresponding effect on the pitot pres-
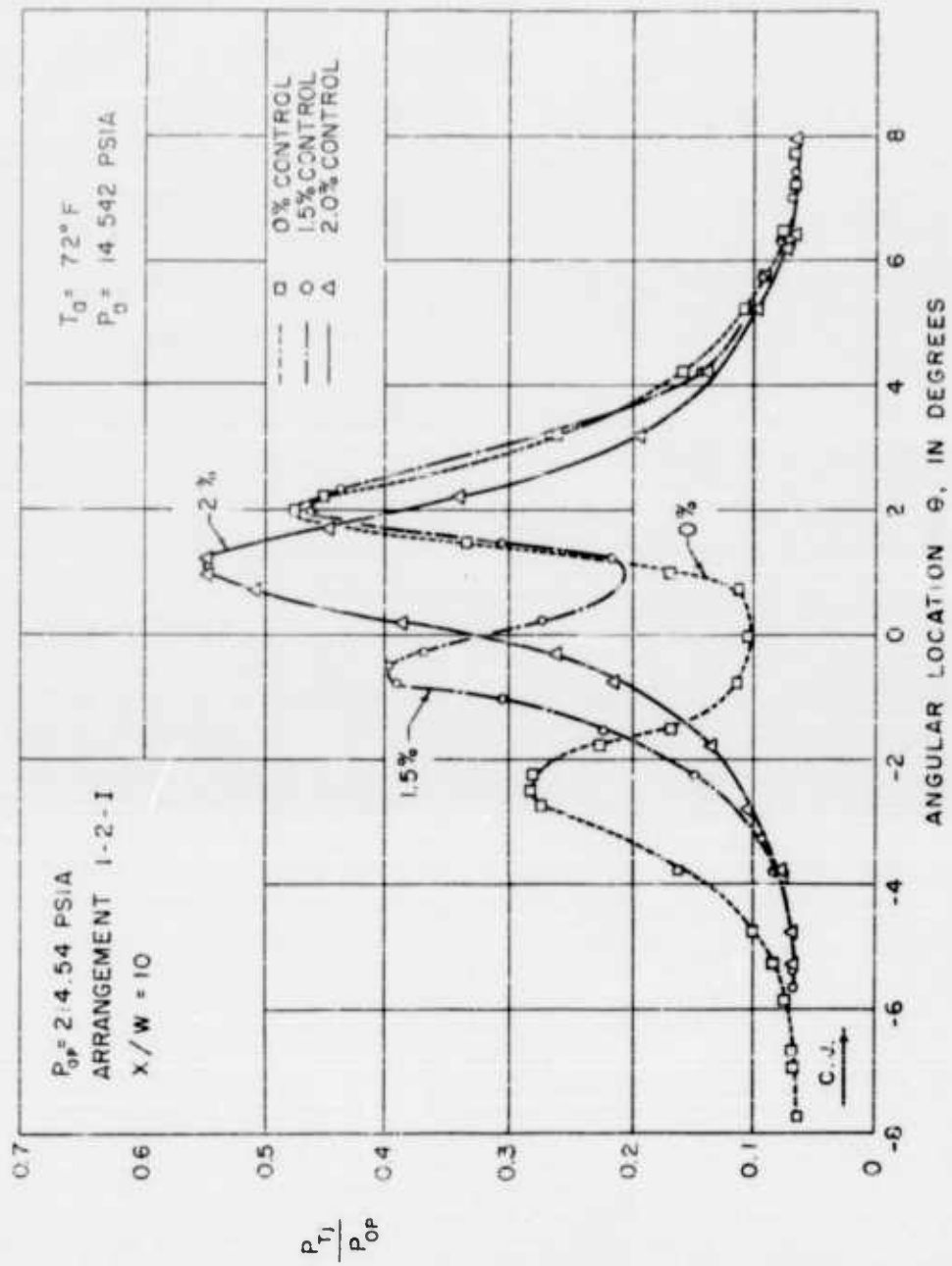
237

Figure 9. Pitot pressure variation with angular location at low
per cent control.

sure at x/w = 10 are shown in Figs. 8b and 9 respectively. A smooth, almost Gaussian, pitot pressure distribution results with a large increase, from 21.5 psia to almost 118 psia, in the jet centerline pitot pressure. Due to the small deflection angles, this could be utilized in a single-receiver pneumatic amplifier yielding a pressure gain of 24.1. With the disappearance of the normal shock, the mixed flow at x/w = 10 because supersonic causing a bow shock wave to form at the probe tip, resulting in the probe sensing a lower than actual jet flow local stagnation pressure. For the zero per cent control power jet flow, however, the centerline pitot pressure of 21.5 psia is very nearly the actual jet stagnation pressure at x/w = 10 since the jet flow downstream of the normal shock is subsonic and thus no bow shock is formed at the probe tip. Thus the increase in the actual jet flow centerline stagnation pressure is even greater than 118 psia. The addition of 1.5 per cent control flow was not sufficient to make the normal shock disappear but it did alter the pressure distribution somewhat, particularly on the control jet side.

It should be mentioned that the peak pressures on either side of the center for zero per cent control in Fig. 9, are different than those recorded earlier and reported in Refs. 7 and 11. This could be due to an initial misalignment of the probe for the transverse shown in Fig. 9. However in the central region of the flow (more important to present investigations), the observed pressures agreed with the previous ones.

Pitot pressure profiles were also recorded at x/w = 5 which is upstream of the normal shock location in the zero per cent control power jet flow. At this location the zero per cent control plot again indicated a low pressure central region with peaks on either side. At this location, however, the low pressure central region corresponded to the uniform flow between the inter-

239

cepting shocks. Since the flow in this central region was supersonic the low pitot pressure recorded was due to the losses through the pitot probe bow shock wave. Considering isentropic expansion into this region[9] the actual jet flow stagnation pressure should have been 214.5 psia as compared to the pitot pressure of 33 psia recorded there. The higher pressure peaks again corresponded to the flow which crossed the intercepting shocks at very oblique angles, the stagnation pressure losses being less severe than through the probe bow shock wave in the central region. The only effect that the addition of the 1.5 and 2 per cent control had at this location was the slight movement toward the center by the pressure peak on the control jet side. The centerline pitot pressure and the pressure distribution on the far side of the jet were unaffected. This behavior indicated that at $x/w = 5$ the addition of the 1.5 and 2 per cent control just affected a slight relocation of the intercepting shock nearest to the control jet. (For a complete discussion of the 10 and 15 per cent control flow addition at $x/w = 10$ and 5 for $\overline{P_{OP}} = 200$ psig, along with the proposed mechanism for the normal shock collapse, see Ref. 11.)

The minimum amount of control jet flow needed to cause the collapse of the normal shock at various power jet settling chamber pressures was shadow-graphically determined. The minimum P_{OC}/P_{OP} needed, decreases linearly with increasing P_{OP}, in the range of power jet settings used (Fig. 10). However, the absolute value of the minimum P_{OC} (or mass flow) increased with increasing P_{OP}. The experimental observations were limited to $P_{OP} > 115$ psia because the normal shock structure is not present at lower pressures. With these experimental observations as a guide, analytical prediction of the minimum control flow needed to cause the collapse of the normal shock structure is being attempted.
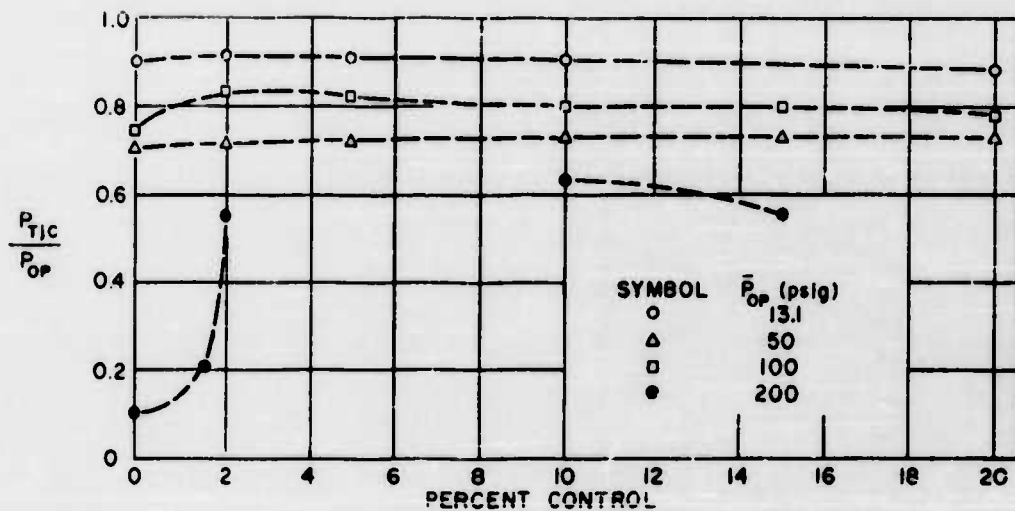
240

FIG. 11 RATIO OF JET CENTERLINE PITOT PRESSURE TO POWER JET SETTLING
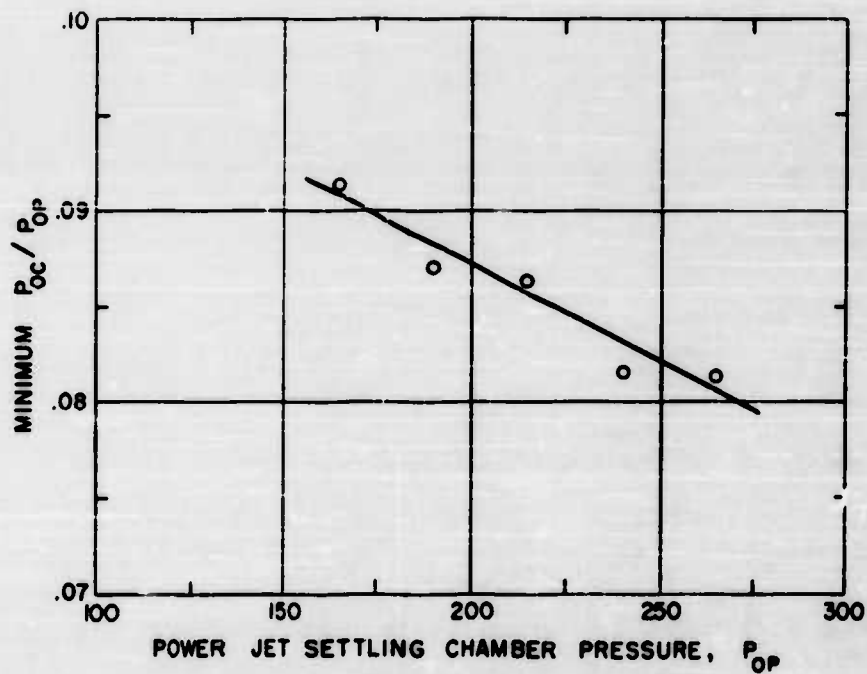CHAMBER PRESSURE AT X/W=10 FOR VARIOUS PERCENT CONTROL.
ARRANGEMENT 1-2-1

FIG. 10 MINIMUM CONTROL JET PRESSURE FOR
COLLAPSE OF NORMAL SHOCK

241

The collapse of the normal shock structure in highly underexpanded flow with the corresponding substantial increase in recovery jet flow stagnation pressure, could have important applications in noise reduction devices, diffusor and turbine design, thrust vectoring, etc., as well as in the design and operation of pneumatic amplifiers. In fact one may generalize and state that this phenomenon may have important practical applications in fluid flow systems when due to the necessity of high operating pressures the dissipative normal shock front is unavoidable while at the same time it is imperative or advantageous to recover the maximum possible flow stagnation pressure.

2. Jet Centerline Recovery Pitot Pressure Variation with Per cent Control

The behavior of the mixed jet flow centerline pitot pressure, P_{TJC}, as a function of per cent control, at $x/w = 10$ for arrangement 1-2-I, is shown in Fig. 11. Due to the Gaussian nature of the pressure distribution, the centerline and maximum pressures for $\overline{P_{OP}} = 15.1$ psig were identical. Since for this just choked jet flow there was hardly any shock structure present in the flow, the slight increase in P_{TJC} with the addition of the 2 per cent control is the result of the added control jet flow momentum to the power jet flow. The subsequent steady decrease of P_{TJC} at the higher per cent control flows may be due to increasing mixing losses, through increased turbulence, nullifying the momentum contribution by the control jet flow. The measurement of the turbulence characteristics of the individual and mixed jet flows are necessary to ascertain the actual mechanism for this decrease in the centerline pitot pressure.

For $\overline{P_{OP}} = 50$ psig, where repetitive diamond shock structure was observed, there was again a slight increase in the jet centerline pitot pressure with

the addition of 2 per cent control flow. With the addition of increased per cent control flow the centerline pitot pressure then remained essentially constant. For this case the jet centerline pitot pressure was not the maximum pitot pressure recovered in the jet flow. For zero and 2 per cent control, higher pressure peaks on either side of the center were present. The pressure difference of 2 psi between the peaks and the centerline, however, is not as severe as for $\overline{P_{OP}}$ = 200 psig. With increasing per cent control the peak on the control jet side of the jet flow was observed to decrease until at 20 per cent control an almost Gaussian shape was achieved for the pitot pressure distribution in the mixed jet flow. If the maximum pressures were plotted versus per cent control, they would show an almost constant value from zero to 20 per cent control. These observations seem to indicate a slight change in the weak diamond structure, but not the radical effects on the pitot pressure distribution noted for the 200 psig case.

For a power jet settling chamber pressure of 100 psig, there was a strong but still repetitive diamond shock structure present in the power jet flow. In this case the addition of the 2 per cent control jet flow resulted in a nearly 10 per cent increase of centerline pitot pressure. The influx of the control jet flow into the first diamond structure cell increased the static pressure there, thus weakening the shocks and increasing the recovered downstream pitot pressure. With further control jet addition, increasing mixing losses steadily reduce the centerline pitot pressure until at 20 per cent control it was only slightly higher than that for zero control. At this P_{OP} and x/w the jet centerline and the maximum jet pitot pressures were the same for all the per cent controls. From the shadowgraphs it appeared that the

vertex of one of the periodic diamond shock structures was located at $x/w = 10$. Traversing through the vertex rather than the cell would account for the absence of multiple peaks. The $\overline{P_{OP}} = 200$ psig case is also shown on this plot to illustrate the large increase in centerline pitot pressure, as discussed earlier.

As would be expected, the jet flow pitot pressure distributions were affected by the entrainment characteristics of the different nozzle arrangements (Fig. 12). At $x/w = 5$, for $\overline{P_{OP}} = 50$ psig, the centerline pitot pressure was not affected by the introduction of the dummy jet; the possible reason being that close to the power jet exit the reduction in entrainment has not yet been felt in the center of the jet flow. However, by $x/w = 17$ lower pitot pressures were recorded for the dummy jet arrangement. For the 1-2-ID arrangement the addition of more than 17 per cent control deflected the power jet flow such that it became attached to the dummy jet nozzle wall; no pressures were recorded once this attachment took place.

Due to the entrainment between the nozzle blocks, a larger P_{TJC} was recovered in the 12-12-0 arrangement, at the lower per cent controls, than that for the 1-2-I arrangement. However, the addition of increased control jet flow steadily reduced this pressure until at 20 per cent control a much lower value was recovered than for the 1-2-I arrangement. The behavior at the higher per cent controls may be the result of the control jet flow impinging at a point further downstream of the power jet exit ($x/w = 12$ instead of $x/w = 1$). This has the effect of increasing both the spread of the mixed jet and the mixing losses. It was seen from the pitot pressure plots that for this arrangement the 20 per cent control mixed jet flow had almost twice the spread of the zero per cent control power jet flow.
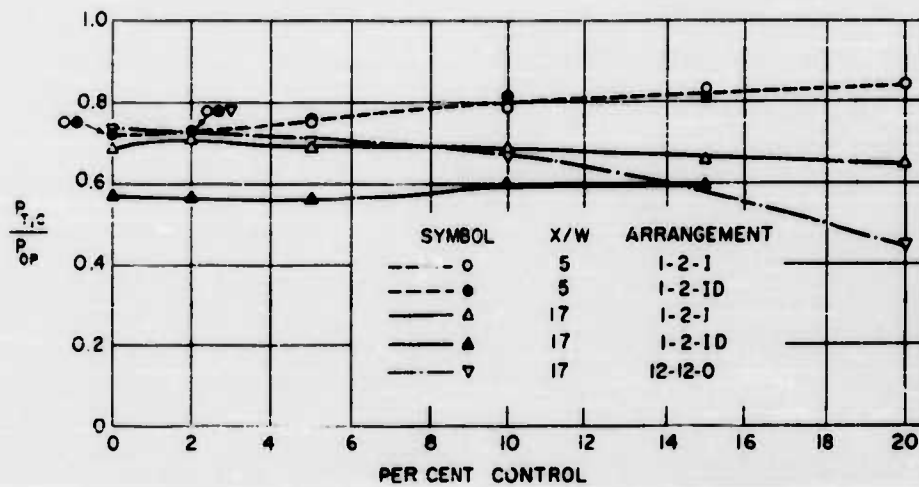
FIG. 12 VARIATION OF THE RATIO OF JET FLOW CENTERLINE PITOT PRESSURE TO POWER JET SETTLING CHAMBER PRESSURE AT $\bar{P}_{op}$ = 50 (PSIG) FOR VARIOUS JET ARRANGEMENTS
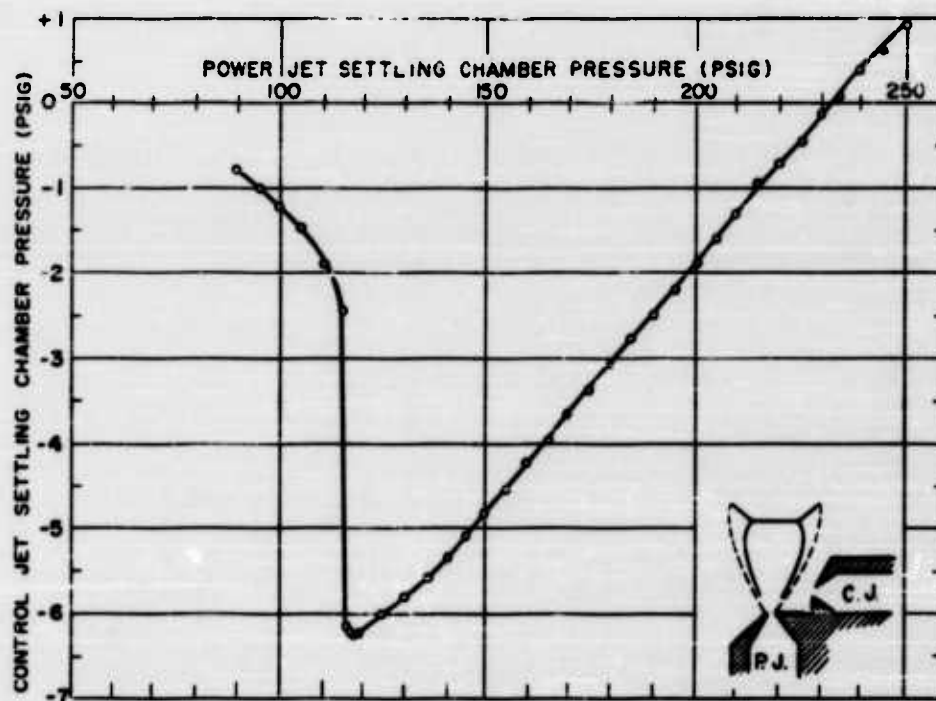

FIG. 13 ENTRAINMENT EFFECTS OF POWER JET FLOW

Another point worth noting is that at $x/w = 5$ the centerline pitot pressure steadily increased with increasing per cent control (see Fig. 12). This differed from the behavior of the centerline pressure for $\overline{P_{OP}} = 50$ psig at $x/w = 10$, as shown in Fig. 11. This difference may be because at $x/w = 5$ the mixing losses, which seem to increase with increasing per cent control, have not completely nullified the momentum contribution of the control jet flow. At $x/w = 17$ the centerline pitot pressure does follow the same behavior as at $x/w = 10$.

3. Entrainment Effects of Power Jet Flow

The entrainment effects of the power jet flow alone, in the 1-2-I arrangement, were recorded. The pressure in the control jet settling chamber, when the supply line to the chamber was shut off, was measured for various settings of the power jet settling chamber pressure (see Fig. 13). The power jet settling chamber was set at a desired constant value. The power jet flow then entrained air from the control jet settling chamber; the resulting pressure in this chamber being recorded. It should be noted that when these data were recorded, at no time was the power jet actually attached to the control jet nozzle as it would in a Coanda type attachment. The interesting point shown by this plot is the sharp increase in the entrainment demand of the power jet flow (as evidenced by sharp decrease in the control jet settling chamber pressure) at the power jet settling chamber pressure of approximately 115 psig. As mentioned earlier, this is the power jet operating pressure at which the normal shock pattern is first established, replacing the repetitive diamond shock structure.

246

Once the normal and intercepting shock structure is established, the steadily increasing pressure in the control jet settling chamber with increased power jet pressure (i.e. decreasing entrainment demand of the power jet flow) can be given a simple possible explanation. As mentioned in Ref. 12, the intercepting shocks divide the jet into two regions; the outer region between the intercepting shocks and the jet boundary being the one influenced by the ambient conditions while the inner region bounded by the nozzle exit, the normal shock and the intercepting shocks is unaffected by the ambient conditions. These regions of the highly underexpanded power jet flow are shown in the insert sketch in Fig. 13 where the solid lines represent the shock waves and the dashed lines the jet boundary. It is the outer region of the jet flow which regulates the entrainment demands of such a power jet flow. As the power jet settling chamber pressure is increased, the jet as a whole expands, while at the same time the extent of the outer region decreases. This decrease of the outer region would explain the decrease in entrainment by the power jet flow as settling chamber pressure is increased. The positive pressure which eventually made its appearance in the control jet settling chamber at the higher power jet settlings was the result of the power jet expanding to such a degree that some of its outer flow actually entered the control jet nozzle.

In the normal and intercepting shock pattern, the intercepting shocks are nearly parallel to the jet boundary thus creating a large inner region of flow which is not exposed to the ambient conditions. However, in the diamond shock structure, present for $\overline{P_{OP}} < 115$ psig, the side shocks are much more oblique to the flow and as the power jet settling chamber pressure is

increased a larger and larger mass of the power jet flow is exposed to the ambient conditions, increasing the mixing entrainment to the jet. This would explain the steady decrease in the control jet settling chamber pressure with increased power jet operating pressures which correspond to a diamond type shock structure.

The sharp increase in the entrainment demand of the power jet when the normal shock structure was first formed at 115 psig is most likely due to the intercepting shock structure not extending far enough upstream toward the nozzle exit (at least not as far as the shocks of the diamond structure) to effectively establish an inner and outer portion of the jet flow. Thus a larger amount of the jet flow is exposed, increasing the entrainment over that for a slightly lower P_{OP} when the diamond structure was present. As the power jet settling chamber pressure is further increased, the intercepting shocks extended farther and farther upstream toward the power jet exit as well as outwards to the jet boundary, creating a larger and larger inner region of jet flow and thus reducing the portion of the jet flow effective in entrainment.

The reduced pressure in the control jet settling chamber on one side of the power jet flow and atmospheric pressure on the opposite side results in a pressure gradient across the power jet flow. The dependence of the magnitude of this pressure gradient on P_{OP} is reflected in the varying deflections of the power jet alone toward the control jet nozzle. It was found that for $\overline{P_{OP}} = 115$ psia (i.e. maximum pressure gradient across the power jet flow) the angle of deflection toward the control jet nozzle was the greatest. A very slight lowering of P_{OP} to a value corresponding to the diamond shock structure resulted in a sharp reduction in this initial deflection angle. This corresponded to the sharp decrease in entrainment in going from the normal shock
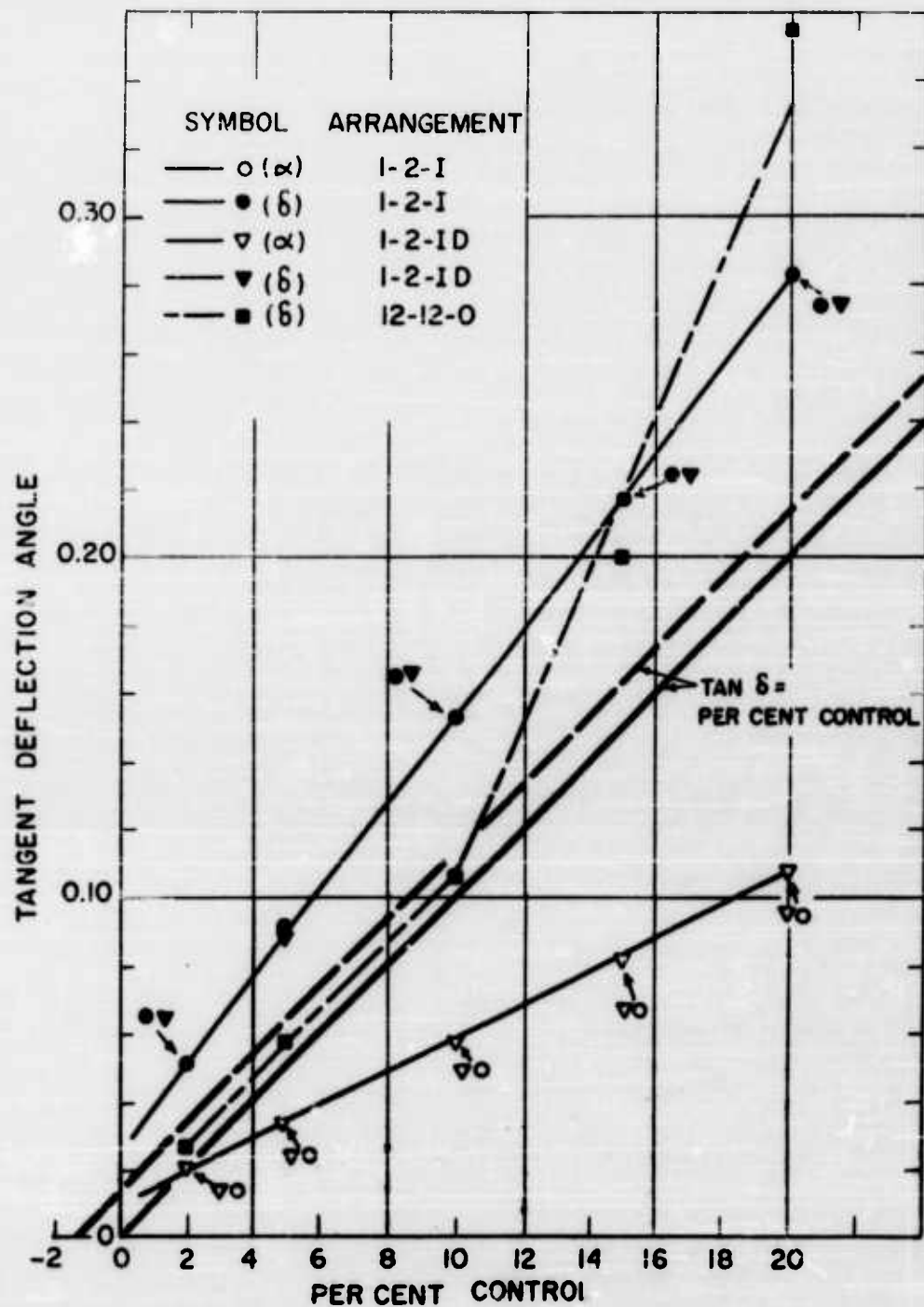
248

FIG. 14 TANGENT OF JET CENTERLINE DEFLECTION ANGLE VS
PER CENT CONTROL FOR P_{op}= 100 PSIG AT X/W =17
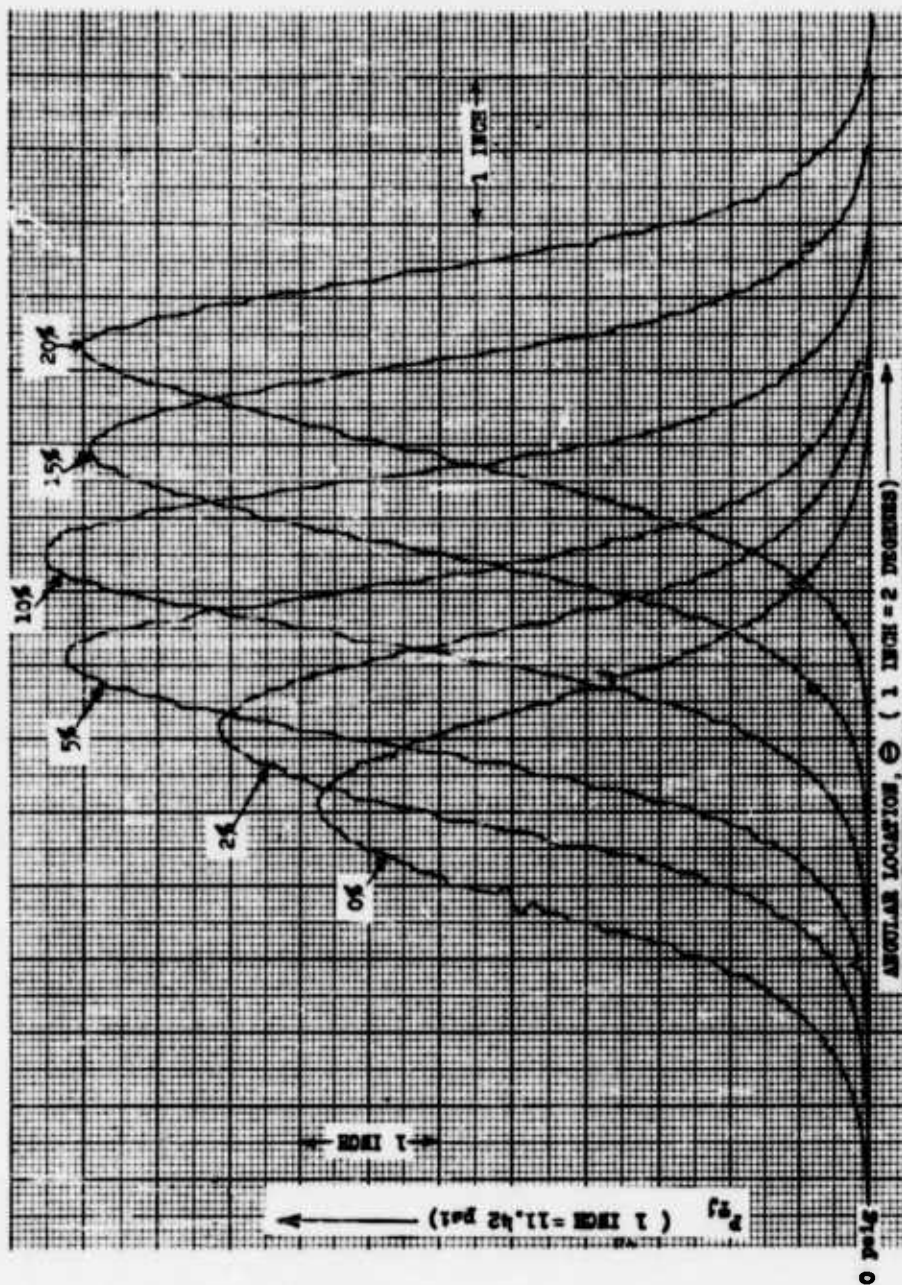
249

FIG. 15 X-Y RECORDER PLOT OF JET FLOW PITOT PRESSURES AT VARIOUS PERCENT CONTROL

$P_a = 29.684$ in. of Hg.

$t_{,p} = t_{,OG} = 69^\circ F$

$\bar{P}_{OP} = 100$ psig

ARRANGEMENT 1-2-10

PROBE TIP AT $X/W = 17$

250

structure to the diamond type structure. Increasing the power jet settling
chamber pressure above 115 psig resulted in a steady reduction in the deflec-
tion angle due to the steady reduction in the entrainment demands of the jet
flow as shown in Fig. 13.

4. Deflection Angles

The deflection angles, α and δ, were measured between the centerline of
the power jet flow alone, which was considered as zero deflection, and the
centerline of the mixed jet flow at the corresponding per cent control. The
tangent of these deflections angles is plotted versus per cent control in
Fig. 14. The deflection angles, α, as measured directly from the pitot pres-
sure versus angular location plots, such as Fig. 15, were with respect to the
pivot point at $x/w = -25$ for the 1-2-I and 1-2-ID arrangements.

To obtain a truer picture of the deflections involved, the deflection
angles should be measured with respect to the effective turning point of the
particular jet flow, rather than with reference to an arbitrary point such
as $x/w = -25$. From purely physical considerations it would seem that the
effective turning point for the deflected mixed jet flows is at the impinge-
ment point of the power and control jet flows ($x/w = 1$ for the 1-2-I and
1-2-ID arrangements). Plots of the deflected mixed jet flow centerlines
confirmed this (Fig. 16), showing that for $\overline{P_{OP}} = 100$ psig the effective turn-
ing point was located at approximately $x/w = 1$. For $\overline{P_{OP}} = 13.1$ psig the effec-
tive turning point appeared to be at $x/w = -1$ while for $\overline{P_{OP}} = 50$ psig it was at
around $x/w = +3.5$. Despite the fact that not all the effective turning
points were at the actual impingement point, they were much closer to it than
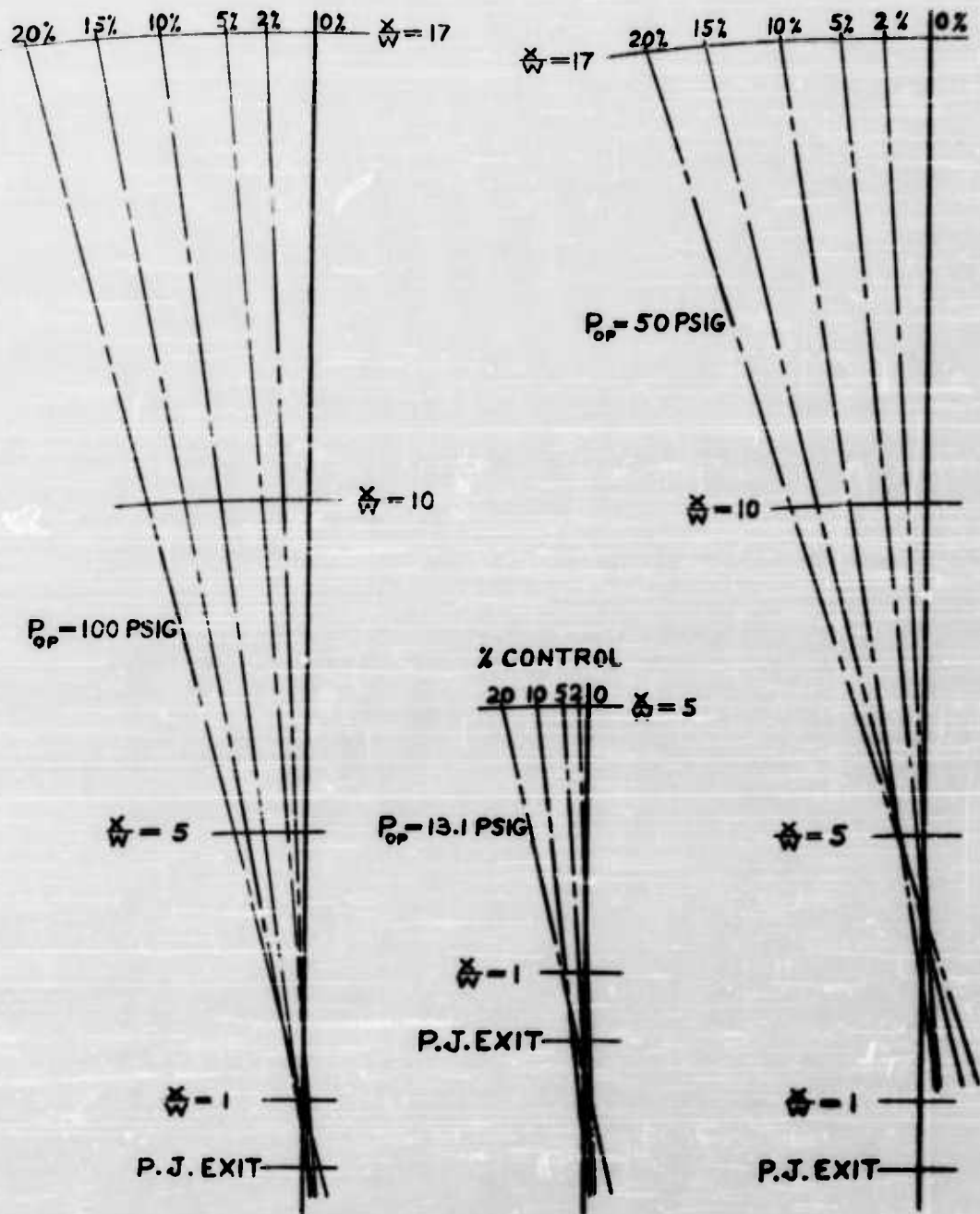to $x/w = -25$ so that the deflection angles δ were calculated with respect to

FIG. 16 Effective Turning Point of Power Jet Flow at Various Percent Control.

the impingement point. The formula for converting the deflection angle α to the larger deflection angle δ can be established, as given in Fig. 17.

Also plotted on Fig. 14 is the tangent relation:

$$\text{Tan } \delta = \frac{\overline{P_{OC}}}{\overline{P_{OP}}} + A \tag{1}$$

where A is a constant. The heavy solid line represents this relation where for zero deflection angle (i.e. power jet flow alone) it is assumed that there is zero per cent control (i.e. $A = 0$). However, as is evident in Fig. 13 there is actually what may be thought of as a negative per cent control at this point due to the entrainment of air from the control jet settling chamber. For $\overline{P_{OP}} = 100$ psig it was -1.2 per cent which is taken into account in the heavy dashed line. In relation (1) it is assumed that the ratio of the jet momenta, $(\rho u^2)_{C.J.}/(\rho u^2)_{P.J.}$, at the point of impingement is equal to the per cent control, $\overline{P_{OC}}/\overline{P_{OP}}$. However, this equality only holds for incompressible free jet flows where no static pressure gradients occur. In high speed compressible jet flows, (used in these investigations) the tangent relation does not hold because $\rho u^2/2$ is no longer simply the difference between the stagnation and static pressures and because static pressure gradients occur in the jet flow when shock structure is present. Thus it would not be expected that the deflection angles measured experimentally would follow the behavior indicated by the tangent relation which was included simply to provide a point of comparison. The δ deflection angles, as calculated from the experimental data, were found to be larger than predicted by the tangent relation for all P_{OP} values used in the investigations with the 1-2-I and 1-2-ID arrangements.

FIG. 17 RELATION BETWEEN δ AND α DEFLECTION ANGLES
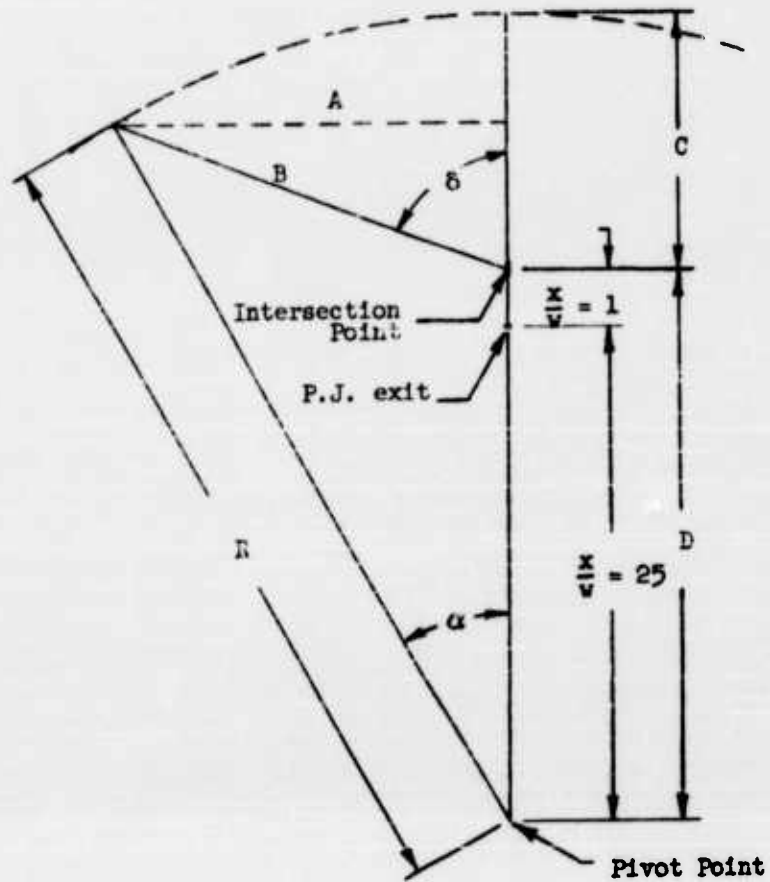
$$\delta = \sin^{-1}\left(\frac{A}{B}\right)$$

$$= \sin^{-1}\left\{\frac{(C + D)\sin\alpha}{(D^2 + R^2 - 2\,DR\cos\alpha)^{1/2}}\right\}$$

where

$$D = \frac{25}{32} + \frac{1}{32} = \frac{26"}{32}$$

$$R = D + C$$

and C is determined by the location of the probe tip from the power jet exit; the values used were $C = \frac{5"}{32}$, $\frac{10"}{32}$ or $\frac{17"}{32}$.

254

This indicates that the ratio of the actual jet flow momenta at the impinge-
ment point was larger than given by the per cent control.

The presence of the dummy jet in the 1-2-ID arrangement did not appear
to have any influence on the deflection angles for the 100 psig power jet, for
the range of per cent controls used. This was not the case for the lower power
jet setting of 50 psig where the deflection angles at the higher per cent con-
trols were larger for the 1-2-ID arrangement. This is due to the fact that
the higher energy jet flow at the 100 psig setting is less susceptible to a
Coanda type deflection introduced by the entrainment blockage of the dummy
jet, than is the lower energy 50 psig power jet flow. This phenomenon was
demonstrated by detaching an actual Coanda attachment of the power jet flow to
the control jet nozzle wall by increasing the power jet settling chamber pres-
sure.

The results from the 12-12-0 arrangement, also shown on this plot, ex-
hibited an entirely different behavior than those of the 1-2-I arrangement.
Of course this was not entirely unexpected because of the considerable entrain-
ment and impingement differences of the two arrangements. At the lower per
cent controls the deflection angles of the 12-12-0 arrangement appear to follow
the tangent relation. However, at the higher per cent controls there appears
to be an increase in slope which would indicate an increase in effective con-
trol. A look at the pitot pressure traverses for this arrangement revealed
that for $\overline{P_{OP}}$ = 100 psig at 15 and 20 per cent control, the Gaussian nature
of the plots was completely destroyed and instead very greatly spread, almost
flat, profiles were recorded. Thus the deflection angles at these larger per
cent controls really had no practical meaning.

255

5. Axisymmetric Jet Interactions

Preliminary shadowgraphs of the interaction of perpendicularly impinging axisymmetric jets were taken to compare any change in shock structure with that observed with the two-dimensional jets. Axisymmetric converging nozzles ($d = 0.12"$) having the same exit area as the two-dimensional nozzles were used and were arranged with their axis intersecting at $x/d = 1$ and $y/d = 2$. In this axisymmetric arrangement the power jet flow freely entrained from all sides while for the corresponding two-dimensional arrangement, 1-2-I, entrainment by the power jet flow from the control jet side was restricted. The axisymmetric arrangement could then be referred to as a 1-2-0 arrangement.

As little as 2 per cent control jet flow was sufficient to cause the disappearance of the normal shock in the two-dimensional jet flow for $\overline{P_{OP}} = 200$ psig. However, in the case of axisymmetric jets, as can be seen from Figs. 18, the impingement of 10 per cent control flow did not effect a complete disappearence of the normal shock. In fact the control jet flow does not seem to even penetrate the cell formed by the normal and intercepting shocks, but only appears to distort and relocate the intercepting shock nearest to the control jet exit and in doing so reduces the extent of the normal shock disc. Even the impingement of 20 per cent control does not completely collapse the normal shock. The above behavior of the shock structure was also noted for $\overline{P_{OP}} = 300$ psig where in the two-dimensional case 10 per cent control was again more than sufficient to completely collapse the normal shock structure. It is felt that the difference in shock structure behavior between the three-dimensional and two-dimensional cases could somehow be the result of their different entrainment characteristics of their arrangements.
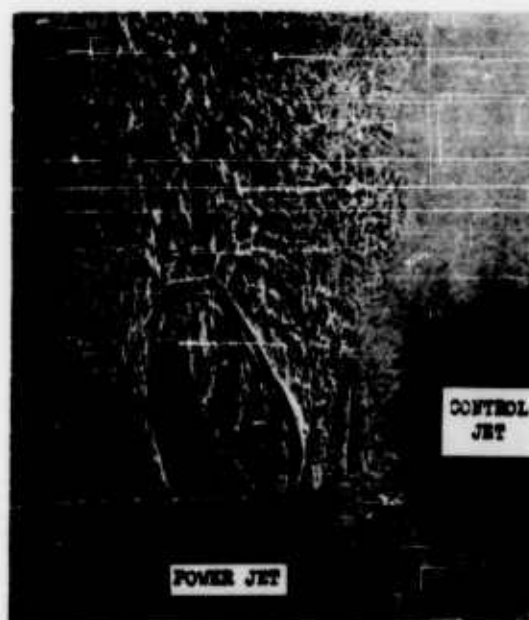
256

Figure 18a. 0 per cent control

Figure 18b. 10 per cent control   Figure 18c. 20 per cent control

Figure 18. Shadowgraph of interacting axisymmetric free jet flows.
Atmospheric pressure = 29.55" of Hg. Room temperature = 71°F

P_{OP} = 214.56 psia T_{OP} = 71°F, T_{OP} = 71°F x/d = 1, y/d = 2

257

6. Miscellaneous Observations

a) Static Pressure Measurements

Attempts were made to measure the static pressure distributions in the mixed jet flow for various P_{OP}'s, per cent controls and x/w's by the use of static pressure probes. However, the response of a standard static probe is greatly influenced by its design[13], the turbulence level of the flow, and the directional changes of the flow[13,14]. Even a few degrees inclination between the probe and the flow direction can cause the recorded static pressure to be in error[14]. Moreover in supersonic flow the presence of the bow shock at the static probe tip changes the actual jet flow static pressure. Because of all these factors the static pressure measurements were not used in any calculations. In such flow fields the density measurements by interferometric technique offers a method free of the above difficulties for obtaining the static pressure distribution[9].

b) Coanda Effect

It was observed that the power jet flow attached itself to the control jet nozzle. This attachment was established soon after the start of the jet flow (i.e. when the P_{OP}, and thus Reynolds Number, was still small). In the 1-2-I arrangement this Coanda attachment was detached by increasing P_{OP} to a value greater than 165 psig. A shadowgraph of the Coanda attachment of a highly underexpanded, $\overline{P_{OP}} = 160$ psig, power jet flow to the control jet nozzle wall is shown in Fig. 19. For $\overline{P_{OP}} < 165$ psig the Coanda attachment could be detached by simply applying control jet flow or by sufficiently restricting the entrainment on the unrestricted side of the jet flow as well. Once this Coanda attachment was detached the power jet flow did not reattach. The only time the Coanda attachment caused any problems was at the higher per cent controls in the 1-2-ID arrangement at $\overline{P_{OP}}$'s of 50 and 13.1 psig when the deflection

258

Figure 19. Shadowgraph of Coanda attachment of power jet flow to control jet nozzle. 0 per cent control; P_a = 29.57 in. of Hg. $\overline{P}_{OP}$ = 160 psig; T_a = 77°F; Arrangement 1-2-1.

with 18 per cent control was sufficient to cause attachment to the dummy jet nozzle. Also the Coanda attachment was so severe in the 12-12-ID arrangement that no systematic results could be obtained. Whenever the probe was traversed toward the dummy jet in this arrangement it caused the mixed jet flow to attach itself to the dummy jet nozzle wall, even at zero per cent control.

c) Jet Noise and Turbulence

As was mentioned earlier in the paper, it was possible to shadowgraphically emphasize the turbulence and the noise phenomena occurring in the interacting jet flows with the film farther from the test section. This is shown in Figs. 20b and c where in Fig. 20c the film was as close as possible to the axisymmetric jet flows (arrangement 1-2-0) and thus the shock structure is emphasized in the shadowgraph. In Fig. 20b the film was mounted approximately 5 inches from jet flow axis, and the turbulence and sound waves are emphasized. The apparent pitting of the nozzles in Fig. 20b is due to the · light rays being greatly refracted by the large density gradients in the jet flows at the exits. In Fig. 20c this apparent pitting does not appear due to the closeness of the film. From these shadowgraphs (Figs. 20), the following general conclusions can be drawn.

1. The sound field emitted by the power jet alone (Fig. 20a) has two modes. The first mode is comprised of spherical discrete (a single characteristic wave length or frequency) wave fronts propagating in all directions. This is often called the screeching frequency of the choked jet flows. For the possible mechanism of generation of this type of sound field see Ref. 15 . These regular patterns of wave fronts seem to be strong in only two quadrants on either side of the jet flow in the downstream direction. The dominant average wavelength $\lambda \approx .062"$ (i.e., $\lambda/d \approx 0.52$). The second mode is comprised of

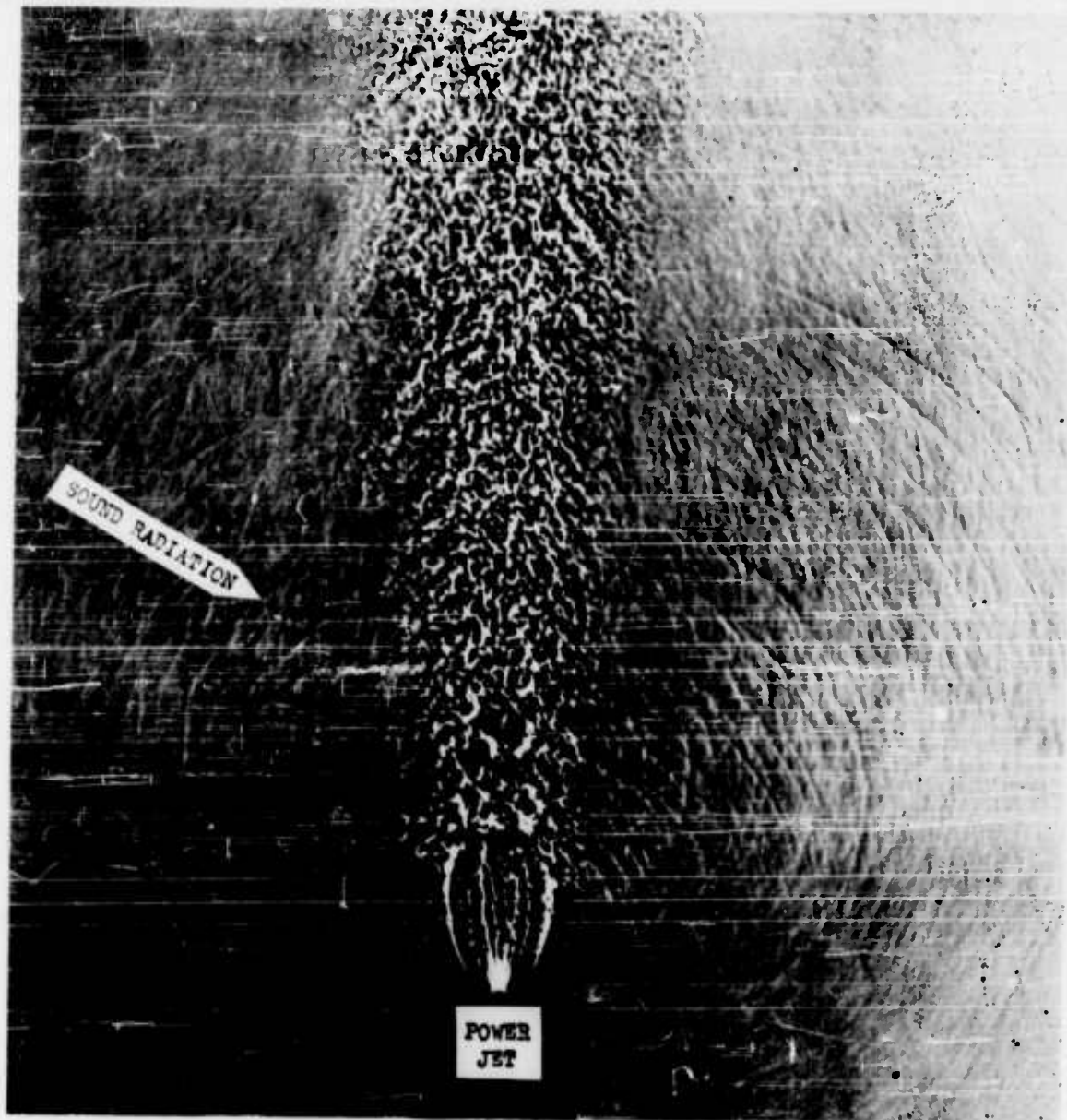Figure 20a. Sound radiation from the power jet.
0 per cent control. P_{OP} = 214.5 psia; P_a = 14.5 psia
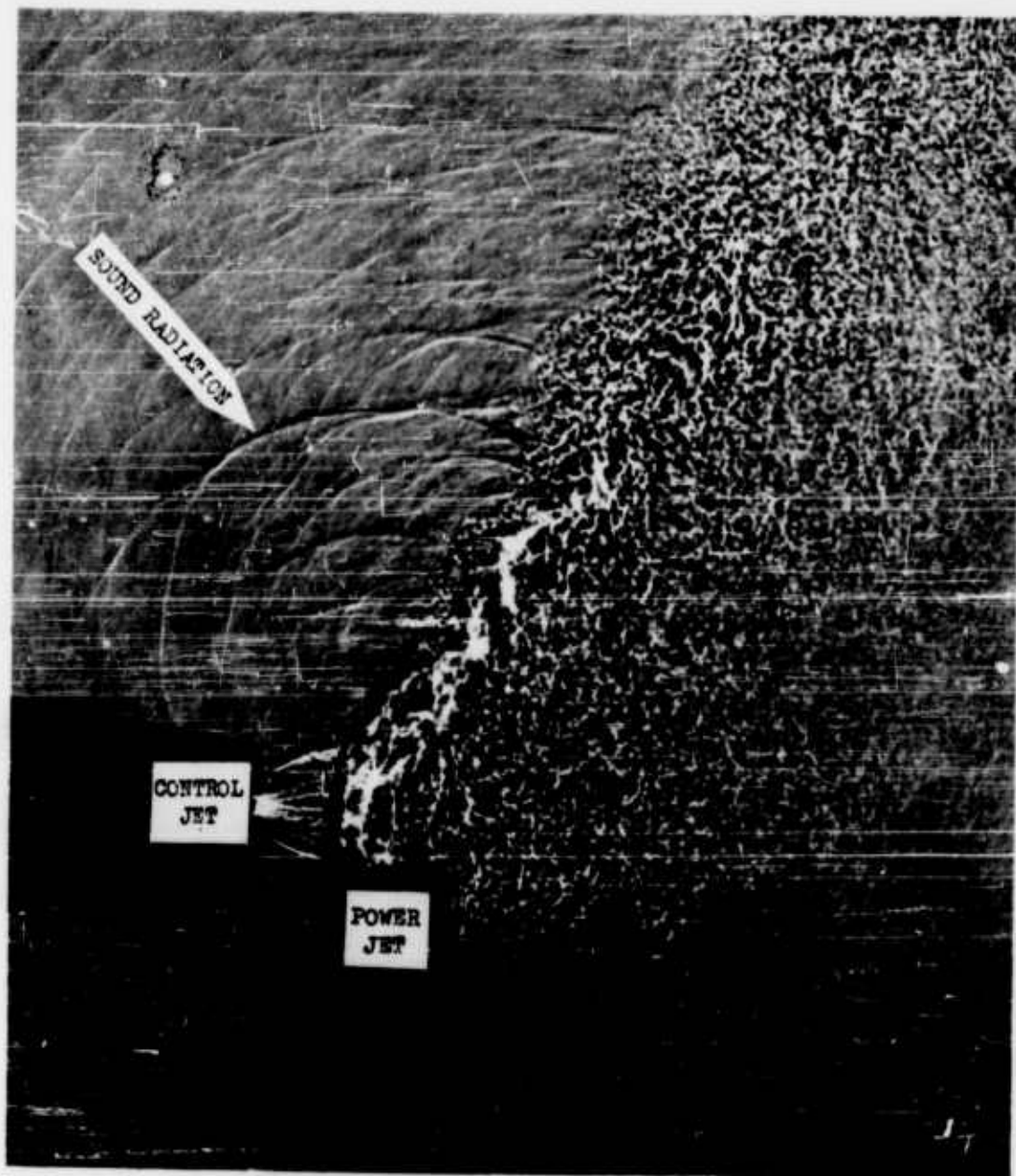Film located 5" from jet centerlines.

261

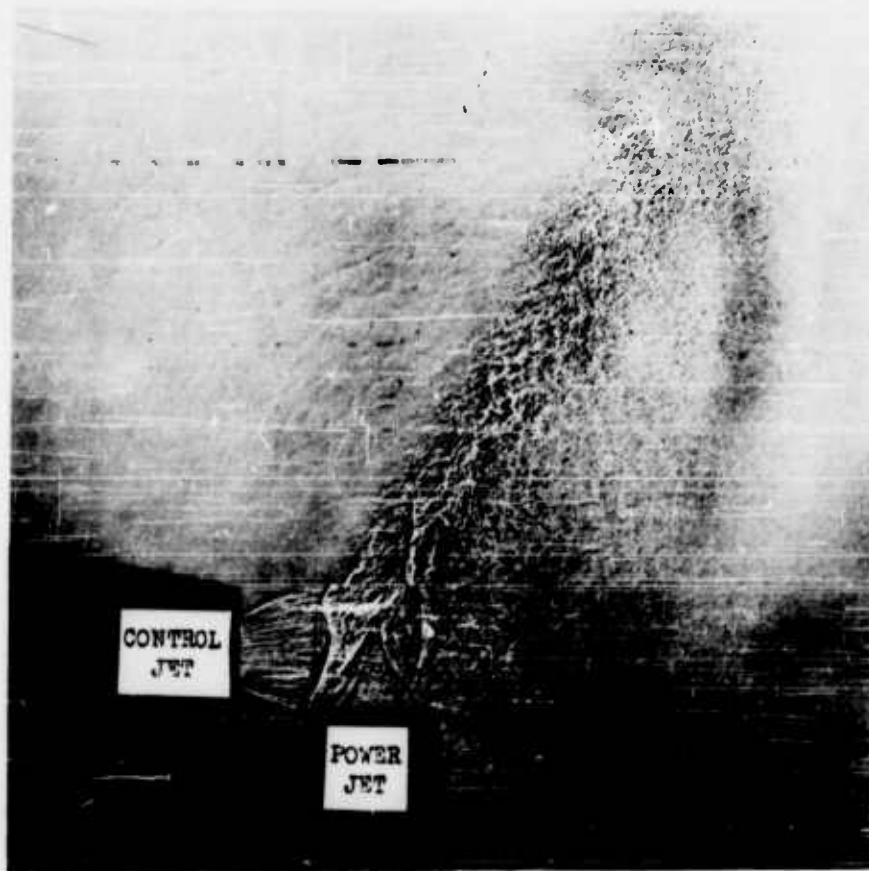Figure 20b.   Film located 5" from jet centerlines.

262

Figure 20c. Film located as close as possible to flow.

Figure 20. Sound radiation from the interacting jet flows.
100 per cent control; P_{OP} = 214.5 psia; P_a = 14.5 psia.

Arrangement 1-2-0

irregular, much higher frequency sound waves generated by the turbulent mixing jet flow field.

2. The sound field emitted by the interacting jet flows (Fig. 20b) also has a predominant characteristic wavelength, or frequency. In this case the average $\lambda \approx .13''$ (i.e. $\lambda/d \approx 1.1$) which is almost twice that for the power jet flow alone. The discrete sources of the predominant radiating wave fronts were traced and found to be distributed along the cellular region of the mixed jet flow. The spherical wave fronts from these discrete sources interact in an interesting pattern. The radiating sound field is strongly evident in only one quadrant. In fact even when the film was close to the jet flow (Fig. 20c), the relatively stronger wave fronts are still evident. Due to the penetration of the control jet flow across the power jet flow an extreme asymmetric spread of the turbulent mixed jet flow is caused. The sound wave system propagating through this quadrant of extended turbulence is dissipated. In this preliminary work no systematic quantitative measurements of either the sound emission or turbulence characteristics of the interacting jet flows were taken.

References

[1] Coles, W. E. and Mihaloen, J. A., "Turbojet Engine Noise Reduction with Mixing Nozzle-Ejector Combinations," NACA TN 4317, 1958.

[2] Spence, D. A., "The Lift on a Thin Aerofoil with Jet Augmented Flaps," Aero Quarterly, Vol. IX, Part 3, August 1958.

[3] Warren, C. H. E., "An Experimental Investigation of the Effect of Ejecting a Coolant Gas at the Nose of a Blunt Body," G.A.L.C.I.T. Report. Memorandum No. 17, December 1958.

264

[4]Eleverum, Jr., G. and Morey, T., "Criteria for Optimum Mixture-Ratio Distribution Using Several Types of Impinging-Steam Injection Elements," Memorandum No. 30-5, Jet Propulsion Laboratory, California Institute of Technology, Pasadena, California, February 1959.

[5]Bowles, R. E. and Others, "Pure Pneumatic Systems," R-310-50-12; Diamond Ordnance Fuze Laboratories, Ordnance Corps, U. S. Army, Washington, D. C. December 1959.

[6]Zalmanyon, L. A. and Semikova, A. I., "Investigations of the Characteristics of Pneumatic Jet Elements," Automatika i Telemekhanica (USSR), Vol. 20, No. 4, April 1959.

[7]Dosanjh, D. S., "Interaction of Confined Two-Dimensional Transversely Impinging Jets," DSL R - 65; Syracuse University Research Corporation, Submitted to Diamond Ordnance Fuze Laboratories, Washington, D. C., August 1961.

[8]Pai, S. I., Fluid Dynamics of Jets; Van Noatrand Co., Inc., New York, 1954.

[9]Ladenburg, R., Van Voorhis, C. C. and Winkler, J., "Interferometric Studies of Faster than Sound Phenomena. Part II. Analysis of Supersonic Air Jets," Physical Review. Vol. 76, No. 5, September 1949.

[10]Love, E. and Grigsby, C., "Some Studies of Axisymmetric Free Jets Exhausting from Sonic and Supersonic Nozzles into Still Air and into Supersonic Streams," NACA RM L54L31, May 1955.

[11]Dosanjh, D. S. and Sheeran, W. J., "Experiments with Two Dimensional, Transversely Impinging Jets," accepted for publication by the Journal of Aerospace Sciences.

[12]Lord, W. T., "On Axisymmetrical Gas Jets, with Application to Rocket Jet Flow Fields at High Altitudes," Report No. Aero. 2626. Royal Aircraft Establishment. (Farnborough, England), July 1959.

[13]Forthmann, E., "Turbulent Jet Expansion," NACA TM No. 789, 1936.

[14]Miller, D. R. and Comings, E. W., "Static Pressure Distribution in the Free Turbulent Jet," Journal of Fluid Mechanics, Vol. 3, 1957-58.

[15]Powell, A, "On the Mechanism of Choked Jet Noise," Proc. Phys. Soc., B 66, 1953.

AN ANALYTICAL AND EXPERIMENTAL STUDY OF
TWO-DIMENSIONAL COMPRESSIBLE SUBMERGED JETS

by

R. E. Olson

of

United Aircraft Corporation
Research Laboratories

ABSTRACT

Analytical and experimental studies of compressible, two-dimensional, turbulent submerged jets were conducted with air as the working fluid. A theoretical flow model is presented and a momentum integral analysis is developed based on this flow model. The analysis employs constant exchange coefficient mixing theory to express the turbulent shear stress and assumes a Gaussian velocity distribution in the mixing zone. Relationships are presented for the length of the inviscid core and the centerline velocity decay in the fully developed portion of the jet in terms of an empirical shear stress constant. Experimental results obtained for jet Mach numbers between 0.66 and 2.0 are discussed and employed to evaluate the shear stress constant which appears in the analysis. These values of shear stress constant are correlated with jet Mach number, and the significance of this correlation is discussed.

INTRODUCTION

In the evaluation of the performance characteristics of pure-fluid elements the characteristics of two-dimensional submerged jets are often desirable. The jet spreading and centerline velocity decay rates are of particular interest since these characteristics effect the size and location of receiving apertures and the power efficiency of these elements. Previous investigations of two-dimensional submerged jets, however, have been limited to incompressible flow (e.g., Ref. 1) and can only be employed qualitatively for compressible fluids. Consequently, the investigation reported herein was performed to study the aerodynamic characteristics of two-dimensional compressible submerged jets and was undertaken as part of a general investigation of the performance of pure-pneumatic elements being conducted for the Diamond Ordnance Fuze Laboratories under Contract DA-49-186-ORD-912.
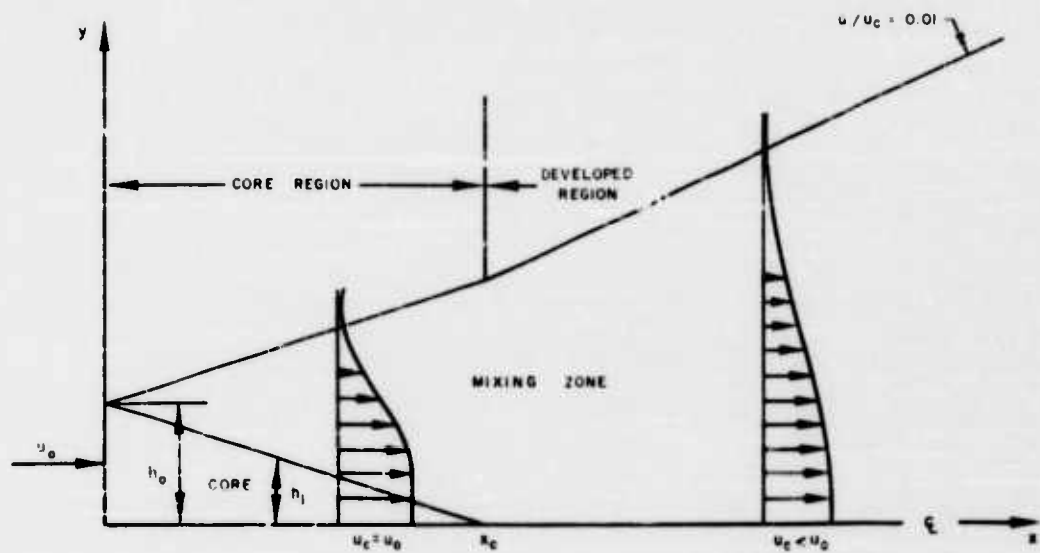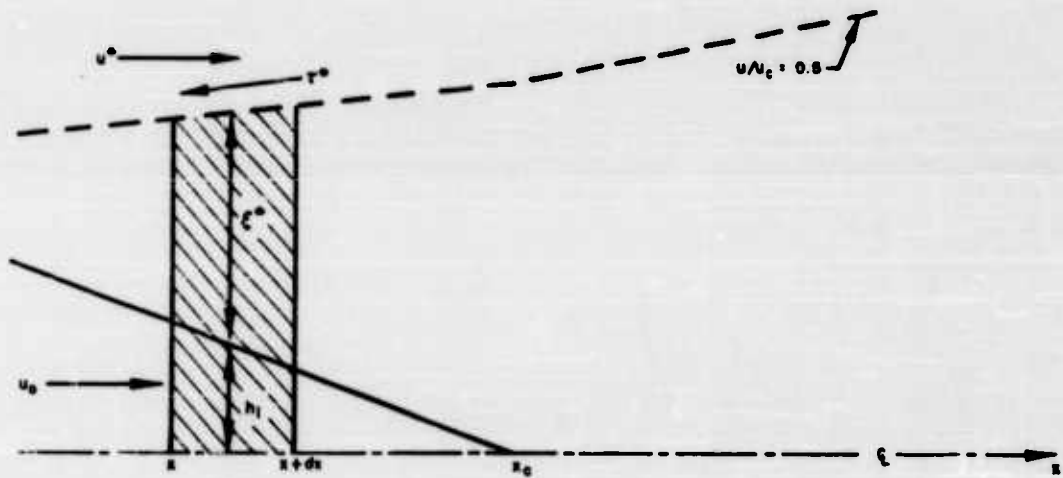
FIGURE 1 SKETCH OF FLOW MODEL

FIGURE 2 SKETCH OF DIFFERENTIAL CONTROL VOLUME

268

THEORETICAL INVESTIGATION

A sketch of the flow model employed for this analysis is presented in Fig. 1. The jet is divided into two regions, the core region and the developed region. The core region consists of an inner inviscid core of constant velocity flow and an outer mixing zone of nonuniform velocity. This mixing zone, which originates at the outer boundary of the jet because of shearing with the quiescent ambient air, spreads inwardly thereby decreasing the core height, and also spreads outwardly entraining flow from the ambient air. At the end of the core region, the inviscid core of constant velocity no longer exists and for subsequent downstream distances the centerline velocity decreases.

From overall conservation of momentum considerations, referring to Fig. 1,

$$\rho_0 u_0^2 h_i + \rho u^2 d\xi + \rho_0 u_0^2 h_0 \tag{1}$$

where,

$$\xi = , \ h_i$$

Consider the differential control volume shown in Fig. 2 between the jet centerline and the location where the velocity is equal to one half of the centerline velocity. For this portion of the jet the change in momentum in the x-direction can be expressed as,

$$\frac{d}{dx}\left(\rho_0 u_0^2 h_i + \int_0^{\xi^*} \rho u^2 d\xi\right) = \left[u^* \frac{d}{dx}\left(\rho_0 u_0 h_i + \int_0^{\xi^*} \rho u d\xi\right)\right] + \tau^* \tag{2}$$

where the bracketed term on the right side of the equation is the momentum gain on the upper boundary of the control volume and τ^* is the shear stress on this boundary.

Using constant exchange coefficient mixing theory and Prandtl's concept that the exchange coefficient, ϵ, at any axial station may be considered to be proportional (1) to the width of the mixing region and (2) to the maximum velocity change at that station, the shear stress term in Eq. (2) can be expressed as,

$$\tau^* = \rho^* \epsilon \left.\frac{\partial u}{\partial \xi}\right|_{\xi=\xi^*} \tag{3}$$

where,

$$\epsilon = \kappa \xi^* \frac{u_c}{2} \tag{4}$$

In Eq. (4) κ is a constant referred to as the shear stress constant, u_c is the jet centerline velocity, and ξ^* is the value of ξ at $u/u_c = 0.5$. Substituting Eqs. (3) and (4) into Eq. (2) and nondimensionalizing yields for the momentum integral equation,

$$\frac{d}{dx}\left[\xi^*\int_0^1 \frac{\rho u^2}{\rho_0 u_0^2} d\left(\frac{\xi}{\xi^*}\right)\right] - 0.5U\,\frac{d}{dx}\left[\xi^*\int_0^1 \frac{\rho u}{\rho_0 u_0} d\left(\frac{\xi}{\xi^*}\right)\right] + \frac{dh_i}{dx}(1-0.5U) =$$

$$\frac{\rho^*\kappa\xi^*}{2\rho_c u_c}\left(\frac{\partial u}{\partial \xi}\right)_{\xi=\xi^*}\frac{\rho_c}{\rho_0}U^2 \tag{5}$$

where $U = u_c/u_0$.

Assuming the velocity profiles in the mixing zone to have a Gaussian distribution as was found for an incompressible two-dimensional jet in Ref. 1,

$$\frac{u}{u_c} = e^{-B(\xi/\xi^*)^2} \tag{6}$$

where, $B = 0.6931$ FOR $u/u_c = 0.5$ AT $\xi/\xi^* = 1$

From the perfect-gas equation of state and the energy equation for isoenergetic mixing (constant total temperature),

$$\frac{\rho}{\rho_0} = \frac{\rho_e}{\rho_0}\left\{1 + \frac{\gamma-1}{2}M_0^2\left[1-\left(\frac{u}{u_0}\right)^2\right]\right\}^{-1} \tag{7}$$

where $\rho_0 = \rho_e = 1$ for a perfectly expanded jet.

Employing Eqs. (6) and (7), Eq. (5) normalized with respect to the initial jet height, h_0, becomes,

$$\frac{d\left[\frac{\xi^*}{h_0}f_1(U)\right]}{d\left(\frac{x}{h_0}\right)} - 0.5U\,\frac{d\left[\frac{\xi^*}{h_0}f_2(U)\right]}{d\left(\frac{x}{h_0}\right)} + (1-0.5U)\frac{d\left(\frac{h_i}{h_0}\right)}{d\left(\frac{x}{h_0}\right)} = -\kappa f_3(U) \tag{8}$$

270

where,

$$f_1(U) = \int_0^1 \frac{\rho u^2}{\rho_0 u_0^2} \, d\left(\frac{\xi}{\xi^*}\right) = \int_0^1 \frac{U^2 \left(\frac{u}{u_c}\right)^2}{1 + \frac{\gamma-1}{2} M_0^2 \left[1 - U^2 \left(\frac{u}{u_c}\right)^2\right]} \, d\left(\frac{\xi}{\xi^*}\right) \tag{9}$$

$$f_2(U) = \int_0^1 \frac{\rho u}{\rho_0 u_0} \, d\left(\frac{\xi}{\xi^*}\right) = \int_0^1 \frac{U \left(\frac{u}{u_c}\right)}{1 + \frac{\gamma-1}{2} M_0^2 \left[1 - U^2 \left(\frac{u}{u_c}\right)^2\right]} \, d\left(\frac{\xi}{\xi^*}\right) \tag{10}$$

and,

$$f_3(U) = \frac{B}{2} \frac{\rho^*}{\rho_0} U^2 = \frac{B}{2} \left[\frac{U^2}{1 + \frac{\gamma-1}{2} M_0^2 (1 - 0.25 U^2)} \right] \tag{11}$$

From Eq. (1) the momentum equation in nondimensional form becomes,

$$\frac{\xi^*}{h_0} = \frac{1 - \frac{h_t}{h_0}}{f_4(U)} \tag{12}$$

where,

$$f_4(U) = \int_0^\infty \frac{\rho u^2}{\rho_0 u_0^2} \, d\left(\frac{\xi}{\xi^*}\right) = \int_0^\infty \frac{U^2 \left(\frac{u}{u_c}\right)^2}{1 + \frac{\gamma-1}{2} M_0^2 \left[1 - U^2 \left(\frac{u}{u_c}\right)^2\right]} \, d\left(\frac{\xi}{\xi^*}\right) \tag{13}$$

For the core region $U = 1$, $f_1(U)$, $f_2(U)$, $f_3(U)$ and $f_4(U)$ are constant. Consequently, combining Eqs. (8) and (12) it can be deduced that

$$\frac{h_t}{h_0} = 1 - \frac{\frac{x}{h_0}}{\frac{x_c}{h_0}} \tag{14}$$

and thereby Eq. (12) can be written as

$$\frac{\xi^*}{h_0} = \frac{\frac{x}{h_0}}{f_4(1) \frac{x_c}{h_0}} \tag{15}$$

Also Eqs. (8) and (12) yield,

$$\frac{x_c}{h_0} = \left\{ \frac{0.5 \left[f_2(1) + f_4(1)\right] - f_1(1)}{f_3(1) f_4(1)} \right\} \frac{1}{\kappa} \tag{16}$$

271

which expresses the length of the core region in terms of an empirically determined shear stress constant, κ , and a constant which is dependent on the initial jet Mach number and the assumed profile shape. Once x_c/h_0 has been determined from Eq. (16), y^* can be determined from Eqs. (14) and (15) noting that $y^* = h_i + \xi^*$.

For the developed region, $h_i = 0$; and combining Eqs. (8) and (12) yields

$$\frac{d}{d\left(\frac{x}{h_o}\right)}\left[g_1(U)\right] - 0.5U \frac{d}{d\left(\frac{x}{h_o}\right)}\left[g_2(U)\right] = -\kappa f_3(U) \tag{17}$$

where,

$$g_1(U) = \frac{f_1(U)}{f_4(U)} \qquad \text{AND} \qquad g_2(U) = \frac{f_2(U)}{f_4(U)}$$

Employing the relation $\frac{d}{dx} = \frac{d}{dU} \frac{dU}{dx}$ Eq. (17) can be written as,

$$\left\{\frac{d}{dU}\left[g_1(U)\right] - 0.5U \frac{d}{dU}\left[g_2(U)\right]\right\}\frac{dU}{d\left(\frac{x}{h_o}\right)} = -\kappa f_3(U) \tag{18}$$

Letting,

$$F(U) = \frac{g_1'(U) - 0.5U g_2'(U)}{f_3(U)} \tag{19}$$

where the derivatives $g_1'(U)$ and $g_2'(U)$ can be determined graphically, Eq. (18) becomes,

$$\int_1^U F(U)dU = -\kappa \left(\frac{x}{h_o} - \frac{x_c}{h_c}\right) \tag{20}$$

where $\int_1^U F(U)dU$ can be evaluated numerically. Therefore, from Eq. (20) the centerline velocity decay can be determined in terms of the empirically determined value of shear stress constant, κ . Once the centerline velocity is known as a function of axial distance the corresponding variation in $y^* = \xi^*$ can be determined from Eq. (12).

Although the above derivation is valid only for the case of perfectly expanded jets (i.e., $p_e = p_0$), the analysis may be made applicable for the case of slightly underexpanded jets by substituting M_{eq} for M_0 and h_{eq} for h_0 where M_{eq} is the Mach number corresponding to isentropic expansion from the

272

Jet total pressure to ambient static pressure and h_{eq} is given by

$$h_{eq} = \left[\left(\frac{h_0}{\gamma M_0^2} \right)\left(1 - \frac{p_e}{p_0} \right) + h_0 \right] \left(\frac{M_0}{M_{eq}} \right)^2 \frac{\rho_0}{\rho_e} \tag{21}$$

which follows from conservation of momentum.

EXPERIMENTAL INVESTIGATION

A schematic diagram and photograph of the test rig employed for these tests are presented in Figs. 3 and 4, respectively. The test rig was two-dimensional throughout its length and was provided with hinged side plates 3 in. apart. A portion of these side plates was glass to enable schlieren observation. Removable nozzle blocks were provided to obtain both subsonic and supersonic jet Mach numbers. Subsonic or sonic jet Mach numbers were obtained with a smooth-approach convergent nozzle. Convergent-divergent nozzles designed for uniform flow at the exit were employed to obtain jet Mach numbers of 1.5 and 2.0. The exit width, w, for all nozzles was equal to 0.25 in., thereby providing an aspect ratio (distance between side plates divided by the nozzle width) equal to 12.0.

Air having a stagnation temperature of approximately 80 F and a dew point of less than -20 F was introduced into the plenum chamber upstream of the nozzle blocks from a 400 psia compressor capable of continuously delivering 5 lb/sec. For these tests the air was throttled to provide total pressures of approximately 22 psia. This upstream pressure corresponds to Reynolds numbers based on the exit width of the jet ranging from 1.4×10^5 (for a jet Mach number of 1.0) to 1.2×10^5 (for a jet Mach number of 2.0). The air was exhausted through nozzle blocks in the center of the test rig into the downstream plenum chamber evacuated by laboratory vacuum pumps. The relatively "dead air" regions on either side of the jet were vented together for pressure equalization on the two sides of the jet. Both the exhaust bellmouth and the vent line between the two unbounded sides of the jet were required to maintain the jet centerline parallel to the longitudinal centerline of the test rig.

The variable-position pitot rake shown in Fig. 4 was employed to obtain surveys through the jet. This probe was located midway between the side plates and was motorized in the directions perpendicular and parallel to the jet centerline. The position of the probe was indicated on a Moseley voltmeter which recorded the output of potentiometers located on the probe actuating mechanism. The probe pressures were measured on mercury manometers.

Tests were conducted at jet Mach numbers of 0.66, 0.895, 1.0, 1.5 and 2.0. For all tests except those for Mach 1.0, the ambient static pressure was equal to the static pressure at the nozzle exit. For the Mach 1.0 tests, the nozzle exit static pressure ratio (ratio of the exhaust static pressure to the nozzle exit static pressure) was equal to 0.87 and 0.59. Exit static pressure ratios

274

REMOVABLE AND ADJUSTABLE
NOZZLE BLOCKS (TO VARY MACH
NUMBER AND ASPECT RATIO)

VENT LINE

FROM 400 PSI
SUPPLY

TO VACUUM PUMPS

EXHAUST BELLMOUTH

FIGURE 3   SCHEMATIC DIAGRAM OF TEST RIG FOR FREE-JET TESTS

EXHAUST BELLMOUTH

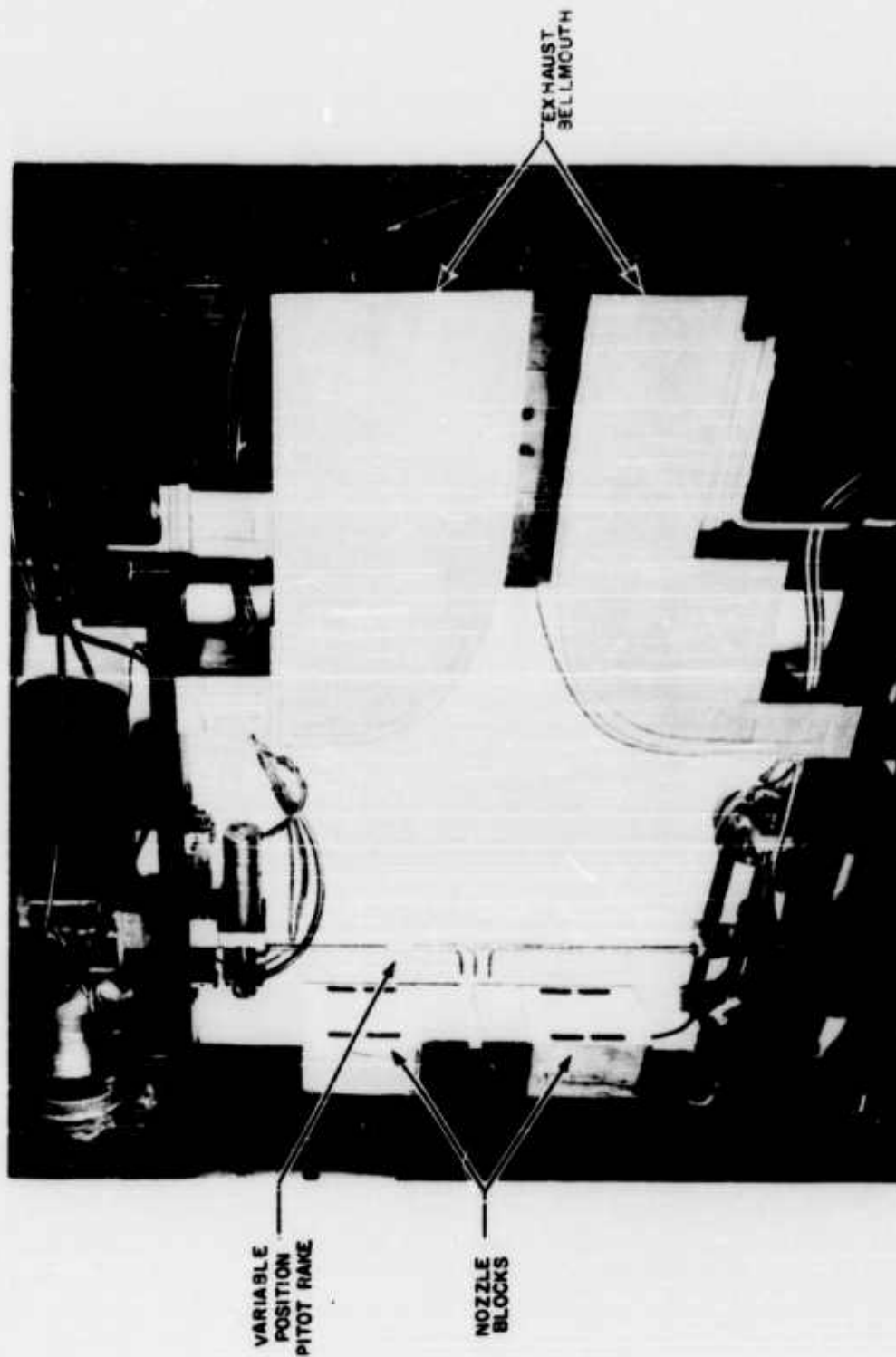VARIABLE POSITION PITOT RAKE
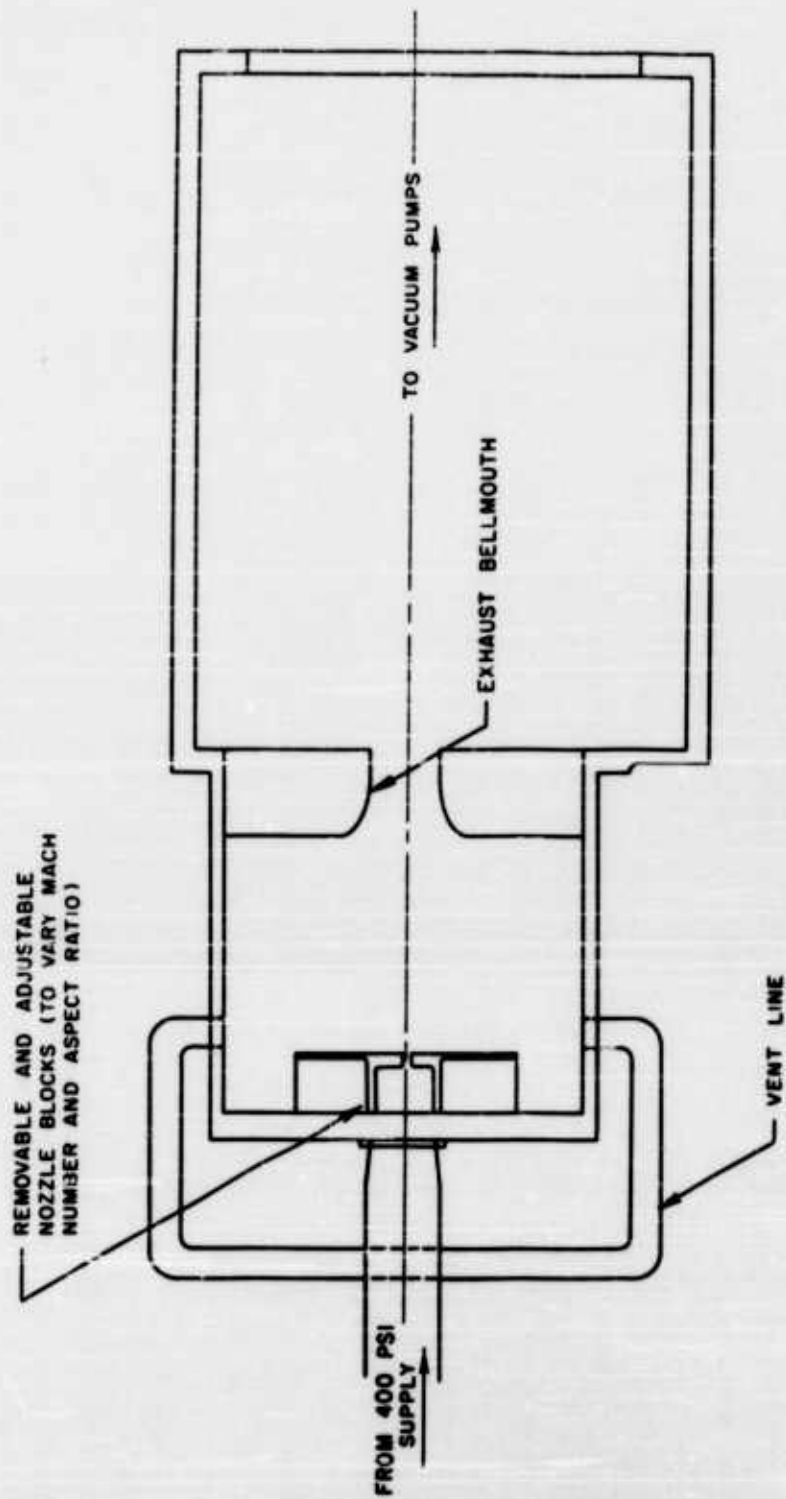
NOZZLE BLOCKS

FIGURE 4 PHOTOGRAPH OF TEST RIG FOR FREE-JET TESTS

275

lower than 1.0 were selected to provide information regarding the characteristics of underexpanded jets.

For each jet Mach number, pitot pressure surveys were obtained at axial stations between 2 and 16 nozzle widths downstream of the nozzle exit. These pitot pressure surveys were obtained from the three-tube rake shown in Fig. 4 which was traversed perpendicular to the jet centerline in the vertical plane. At two locations in the jet (one above and one below the centerline), readings were obtained with both the outer probes and the center probe. A comparison of these readings provided a means of matching the profiles obtained from the three probes to form a continuous single profile and also enabled an evaluation of probe interference effects. The static pressure in the relatively "dead air" region on the unbounded sides of the jet was adjusted by varying the pressure in the plenum downstream of the exhaust bellmouth.

The Mach number and velocity distributions in the jet were computed from the measured pitot profiles using one-dimensional compressible-flow relations assuming a constant static pressure and total temperature throughout the stream. For all cases the static pressure througout the jet was assumed equal to the ambient pressure and the total temperature was taken equal to the temperature of the supply air.

A comparison of the experimental nondimensional velocity profiles in the mixing zone of the core and developed regions with the profile shape assumed in the analysis is presented in Figs. 5 and 6. Presented in the upper portion of Fig. 5 are the profiles for Mach number 0.66 at various axial stations within the core and in the lower portion are the profiles for various Mach numbers at one axial station in the core. The nondimensional velocity profiles for the developed region are presented in a similar manner in Fig. 6. For both the core and developed regions, good agreement is shown between the experimental profiles and the assumed Gaussian profile except near the outer edge of the jet. In this portion of the profile, however, the scatter in the experimental velocities precludes any valid comparison. This scatter is probably due principally to the extreme sensitivity of the calculated velocities to the values of static pressure employed.

A comparison between the theoretical and experimental centerline velocity decay characteristics for all the jet Mach numbers investigated is presented in Fig. 7. The theoretical decay curves were calculated using Eqs. (16) and (20). Good agreement is shown between the analytical and experimental values of centerline velocity ratio except near the transition between the core region and developed region. As would be expected, this transition is not discontinuous as assumed in the analysis but occurs over a finite distance.

A comparison between the theoretical and experimental jet velocity spreading characteristics is presented in Fig. 8. The theoretical values of y^*/w presented in this figure were calculated from Eqs. (12) and (15), employing

FIGURE 5 NONDIMENSIONAL VELOCITY PROFILES FOR CORE REGION

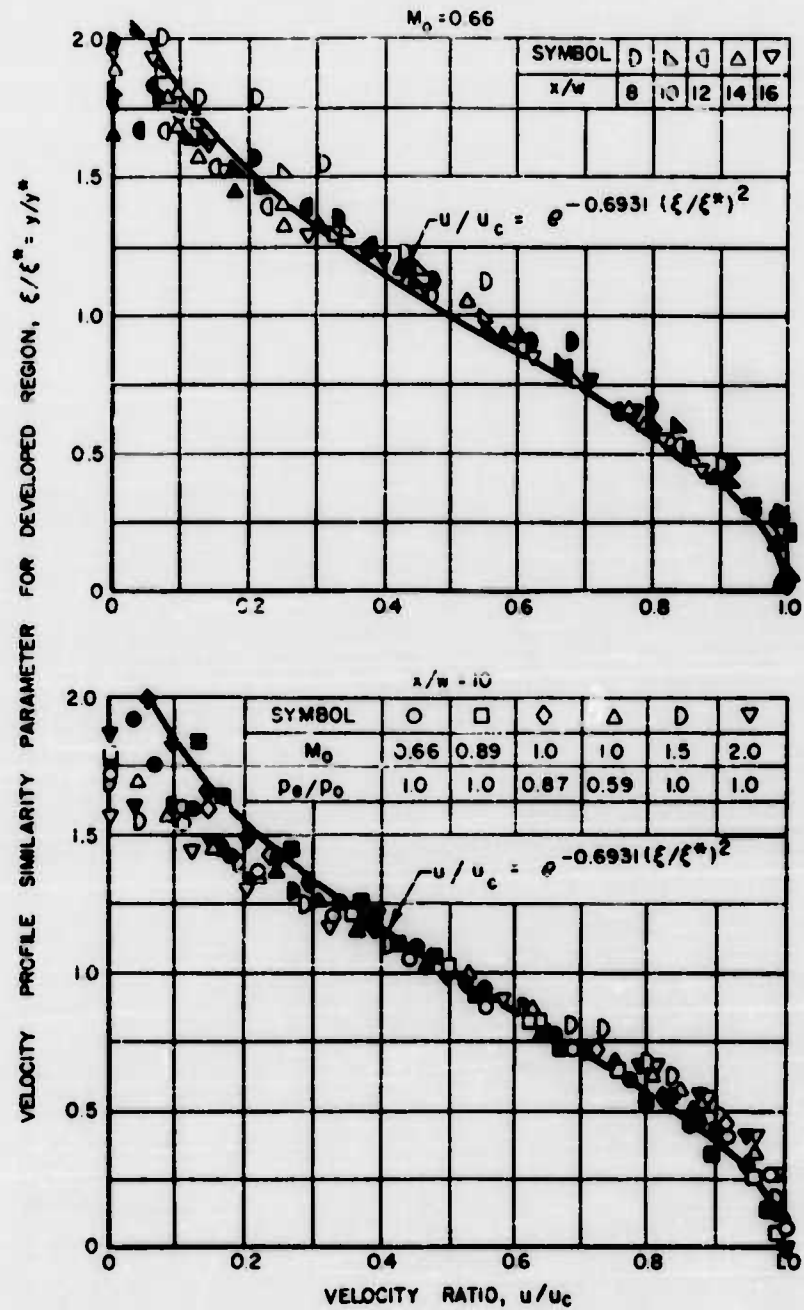FIGURE 6 NONDIMENSIONAL VELOCITY PROFILES FOR DEVELOPED REGION
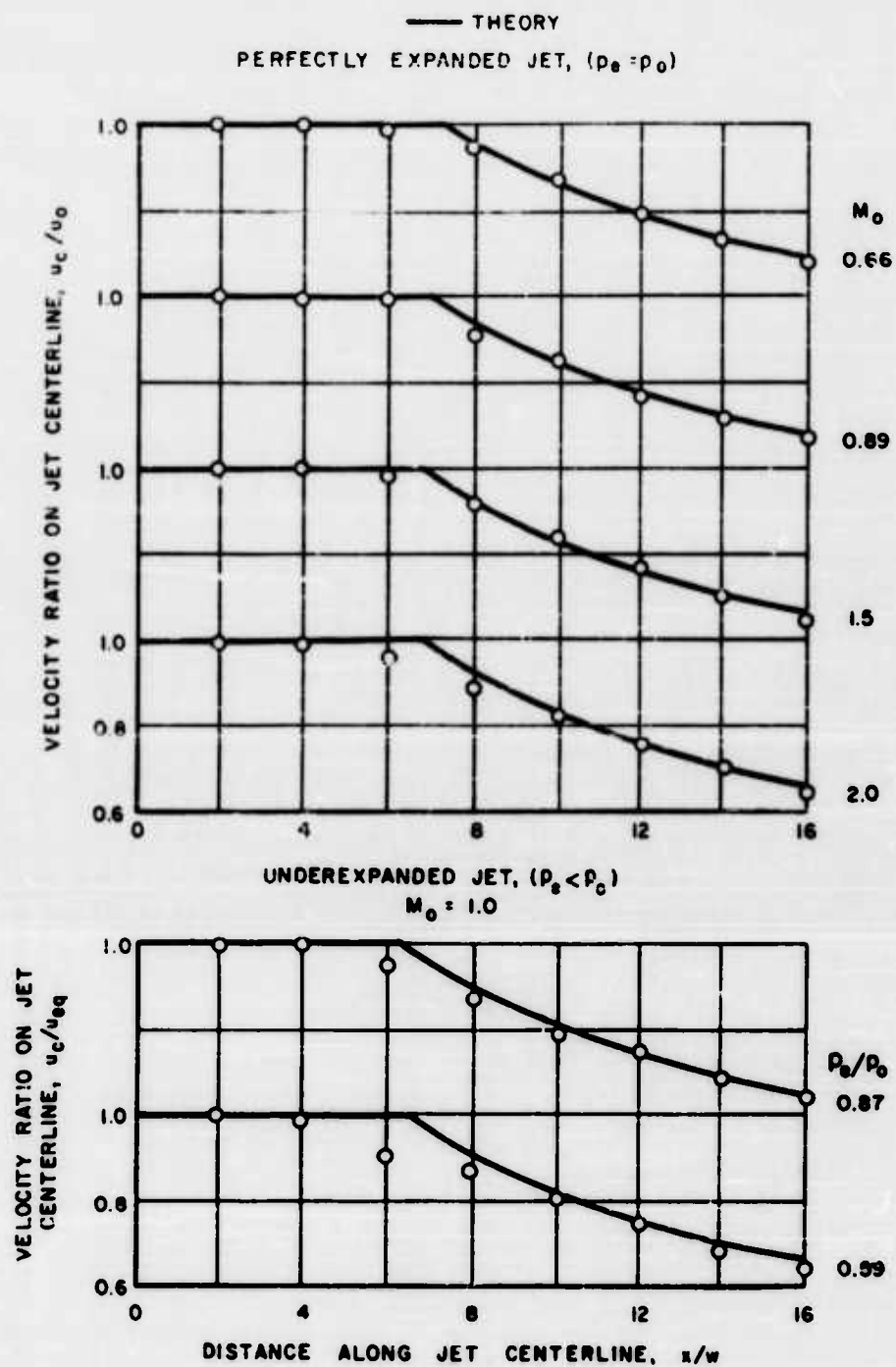
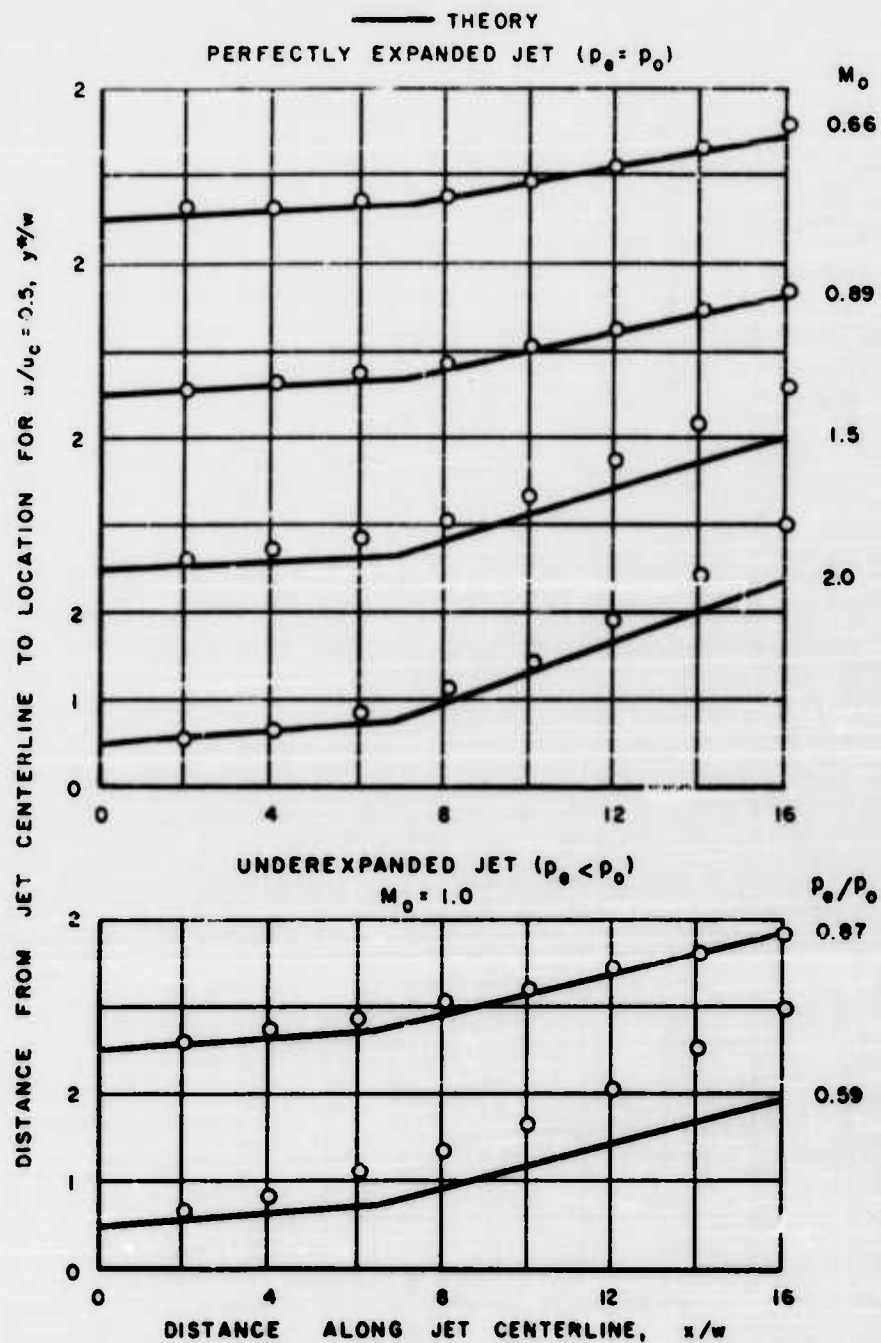FIGURE 7 CENTERLINE VELOCITY DECAY CHARACTERISTICS

FIGURE 8 VELOCITY SPREADING CHARACTERISTICS

$$\tau = \epsilon \frac{\partial u}{\partial y}$$

WHERE,

$$\epsilon = \kappa \frac{u_c}{2} \xi^*$$

OPEN SYMBOLS DENOTE $M_{eq} = M_0$
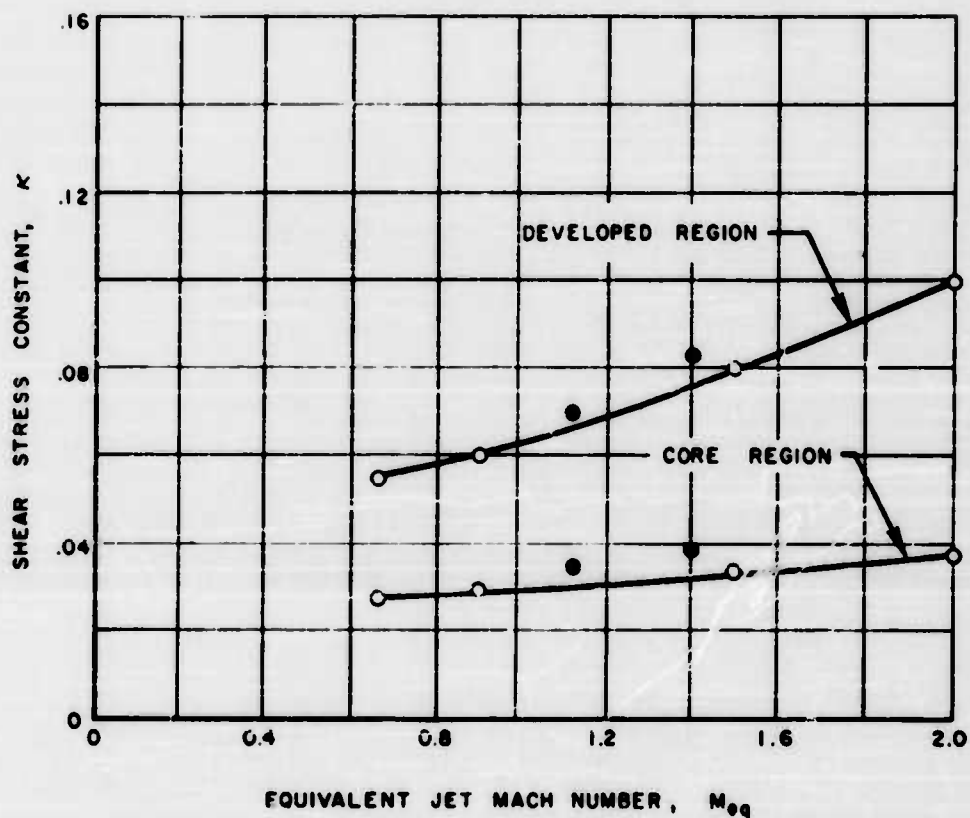CLOSED SYMBOLS DENOTE $M_{eq} > M_0$

FIGURE 9 VARIATION OF SHEAR STRESS CONSTANT WITH JET MACH NUMBER

the theoretical results presented in Fig. 7. For the underexpanded jets, Eq. (21) was used to define an equivalent exit height of the nozzle. Good agreement is also shown between the analytical and experimental values of jet spreading rate for the subsonic jets and for the slightly underexpanded Mach 1.0 jet. Somewhat poorer agreement is shown for the higher Mach number supersonic jets. It is believed that the discrepancies shown for the supersonic Mach number jets are due principally to static pressure distributions existing in the jet which were not accounted for in either the calculation of the experimental velocity profiles or in the development of the momentum integral equation for computing the theoretical jet characteristics. The static pressure gradients could be caused by small inaccuracies in the nozzle contours or possibly by increased shear in the jet. The effect of static pressure gradient is even more pronounced for the underexpanded Mach 1.0 jet having an exit static pressure ratio, p_e/p_0, equal to 0.59. For this case the static pressure gradients are caused by the series of shocks and expansions characteristic of the pattern for an underexpanded jet.

For each jet Mach number the value of shear stress constant, κ , employed in the determination of the theoretical results presented in Figs. 7 and 8 was the value which produced the best match to the data. The values of κ used are presented in Fig. 9 as a function of equivalent jet Mach number. It is seen from this figure that different values of shear stress constant were employed for the core and developed regions. The reason for this difference is not completely understood. Two possible explanations are (1) that these differences arise because of the assumptions made in the integral analysis employed or (2) that actual differences exist in the momentum exchange rates in the two regions. These differences are also suggested by comparing the results of the incompressible analyses for a jet boundary and a two-dimensional jet presented in Ref. 2. More detailed investigations of the mixing processes involved are required to resolve these differences indicated above.

The increase in κ with increasing Mach number in both regions indicates that the increased momentum transferring ability of the jet with increasing Mach number is apparently greater than that predicted by the analysis which assumes κ is a constant. This dependence of κ on jet Mach number has also been shown for axisymmetric jets in Ref. 3. For the axisymmetric jet studies, however, κ was found to decrease with increasing Mach number. It should also be noted that the value of κ for each Mach number could be appreciably effected by the Reynolds number. This effect of Reynolds number for a two-dimensional incompressible jet is shown in Ref. 4 where the core length was found to increase with increasing Reynolds number. This increase in core length corresponds to a decrease in the value of κ . Further investigations are necessary to determine the effect of Reynolds number for compressible two-dimensional jets.

In summary, it has been shown that the integral analysis presented herein provides a quantitative method for predicting the velocity profiles for perfectly expanded and slightly underexpanded two-dimensional, turbulent, compressible submerged jets over a range of Mach numbers. As pointed out previously, however, additional investigations are required to determine the effect of Reynolds number on the values of the empirical shear stress constant employed in the analysis.

LIST OF REFERENCES

1. Albertson, M. L., Y. B. Dai, R. A. Jensen and Hunter Rouse: Diffusion
    of Submerged Jets. American Society of Civil Engineers Proceedings,
    Vol. 74, No. 10, December 1948.

2. Schlichting, Hermann: Boundary Layer Theory. McGraw-Hill Series in
    Mechanical Engineering. Fourth Editions, 1960.

3. Warren, Walter R.: An Analytical and Experimental Study of Compressible
    Free Jets. Aeronautical Engineering Laboratory Report No. 381, Princeton
    University, Princeton, New Jersey, 1957.

LIST OF SYMBOLS

B	Constant in Eq. (6)
h_i	Distance between jet centerline and outer boundary of core
h_o	Distance between nozzle centerline and inner contour at nozzle exit
M	Mach number
p	Static pressure
p_e	Static pressure on free boundary of jet
u	Velocity parallel to jet centerline
u_c	Velocity on jet centerline
U	Ratio of local centerline velocity to initial jet velocity
w	Total height of nozzle at exit
x	Distance along jet centerline
x_c	Distance between nozzle exit and end of core region
y	Distance perpendicular to jet centerline
γ	Ratio of specific heats
ϵ	Turbulent exchange coefficient
κ	Shear stress constant
ξ	Transformed coordinate perpendicular to jet centerline
ρ	Density
ρ_c	Jet centerline density
τ	Shear stress

Subscripts

eq   Denotes equivalent conditions

o   Denotes conditions at nozzle exit

Superscripts

*   Denotes conditions where $u/u_c = 0.5$

286

A SOLUTION OF THE TWO-DIMENSIONAL TURBULENT VISCOUS CURVED JET USING THE IBM 7090 COMPUTER

by

Professor G. D. Boehler

of

The Catholic University of America
and
Aerophysics Company
Washington 6, D. C.

ABSTRACT

A numerical solution of the two-dimensional curved turbulent and incompressible jet flow, using the IBM 7090 computer, is presented. This solution is a straight-forward extension of the classical straight jet solution. Its only limitation is that it assumes similar velocity profiles.

The solution is obtained by reducing the Navier Stokes partial differential equations of the curved jet flow to a third-order total differential equation of the Jartree-Skan type. This equation is integrated numerically on the IBM 7090 computer using a Runge-Kutta subroutine. The boundary conditions are carefully established and discussed. Typical numerical results, in the form of velocity and pressure distribution across the jet are presented and discussed.

CHARACTERISTICS AND CONTROL OF FREE LAMINAR JETS

by

Alan Powell

University of California, Los Angeles

The operation of certain classes of fluid flow devices depends upon the character of and response to applied disturbances of jet flows. This paper describes some relevant basic features of laminar incompressible jet flows as a separate element free of the effects of adjacent solid walls. The characteristics of the steady flow are well established, theoretically and experimentally. Results are given showing how the main jet is deflected by side jets, the deflection angle being dependent upon the geometry. Classical instability theory of periodically disturbed "psuedo-laminar" jets has been supplemented by recent experimental work which has disclosed the frequency range for disturbance growth is real, spreading, laminar jets. This work is now extended to the case of the main jet being disturbed by periodic (modulated) side jets. The classical oscillatory feedback of edgetones from a wedge-like obstruction lying in the jet back to the orifice, is discussed, as is also the case when a resonating element is in the feedback path.

1. INTRODUCTION

The great attraction of the wide class of fluid flow devices as typified by the fluid amplifier is their extreme physical simplicity; it is somewhat ironic that the challenge of thoroughly understanding the details of the flow is one beset with great complication. Progress so far has been along almost purely empirical lines, in that singularly few characteristics can be predicted by entirely theoretical reasoning, or even with the aid of the limited experimental observation of that type so typical to fluid mechanics.

This paper concentrates upon the fundamental properties of one of the several major flow phenomena involved, namely upon the behavior of the jet flow. The most simple situation is taken, in that the complicated (and admittedly very interesting!) effects of side walls are presently deliberately avoided. Further, attention is limited to laminar flows, so that this area may be reasonably explored before entering into questions of turbulent or compressible flow fields.

2. THE STEADY LAMINAR JET

The steady two-dimensional laminar jet is one of the few flow problems which have been solved explicitly and exactly, even though this concerns flow from an infinitely narrow slit.[1] For this flow, the cross-sectional velocity profiles are similar, actually like secant curves. The only variation from cross-section to cross-section is the decay of the centerline velocity with distance raised to the inverse third power and the corresponding spread in the jet width with distance, actually to the two-thirds power so that the momentum flow remains constant.

In practice the jet must emerge from an exit of finite width, so a transitional region occurs between the exit velocity profile and that of the theory, the latter being found some distance downstream. Careful experiments have shown that this transitional region must unfortunately be considered to occupy certainly most, if not all, of the distance of greatest interest in the fluid amplifier field, say up to a distance of ten slit widths from the exit.[2] Nevertheless, the existence of the explicit solution has enabled much theoretical progress to be made on the important and highly relevant question of jet instability, to which we return later.

If a steady laminar jet flows into a field of virtually unlimited extent it always sooner or later loses its steady character and becomes turbulent. Even if very carefully guarded from disturbances, very minute disturbances are inevitably communicated to the jet and are carried along with it, sooner or later to reach an area of the jet where the width is such that these disturbances are highly unstable. They then become enormously amplified into violent eddying motions, as can be seen in the drawing of Fig. 1 (which was prepared from a photograph of a smoke jet); this is immediately followed by collapse to ragged turbulence.[2] Here we are concerned with the flow region prior to such transition to turbulence (which occurs less spectacularly and very close to the exit for turbulent jets.)

3.   DIRECTIONAL CONTROL BY STEADY SIDE JETS

The main jet flow may be deflected by imparting lateral momentum to it by the impingement of a side jet, which in fluid amplifier language is termed a control jet.[3] One geometry to achieve this is shown in Fig. 2, together with the resultant local flow pattern. The momentum flow in the original axial direction is virtually unaffected by the presence of the control jet; however the control jet, in pushing the main jet from the adjacent wall, results in a modified pressure distribution on that wall, so that the lateral jet momentum is not simply that of the control jet flow itself.

The experimental results of Fig. 3 show how the deflection angle depends on the flows of the two jets, the main jet and the control jet; the geometry for these results is that of Fig. 2, the main jet being 0.635 cm wide and the control jet 0.0508 cm wide, both of them having a length normal to the paper plane of 15.25 cm.

A second control jet may be placed on the left side of the main jet of Fig. 2, but then the presence of the upper lip of the second control jet clearly impedes the deflection of the jet by the first control jet. Further, the confined flow from the control jet causes an effective narrowing of the main jet flow, and this may be considered to be an undesirable feature for certain applications. With this geometry the control jet flow must be doubled to achieve the same deflection as when the second control jet nozzle is absent. These two situations are represented by the uppermost and lowest curves in Fig. 4.

The constriction in the main flow caused by the pair of control jet flows may be relieved partially by set-back of the upper lip of the nozzles; but the deflection angles are still considerably less for the single control jet of Fig. 2, even with only one set-back nozzle present. This is also shown in Fig.4, the curves marked 2 and 4 being for two and one control nozzle with set back respectively.

If both the top and bottom of the nozzle (see Fig. 2) is set back then the apparently favorable pressure distribution on the wall is lost, so the curve marked 3 results. But now the presence of a second set-back control nozzle results in a local flow pattern in the additional flow cavity so formed in such a way that the deflections achieved, curve 5, are almost as large as for the single control jet system of Fig. 2.

The question naturally arises as to what amount of set-back results in maximum deflection. The indications are that there is such an optimum, for Fig. 5 shows how, for a number of main jet flows, the control jet flow must vary with set-back in order to maintain a constant flow deflection of 20°. The minimum occurs at almost the same value of the set-back for all the flow rates considered.

4. QUASI-STEADY RESPONSE

If the flow rate of a control jet is varied very slowly, the resultant jet flow is almost straight for a distance of several nozzle widths: this we may call the quasi-steady case. The angular deflection, at any instant, in the immediate neighborhood of the orifice is virtually the same as if the control jet were a steady one of that instantaneous flow rate. An example of the flow is shown in Fig. 6; here the jet is swinging from right to left. In this partic-ular case the flow rate varies in more of a square-wave fashion than sinusoidally. As the switching action commences a vortex forms where the jet begins to move from the extreme position, the vortex naturally moving away from the nozzle exit.

The Strouhal number is a very important factor in the dynamic case. It is defined as the product of the frequency and the jet width divided by the mean jet velocity. Thus, a high Strouhal number indicates closely spaced jet dis-turbances, and a low Strouhal number indicates a relatively large spacing. In the case of Fig. 6, $S = 0.00465$.

5. DYNAMIC RESPONSE

When the flow of the control jet or jets is cycled relatively rapidly, two new effects appear. Firstly, because the control jet interacts with a fin-ite region of the main jet, some local averaging out must be expected. Secondly, and much more important, is that the combined jet takes on a wavy form, and this is very unstable for wavelengths of intermediate length, the instability being greatest for wavelengths equal to about six jet widths. In other words, the inherent instability of the jet results in a nearly exponential growth of the disturbance amplitude far in excess of the almost linear one arising from the jet merely being directed in differing directions. The Strouhal number is a crucial parameter in determining the flow pattern. At a value of 0.073 the flow is unstable, but not greatly so, and the wavelength is long. Thus the flow pat-tern, Fig. 7, is virtually that of a quasi-steady jet.

At $S = 0.27$ the flow is extremely unstable, Fig. 8.

At higher Strouhal numbers the instability decreases and then becomes stable, see Fig. 9 and 10 where $S = 0.71$ and 1.9 respectively. The Strouhal number for the neutrally stable case is difficult to locate exactly, since the degree of instability actually varies along the length of the spreading jet, and in any case, the overall effect varies rather slowly with frequency. Under different conditions

of excitation a value of about 0.5 was found to correspond to neutrally stable conditions.

6. EFFECT OF OBSTACLE IN STREAM - SELF-EXCITED OSCILLATIONS

If an object is placed on the initial centerline so as to divide the flow, one of several flow patterns may result even in the absence of flow from the control jets.[4] If the object--a cylinder or wedge--is relatively close to the edge the steady flow may become completely bifurcated even if the object is quite small: if the object is very small, however, the flow will recombine on the downstream side. Fig. 11 illustrates these basic flows.

But if the spacing between orifice and object exceeds a certain critical distance, violent self-excited oscillations ensue. This action takes place both in a liquid and in a gas; in air the fluctuating force on the object results in sound generation known as the edgetone. This is a natural feedback, the interaction of the eddying flow at the object disturbing the jet as it leaves the orifice, see Fig. 12. As one would expect, such self-excited oscillations occur in the frequency range of greatest jet instability. The conditions and amplitude of the oscillations have received much attention at low speeds.[5,6] For example, we now know that the amplitude of the disturbance caused at the exit may be amplified several thousand times before reaching the obstacle in the stream. One of the interesting features is that smooth variations of the frequency with jet velocity and with spacing are separated by quite sudden discontinuities; these occur so as to bring the frequency back closer to that for maximum instability.

7. FEEDBACK VIA A RESONATOR

A second feedback path may be introduced in several ways. One method is shown in Fig. 14, in which a cylindrical pipe resonator reminiscent of an organ pipe has been added to the basic system. In this case, the working fluid is air. With the Q-factor of the resonator high enough, the oscillation is not only forced to occur very close to one of the resonant frequencies of the pipe, but the self-excited oscillation occurs over a much greater range of parameters. Although the organ pipe is of ancient origin, it has only very recently become possible to predict which of the several resonant frequencies will be generated and with what power[7]; the action at the open ends of the resonator is, of course, greatly amplified.

REFERENCES

1. W.G. Bickley, "The Plane Jet," Phil. Mag. Vol. 23, 727, 1937.
2. R.C. Chanaud and Alan Powell, Experiments concerning the Sound Sensitive Jet, J. Acoust. Soc. Am. Vol. 34, No. 7, 907-195, 1962.
3. J.E. Wuerer and Alan Powell, unpublished work.
4. Alan Powell and R.C. Chanaud "Some Observations of Plane Laminar Jet Flows Impinging on Fixed Objects," Dept. of Engineering Report 62-8, University of California, Los Angeles, 1962.
5. Alan Powell, "On the Edgetone," J. Acoust. Soc. Am. Vol. 33, 305-409, 1961.
6. Alan Powell, "Vortex Action on Edgetones," J. Acoust. Soc. Am., Vol. 34, 163-166, 1962.
7. Alan Powell, "Nature of the Feedback Mechanism in Some Fluid Flows Producing Sound," Proceedings of the Fourth International Congress on Acoustics, Copenhagen, 1962.
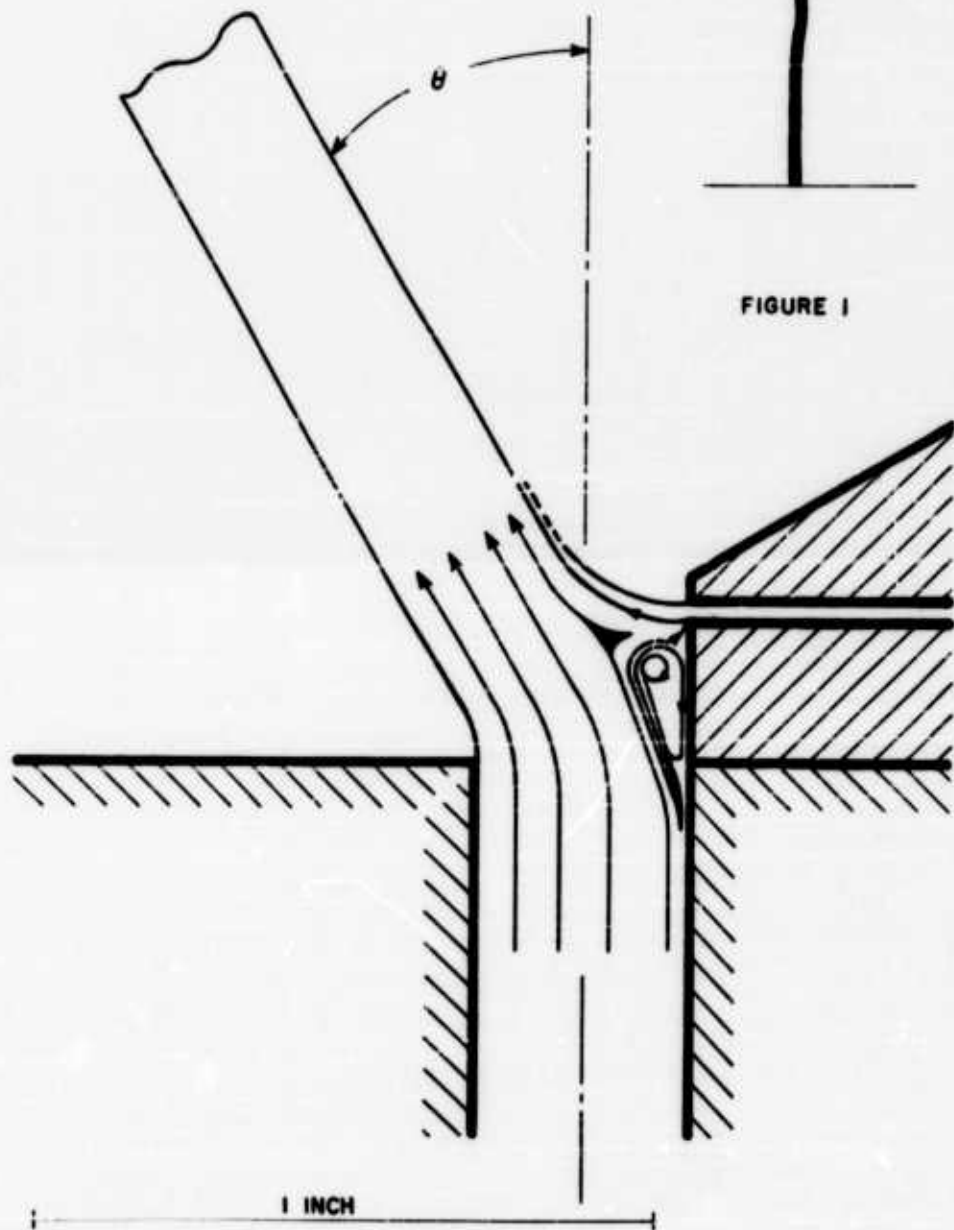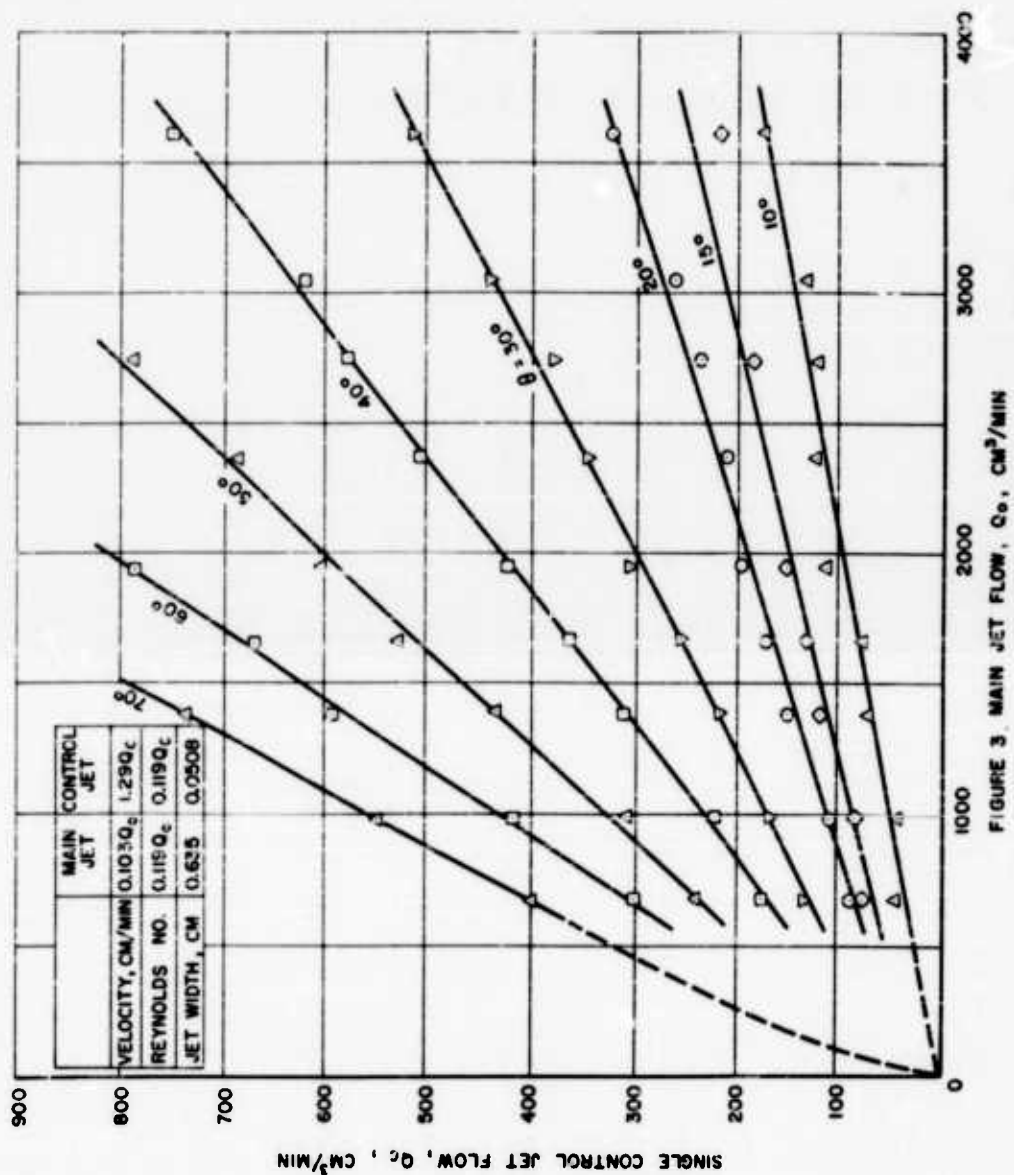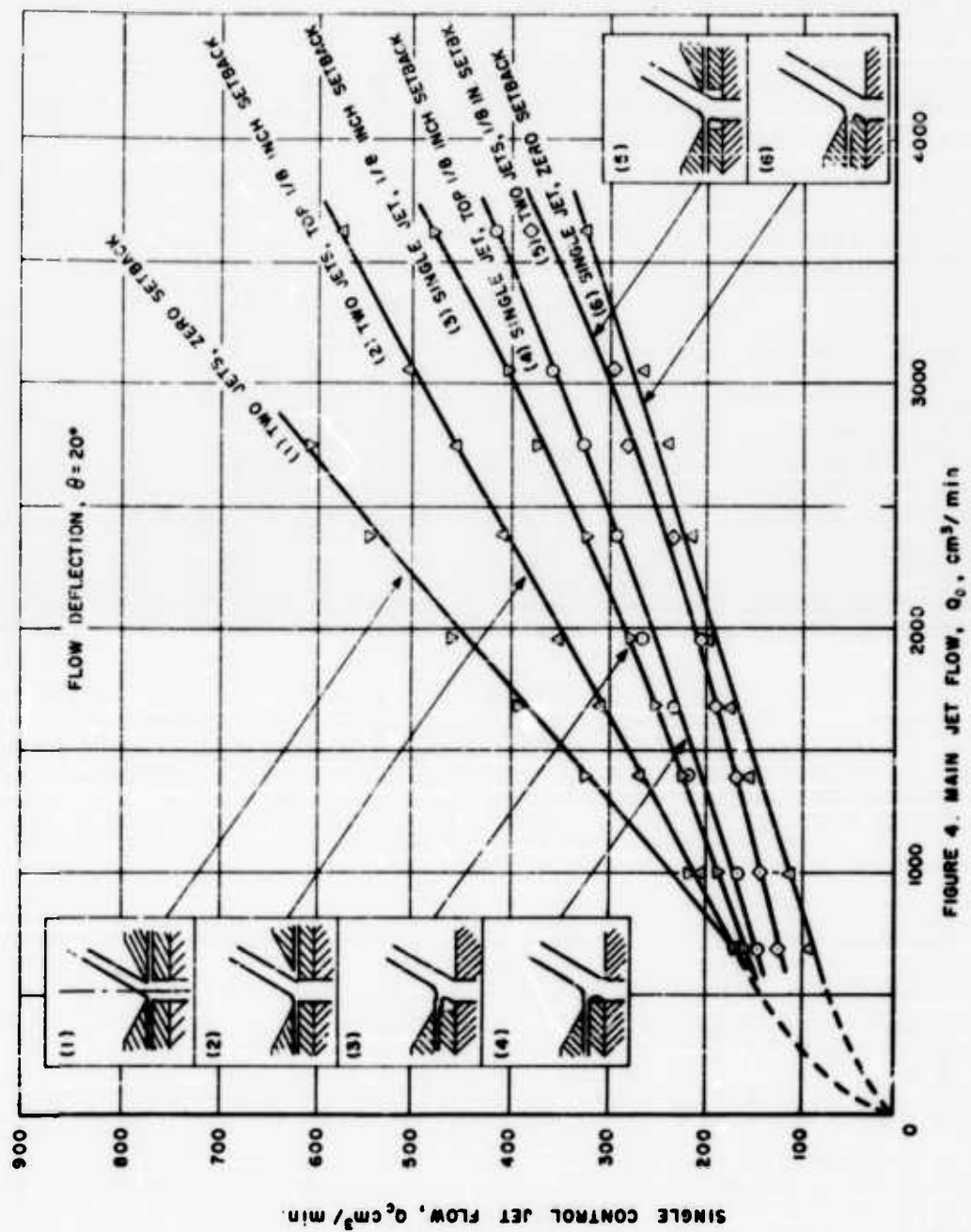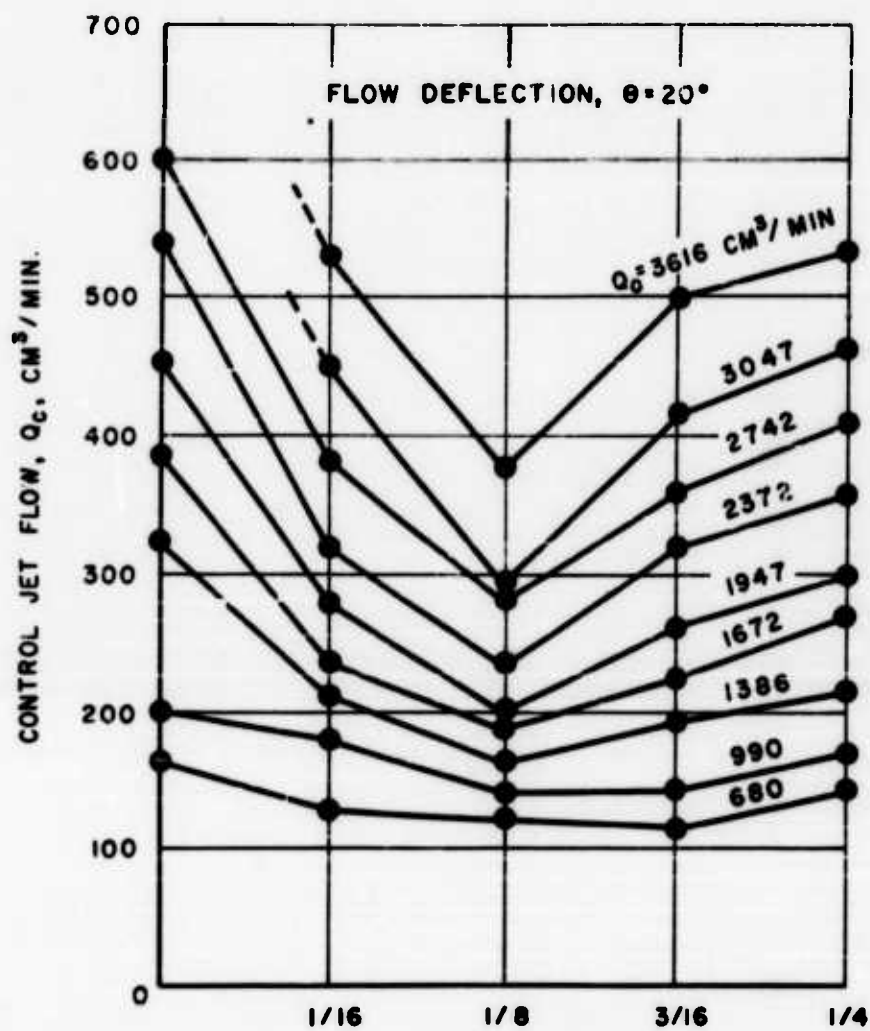
FIGURE 1

1 INCH

FIGURE 2.

293

FIGURE 3. MAIN JET FLOW, Q_e, CM^3/MIN
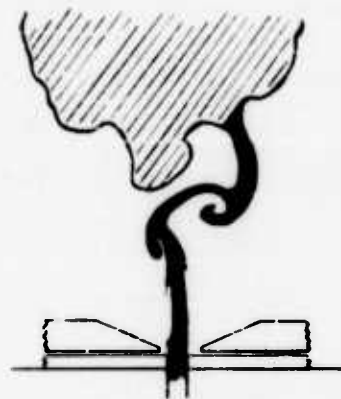
FIGURE 4. MAIN JET FLOW, q_0, cm³/min

FIGURE 5. SETBACK, INCH

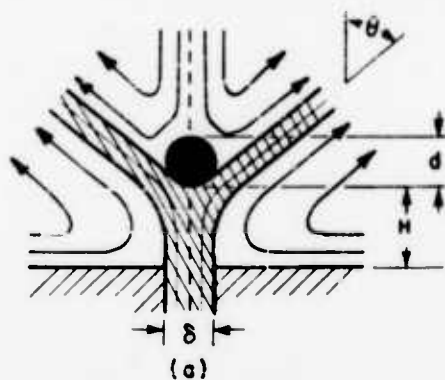296

FIGURE 6

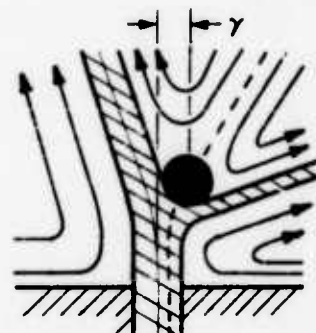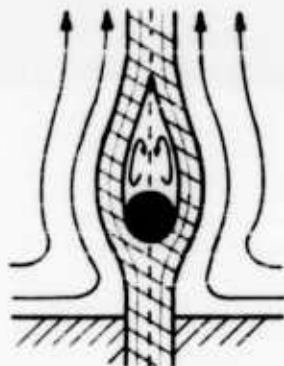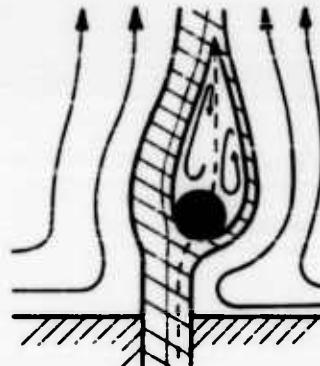FIGURE 7

FIGURE 8

FIGURE 9
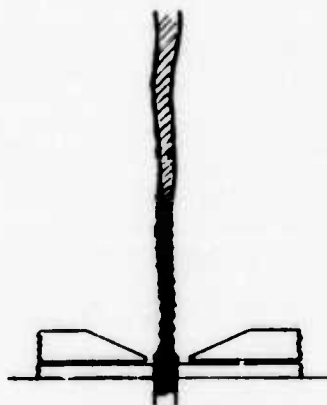
FIGURE 10

(a)
SYMMETRIC BIFURCATED JETS

(b)
ASYMMETRIC BIFURCATED JETS

(c)
SYMMETRIC CONFLUENT
JETS

(d)
ASYMMETRIC CONFLUENT
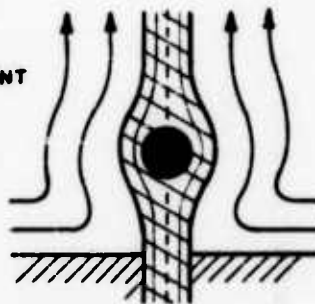JETS

(e)
FIGURE II. SYMMETRIC UNSEPARATED JET FLOW
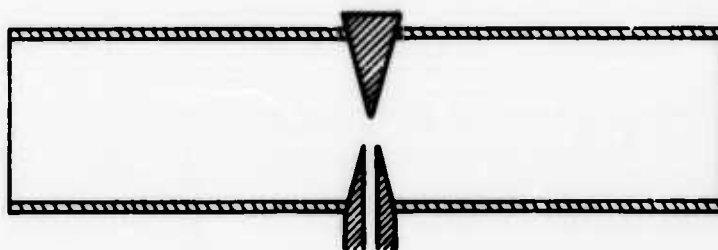
298

i

FIGURE 12

FIGURE 13

299

PNEUMATIC LINEAR CIRCUITS

by

Beatrice A. Hicks
Evelyn S. Jetter

of

Newark Controls Company

INTRODUCTION

The importance of demonstrable analogies between pneumatic and electrical and mechanical systems is that we can apply the same kinds of circuit theory to predict the behavior of a given pneumatic system and to design for desired performance characteristics.

FLOW OF GASES

Flow rate of gases in pneumatic circuits corresponds to current in electrical circuits or velocity in mechanical analysis. It is the rate of movement. In a pneumatic circuit which is in temperature equilibrium, flow rate is the number of cubic inches of gas passing a given point in one second when that gas is measured at unit pressure. For example: if 35 cubic inches at 12 psia pressure were to flow past a point in 3 seconds time, the flow would be $\frac{35 \text{ in}^3 \times 12 \text{ psia/psia}}{3 \text{ sec.}} = 140$ cu. in./sec. In multiplying directly by 12 psia/psia to obtain the cubic inches of gas at 1 psia we assume the application of the perfect gas law $PV = NRT$, which is a linear relationship.

Flow rate may vary with time and be an alternating flow just as current or velocity in electrical and mechanical systems may. Alternating or variable flow rate is symbolized by $u(t)$ and steady flow

301

rate by U. Its integral, charge, is symbolized by X and x(t), the equivalent volume at unit pressure in a specified geometric volume.

To compare two linear circuits each of which is at a different temperature, it is convenient to convert the quantity of flow to molal units. For example: a flow rate of 80 cu.in./sec. at 70°F. The volume is transformed by use of the equation PV=NRT.

$$N = \frac{PV}{RT}$$

$$N = \frac{1 \times 80}{18,510 \times (460+70)}$$

$N = 8.16 \times 10^{-6}$ lb.mols

Therefore 80 cu. in./sec at 70°F is equivalent to 8.16×10^{-6} lb-mols/sec.

where P = unit pressure, psia

V = volume, cu. in.

T = Absolute temp. °Rankine

N = Quantity of Gas, lb-mols

R = Gas Constant, 18,510 lb in./(lb-mols)-°R

Analysis of pneumatic circuits that are not in temperature equilibrium must include this factor. As an example, analysis of a system involving the movement of a hot gas to a cooler volume must reflect the effect of temperature transients. Elimination of the consideration of temperature and temperature transients from the equations and measurements in a linear pneumatic system is treated separately in molal units. The principle limitation in the application of this approach has been the lack of adequate measuring instruments.

PRESSURE

Pressure or, in the English system, the pounds of force exerted on each square inch of area corresponds to voltage in electrical circuitry or force in mechanical systems. The net effective pressure, or the difference in pressure between two points, may vary with time in the

302

same manner as voltage and is symbolized by $p(t)$, or by P for steady non-varying pressure. The basic reference pressure does not have to be absolute zero just as ground in an electrical system can have a voltage and force can be the resultant after a counter force is taken into account.

A centrifugal compressor, a source of constant pressure, is analogous to a battery supply of dc voltage and a piston compressor supplying variable pressure to an ac voltage supply.

Because of its extent the open atmosphere and its constant supply of non-varying pressure is also equivalent to a constant pressure source or, in electrical terms, a battery. The level of this atmospheric pressure source varies with altitude and weather conditions.

Terms, Definitions, Units and Dimensions for the parameters of a pneumatic circuit are shown in table I. Circuit element analogies for pneumatic, electrical and mechanical systems appear in table II.

CIRCUIT ELEMENTS

Resistance to the flow can be represented by an orifice in a line. If a unit difference of pressure between the two sides of an orifice causes a unit flow of gas of 1 cubic inch per second through the orifice, the orifice is one unit of resistance.

A pneumatic capacitor is a simple geometric volume and its capacity is the ratio of the charge in cubic inches of gas in the volume when measured at 1 psia to the pressure in psia in the volume. For perfect gases this ratio is the geometric volume of the capacitor in cubic inches.

303

Again we see the similarity to electrical parameters where electrical capacitance is the ratio of the charge on the capacitor to the voltage across the capacitor. In the mechanical system the spring rate of a spring is the force required on the spring for every inch of compression; this is the reciprocal of capacitance.

Leakage of molecules of gas through the walls of a closed volume is analogous to the leakage of electrical charge from a condenser or, in the mechanical system, to the creep in the metal of a spring subjected to compression over a long period of time.

The energy due to the flow or velocity of the molecules of gas is stored in an inductive field. An inductance element can be provided by a channel or tube in which gas flows. If it is desired to increase the flow by accelerating the volumetric movement of the gas at one cu.in./sec.^{2} a counter pressure of one psia must be overcome. Or conversely if the flow decreases or the gas decelerates at one cu.in./sec.^{2} there will be an induced pressure of one psia.

The kinetic energy expended in the movement of a gas in a pneumatic circuit is transferred to this inductive field. It is equal to $1/2\ Lu^2$. In the units we are using this is in lb. in. and is analogous to the stored magnetic field energy of an electrical inductance or in the mechanical analogy $1/2\ mv^2$. The equation is derived from the work done to push a charge of gas through an inductance. This work is the pressure times the charge.

Since total charge is flow times time or u dt, we have.

304

$$P = L \frac{du}{dt}$$

$$p \cdot u \, dt = L \frac{du}{dt} \cdot u \, dt$$

since $pu \, dt = p \, dx = dE_k$

$dE_k = p \, dx = Lu \, du$

$$E_k = \frac{1}{2} Lu^2$$

The potential energy of a pneumatic circuit is stored in the gas charge in the capacitance. It is analogous to the storage of charge on an electrical condenser or the storage of potential energy in a compressed mechanical spring. It is the work initially necessary to charge the capacitance to its pressure and is equal to one half of the product of the pressure and the charge. It is derived in the standard manner.

The energy units are lb. in. when pressure is in lbs per sq. in. and charge in cu. in.

ANALOGIES

Taking the parameters we have discussed we can build several interesting analogies between pneumatic, electrical and mechanical circuits. These are shown in table III.

PRESSURE DRIVING FORCES

Flow through these circuit elements will occur when a driving force is applied. Since pressure variations result from many varied causes, the resulting pressure versus time curves can be very complex. We will briefly consider a few simple examples. Pressure curves encountered in actual practice can in many instances be described by these forms, or superpositions of them.
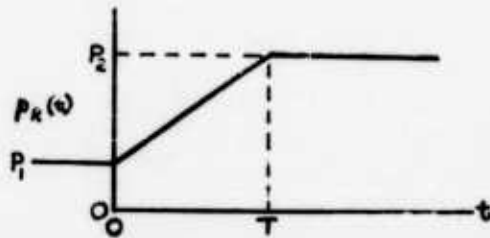
wheres $p_R(t)$ = Absolute Pressure of Disturbance

P_1 = Lower of Two Constant Pressure Levels

P_2 = Higher of Two Constant Pressure Levels

P = Pressure Difference between the Two Constant Pressure Levels = $P_2 - P_1$

t = Time measured from onset of Pressure Driving Force at $t = 0$.

$$p_R(t) = P_1 + Kt$$

$$K = \text{Slope} = \frac{(P_2 - P_1)}{T} = \frac{P}{T}$$

at $t < 0$ $p_R(t) = P_1$

This represents a system operating at a constant pressure, upon which a constant linear rate of change of pressure is imposed.

Example: filling of a tank under conditions of constant flow rate.
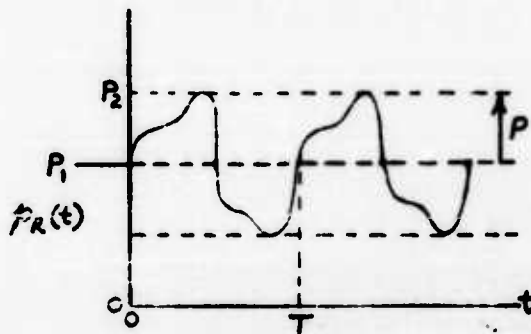
$$p_R(t) = P_1 + \sum_{n=1}^{n=\infty} C_n \sin nwt, \quad \text{a Fourier Series}$$

wheres $w = 2\pi f = \frac{2\pi}{T}$

for sinusoidals $p_R(t) = P_1 + P \sin wt$

at $t < 0$ $p_R(t) = P_1$

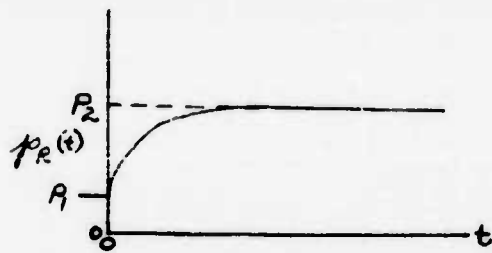A system normally at constant pressure (P_1) upon which an oscillating disturbing force acts. A sound wave would be such an example.

306

$$p_R(t) = P_1 + P(1 - e^{-\alpha t})$$

$$\text{at } t < 0 \quad p_R(t) = P_1$$

This represents the transient pressure curve for a system normally operating at a constant pressure (P_1) when it is connected to a system of higher pressure (P_2) through an orifice. A leak in a vacuum system would produce such a pressure characteristic; α is the characteristic of the system.

This last varying pressure curve is of particular interest because it represents a physical situation frequently encountered. When a disturbance from an equilibrium condition occurs, in this type of system, a new equilibrium is approached exponentially.

EXAMPLE

As an example of the effect of a disturbing force upon a pneumatic system take the second system shown in the table of analogies, table III.

It includes an enclosed geometric volume (representing capacitance) with an orifice (representing resistance). The system is, for the present, considered to be free of inductance.

The schematic and governing equations are shown below.
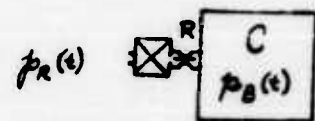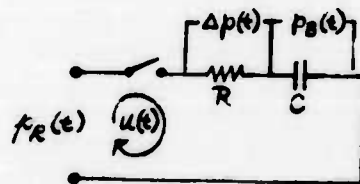
$P_R(t)$ = Applied Pressure.

$p_R(t)$ = Pressure in Enclosed Volume, C.

$\Delta p(t)$ = Difference in Pressure between p_R and p_B.

$u(t)$ = Instantaneous Volume Flow through Orifice.

R = Resistance of Orifice, a constant.

C = Capacitance of Volume, a constant

β = Circuit Characteristic = $\dfrac{1}{RC}$, a constant.

t = Time Measured from Onset of Pressure Disturbance at t = 0

Under steady-state conditions:

1) $p_R(0) = p_B(0)$ = a constant system pressure.

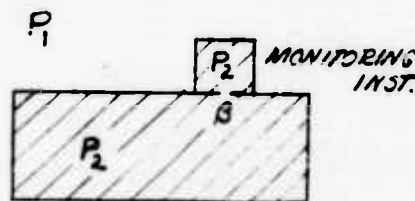$P_R(t)$, Time varying pressure is imposed upon the system.

Whatever the nature of the disturbing force:

2) $p_B(t) = p_B(o) + \dfrac{1}{c}\displaystyle\int_{o}^{t} u(t)\, dt$

3) $\Delta p(t) = p_R(t) - p_B(t) = R\, u(t)$

As a particular example of the use of this pneumatic system consider an instrument designed to monitor the rate-of-change of pressure in a closed vessel.
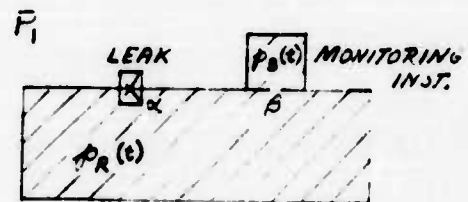
$t < 0$ $t > 0$

The constant pressure, P_2, in a sealed pressurized vessel is being monitored by this instrument. The parameters of the instrument must be of such magnitude as not to influence the effect being observed beyond acceptable limits. This vessel is immersed in another system of constant but lower pressure P_1 (this could be atmospheric pressure). Now an opening is made in the vessel resulting in an exponentially decreasing pressure, $p_R(t)$, dependent upon the resistance of the leak and the capacitance of the vessel.

$$p_R(t) = P_1 + Pe^{-\alpha t}$$

$$p = P_2 - P_1$$

α = Characteristic of the fault and capacity of the pressurized vessel, $\frac{1}{RC}$
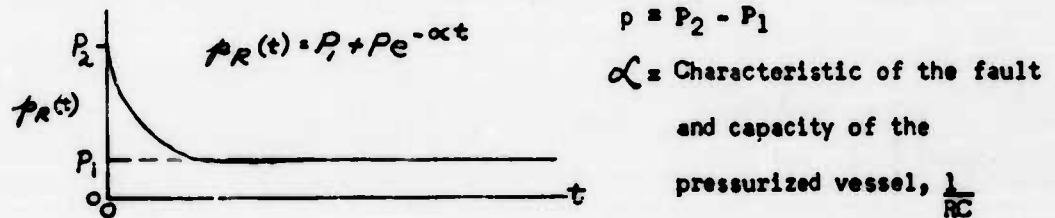
at $t = 0$ $p_R(0) = p_B(0) = P_2 = P_1 + P$

The monitoring system whose circuit characteristic is β, $(\frac{1}{RC})$, is responding to this exponentially declining pressure $p_R(t)$ in the following manner.
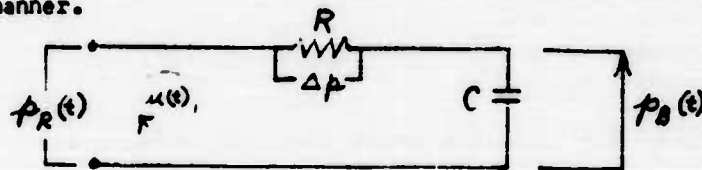
The circuit equation is:

$$R u(t) + p_B(t) = p_R(t)$$

with the solution:

$$R u(t) + \frac{1}{C} \int_0^t u(t)\, dt = (P_1 + P_e^{-\alpha t}) - p_B(0)$$

$$R u(t) + \frac{1}{C} \int_0^t u(t)\, dt = -p (1 - e^{-\alpha t})$$

$$u(t) = -\frac{1}{R} \frac{P}{1 - \beta/\alpha} (e^{-\beta t} - e^{-\alpha t})$$

Note that the true direction of flow is reversed from that shown in
the circuit diagram, therefore:

$$\Delta p(t) = p_B(t) - p_R(t)$$
$$\Delta p(t) = - R u(t)$$

The important result is the pressure difference $\Delta p(t)$ developed
between the monitoring instrument and the vessel, because it is this
quantity Δp that is used to actuate an indicating system.

Graphically, the results can be shown as follows:
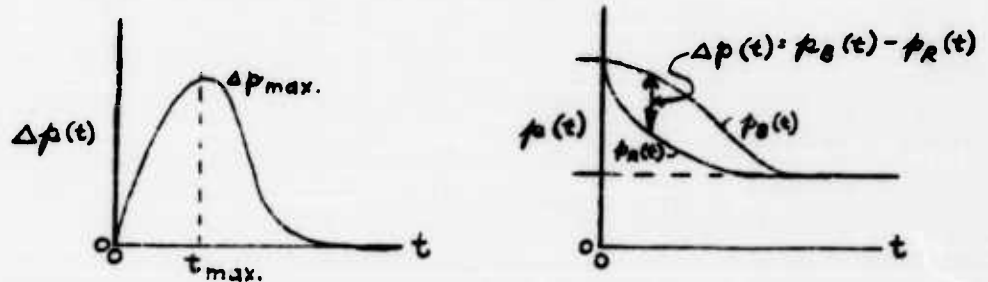
The value for maximum $\Delta p(t)$ can be related to the α and β
characteristics.

$$\Delta P_{max} = p \frac{\alpha}{\beta} e^{-\alpha t_{max}}; \text{ where } t_{max} = \frac{\ln \alpha/\beta}{(\alpha - \beta)}$$

The significance of these results can be discussed as follows:

The monitoring instrument (capacitance with orifice) can be built
to have a desired characteristic β. Then, for a given known P_1,
P_2 system actuation of the instrument can be achieved for a designated
α value. This suggests use for controlled flow at a desired rate as
well as use as an alarm to signal leaks.

The problem of measuring a fault in a continuous flow pipe would be
different from this example, α would be different, and would be

310

related to the characteristic impedance as in an electrical transmission line.

A fundamental, if obvious, point is that we are dealing with a transient response and using the temporary effect of the disturbance as our signal or driving force for the monitoring instrument.

The extension of the preceding analysis to a pneumatic system including inductance will obviously result in more complex equations because we must now consider Δp through the inductance as well as through the resistance of the orifice. Basically the approach is similar. The solutions of the analogous electrical RLC circuits can be found in standard texts on transient analysis.

311

One of the circumstances that led to the original rapid development of electrical circuit theory was the ability to experimentally substantiate theoretical equations. This was due to our ability to lump and thus orient and control the electrical circuit constants at low frequencies. It is much more difficult in pneumatic work to lump the circuit constants. Most circuit elements contain significant values for the three parameters: inductance, capacitance and resistance.

Advances in the meteorological field and new instrumentation in the rocket and missile field exemplify this progress. The work here at DIAMOND ORDNANCE FUZE LABORATORIES gives us an insight into the potential applications of fluid control. In terms of power alone, the movement of terrestrial and extra terrestrial gases is tremendous; direct control of pneumatic forces, without recourse to conversion processes is another new and challenging area.

BIBLIOGRAPHY

Dynamical Analogies, Olson, Harry F., Van Nostrand

Princeton, 1958

Stress-Strain-Time Relationships for Idealized Materials,

B. J. Lazan, University of Minnesota

Introductory Paper at June 1962 Symposium

of ASTM Material Sciences Division.

TABLE I

PNEUMATIC SYMBOLS, TERMS, UNITS, DEFINITIONS & DIMENSIONS
with corresponding analogies in the mechanical and electrical systems.

MECH-ANICAL SYMBOL	ELEC-TRICAL SYMBOL	PNEU-MATIC SYMBOL	TERM	UNIT	DEFINITIONS	DIMENSIONS
F,f(t)	E,e(t)	P,p(t)	Pressure	lbs/in²	Force exerted by a gas on a unit area.	$ml^{-1}t^{-2}$
t	t	t	Time	Sec.	Time.	t
S,s(t)	Q,q(t)	X,x(t)	Charge	In³	Volume* of gas in a specified geometric volume.	l^3
V,v(t)	I,i(t)	U,u(t)	Flow Rate	In³/sec.	Volume* of gas flowing in unit time.	l^3t^{-1}
R	R	R	Resistance	$\dfrac{lbs/in^2 \ sec.}{in^3}$	Resistance of an orifice through which a unit pressure difference will provide a unit flow of gas.	$ml^{-4}t^{-1}$
M	L	L	Inductance	$\dfrac{lbs/in^2 \ sec.^2}{in^3}$	Induced pressure produced when the flow of gas is decreased at a unit rate or the charge of gas is decelerated at a unit rate; or the counter pressure that must be overcome when the flow of gas is increased at a unit rate or the charge of gas is accelerated at a unit rate.	ml^{-4}
K	C	C	Capacitance	$\dfrac{in^3}{lbs/in^2}$	Volume* capacity of a specified geometric volume for every unit of pressure in the specified geometric volume.	$m^{-1}l^4t^2$
E_p	E_p	E_p	Potential Energy	lb.in.=1/2 $\dfrac{x^2}{C}$	Energy of the gas charge stored in a capacitor.	ml^2t^{-2}
E_k	E_k	E_k	Kinetic Energy	lb.in.=1/2 Lu^2	Energy due to the velocity of gas in a channel; the inductive fields energy.	ml^2t^{-2}

- 14 -

314

TABLE I (continued)

PNEUMATIC SYMBOLS, TERMS, UNITS, DEFINITIONS & DIMENSIONS

* Volume of Gas is defined as its equivalent volume at unit pressure.

NOTE: Volume is related to temperature. To calculate and compare Flows and Charges in circuits at different equilibrium temperatures it is required that they be converted to molal units using $PV = NRT$. For example: 70 cu in. at 68° F is equivalent to:

$$N = \frac{PV}{RT}$$

$$N = \frac{1 \times 70}{18,510 \times (460 + 68)}$$

$$N = 7.17 \times 10^{-6} \text{ lb mols}$$

where: P = unit pressure, psia

V = volume, cu. in.

T = Absolute Temperature, °Rankine

R = Gas Constant, 18,510 lb.in./lb.mols °K

N = Quantity of Gas, lb-mols.

315

TABLE II

ANALOGIES OF PNEUMATIC, ELECTRICAL & MECHANICAL CIRCUIT PARAMETERS
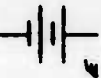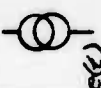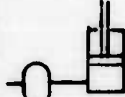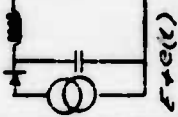
PNEUMATIC	ELECTRICAL	MECHANICAL
SWITCHES Valve opens or closes circuit.	Switch opens or closes circuit.	Actuator or release mechanism.
POWER SOURCES Open atmosphere or other large volume storage supplies steady state pressure. P	Battery supplies dc voltage.	Steady Force. F
Centrifugal compressor supplies steady state pressure. P	dc Generator supplies dc voltage.	Steady Force. F
Piston Cylinder supplies alternating pressure supply. $p(t)$	a.c. Generator supplies ac voltage. $e(t)$	Alternating Force supplied by a reciprocating engine. $f(t)$
Piston pump with tank supplies dc pressure with a small alternating component. $P+p(t)$	a.c. Generator with a rectifier supplies dc voltge with a small alternating component. $E+e(t)$	Force from reciprocating engine rectified by a flywheel. Output is steady shaft rotation with a small alternating component. $F+f(t)$
CHARGE $X, x(t)$ Amount of stored gas molecules.	$Q, q(t)$ Amount of stored electrons.	$S, s(t)$ Amount of displacement from equilibrium.

316

- 16 -

TABLE II   (Continued)

ANALOGIES OF PNEUMATIC, ELECTRICAL & MECHANICAL CIRCUIT PARAMETERS
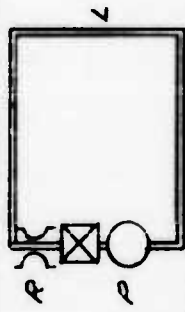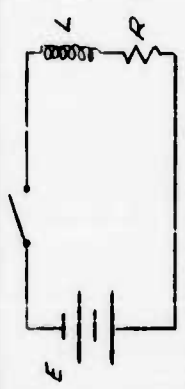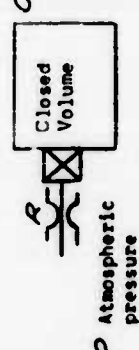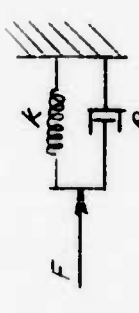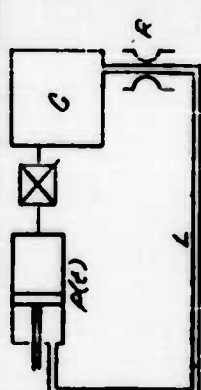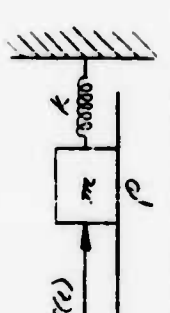
PNEUMATIC	ELECTRICAL	MECHANICAL
FLOW RATES $U, u(t)$ Rate of flow of molecules	$I, i(t)$ Rate of flow of electrons.	$V, v(t)$ Rate of movement
CIRCUIT ELEMENTS Orifice offers Resistance to flow of gas. All circuit elements have some resistance. R	Electrical Resistor offers resistance to electrical current. All circuit elements have some resistance. R	Friction offers resistance to movement of the parts of the system. All circuit elements have some friction. ρ
A capacitance of specified geometric volume capable of holding a charge of gas. All circuit elements are capable of holding some charge although insubstantial. C	A capacitor capable of holding a charge of electrons. All circuit elements are capable of holding some charge although insubstantial. C	A spring capable of being displaced from its equilibrium position. All materials have some flexibility although insubstantial. 1/k
A choke through which a flow of gas is directed. All circuit elements are capable of directing some flow of gas. L	A coil about which a magnetic field is formed. All circuit elements are capable of building some magnetic field. L	A mass capable of movement. All circuit elements have mass. m

- 17 -

317

TABLE III

ANALOGIES OF PNEUMATIC, ELECTRICAL & MECHANICAL CIRCUITS

GAIN ANALYSIS OF THE PROPORTIONAL FLUID AMPLIFIER

by

S. J. Peperone

Silas Katz

John M. Goto

of

Diamond Ordnance Fuze Laboratories

319
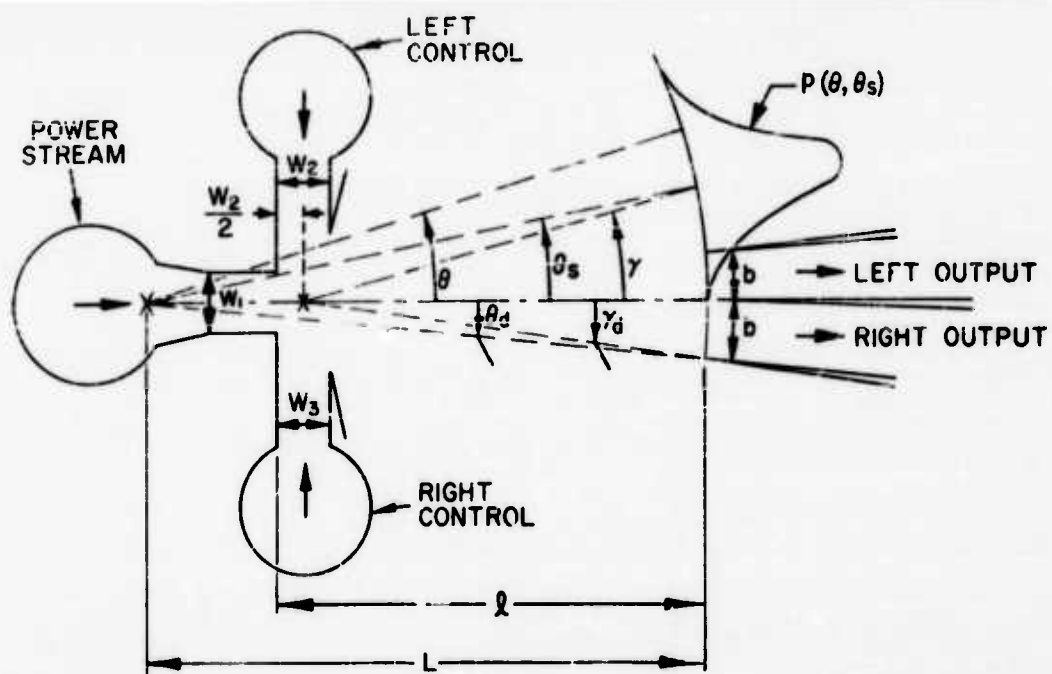
Figure 1. Proportional fluid amplifier -- basic design.
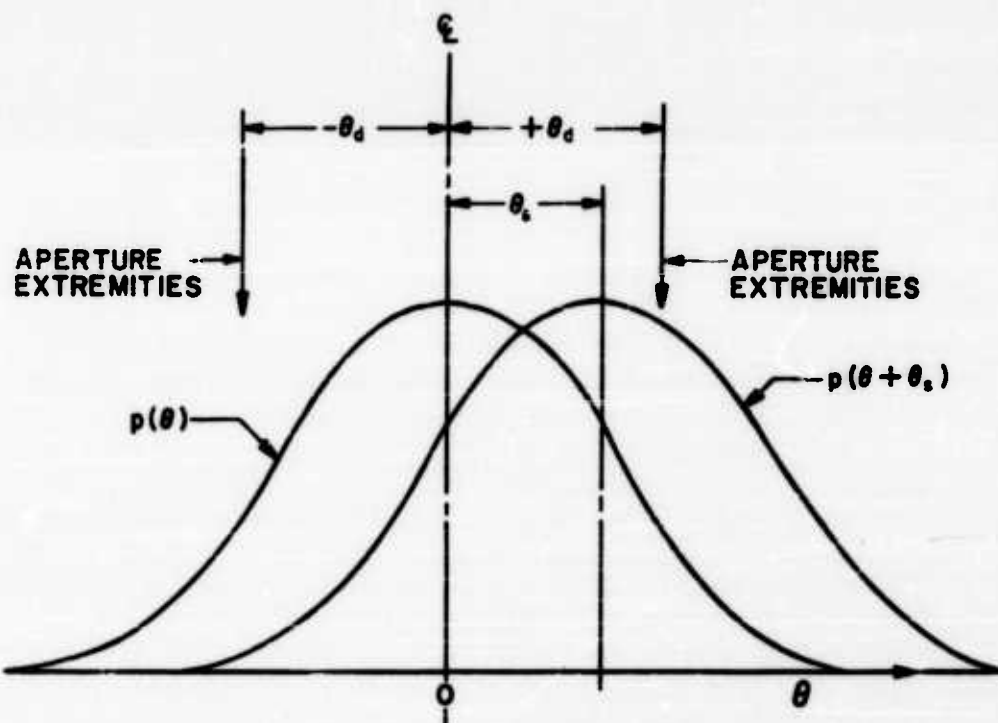
Figure 2. Power-jet pressure profile at entrance to output apertures.

320

1. INTRODUCTION

To achieve fluid amplification without mechanical moving parts, a power nozzle is used to transform the energy initially stored in static pressure into dynamic pressure. This power stream of high energy fluid passes through an interaction region and is partitioned into two output apertures as shown in fig. 1. Control streams placed at each side and usually normal to the power stream determine the direction of flow of the power stream. Variations in the net thrust of the control streams change the deflection of the power stream, and thereby change the division of fluid between the two output apertures (fig. 2).

The gain of a proportional amplifier is defined as the ratio of the change in the variable of interest at the output to the change of this variable at the input - that is, the ratio of output to input signal. A theoretical analysis that follows was made of the gains in pressure, volume flow, and power; predictions were compared with experimental data. An incompressible fluid was assumed in this analysis and the measurements were made using air at less than 5 psig.

2. CHARACTERISTICS OF JET STREAMS

The operation of a proportioning fluid amplifier is dependent upon controlling and collecting the fluid stream issuing from a nozzle. To understand fluid amplification, therefore, some knowledge of jet-stream characteristics is necessary.

A fluid stream discharging into a fluid initially at rest undergoes both lateral diffusion and deceleration (ref. 2) while the surrounding fluid is brought into motion. The reason for this is that, at the exit of the
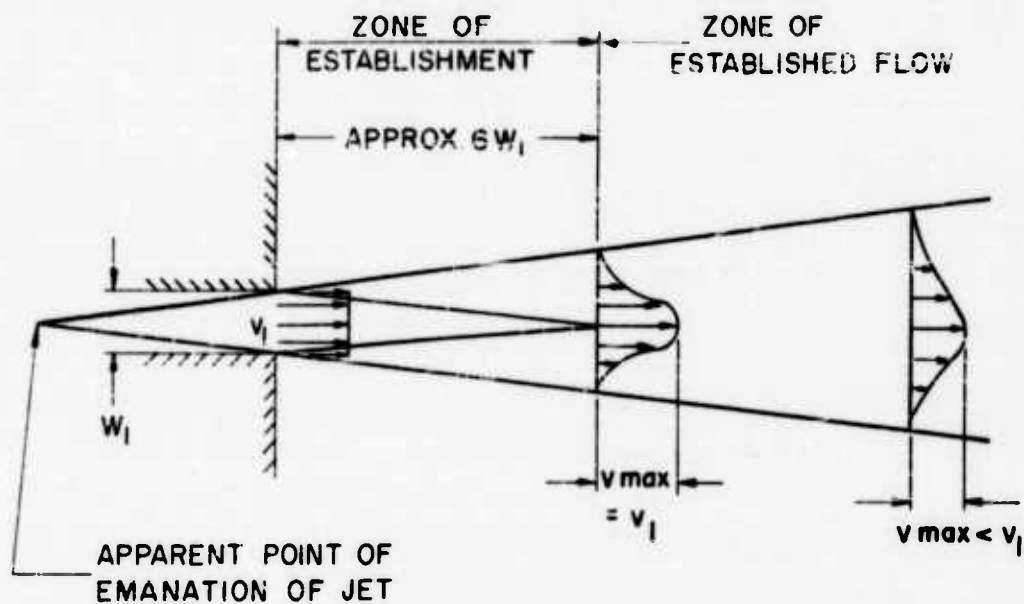
Figure 3. Schematic diagram of jet diffusion.
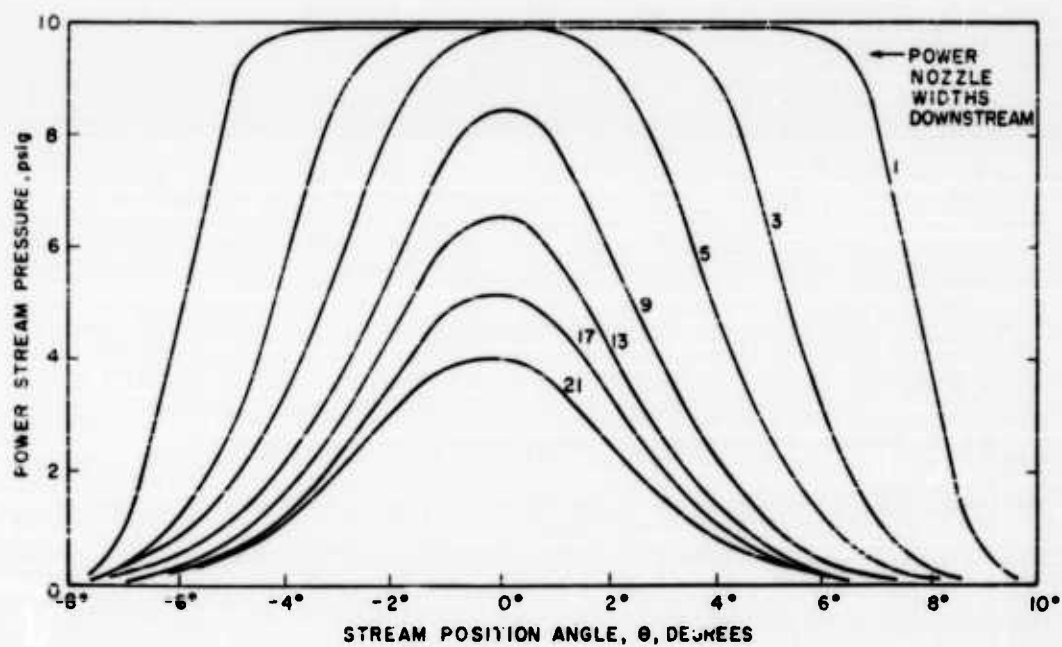
Figure 4. Experimental profiles.

322

nozzle, a high velocity gradient exists between the stream and the surrounding fluid. Eddies generated in this region produce a lateral mixing process resulting in the formation of two distinct regimes (fig. 3), the zone of establishment and the zone of established flow. Over an extremely wide range of Reynolds number (ref. 2), the stream characteristics remain essentially unchanged. The zone of establishment ends about 6 nozzle widths downstream from the nozzle exit for the conditions of interest here. In this zone the mixing process has not penetrated to the center line of the jet stream, and the conditions at the center line are still the same as at the nozzle exit. At approximately 6 nozzle widths the fluid enters the zone of established flow. In this region the velocity throughout the stream decreases as the distance from the nozzle exit increases.

The fluid in the amplifier under consideration differs from the stream described above, because it is confined between parallel plates. In the unconfined stream, only the tangential shear within the mixing region decelerates the jet stream, and since this process is completely internal, momentum flux is conserved. In the confined stream, the top and bottom plates exert a shearing force on the stream. This process is external to the stream, and momentum flux is not conserved. Consequently, the zone of established flow appears to emanate from a point on the center line farther upstream from the nozzle than the apparent point of emanation of an unconfined stream (ref. 3).

Dynamic pressure profiles (taken at DOFL) of a two-dimensional (2-D) stream confined between parallel plates are shown in fig. 4. The ratio of the distance between plates to the nozzle width (aspect ratio) was 8.

Integration of these profiles confirms the fact that momentum flux is not conserved, but decreases with increasing distance from the nozzle exit. In this case, the stream appears to emanate from a point 4 nozzle widths upstream from the exit. As the aspect ratio is lowered this distance is expected to increase.

The maximum pressure of these experimental profiles occurs on the center line of the stream. These data show that the maximum pressure 7 nozzle widths downstream of the exit dropped to 95 per cent of the exit pressure; at 11 nozzle widths, to 68 per cent of the exit pressure. The shape of these profiles is similar to those found in ref. 2 for 2-D jets without parallel plates.

It is to be noted that the experimental profiles were obtained in the absence of output apertures. Experimental evidence indicates that the static pressure throughout the zones of motion is constant if no obstructions are present. The stagnation pressure at the edges of the apertures affects the profiles; however, if the edges are sharp, this effect is believed to be small.

3. ANALYSIS OF POWER-JET DEFLECTION

The following analysis of the power-jet deflection by means of the control stream is based on three assumptions:

      (1) The fluid is incompressible and frictionless.

      (2) The flow is steady.

      (3) The impingement of the control stream on the power stream may be viewed as a 2-D potential motion problem where the power jet is considered as a nondeformable wall. This means that there is no mixing between the control and power streams.

324
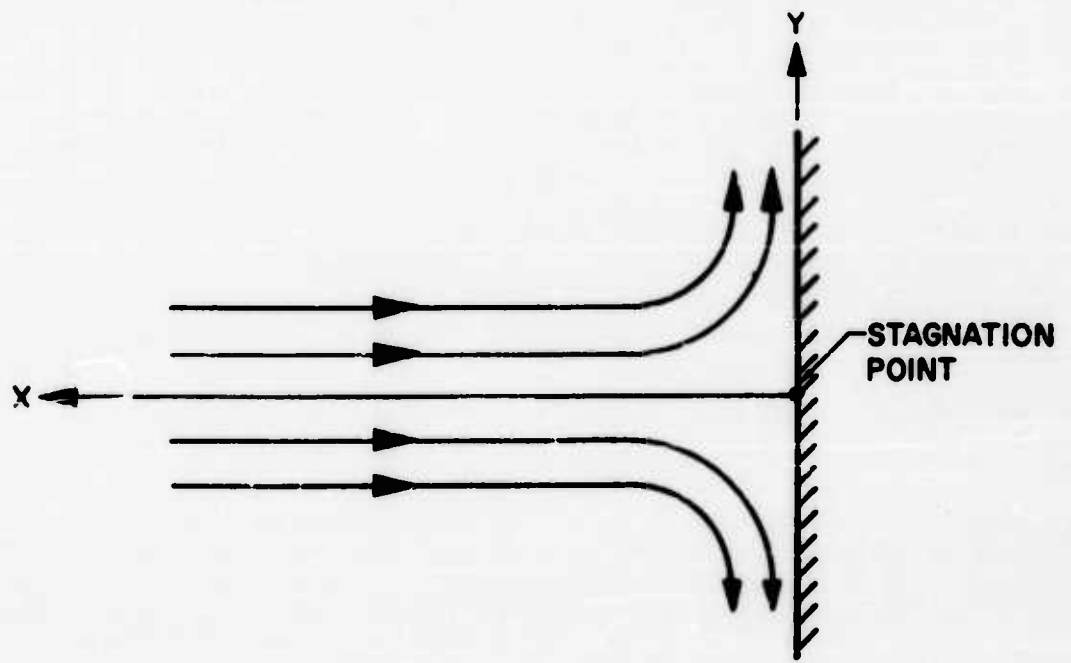
Figure 5(a). Jet impinging on a flat wall.
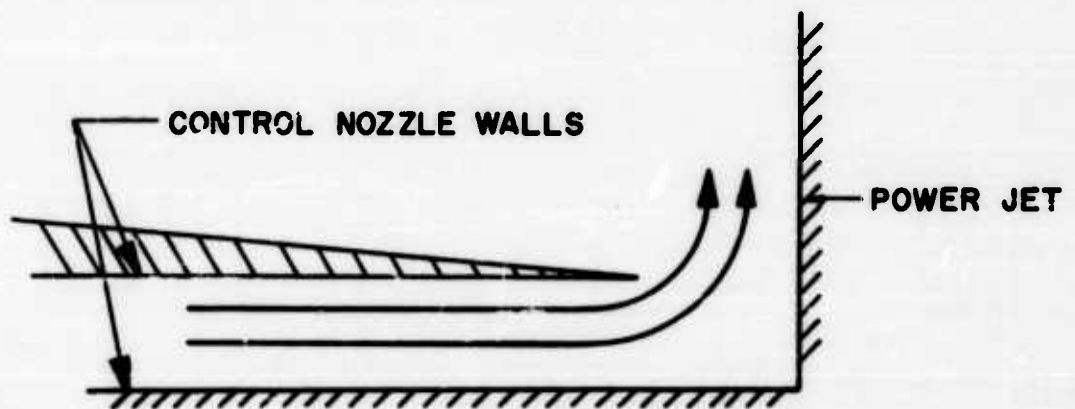
Figure 5(b). Fluid amplifier interaction region.

325

The thrust exerted by the control stream on the power jet is computed from Newton's second law, which for a frictionless fluid in steady motion may be written as

$$\Sigma \vec{F} = \oiint_{surface} \frac{\rho}{g_c} (\vec{v} \cdot d\vec{A}) \vec{v} + \oiint_{surface} p_s \, d\vec{A} \qquad (1)$$

where ρ and $\vec{v}$ are the density and velocity of the control stream, $d\vec{A}$ is incremental area, p_s is static pressure, and g_c is the gravitational conversion factor. This equation simply states that the sum of the external forces acting on the system is equal to the rate of change of momentum of the bounded mass system.

Assuming that the problem of determining the velocity $\vec{v}$ is similar to the classical problem of the impingement of an incompressible, frictionless, steady stream on a flat wall, the result is given by the curves of fig. 5a.

The solution shows (ref. 4) that the streamlines are hyperbolas whose asymptotes are the x and y axes. The control stream, therefore, follows along the side of the power jet with no bounce. If the configuration in fig. 5a is modified by inserting walls at the middle and edge filaments, and if the power jet replaces the wall, the streamlines remain essentially unchanged (fig. 5b).

The geometry of the classifcal problem now conforms to the interaction region of the fluid amplifier and $\vec{v}$ is determined. The desired relation between stream thrust and deflection angle is derived in App. A.

4. THEORETICAL DEVELOPMENT OF GAIN

4.1 Flow Gain

The flow gain G_Q of a proportional amplifier is defined as the ratio of the change in the output volumetric flow difference ΔQ_o to the change in

326

input volumetric flow difference, ΔQ_i so that

$$G_Q = \frac{\Delta Q_o}{\Delta Q_i} \qquad (2)$$

or

$$G_Q \equiv \frac{\Delta(Q_L - Q_R)}{\Delta(Q_2 - Q_3)} \qquad (2a)$$

where the subscripts L and R refer to the left- and right-output apertures, and 2 and 3 refer to the left- and right-control nozzles, respectively.

The output-flow difference Q_o is a function of the pressure profile $p(\theta, Q_s)$, the angle subtended by the apertures θ_d and the downstream distance of the apertures ℓ where θ is an arbitrary angle and θ_s is the stream deflection angle:

$$Q_o = Q_o\,(\theta, \theta_s, \theta_d, \ell) \qquad (3)$$

The total differential of equation (3) is

$$dQ_o = \frac{\partial Q_o}{\partial \theta}\,d\theta + \frac{\partial Q_o}{\partial Q_s}\,d\theta_s + \frac{\partial Q_o}{\partial \theta_d}\,d\theta_d + \frac{\partial Q_o}{\partial \ell}\,d\ell \qquad (4)$$

For small increments, the flow gain may be written as

$$G_Q = \frac{dQ_o}{dQ_i} = \frac{\partial Q_o}{\partial \theta}\frac{d\theta}{dQ_i} + \frac{\partial Q_o}{\partial Q_s}\frac{d\theta_s}{dQ_i} + \frac{\partial Q_o}{\partial \theta_d}\frac{d\theta_d}{dQ_i} + \frac{\partial Q_o}{\partial \ell}\frac{d\ell}{dQ_i} \qquad (5)$$

Assuming that the pressure profile does not change for small control inputs, $\frac{d\theta}{dQ_i} = 0$; and since θ_d and ℓ are independent of Q_i, the gain expression reduces to

$$G_Q = \frac{\partial Q_o}{\partial \theta_s}\,\frac{d\theta_s}{dQ_i} \qquad (6)$$

327

From the definition of flow rate, the output flow difference may be written as

$$Q_o = A_L v_{av\,L} - A_R v_{av\,R} \tag{7}$$

where A_L, for example, is the area of the left aperture and v_{av} is the average velocity. For an incompressible fluid, the total pressure at the entrances and exists of the apertures is the sum of the static and dynamic pressure; moreover, the static pressure of the fluid stream approaching nonloaded apertures is ambient, so that the output volume flow rate may be computed from $p = \dfrac{\rho}{2g_c} v^2$. In terms of the pressure profile $p(\theta + \theta_s, \ell)$ the average velocity is

$$v_{av} = \sqrt{\frac{2g_c}{\rho}} \; \frac{1}{\theta_d} \int_{-\theta_d}^{\theta_d} p^{1/2}(\theta + \theta_s, \ell) \, d\theta \tag{7a}$$

and the output volume flow rate is

$$Q_o = \frac{1}{\theta_d} \sqrt{\frac{2g_c}{\rho}} \left[A_L \int_0^{\theta_d} p^{1/2}(\theta + \theta_s, \ell) \, d\theta - A_R \int_{-\theta_d}^{0} p^{1/2}(\theta + \theta_s, \ell) \, d\theta \right] \tag{8}$$

The relation between stream deflection γ and input-flow difference is derived (App. A) by applying the momentum equation to the interaction region. If the left and right control areas are equal, the relation is approximately

328

$$\tan \gamma = \frac{\rho (1+\alpha_2)(1+\sin \phi)(Q_i^2 + 2 Q_i Q_3)}{2 g_c \alpha_2 A_1 A_2 (1+\alpha_1) p_1} \tag{9}$$

where α is the ratio of dynamic to total pressure, ϕ is the difference in deflection between power stream and control stream, and the subscript 1 refers to the power nozzle.

It should be noted that the angles θ_s and γ are measured from different vertices. Experiments have shown that the power stream appears to radiate from a source approximately 4 nozzle widths upstream of the power-jet exit (for an aspect ratio of 8), but it is deflected about the point of intersection of the power- and control-nozzle center lines.

From fig. 1, the geometrical relation between angles θ_s and γ is

$$\tan \theta_s = \frac{\ell - \frac{w_2}{2}}{L} \tan \gamma \tag{10}$$

where L is the downstream distance from the point of apparent emanation to the apertures and w_2 is the control-nozzle width.

If the areas of the left and right apertures are equal, the theoretical flow gain obtained by combining eq. (6), (8), (9), (10) and normalizing the pressure is

329

$$G_Q = \frac{K Q_2 A_1 A_d \, p_m^{1/2}(\ell)}{Q_1 A_2^2 \, \theta_d \, p_1^{1/2}} \left[\frac{p^{1/2}(\theta_d + \theta_s, \ell)}{p_m^{1/2}(\ell)} + \frac{p^{1/2}(-\theta_d + \theta_s, \ell)}{p_m^{1/2}(\ell)} - \frac{2 \, p^{1/2}(\theta_s, \ell)}{p_m^{1/2}(\ell)} \right] \quad (11)$$

where $p_m(\ell)$ refers to the maximum pressure of the profile,

$$K = \frac{2 A_2 \left(1 - \frac{w_3}{2}\right)\left(1 + \alpha_3\right)\left(1 + \sin\phi\right)\cos^2\theta_2}{A_1 L \, \alpha_2 \left(1 + \alpha_1\right)}$$

and

$$Q_1 \cong A_1 \sqrt{\frac{2 a_o \, p_1}{\rho}}$$

and where it must be kept in mind that $\quad \dfrac{\partial p(\theta + \theta_s)}{\partial \theta_s} = \dfrac{\partial p(\theta + \theta_s)}{\partial \theta}$

4.2 Pressure Gain

The pressure gain of a proportional fluid amplifier is defined as the ratio of change in total output pressure difference, to the change in total input pressure difference. This may be written as

$$G_p \equiv \frac{\Delta p_o}{\Delta p_i} \quad (12)$$

330

or

$$G_p \equiv \frac{\Delta\left(p_L - p_R\right)}{\Delta\left(p_2 - p_3\right)} \tag{12a}$$

The output pressure difference p_o is a function of the pressure profile, $p(\theta, \theta_s)$, the width of the aperture θ_d, and the downstream distance of the apertures ℓ ; that is

$$p_o = p_o\left(\theta, \theta_s, \theta_d, \ell\right) \tag{13}$$

The total differential of equation (13) is

$$dp_o = \frac{\partial p_o}{\partial \theta}d\theta + \frac{\partial p_o}{\partial \theta_s}d\theta_s + \frac{\partial p_o}{\partial \theta_d}d\theta_d + \frac{\partial p_o}{\partial \ell}d\ell \tag{14}$$

For small increments, the pressure gain may now be written

as

$$G_p = \frac{dp_o}{dp_i} = \frac{\partial p_o}{\partial \theta}\frac{d\theta}{dp_i} + \frac{\partial p_o}{\partial \theta_s}\frac{d\theta_s}{dp_i} + \frac{\partial p_o}{\partial \theta_d}\frac{d\theta_d}{dp_i} + \frac{\partial p_o}{\partial \ell}\frac{d\ell}{dp_i} \tag{15}$$

331

Assuming that the pressure profile does not change for small control inputs, and since θ_d and ℓ are independent of p_i, the gain expression reduces to

$$G_p = \frac{\partial p_o}{\partial \theta_s} \frac{d\theta_s}{dp_i} \tag{16}$$

From the assumptions, the output pressure is in the form of dynamic pressure; therefore,

$$p_o = \frac{\rho}{2g_c} V_{avL}^2 - \frac{\rho}{2g_c} V_{avR}^2 \tag{17}$$

By using the expression for average velocity, the output pressure difference is

$$p_o = \left[\frac{1}{\theta_d} \int_0^{\theta_d} p^{1/2}(\theta + \theta_s, \ell)\, d\theta\right]^2 - \left[\frac{1}{\theta_d} \int_{-\theta_d}^{0} p^{1/2}(\theta + \theta_s, \ell)\, d\theta\right]^2 \tag{18}$$

332

The relation between stream deflection and input pressure difference is derived in App. A. If the left and right control areas are equal, the relation is approximately

$$\tan \gamma = \frac{A_2 (1+\alpha_2)(1+\sin\phi)\, \varphi_i}{A_1 (1+\alpha_1)\, \varphi_1} \tag{19}$$

From the geometrical relation in equation (10), equation (19) may be written as

$$\tan \theta_s = \frac{A_2 \left(\ell - \frac{\omega_c}{2}\right)(1+\alpha_2)(1+\sin\phi)\, \varphi_i}{A_1 L (1+\alpha_1)\, \varphi_1} \tag{20}$$

A theoretical expression for pressure gain is obtained by combining equations (16), (18), (20), and normalizing the pressure so that

$$G_p = \frac{\alpha_2 K \varphi_m(\ell)}{\theta_d \varphi_1} \left\{ \left[\frac{\varphi^{1/2}(\theta_d + \theta_s, \ell)}{\varphi_m^{1/2}(\ell)} - \frac{\varphi^{1/2}(\theta_s, \ell)}{\varphi_m^{1/2}(\ell)} \right] \left[\frac{1}{\theta_d} \int_0^{\theta_d} \frac{\varphi^{1/2}(\theta + \theta_s, \ell)}{\varphi_m^{1/2}(\ell)} d\theta \right] - \left[\frac{\varphi^{1/2}(\theta_s, \ell)}{\varphi_m^{1/2}(\ell)} - \frac{\varphi^{1/2}(-\theta_d + \theta_s, \ell)}{\varphi_m^{1/2}(\ell)} \right] \left[\frac{1}{\theta_d} \int_{-\theta_d}^{0} \frac{\varphi^{1/2}(\theta + \theta_s, \ell)}{\varphi_m^{1/2}(\ell)} d\theta \right] \right\} \tag{21}$$

333

where, as before,

$$K = \frac{2A_2 \left(\ell - \frac{\omega_2}{2}\right)(1-\alpha_2)(1-\sin\phi)\cos^2\theta_2}{A_1 L \alpha_2 (1+\alpha_1)}$$

4.3 Power Gain

The power gain may be defined in terms of pressure gain and flow gain, so that

$$G_{pQ} \equiv \left|\frac{\Delta p_o \, \Delta Q_o}{\Delta p_i \, \Delta Q_i}\right| \tag{22}$$

or

$$G_{pQ} = \left| G_p \, G_Q \right| \tag{22a}$$

The theoretical expression for power gain is, therefore, obtained by multiplying equation (11) by equation (21).

334

5. APPLICATION OF THEORY

5.1 Predicting the Gain of a Fluid Amplifier

The theoretical expressions for flow and pressure gain are given in equations (11) and (21). Gains are calculated from these equations by specifying:

(a) The shape of the pressure profile at the entrance to the apertures;

(b) The physical dimensions of the amplifier;

(c) The ratio of dynamic pressure to total pressure for control (α_2) and power (α_1) streams; and

(d) The turning angle of the control stream ϕ.

Experimental (fig. 4) and theoretical analyses (ref. 2) of 2-D submerged jets show that the pressure profile is approximately Gaussian in the region of established flow. This may be expressed mathematically as

$$p(\theta) \approx p_m \ exp\left[\frac{-(\theta-\theta_1)^2}{2\sigma^2}\right] \qquad (23)$$

At power-stream pressures of 5 psig, and an aspect ratio of 8:1, these data gave a peak pressure p_m of 3.5 psig and a standard deviation σ of approximately 2.40 deg at 11 nozzle widths downstream. Since the value of σ depends to some extent on aspect ratio, the dependence of pressure and flow gains on σ is also considered.

The ratios α_1 and α_2 were determined experimentally as $\alpha_1 = 0.84$ and $\alpha_2 = 0.44$ at the operating pressures of the amplifier. These operating

335

pressures were chosen below 5 psig so that the assumption of incompressibility would be valid.

The turning angle ϕ has been taken as 8 deg, since the power stream spreads at approximately this angle in the interaction region. The direction of flow of the control stream as it leaves the interaction region therefore differs from the axis of the power stream by this angle.

When these σ values are employed in equations (11), (21), and (22), the theoretical flow, pressure, and power gains are determined. Fig. 6, 7, and 8 show the theoretical gains plotted against deflection angle for a Gaussian profile.

5.2 Optimization of Gain

Consideration will now be given to the effect of varying certain physical dimensions of the amplifier to optimize the gain using measured pressure profiles.

It should be noted that the pressure gain given by equation (21) is not directly proportional to the ratio of control area A_2 and power area A_1 alone, since the α's are also functions of the areas. This applies also to the ratio of flow rates Q_2/Q_1 in the flow gain expression (eq. 11). Since the functional relation between the areas (or flow rates) and the α's is not analyzed here, the effects of varying the area ratio or flow rate control to power ratio is not considered.

5.2.1 Constant-Width Apertures—Varying Distance Downstream

As the downstream distance of constant-width apertures is increased, each aperture accepts a smaller percentage of the total stream.

336
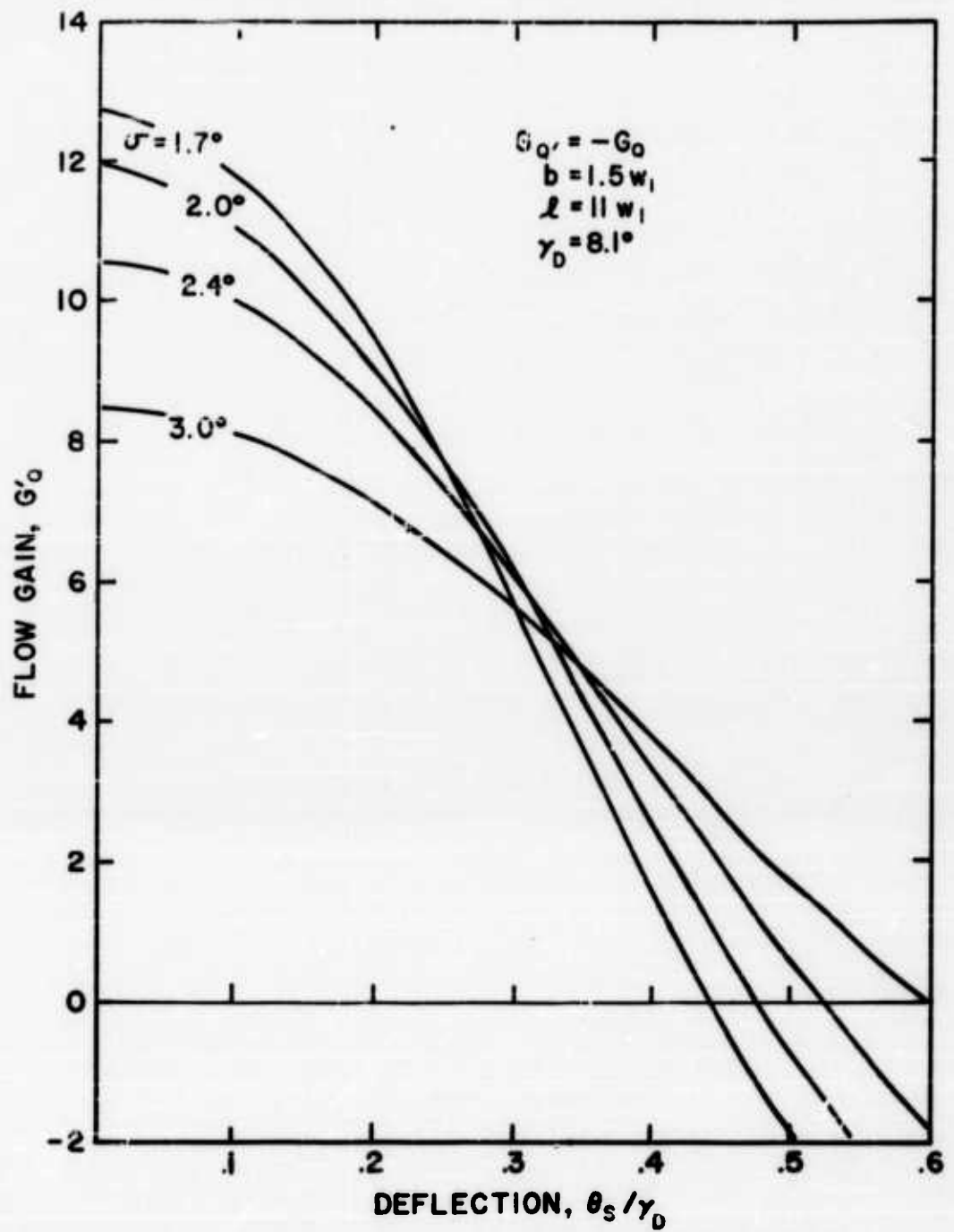
Figure 6. Theoretical flow gain versus stream deflection
with stream width as a parameter.
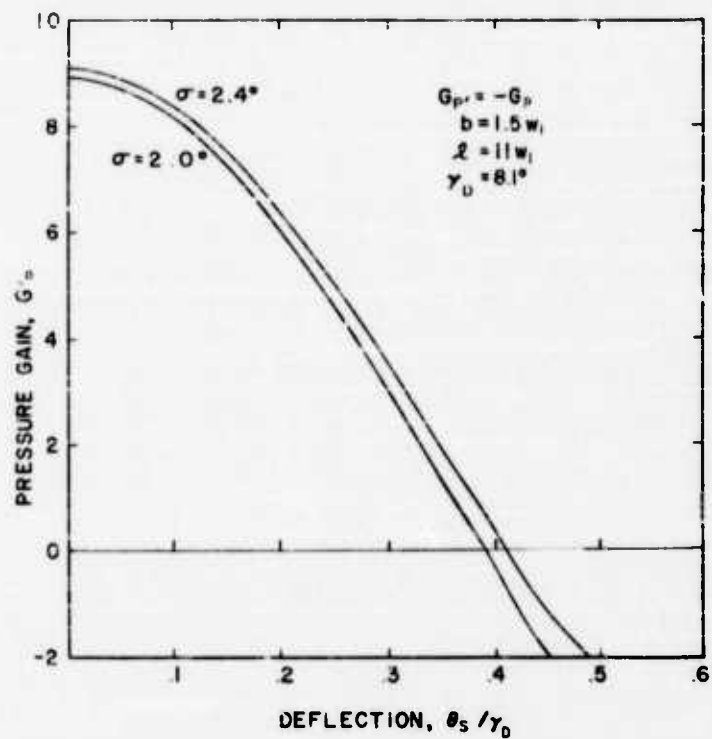
Figure 7. Theoretical pressure gain versus stream deflection
with stream width as a parameter.
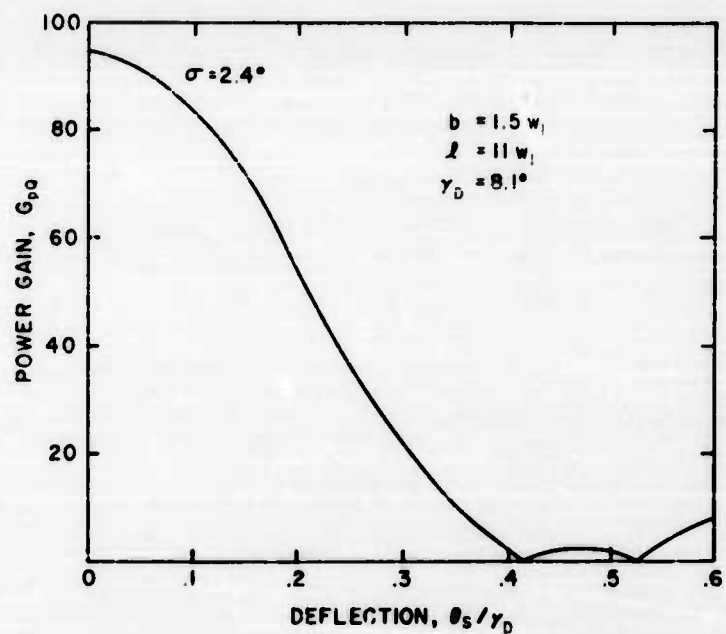
Figure 8. Theoretical power gain versus stream deflection with
stream width as a parameter.

338

The peak pressure is also decreasing with increasing downstream distance. Using experimental profile data taken at DOFL, these quantities may be related to downstream distance. Fig. 9 is a plot of theoretical pressure, flow, and power gains versus downstream distance for the case of a constant width aperture equal to 1.5 power nozzle widths and a stream deflection $\theta_s = 0$. The theoretical gains maximize at 11 nozzle widths downstream.

5.2.2 Constant-Deviation Apertures - Varying Distance Downstream

If the apertures are constrained to subtend a fixed angle, the aperture width must increase with increasing downstream distance. Fig. 10 shows the relation between theoretical pressure, flow, and power gains, and downstream distance for a fixed aperture angle of 2.50 σ at a stream deflection of $\theta_s = 0$. The pressure gain decreases monotonically in the region of established flow, whereas the flow gain increases monotonically. The power gain, however, exhibits a maximum at about 11 nozzle widths downstream.

5.2.3 Varying Width Apertures-Fixed Downstream Distance

Varying the width of apertures at a fixed downstream position varies their position with respect to the pressure profile. Fig. 11 is a plot of theoretical pressure, flow, and power gains versus the equivalent σ width at 11 nozzle widths downstream and $\theta_s = 0$. The flow gain increases monotonically until the apertures increase to the width of the power stream; thereafter, increasing the aperture width does not change the gain. The pressure gain is a maximum at an aperture width of 1.7 σ, and the power gain is a maximum at approximately 2.5 σ.

339
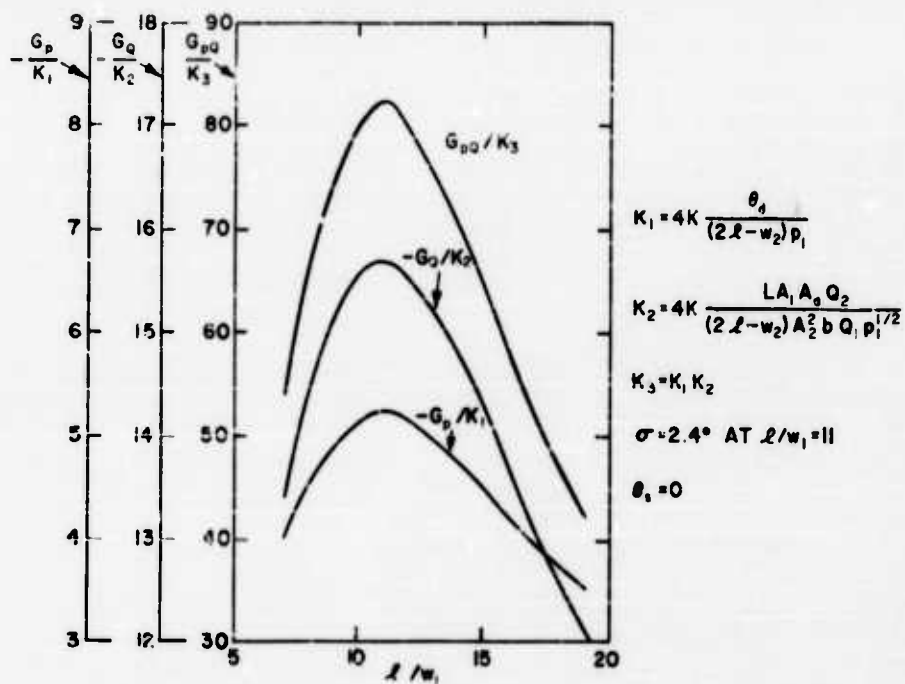
Figure 9. Theoretical gain versus downstream distance constant-width aperature ($\Theta = 0$).
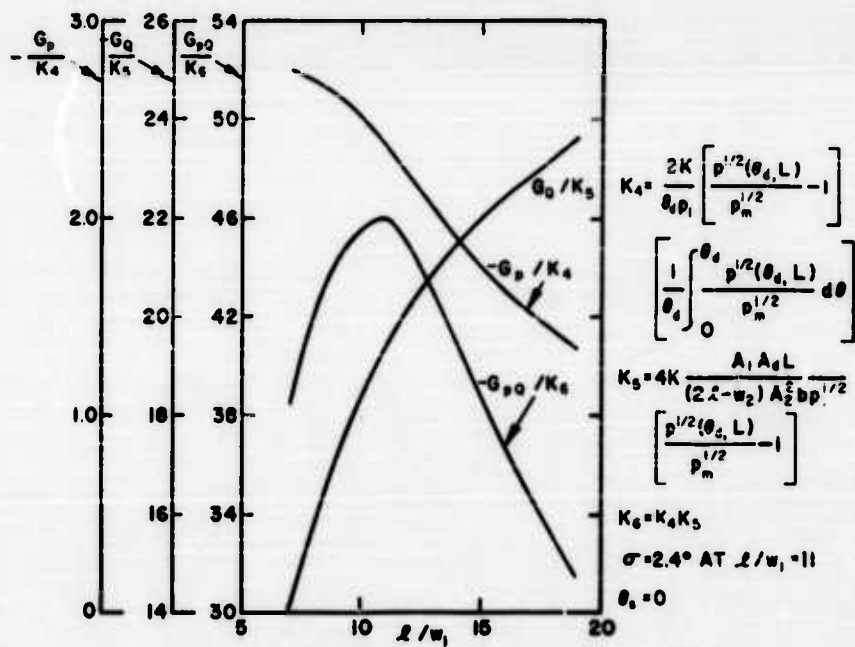
Figure 10. Theoretical gain versus downstream distance constant-deviation apertures ($\Theta = 0$).

340

$K_7 = 2K \dfrac{p_m}{p_1}$

$K_8 = \dfrac{2A_1 A_d L Q_2 p_m^{1/2}}{A_2^2 b Q_1 p_1^{1/2}} K$

$K_9 = K_7 K_R$

$\theta_S = 0$

$\ell/w_1 = 11$

W
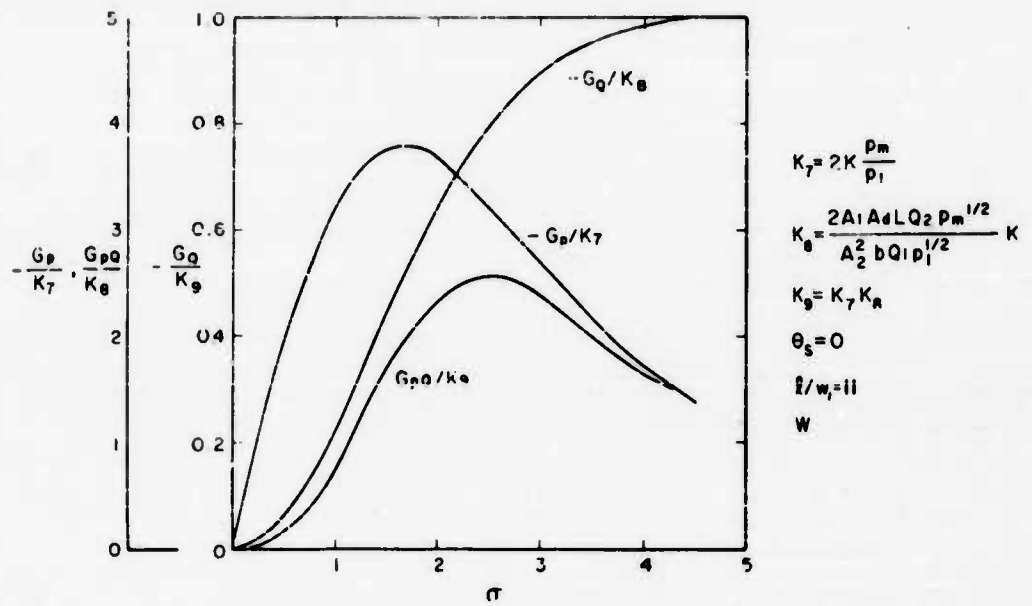
Figure 11. Theoretical gain versus aperture width fixed distance downstream ($\Theta = 0$).
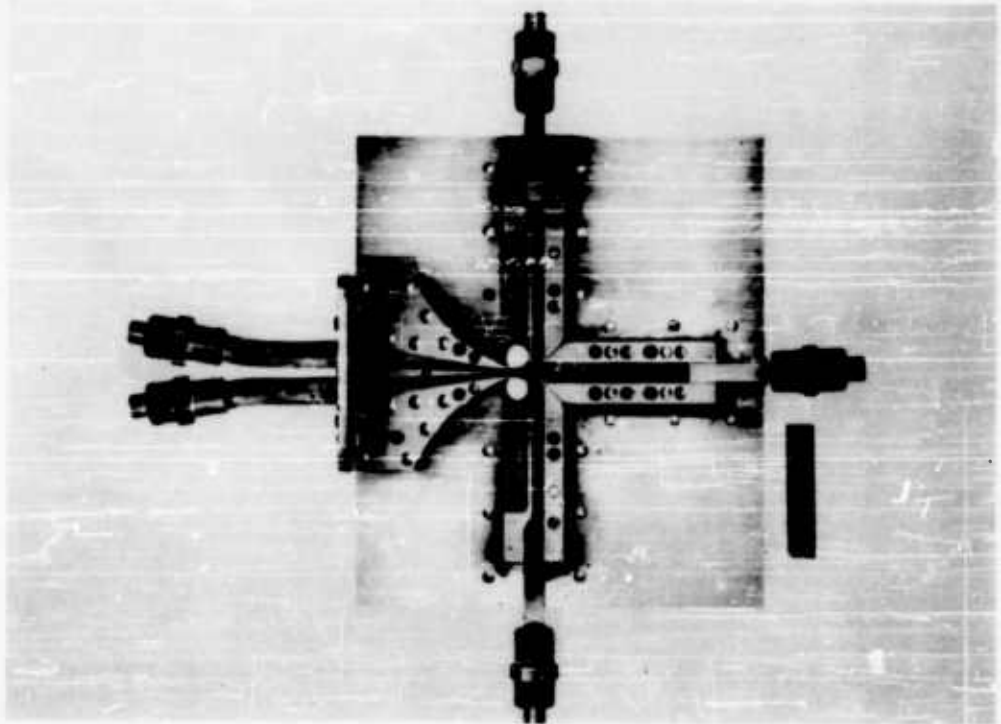
Figure 12. Proportional amplifier.

341

6. TEST SETUP AND PROCEDURE

To check the theoretical analysis, tests were performed on the amplifier shown in fig. 12. This amplifier has the following dimensional features:

(a) The nozzle widths of power and control streams are approximately equal.

(b) The entrance width b of each output aperture is 1.5 power nozzle widths.

(c) The entrance of the apertures is fixed at 11 power nozzle widths from the exit of the power nozzle.

(d) The ratio of nozzle height to power nozzle width (aspect ratio) is 8.

A functional diagram (fig. 13) shows the test arrangement used with this amplifier. The test setup consists of a regulated air supply to each nozzle and the means of measuring input and output conditions. The flow rate into the nozzles and out of the apertures is measured with rotameters that have a full-scale accuracy within 2 per cent. The pressure in the control-input tanks is measured with manometers.

During a test, the power stream settling tank was maintained at a constant pressure of 3 or 5 psig. One of the control tanks was also kept at a constant pressure, which is 0 to 20 per cent of the power-stream pressure. Small changes were then made in the other control pressure. The flowmeters at the input and output were read at each control-pressure point.

It may be seen in fig. 12 that there are through-holes on each side of the power stream in the region between the control jets and apertures. This effectively short circuits any pressure difference across the stream, thereby insuring stream stability.

342
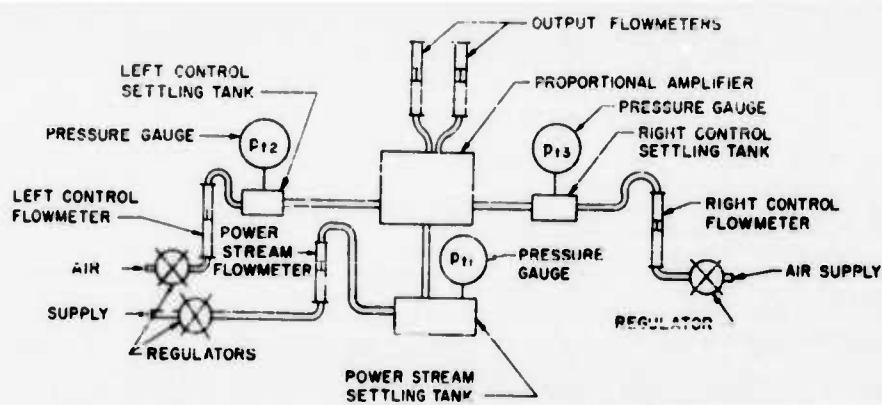
Figure 13. Functional diagram of test set-up.
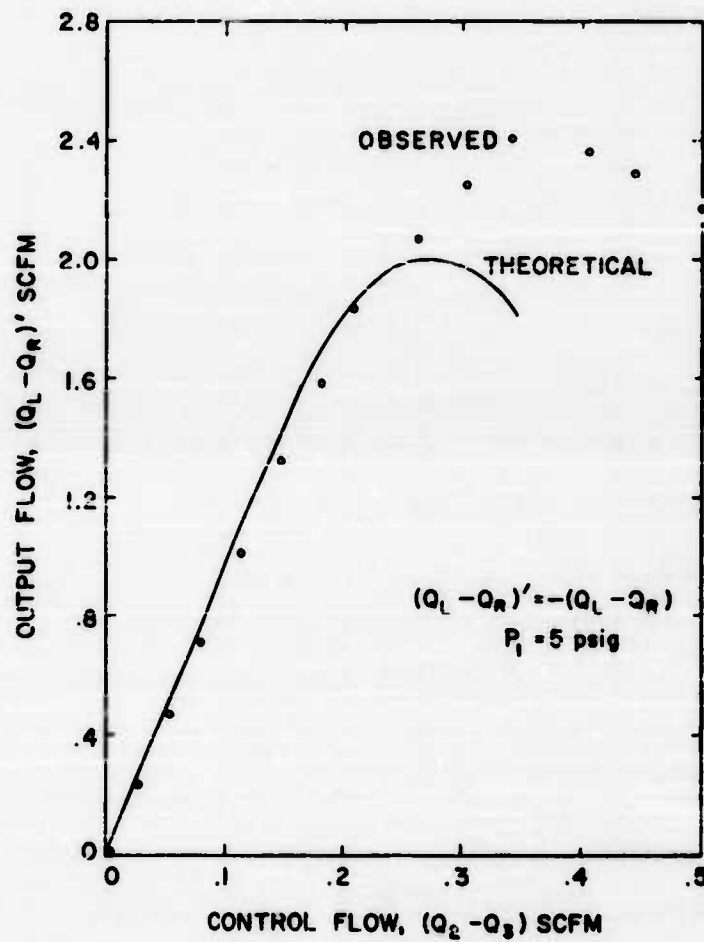
Figure 14. Comparison of experimental and theoretical
flow differences.

7. COMPARISON OF THEORETICAL AND EXPERIMENTAL RESULTS

In comparing the theoretical and experimental results, it is advantageous to plot output difference versus input difference rather than gain versus deflection angle, since claculation of experimental gain requires division by small differences, which reduces the accuracy of the results. Equations (2) and (12) show that the slope of the curve that has the output difference as ordinate and input difference as abscissa will be the gain of the amplifier.

7.1 Flow Difference

If the conditions given in section 5.1 are assumed again, a theoretical relation between aperture-flow difference Q_L - Q_R and control-flow difference Q_2 - Q_3 can be calculated from equations (8), (9), and (10). The theoretical and experimental flow difference results are shown in fig. 14 and 15.

The theoretical and experimental results are in close agreement until the control flow difference reaches 10 per cent of the power stream flow. As the control flow increases above this value, the experimental results become higher than predicted by the theory.

7.2 Pressure Difference

The theoretical relation between aperture pressure difference p_L - p_R and control pressure difference p_2 - p_3 can be calculated from equations (18) and (20) by using the conditions given in section 5.1. This relation is shown in figs. 16 and 17 for both theoretical and experimental results. In the experimental results, the dynamic pressure at the entrance to the apertures is computed from the output flowmeter readings by relating dynamic pressure to average velocity and using the equation of continuity.

344

Figure 16. Comparison of experimental and theoretical pressure differences.

Figure 15. Comparison of experimental and theoretical flow differences.

345
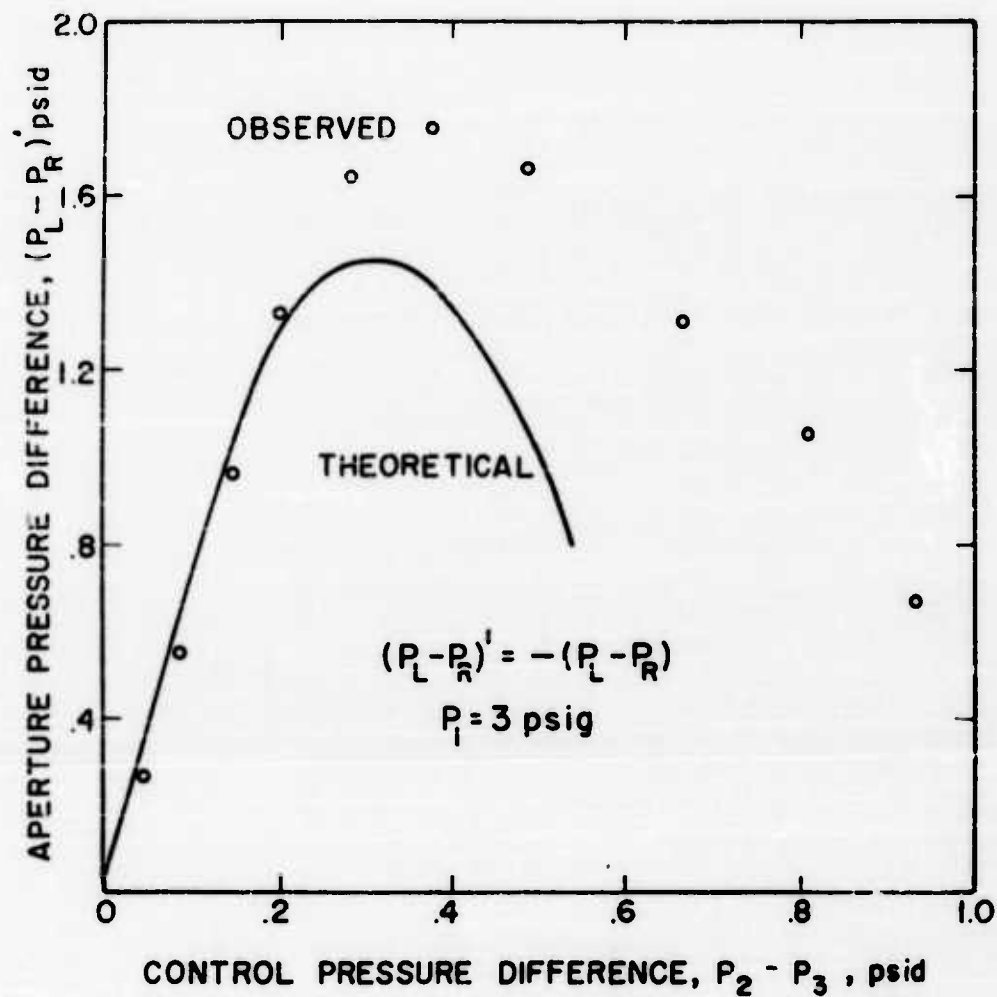
Figure 17. Comparison of experimental and theoretical
pressure differences.

346

The experimental and theoretical curves have essentially the same shape. For small control pressure differences the agreement is good. As the control pressure difference increases the experimental aperture pressure difference becomes larger than predicted by the theory. The maximum value, or point of zero gain, occurs when the control pressure difference is approximately 10 per cent of the power stream pressure.

8. DISCUSSION

To obtain the theoretical output differences a Gaussian pressure profile was assumed. This profile was selected from those found experimentally by specifying the same standard deviation and maximum value. Increasing the standard deviation of the theoretical profile as much as 20 per cent caused only a negligible change in the output difference functions, P_L - P_R and Q_L and Q_R, because all apertures were almost equally affected. This was also confirmed experimentally. The experimental profile was broadened by increasing the percentage of control pressure; tests made at 10 per cent, 20 per cent, and 30 per cent control pressure yielded close results. If the maximum value of the Gaussian is changed, the output difference functions are also changed. According to the theory, the aperture difference pressure is directly proportional to the maximum pressure. The experiments made with power stream pressures of 3 psig and 5 psig tended to confirm this. At a power stream pressure of 5 psig, the maximum aperture pressure difference was 2.78 psig. At 3 psig, the aperture pressure difference was 1.75 psig. The ratio of these is 0.63 compared with the prediction of 0.60 from the theory. In addition, experimental profile data of undeflected streams obtained at DOFL were substituted in the theoretical equations. The result was within 5 percent of the result obtained with the Gaussian profile. It must be concluded

347

then, that the use of Gaussian profiles in place of actual undeflected profiles leads to relatively small errors in the theoretical results.

To obtain the theoretical input differences, the momentum equation was applied to the interaction region (App. A). An approximate relation has been employed to give the input-pressure difference $p_2 - p_3$ in equation (20) and the input-flow difference $Q_2 - Q_3$ from equation (9). At present there are no experimental data available to check the accuracy of this relation.

As the control differences increase, the experimental output differences become greater than the theory predicts. The theoretical output differences were based on the assumption of a Guassian profile. At present, profiles of highly deflected streams have not been taken but they are not expected to remain Guassian; therefore, the use of a profile that remains Gaussian restricts the theoretical results to conditions where the stream deflections are small.

The experimental difference functions are greater than the theory predicts. In the present tests the total output flow was greater than the profile indicated, even when the stream was not deflected. This occurs because a fluid whose velocity is nonuniform at the input to an aperture continues to entrain fluid after the fluid has entered the collectors. In this analysis, all calculations were made under the assumption that the velocity profile at the input to an aperture is unaffected by the presence of the aperture.

9. CONCLUSIONS

A theory has been presented that predicts small signal pressure, flow, and

348

power gain of a single amplifier stage. The theory indicates that a power gain of about 100 is easily achievable with pressure and flow gains of about 10.

All gains are at maximum when the power stream is evenly divided by the two output apertures. The gains decrease with deflection angle and become zero when the stream is approximately centered in one of the apertures.

The power gain maximizes at about 11 power-jet nozzle widths downstream with aperture widths 1.5 times the power-jet nozzle width.

Comparison of those aspects of the theory, which could be checked on a single laboratory model showed good agreement within the experimental error.

On this model the pressure gain was calculated to be 9.1 and measured 8.4; the flow gain was calculated to be 10 5 and measured 9.4.

10. REFERENCES

(1) DOFL TR-1039, "Fluid Amplification - No. 1: Basic Principles", R. W. Warren and S. J. Peperone, 15 Aug 1962 (Part II).

(2) M. J. Albertson, Y. B. Dai, R. A. Jensen and H. Rouse, "Diffusion of Submerged Jets", Proc. Am. Soc. Civ. Engrs., Dec 1948.

(3) B. G. Newman, "The Deflection of Plane Jets by Adjacent Boundaries - Coanda Effect", Pergamon Press, 1961 (Boundary Layer and Flow Control, Vol 1).

(4) Prandtl and Tietjens, "Fundamentals of Hydro- and Aero-mechanics", Dover Publications, Inc. (1957).

APPENDIX A

THEORETICAL ANALYSIS OF INTERACTING STREAMS--MATHEMATICAL DERIVATIONS

To formulate the expression for gain in equations (6) and (16), it is necessary to have a relationship between input difference and the stream deflection. This relation can be obtained by the application of the momentum equation to the control and power streams.

In the derivation it is assumed that the fluid is incompressible, the flow is steady, there is no energy loss, and the change in momentum is due only to the change in direction of the interacting streams. Experiments have shown that the axes of the power stream and control streams are not parallel after interacting because of the characteristic spreading of a jet stream. This fact is considered in the derivation.

From the above assumptions and neglecting body forces, the momentum equation

$$-\int p_s \, d\vec{A} = \int \frac{\rho}{g_c} (\vec{v} \cdot d\vec{A}) \vec{v} \qquad \text{(A-1)}$$

may be written as Newton's second law

$$\sum \vec{F} = \frac{d\vec{M}}{dt} \equiv \dot{\vec{M}} \qquad \text{(A-2)}$$

where $\vec{M}$ is the momentum vector and $\vec{F}$ is the force vector.

350

From the free body diagrams shown in fig. A-1, the following component equations are obtained (where the subscript w denotes the wall):

Left-Control Stream

$$\Sigma F_x = \dot{M}_x$$

$$P_{s2} A_2 \cos\beta + P_{s2} A_2 \sin(\phi-\gamma) - F_{x_2} = \frac{\rho}{g_c} A_2 \nu_2^2 \sin(\phi-\gamma) - \frac{\rho}{g_c} A_2 \nu_2^2 \cos\beta \qquad (A-3)$$

$$\Sigma F_y = \dot{M}_y$$

$$P_{s2} A_2 \sin\beta + F_{yw2} + F_{y2} - P_{s2} A_2 \cos(\phi-\gamma) = \frac{\rho}{g_c} A_2 \nu_2^2 \cos(\phi-\gamma) - \frac{\rho}{g_c} A_2 \nu_2^2 \sin\beta \qquad (A-4)$$

Right-Control Stream

$$\Sigma F_x = \dot{M}_x$$

$$F_{x3} - P_{s3} \cos\beta - P_{s3} A_3 \sin(\phi+\gamma) = \frac{\rho}{g_c} A_3 \nu_3^2 \sin(\phi+\gamma) + \frac{\rho}{g_c} A_3 \nu_3^2 \cos\beta \qquad (A-5)$$

$$\Sigma F_y = \dot{M}_y$$

$$P_{s3} A_3 \sin\beta + F_{yw3} + F_{y3} - P_{s3} A_3 \cos(\phi-\gamma) = \frac{\rho}{g_c} A_3 \nu_3^2 \cos(\phi+\gamma) - \frac{\rho}{g_c} A_3 \nu_3^2 \sin\beta \qquad (A-6)$$

Power Stream

$$\Sigma F_x = \dot{M}_x$$

$$F_{x2} - F_{x3} - P_{s1} A_1 \sin\gamma = \frac{\rho}{g_c} A_1 \nu_1^2 \sin\gamma \qquad (A-7)$$

$$\Sigma F_y = \dot{M}_y$$

$$P_{s1} A_1 + \frac{\rho}{g_c} A_1 \nu_1^2 - F_{y2} - F_{y3} - P_{s1} A_1 \cos\gamma = \frac{\rho}{g_c} A_1 \nu_1^2 \cos\gamma \qquad (A-8)$$
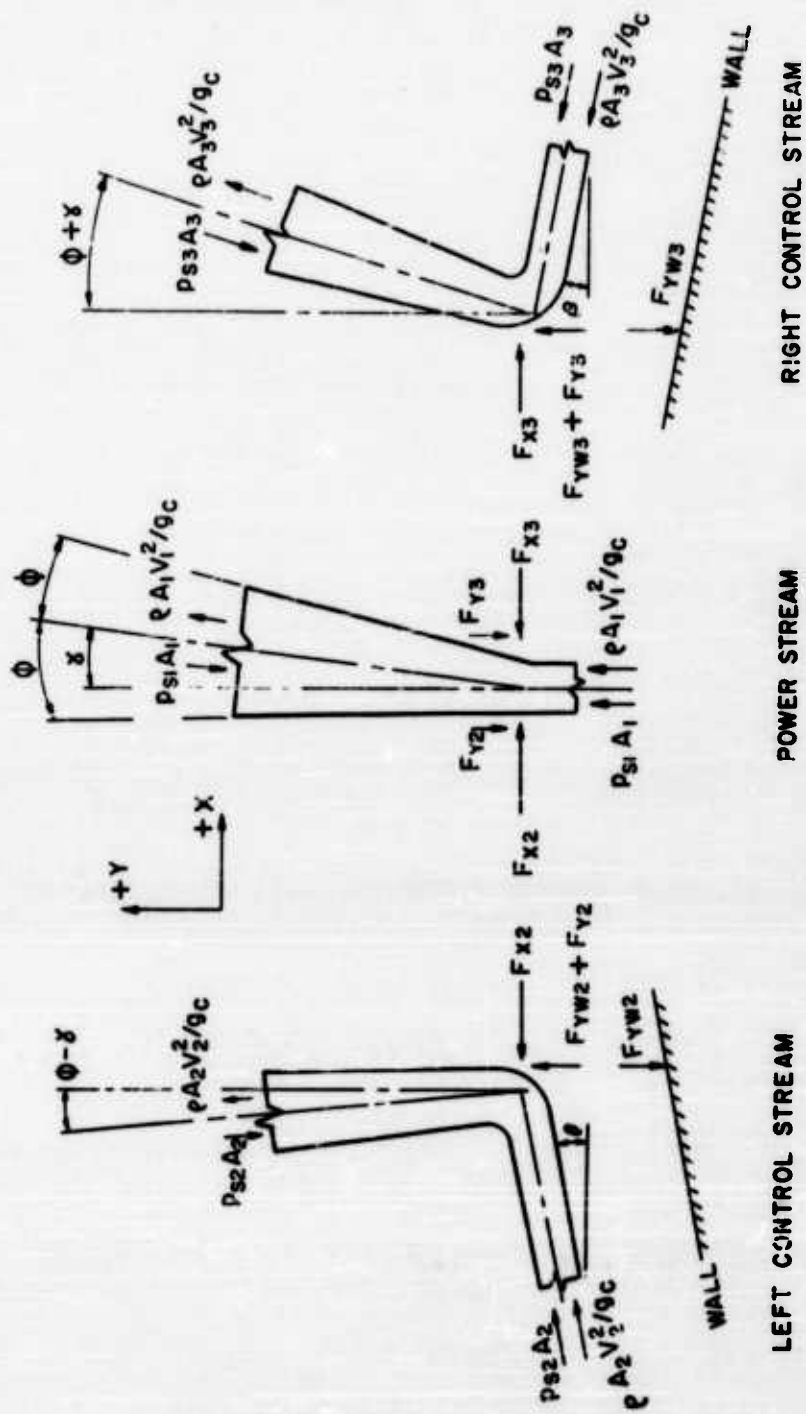
Figure A-1. Free body diagrams of the interacting streams.

352

$$F_{yw3} = p_{s3} A_3 \quad ; \quad F_{yw2} = p_{s2} A_2 \tag{A-9}$$

Now if eq. (A-7) is divided by ea. (A-8)

$$\tan \gamma = \frac{F_{x2} - F_{x3}}{p_{s1} A_1 + \frac{\varrho}{g_c} A_1 v_1^2 - F_{x2} - F_{y3}} \tag{A-10}$$

Substituting equations (A-3), (A-4), (A-5), (A-6), and (A-9) into (A-10) the result is

$$\tan \gamma = \frac{\left[p_{s2} A_2 + \frac{\varrho}{g_c} A_2 v_2^2\right]\left[\cos\beta + \sin(\phi-\gamma)\right] - \left[p_{s3} A_3 + \frac{\varrho}{g_c} A_3 v_3^2\right]\left[\cos\beta + \sin(\phi+\gamma)\right]}{\left[p_{s1} A_1 + \frac{\varrho}{g_c} A_1 v_1^2\right] + \left[p_{s2} A_2 + \frac{\varrho}{g_c} A_2 v_2^2\right]\left[\sin\phi - \cos(\phi-\gamma)\right] + \left[p_{s3} A_3 + \frac{\varrho}{g_c} A_3 v_3^2\right]\left[\sin\phi - \cos(\phi-\gamma)\right] + p_{s2} A_2 + p_{s3} A_3} \tag{A-11}$$

In general, the control streams are perpendicular to the power stream ($\hat{\beta} = 0$) so that eq. (A-11) becomes

$$\tan \gamma = \frac{A_2\left[p_{s2} + \frac{\varrho}{g_c} v_2^2\right]\left[1 + \sin(\phi-\gamma)\right] - A_3\left[p_{s3} + \frac{\varrho}{g_c} v_3^2\right]\left[1 + \sin(\phi+\gamma)\right]}{A_1\left[p_{s1} + \frac{\varrho}{g_c} v_1^2\right] - A_2\left[p_{s2} + \frac{\varrho}{g_c} v_2^2\right]\left[\cos(\phi-\gamma)\right] - A_3\left[p_{s3} + \frac{\varrho}{g_c} v_3^2\right]\left[\cos(\phi+\gamma)\right] + p_{s2} A_2 + p_{s3} A_3} \tag{A-12}$$

For power-stream deflection angles γ small compared with ϕ, the stream deflection is approximately

$$\tan\gamma = \frac{\left[A_2\left(p_{s2}+\frac{\rho}{g_c}v_2^2\right)-A_3\left(p_{s3}+\frac{\rho}{g_c}v_3^2\right)\right]\left[1+\sin\phi\right]}{A_1\left[p_{s1}+\frac{\rho}{g_c}v_1^2\right]+\left\{p_{s2}A_2+p_{s3}A_3-\left[A_2\left(p_{s2}+\frac{\rho}{g_c}v_2^2\right)+A_3\left(p_{s3}+\frac{\rho}{g_c}v_3^2\right)\right]\cos\phi\right\}} \tag{A-13}$$

In the denominator of eq. (A-13), the bracketed term is at least an order of magnitude smaller than the first term. Neglecting this term leads to the further approximation

$$\tan\gamma = \frac{\left[A_2\left(p_{s2}+\frac{\rho}{g_c}v_2^2\right)-A_3\left(p_{s3}+\frac{\rho}{g_c}v_3^2\right)\right]\left[1+\sin\phi\right]}{p_{s1}A_1+\frac{\rho}{g_c}A_1v_1^2} \tag{A-14}$$

Using Bernoulli's equation

$$p = p_s + \frac{\rho}{2g_c}v^2 \tag{A-15}$$

eq. (A-14) becomes

$$\tan\gamma = \frac{\left[A_2\left(p_2+\frac{\rho}{2g_c}v_2^2\right)-A_3\left(p_3+\frac{\rho}{2g_c}v_3^2\right)\right]\left[1+\sin\phi\right]}{A_1\left(p_1+\frac{\rho}{2g_c}v_1^2\right)} \tag{A-16}$$

354

If $A_2 = A_3$ eq. (A-16) takes the form given in eq. (19) with $p_1 = p_2 - p_3$; that is,

$$\tan \gamma = \frac{A_2(1+\alpha_2)(1+\sin\phi)\, p_3}{A_1(1+\alpha_1)\, p_1}$$ (A-17)

where, by definition,

$$\alpha_1 \equiv \frac{\rho\, v_1^2}{2 g_c\, p_1} \quad ; \quad \alpha_2 = \alpha_3 \equiv \frac{\rho\, v_2^2}{2 g_c\, p_2} = \frac{\rho\, v_3^2}{2 g_c\, p_3}$$

For the flow-gain expression, it is convenient to express eq. (A-17) in terms of control flow rather than control pressure.

Expressing p_2 and p_3 in terms of α_2, N_2 and N_3 and still assuming that $A_2 = A_3$ gives

$$p_2 - p_3 = \frac{\rho}{2 g_c \alpha_2}(v_2^2 - v_3^2) = \frac{\rho}{2 g_c \alpha_2 A_2^2}(Q_2^2 - Q_3^2)$$ (A-18)

By definition $Q_1 = Q_2 - Q_3$ so that

$$p_2 - p_3 = \frac{\rho}{2 g_c \alpha_2 A_2}(Q_1^2 + 2 Q_1 Q_3)$$ (A-19)

Substituting eq. (A-19) for p_1 in eq. (A-17) gives

$$\tan \gamma = \frac{\rho \left(1+\alpha_2\right)\left(1+\sin \phi\right)\left(Q_1^2 + 2Q_1 Q_3\right)}{2 g_c \alpha_2 A_1 A_2 \left(1+\alpha_1\right) \rho_1} \qquad \text{(A-20)}$$

which is equivalent to eq. (9).

356

TURBULENCE AMPLIFIER DESIGN AND APPLICATION

by

Raymond N. Auger

of

Fluid Logic Control Systems
New York 27, New York

The turbulence amplifier is a pneumatic or hydraulic no-moving-parts fluid amplifier with many unique properties which suit it for use in logic circuits and as a primary sensor of low velocity fluid streams and low energy acoustic waves. The turbulence amplifier produces signal amplification by the disturbance of a laminar flow in a submerged jet. Figure 1 illustrates the basic configuration of the device.

If a fluid stream is sent through a smooth-walled pipe of small diameter at a sufficiently low velocity, the pipe's walls will induce laminar flow. If this flow is sufficiently laminar, it can then be projected a distance of over 100 times the diameter of the pipe and remain in a laminar state until it becomes turbulent. The distance over which the stream can be projected in a laminar state decreases as the velocity of the stream is increased. If an orifice is placed in a laminar stream, as in the tube "0" in Figure 1, it will obtain a static pressure which is the result of the average velocity of the portion of the stream received. If the velocity of this stream is increased so that turbulence occurs between the supply tube and the output orifice, as seen in the lower half of Figure 1, the pressure in the output drops because a smaller proportion of the fluid in the supply stream enters the output tube. When the supply stream's velocity is increased to a degree that the point of turbulence of the stream is at the exit of the supply tube, the output pressure of the device slowly increases because the fraction of the supply fluid reaching the output tube remains constant while the velocity of the supply fluid continues to rise. Output pressure as a function of input pressure for this arrangement is shown at the top of Figure 1. The peak of this curve marked "m" represents the supply velocity at which the cone of turbulence appears immediately before the output tube. If the distance between the supply and output tubes has been properly selected, small disturbances of the supply stream near its point of exit from the supply tube will be amplified by phenomena within the laminar stream, causing it to become turbulent at a point nearer the supply exit, and producing large pressure variations in the

357

output tube. Power gains of 100 and higher are possible by this
arrangement. The disturbances introduced into the laminar stream may
be the result of acoustic waves or other fluid streams directed into
the laminar stream. The greater the distance between the supply and
output tube, the greater the sensitivity of the device, but as the
maximum velocity of a laminar stream decreases with distance, the
selection of the distance between supply and output for a practical
device must represent a balance of sensitivity and useful output.

The arrangement of Figure 1 provides a means of using the well-
known sound-sensitivity of laminar jets for the actuation of pneumatic
amplifiers or pressure switches. Fortunately, sound sensitivity
becomes significant at distances between supply and output which are
much greater than required for the design of practical amplifiers of
fluid streams. Using a 0.030 inch diameter supply jet, pneumatic
turbulence amplifiers are practical fluid stream amplifiers when the
supply-output distance ranges between 0.7 to 1 inch, while significant
sound sensitivity begins at about 1.3 inches. High frequency sensitivity
is high at 1.7 inches, with relative insensitivity to low frequency
sounds (below 10,000 cps), while at a distance of from 1.8 and greater
sound sensitivity rivals that of high-gain electronic devices in the high
and mid-frequency range. At a supply-output distance of 1.9 inches, an
output pressure of approximately 0.9 inches of water column is obtainable
while the stream is laminar, and an output pressure of less than 0.2
inches results when the stream is upset by the sound of a high-frequency
dog whistle blown by a human being with fair lung power at a distance of
30 feet. With the output of the amplifier directed into the input of a
non-microphonic fluid stream amplifier, pressure outputs sufficient to
drive pressure switches responding to 1 inch of water column can be
obtained from distances of 300 feet by means of a man-operated whistle.

When the distance between supply and output is reduced below the
range of significant sound sensitivity, turbulence amplifiers can be
used to sense fluid flows directed approximately at right angles to the
laminar jet. Sensitivity to such flows is very great, and enables
practical amplifiers to be constructed with power gains in the range of
40 to 80. By "practical amplifiers" it is meant that devices can be
built which have outputs that can be easily used to operate other
devices, such as other amplifiers or pressure switches. Air flows
producing a pitot tube static pressure of less than 0.02 inches of water
can be used to operate turbulence amplifiers with an output range from
0.1 to 1 inches of water. If some sound-sensitivity can be tolerated
for a given air-stream detector application, pressure gains of 1,000 can
be obtained by a single device. The very high sensitivity of this device
enables it to be used for fluid stream detection in much the same way as
photoelectric devices are used to sense light beams, their interruption
and reflection. The air streams produced by small blowers can be
detected many feet from their source in an open atmosphere.

358

The use of projected air streams as input signals to turbulence amplifiers indicates the possibility of their use in complex circuits where they can be interconnected and used for multi-stage signal amplification or as switching devices in logic and control circuits. Figure 2 illustrates a turbulence amplifier with a control jet used to introduce disturbances in the laminar stream. For this arrangement to be practical for use in complex circuits, its output must be capable of direct coupling with the input of an identical device. This has been achieved with the realization of amplifier configurations which produce input-output functions such as shown at the top of Figure 2. Because the output of turbulence amplifiers never drops completely to zero, except for very large signals, for one amplifier to be directly coupled to a second it is essential that the second amplifier be unresponsive to very small signals. As the curve of Figure 2 indicates, this is the case for a properly designed turbulence amplifier. The range of unresponsiveness is a result of simple design parameters and can be made as great as desired. The simplest design technique for controlling the range of unresponsiveness is to use a configuration which projects a stream which is so stable that it is undisturbed by the time it reaches the output during the range of input to be ignored.

Air-operated turbulence amplifiers in an atmosphere of approximately sea-level pressure can be built in a limited range of sizes. There is only one size supply jet which produces maximum power gain, and this is approximately 0.040 inch in diameter. Acceptable gain for logic circuit applications exists through a range of supply diameters running from approximately 0.010 inch to 0.070 inch. The importance of proper supply tube configuration (diameter taper, if any, and straight length) increases significantly with tube diameter.

Supply jet diameters of 0.030 inch have proven to be practical from the point of view of power consumption and pressure, output volume, amplifier gain, fabrication convenience and size. These units are now commercially available in limited quantities. They operate with a supply pressure of approximately four inches of water, produce an output of approximately 2 inches with a no-load volume of 20 cu. in. per minute. The input or control signal volume is about 3 cu. in. per minute with a control pressure range of approximately 0.3 inches. Signal transmission between amplifiers and within them is at approximately 1 inch per millisecond. Connecting an amplifier input to output with a 3 inch circuit path results in oscillations of approximately 350 cps. Some care must be exercised in constructing high-speed circuits not to overdrive amplifiers because the resumption of laminar flow after very strong turbulence will be delayed to a variable degree. The degree to which this occurs is readily observable in oscillators.

The turbulence amplifier has a number of advantages when used as a switching element in logic circuits. It is a major convenience in constructing such circuits to use an element which is free of impedance matching problems and which exhibits the large fan-out ratio (1:10) of

these units. The complete isolation of turbulence amplifier inputs and the fact that a single amplifier can have an almost unlimited number of inputs is a major advantage in many practical circuits. A third major advantage of turbulence amplifiers is the fact that each amplifier performs the logical NOR function, which can be used as the basis for all of the other logic functions, such as AND, OR, MEMORY (flip-flop), and counting circuits. Figure 3 illustrates the circuit for the flip-flop and the AND. The flip-flop circuit is one of the few which requires some consideration of output load. For a flip-flop to be symmetrical its outputs must be connected to approximately equal loads: either dead-ends, such as manometers, or groups of amplifiers.

The power supplies for fluid logic systems are generally regarded as one of the problems in their application. The fact that turbulence amplifiers operate with both very low pressures and volumes is an asset from the power supply point of view. Small systems using from one to 20 amplifiers may be powered by inexpensive vibratory diaphragm type pumps. Larger systems can use centrifugal blowers or vane type pumps. Totally closed systems can be used to limit contamination. The low pressure drops in turbulence amplifiers minimizes the possibility of moisture condensation. Complex logic circuits have been operated over temperature ranges from 20 to 130 degrees farenheit, with relative humidity up to 99%.

Turbulence amplifiers can be fabricated by a wide variety of techniques, ranging from soldering together short lengths of brass tubing to molding complete amplifiers and interconnections in plastic. At the present time they are being made by casting brass tubes in plastic. The tubes provide both precise passages for air flows and convenient terminals for attaching plastic tubing. These amplifiers are being used in consoles, such as in Figure 4, which provide a built-in power supply, manometer-type indicators. back-pressure push-buttons, in addition to 24 two-input amplifiers with a rated output of 1.5" w. The purpose of these consoles is to provide a convenient means for the study of turbulence amplifier operation and circuit design. In the future, individual sets of amplifiers will be available either for mounting as a ganged assembly for plastic-tubing interconnection, or as plug-in units for assembly into circuits cast, milled or photoetched into sheets of plastic or glass.

Figure 5 illustrates a variety of components which can be integrated into turbulence amplifier control systems. The microphone, shown at the top of the group of inputs, combines the properties of a very sensitive sound detector and a high-pass filter. It provides a pneumatic output sufficient to directly operate pressure switches or other turbulence amplifiers from very weak acoustic signals above 10 kc. A very inexpensive and simple device to build, it may be used for the remote control of toys, garage door openers, or industrial alarm systems, with the remote control "transmitter" being simply a high-frequency whistle.

360

The air-stream sensor can be used in two ways: the jet of laminar air thrown between its supply jet and curved output "collector" can be mechanically interrupted or made turbulent by means of very low velocity cross-currents.

The whisker-valve is a new sub-miniature valve operated by means of deflection of a wire feeler by means of very light mechanical forces. The characteristics of this valve suit it for producing inputs to fluid logic systems.

Small diaphragms can provide enough air flow when depressed 1/16 inch to trigger flip-flops. Thus, they can be used as push-buttons or limit switches for totally enclosed systems.

Sensing holes in perforated tape by air flows is a familiar technique. The availability of logic elements to work with tape reader signals, either for code conversion or other roles, eliminates the need for immediate pneumatic-to-electric conversion.

Analog-to-digital code disks with the same resolution as their electromechanical counterparts and with inherently greater accuracy due to the absence of brushes or lights sources and photoelements can be offered at a fraction of the cost of their electrical counterparts.

Just as no-moving-parts push-buttons can be made by venting a small amount of air to atmosphere and then sensing the increase in line pressure by blocking the line with light finger pressure, electric-to-pneumatic conversion can be accomplished using conventional relays with one or more contacts modified to act as armature-closed orifices. Many relays can be modified and continue to carry electric contacts at the same time.

Thanks to the ease with which turbulence amplifiers are constructed and inter-connected, their use in practical applications is an immediate possibility.

362

FIG.1

FIG. 2

FIG. 3

364
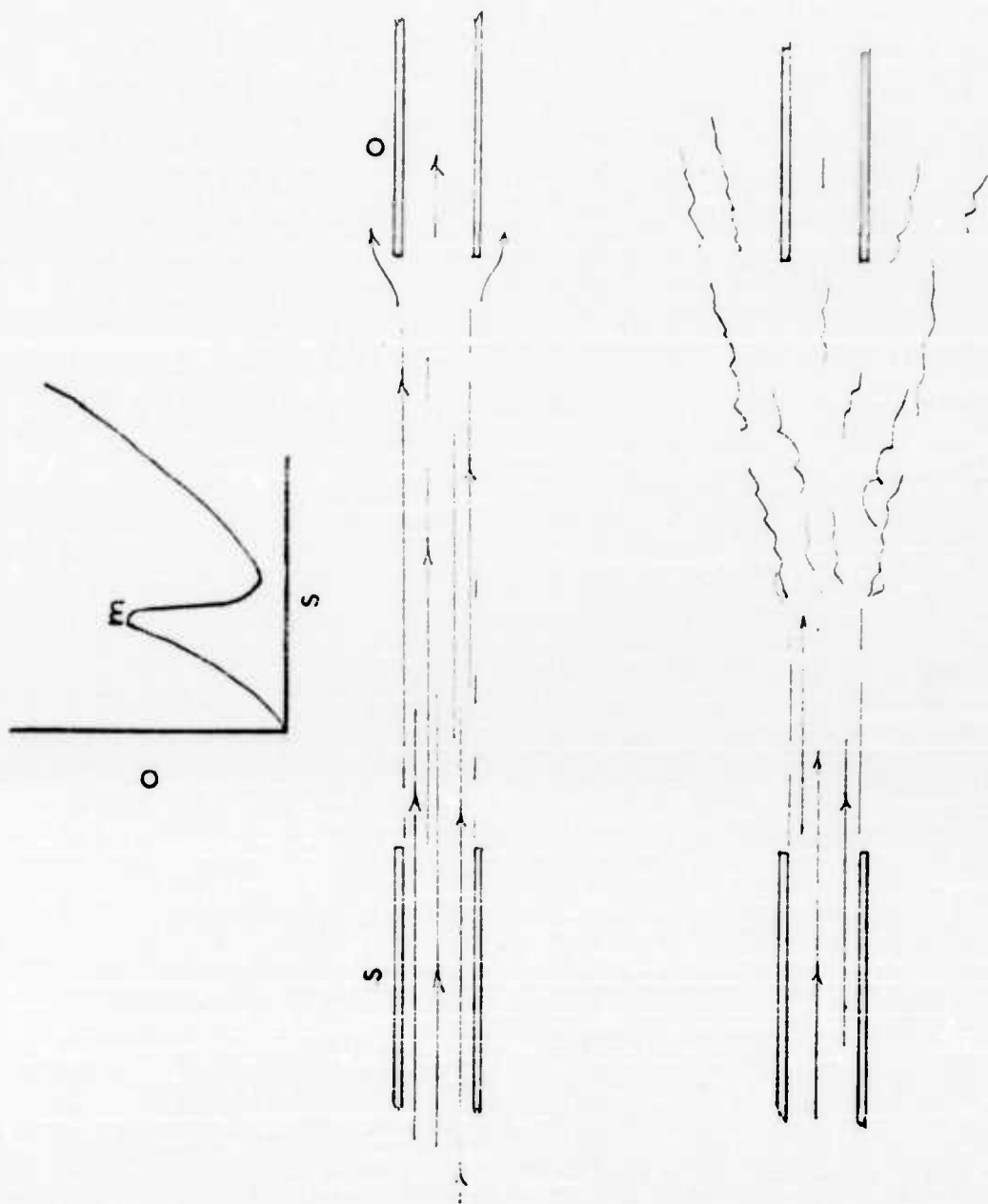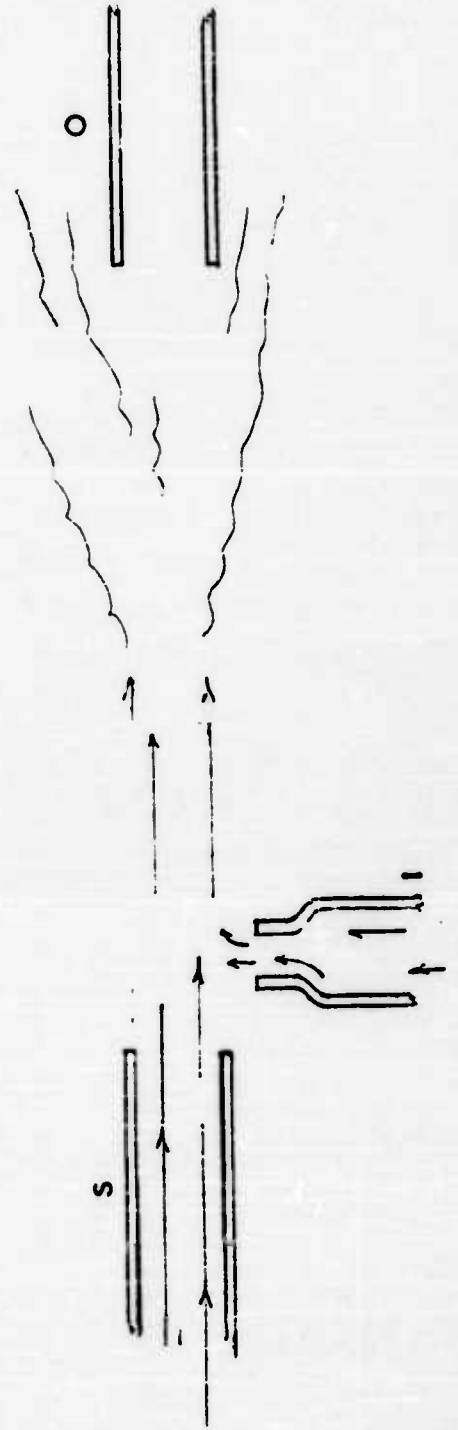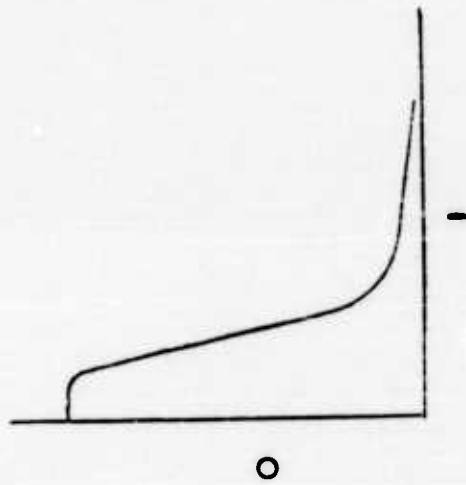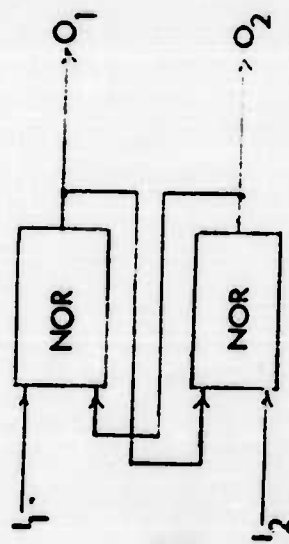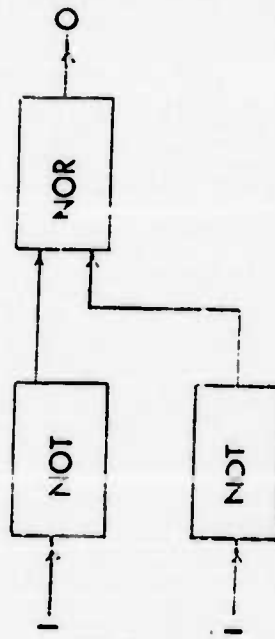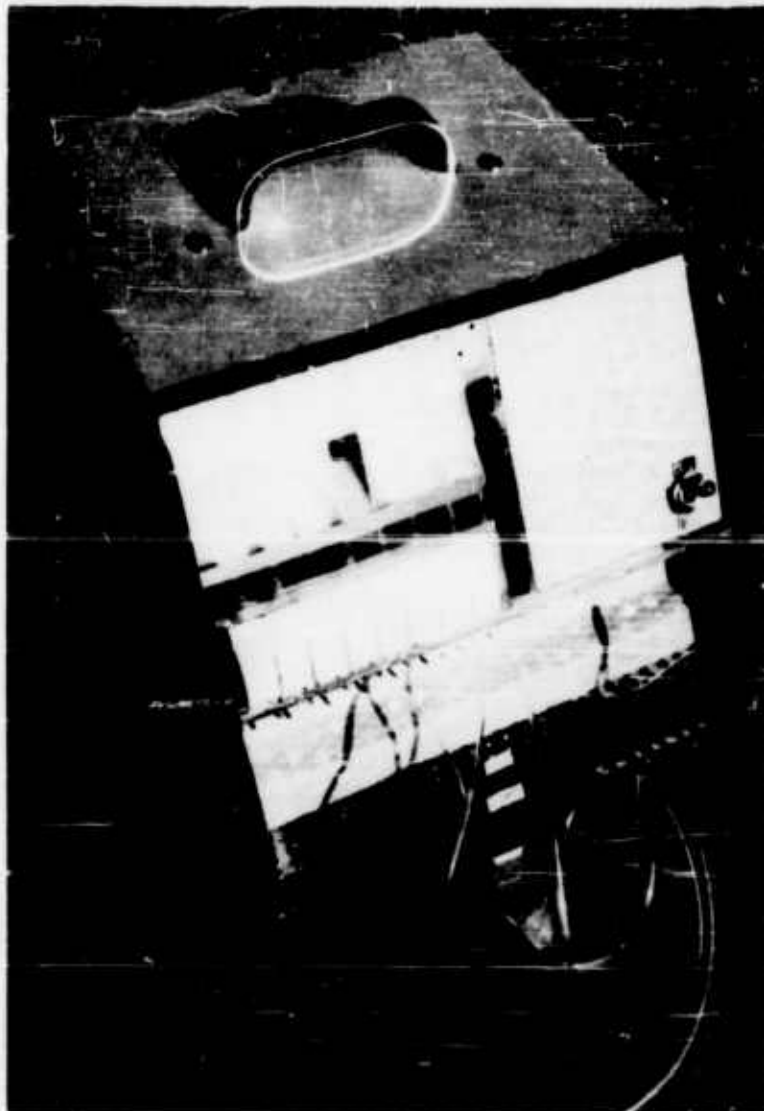
Figure 4. A 24 amplifier console used to study turbulence amplifier circuits. It contains a vane type pump, eight manometers which can be connected to the output of any amplifier, plus one manometer to indicate supply pressure, and eight back-pressure type push-buttons. Two of the 24 amplifiers have four inputs, the others have two inputs.

Fig. 5

FLUID LOGIC CONTROL SYSTEM COMPONENTS
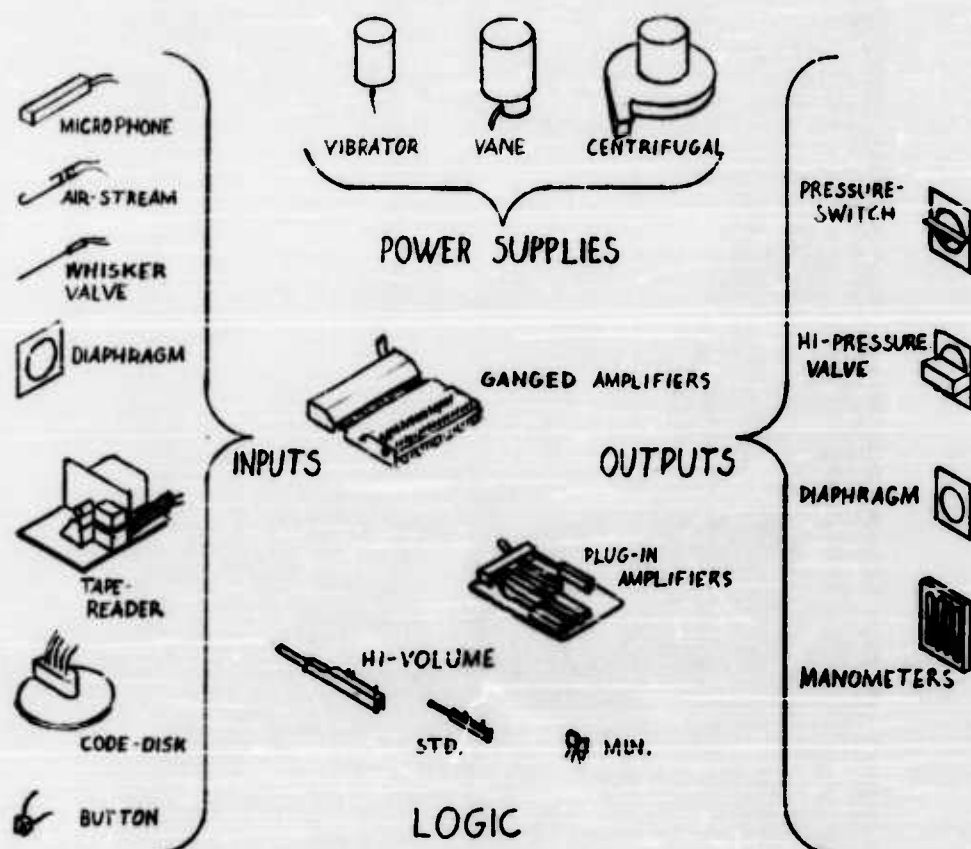
AMPLIFIER SPECIFICATIONS

	HI-VOLUME	STANDARD	MINIATURE
NO. OF INPUTS (STD.	1, 2, 3, 4, 5 OR 6	1, 2, 3, OR 4	2
SUPPLY PRESSURE	3"-6" W.C.	3"-5.5" W.C.	7"-9 W.C.
" VOLUME (MAX.)	80 CU. IN./MIN.	40 CU. IN./MIN.	12 CU. IN/MIN
INPUT RANGE (STD)	0.2"-0.4" W.C.	0.2"-0.35 W.C	0.15"-0.3" WC
INPUT VOLUME (MAX.)	3.5 CU. IN/MIN.	3 CU. IN/MIN.	2 CU. IN/MIN.
OUTPUT PRESSURE (MAX.)	2" W.C.	1.5" W.C.	1" W.C.
OUTPUT VOLUME (MAX.)	40 CU. IN./MIN.	20 CU. IN./MIN.	6 CU. IN./MIN.

366

ON THE INHERENT LIMITATIONS IN FLUID-JET MODULATORS

by

F. T. Brown

Assistant Professor
Department of Mechanical Engineering
Massachusetts Institute of Technology

Abstract

The manner in which wave motion, energy dissipation, and gross jet turbulence produce inherent limitations in fluid-jet modulators is qualitatively discussed. Topics include surge impedance matching at input and load ports, the possibility of nearly infinite pressure and power gains of "momentum-controlled" and "pressure-controlled" jet amplifiers, and the effect of nozzle design on jet noise with implications on the signal-to-noise ratio and other operating conditions.

Introduction

Fluids used in fluid-jet modulators have three significant properties: mass, viscosity, and compressibility. Aside from the basic energy flux associated with the jets, significant manifestations of these properties include wave motion, energy dissipation, and gross turbulence. These phenomena are partially beneficial, and yet also introduce inherent limitations to the operation of the devices. The purpose of this paper is to outline this concept, with emphasis on the gross turbulence in jet flows.

Wave Motion

Wave motion in fluid-jet modulators is the factor most frequently causing unsatisfactory operation. Its mechanism is usually not well understood, but the seriousness of the dynamic instabilities which result certainly are. Most effects can be analyzed in terms of the interaction of the device with its inputs (source impedance matching) or with its outputs (load impedance matching).

Perfect dynamic or surge matching exists when a wave, travelling down a

control passage or up a load passage, is completely absorbed at the port, with no reflection. This condition has been realized at the input or control ports of certain pressure-controlled proportional amplifiers (1,2), and conceptually can be nearly realized at the input of momentum-controlled proportional amplifiers (2). The problem is more difficult in bistable relays, as the control port must have identical pressures and flows, in the absence of a control signal, for both states of the device. Though conceptually possible (2), this has not been realized. To the author's knowledge no one has succeeded in, or even expressly directed his intention toward, matching the output surge impedance of the jet with the load receiver ports. An effort in this direction is starting at M.I.T.

Dynamic stability in the face of a poorly matched input surge impedance can be exceedingly difficult to achieve, especially if the wave time of the control lines is long compared with the response time of the device itself, although it is possible (3). Specifications of the load, however, often preclude stability in the face of severe impedance mis-matching. For example, if the load involves somewhat long lines leading to an essentially blocked load, waves generated at the jet receiver-port travel to the load and back with only slight attenuation, to be reflected at the mis-matched load by a larger wave than initially, which in turn travels down the line and back with increasing amplitude at each cycle. The result: severe oscillations. This wave phenomenon implies apparently inherent limitations on possible designs, although much effort needs to be expended to properly determine the true extent of the problem and possible compensations.

Energy Dissipation

Viscous dissipation of energy in fluid-jet modulators is, in fact, essential to their operation. It enables partial-admission jet diffusers to work, causes the flow entrainment which produces bistability in pressure-controlled relays, and provides damping necessary for the stability of flow in jets and lines (4) in the face of wave motion. At the same time it causes inherent limitations in the pressure and power recovery or efficiency of the devices. The lower bound of these limitations in general has not been established.

Energy dissipation alone imposes no limitation on the pressure and flow gains which can be achieved in continuous and bistable relays, however. To consider this significant statement two types of amplifiers, "momentum-controlled"

368

and "pressure-controlled," are discussed.

"Momentum-Controlled" Amplifiers

The control force on the jet of a "momentum-controlled" amplifier, Fig. 1, results primarily from the momentum-flux of the control jets. The gain of such an amplifier can be increased by feeding back some of the received flow on the left to the input on the right, and vice-versa (positive feedback). The feedback can be increased until the gain becomes infinite, barring wave motions which might well cause violent oscillations. A further increase in the feedback produces bistable operation with an increasing width of the hysteresis loop.

"Pressure-Controlled" Amplifiers

The control force on the jet of "pressure-controlled" amplifiers, Fig. 1, results primarily from the pressure gradient across a relatively long extent of the jet. Techniques for developing continuous and bistable amplifiers of this type have been described (2,5). That infinite gain can be achieved was demonstrated by the amplifier shown in Figs. 2 and 3. This amplifier, discussed in detail elsewhere (2), has two stages, the first of which is always continuous and the second of which is continuous or bistable, depending on the two nozzle supply pressures.

The second-stage jet receiver is described more fully in Fig. 4. Its design successfully eliminated essentially all feedback effects of the push-pull piston-cylinder load, Fig. 5, on the second-stage jet. The entire mechanism acted as a receiver-decoder-actuator for pulse-position-coded input pneumatic pulses.

The output differential pressure is plotted against the input pressure in Fig. 6. All the data was taken for a specific supply pressure for the second-stage jet, but the different curves represent operation with different first-stage control pressures. Note the continuous transition from bistable operation through metastable operation (infinite gain) to continuous operation. This conformed to predictions based on the characteristics of individual components of the system determined separately by analysis and experiment.

There is of course a fallacy in the concept of infinite gain in fluid-jet amplifiers, which takes the same form as in their electronic counterparts: signal-to-noise ratio. The effect of the inherent limitation of jet noise on the behavior of the two-stage amplifier was reflected in an effective randomness of the input

369

a) "MOMENTUM—CONTROLLED" AMPLIFIER

b) "PRESSURE CONTROLLED" AMPLIFIERS

Fig. 1. Fluid-Jet Amplifiers

for side view,
see Fig. 11.1

model uncovered

model covered

depth of passage

passage same depth as
transmission line

shallow relief grooves

second-stage
supply pressure

transmission line
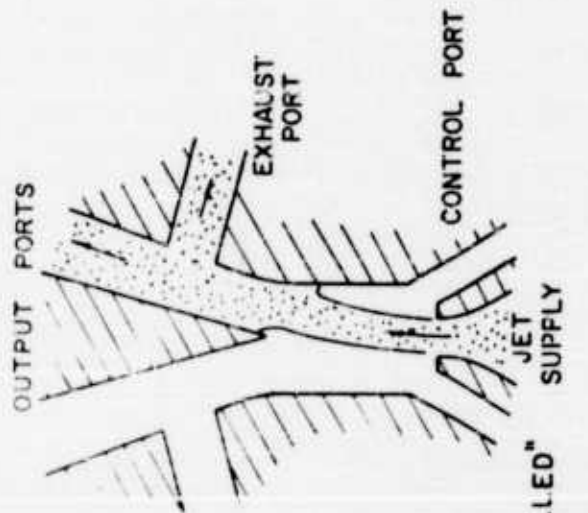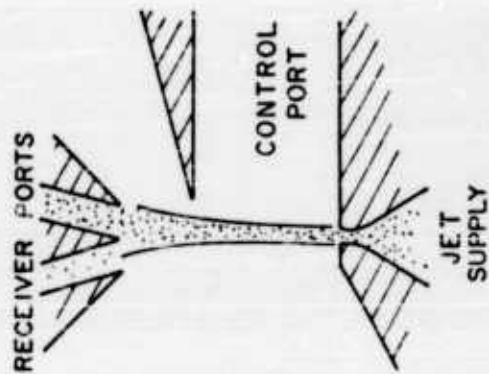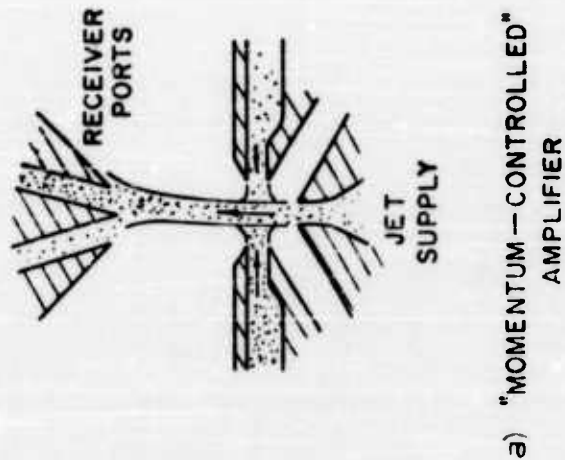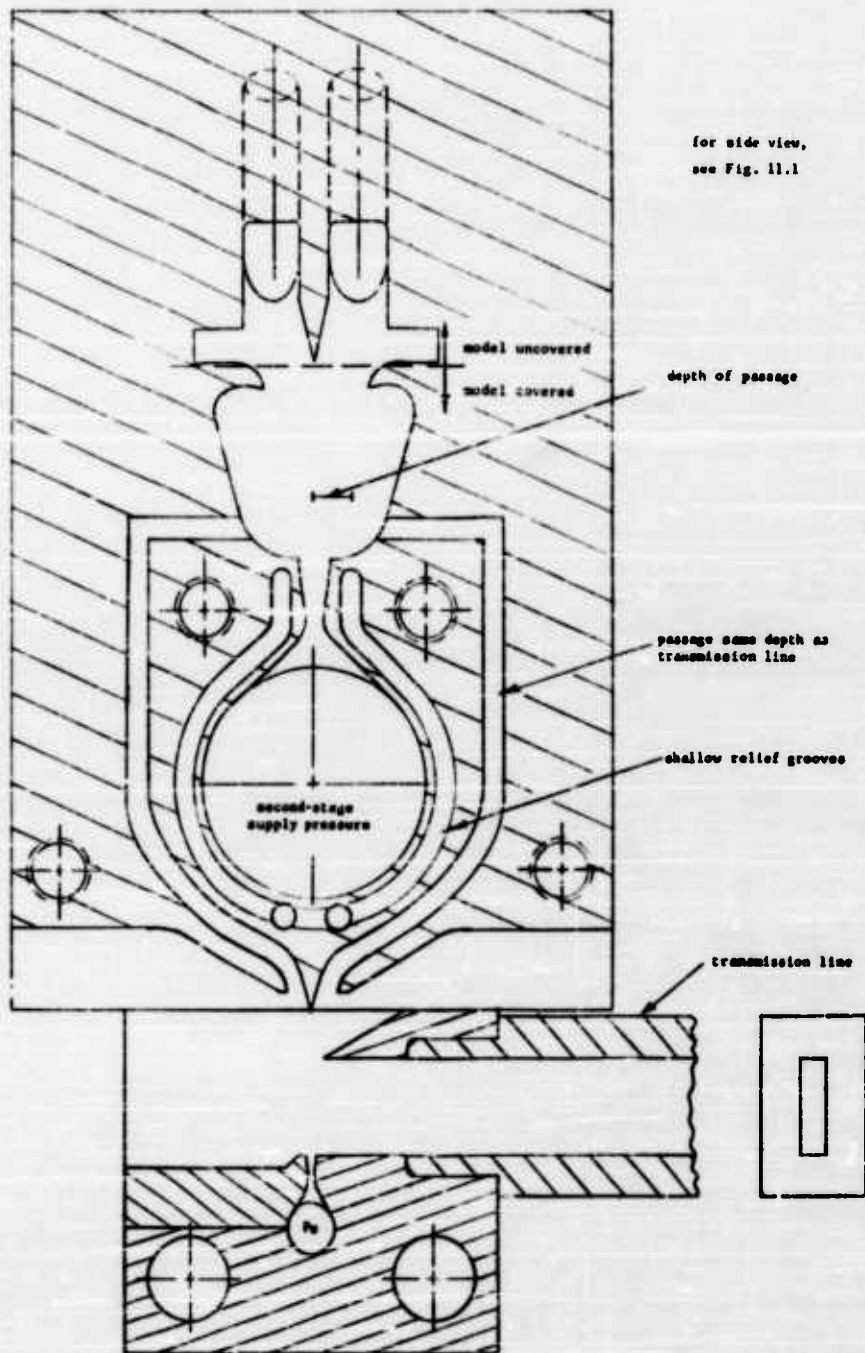
Fig. 2. Two-Stage Fluid-Jet Amplifier (machined with 1/32 inch end mill)

371
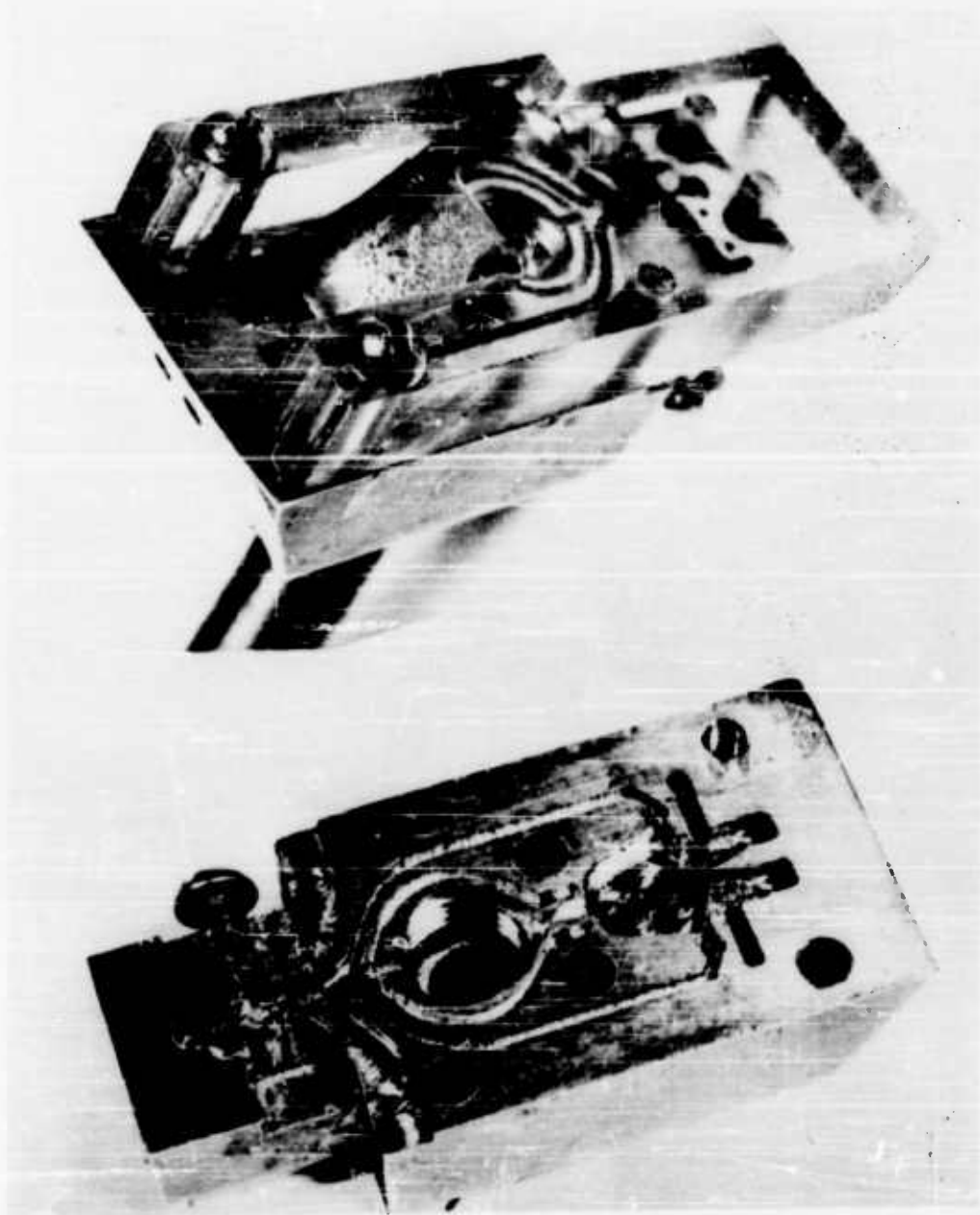
Figure 3. Photographs of amplifier.

372
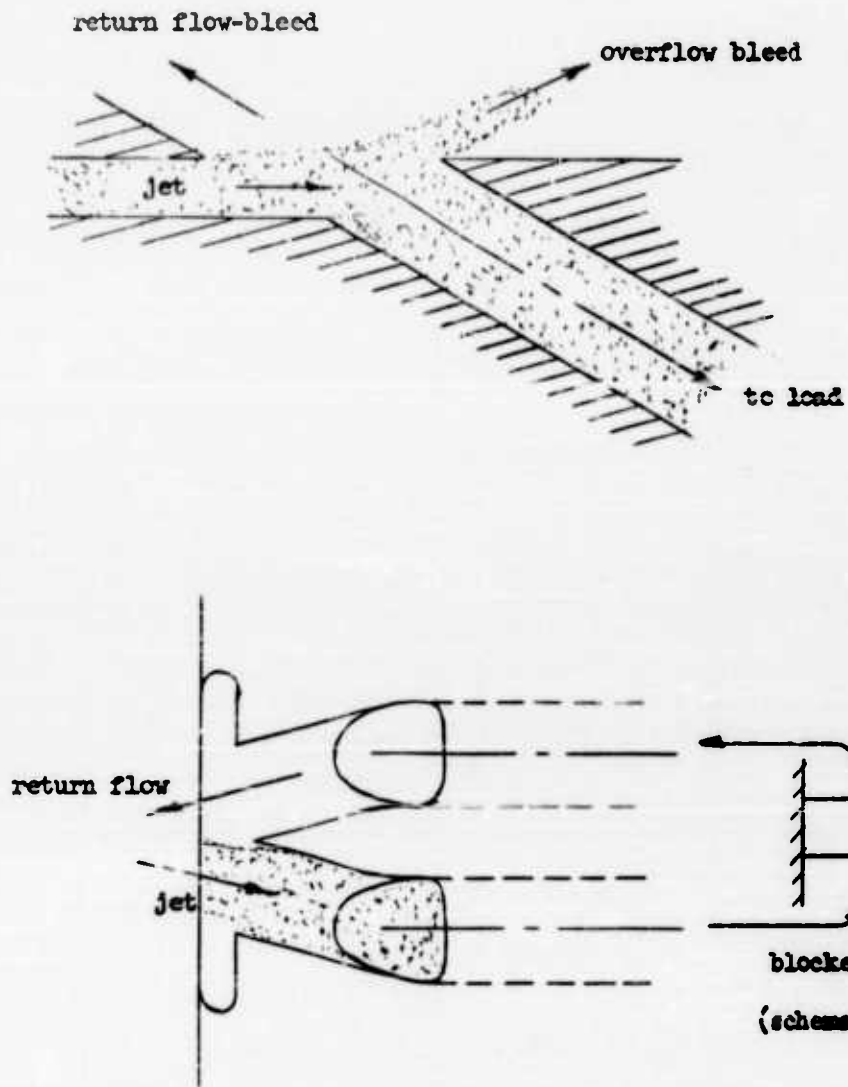
Fig. 4. Jet-Receiver Ports of Amplifier

373

output shaft

±24° rotation

θ

flow from jet relay

L

full scale

screws and pressure
taps not shown
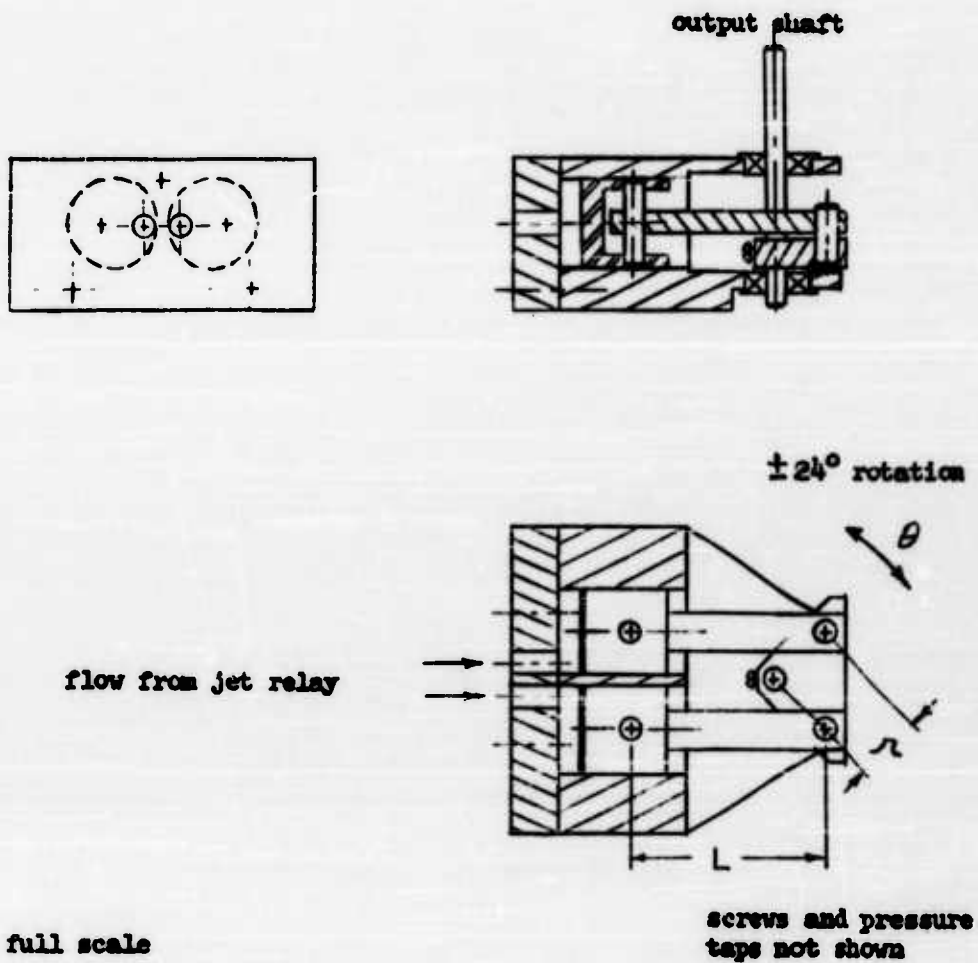
Fig. 5. Piston-Cylinder Load

374
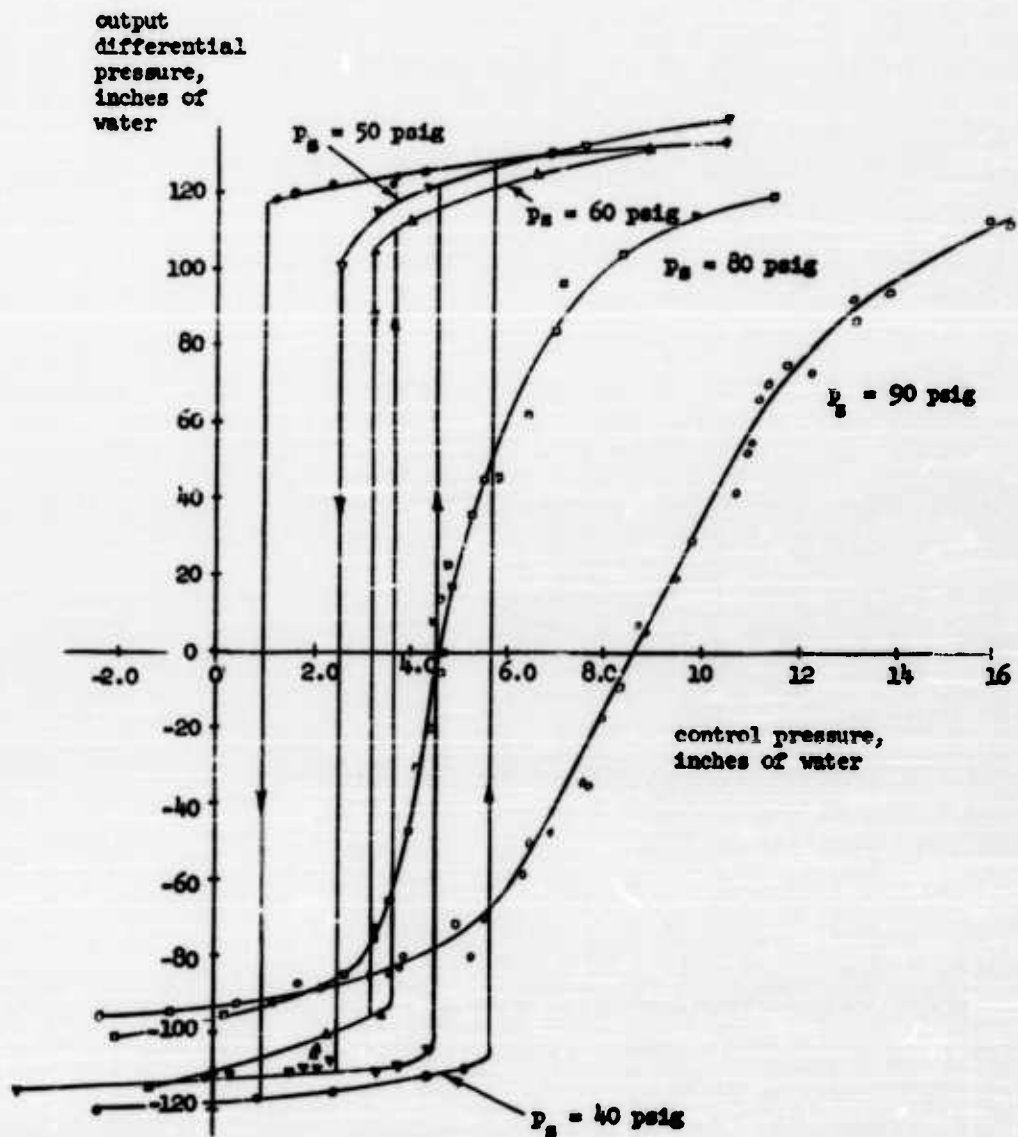
Fig. 6. Steady-State Pressure Characteristics of Amplifier,
Second-Stage Supply Pressure 40 PSIG

with a pressure amplitude of about one-half inch of water. Thus the bistable mode with the hysteresis loop only one-half inch of water wide was a totally impractical condition; the jet oscillated in a slow, random (noncyclic) manner. Similarly, when the device was continuous but with very high gain the output would wander about randomly within a constrained band.

Jet Noise

The most curious aspect of the random oscillations of the jet is the low frequencies which are prevalent. This leads one to suspect various standing waves travelling, for example, in the long control line. The superposition of standing waves travelling at different frequencies, although strictly speaking a cyclic phenomenon, could appear random.

An alternate explanation is simply that the jet contains significant noise at frequencies as low as the observed phenomenon. The jet might shed large chunks of fluid at random intervals, and occasionally several of these might be shed in an unusually short period, causing the control force on the jet to change markedly. Waves generated by the vortex shedding would play a significant role.

In Fig. 7 several frames of a moving picture demonstrating jet randomness are shown. The model is a water table with water three inches deep, with dye injected into the boundary layer of the three-quarter inch wide converging nozzle. Vortices were shed in an initially symmetric pattern, but further downstream they interacted strongly with one another in a random manner; occasionally a large chunk of fluid was transported from one side of the jet to the other, or flung away from the jet entirely. Downstream receiver ports and other obstacles tended to increase the size of the vortices, and hence increase the low-frequency disturbance forces on the jet.

Actually in this demonstration there were small waves travelling back and forth in the nozzle which generated tiny vortices in the slip planes on either side of the nozzle. These vortices were unstable, and grew with energy supplied by the jet itself. Generally the vortices in a jet are symmetric when the nozzle is short and anti-symmetric when the nozzle is long (6). The significant effects here are the damping of distrubances in a long nozzle, and the more nearly parabolic velocity distribution of the jet emanating from it.

Most basic experiments on jets have been performed with large settling chambers and very long nozzles with parallel walls, as only then are the

376

Re about 800
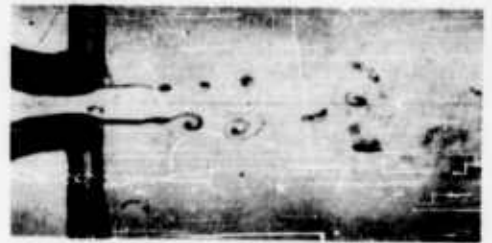
Re about 2500
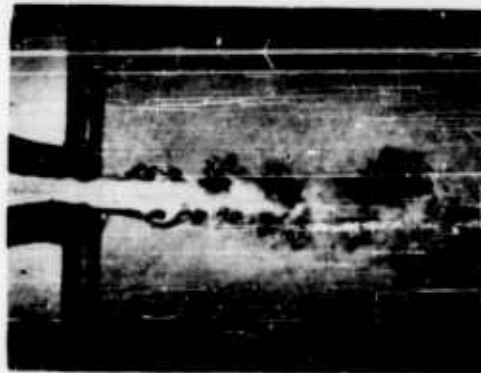
Re about 10,000

Re about 2500

Re about 2500

Figure 7. Photographs of free jets and jets impinging on blocked receivers.

phenomena essentially independent of upstream conditions (7). In these instances jets remain basically laminar for several nozzle-widths downstream, even for relatively high Reynold's numbers, say 1000. Actually waves are growing essentially exponentially (6) in the boundary layer, but are not noticeable until suddenly the jet nearly explodes into violent turbulence. Under such conditions small sound disturbances in the surrounding fluid can excite strong turbulence much earlier (6,7), as was vividly demonstrated at this symposium by Raymond Auger. The level of stability of a small disturbance in the jet depends on the local effective Reynold's and Strouhal numbers of the jet and distrubance.

Fluid-jet modulators typically involve very short nozzles and small upstream chambers, however, increasing the level of turbulence by an order of magnitude. This grossly effects the average entrained flow and the pressure and power recoveries, as well as the signal-to-noise level, and deserves considerable attention in basic and applied work on these devices. Unfortunately most work on turbulent jets involves only average pressure and velocity profiles (8,9,10).

Much sound work remains before the inherent limitations of the various classes of fluid-jet modulators can be expressed quantitatively. First the basic phenomena must be much better understood and the devices optimized.

References

1. R. W. Crossley, "An Experimental Investigation of Pneumatic Jet-Type Amplifiers and Relays," S.M. Thesis, Engineering Projects Laboratory, Department of Mechanical Engineering, M.I.T., September 1961.

2. F. T. Brown, "Pneumatic Pulse Transmission with Bistable-Jet-Relay Reception and Amplification," Sc.D. Thesis, Engineering Projects Laboratory, Department of Mechanical Engineering, M.I.T., May 1962.

3. A. R. VanKoevering, "Experimental Load Characteristics of Fluid-Jet Amplifiers," S.M. Thesis, Engineering Projects Laboratory, Department of Mechanical Engineering, M.I.T., August 1962.

4. F. T. Brown, "The Transient Response of Fluid Lines,"to be published in the Journal of Basic Engineering, ASME Transactions, Vol. 84, Series D, No. 4, December 1962.

5. F. T. Brown, "A Combined Analytical and Experimental Approach to the Development of Fluid-Jet Amplifiers," to be presented at the Symposium on Fluid Jet Control Devices, ASME Winter Annual Meeting, November 26, 1962, and published in the Journal of Basic Engineering.

6. Hiroshi Sato, "The Stability and Transition of Two-Dimensional Jet," Journal of Fluid Mechanics, Vol. 7, Part 1, January 1960.

7. R. C. Chanaud and Alan Powell, "Experiments Concerning the Sound-Sensitive Jet," The Journal of the Acoustical Society of America, Vol. 34, No. 7, July 1962.

8. Hermann Schlichting, Boundary Layer Theory, McGraw-Hill Book Company, Inc., 4th Ed., 1960.

9. S. I. Pai, Fluid Dynamics of Jets, Van Nostrand, 1954.

10. G. Birkhoff and E. H. Zarantonello, Jet, Wakes and Cavities, Academic Press, New York, 1957.

by

Thomas J. Lechner
Martin W. Wambsganss

of

Johnson Service Company

1. Introduction

This paper is concerned with proportional pure fluid amplifiers of the three dimensional type shown in Fig. 1. This type is based on the interaction of two streams: a supply or power stream and a signal or control stream. The principle of operation of such a pure fluid amplifier is a transfer of momentum at the point of intersection of the two streams. The supply stream is deflected by the control stream and a proportionate amount of pressure is collected at the output.

Pure fluid amplifiers of the above mentioned type can be designed to have high pressure gains such as shown in Fig. 2. However, the output impedance of such a device is high and the input

---- NOMENCLATURE ———————————————————————

Dimensional Terms

g, ℓ, r = geometric parameter referred to Fig. 1

p = pressure, psig

q = volumetric flow (referred to atmospheric pressure), in^3/min.

u = power, ft.lb./sec.

impedance low making it difficult to directly cascade the stages.
The stages can be successfully cascaded with the use of isolation
relays. However, in pure fluid systems there is a definite need
for intermediate stages of impedance matching to eliminate the
need for isolation relays. This is the subject considered in this
paper.

────── NOMENCLATURE ─── ──── ──────────────── ── ───

Subscripts   refer to

     s   signal

     p   supply

     o   output

     r   recovery (no signal)

     c   cutoff (no output)

<u>Nondimensional</u> <u>Ratios</u>

$$R_o = r_o/r_p \qquad\qquad U_o = u_o/u_p$$

$$R_s = r_s/r_p \qquad\qquad U_s = u_s/u_p$$

$$L = \ell/r_p \qquad\qquad\quad Q_o = q_o/q_p$$

$$G = g/r_p \qquad\qquad\quad Q_s = q_s/q_p$$

$$U_r = U_o\Big|_{u_s = o} = \text{power recovery ratio}$$

$$U_c = U_s\Big|_{u_o = o} = \text{power cutoff ratio}$$

$$Q_r = Q_o\Big|_{q_s = o} = \text{flow recovery ratio}$$

$$Q_c = Q_s\Big|_{q_o = o} = \text{flow cutoff ratio}$$

$$R^* = R_s/R_c = r_s/r_o$$

$$U^* = U_r/U_c = \text{overall power ratio}$$

$$Q^* = Q_r/Q_c = \text{overall flow ratio}$$

382

In cascading these stages, maximum power transfer between each stage and the following one is desired. Maximum power transfer is obtained when the output impedance is equal to the load impedance or, in this case, equal to the input impedance of the following stage. Therefore, the stages will be cascaded by making the output orifice integral with the input orifice of the next stage as shown in Fig. 3.

2. Overall Power Ratio

In a cascaded unit, the output of any one stage is the signal for the next stage. The signal stream does work in deflecting the supply stream. Therefore, the power represented by the kinetic energy of the streams is pertinent. The power represented by the kinetic energy of a stream issuing from an orifice can be expressed as

$$(2.1) \qquad u = \frac{w v^2}{2} \ .$$

Since only pressures of 20 psig or less will be considered, the fluid is assumed to be incompressible. Equation (2.1) can then be written

$$(2.2) \qquad u = \frac{\rho}{2 A^2} q^3 ,$$

or,

$$(2.3) \qquad u \propto q^3 / r^4 .$$

The power ratio from signal to output can now be expressed as

$$(2.4) \qquad U = \frac{u_o}{u_s} = \left(\frac{r_s}{r_o}\right)^4 \left(\frac{q_o}{q_s}\right)^3 = \frac{U_o}{U_s} \ .$$

Since the cascading of these stages is being studied, only their overall power ratios need be considered. The overall power ratio

383

is the ratio of output power with no signal $\left(U_o\Big|_{u_s\,=\,o} = U_r\right)$

to the signal power required to drive the output to zero $\left(U_s\Big|_{\mu_o\,=\,o} = U_c\right)$. The overall power ratio for a particular stage

can be written as

(2.5) $U^* = U_r/U_c$,

i.e., the ratio of the power recovery to power cutoff ratios.

3. Power Recovery Ratio

The power recovery ratio is defined as the ratio of output power with no signal to supply power, i.e.,

(3.1) $U_r = U_o\Big|_{u_s\,=\,o} = \dfrac{Q_r^{\,3}}{R_o^{\,4}}$.

The flow recovery ratio, Q_r, is a function of the geometric ratios, R_o and G.

To determine Q_r as a function of R_o and G, a test fixture was designed and built. The test fixture consisted of a pair of opposing, interchangeable orifices with a variable gap. Various combinations of the ratios R_o and G were used and the flow recovery ratios recorded and plotted versus G in Fig. 4. It was found that the flow recovery ratio was somewhat independent of the supply pressure. From Fig. 4 it can be seen that for the ranges

(3.2) $5 \leq G \leq 22$,

and

(3.3) $0.8 \leq R_o \leq 1.6$,

384

the flow recovery curves can be approximated by straight lines. This approximation was made and it was possible to derive the following empirical equation for the flow recovery ratio as a function of R_o and G,

(3.4) $Q_r = 1.344 R_o - 0.0257G - 0.292$.

Based on experience, the stages are designed such that the distance from the supply wall to the center line of the signal orifice is equal to $2r_s$. Therefore, the following relationship can be written for G

(3.5) $G = L + 2R_s$.

Substituting (3.5) in (3.4) yields

(3.6) $Q_r = 1.344R_o - 0.055R_s - 0.0275L - 0.292$.

Further substituting (3.6) in (3.1) gives an expression for the power recovery ratio as a function of the geometry,

(3.7) $U_r = \left(\dfrac{1}{R_o}\right)^4 (1.344R_o - 0.055R_s - 0.0275L - 0.292)^3$.

4. <u>Power Cutoff Ratio</u>

In order to determine the power cutoff ratio it was first necessary to find the relationship between the signal flow (q_s) and the flow from the power jet (q_p). From this relationship the power cutoff ratio U_c was found from:

(4.1) $U_c = \left(\dfrac{r_p}{r_s}\right)^4 \left(\dfrac{q_s}{q_\rho}\right)^3 = \dfrac{Q_c^3}{R_s^4}$.

The analysis of Q_c was divided into two parts. The first part relating the cutoff conditions with the deflecting angle φ, and the stream tube radius η. The second part relating φ and η with the

385

two flows, q_s and q_p, and the geometric parameters, using the
momentum exchange equation.

4a. The pressure distribution equations

Consider a stream tube of radius η, approaching a flat wall
at an angle Φ with the normal to the wall. Assume that the velocity
vectors in the stream are all parallel previous to their being in-
fluenced by the wall. The force exerted on the wall by the stream
tube is a maximum at the point where the axis of the tube intersects
the wall, and it decreases in all directions from that point.

Now consider the three dimensional space with the x, y, axis
set up at the intersection of the wall and the axis of the stream
tube, and the z axis as a measure of the pressure exerted at any
point. The loci of constant pressures are continuous closed paths
regardless of the angle Φ. If $\infty = 0$, the distribution would be
axially symmetrical about the z axis, and the loci of constant
pressures would be circular. Therefore, it seems quite logical
that these loci of constant pressures be described by ellipses for
all values of Φ, where the ellipses become circles in the special
case when $\infty = 0$.

We now define the boundary of the three dimensional space as
the loci of pressures where the pressure $p = \epsilon\, p_m$ (where p_m is
the maximum pressure exerted in that space, and ϵ is a very small
number).

If, as the angle ∞ is changed, the intersection of the center
of the stream tube and the wall always occurs at $x = 0$, then the
equation that describes the boundary ellipse can be given by:

386

$$(4a.1) \qquad 1 = \frac{x^2}{a^2(\eta, \varphi)} + \frac{[y+\Delta(\eta, \varphi)]^2}{b^2(\eta, \varphi)}$$

where: $\Delta(\eta, \varphi)$ = distance from the point of maximum pressure to the center of the ellipse

$a(\eta, \varphi)$, $b(\eta, \varphi)$ = the half widths of the minor and major axes respectively.

As φ is increased from zero the ellipse that describes the boundary elongates in the direction of φ (and thus in the direction of y), and contracts along the normal to the path of φ (x exis), so that the area enclosed by a particular locus would appear unchanged. On this basis it is proposed that the area enclosed by any boundary is constant with respect to φ. If this area is chosen as α^2 times the area of the stream tube, i.e. $\alpha^2 \pi \eta^2$, equation (4a.1) becomes:

$$(4a.2) \qquad \frac{\alpha^2 \eta^2}{a^2(\eta, \varphi)} x^2 + \frac{a^2(\eta, \varphi)}{\alpha^2 \eta^2} [y+\Delta(\eta, \varphi)]^2 = \alpha^2 \eta^2$$

Since a is the half width of the minor axis normal to the plane of the angle φ, it can be seen that:

when $\qquad \varphi = 0 \qquad a = \alpha \eta$

and when $\quad \varphi = \dfrac{\pi}{2} \qquad a = \eta$

so that a could depend on φ in the following manner:

$$(4a.3) \qquad a = \eta[1+(\alpha-1)\cos\varphi]$$

Thus the boundary can be described by

$$(4a.4) \qquad \left(\frac{x}{\sigma(\varphi)}\right)^2 + \left(\sigma(\varphi)\left\{y+\Delta(\eta, \varphi)\right\}\right)^2 = [\alpha\eta]^2$$

where $\qquad \sigma(\varphi) = \dfrac{1+(\alpha-1)\cos\varphi}{\alpha}$

Since the point of maximum pressure appears in the center of the circular distribution when $\varphi = 0$, and shifts very much like the major focus as ω is increased, it was assumed that they were coincidental. Thus

(4a.5) $\Delta(\eta,\varphi) = \sqrt{b^2 - a^2} = \frac{\alpha\eta}{\sigma(\omega)}\sqrt{1 - \sigma^4(\omega)}$

Thus (4a.4) becomes:

(4a.6) $\left(\frac{x}{\sigma(\omega)}\right)^2 + \left(\sigma(\omega)\left\{y + \frac{\alpha\eta}{\sigma(\varphi)}\sqrt{1 - \sigma^4(\omega)}\right\}\right)^2 = (\alpha\eta)^2$

Since the cutoff flow ratio (Q_c) is defined as that ratio that causes non-inclusive tangency between the output orifice and the ellipse locus, it is possible to find the relationship between η and ω. From Fig. 5, it can be seen that:

$\ell \tan\omega - r_0 = b - \Delta(\eta,\varphi)$

(4a.7) $= \frac{\alpha\eta}{\sigma(\omega)}\left[1 - \sqrt{1 - \sigma^4(\varphi)}\right]$

where $\sigma(\varphi) = \frac{1 + (\alpha-1)\cos\omega}{\alpha}$.

Thus the deflecting angle ω is related to the stream tube radius η.

4b. The momentum exchange equations

In order to form the equations relating η and ω to the applied pressures and geometric parameters, three important assumptions were necessary. The first two were based on density photographs taken at the University of Wisconsin. The third is somewhat of a restriction on the geometry. They are:

  a. The pressure in the mixing region of the gap is everywhere atmospheric. The photos showed that this was approximately true as long as the power and signal streams were below 30 psig.

388

b. The two streams merge so that the resulting stream contains the sum of the masses of the individual streams. The photos showed a definite union of the two streams.

c. The distance from each of the orifices to the point of contact should be short enough so that the velocity vectors can be assumed parallel and unretarded before contact with the other stream.

Thus if $q_s/\pi r_s^2$ is the velocity of the signal stream, the rate of momentum acting on the control volume due to the signal stream is:

$$\text{(4b.1)} \qquad \frac{dM_s}{dt} = \rho \, \frac{q_s^2}{\pi r_s^2}$$

If $q_p/\pi r_p^2$ is the velocity of the supply stream, its rate of momentum is:

$$\text{(4b.2)} \qquad \frac{dM_p}{dt} = \rho \, \frac{q_p^2}{\pi r_p^2}$$

Since the signal stream is perpendicular to the power stream, the total momentum in the direction of the power stream becomes:

$$\text{(4b.3)} \qquad \frac{dM_T}{dt} = \frac{dM_p}{dt} + j \, \frac{dM_s}{dt}$$

Since the resultant flow is in the direction of the momentum it can be shown that:

$$\text{(4b.4)} \qquad \varpi = \arctan \left[\frac{r_p}{r_s} \, \frac{q_s}{q_p} \right]^2$$

$$= \arctan \, \frac{Q_c}{R_s}^2$$

Since the absolute value of the momentum given in equation (4b.3) is:

$$(4b.5) \qquad \left|\frac{dM_T}{dt}\right| = \frac{\rho(q_s + q_p)}{\pi\eta^2}$$

It can further be shown that:

$$(4b.6) \qquad \eta = r_s\left[\frac{R_s(1 + Q_c)}{[Q_c^4 + R_s^4]^{1/4}}\right]$$

Thus equations (4b.4) and (4b.6) relate η and m to the flows, q_s and q_n, and the geometric parameters.

4c. Flow cutoff ratio

In order to determine Q_c, equations (4b.4) and (4b.6) were substituted into (4a.7), and the following equation resulted:

$$(4c.1) \qquad \frac{\alpha^2\delta^{1/2}}{[1+(\alpha-1)\delta]}\sqrt{1-\left(\frac{1+(\alpha-1)\delta}{\alpha}\right)^4} = \frac{L\left(\frac{Q_c}{R_s}\right)^2 - R_0}{1+Q_c}$$

where

$$\delta = \frac{1}{\sqrt{1+\left(\frac{Q_c}{R_s}\right)^4}}$$

For various values of α, the right side of (4c.1) is plotted versus Q_c/R_s in Fig. 6. Several power stages were designed and built in order to choose a value for α. Experimental points obtained from these stages are also shown in Fig. 6, whereby $\alpha = 4.0$ was chosen. To obtain the experimental points an ϵ of 0.03 was arbitrarily chosen.

For all of the power stages designed, the value of Q_c/R_s was always in the range

$$(4c.2) \qquad 0.30 \leq \frac{Q_c}{R_s} \leq 1.0$$

390

For the range given in (4c.2), (4c.1) can be approximated by the simplified equation:

(4c.3)
$$\frac{L\left(\dfrac{Q_c}{R_s}\right)^2 - R_o}{(1+Q_c)} = 4.7 - 3.92 \frac{Q_c}{R_s}$$

(see dotted line in Fig. 6).

Solving (4c.3) for $1/Q_c$,

(4c.4)
$$\frac{1}{Q_c} = \gamma \left(-\beta + \sqrt{\beta^2 + 3.92 R_s + L} \right)$$

where
$$\gamma = \frac{1}{R_s \sqrt{4.7 + R_o}} \ ,$$

$$\beta = \frac{4.7 R_s - 3.92}{2 \sqrt{4.7 + R_o}}$$

From equation (4c.4) the power cutoff ratio can be given as:

(4c.5)
$$\frac{1}{U_c} = \frac{R_s^4}{Q_c^3} = R_s^4 \left[\gamma \left(-\beta + \sqrt{\beta^2 + 3.92 R_s + L} \right) \right]^3$$

Thus the power cutoff ratio has been determined as a function of the geometric parameters.

5. Impedance Matching for Optimum Power Transfer

Expressions have been derived for U_r and U_c as functions of the geometry; (3.7) and (4c.5) respectively. Substituting (3.7) and (4c.5) in (2.5) yields, for the overall power ratio,

(5.1)
$$U^* = [R^*]^4 [0.0275(2\lambda - L)\gamma(-\beta + \sqrt{\beta^2 + 3.92 R_s + L}\ )]^3$$

where,
$$\lambda = 24.429 R_o - R_s - 5.30,$$

$$\beta = \frac{4.7 R_s - 3.92}{2\sqrt{4.7 + R_o}} \ ,$$

3,1

$$\gamma = \frac{1}{R_s \sqrt{4.7 + R_o}} \ .$$

The overall power ratio as given by (5.1) is a function of three geometric ratios; R_o, R_s, and L. A typical set of overall power ratio curves can be obtained by letting R_o equal R_s and plotting U^* versus L for various values of the radius ratios; see Fig. 7. Several power stages were designed and built to experimentally obtain a particular power ratio curve and check the derived equation. These stages were designed for $R_o = R_s = 1.25$ with the experimental points shown on Fig. 7.

From Fig. 7 it can be seen that the overall power ratio curves exhibit maximums. The optimum values of the length ratio, L, at which these maximums occur can be obtained from (5.1) by taking the partial derivative of U^* with respect to L, setting it equal to zero, and solving for L_{opt}. This yields the following relationship for L_{opt}.

$$(5.2) \qquad L_{opt.} = \frac{2}{3} \left[\lambda - \frac{2}{3} \beta^2 + 3.92 R_s + \sqrt{\frac{2}{3} \beta^2 \left(\lambda + \frac{2}{3} \beta^2 + \frac{3.92}{2} R_s \right)} \right].$$

It should be noted that the optimum length ratio to give a maximum overall power ratio is also the length ratio to give a maximum overall flow ratio.

In Fig. 8, $L_{opt.}$ is plotted versus R_s for constant values of the ratios, R_o and R^*. Thus, for given values of the radius ratios, R_s and R_o, the length ratio to give a maximum overall power ratio can be read from Fig. 8.

Substituting (5.2) into (5.1) gives an equation for the overall power ratio optimized with respect to the length ratio. Further optimizing, with respect to either R_o or R_s yields expressions too complicated to handle.

392

The equation for the overall power ratio optimized with respect to the length ratio is now a function of only two variables, R_o and R_s. Therefore, the overall power ratio optimized with respect to L can be plotted versus R_s for constant value of R_o and R^* as in Fig. 9. From Fig. 9 it can be seen that there are no optimum values of radius ratios within the range for which the equations were derived.

6. Example Problem

Given two amplifier stages of mismatched impedance, it is desired to design the intermediate buffer stage(s). These stages are cascaded by making the output orifice of one integral with the signal orifice of the following one.

The given amplifier stages are shown in Fig. 10. The maximum available output flow from stage (1) is c. The signal flow required by stage (2) to obtain cutoff is 1.1c. Therefore, the buffer stage(s) has the following requirements:

$$R_b{}^* = \frac{r_{o1}}{r_{s2}} = \frac{1.1k}{k} = 1.1,$$

and

$$Q_b{}^* = \frac{q_{s2}}{q_{o1}} = \frac{1.1c}{c} = 1.1.$$

The overall power ratio required is

$$U_b{}^* = R_b{}^{*4} Q_b{}^{*3} = 1.61.$$

With $R_b{}^* = 1.1$ and $U_b{}^* = 1.61$ enter Fig. 9. The curve of Fig. 9 is satisfied when $R_{sb} = 1.25$. Therefore, one buffer stage is sufficient. To determine the geometry of the buffer stage enter Fig. 8 with $R_b{}^* = 1.1$ and $R_{sb} = 1.25$ and read

$$L_{opt} = 11.8$$

393

The remaining geometry is determined as

$$R_{sb} = 1.25 = \frac{r_{sb}}{r_{pb}} = \frac{r_{o1}}{r_{pb}} ,$$

$$r_{pb} = \frac{1.1k}{1.25} ;$$

and
$$G_b = L_b + 2R_{sb},$$

$$G_b = 11.8 + 2(1.25)$$

$$g = r_{pb}G = 13.68k.$$

The supply pressure, p_{pb}, required for the buffer stage can be determined knowing r_{pb} and q_{pb}. q_{pb} is deduced with the aid of Fig. 4.

If the overall power ratio required by the buffer stage lies outside the field of Fig. 9, the need for more than one stage is indicated. Thus, assuming the ranges for which the equations were derived to be the limits of physical realizability, the minimum number of buffer stages can be determined.

7. Concluding Remarks

It should be pointed out that the aim of this paper is to present a method of approach, rather than an exacting analysis. The equations that represent the flow ratios are only approximate but the results give direction and insight as to the compatibility of pure fluid devices.

It should be noted that while restrictions were placed on the geometric parameters, (i.e., $5 \leq G \leq 22$, $0.5 \leq R_s \leq 2.0$, etc.) these restrictions do not contradict the physically realizable range. If the equations for the flow ratios were improved these limits could be increased to cover almost any range that would be desired.

394
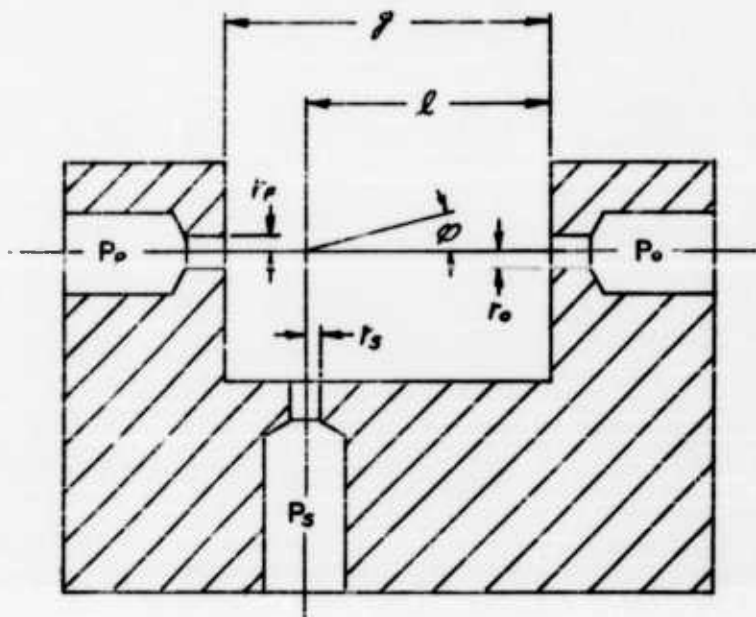
PROPORTIONED PURE FLUID AMPLIFIER

FIGURE I

HIGH GAIN PRESSURE STAGE
FIGURE 2
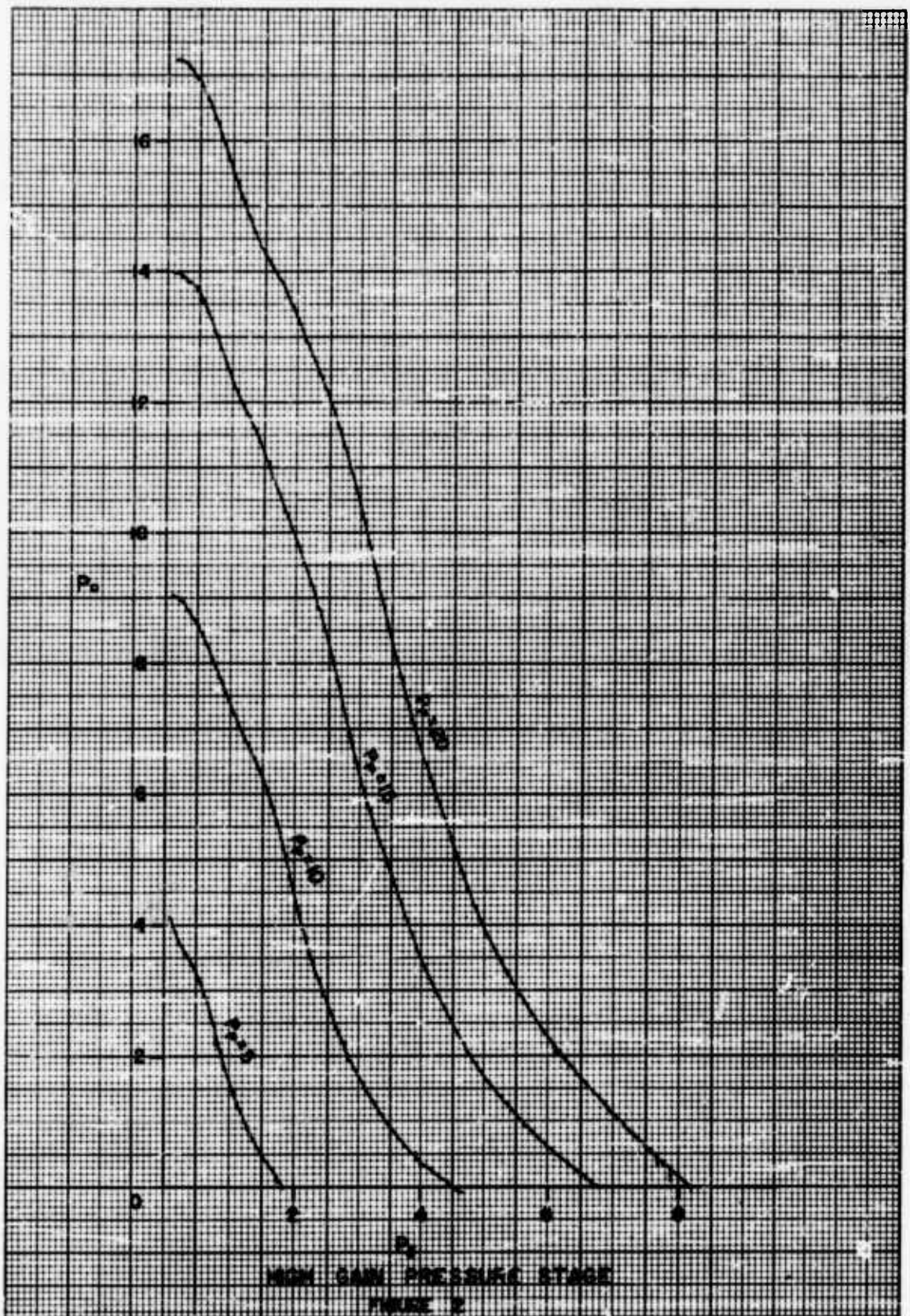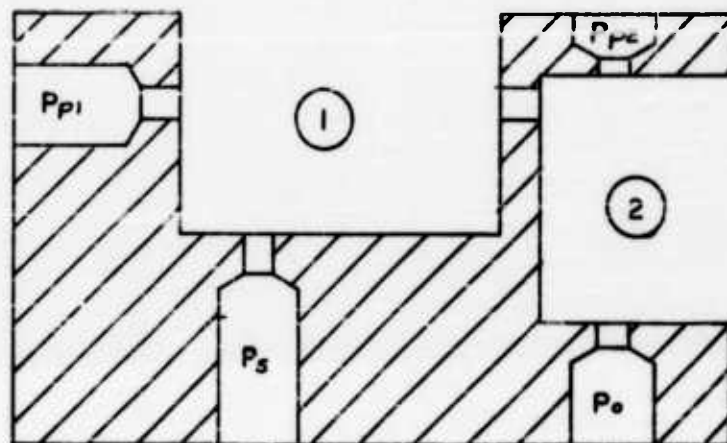
TWO STAGES CASCADED

FIGURE 3
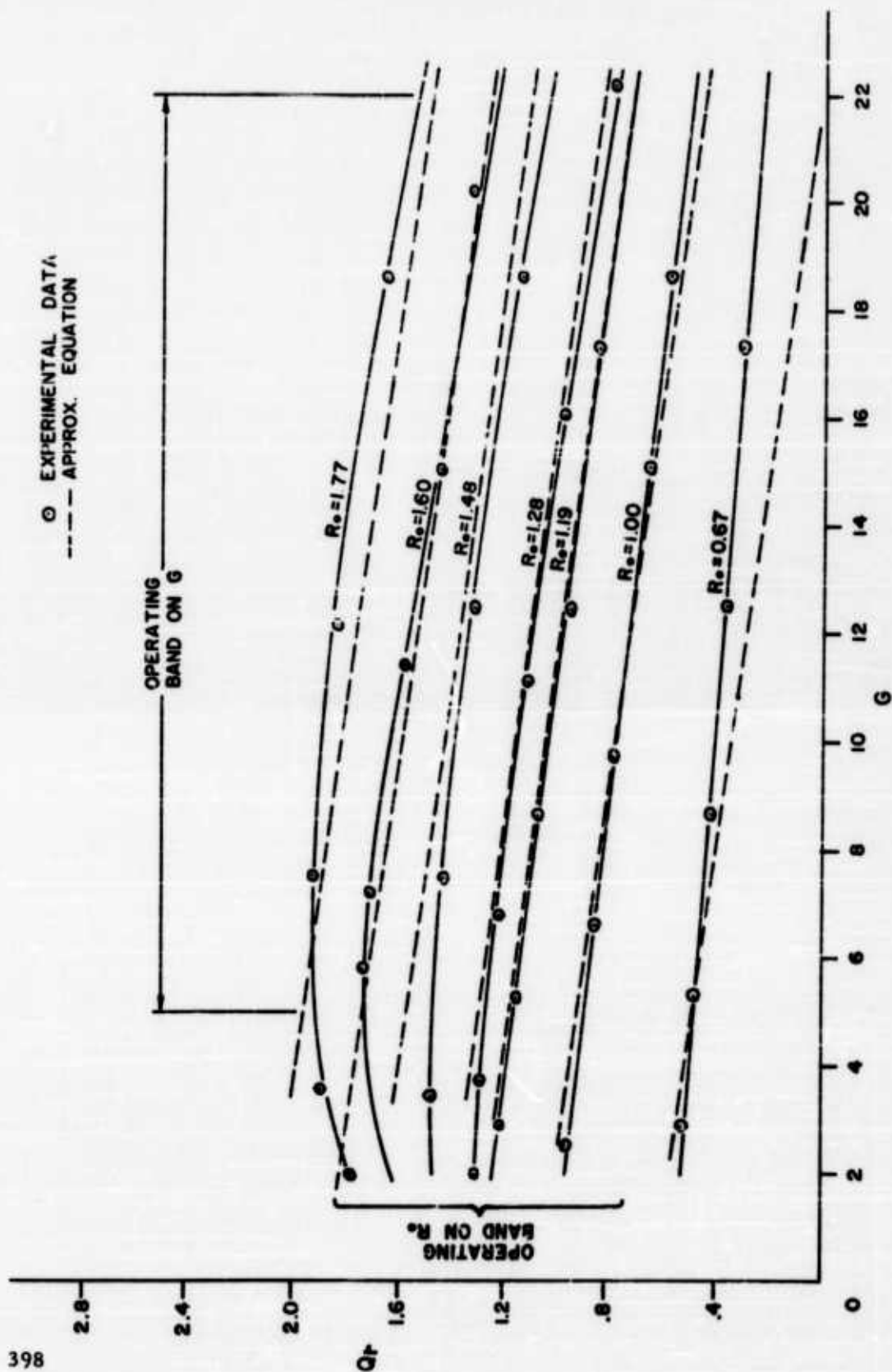
FLOW RECOVERY RATIO

FIGURE 4

398
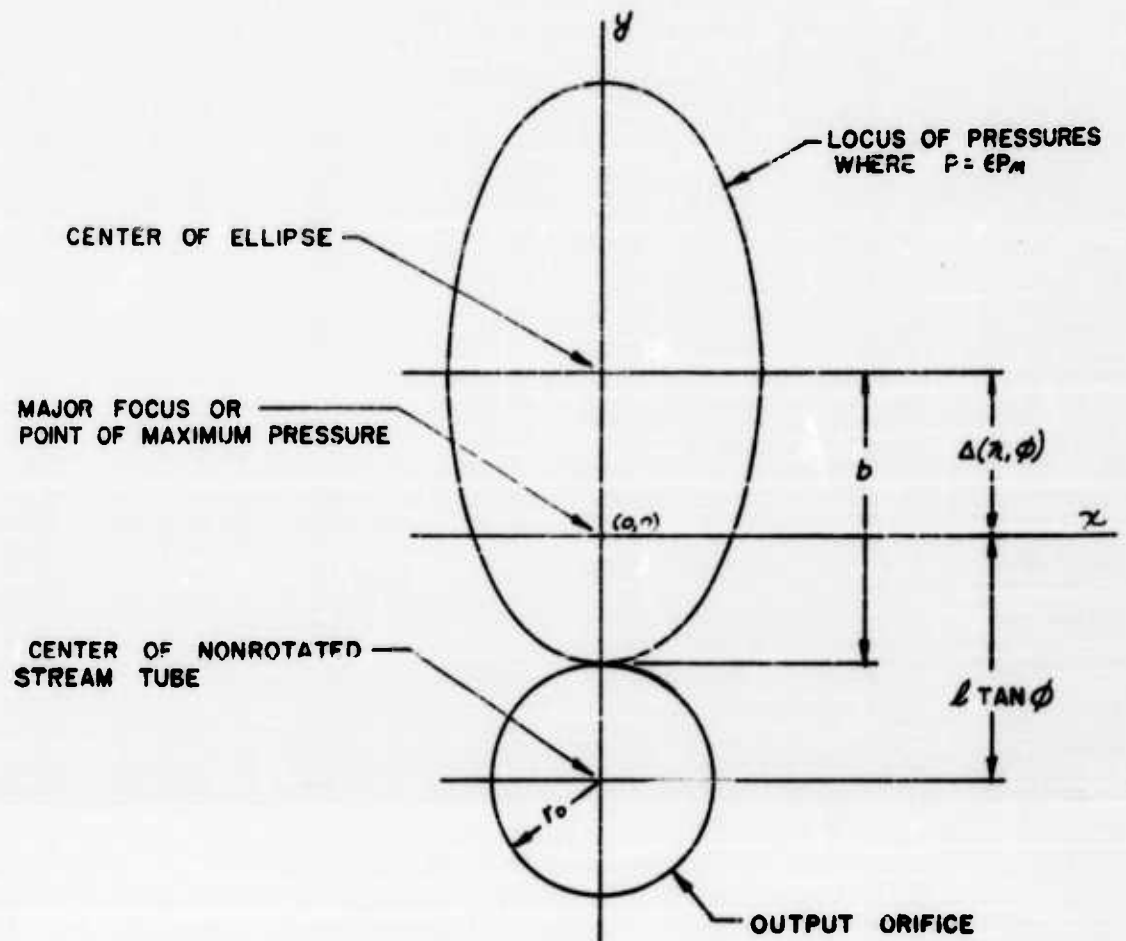
PRESSURE DISTRIBUTION DIAGRAM

FIGURE 5

399

FIGURE 6

400

OVERALL POWER RATIO

FIGURE 7

401
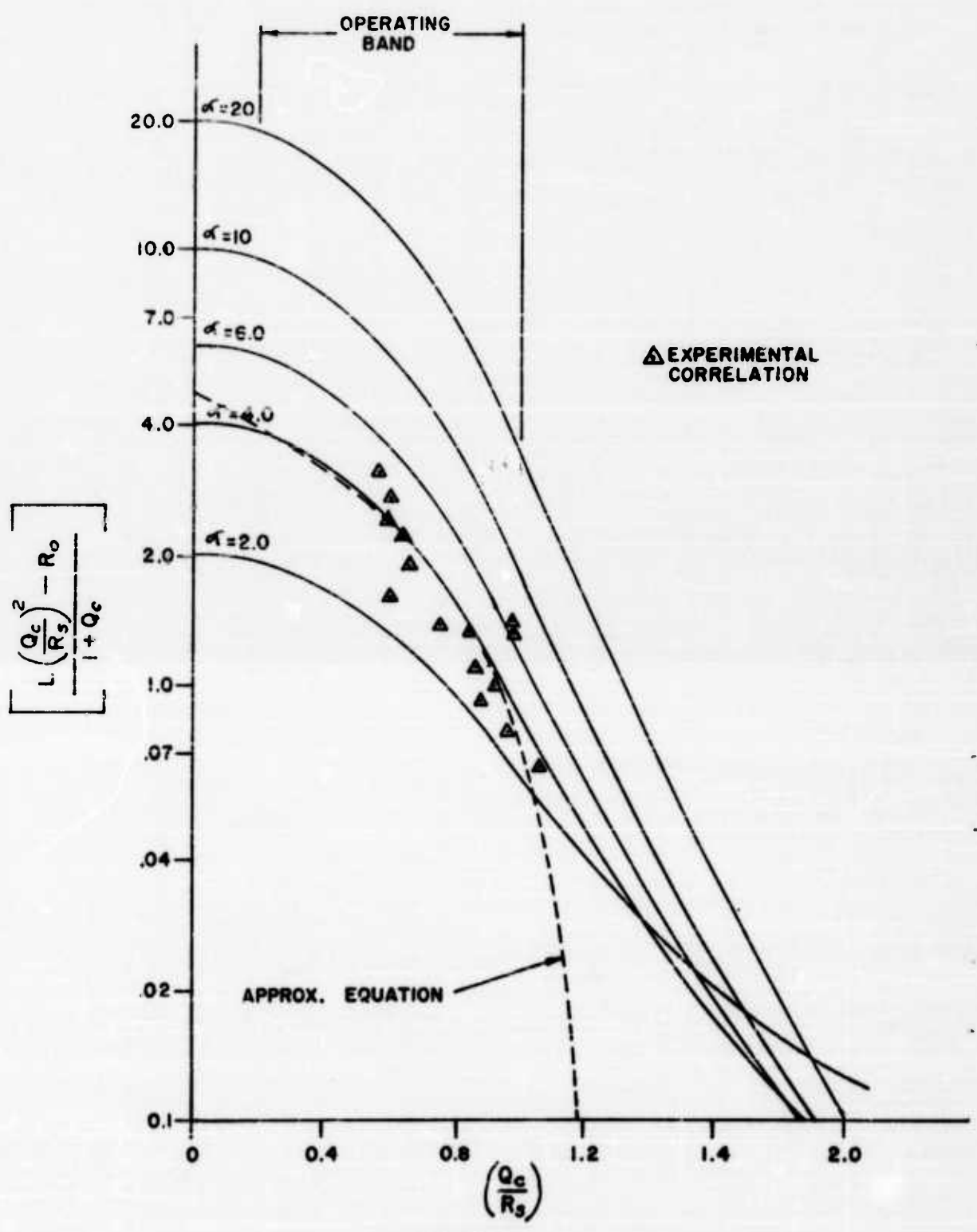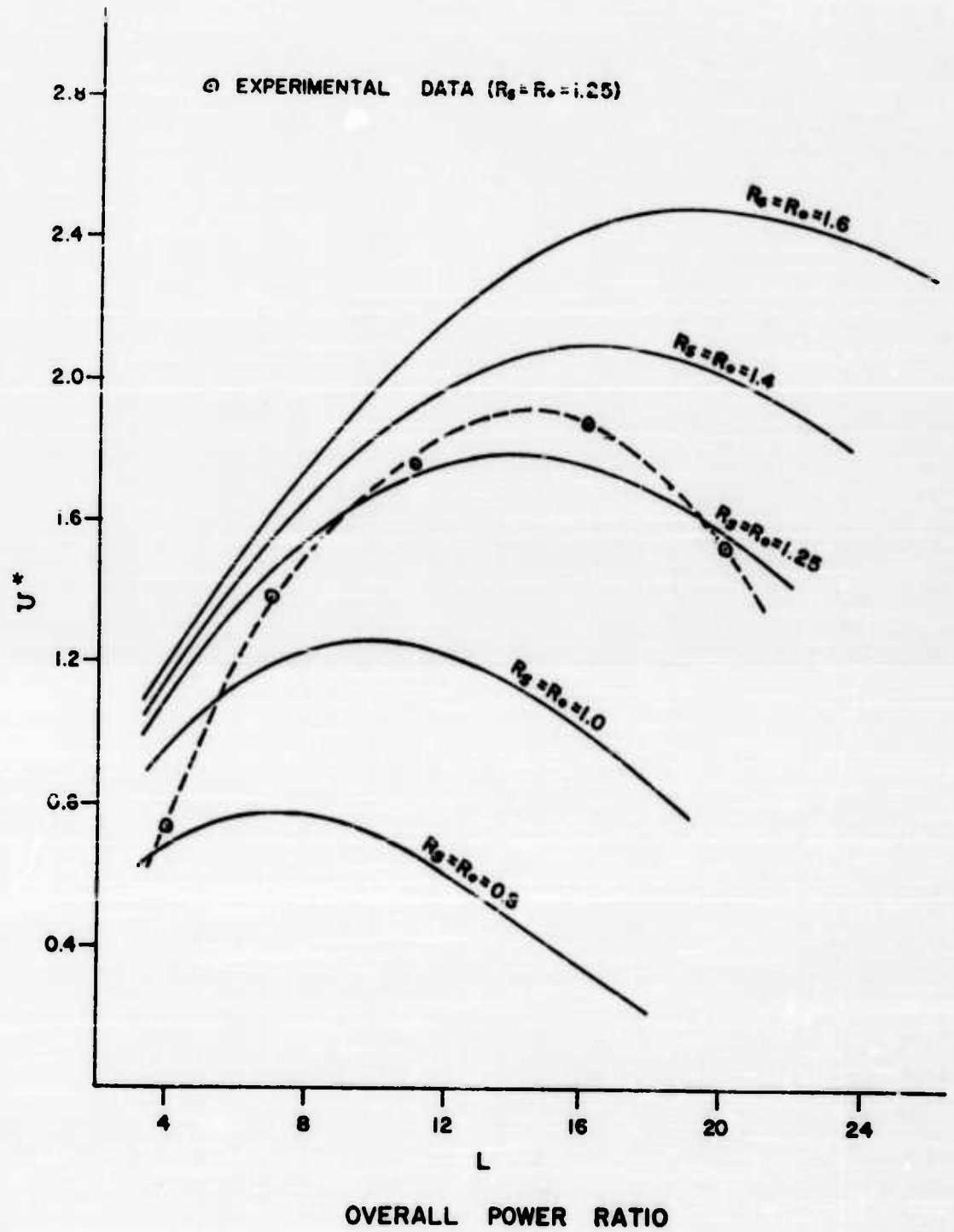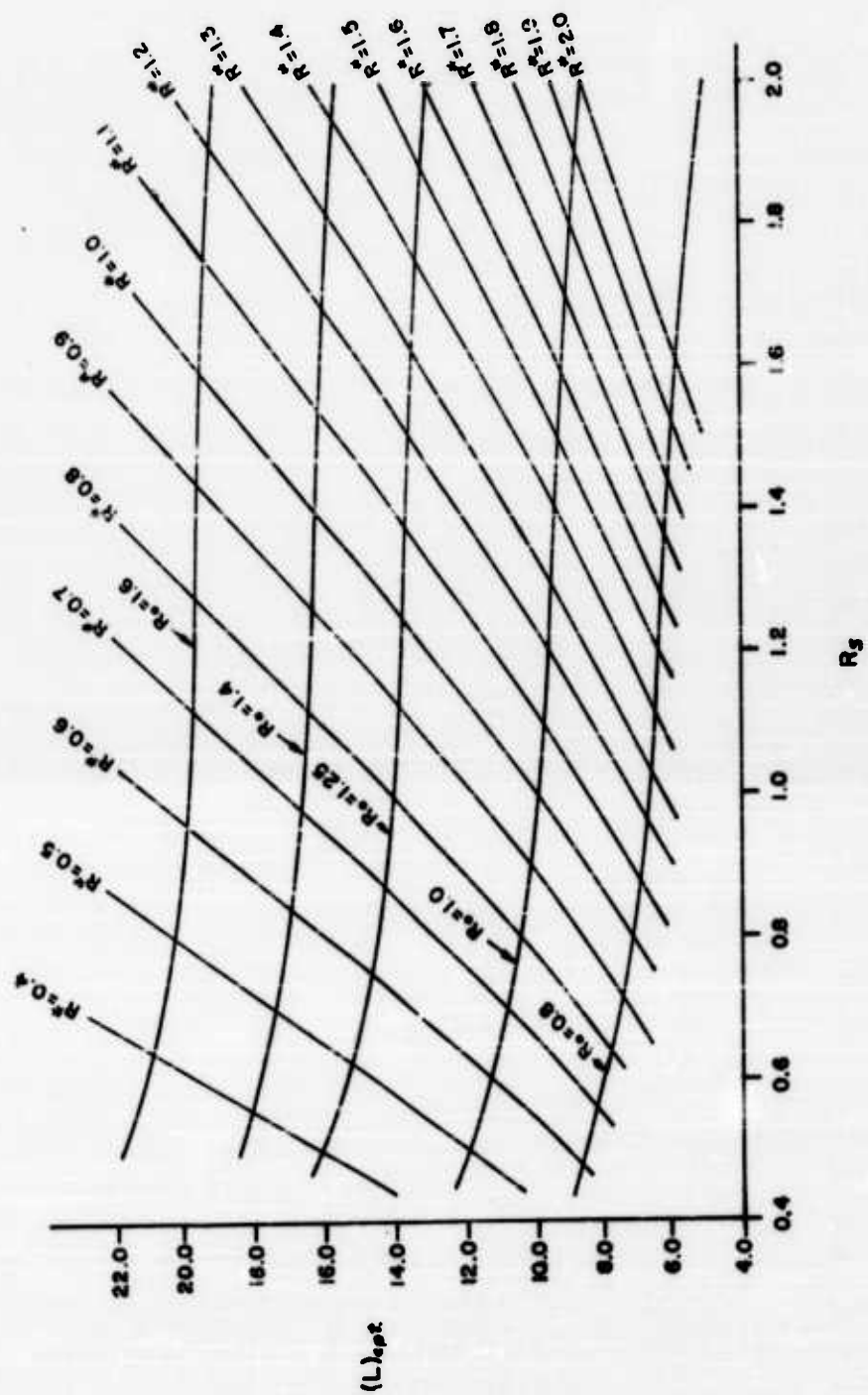
OPTIMUM LENGTH RATIO

FIGURE 8
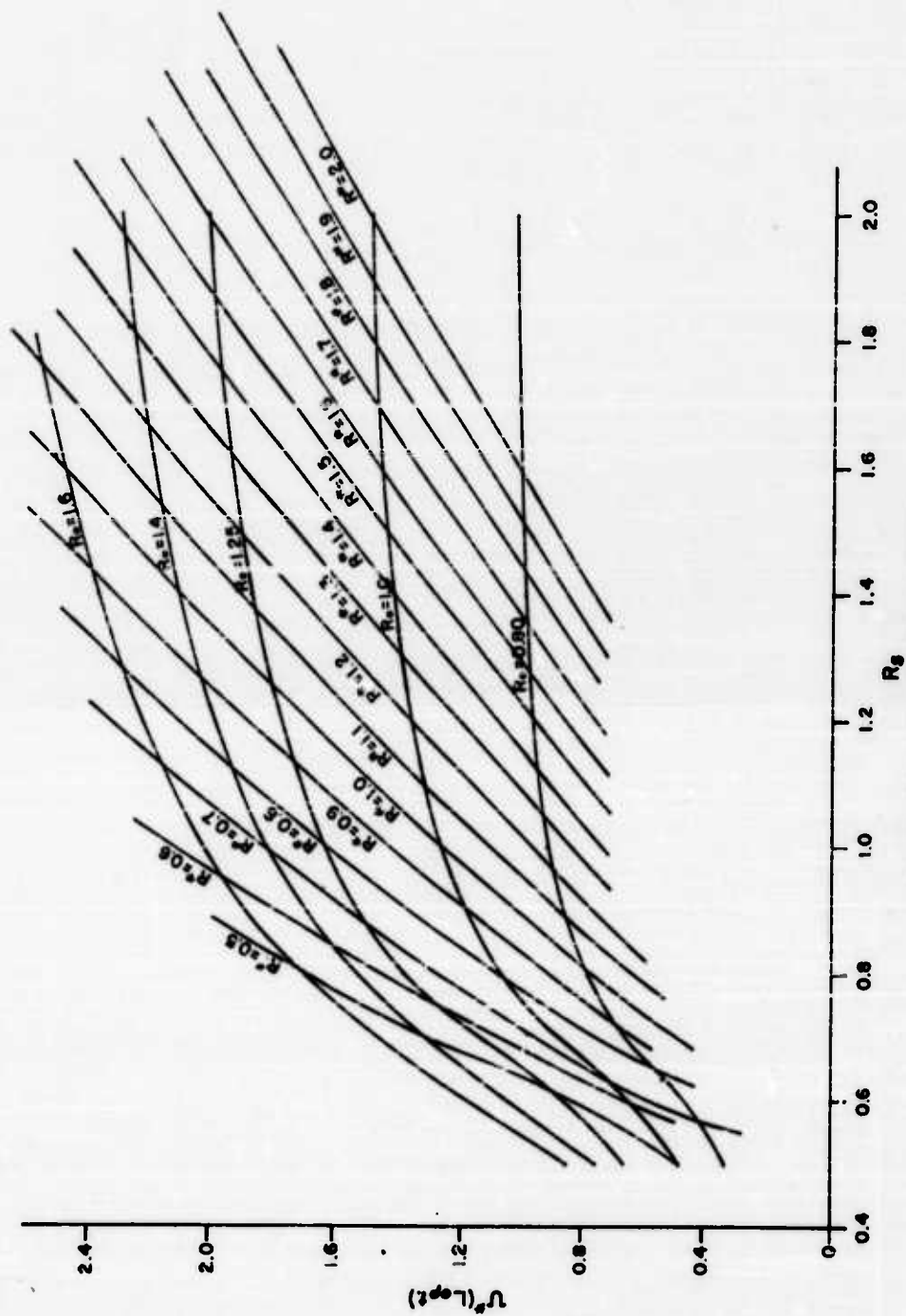
IMPEDANCE MATCHING CURVES
FIGURE 9

STAGE I

$2r_o = 2.2K$

STAGE II

$2r_s = 2K$
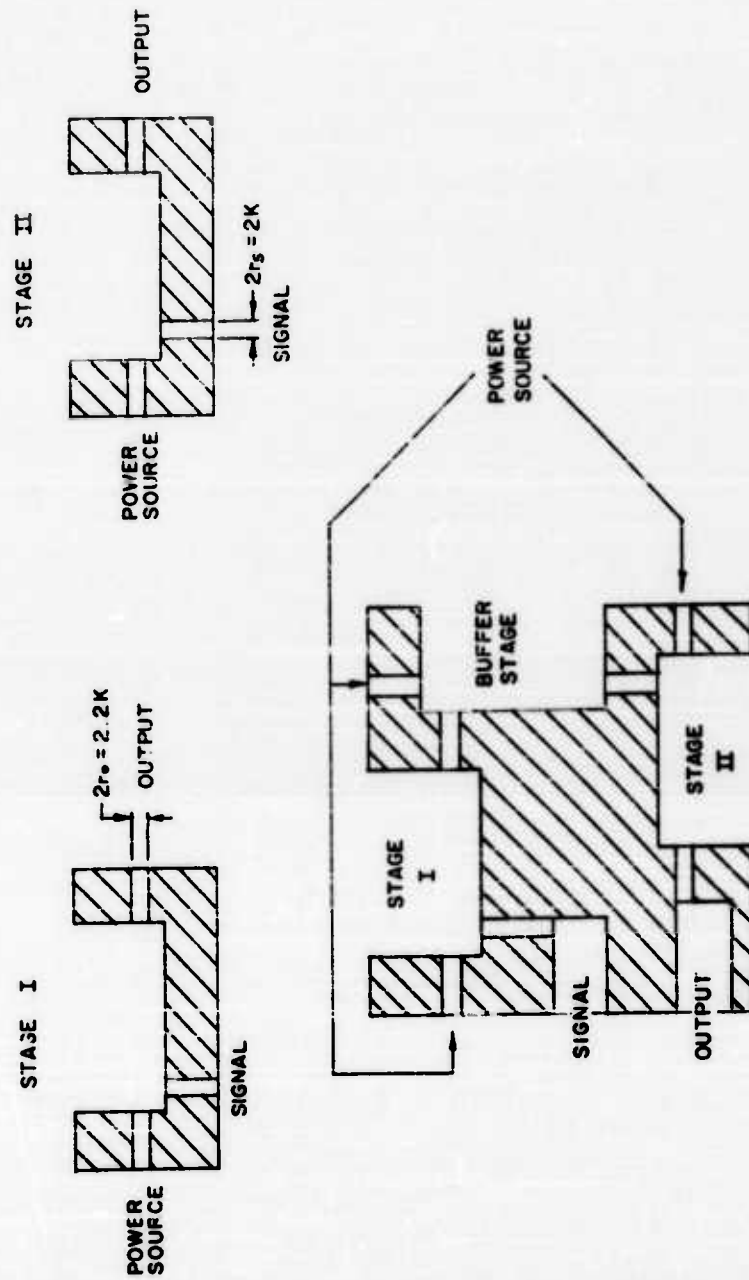
BUFFER STAGING

FIGURE 10

404

PURE FLUID DIGITAL LOGIC WITH A SINGLE SWITCHING ELEMENT

by

Peter Bauer

of

'Bowles Engineering Corporation

ABSTRACT

The advent of pure fluid amplifiers has introduced the question of economy in the development, design, manufacture, and test of pure fluid circuits and systems. The principles of conventional electronic logic design (such as "NOR" logic) were employed as the basis for the development of one universal digital element to serve a multitude of logic functions, singly and in combinations. Definite and conclusive evidence was desired to prove the objective not only feasible but practical as well. With this aim in mind, no particular attempt was made to optimize the performance of the element alone.

Thoughts on the selection of the kind of element used in this study are discussed, and preliminary specifications, based on these, are given. The design and operation of the fluid element selected is described, and pertinent performance characteristics are presented. The principles on which circuit and circuit assembly design were based are discussed and examples of the main logic functions performed by this element, when used in digital circuits, are given. Circuits which were tested are described together with element interconnection characteristics obtained. Some results of in-circuit measurements, steady state as well as transient, are given. Conclusions are drawn from characteristics. The breadboard circuit assembly, developed during this program, performing the principal logic operations including amplification, inversion, "OR", "NOR", and "AND" gating, is described. Fabrication techniques used and later advances made are mentioned.

The feasibility as well as practicability of employing one fluid element to provide most of the basic logic functions needed in digital systems is demonstrated and the direction of future development is indicated.

The advent of pure fluid amplifiers has introduced the question of economy in the development, design, manufacture, test, and maintenance of pure fluid elements and systems. A survey of conventional digital logic and logic design methods on one hand, and an evaluation of possible development and manufacturing techniques on the other hand, has shown the need for a standardization of fluid element designs. The program described in this report was initiated to demonstrate that a single digital switching element could be employed to perform a variety of logic functions in digital circuits. Conventional logic design suggested the "NOR" gate as one of the most universally useful elements.

LOGIC

A schematic diagram of a "NOR" gate is shown in Figure 1. It consists of a power stream (P+), two control inputs (C_1 and C_2), and two output lines. This element is stable on one side; if neither C_1 nor C_2 is providing an input signal, the power stream will issue from the "NOR" output. If a control signal is provided by either C_1 or C_2 or both, the power stream will be directed into the other output line for the duration of the control signal and no output will be present at the "NOR" output line.

Figure 2 presents schematics of some of the possible basic uses for the "NOR" gate. The first schematic represents the standard "NOR" gate, the second the standard "OR" gate. The element should be able to serve both functions if the fluid considerations are properly taken into account during design. The corresponding schematics of a "NOT" unit (inverter) and a "RELAY" (amplifier) are also shown. Both use a single control input. The unused output

Fig. 1 "NOR" GATE SCHEMATIC
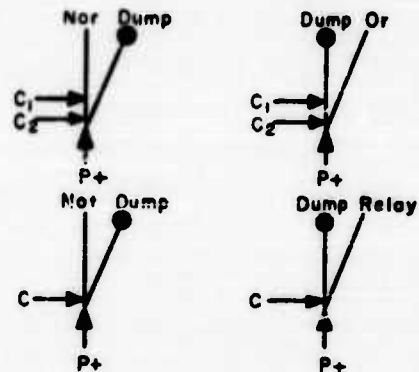
Fig. 2 "NOR" GATE USES (SCHEMATIC)

406

line returns to "DUMP" or "power return" in every case. However, it is possible, by suitable design, to use both outputs simultaneously where the number of elements used must be reduced to the absolute minimum. In this program, the assumption was made to use one output line only for the sake of a simplified design.

DESIGN AIM

The objective of this program was to demonstrate the feasibility of employing a single fluid element to provide a variety of digital functions alone and in combinations. The element design was based on techniques available at the time and no attempt to optimize or improve performance was made. The following general specifications for the fluid element were established to accomplish the objective of the program.

Power consumption:	as low as possible
Size:	as small as possible
Fan-out ability:	one output must be able to control at least two inputs of the same type of element
Control inputs:	at least two
Switching speed:	as high as possible

Air was chosen as the fluid which could be handled easiest. A supply pressure of 1 psig was chosen to insure definite operation and to facilitate measurements without an unnecessarily high power level. The size (20 mil width for power nozzle) was compatible with power consumption requirements and ease of fabrication, handling and measurement. The fan-out ability and the number of inputs required represent the minimum properties to achieve the objective. The switching speed obtained was accepted without reservations.

DESIGN

Figure 3 shows the type of configuration which was chosen and the main paths of fluid. In the absence of a control input signal (C_1, C_2) the power stream (P+) locks onto the left-hand wall and is stable on the side designated

as "NOR". If a signal is provided
by one or both control inputs, the
power stream is deflected into the
other output line designated as
"OR". A small part of the power
stream is diverted into the round
chamber, where it forms a vortex
and provides a negative feedback.
This feedback insures a fast and
definite returning of the power
stream to its stable position (NOR)
when the control signal is discon-
tinued.

Fig. 3 ELEMENT CONFIGURATION

CHARACTERISTICS

Typical steady-state char-
acteristics of the designed element,
reference table I, operating at 1
psig supply pressure and 0 psig
dump pressure, are shown in
Figure 4. The characteristic areas
shown encompass the various
possible operating conditions and
different interconnections.
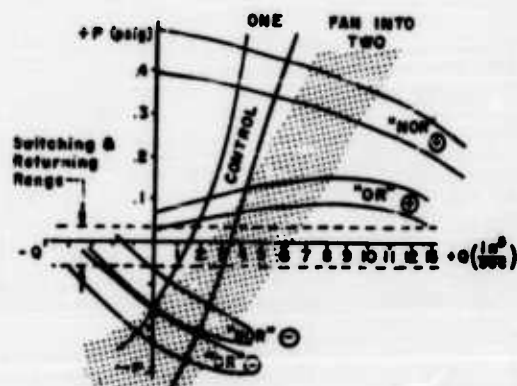
Fig. 4 "NOR" ELEMENT-STEADY STATE
CHARACTERISTICS

The "NOR$_\oplus$" characteristic
shows the pressure/flow relation-
ship at the "NOR" output for
various output loads in the absence
of a control signal, i.e., when the
power stream is feeding the "NOR"
output. The "OR$_\ominus$" characteristic gives the pressure/flow relationship at the
"OR" output for various loads when the element is in the same state, i.e.,
in the absence of a control signal. The "OR$_\oplus$" and the "NOR$_\ominus$" characteristics
are similarly measured when the element is switched to the "OR" output, i.e.,
in the presence of the minimum control signal to cause such switching. The
"CONTROL" input characteristic represents the pressure/flow relationship at
one input for various output conditions when the element is in both states
(and passing through switching and returning conditions). The switching and
returning range (horizontal dashed lines) encompasses switching and returning
parameters under the same varied conditions.

408

The characteristics of the "NOR" and "OR" outputs and the control input characteristic are superimposed. If the output of one unit is connected to another unit's input, the equilibrium conditions are in the coordinates of the common (crossover) areas of the two respective curves. The switching and returning range for the control characteristic lies between any such two conjugate common areas, as required for satisfactory operation. Fanning out from one unit into two control inputs, one obtains the second control characteristic, shown as a dotted region. (This is obtained by doubling all the measured single control input flows.) In the same manner, as before, one can find equilibrium conditions for such an interconnection.

These characteristic curves show whether or not an element will operate satisfactorily within a circuit; they give the fan-out ability, the equilibrium conditions, and many other pertinent data. Furthermore, conclusions as to allowable tolerances and safety margins can be drawn from these curves, as well as some indications about the element's probable transient behavior and its stability.

From general past experience it is known that steady-state characteristics are usually conservative in describing some aspects of the actual operation of fluid elements, such as switching and returning. An element will not switch and return under steady-state control conditions if the controlling switching pressure is less and the controlling returning pressure is more than the characteristic measured values. However, the element may operate satisfactorily when controlled by transients of the same peak amplitude values. Such transient switching characteristics become important when steady-state switching would predict marginal operation under some circuit conditions.

Figure 5 shows characteristic wave forms within a circuit with short interconnecting channels. They were measured with a hot-wire anemometer system developed for such purposes by the Bowles Engineering Corporation (Reference 1). The first picture shows a single pulse of approximately 20 milliseconds duration, the second one a repetitive wave form of 250 pps. Characteristic pulse rise times are of the order of 5 milliseconds, necessarily becoming shorter at higher frequencies, mainly due to the loss in pulse amplitude. The third wave form is the result of a
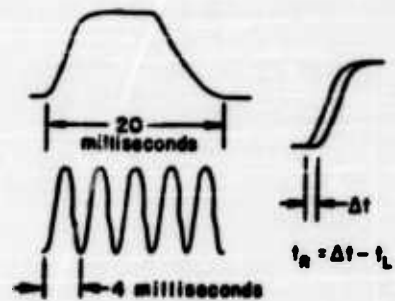
Fig. 5   CHARACTERISTIC WAVE FORMS

switching or signal transfer time measurement. The "Δt" shown is measured between a point just before entering a control input of an element within a circuit and just downstream from the output of the same element. It consists of the signal transport time within the element channels and the actual reduced switching time. If, for simplicity's sake, we define "t_L" as the sonic velocity transport time along the measured average channel lengths between the points of measurement, the reduced switching time ("t_r") is the difference between the measured "Δt" and the calculated sonic transport time ("t_L"). This value for the "NOR" element is approximately 0.5 milliseconds under normal in-circuit conditions.

TABLE I

A summary of characteristics of molded models of the universal element is given below.

Active area	$1/4$ in^2
Depth	0.120 in
Nozzle width	0.020 in
Aspect ratio	6
Power consumption	less than 1 watt
Supply pressure	1 psig
Dump (return) pressure	0 psig
Fan-out ability	2 to 3
Number of control inputs	2
Reduced switching time	approximately 0.5 milliseconds

Besides many different circuit tests made with this designed "NOR" element, a breadboard circuit assembly was constructed. Figure 6 gives the schematic circuit diagram. The various basic logic circuits employed can be seen, and the flexibility of interconnecting "NOR" elements and of interconnecting "NOR" and other elements is clearly demonstrated. The operation of the circuit is monitored electrically by means of two thermistor (TH) flow/no flow indicators (Reference 1) and one pneumatically operated reed switch (RS) and lamp circuit.
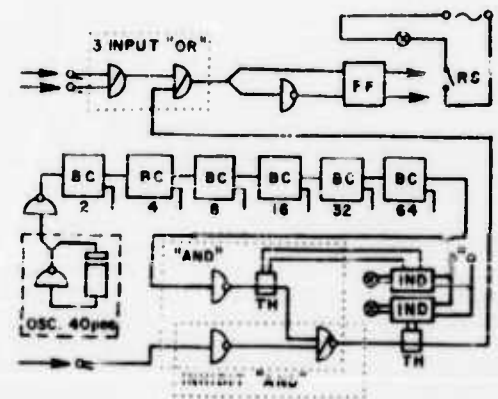
Fig. 6 LOGIC CIRCUIT DIAGRAM

An oscillator (40 pps), consisting of a "NOT" element with a delayed feed-back, drives (through an amplifier inverter) a modular six-stage binary counter (BC), which in turn is feeding one input of a two-input "AND" gate. The second input to this "AND" gate consists of two inverters and one "NOR" gate. The output of this "AND" gate is fed to one input of a 3-input "OR" gate at the top of the diagram. The other two inputs are from a manual pure fluid keyboard to a second "OR" whose output feeds the other input of the same "OR" fed by the "AND" gate at the bottom of the figure. If a signal is provided by any one or more than one of the 3 inputs, the "OR" provides a signal which operates the flip-flop (FF) push pull by dividing and inverting the "OR" gate output.

The pulse rate divided by 64 in the binary counter feeds the "AND" assembly, is gated through it by the signal from the manual actuator and operates the flip-flop and the electrical read-out through the rest of the circuitry. The manual "OR" inputs can, of course, override this pulse transfer. In absence of a signal gated through the "AND" assembly, the manual "OR" inputs can actuate the flip-flop as well. The electrical read-out circuits monitor signal transport and gating in the "AND" circuit. Various uses of the universal "NOR" element can be clearly seen and demonstrated. "NOR", "NOT", "AND", "INHIBIT AND", and "OR" functions are shown.

411

Figure 7 is a photograph of the actual breadboard panel as described. With the exception of the oscillator circuit, the power distribution, and the electrical circuitry, which are located behind the panel, all circuits are as shown in the schematic diagram in Figure 6. The modular binary counter has provision for an electrical read-out at every stage, but it was not used in this case.
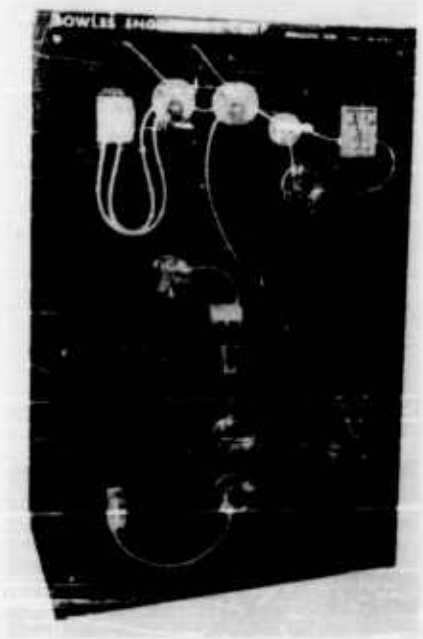
Fig. 7 PNEUMATIC NOR-LOGIC CIRCUITS

Typical examples of other circuits tested are shown in Figure 8. The half-adder, a flip-flop, and leading edge and trailing edge differentiators were constructed using exclusively universal "NOR" elements.

HALF ADDER

FLIP-FLOP

L.E. DIFFERENTIATOR

T.E. DIFFERENTIATOR
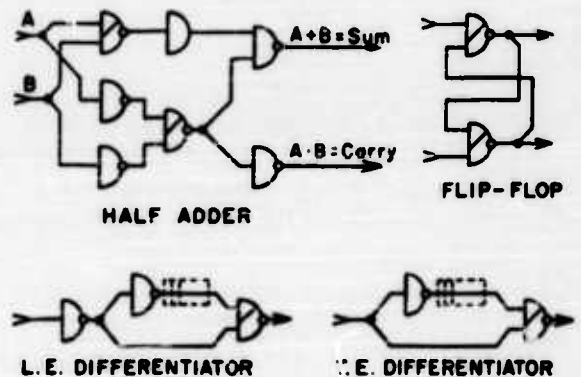
Fig. 8 EXAMPLES OF BASIC CIRCUITS TESTED

FABRICATION

Molding

At this stage it may be pertinent to mention something about the fabrication of the elements. A drawing of the proposed design was scaled up to produce a large master template for use during milling of the element in an

engraving machine. The obtained unit was used as a master for the proprietary "moldform" process to cast the final element from epoxy resin. This low cost fabrication method has proven quite suitable for laboratory purposes and for short or medium production runs. Molded units of several aspect ratios were prepared and tested. The data presented are for the unit described in Table I having an aspect ratio of 6.

Optiform

The silhouette of the universal "NOR" gate was also used to make elements utilizing the proprietary "Optiform Process A" (Reference 2). This is an optical machining process. The large scale silhouette is photographically reduced to the finally required size and optically transferred to photosensitive plastic, which, after processing, provides the finished element.

Comparison tests were made with regard to performance of molded and Optiform models, which had the same aspect ratio (=2). No measureable differences were detected. Also, the optically machined element has been subjected to a life test, being switched at a rate of 33 pulses per second. It has accumulated to date over 70 million switching cycles without a detectable degradation of performance. This test is continuing.

SUMMARY

We have made use of conventional logic experience to simplify logic circuit design with pure fluid devices, by standardizing basic elements to the point of a single universal digital element, the "OR"/"NOR" gate. This element has been designed, made, and replicated. Its characteristics were determined and it was interconnected into various basic logic circuits. The feasibility as well as the practicability of such a scheme was proven. Improved units and circuits using these elements are being designed.

REFERENCES

1. Humphrey, R. I., Metzger, E. E.: Instrumentation for Research and Development in Pure Fluid Systems. Paper presented at DOFL Fluid Amplification Symposium, October 2-4, 1962.

2. Bowles, R. E., Colston, J. R.: "Optiform," Optical Machining of Pure Fluid Systems in Plastics. Paper presented at DOFL Fluid Amplification Symposium, October 2-4, 1962.

414

HIGH SPEED PNEUMATIC DIGITAL
OPERATIONS WITH MOVING ELEMENTS

by

H. E. Riordan

of

Kearfott Division
General Precision, Inc.

Origin of the Concept

Kearfott first became interested in pneumatic digital computers in conjunction with a feasibility study on an all-pneumatic guidance system. Such a system is of interest for applications presenting a severe thermal or radiation environment. Digital data processing was selected for the pneumatic system because it presented no accuracy limitations (as opposed to analog computation), and because it was felt that the digital approach offered greater flexibility of application and design.

A set of performance and design requirements was prepared for the computer, based both on the results of the guidance system feasibility study and on the desire for an approach which would be adaptable to as broad a range of applications as possible.

These requirements were:

1. Adequate speed of operation (10 to 100 μsec)
2. Simplicity of operating principles
3. Small size
4. Flexibility of function
5. Ease of converting between electrical and pneumatic signals
6. Ease of testing
7. Compatibility with existing manufacturing techniques
8. Reasonable cost
9. Moderate power consumption
10. Reliable operation in adverse environments.

From this set of requirements it appeared that the basic approach would have to have the following characteristics:

1. Small size -- since the speed of sound would be one of the limiting conditions on response speed -- and because a compact system with low power consumption was required

415

2. A moving element -- to permit easy testing with existing electrical digital equipment and ready conversion between electrical and pneumatic signals
3. Modular Construction -- requiring only simple repetitive operations for fabrication and providing maximum flexibility of circuit configuration.

Basic Circuit Element

The basic Kearfott pneumatic computer element appears to meet all of the preestablished requirements. It consists of a ball moving freely in a cylinder having two axial connections at the ends and two or more radial connections (Figure 1).

When the ball is at either end of the cylinder, it closes the axial connection at that end.

If such a device is connected to a pressure source as shown. it will behave as a bistable element, accepting as input signals either the application of a pressure change or a closure to the input connections. The output appears as a pressure change at the axial connections or as a flow change through the radial connections.

If an additional central radial connection is used, the device exhibits three stable states, and may be used in preference to the bistable element to simplify some types of circuits. The basic element provides both pressure and flow gain and hence is a true amplifier.

It can be shown that all of the fundamental logic and arithmetic functions can be instrumented with simple combinations of one or more bistable elements. Examples of some simple logic and oscillator circuits are shown in Figures 2 through 5.

The first working model was built up of plexiglass plates and plastic balls (Figures 6 and 7). This unit is approximately eight times the size (linear dimensions) of one scaled for optimum response speed and manufacturability. It represents, however, a size which would be useful for process control and other relatively low speed applications.

The second model (Fig. 8) was an instrumentation of the two stage circuit shown in Figure 4. It is an "and" followed by an inverter or "not" and is about three times the size of a normal element.

Construction

The use of simple drilled and grooved plates to build up modules containing a number of elements with their interconnecting circuitry is shown in Figures 9 and 10.

It has been a pleasant surprise to find that even up to rather high operating pressures, no precaution against leakage other than clamping of the plates has been necessary.

The choice of materials is conditioned by operating temperature, response speed (since the mass of the ball is important), and ease of manufacture. Photoceram appears ideally suited to many classes of applications. Photo-etched metal also appears to be quite suitable. The balls may be of any suitable metal, ceramic, or even plastic.

Tolerances are quite reasonable since normal operation assumes leakage past the ball and is possible even with leakage at the axial end ports.

Development Program

Following the demonstration of basic feasibility, effort has been concentrated on obtaining fundamental information on the behavior of the device. The first concern has been to establish a valid mathematical model of sufficient simplicity to permit the design of circuits with reasonable facility.

Since the equations of gas flow are non-linear and inconvenient in form, a search has been made for a useful set of linearizing assumptions which could be made compatible with the mathematical structure used in conventional electrical circuit analysis.

The problem is somewhat complicated by the existence of size effects which tend to invalidate some of the assumptions made in conventional orifice flow analysis. The size effects are associated with the velocity of approach, the significance of viscous friction, and the effects of discontinuous geometry in the flow channels. An additional complexity is introduced by the necessity of considering the effects of compressibility and the finite speed of sound in the working medium.

We have attacked the design problem by assuming a very simple model initially and introducing such corrective terms as the experimental results might suggest.

One highly simplified view is represented by the equations shown in Figure 13. For certain choices of orifice size ratios and operating pressures, this representation is quite useful.

In order to check the validity of a given representation of the device, the following criteria were adapted because of the relative ease of making the necessary measurements:

1. Effect of supply pressure on stability
2. Effect of supply pressure on transit time
3. Effect of orifice size ratios on transit time
4. Effect of ball clearance on transit time.

Transit time has been measured electrically, using the single element test unit shown in Figures 11 and 12. This unit has an 0.020 diameter cylinder and a ball travel of 0.008 inch. For investigative work, however, photographic measurement of ball position has proved more accurate. In addition, the use of a transparent model is helpful in detecting anomalous operation such as might be caused by leaks, bad end-seat geometry, or incorrect orifice sizing.

The photographic setup is shown in Figures 14 and 15. This unit has a cylinder bore of 0.0244 inch and is used with various ball diameters and travel distances.

The photographic test unit is shown set up as a tuned multivibrator in Figure 16. A typical set of transit time data is plotted in Figure 17. For the scaling used, the transit time correlates quite well with the semi-empricial formula of Figure 13. if the effective pressure drop across the ball is computed from the supply pressure on the basis of simple orifice theory.

It will be seen that the shortest transit time with a brass ball in this series of tests was 169 microseconds. An aluminum or ceramic ball will give about 100 microseconds. With the shortest practical ball travel, this can be further reduced to 70 microseconds. For transit times shorter than this, it is necessary to go either to higher supply pressures or to moving elements of special geometry.

Performance Capabilities

Since the basic bistable element will change state and produce a useful power output when a pressure is applied to the input without any accompanying input flow, it is difficult to define the power gain. However, pressure gain may be related to the ratio of the projected area of the ball to the cross sectional area of the axial end ports.

A pressure gain of ten is readily obtainable. The practical upper limit has not yet been established. Pressure gain and response speed are, however, inversely related.

In view of the experimental data thus far obtained, it is calculated that a transit time in the vicinity of 20 microseconds should be achievable at reasonable supply pressures with special geometry of the moving element. For the packaging techniques being developed, the transmission delay between units will be about 8 microseconds. The input time constant will be in the neighborhood of 10 microseconds; hence overall operating times of 40 to 50 microseconds appear to be achievable.

This speed corresponds to clock frequencies in the range of 20 to 25 kilocycles per second. This is a usable frequency for a sizable class of guidance and control computers, and is more

than adequate for many industrial control and computing applications.

Since the basic element is small and relatively inexpensive, improvement in overall computing speed can be achieved at reasonable cost by employing parallel, rather than serial, logic and arithmetic.

There is no upper limit on the size of the elements. Thus, direct conversion from signal level to power outputs capable of performing useful mechanical work is accomplished simply by using larger units as output power amplifiers.

No internal temperature rise occurs in the computing circuits, so that full advantage can be taken of the high packaging density.

Direct electrical inputs are accepted by using small coils to magnetically force ball motion. Electrical readout is obtained by direct contact with the ball or by using capacitive or magnetic sensing of ball position. Present planning envisions the provision of built-in electrical test circuits for checkout and trouble-shooting.

Potential Applications

The most obvious applications of pneumatic digital equipment are those in which a severe thermal or radiation environment precludes or seriously hinders the use of electrical equipment.

Examples of such situations are:

Reactor control
Control of reactor-power devices
Control of re-entry or other very high mach number vehicles.

Other applications involve the absence of electrical power, unwillingness to rely on auxiliary electrical power supplies, or existing use of pneumatic data transmission and power devices; for example:

Steam generator controls
Chemical process controls and data systems
Low cost tactical weapon control
Machine tool control
Submarine controls.

If low cost and high packaging density are realized to the anticipated extent, some penetration into fields normally reserved for electrical computation can also be anticipated.

Conclusion

It has been possible to devise a pneumatic digital computing element providing adequate response speed, ready conversion

between pneumatic and electrical signals, and high packaging density.

Tests have thus far verified the design assumptions. Experience with working units has revealed additional advantages arising from the use of plate type construction. The very simple basic geometry and good freedom from tolerance sensitivity of the moving ball element help provide assurance that production costs will be reasonable.

Work is being concentrated on the development of basic understanding of the device and of convenient mathematical descriptions and circuit design techniques. Kearfott is ready at this time to undertake the design and development of useful pneumatic computing and control devices based on the moving element bistable device.
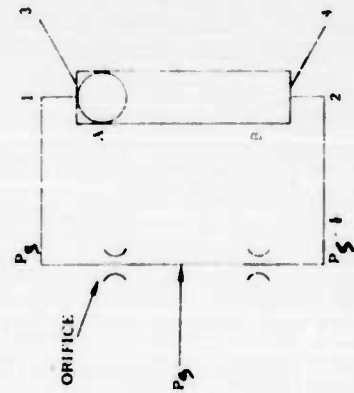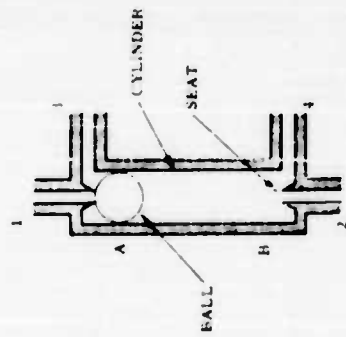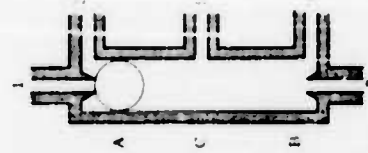
BASIC ELEMENTS AND CIRCUITS

FIGURE 1

421
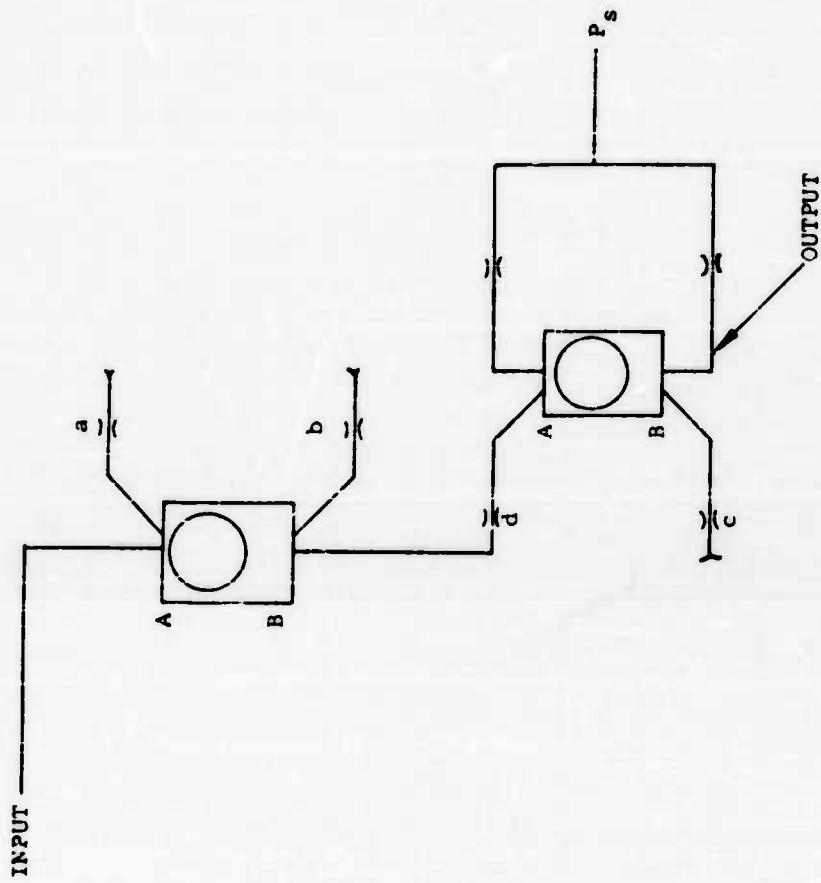
PULSE RESHAPER

FIGURE 2

422

MULTIPLE INPUT "OR"

FIGURE 3

423
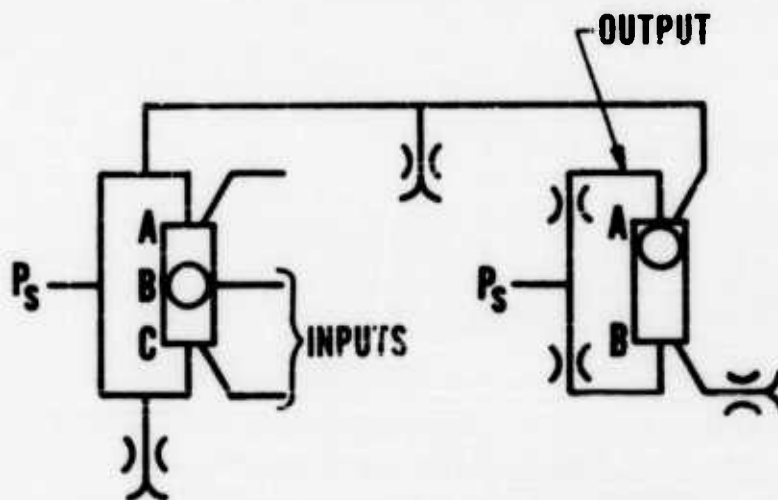
SCHEMATIC OF TYPICAL 2 STAGE CIRCUIT

FIGURE 4
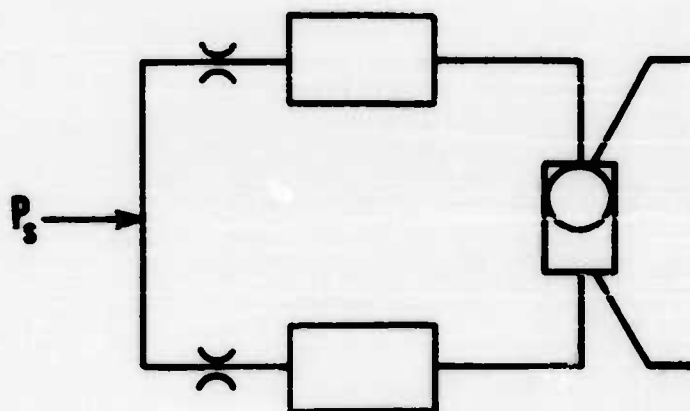
SCHEMATIC OF TUNED MULTIVIBRATOR

FIGURE 5

424
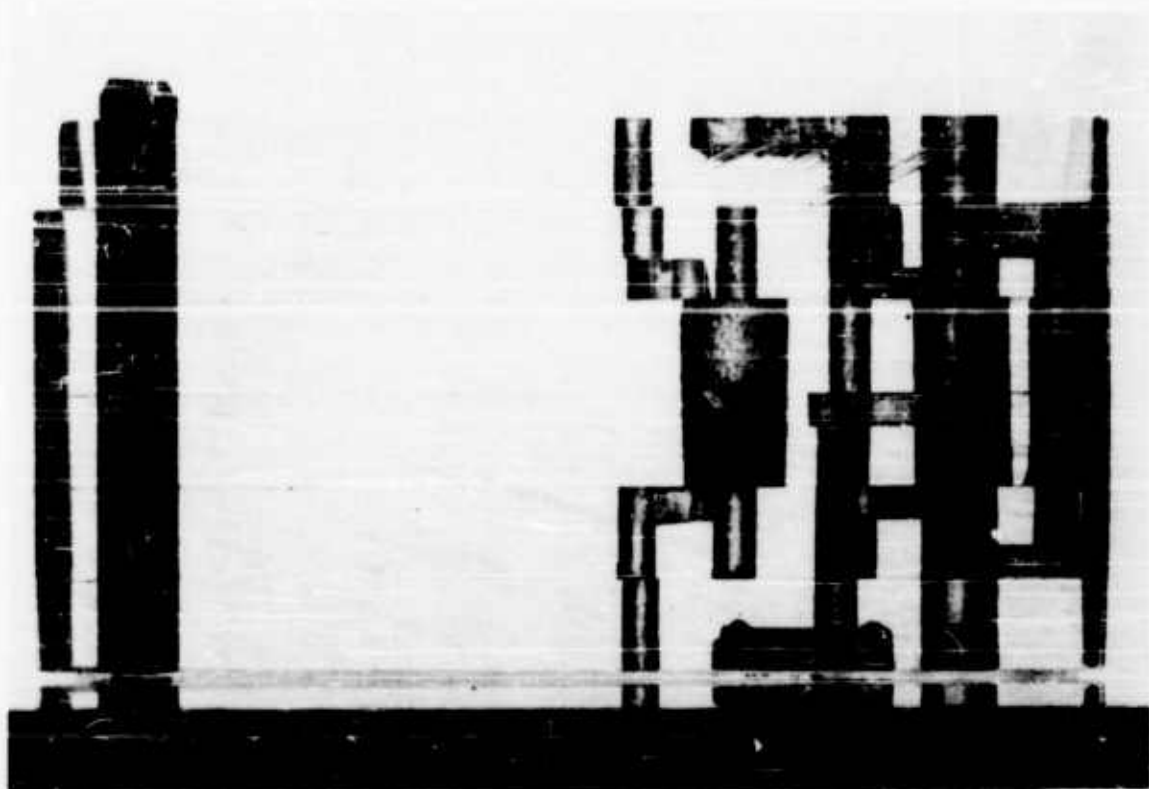
FIRST WORKING MODEL (SECTION)

FIGURE 6
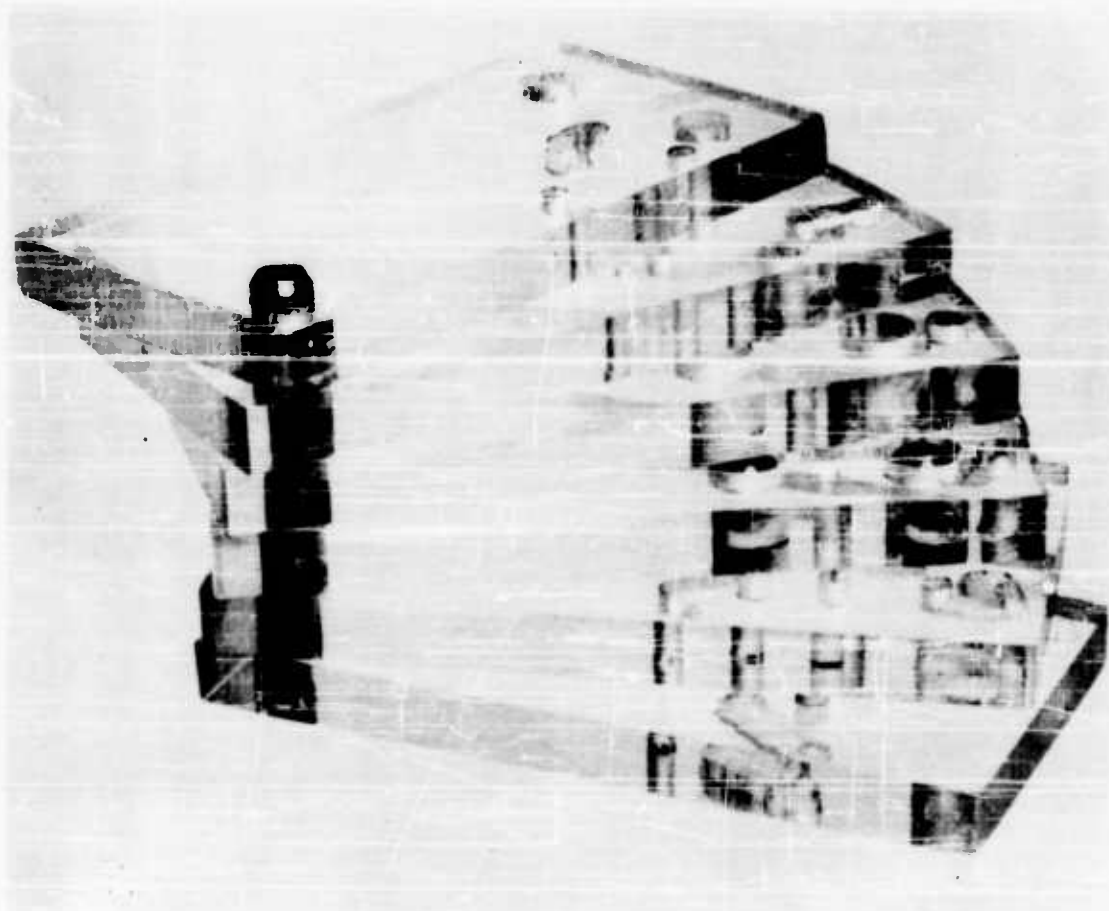
FIRST WORKING MODEL (EXPLODED VIEW)

FIGURE 7

SECOND MODEL

FIGURE 8

427
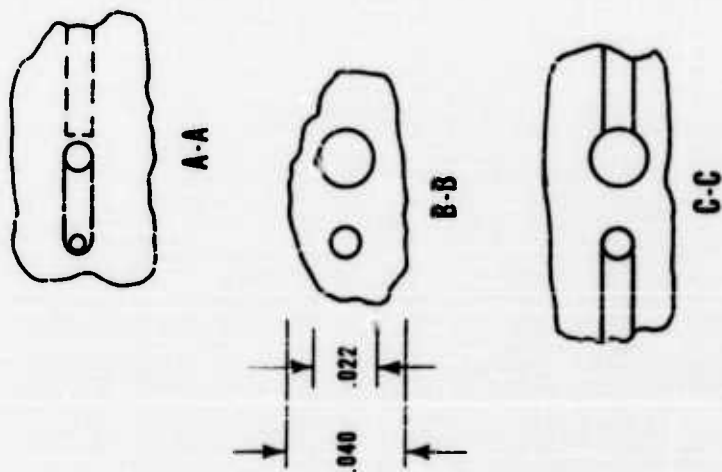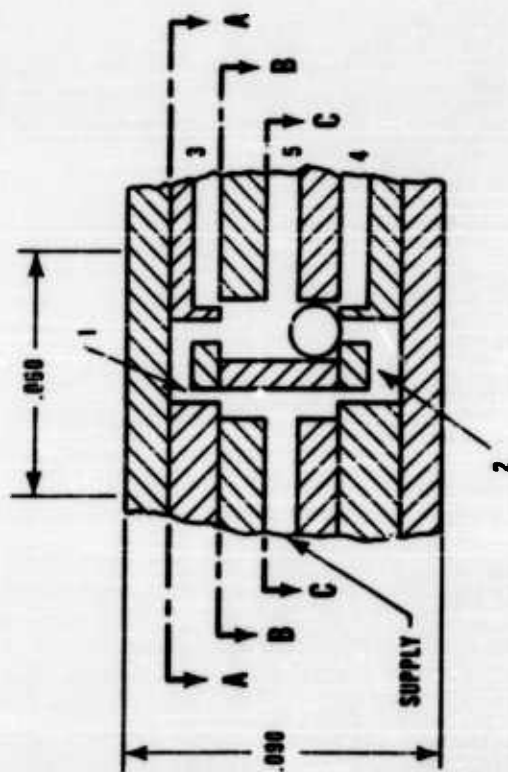
TYPICAL PLATE CONSTRUCTION

FIGURE 9

A-A

B-B

C-C

.022

.040

ACTUAL SIZE

PACKAGING DENSITY
4,640 UNITS/in³

.050

.090

SUPPLY

428
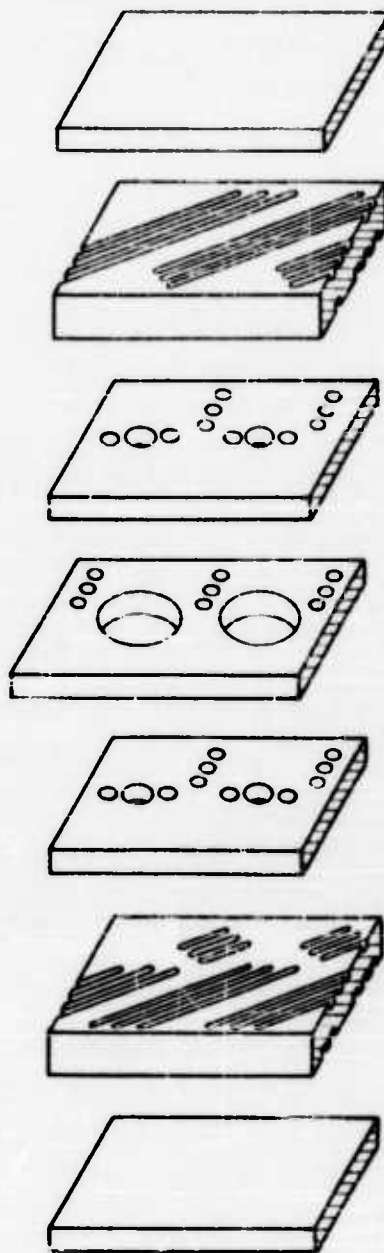
MATRIX CONSTRUCTION

FIGURE 10
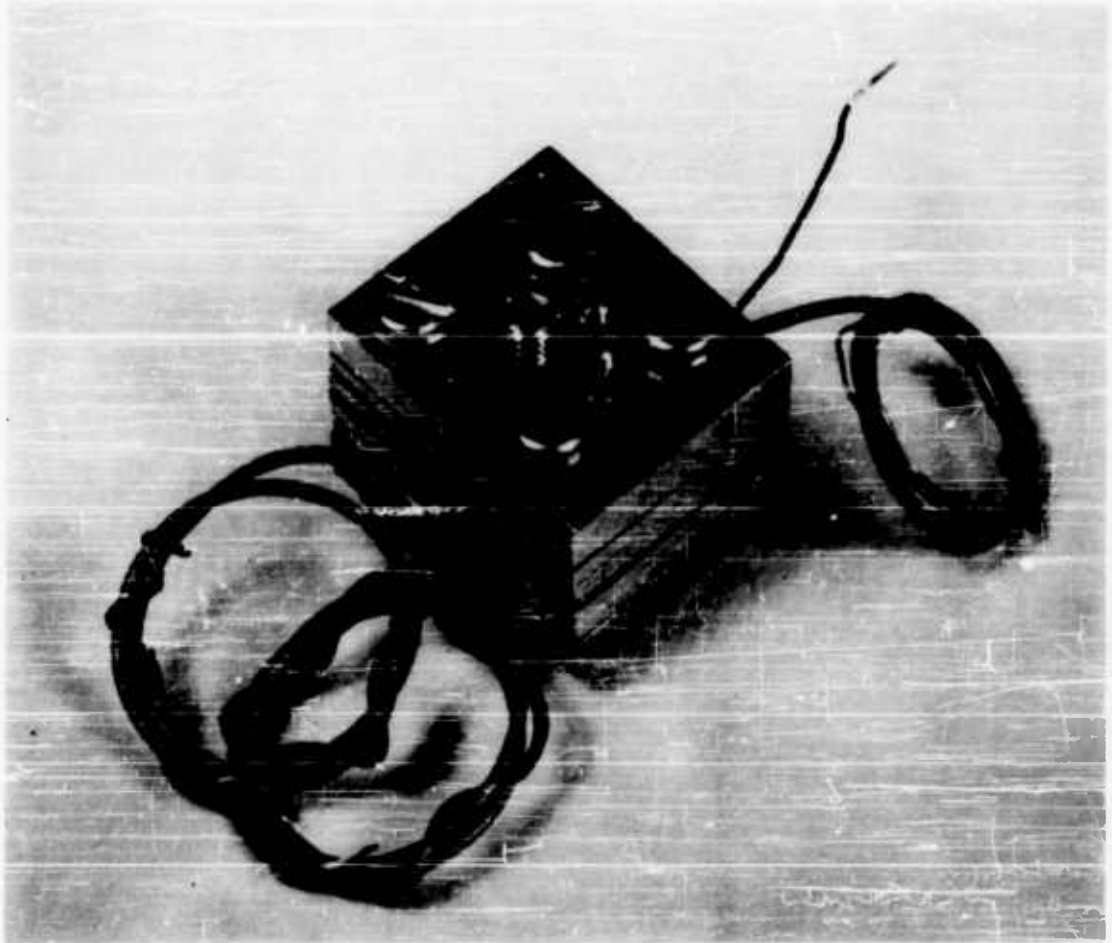
TEST MODEL WITH ELECTRICAL OUTPUT

FIGURE 11

430

PNEUMATIC COMPUTER
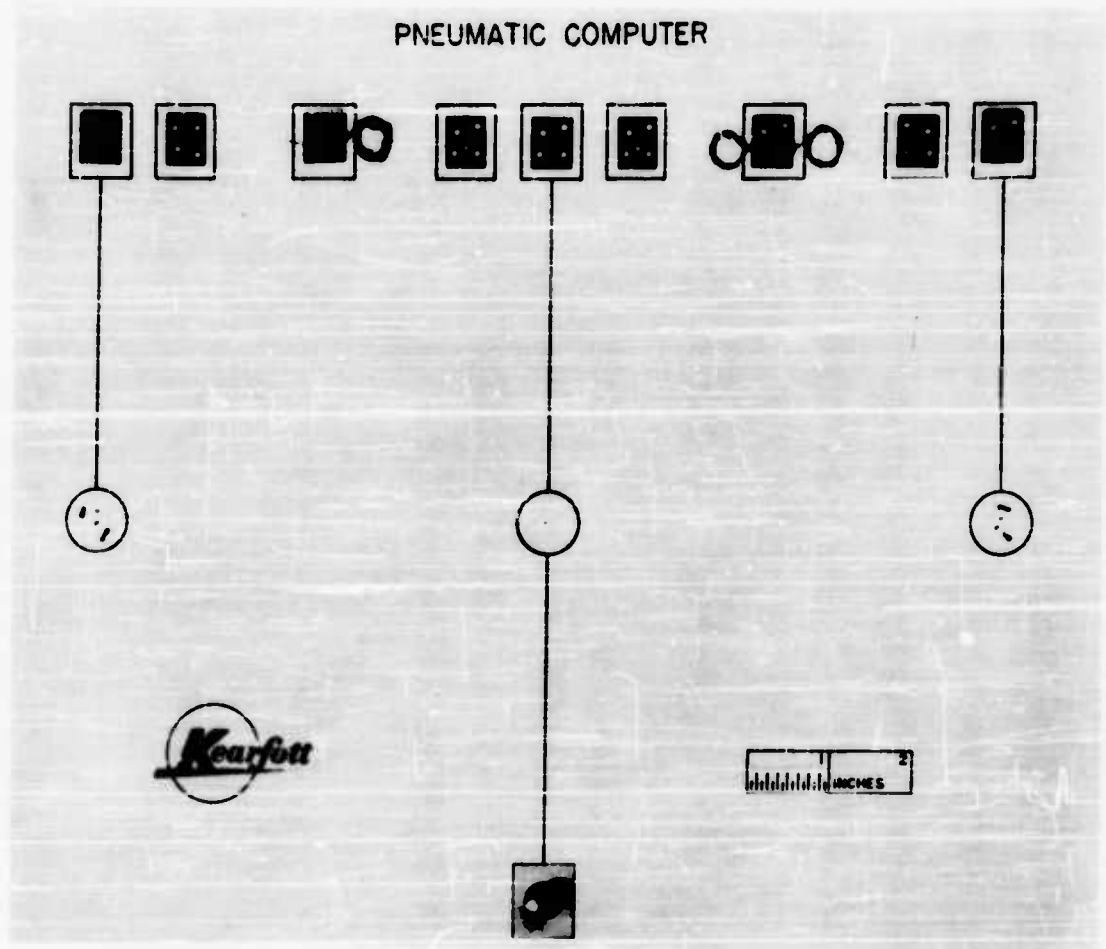
EXPLODED VIEW - ELECTRICAL OUTPUT MODEL

FIGURE 12

431

$$t_r = t_l + t_i + t_t = \text{TOTAL RESPONSE TIME}$$

$$t_l = \text{LINE DELAY} = \frac{l}{v}$$

$$t_i = \text{INITIATION TIME} = R_i C_i$$

$$t_t = \text{TRANSIT TIME OF BALL} = K\sqrt{\frac{4}{3}\frac{X d \gamma}{P_d}}$$

l = INPUT LINE LENGTH

v = SPEED OF SOUND

R = EQUIVALENT INPUT RESISTANCE OF ELEMENT

C = EQUIVALENT INPUT CAPACITANCE OF ELEMENT

X = BALL TRAVEL

d = BALL DIAMETER

γ = BALL DENSITY

Pd = DIFFERENTIAL PRESSURE ACROSS BALL

K = EMPIRICAL CONSTANT = 2

RESPONSE TIME FORMULAS

FIGURE 13
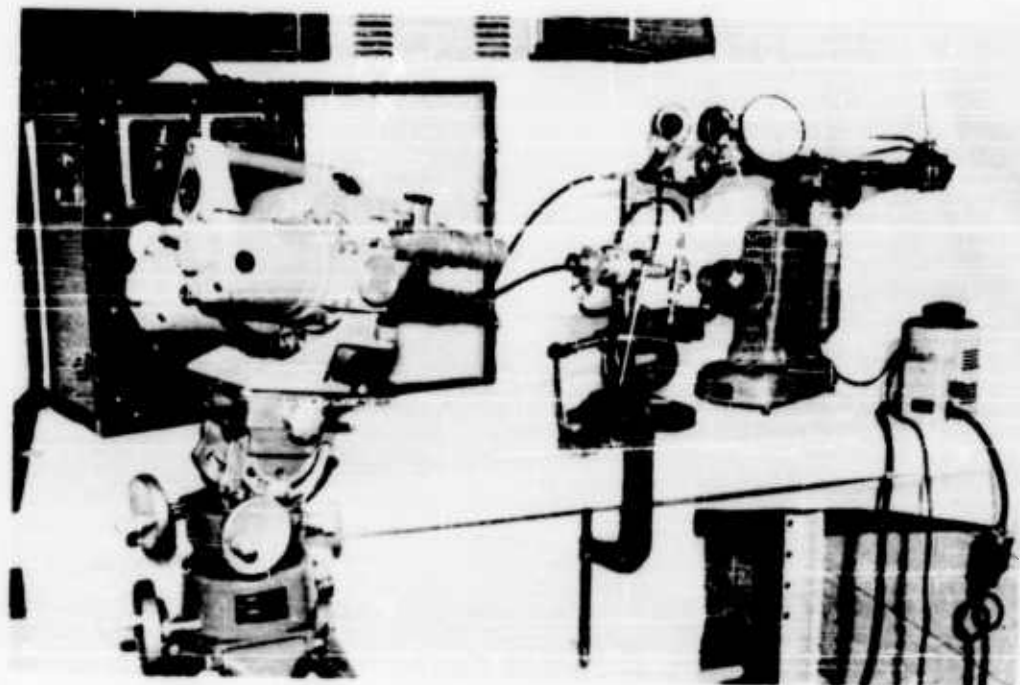
RESPONSE TIME SETUP

FIGURE 14
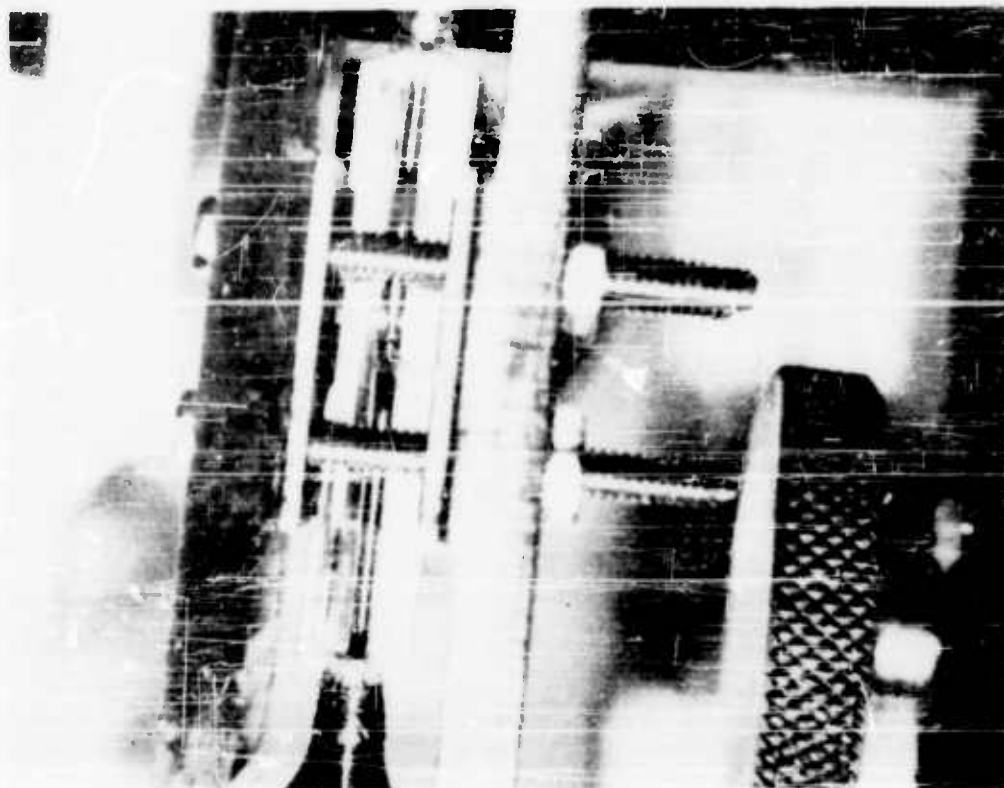
CLOSE UP OF RESPONSE TEST UNIT

FIGURE 15

434
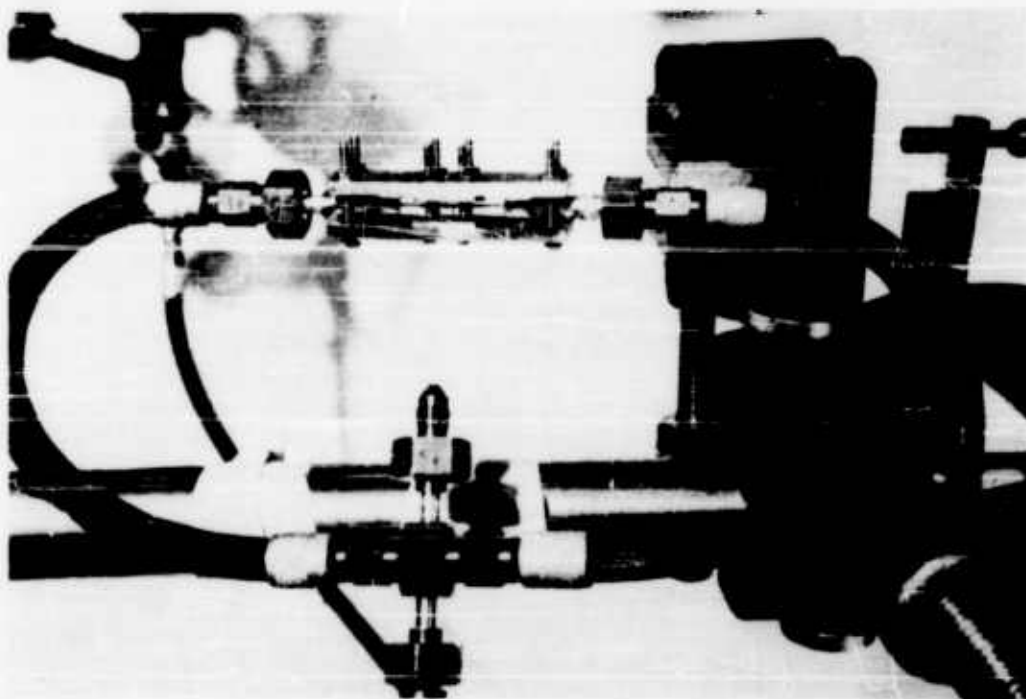
TUNED MULTIVIBRATOR TEST SETUP

FIGURE 16
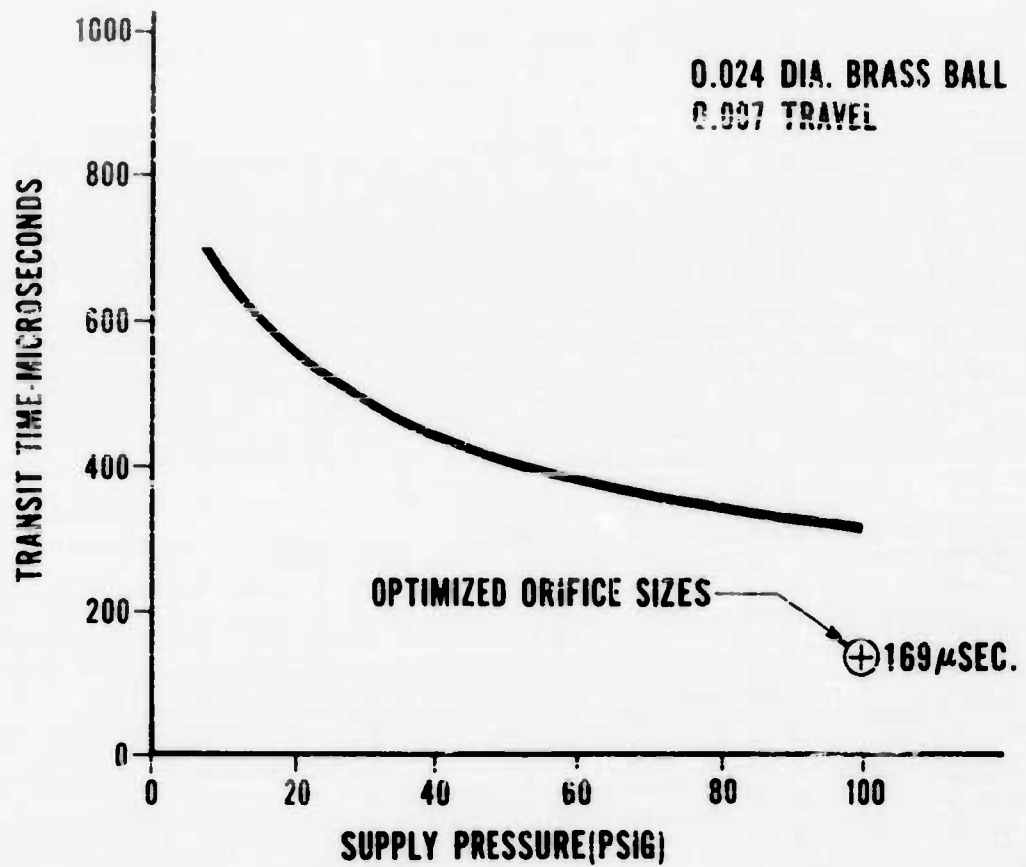
TRANSIT TIME VS. PRESSURE GRAPH

FIGURE 17

A SUGGESTED SYSTEM OF SCHEMATIC SYMBOLS

FOR

FLUID AMPLIFIER CIRCUITRY

By

W. A. Boothe
Dr. J. N. Shinn

General Electric Company
General Engineering Laboratory
Schenectady, New York

ABSTRACT

This paper proposes a system of short-hand symbols that effectively differentiates between analog and digital devices, beam deflector and vortex amplifiers and passive versus active types of valves. A means of designating the memory and no-memory digital amplifier is also provided. On this simple base it is possible to build symbols representing the more sophisticated logic and control components. Examples given include an operational amplifier, simple flip-flop, counter, half adder (or exclusive OR), AND, OR and NOT elements.

Representation is also suggested for the commonly used circuit elements such as resistance, capacitance and inductance. Some of the common pitfalls of electrical analogies to these elements are outlined. Examples of schematic circuits using these suggested symbols are also presented.

INTRODUCTION

Some risk must be involved in proposing a system of standard symbols or nomenclature for a technology as young and explosive as fluid amplifiers. It is impossible and unwise to try to anticipate all possibilities, since new developments are popping up at a phenomenal rate. At the same time, fluid amplifier circuits are becoming more complex and a real need now exists for schematic presentation of circuits. This meeting presents a fitting opportunity to broach the subject of adopting a standard set of symbols before the many firms and individuals in this field develop too widely diverging a set of symbols of their own. The symbols suggested in this paper are offered for discussion and it is hoped they will lead to a better means of communicating ideas in this field.

The symbols are simple and flexible, permitting the "building block" approach so necessary to a technology of this type, where standards should definitely not limit freedom in representation. This paper will deal primarily with symbols although some suggestions for standard performance specs and element designation are in order. It is understood that DOFL is developing a system of nomenclature for fluid amplifiers to permit presentation of analyses in a more standard form.

FUNDAMENTAL DELINEATIONS

Fluid amplifiers can be categorized in many ways. However, several basic questions about a fluid amplifier element come to mind immediately. Is it digital or analog in nature? Is it a beam deflector type element or a vortex element? Is it active or passive? These questions can be answered quite simply in schematic form. Our usage has been to denote the flow path of the power jet of an analog valve with a dashed line whereas a digital element is represented with solid lines throughout. Figure 1 shows this usage applied to simple beam deflector amplifiers. The use of the enclosing circle around the element has been optional with us. In simpler schematics it is not used, while in more complicated ones it makes the element stand out from the connecting lines. The input and output lines of the elements appear in the schematic at the same points where they normally would on the actual element, as pointed out in Figure 1. Figure 2 shows the symbols used for vortex amplifiers which may also be digital or analog in form.

As shown in Figure 3, the designation as to whether a valve is active or passive is done by means of a solid circle at the base of the power nozzle line to indicate that this line is connected to the circuit supply pressure. If more than one pressure supply level is used in a circuit, a letter or number code can be used to differentiate between those used.

SCHEMATICS FOR ANALOG DEVICES

The basic form of analog valve symbols are given in Figures 1 (b) and 2 (b), where the main distinguishing feature is the dashed line to represent the flow path of the power jet. The possible variations of these basic representations are so numerous that they can not be covered completely in this paper. However, one short-hand representation believed worth mentioning is that of the operational amplifier. Figure 4 (a) shows an arbitrary example of a schematic for a high gain four stage operational amplifier. The outputs in this example will be a function of the difference between input A and input B, the function depending on the feedback impedances Z_1 and Z_2 which provide in this instance negative and positive feedback, respectively. Figure 4 (b) shows the short hand symbol for the same circuit. In this symbol the asterisk is used to indicate the sense or polarity. For example, in Figure 4(b) this notation indicates an increase in input A results in an increase in output C to correspond with the circuit in Figure 4(a). If an odd number of stages were used the asterisk would, of course, appear behind D.

438

This convention permits the schematic to have close correspondence with the physical circuit layout.

SCHEMATICS FOR DIGITAL DEVICES

The schematic for a basic flip-flop, shown in Figure 5, is quite similar to the physical layout of the device. An input of A will cause an output at D and an input at B will switch the flow to C. The symbol for a fluid source indicates that the flip-flop in the example is an active device. The schematic for the binary flip-flop, such as the counter stage developed by R. W. Warren at DOFL, is shown in Figure 6. Input pulses at A switch the flow alternately to outputs C and D. A re-set signal pulse applied at the RS input will switch the second stage jet to output D. The schematic indicates the second stage of the binary flip-flop to be an active device.

The schematic for an active or-nor element is shown in Figure 7 (a). Inputs at C or D or E will cause an output at B, thus performing the "or" function. With no input signal the output is at A, performing the "nor" function. Using conventional logic notation the element is identified as an or-nor by including the + sign. The choice of three inputs for the example in Figure 7 (a) was arbitrary; an "n" input element would be shown schematically with "n" input lines. Figure 7 (b) shows a passive "or" element.

Figure 8 shows the schematic for the active and passive "and" elements. Using standard logic notation for an "and", the function of the element is identified by a dot. An output at B will occur only when inputs C and D and E all are present.

The "half adder" or "exclusive or" schematic is shown in Figure 9. An input at either C or at D, but not both simultaneously, will provide an output at B while simultaneous inputs at C and D provide an output at A. The half adder can also be used as a two input "and" element. This schematic follows closely the general physical layout of one form of a half adder now in use. Although half adders quite different from that shown in the schematic have been devised, this schematic was chosen because it is believed to represent simply and clearly the functioning of the half adder element.

MEMORY AND BIASING

Some devices have memory and thus can operate with input signals in pulse form while others require a continuous input signal for operation. This difference in operating characteristics is delineated on the schematics as illustrated in Figure 10. The arrowheads on the input lines indicate that a continual flow is required to maintain the state of the element. Note that in Figures 7, 8, and 9 this notation was used to indicate steady state inputs are required to provide the desired performance.

Bias signals are often used to provide desired characteristics. Fig. 11 illustrates how a bias signal would be represented schematically on a flip-flop and an "or" element. If an "and" or "or" element is shown without the biasing input line then it is implied to be geometrically biased.

OTHER CIRCUIT ELEMENTS

A fluid circuit would not be complete without the many passive impedance elements such as orifices or restrictions and without showing connections such as vents or drains. To do this we have drawn heavily on JIC practice where practical.

Figure 12 (a) shows the general symbol for impedance. Figure 12 (b) shows the representation for an ofifice which would obey a square-law relationship if an incompressible fluid is used. (No attempt is made here to differentiate between a choked and unchoked flow if the fluid is compressible). Figure 12 (c) represents a laminar restriction where pressure drop varies linearly with flow and where friction effects predominate over inertial effects. Figure 12 (d), in turn, shows fluid inductance where inertial effects predominate over friction. A relatively pure fluid inductance is found primarily in liquid circuits.

Figure 12 (e) shows the symbol for a fluid capacitor which, in some instances, is analogous to an electrical capacitor. A fluid capacitor consists of a fixed volume if the fluid is compressible, or a hydraulic accumulator or equivalent for an incompressible fluid. In drawing an electrical analogy, where voltage and current are analogous to pressure and flow, respectively, a fluid capacitor such as the volume or accumulator can only be the equivalent to shunt capacitance from the point in question to ground. It is never the equivalent of a blocking capacitor. The equivalent of blocking capacitors must be obtained by using other devices.

Figure 12 (f) shows the symbol for a fluid delay line which has the characteristic of providing a pure time delay in the signal transmitted with a minimum of attenuation.

Figures 13 (a) and 13 (b) show that crossing and connecting lines follow a practice identical to JIC hydraulic practice as well as some electrical standards.

Vent connections are shown in Figure 13 (c) and should be used in any open cycle circuit where the excess fluid is merely vented to atmosphere or drained off.

If a closed cycle circuit is used, the excess and exhaust fluid must be returned to the reservoir. To decrease the number of lines in the schematic, it is recommended that the JIC symbol of Figure 13 (e) be adopted.

USE OF SCHEMATICS -- EXAMPLE

Figure 14 is a hypothetical example of the use of the above symbols. In this circuit, a multivibrator drives a power flip-flop through an "or" gate on the fourth actuator stroke. When the "or" gate opens, the actuator is held in the down position until a re-set signal reactivates the circuit.

CONCLUSIONS

The schematic representations presented above are not claimed to be complete or adequate for every situation. Modifications, changes and revisions will be necessary in order to evolve a convenient and universal system. It is believed, however, that the representations suggested above can serve as a basis for initiating standardization.

Further it is recommended that work be initiated now on standardizing the performance parameters and the presentation of their characteristics. The goal of this effort would be data for elements presented in a fashion similar to electron tube or transistor characteristics. For example, normalized pressure-flow curves for the output of an element would be quite useful in determining optimum sizes for staging and circuit work. Furthermore from the flow and pressure recovery values shown by these curves, the efficiency of the element can be deduced. These output characteristics are used, in addition to gain characteristics, because usable output signal level is an important parameter in any circuit design. High gain is certainly desirable but a trade-off often must be made between gain and output power or pressure recovery for a practical application. A standard format such as this for presentation of these kinds of data will minimize the language barrier and will provide better and earlier interchanges of information. Also, standards will eventually be needed for element designations along the same lines now used for electron tubes and transistors.

In conclusion, it is believed timely to initiate standardization in this new field. The schematic representations suggested above cannot fit every situation but are believed adequate for most pure fluid amplifier elements presently being developed. It would be quite satisfying to the writers if representations suggested above result only in the impetus to initiate work on more complete and thorough schematic representation.
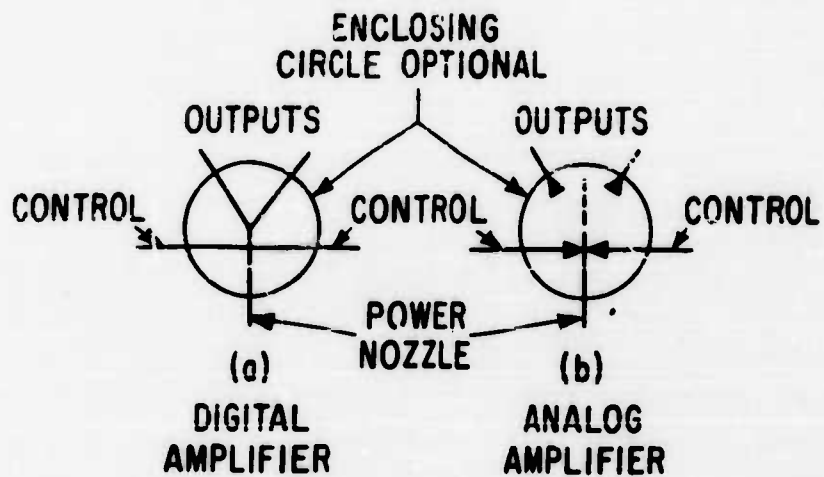
Figure 1. Beam deflector amplifiers.
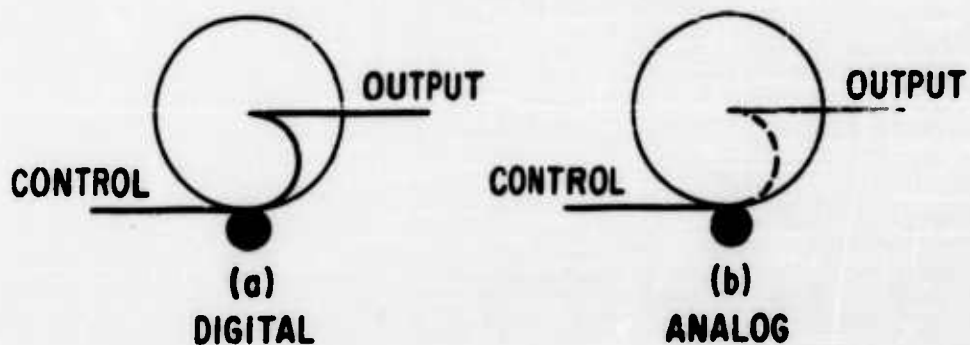
Figure 2. Vortex amplifiers.
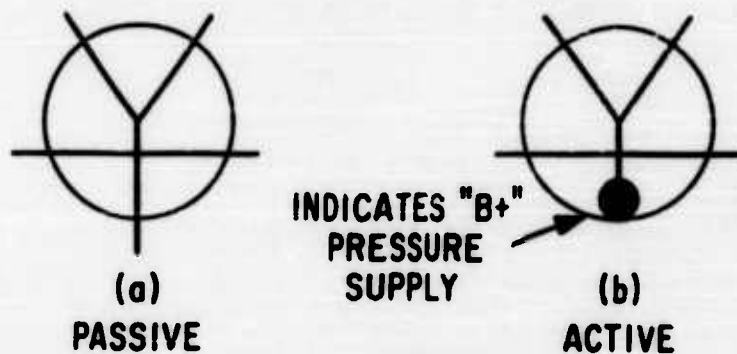
Figure 3. Designation of active vs passive elements.
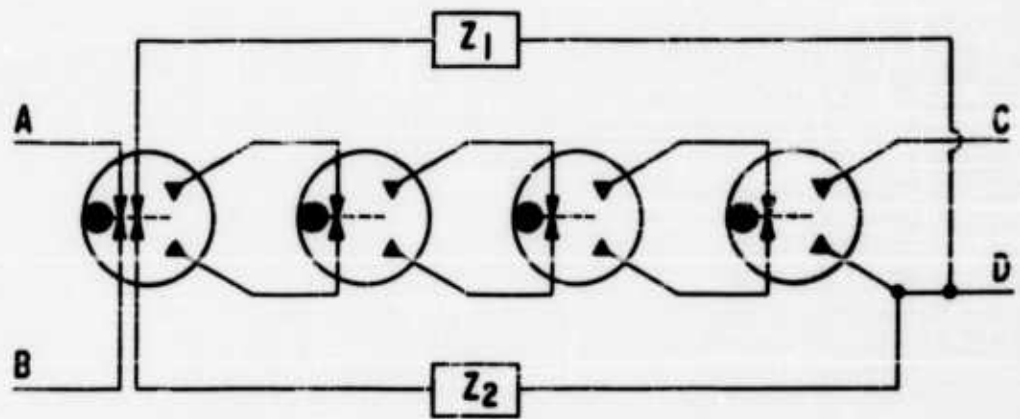
Figure 4a. Schematic of 4 stage operational
amplifier.
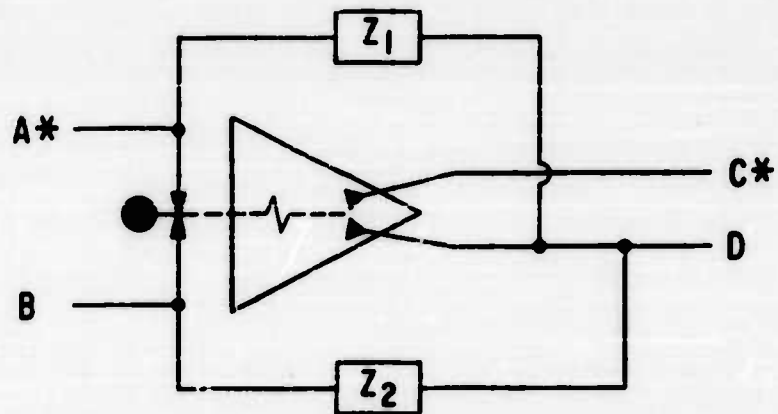
Figure 4b. Simplified diagram for operational
amplifier.
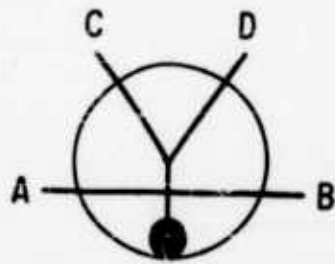
Figure 5. Basic flip-flop.
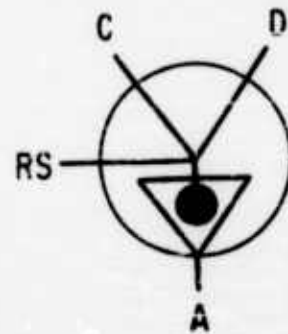
Figure 6. Binary flip-flop.
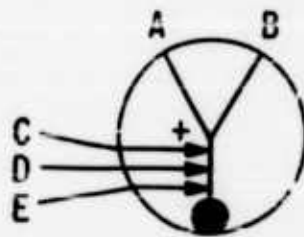
(a)
ACTIVE
OR-NOR
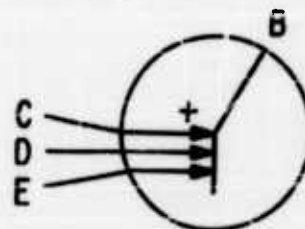
(b)
PASSIVE
"OR"

Figure 7. "OR" logic elements.
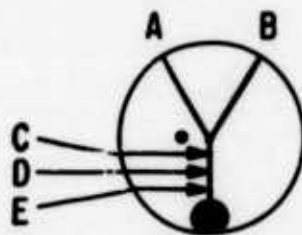
(a)
ACTIVE
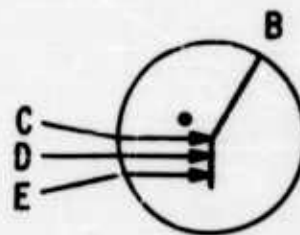
(b)
PASSIVE

Figure 8. "AND" logic element.

444
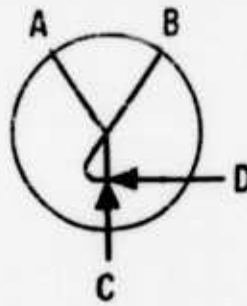
Figure 9. Half-adder, exclusive or.
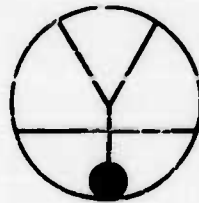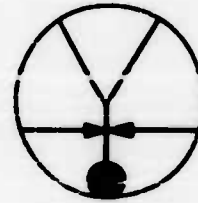
Figure 10. Flip-flops with and without memory.
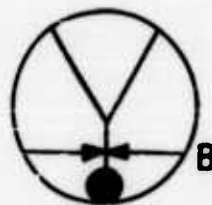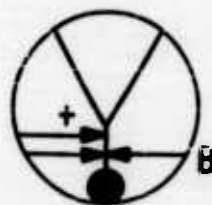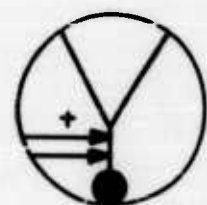
Figure 11. Representation of biasing signals.

445

(a) GENERAL IMPEDANCE

(b) ORIFICE

(c) CAPILLARY (LAMINAR) RESTRICTION

(d) INDUCTANCE

(e) VOLUME OR ACCUMULATOR

(f) DELAY LINE
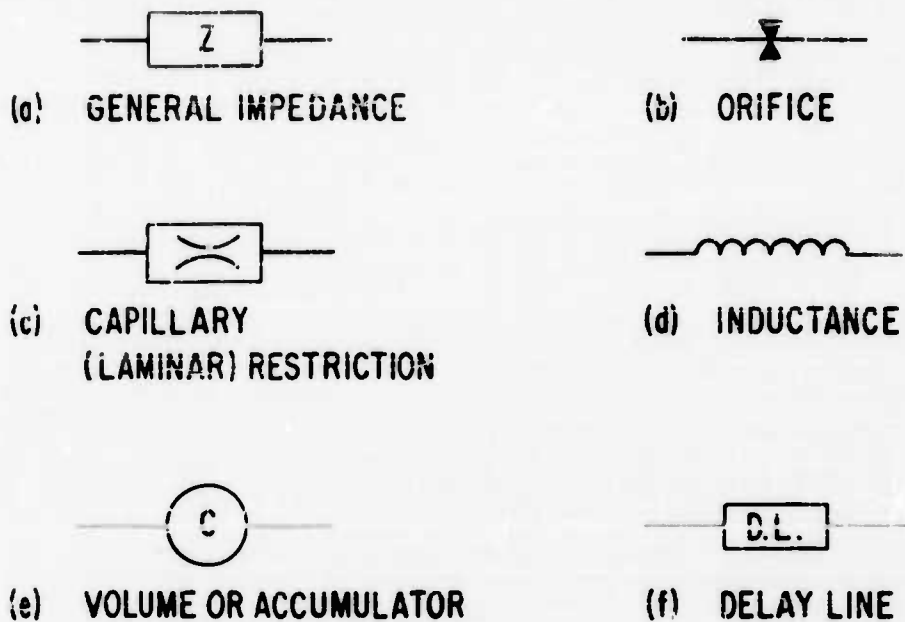
Figure 12. Symbols for line impedances.

(a) CROSSING LINES

(b) CONNECTING LINES

(c) VENT CONNECTION

(d) EXAMPLE OF VENT

(e) RETURN TO RESERVOIR

(f) EXAMPLE OF RESERVOIR RETURN
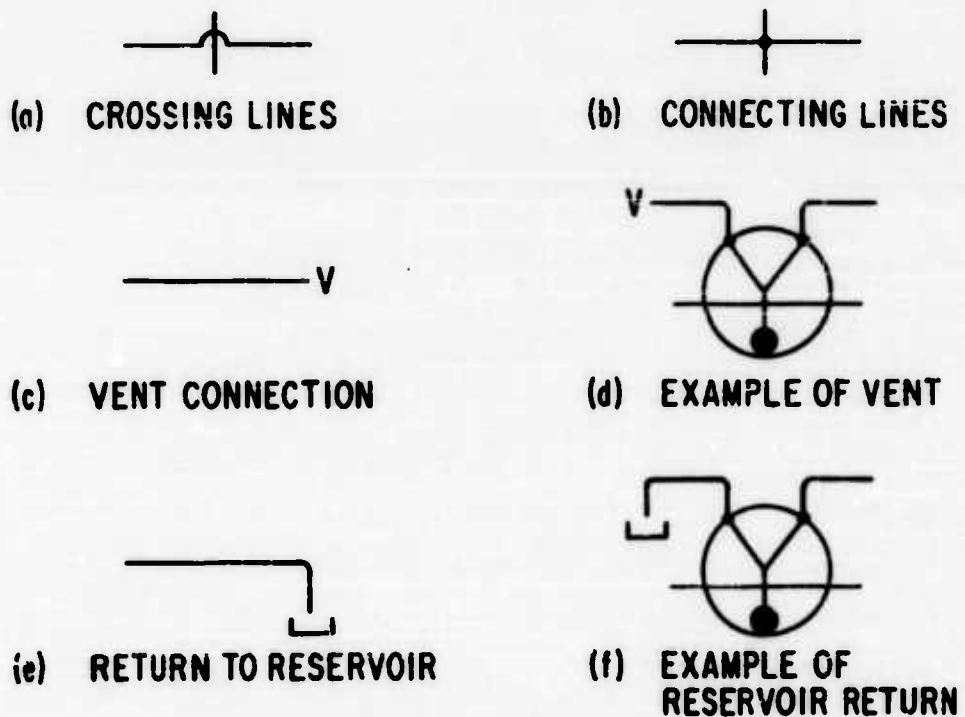
Figure 13. Symbols for connections.

446
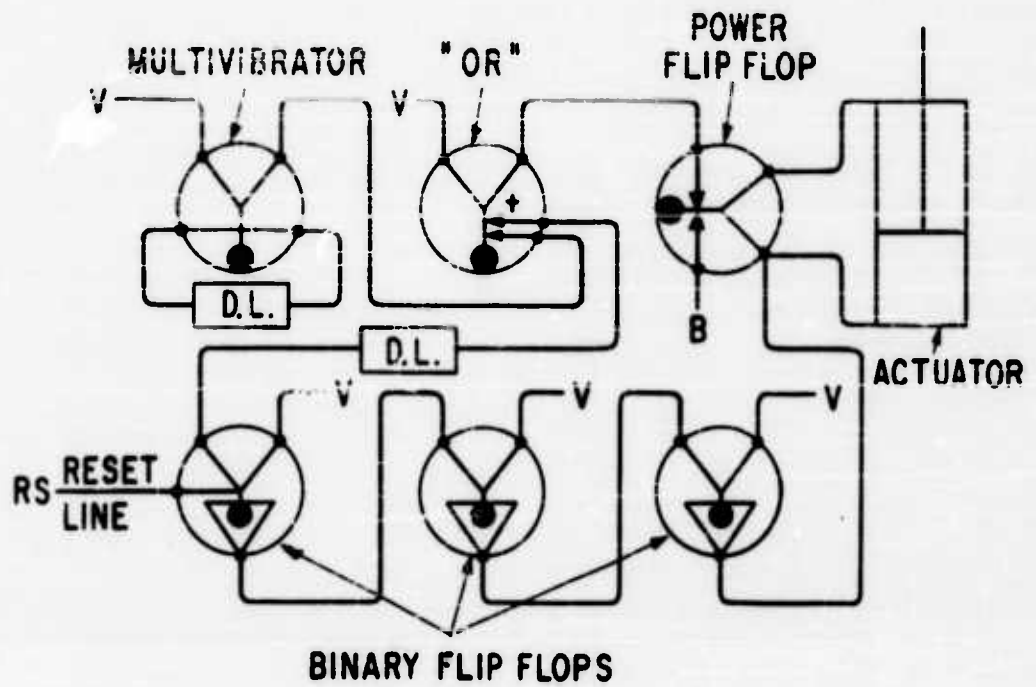
Figure 14. Example circuit.

A TECHNIQUE FOR MATCHING PURE FLUID COMPONENTS
APPLIED TO THE DESIGN OF A SHIFT REGISTER

by

Edwin M. Dexter

of

Bowles Engineering Corporation

INTRODUCTION

In the breadboarding and subsequent testing as well as in quality control of Pure Fluid circuits it is desirable to have available a simple quick method of evaluating the performance of elements in a circuit. An example of the problem is the shift register a section of which is shown in silhouette in Figure 1.

In this figure the section of the shift register shown comprises three MEMORY units and two AND gates. Initially this circuit was assembled from individual breadboard units connected with tubing. It was desired to determine if the output from the MEMORY unit was sufficient to operate the AND gate and subsequently if the AND gate output was sufficient to operate the MEMORY element. In addition it was desired to provide a reference for testing individual elements before assembly. Later it was necessary to probe the circuit to locate the source of problems.

In each of these cases it is necessary to know what to expect from the performance of each element, also it is desirable to limit the test to a pressure measurement as this is usually the easiest to perform.

It is the objective of this discussion to describe an approximate scheme which has proven useful in evaluating the matching possibilities of units, quality control, and circuit testing. The first assumption was that a considerable safety factor is desired with digital elements, i.e., it is desired to have somewhat more pressure available to flip a unit than required. Secondly, allowance must be provided for the differences between elements to be encountered in practice. Perhaps it will be said that these methods are restricted to a particular family of elements and this is true. However, it appears that the resulting family chosen may have distinct advantages. Under these conditions the method to be outlined lends some facility to the description of units and is an aid in quick evaluation of matching for steady state operation. The shift register circuit is used as an example to describe this technique.

449

Figure 1 is a silhouette of the pneumatic shift register showing three MEMORY units and two AND gates. The center MEMORY unit is the intermediate storage. The AND units are referred to as TWIN-AND because they, in a sense, are a combination of two AND gates. Supply pressure P+ is applied to all three of the MEMORY units continuously. A "bit" of information is placed in the first MEMORY unit by applying a pulse of pressure to either control, for example, a-. The MEMORY unit will now be switched to the right output leg, b+. The pressure in the left output leg will be negligible, and can be positive or negative depending on the element design. The flow resulting from the pressure b+ will go to the left of the receivers into the large open area which is vented. Now, if a pressure pulse of the proper magnitude is applied at the center control, T_1, of the first TWIN-AND, the combined momentums of the two streams will be directed toward its left receiver, raising the pressure at c-. One objective of the graphic analysis is to determine if the recovered pressure at c- will be enough to flip the second memory unit. In addition, it is desired to show that this technique can be applied to systems of other elements that are within the family of performance characteristics selected.

ADMITTANCE

The basis for this technique is in approximating the steady state control input admittance of elements with an equivalent orifice which performs in the manner of the hydraulic square law; $Q = KP^{1/2}$. This is a reasonably valid assumption but is an approximation. Pressure flow tests of passages and orifices of the types expected in pure fluid circuits show that the relation is surprisingly often $Q = KP^{.63}$. We have found it convenient to use units where Q is the flow in inches^3 per second and pressure is psig. If a value of K is determined within the pressure region to be used the assumption of a hydraulic square law performance does not lead to excessive error. Under these conditions the ratio of Q^2/P remains constant and can be used as an admittance. Since the nominal pressure is often 1 psig the admittance Q^2/P under this condition is numerically equivalent to Q^2, for example, an orifice with an admittance of 9 passes 3 in^3 per second at a pressure drop of 1 psi.

The pressure flow relationships for the control inputs of elements have a wide variety, some are quite linear while others conform closely to the orifice characteristic. Figure 2 shows the control input pressure-flow relationship for three different elements; a COUNTER, a MEMORY, and an OR. The input relationships for the OR element are given for two load conditions. In addition the dashed lines show the performance of orifices that have corresponding admittances in the important ranges of operation.

450

The dots shown are the points at which the element changes state. For the FLIP-FLOP, for example, the pressure and flow is increased to .09 psi at .7 in^3 per second to effect flipping. The upper pair of curves represent the control input characteristics before and after flipping for an OR element that is driving another OR element. The pressure and flow are increased to .22 psig and .7 in^3 per second to effect flipping and following this the input characteristic is given by the upper curve. Reducing the pressure and flow to .2 psig and .5 in^3 per second allows the unit to reset.

It is seen that the COUNTER input characteristic is exactly that of an orifice with an admittance of 6.2. The FLIP-FLOP or MEMORY element can also be approximated by an admittance of 6.2 at the point where flipping is expected. The OR unit deviates from the orifice considerably but can be approximated by admittances of 2.2 or 2.9 respectively for the load conditions given and at the points of flip and reset.

It is noted that describing an input characteristic with an orifice is limited to elements that have positive values of pressure and flow in the control region. It appears likely that most elements will perform in this manner.

ELEMENT PERFORMANCE

Since it appears possible to represent input characteristics with equivalent orifices and as the input characteristics are loads to the preceding elements it is possible to evaluate the performance of elements on the basis of orifice load tests.

Memory

In the shift register circuit of Figure 1 it is seen that the MEMORY element output loads are equal on each leg and only one input control is pressurized, the other is vented. The test data for a MEMORY element with equal orifice loads and one control vented is shown in Figure 3. The output pressures and the input control pressure and flow are plotted as a function of the load admittance. It is seen that the control admittance with a load admittance between 10 and 80 averages about 6 (Q_c^2/P_c).

Twin-And

A similar characteristic performance is given for the TWIN-AND in Figure 4. In addition and because it has an analog characteristic it is necessary to add the results of test with various control pressures. Figure 4 is the result of this test with control pressures of 0.5, 1.0, 1.5, and 2 psi. Since the unit is analog, the control pressure can be interpreted as a differential control pressure as well.

451

It can be seen from the curves of Figure 4 that the maximum output is obtained when the ratio of control to center inlet pressure is 1.5/5 or 0.3, but this is not a requirement for its use. A test of the input admittance of the TWIN-AND shows that it is about 20 $in^8/lb-sec^2$.

MATCHING

From this data it is possible to determine the steady state matching capability of the MEMORY element and the TWIN-AND. Referring to the shift register circuit of Figure 1, a MEMORY element with a load admittance of 20 has a differential output pressure of about .9 psi and requires a pressure to flip of about .6 psig. In this range of load it has a control input admittance of about 6.

The TWIN-AND with this load admittance, 6, and a differential control pressure, P_c, of .9 psi has an output pressure of about .9 psi. This output is .3 psi greater than the necessary .6 psi for flipping the MEMORY element.

SUMMARY

From this it can be seen that the admittance characteristics, Q^2/P, can be used to select elements to perform a desired function as well as to establish the expected performance of elements in a circuit during trouble-shooting. Tests for quality control purposes can also be made effectively with this method to check performance at specific operating conditions. Experience to date indicates this technique to be satisfactory and extremely useful.

Fig.1 SHIFT REGISTER
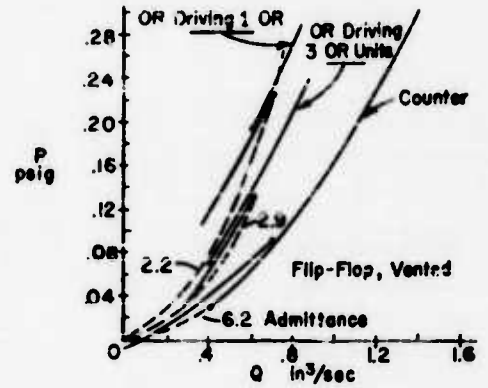
Fig.2 CONTROL IMPEDANCE
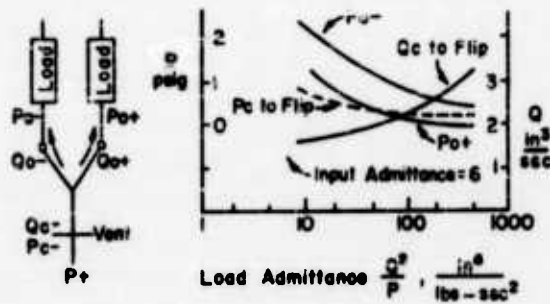
Fig.3 MEMORY UNIT

Fig.4 TWIN "AND"

453
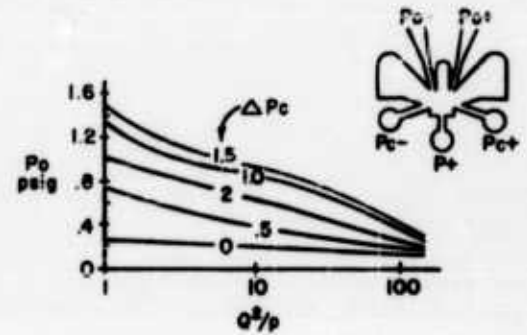
A COMPARISON OF THE RELIABILITY OF ELECTRONIC COMPONENTS AND PURE FLUID AMPLIFIERS

by

Harold L. Fox

of

Sperry Utah Company
Division of Sperry Rand Corporation

ABSTRACT

Current achievements in attaining high reliability for electronic components are compared to the predicted reliability of pure fluid amplifiers. Figures for electronic components are presented for various environmental regimes which may be encountered in industrial, field, and aero-space applications.

Due to the lack of statistical data on pure fluid devices, the predicted reliability results from certain assumptions. The assumptions are discussed. Reliability of pure fluid amplifiers under severe conditions of temperature, vibration, shock and radiation is predicted.

The results of the comparisons of the reliability of electronic components and pure fluid amplifiers are applied to a typical system problem. Predicted system failure rates are given for both electronic and fluid systems.

I. INTRODUCTION

There is much interest today in the design and fabrication of control and computer systems which have an inherent high reliability. The difficulty of maintaining the somewhat ordinary military field weapon system is a serious problem requiring the careful consideration of industry. An even more difficult problem is involved in the maintenance of an orbiting control or computer system. These problems can be lessened or resolved by the use of sufficiently reliable equipment.

To find and utilize suitable control and computer system components is a goal worth achieving. It is to this end that many corporate and government projects are being directed. Does the pure fluid component provide the degree of reliability which is necessary to enable the engineers of both government and industry to design and fabricate control and computer systems to meet today's requirements in field, air and space? To this question this paper is addressed.

It is not the intent of this presentation to explore the more mundane factors involved in the use of pure fluid logic devices, such as, do they function properly in circuits. It would be surprising indeed if the ingenuity of American scientists had not at least partially resolved this problem. Neither is

it the purpose of this paper to define all areas of application of pure fluid systems. This problem we leave to others.

Fluid devices are slower than electronic devices. Nevertheless, it must be mutually recognized that there are control and computer system requirements which are sufficiently time-wise unrestricted that pure fluid logic devices will suffice. Similarly, it is recognized that there are system requirements for high speed data processing which the pure fluid system will never meet. The gray area between these extremes of low speed black and high speed white, is left to present and future fluid system designers.

For those agreed upon areas of application (the area of relatively low speed applications) this paper will compare the reliability of pure fluid logic devices with the present state of the art of reliability of similarly functioning electronic devices. While there is probably no reliability engineer who will admit to having sufficient data for his needs, even in the electronic field, at least there exists a body of electronic experience and data upon which to base quite accurate reliability information.

Accurate reliability information in pure fluid devices is almost non-existent. It is the problem of this paper to indicate the means whereby experience in the use of various materials under various environmental regimes can be used to predict the reliability of a group of pure fluid devices. It has been the author's intent to be conservative in the determination of predicted reliability figures so as to circumvent the apriori determination of a consciously desired high reliability figure. To prevent enthusiasm for pure fluid systems from influencing the predicted reliability of pure fluid devices, the assumptions made and the method used to arrive at predicted reliability figures will be carefully presented.

II. CURRENT ACHIEVEMENT IN RELIABILITY FOR ELECTRONICS

Out of the hoard of books and papers relating to electronic component reliability, one has been selected to represent the current state of the art. By the selection of one listing, at least some degree of selfconsistency in reliability data is achieved. The publication which has been selected is Earles and Eddins, "Reliability Engineering Data Series - Failure Rates". From this publication will be extracted all the necessary reliability information for our electronic circuitry.

To establish a reliability figure for an electronic flip-flop, a selected circuit of transistors, diodes, resistors and appropriate connections is chosen. To establish one of the "best" reliability figures for electronic devices, the "best" data is selected from the list of failure rates of the best components. The following list will give the basic failure data to be used:

<div align="center">

Electronic Reliability Data

</div>

Component	Failure Rate (per 10^6 hrs)[*]
Transistors, silicon	0.01 failures per 10^6 hrs.
Diodes	0.001 failures per 10^6 hrs.
Resistors	0.005 failures per 10^6 hrs.
Connections, per pin or per joint	0.0001 failures per 10^6 hrs.

456

These figures combine both the generic failure rate (GF_r) with an application factor (K_A).

The basic electronic circuitry which is considered for obtaining a reliability figure is:

1. An R S Flip - Flop (2 active, 8 passive elements) (Figure 1)
2. A 4 Input NOR gate (1 active, 6 passive elements) (Figure 2)

Using the failure rate figures for the electronic components given above, a figure of merit can be determined for the electronic flip-flop and the four input NOR gate as follows:

Reliability Calculations

Flip-Flop	Failures per 10^6 hrs. *
2 transistors	.02
8 resistors	.04
20 solder joints	.002
	.062

4 Input NOR Gate	Failures per 10^6 hrs. *
1 transistor	.01
6 resistors	.03
14 solder joints	.0014
	0.0414

* Note that these figures combine the generic failure rate (GF_r) with an application factor (K_A).

A figure of merit (in terms of failures per million hours of operation) for simple electronic circuits has now been established. The failure rates have been selected from the lower limits of the available data. It can, therefore, be expected that the circuits generated are extremely reliable from today's state of the electronic art. (It might be mentioned that this flip-flop compares very favorably with Minuteman circuitry).

III. RELIABILITY FACTORS FOR ELECTRONIC EQUIPMENT FOR VARIOUS ENVIRONMENTAL REGIMES

By making use of the data compiled by Earles and Eddins, figures are determined which indicate the amount of increase in failure rates which is caused by operating electronic equipment in other than laboratory type environments.

It is known by experience and data that if electronic circuitry is operated in environments having increased temperatures that the reliability is less.

457

FIGURE 1
R S FLIP-FLOP

FIGURE 2
4-INPUT NOR GATE

OUTPUT
$$\bar{A} \cdot \bar{B} \cdot \bar{C} \cdot \bar{D} = \overline{A+B+C+D}$$

INPUT

158
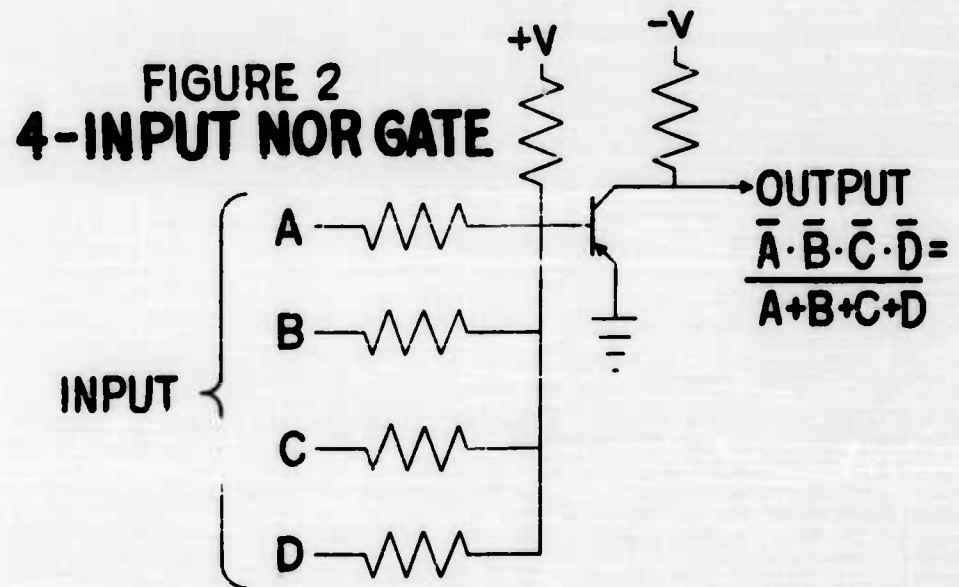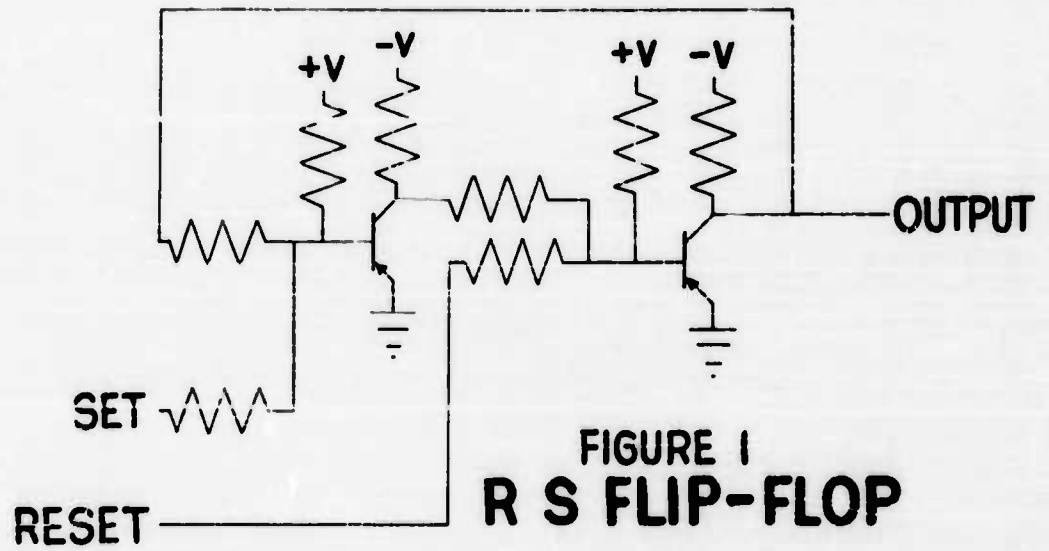
Similarly, if circuits are operated in low temperatures, increased failure rates are experienced. Similar results are observed for radiation environments and for vibration or shock environments.

Table I presents factors which can be used in conjunction with failure rate data to express the increased failures to be expected by operating in various environments.

TABLE I.
EQUIPMENT USAGE FACTORS

Circuit	Lab Conditions	Temp of +150°C	Temp of -50°C	Missile Vibration
Flip-Flop	1	10	5	900
4-Input NOR Gate	1	10	5	900

Radiation Environments. The data relating to degradation of electronic components and their increased failure rates in radiation environments is more difficult to use. The problem is that the duration and intensity of the radiation must be known; the spectrum of the radiation must be specified; and the particular components must be specified. By this time it would probably be necessary to run an actual test to come up with the factor we need. For the purpose of this paper engineers of the reliability department have made the following determinations (best technical judgements) of radiation failure factors:

USAGE FACTOR - RADIATION

Radiation Type	Factor Indicating Increased Failure Rates
Partially shielded Control System for Nuclear Reactor	1000
Vicinity of Atomic Blast (5 miles from 20 megaton)	100
Solar Flare in Cislunar Space	10
Cislunar Space	2

For the purposees of this paper, a 90-day period of operation in these environments is assumed, except that only one nuclear blast or one solar flare is considered.

To make use of these failure rate factors, multiply the failure rate for the flip-flop or NOR gate circuit by the appropriate factor. The resulting

459

product is the new failure rate per 10^6 hours to be expected in these environments.

IV. PREDICTED RELIABILITY FOR PURE FLUID DEVICES

a. The Approach

Within the next few months there will be papers and data published which will start the accumulation of reliability data on pure fluid components, systems, and associated equipment. Today, however, there is not sufficient available data from which to extract failure rate information. This lack of data is not a new problem for reliability analysis, and a means of predicting reliability so as to obtain useful preliminary estimates does exist.

It will be the "piece de resistance" of this paper to demonstrate that by a series of logical considerations useful predicted reliability figures of merit for pure fluid components can be obtained.

Briefly, the approach will be to carefully define the modes of failure which are expected to occur. To do this, some reasonable assumptions as to the methods of fabrication and testing of pure fluid devices must be made. This process involves certain assumptions which will be carefully stated. Then, using the wealth of experience in producing similar items, we shall extrapolate from the known to this new field. It should be emphasized that in using this technique of predicting reliability, this paper will present the conservative approach. In other words, it is to be expected that the predicted figures for failure rates must be interpreted to mean: "We have great confidence that we can do at least this good with today's state of the art of fabrication and testing".

Should it turn out that the conservative figures of merit for pure fluid devices and systems are superior to the optimistic figures of merit for electronics, THEN, we can be confident that the pure fluid devices are indeed a possible answer to the reliability problem. However, should it be shown that the pure fluid devices are not better than the electronic devices, then, it will be necessary to take a better look at the pure fluid devices by appeal to actual test data before these devices are hailed as being ultra-high-reliability elements.

b. Assumptions

The following assumptions will define the approach to the problem of predicting failure rates for pure fluid components. The assumptions are related to the manner in which the components are to be fabricated and used. As a basis for all of these assumptions, today's state of the art in methods of fabrication, inspection and test will be used.

1. It is assumed that the size of each component is such that it will occupy no more than 1/2 cu. inch of volume, including interconnections and packaging.

2. It is assumed that the pure fluid components will be fabricated into a sheet of material such that all components and interconnections

460

will be fabricated into one combination of two joined sheets, and that the inputs and the outputs for these 100 components will be arranged along the edges of the joined sheets.

3. It is assumed that the material used for the fabrication is suitable for the environment in which the material will be used. (For example, high temperature environments will require metal or ceramic materials, high radiation environments will require materials immune to damage by radiation, and high vibration environments will require materials that are resistant to vibration induced failures.)

4. It is assumed that design techniques for packaging will be suitable for the environment in which the package is used. Only today's state of the art design techniques are to be utilized.

5. It is assumed that a prototype unit can be built and tested and minor redesign changes made as determined by tests. This is to say that an ordinary R & D program will be allowed for the development of any particular pure fluid system application.

6. It is assumed that assembly of the pure fluid system is accomplished in a "clean room".

7. It is assumed that appropriate inspection and assembly techniques will be utilized to insure that no incipient failures are present in the material or in the machining or forming of that material.

8. It is assumed that each assembly of 100 components will be appropriately tested to insure that the assembly functions in the manner specified by the designer. This assumption also implies test modes to insure that the assembly operates properly within the range of fluid power, fluid signal pressures, and fluid flows which are part of the system specifications.

9. It is assumed that all fluid used for test or operation of the pure fluid system at all stages of assembly and test is free from any particles which are larger than one hundredth the size of the smallest duct, orifice, or connector dimension.

In the above assumptions, it will be recognized that items 1 through 6 have no statistical nature. It is agreed that these things either can or cannot be accomplished. Therefore, the problems have not been resolved by the assumptions made. Items 7, 8 and 9, however, present a different problem. It is easy to say that no incipient failures exist. To make this statement indicates perfection in inspection techniques. By the same method of making assumptions, any degree of reliability can be assumed into any product which is to be manufactured.

The last three "assumptions" therefore, must be given some statistical evaluation. It is necessary to express in some statistical fashion our confidence that these things can be accomplished within certain confidence levels.

How are these confidence levels for fabrication, assembly and test procedure established? To explore this query, consider how this problem is taken

care of in the electronic gear with which we are familiar. Assume that in the electronic production line printed circuit boards are fabricated and later used in a system. If there exists an incipient failure in a PC board, it may easily develop into a fracture, and if this fracture occurs in the vicinity of a printed conductor, a failure can be expected to occur sooner or later in the system. Inspection and test techniques are therefore geared to this type of problem. The best techniques are used to locate any defects before they become a part of the system.

How do we assess our ability to locate these defects? The answer - by the reliability of the system which is produced! It is true that from many system failures some failures which are pinpointed to such items as PC board fractures can be isolated. However, it is a difficult and sophisticated reliability problem to determine accurately that a particular sequence of test events will insure a given degree of reliability for printed circuit boards. Rather, the reliability expert is reasonably content if the "model" he is using to determine a system mean time between failure is in close agreement with the reported data he receives from systems in use.

The question still remains: Can experience in making today's systems be used to predict our ability to make reliable pure fluid systems? The contention of this paper is that the answer is YES.

Before continuing with the assessment of our ability to turn out reliable pure fluid systems, the modes of failure which might be expected must be described.

c. Modes of Failure

There are three modes of failure which are immediately apparent:

1. The failure of connectors between sheets of components. However, failure rate data is available for such connectors, so predicted failure rates for connectors need not be made.

2. If the fluid contains particles which are large enough to obstruct a duct, orifice, or component failure will probably occur.

3. If the material in which the components are formed separates, cracks, ruptures, peels, fragments, creeps, flows, disintegrates, warps, or twists beyond certain limits, then failure will occur.

No other failure modes are evident. If the pure fluid components are not clogged from particle build-up or improperly vented by fracture of the material, of failure of connectors, then they will work as designed.

The reader will note that the problem of power supply design for maintaining fluid flow has not been examined. Similarly, power supply problems in the electronic circuitry have been ignored. This approach can be justified by remembering that the logical components will be used in far greater number than will power supplies. Therefore, the greater reliability problem is associated with the logical components.

462

d. Predicted Failure Rates

It is contended that experience in fabricating other devices can be used to predict our ability to fabricate pure fluid devices. Examine first the problem involved in the mode of failure which will allow the escape of fluid from or into a duct or component. The Reliability Department engineers suggest that the most likely failure mode will be the separation problem involved in sealing two plates together. Therefore, the following data on somewhat similar problems is submitted:

Failure Rates of Similar Devices

Item	Failure Rates Per 10^6 Hours		
	lower limit	mean	upper limit
Phenolic Gasket	0.01	0.05	0.07
Sliding Seal	0.11	0.3	0.92
Tanks, Hi Pressure, Small	0.044	0.08	1.44
Valves, Air	0.112	0.212	2.29

The reader will agree that today's state of the art permits the sealing of two flat plates together with at least the reliability of an air valve. Similarly, it would not be expected that the failure rates of a phenolic gasket could be reduced (at least not immediately). Therefore, a failure rate one magnitude worse than a phenolic gasket will be predicted. Inasmuch as the electronic failure rates were selected from the lower limit, the figure of 0.01 x 10 or 0.1 will be used for the predicted failure rate for the pure fluid sealing problem.

Inasmuch as the reliability experience indicates that the problems of sealing will be worse than the problems of fracturing or cracking, the figure of 0.01 will be used as the failure rate for fracturing or cracking. The total failure rate as predicted for the failure mode of "improperly ducting" the fluid is 0.11 failures per 10^6 hours.

Next, examine the failure mode related to contamination of the fluid. The internal combustion engine industry has developed some remarkable filters to filter contaminants out of the fuel prior to the time that the fuel flows through the small orifices involved in carburetors or fuel injectors. Similarly, other types of filters have been developed for removing contaminants from gases (even to the extent of the CBR filters). The fluid circulation system can be designed so that the filtered fluid is returned to the pump intake after use in the pure fluid system. By this means, the amount of particle buildup that may occur in the filtering system will be definitely lessened.

This area of predicting the failure rate of fluid systems due to particle contamination, results more in placing design restrictions on the power supply than in anticipating failure rates. However, with the state of the art as it exists, it is submitted that the fluid can be filtered sufficiently well so that the failure rate due to contamination is no greater than 1.0 failures per component board per 10^6 hours. Our engineering staff is confident that this is a reasonable and achievable requirement. A failure rate of 1.0 failures per 10^6 hours is in effect stating that the problem of fluid contamination is an order of magnitude worse than the problem of fluid escape.

The other mode of failure for which, fortunately, there exists data, is the failure of pneumatic joints. For this failure mode the figure of 0.02 failures per 10^6 hours per joint is used (from Earles & Eddins).

463

e. Predicted Failure Rate Per Fluid Component

To predict failure rates per fluid component, it is necessary to determine the number of fluid joints which will be used (on the average) per component plate. The number of inputs and outputs will, of course, vary with the logic fabricated into a component plate. It would be a nominal estimate to assume that ten inputs and ten outputs could be used. We shall be conservative and suggest that 50 inputs and 50 outputs are used. This is an average of one input or output per component. This figure is conservative and errs on the side of larger failure rates per component than would be expected.

The summary of fluid failure rates may now be made:

Fluid Device Reliability

Item	Failure Rates Per 10^6 Hours
Fluid Connectors (100)	2.00
Contamination of a Board	1.00
Fracture or Separation of Board	0.11
Total for One Board of 100 Components	3.11
Average Predicted Failure Rate Per Component	.0311

Table II compares the reliability of two simple electronic circuits with the equivalent pure fluid devices.

TABLE II.
FAILURE RATE COMPARISON

Item	Electronic Calculated	Fluid Predicted
Flip-Flop	0.062	0.0311
4-Input NOR Gate	0.0414	0.0416

f. Application Factors for Fluid Devices Under Extreme Environments

A factor to consider is the change in the failure rates when the fluid devices are subjected to environmental extremes. In the case of electronic equipment, the change in characteristics as a function of temperature is well documented. In the case of pure fluid devices, the problem becomes one of assessing the effect of different temperature regimes on the problem of component board fracture or separation and fluid contamination. While it is readily apparent to the reader that there is some difficulty in predicting an exact factor to represent the increase in failure rates, it is also apparent that a much simpler type of phenomena is being considered in the case of the pure fluid components than in the case of the intricately made and assembled electronic components.

It is the opinion of several of my colleagues that an increase of 100°C in the temperature should no more than double the fluid device failure rate. This predicted factor is presented as being conservative for at least the first 100C°. Operating environments higher than 1000° C are a bit outside of our realm of experience and is left for further evaluation.

A similar estimate of the increase of failure rates for low temperature is that the failure rates double for each reduction of 100° C. This is presented as a reasonably conservative figure down to -200° C. Below this figure, the author would have consult the cryogenics specialists.

A look at the radiation environments leads to the conclusion that appropriate materials can be selected such that the radiation effects are negligible. But to be conservative, a factor of 10, by which to multiply failure rates, is selected when fluid systems are used in the vicinity of a nuclear reactor.

For the environments of vibration, the argument is that it is much easier to protect packaged fluid elements than it is to protect the more delicate electronic components. A conservative factor for increasing the failure rates is ten.

Table III summarizes the usage application factors. To obtain system failure rates for systems used in various environments, multiply the component or system failure rates by the appropriate application factor.

V. SYSTEM APPLICATION OF FAILURE RATES

While the previous section indicates the predicted failure rates for fluid components and application factors for determining failure rates for various environments, it does not indicate the results of system application of the data. To adequately carry out the comparison of electronic versus pure fluid reliability, it is necessary to go one step farther.

In the application of fluid devices in a control or computer system, it is necessary to know the task for which the system is designed. In many cases, a fluid system will require a much larger number of components than will the electronic system due to the higher speed of the electronic elements. Therefore, to properly compare the two systems, it is necessary to take into account the logical design of the control or computer system.

A good example is the case of an electronic fire control computer which has the task of providing the firing program necessary to prepare and launch a missile. An electronic system to do this task can be made with far fewer flip-flops and NOR gates than if the 100 times slower fluid flip-flops and NOR gates are used. An analysis of the two computers provides the basic data found in Table IV. By comparison of the two systems designed to accomplish the same function (in this case a fire control function), the electronic system is 16 times as good as the fluid system.

However, the case for fluid systems versus electronic systems is not as bad as it first appears when we consider also the effect of usage factors. Table IV presents the case for the two systems used in the environment of a laboratory type computer. Table V summarizes the failure rates which would be expected if we used these same two systems in various environments.

TABLE III.

USAGE APPLICATION FACTORS

Application	Electronics Application Factors	Pure Fluid Devices Application Factors
Laboratory Computer	1	1
Ambient Temperature		
$+ 150^o$ C	10	2
$- 50^o$ C	5	2
$+ 250^o$ C	Transistors fail to function	3
$- 150^o$ C	" "	4
Radiation		
Cislunar Space	2	1
Solar Flare	10	2
Nuclear Blast	100	5
Nuclear Reactor Vicinity	1000	10
Missile (Vibration Environment)	900	10

466

TABLE IV.

SYSTEM COMPARISON

Specifications: NOR Logic
14-Bit Word Length
Perform fire control computation functions
in sixty seconds.

Electronic	Fluid
Basic components are 100 times as fast as fluid components.	Slower components
Use serial operation	Use parallel operation
Use sequential control of arithmetic unit.	Use polymorphic operation for computation.

Failure Rates

2.6 failures per 10^6 hours   41.4 failures per 10^6 hours

Note: The reader will recognize that the electronic system has an exceptionally low failure rate, and that the predicted failure rate for the fluid system is extremely good.

As is shown in Table V the fluid system with our conservatively predicted failure rates is superior to the optimistic electronic system in the areas of extremes of temperature, high radiation and high vibration environments. It should also be pointed out that the demand on the system was a fairly severe one and for systems in which the demands are relaxed (timewise), the fluid systems could be designed with fewer components and therefore experience lower failure rates.

In summary, it is predicted that pure fluid devices are here to stay and this new engineering area deserves your further research and development efforts.

TABLE V.

SYSTEM COMPARISON SUMMARY

Usage	Failure Rates		
	Electronic	Fluid	Ratio (Elec/Fluid)
Laboratory Computer	2.6	41.4	1:16
Temperature			
+ 150° C	26	83	1:3
- 50° C	13	83	1:6
+ 250° C	large	124	5:1
- 150° C	large	165	5:1
Radiation			
Cislunar Space	5.2	41.4	1:8
Solar Flare	26	83	1:3
Nuclear Blast	260	207	1.2:1
Nuclear Reactor	2600	414	6:1
Vibration			
Missile Guidance	2340	414	6:1

Note: Where the ratios are underline the fluid system is superior.

468

BIBLIOGRAPHY

Blundell, L. and Brashear, R., "On the Successful Application of a Repeated Test to Failure Program for Sergeant Missile Assemblies". A Sperry Utah Company paper presented at the Seventh Military-Industry Missile and Space Reliability Symposium. NAS North Island, June 18-21, 1962.

Brett, J., "Grain Boundary Cracking in Metals Under Stress at Elevated Temperatures", General Telephone and Electronics Laboratories, Bayside, N.Y., Final Report, June 15, 1961.

Earles, D. R. and Eddins, M. F., "Reliability Engineering Data Series - Failure Rates", Reliability Analysis Section; Research and Advanced Development Division, Avco Corporation, Wilmington, Massachusetts, April 1962.

Firth, W.G., "Effects of Nuclear Radiation Burst On the Minuteman Guidance and Control Transistor Flip-Flop", The Boeing Company, Seattle, Washington, Report No. D7-2641.

Sante, D. P., "Ultrareliability Techniques for Communication Equipment", Sylvania Electronic Systems, Buffalo, N. Y., September 1960.

"Development and Evaluation of High-Temperature Resistant Composite Plastic Plates", Midwest Research Institute, Quarterly Progress Report #3, MRI Project No. 2380-C, November 11, 1960.

469

Robert B. Adams	Moore Products Co.	H & Lycoming Streets Philadelphia 24, Pa.
Clifford Allen	Westinghouse Air Brake Co.	Wilmerding, Pa.
Laird R. Allen	Westinghouse Electric Corp.	1310 Beulah Road Churchill Boro. Pittsburgh 35, Pa.
Louis Aronica	The Library of Congress Science and Tech. Div.	Washington 25, D. C.
Clarence W. Asche	Autonetics	Box 661, Anaheim, Calif.
Raymond N. Auger	Fluid Logic Control Systems	456 Riverside Drive New York 27, New York
Gene Bahniuk	The Weatherhead Company	300 East 131 Sstreet Cleveland 8, Ohio
Capt. V. Bailey	Army Materiel Command	Washington 25, D. C.
Howard Barry	Bowmar Instrument Corp.	8000 Bluffton Road Fort Wayne, Indiana
Kenneth Becker	Vickers Inc.	Troy, Michigan
B. B. Beeken	Pitney-Bowes Inc.	Walnut and Pacific Sts. Stamford, Conn.
Charles A. Belsterling	The Franklin Institute	Philadelphia 3, Pa.
Lt Charles F. Bentz	Air Force Systems Command	Wright-Patterson AFB Ohio
Stanley G. Best	Hamilton Standard Div. United Aircraft Corp.	Windsor Locks, Conn.
A. W. Blackman	United Aircraft Corp. Research Laboratories	East Hartford 8, Conn.
William B. Blesser	Fluid & Electro Devices Corp.	11-11 131st Street College Point 56, N. Y.

Dr. Gabriel D. Boehler	AEROPHYSICS CO.	17 Dupont Circle Washington 6, D. C.
W. A. Boothe	General Electric Co.	One River Road Schenectady 5, N. Y.
Allen Atvill Bowers	University of Maryland	College Park, Md.
R. E. Bowles	Bowles Engineering Corp.	9347 Fraser St. Silver Spring, Md.
George Boyadjieff	University of California Lawrence Radiation Lab.	P. O. Box 808 Livermore, Calif.
Mr. William T. Bradley	Research and Engineering Support Division Institute for Defense Analyses	1825 Conn. Ave., N.W. Washington 9, D. C.
Professor Forbes T. Brown	Mass. Institute of Technology	Cambridge, Mass.
Wm. J. Brown	R&D Directorate Army Materiel Command	Washington 25, D. C.
W. Kenneth Bullivant	Munitions Development Div. Chemical Corps Biological Laboratories	Fort Detrick, Md.
O. R. Burggraf	Lockheed Missiles & Space Co.	3251 Hanover St. Palo Alto, Calif.
Joe L. Byrd	Redstone Arsenal	Alabama
Frank J. Coldwell	National Cash Register	Main & K Sts. Dayton 9, Ohio
Richard S. Carlson	Applied Physics Laboratory The Johns Hopkins University	8621 Georgia Ave. Silver Spring, Md.
Charles F. Cartledge, Jr.	American Bosch Arma Corp.	Springfield 7, Mass.
Mr. Robert Chamberlain	General Precision, Inc. Kearfott Division	808 17th St., N. W. Washington 6, D. C.
Professor Paul K. Chang	The Catholic University of America	Washington 17, D. C.
B. J. Clayton	Redstone Arsenal	Alabama
H. A. Clutz	LTV Chance Vought Corp.	P. O. Box 5907 Dallas 22, Texas

472

Whitney Levander Cochran	Corning Glass Works	Bradford, Penn.
Bernard C. Coffin	Minneapolis-Honeywell	2600 Ridgway Road Minneapolis 40, Minnesota
John R. Colston	Bowles Engineering Corp.	9347 Fraser St. Silver Spring, Md
C. E. Coon	Tung-Sol Electric Inc.	1 Summer Ave. Newark 4, N. J.
Ray E. Cooper	Southwest Research Institute	8500 Culebra Rd. San Antonio 6, Texas
Dr. Arvid Corneliussen	Applied Mechanics Div. Sperry Rand Research Center	North Road (Route 117) Sudbury, Mass.
Dr. G. T. Croft	Pitney-Bowes Inc.	Walnut and Pacific Sts. Stamford, Conn.
Felix Crommie	U. S. Army Munitions Command	Picatinny Arsenal Dover, N. J.
Howard A. Curtiss	Giannini Controls Corp. Berwyn, Pa	8 Leopard Rd.
Charles Daniel	Martin Marietta Corp.	Baltimore, Md
Norman C. Davis	Central Intelligence Agency	Washington 25, D. C.
A. H. Delmege	Corporate Research and Development, Vickers Inc.	Troy, Michigan
George Demitrack	Picatinny Arsenal	Dover N. J.
Russell Ernest Denker	Telecomputing Corp. Whittaker Controls & Guidance	16217 Lindburgh St. Van Nuys, Calif.
Edwin M. Dexter	Bowles Engineering Corp.	9347 Fraser St. Silver Spring, Md
Mr. Robert Dockery	National Bureau of Standards	Conn. Ave. & Van Ness Sts. Washington 25, D. C.
Charles Doolittle	Westinghouse Air Brake Co.	Wilmerding, Pa
Stanley Doroff	Office of Naval Research	Washington 25, D. C.

Dr. Darshan S. Dosanjh   L. C. Smith College of Engrg.   Syracuse 10, New York
Syracuse University

Angelo Doumcoucos   General Electric Company   Lakeside Avenue
Burlington, Vermont

Victor L. Dowdell   Taylor Instrument Company   Rochester 1, New York

Verner Egli   Minneapolis-Honeywell   2600 Ridgway Road
Regulator Company   Minneapolis, Minnesota

John J. Eige   Stanford Research Institute   Menlo Park, California

E. J. Ellis   International Business Mach.   1701 North Street
General Products Division   Endicott, New York

Gerald Elsbach   Ampex Corporation   934 Charter Street
Redwood City, California

F. Richard Emmons   United Aircraft Corporation   Windsor Locks,
Hamilton Standard Division   Connecticut

Dr. Robin Esch   Sperry Rand Research Center   North Road (Route 117)
Applied Mechanics Division   Sudbury, Massachusetts

Kenneth Evans   Redstone Arsenal   Huntsville, Alabama

R. A. Evans   Minneapolis-Honeywell   2600 Ridgway Road
Regulator Company   Minneapolis, Minnesota

T. K. Faison   National Bureau of Standards   Conn. Ave. & Van Ness St.
Washington 25, D. C.

Andrew D. Farrell   The Bendix Corporation   1730 K Street, N.W.
Washington, D. C.

Delbert C. Faust   Norgren Company   3400 South Elati Street
Englewood, Colorado

Frank Feoranz   Curtiss-Wright   35 Market Street
Electronics Division   East Paterson, New Jersey

Hugh M. Fitzpatrick   Systems Engineering Division   4936 Fairmont Avenue
Pneumodynamics Corporation   Bethesda 14, Maryland

H. L. Fox   Sperry-Utah Company   322 North 21st West
Salt Lake City 16, Utah

Samuel A. Francis   Francis Associates   Bradford, Pennsylvania
Corning Glass Works

Fred Frishman,	Sciences Div. Army Research Office	Washington 25, D. C.
William G. B. Gardner	Pratt & Whitney Aircraft	East Hartford 8, Conn.
William F. Gesell	Mechanical Dept. Research & Development Sheffield Corp.	Dayton 1, Ohio Box 893
Admiral Frank Giambattista	Plasmadyne Corporation	3839 S. Main Street Santa Ana, Calif.
Stuart D. Gilchrist	Martin Company	Orlando, Florida
Fabio Goldschmied	Remington Rand Univac Division of Sperry Rand Corp.	P. O. Box 500 Blue Bell, Pa.
S. John Gorman	Bureau of Naval Weapons	Washington 25, D. C.
Gunars Grabis	Tracerlab, Div. of Laboratory for Electronics Inc.	1601 Trapelo Road Waltham 54, Mass.
Lucius P. Gregg, Capt USAF	Mechanics Div. Directorate of Engineering Sciences Air Force Office of Scientific Research	Washington 25, D. C.
Charles J. Grimland	The Geotechnical Corporation	3401 Shiloh Rd. Garland, Texas
Richard J. Gurski	Mass. Inst. of Technology	Cambridge, Mass.
Lt. J. F. Hall	Aeronautical Systems Div. Air Force Systems Command USAF	Wright-Patterson AFB Ohio
Roy Tyler Hardin	General Electric Co.	Lakeside Ave. Burlington, Vermont
John L. Harned	General Motors Research Lab.	Warren, Michigan
R. Barnett Harper	Sperry Utah Co., Sperry Rand	322 North 21st West Salt Lake City, Utah
F. Jack Hartley.	Bowmar Instrument Corp.	800 Bluffton Road Fort Wayne, Indiana

Ralph J. Havens.	Pegann Air Inc.	P. O. Box 3497 Glendale 1, California
Russel W. Henke	Fluid Power Institute Milwaukee School of Engineering	1025 N. Milwaukee St. Milwaukee 1, Wisc.
Dr. Beatrice Hicks	Newark Controls Co.	15 Ward Street Bloomfield, New Jersey
P. T. Higgins	Bendix Corporation, Research Lab.	Southfield, Michigan
A. H. Hobelmann	Kidde Aero-Space Division Walter Kidde & Co. Inc.	Belleville 9, New Jersey
Alton V. Hooper	Plasmadyne Corporation	3839 S. Main St. Santa Ana, Calif.
Richard H. Hronik	Melpar, Inc.	3000 Arlington Blvd. Falls Church, Va
Ronald L. Humphrey	Bowles Engineering Corp.	9347 Fraser St. Silver Spring, Md
Theodore Sanford Insland	Bailey Meter Company	1050 Ivanhoe Rd. Cleveland 10, Ohio
Lt. Col. R. S. Isenson	Physical Sciences Div. Army Research Office	Washington 25, D. C.
Paul E. Jaquish	Defence Research Labs. General Motors Corp. Box T	Santa Barbara, Calif.
Norman L. Jeglum	Director Research and Dev. The Sheffield Corporation	The Sheffield Corporation Dayton 1, Ohio
Evelyn S. Jetter	Newark Controls Co.	15 Ward Street Bloomfield, New Jersey
Frederick D. Joesting	Minneapolis-Honeywell Regulator Co.	8330 No. Austin Ave. Morton Grove, Illinois
F. T. John	Zygon Corporation	16900 Scenic Place Pacific Palisades, Calif.
Andrew I. Johnson	Continental Aviation and Engineering Corp.	12700 Kercheval Detroit 15, Michigan
Charles Jones	General Precision, Inc.	Kearfott Div. 808 17th Street, N. W. Washington 6, D. C.

476

Roger Clyde Jones	Melpar Inc.	3000 Arlington Blvd. Falls Church, Va
Ronald Jones	Bowles Engineering Corp.	9347 Fraser Street Silver Spring, Md
Mr. John A. Kallevig	Minneapolis-Honeywell	2600 Ridgway Rd. Minneapolis 40, Minn.
Dr. David Katsanis,	U. S. Army Munitions Command Frankford Arsenal	Philadelphia 37, Pa
Julius Kendall,	Kendall & Associates	44 East 53rd Street New York 22, N. Y.
S. E. Ketner	W. R. Grace & Co.	Washington Research Center, Clarksville, Md
B. G. Kibby	Temco Electronics Div.	P. O. Box 6118 Dallas 22, Texas
David B. Kirk	Moore Products Co.	H & Lycoming Sts. Philadelphia 24, Penna.
Howard Knoer	Avco Corp.	2630 Glendale-Milford Rd. Cincinnati 15, Ohio
Herman N. Knoll	Radio Corporation of America Defense Electronic Products	Camden, New Jersey
Edward J. Kompass	Control Engineering	330 West 42nd St. New York 36, N. Y.
Joseph Packard Laird, Jr	Engineering Dept. E. I. du Pont de Nemours & Co.	Wilmington 98, Delaware
H. J. Lamon	Minneapolis-Honeywell	2600 Ridgway Rd. Minneapolis 40, Minnesota
R. P. Lawler	The Foxboro Company	Foxboro, Massachusetts
Thomas J. Lechner	Johnson Service Co.	507 East Michigan St. Milwaukee 1, Wisc.
Frank C. Legler	Atomic Energy Commission	Washington 25, D. C.
William S. Lemire, Jr.	Leslie Co.	Lyndhurst, N. J.
Guido A. Lemke	IBM Room 12-154	P. O. Box 218 Yorktown Heights, N. Y.

G. V. Lemmon	Sandia Corporation	Sandia Base Albuquerque, N. M.
David J. Liquornik	Giannini Controls Corp.	8 Leopard Rd. Berwyn, Pa
H. H. Long	Research and Dev. Division E. I. Du Pont De Nemours & Co	Wilmington, Delaware
Melvin E. Long	Machine Design Magazine	Penton Bldg. Cleveland 13, Ohio
Herman H. Lowell	National Aeronautics and Space Administration	Washington 25, D. C.
J. P. Madurski	Bendix Corporation	Southfield, Michigan
Francis M. Manion	Bowles Engineering Corp.	9347 Fraser St. Silver Spring, Md
John Mattern	Westinghouse Electric Corp.	Box 1897, Baltimore 3, Md
Capt. David C. May, Jr.	Aeronautical Systems Div. Air Force Systems Command USAF	Wright-Patterson Air Force Ohio
Thomas McBirney	Applied Physics Lab. The Johns Hopkins Univ.	8621 Georgia Ave. Silver Spring, Md
Maurice W. McCabe	Aeronautical Systems Div. Air Force Systems Command	Wright Patterson Air Force Base, Ohio
Major McLeary	Missiles Div. OCRD Headquarters Dept. of the Army	Office of the Chief of Research and Development, Wash. 25, D. C.
Edward W. McGraw	Goodyear Aircraft Dept. 473	Akron 15, Ohio
George F. McKay	Central Intelligence Agency	Washington 25, D. C.
John C. Mentzell	Westinghouse Electric Corp.	Box 1897 Baltimore 3, MD
Dr. Wolfgang Menzel	National Aeronautics and Space Administration	Washington 25, D. C.
Eric E. Metzger	Bowles Engineering Corp.	9347 Fraser St. Silver Spring, Md
C. C. Miesse,	Westinghouse Astronuclear Lab.	P. O. Box 10864 Pittsburgh 36, Pa

Robert Mockenhaupt	Minneapolis-Honeywell	2600 Ridgway Rd. Minneapolis 40, Minn.
Robert G. Moore,	Bendix Corp.	South Bend 20, Indiana
Robert V. Muffley	Stanford Research Institute	Menlo Park, Calif.
John T. Muller,	Leslie Co.	Lyndhurst, N. J.
Walter Munch	The Baldwin Piano Co.	1801 Gilbert Ave. Cincinnati 2, Ohio
Desmond Joseph Nelson	Marquardt Corporation	16555 Saticoy St. Van Nuys, California
O. B. Noren	Parke Davis	Detroit, Michigan
Howard North, Jr.	Gas Turbine Dept. Lycoming Div. of AVCO Corp.	Stratford, Conn.
Richard E. Norwood	IBM General Products Div.	Endicott, New York
Henry M. O'Bryan	Bendix Corp.	1730 K Street, N. W. Washington, D. C.
R. E. Olsen	United Aircraft Corp. Research Lab.	East Hartford 8, Conn.
William C. O'Neill	Thermo Dynamics Systems Engineering Div.	4936 Fairmont Ave. Bethesda 14, Md
Stanley Ostrow	Sensonics Inc.	3831 Plyers Mill Road Kensington Maryland
Dr. Paul Pagerey	Taylor Instrument Co.	Rochester 1, New York 95 Ames Street
Dr. Gene Parrish	U. S. Army Research Office	Box CM Duke Station Durham, North Carolina
Robert H. Pettey	Redstone Arsenal	Redstone, Alabama
Charles R. Phillips	DEP, Radio Corporation of America	Moorestown, N. J.
Wayne E. Phillips	Beckman Instruments	2500 Harbor Blvd. Fullerton, Calif.
J. Pimlott	Army Materiel Command	Washington 25, D. C.
Dr. Alan Powell	Aerosonics Lab.	University of California Los Angeles 24, Calif.
Stanley V. Preskitt	The Geotechnical Corporation	3401 Shiloh Rd. Garland, Texas

Mr. Albert Ragati	Curtiss-Wright	35 Market Street East Paterson, N. J.
Mr. Edward Kenneth Renke	Holley Carburetor Company	11955 E. Nine Mile Rd. Warren, Michigan
R. F. Rasmussen	Minneapolis-Honeywell	2600 Ridgway Rd. Minneapolis 40, Minn.
Charles F. Rees,	Weston Hydraulics	7500 Tyrone Ave. Van Nuys, Calif.
Karl N. Reid	Mass. Inst. of Technology	Cambridge, Mass.
R. J. Reilly	Minneapolis-Honeywell	2600 Ridgway Rd. Minneapolis, Minn.
Richard A. Retta	Navy Bureau of Weapons	Washington 25, D. C.
J. L. Reynolds	Marquardt Corp.	Van Nuys, Calif.
T. Kenneth Riggs	General Kinetics Incorporated	2611 Shirlington Rd. Arlington 6, Va
Ronald L. Ringo	Aeronautical Systems Div.	USAF Wright-Patterson Air Force Base, Ohio
Hugh E. Riordan	Kearfott Div. General Precision, Inc.	808 - 17th St. N. W. Washington 6, D. C.
Eugene S. Rocks	Sperry Gyroscope Co.	Garden City, New York
Gilbert M. Rosenberg	Army Material Command Development Div. R. & D. Directorate	Washington 25, D. C.
Wm. T. Sacket Jr.	Minneapolis-Honeywell	2600 Ridgway Rd. Minneapolis 40, Minn.
George Salume	Springfield Armory	Springfield, Mass.
Robert M. Salemka	The Bendix Corporation	South Bend 20, Indiana
Dr. Turgut Sarpkaya	Bancroft Hall 219	University of Nebraska Lincoln 8, Nebraska
Mr. T. T. Sawyer	Thiokol, Chemical Corp.	Huntsville Plant Huntsville, Alabama
Ted K. Scarff	National Water Lift Co. A Division of Pneumodynamics	2220 Palmer Ave. Kalamazoo, Michigan

Robert E. Schaffer	IBM, General Products Division, Development Lab.	Endicott, New York
Alfred Scheide	The Baldwin Piano Co.	1801 Gilbert Ave. Cincinnati 2, Ohio
Dr. A. E. Schmidlin	Kidde Aero-Space Div.	Belleville 9, N. J.
Col. R. Schnittke	Army Materiel Command R. & D. Directorate	Washington 25, D. C.
Zolly Carleton Van Schwartz	Zolly C. Van Schwartz M.S. - M.E.	2509 East Floyd Ave. Cherry Hills Heights Englewood, Colorado
Marvin Schweiger	Bowles Engineering Corp.	9347 Fraser St. Silver Spring, Md
Morton Russell Shaw	Corning Glass Works	Bradford, Pennsylvania
William Sheeran	Syracuse University Department of Mechanical Engineering	Syracuse 10, New York
Dr. J. N. Shinn	General Electric	One River Road Schenectady 5, New York
Charles A. Shreeve	Bowles Engineering Corp.	9347 Fraser St. Silver Spring, Md
Dr. Bennett L. Silverstein	Office of Naval Research	Washington 25, D. C.
Anton K. Simson	Massachusetts Institute of Technology	Cambridge, Mass
Dr. Turner L. Smith	Aberdeen Proving Grounds	Ballistic Research Lab. Aberdeen, Md
Edwin U. Sowers	Bowles Engineering Corp.	9347 Fraser St. Silver Spring, Md
Roy R. Stevens	Westinghouse Air Brake Co. Industrial Products Div.	916 Ring Bldg. 1200 - 18 St. N. W. Washington 6, D. C.
A. Rivington Stone	Applied Physics Laboratory Johns Hopkins University	8621 Georgia Ave. Silver Spring, MD
Charles K. Taft	Case Institute of Technology	Cleveland Ohio
L. D. Taylor	Vickers Incorporated	Troy, Michigan

Theodore C. Taylor	Massachusetts Institut of Technology, Dept. of Aeronautics and Astronautics	Instrumentation Lab. Cambridge, Mass.
Walt Thomas	Univac Division Sperry Rand Corporation	P. O. Box 500 Blue Bell, Pa
R. Thorkildson	Army Materiel Command R. & D. Directorate	Washington 25, D. C.
Leonard Trugman	Bendix Corp. York Division	York, Pennsylvania
Henry Bell Tryon	Bailey Meter Company	1050 Ivanhoe Road Cleveland 10, Ohio
Marshall P. Tulin	Hydronautics Inc.	200 Monroe Street Rockville, Md
Robert F. Turek	Hamilton Standard Division United Aircraft Corporation	Windsor Locks, Conn.
Robert Wyant VanTylburg	Corning Glass Works	Bradford, Pennsylvania
W. Geoffrey Wadey	Bowles Engineering Corp.	9347 Fraser Street Silver Spring, Md
Alexander Wagnecz	U. S. Army Munitions Command Picatinny Arsenal	Dover, New Jersey
Ronald E. Walker	Applied Physics Laboratory The John Hopkins University	8621 Georgia Ave. Silver Spring, Md
Mr. Martin W. Wambsganss	Johnson Service Company	507 East Michigan St. Milwaukee 1, Wisconsin
R. L. Warren	Temco Electronics Div.	P. O. Box 6118 Dallas 22, Texas
Dr. William F. Warren	U. S. Naval Ordnance Laboratory	White Oak, Silver Spring, Md
Dr. Richard R. Weber	Cincinnati Milling Machine Co.	Cincinnati 9, Ohio
Manuel Weinstock	Ballistics and Supporting Research Branch	U. S. Army Munitions Command, Frankford Arsenal, Philadelphia 37, Pennsylvania
Paul Whitmarsh	Systems Development Engineer Minneapolis Honeywell Brown Div.	Grace Rd., Star Rt. Pottstown, Penna.

Richard V. Wible	Aeronautical Systems Div. Air Force Systems Command USAF	Wright-Patterson AFB, Ohio
William H. Wilkinson	Battelle Memorial Institute	505 King Ave. Columbus 1, Ohio
James G. Williams	U. S. Army Missile Command	Redstone Arsenal, Alabama
Richard Isaac Windsor	Assistant Director University of Maryland	Colleg Park, Md
Philip Eugene Wood	Continental Aviation and Engineering Corp.	12700 Kercheval Detroit 15, Michigan
Seth A. Young	Aeronautical Systems Division Air Force Systems Command	USAF, Wright-Patterson Air Force Base, Ohio
Samuel Rudewitz, P. E.	Samuel Rudewitz Co.	2789 Valentine Ave. New York 58, N. Y.
Brig.Gen. John G. Zierdt	Deputy Director, Research and Development, Army Materiel Command,	Washington 25, D. C.
Hermann Ziermann	United Aircraft Corp. Corporate Systems Center	Windsor Locks, Connecticut
Ward H. Zimmerman	Boeing Comapany, Aero Space Div.	P. O. Box 3707 Seattle 24, Wash.
Melvin Bernard Zisfein,	Giannini Controls Corp. Astromechanics Research Div.	#8 Leopard Rd. Berwyn, Penna.
Dr. Glen W. Zumwalt,	Oklahoma State University Dept. of Mechanical Engineering	Stillwater, Oklahoma

483

Office of the Director of Defense Research & Engineering
AMC Detachment No. 1, Temporary Bldg I
  Attn: Technical Library (2 copies)

Commandant
U.S. Army Artillery & Guided Missile School
Fort Sill, Okla
  Attn: Combat Development Department

Commander
U.S. Naval Ordnance Laboratory
White Oak, Silver Spring 19, Md.
  Attn: Technical Library (2 copies)

Commanding General
White Sands Missile Range
White Sands, New Mexico
  Attn: ORDES-OM, Tech Library

Commanding Officer
Watervliet Arsenal
Watervliet, New York
  Attn: Technical Library

Transportation Research Command
Ordnance Liaison Officer
Fort Eustis, Va.

Commanding Officer
Picatinny Arsenal
Dover, New Jersey
  Attn: Technical Library (3 copies)

Commanding General
Ordnance Weapons Command
Rock Island, Ill
  Attn: Technical Library

Ordnance Technical Intelligence Agency
Arlington Hall Station
Arlington 12, Virginia
  Attn: Technical Library

Commanding Officer
Ordnance Special Weapons
Ammunition Command
Dover, New Jersey
  Attn: Technical Library

Commanding Officer
Ordnance Materials Research Office
Watertown Arsenal
Watertown 72, Mass.
   Attn: Director's Office

Director, Special Weapons
Office of the Chief of Research & Development
Department of the Army
Washington 25, D. C.

Commanding General
U.S. Army Electronics Proving Ground
Fort Huachuca, Arizona
   Attn: Technical Library

Director, Army Research Office
Office of the Chief of Research & Development
Department of the Army
Washington 25, D. C.
   Attn: Technical Library

Commanding Officer
Department of the Army
Springfield Armory
Springfield 1, Mass.
   Attn: TIU

Commanding Officer
AMC Detachment No. 1 Temporary Bldg 1
Washington 25, D. C.
   Attn: ORDTU
   Attn: ORDTS
   Attn: ORDTN
   Attn: ORDTB
   Attn: ORDTX
   Attn: ORDTW

Commanding General
Headquarters, U.S. CONARC
Materials Developments Section
Fort Monroe, Virginia
   Attn: MD-1

Commanding Officer
New York Ordnance District
770 Broadway
New York 3, N. Y.
   Attn: William P. Blake

Commanding Officer
Los Angeles Ordnance District
55 S. Grand Avenue
Pasadena, California
     Attn: V. V. Barker

Commanding Officer
Frankford Arsenal
Philadelphia 37, Pennsylvania
     Attn: Reference Librarian (3 copies)

Commanding General
Engineering Research & Development Laboratory
Fort Belvoir, Virginia
     Attn: Technical Library

Department of the Army
Office of the Chief of Research & Development
Washington 25, D. C.
     Attn: Chief, Combat Material Div

Department of the Army
Army Research Office
The Pentagon, Washington 25, D. C.
     Attn: Lt Col J. T. Brown, Office, Chief of R & D

Commanding General
OTAC
Detroit Arsenal
Centerline, Mich
     Attn: Technical Library

Commandant
Command & General Staff College
Archives
Fort Leavenworth, Kansas

Commanding Officer
Chemical Warfare Laboratories
Army Chemical Center, Md.
     Attn: Technical Library

Commanding Officer
Camp Detrick
Frederick, Maryland

Commanding Officer
U.S. Army Signal Research & Development Laboratory
Fort Monmouth, N. J.
     Attn: Technical Library
     Attn: Arthur Daniel

487

Commanding Officer
Army Research Office (DURHAM)
Box CM, Duke Station
Durham, N. C.

Commanding General
U.S. Army Ordnance Missile Command
Redstone Arsenal, Alabama
  Attn: Technical Library (3 copies)
  Attn: ORDXM-REE, Bldg 7446, Charles Schriener

Commanding General
Aberdeen Proving Ground
Branch 3, Bldg 400
Aberdeen, Maryland
  Attn: Tech Library (4 copies)

U.S. Army Artillery Board
Missile Division
Fort Bliss, Texas
  Attn: Technical Library

U.S. Naval Underwater Sound Laboratory
Fort Trumbull
New London, Conn.
  Attn: Technical Library
  Attn: Research Division, Dr. R. Berman

Department of the Navy
Chief, Office of Naval Research
Washington 25, D. C.

Department of the Navy
RRRE-3L
Bureau of Naval Weapons
Washington 25, D. C.
  Attn: S. J. Gorman

Commander
Naval Ordnance Laboratory
White Oak, Silver Spring, Maryland
  Attn: B. Gilbert

Commander
U.S. Naval Ordnance Laboratory
Corona, California
  Attn: Technical Library

Commander
U.S. Naval Ordnance Test Station
China Lake, California
  Attn: Technical Library

488

Commanding Officer
U.S. Army Limited War Laboratory
Aberdeen Proving Ground, Maryland
    Attn: Lt Col J. T. Brown

Mr. W. S. Hinman, Jr.
Deputy Assistant Secretary of the Army
Research & Development
Room 3E390, The Pentagon
Washington 25, D. C.

Office of the Director of Defense
Research & Engineering
Asst. Dir of Research Engineering (Defense)
The Pentagon, Washington 25, D. C.

Institute for Defense Analysis
Gordon Rausbeck
Advanced Research Projects Div
The Pentagon,
Washington 25, D. C.

Commander
U.S. Naval Ordnance Laboratory
Corona, California
    Attn: Technical Library

 Jet Propulsion Laboratory
 Pasadena, California
    Attn: Library

USCONARC
Liaison Group
The Pentagon (Rm 3E366)
Washington 25, D. C.

Office of the Director of Defense Research & Engineering
AMC Detachment No. 1
Temporary Bldg I
Washington 25, D. C.
    Attn: Director of Weapons Systems Evaluation Group (Rm 2E812)

Commander
U.S. Naval Ordnance Test Station
China Lake, California
    Attn: Technical Director

Commander
Edwards Air Force Base, Calif
    Attn: AFTTC(FTOOT)

Commander
Naval Research Laboratory
Washington 25, D. C.
    Attn: Technical Library

Commandant
U.S. Marine Corps
Code A04F
Washington 25, D. C.

Department of the Navy
Bureau of Naval Weapons
Washington 25, D. C.
    Attn: Code CACF-3

Department of the Navy
Chief of Naval Operations
R & D Planning Group
The Pentagon, Washington 25, D. C.

Commander
Aeronautical Systems Division
Wright-Patterson Air Force Base, Ohio
    Attn: Technical Library

Department of the Air Force
Deputy Chief of Staff for Development
Director of R & D
The Pentagon, Washington 25, D. C.

Commander
Armed Services Technical Information Agency
Arlington Hall Station
Arlington 12, Virginia
    Attn: TIPDR (10 copies)

Commander
Armed Services Technical Intelligence Agency
Arlington Hall Station
Arlington 12, Virginia
    Attn: TIPDR-B

Commander
Air Research & Development Command
Andrews Air Force Base
Washington 25, D. C.
    Attn: Technical Library - B

490

Commander
Air Proving Ground Center
Eglin Air Force Base, Florida
    Attn: Technical Library

Commander
Air Material Command
Wright-Patterson Air Force Base, Ohio
    Attn: LMDN

Air Force Systems Command
Space Systems Division
Los Angeles 45, California
    Attn: Technical Data Center

Commander
Air Force Ballistic Missile Division
Inglewood, California
P.O. Box 262
    Attn: WDSOT

Air Force Special Weapons Center
Kirtland Air Force Base
Albuquerque, New Mexico

Aeronautical Systems Division
Wright-Patterson Air Force Base, Ohio
    Attn: WWRMCO (M. Schorr)

Scientific and Technical Information Facility
P. O. Box 5700
Bethesda, Maryland
    Attn: NASA Representative (S-AK/DL)
National Aeronautics & Space Administration
Langley Research Center
Langley, Station, Hampton, Va.
    Attn: Technical Library

National Aeronautics & Space Agency
Lewis Research Center
2100 Brookpart Road
Cleveland 35, Ohio
    Attn: K. Hiller

Marshall Space Flight Center
Advanced Propulsion Section
Huntsville Alabama
    Attn: M-S&M-PA

Marshall Space Flight Center
Computation Division
Huntsville, Alabama
      Attn: Dr. Walter P. Krause

Chief, Defense Atomic Support Agency
Washington 25, D. C.
      Attn: DASAG/Library

U.S. Atomic Energy Commission
Washington 25, D. C.
      Attn: Technical Reports Library

U.S. Atomic Energy Commission
Division of Military Applications
Germantown, Md.

Advisory Group on Elec Parts
Moore School Building
200 S. 33rd St.
Philadelphia 4, Pennsylvania
      Attn: Allen M. Hadley

Director
Advanced Research Projects Agency
Washington 25, D. C.
      Chief, Technical Operations Division

Atomic Energy Commission
Space Nuclear Propulsion Office
Washington 25, D. C.
      Attn: F. C. Schwenk

University of Maryland
Director, Wind Tunnel
College Park, Maryland
      Attn: Donald S. Gross

United Aircraft Corporation
Research Division
East Hartford 8, Connecticut
      Attn: Mr. R. Olsen

Los Alamos Scientific Laboratory
Los Alamos, New Mexico
      Attn: Library

U.S. Library of Congress
Washington 25, D. C.
      Attn: Science & Technology Division

492

Army Engineer Research & Development Laboratories
Fort Belvoir, Virginia
      Attn: Chief, Mechanical Dept

University of New Mexico
Albuquerque, New Mexico
      Attn: Dr. Richard Moore

University of Michigan
Institute of Science & Technology
2038 E. Engr Bldg
Ann Arbor, Mich
      Attn: K. R. White, Director

University of Maryland
College of Aeronautical Engineering
College Park, Maryland
      Attn: W. Sherwood

University of Florida
Physics Department
Gainesville, Florida
      Attn: Technical Library - Alex G. Smith
      Attn: L. H. Roberts

Engineering Library
University of California
405 Hilgard Avenue
Los Angeles 24, California
      Attn: Mrs. J. E. Tallman

Engineering Library
University of California
Berkeley, California
      Attn: Mrs. Blanche Dalton

University of Arizona
Physics Department
Tucson, Arizona
      Attn: Professor Ulrich H. Bentz

Sandia Corporation
Sandia Base
Albuquerque, New Mexico
      Attn: Technical Library

Rensselaer Polytechnic Institute
Dept of Aeronautical Engineering
Troy, New York
        Attn: Mr. K. T. Yen

Patent Office
Washington 25, D. C.
        Attn: Scientific Library

Ohio State University
576 Melrose Avenue
Columbus 2, Ohio
        Attn: Technical Library

New York Naval Shipyard
Bldg 291, Code 91?F
Brooklyn 1, New York
        Attn: Library

National Physical Laboratory
Teddington, Middlesex, England
        Attn: Technical Library
        Thru: AMC Detachment No. 1, Washington 25, D. C.
               Attn: ORDTK

National Bureau of Standards
Bldg 16 - Rm 310
Washington 25, D. C.
        Attn: Chief Section 1.06

National Bureau of Standards
Boulder, Colorado
        Attn: Technical Library

National Bureau of Standards
Washington 25, D. C.
        Attn: Library

Minneapolis-Honeywell Regulator Company
2753 Fourth Avenue, S.
Minneapolis 8, Minn.
        Attn: Mr. H. Sparrow

Massachusetts Institute of Technology
Dept of Mechanical Engineering
Cambridge, Mass.
        Attn: L. Shearer

Linda Hall Library
Joseph C. Shipman
5109 Cherry Street
Kansas City 10, Missouri

494

Johns Hop. University
Applied P: es Laboratory
8S21 Georg Avenue
Silver Sp , Maryland
        Attn: ch Library (2 copies)

Franklin l st to e of the State of Pennsylvania
Philadelp , Pennsylvania
        Attn: C. W. Hargens, Tech Director

Mr. Charle A. Belsterling
Franklin I stitute of the State of Pennsylvania
Philadelph a 3, Pennsylvania

Engineer) Societies Librar
29 W. 39th St.
New York 1d, New York
        Attn: Mr. John Herling, Order Li an

Dayton & Montgomery County Public Libre
215 East Third Street
Dayton 2, Ohio
        Attn: Circulation Department

Corning Glass Works
Corning, New York
        Attn: James K. Davis

Cornell University
Ithaca, New York
        Attn: Dr. Ed Resler, Jr.

John Crerar Library
86 E. Randolph Street
Chicago 1, Illinois
        Attn: H. Henkle

Battelle Memorial Institute
Chief Systems Engr Div
505 King Avenue
Columbus 1, Ohio
        Attn: Chief Systems Engr. Div.

Armour Research Foundation of Illinois Ir s. of Tech Cent
10 W 45th Street
Chicago 16, Ill
        Attn: Mr. George T. Jacobi